Physics
Saxon

THE JOURNAL
OF
CHEMICAL PHYSICS

VOLUME 20, NUMBER 1 JANUARY, 1952

The Microwave Spectrum of a Slightly Aspherical Top—The Structure and Dipole Moment of Sulfuryl Fluoride*

ROBERT M. FRISTROM†
Mallinckrodt Chemical Laboratory, Harvard University, Cambridge, Massachusetts
(Received September 10, 1951)

The microwave spectrum of the slightly aspherical rotor, sulfuryl fluoride, has been investigated. Seven lines were found in the twenty to thirty thousand megacycle region. Six of these lines were assigned to $J=1\rightarrow2$ and $2\rightarrow3$ rotational transitions of the molecule $S^{32}O_2F_2$ and the other to the $1_{11}\rightarrow2_{12}$ transition of $S^{34}O_2F_2$. These lines can be fitted to within the limits of experimental error (0.002 percent) with the following reciprocal moments of inertia:

$a_{32}=5139.77$ mc $\quad a_{34}=5139.77$ mc
$b_{32}=5077.81$ mc $\quad b_{34}=5073.00$ mc
$c_{32}=5057.22$ mc $\quad c_{34}=5052.51$ mc

Structural parameters were determined from these moments and the assumption of C_{2v} symmetry. The latter was confirmed by intensity measurements.

S—O 1.370±0.01A S—F 1.570±0.01A O—S—O angle 129°38′±30′
F—S—F angle 92°47′±30′

The S—O distance differs by −0.06A from the published electron diffraction value.

Measurements on stark lobes of the three $1\rightarrow2$ transitions of $S^{32}O_2F_2$ gave a quantitative check of the assignment and a value of 0.228 Debye units for the dipole moment.

INTRODUCTION

THE slightly aspherical top is a somewhat uncommon type of molecule which has not been previously studied by microwave techniques. For such a molecule the difference between the greatest and least reciprocal moments is small compared with the reciprocal moments themselves. Consequently, the asymmetry splitting will be small regardless of the value of the asymmetry parameter, κ. The spectrum is thereby simplified. See Fig. 1.

Sulfuryl fluoride, the example chosen for this study, is noted for its chemical inertness, being stable to a red heat in metal containers.[1] Its relationship to better known molecules can be visualized by considering it as the acid fluoride of sulfuric acid or as a fluorine substitution of sulfur trioxide.

* This work was supported by the Navy Department through the ONR under Task Order V of Contract N5ori-76.

† Present address: The Johns Hopkins University, Applied Physics Laboratory, Silver Spring, Maryland.

[1] M. Trautz and E. A. Ehrman, J. prakt. Chem. **142**, 79 (1935).

EXPERIMENTAL

Preparation of Sulfuryl Fluoride

The first method used for the preparation of SO_2F_2 was the decomposition of barium fluorosulfonate, ($Ba(FSO_3)_2$) in an iron vessel.

$$Ba(FSO_3)_2 \xrightarrow{\Delta} BaSO_4+SO_2F_2\uparrow.$$

The second method was the fluorination of sulfur dioxide (SO_2) using silver difluoride (AgF_2) as the fluorinating agent.[2]

$$SO_2+2AgF_2\rightarrow 2AgF+SO_2F_2\uparrow.$$

The second procedure proved to be the more satisfactory. Samples were purified by allowing them to stand over water for twenty-four hours with redistillation at low temperature (−100°C). This procedure was repeated until the infrared spectrum (rocksalt region) remained unchanged. The final infrared spectra ob-

[2] H. J. Emeleus and J. F. Wood, J. Chem. Soc. **60**, 2183–88 (1948).

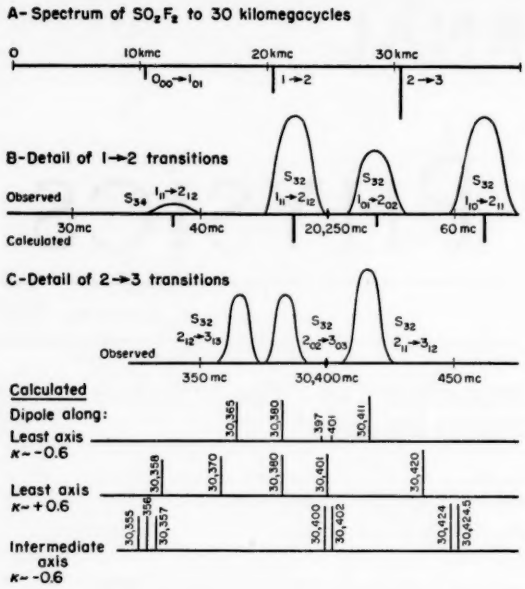

FIG. 1. Microwave spectrum of sulfuryl fluoride.

tained from the two samples were identical. In the ensuing study of the microwave absorptions, the samples were also found to be identical and were used interchangeably.

SPECTROSCOPY

The microwave measurements were made with a sixteen foot Stark effect spectrograph of the type described by McAfee, Hughes, and Wilson.[3] Since the lines proved to be weak (it was estimated that the strongest transition $1_{10}\rightarrow2_{11}$ $S^{32}O_2F_2$ had an intensity of the order of 10^{-7} cm^{-1} at room temperature), it was found desirable to increase the population differences in the lower levels by cooling the absorption cell with dry ice (−80°C). Frequency measurements were made by comparison with a microwave frequency standard which was periodically calibrated with the five megacycle standard signal broadcast by station WWV. Stark effect measurements were made using zero-based, square-wave modulation; voltmeter readings were calibrated by direct comparison with the splittings produced in the $J=1\rightarrow2$ transition of $O^{16}C^{12}S^{32}$ in the ground vibrational state, the dipole moment of which has been given by Shulman and Townes.[4] Relative intensities were measured by comparison with a one hundred kilocycle signal from a calibrated attenuator using a method developed in this laboratory by Dr. D. H. Baird.[5]

DATA

A search of the microwave spectrum in the region from 19,000 to 31,000 mc revealed a number of absorptions whose frequencies are recorded in Table I along with their apparent relative intensities, temperature coefficients of intensity, and assignments. All of these transitions were observed in normal isotopic abundance.

ANALYSIS OF DATA

The energy levels for an asymmetric rotor are given by reference 6.

$$E=\tfrac{1}{2}(a+c)J(J+1)+\tfrac{1}{2}(a-c)E^J{}_{K-1\ K+1}(\kappa). \quad (1)$$

E is the energy of the level in question expressed here in megacycles per second. a and c are the reciprocals of the least and greatest moments of inertia, respectively, expressed in the same units as E, megacycles per second. $E^J{}_{K-1\ K+1}(\kappa)$ is a function of the asymmetry parameter $\kappa=(2b-a-c/a-c)$. Explicit algebraic expressions[6,7] are available for this function for levels up to $J=7$.

For pure rotational transitions the selection rule for total angular momentum is $J=0,\pm1$. Therefore, possible transitions are given by

$$\Delta E=J^*(a+c)+\tfrac{1}{2}(a-c)\Delta E^J{}_{K-1\ K+1}(\kappa) \quad (2)$$

$$\Delta E=\tfrac{1}{2}(a-c)\Delta E^J{}_{K-1\ K+1}(\kappa). \quad (3)$$

J^* represents the upper principal rotational quantum number.

In this application, $\frac{1}{2}(a-c)$ is small (<50 mc) and $\Delta E^J{}_{K-1\ K+1}(\kappa)$ is not large (approximately J^2), so we would not expect to find transitions of the type described by Eq. (3) with J less than 25. Populations of such levels at dry ice temperature are low. Hence, we would not expect to see these transitions with our apparatus. The lines which are observed should, therefore, be transitions with the selection rule $\Delta J=\pm1$. The term $(a+c)$ is expected to be large compared with $(a-c)$, hence the predicted spectrum should consist of a series of roughly equally spaced groups of lines appearing, in the case of SO_2F_2, every ten thousand megacycles. Within each group of lines the pattern is governed by the function $\Delta E^J{}_{K-1\ K+1}(\kappa)$. The term $(a-c)$ is a scale factor and does not affect the qualitative appearance of the pattern. The ultimate assignment of the lines depends upon fitting these patterns. The theoretical splitting of the $J=1\rightarrow2$ transitions are

TABLE I. Microwave absorption frequencies of sulfuryl fluoride.

Molecule	Assignment	Frequency (mc) obs	calc	Dev.	Rel. int. obs	calc	Temp. coef. intensity
$S^{32}O_2F_2$	$1_{01}\rightarrow2_{02}$	20,258.12	20,257.63	0.49	0.5	0.48	neg.
	$1_{10}\rightarrow2_{11}$	20,276.09	20,275.61	0.48	(1.0)	(1.0)	neg.
	$1_{11}\rightarrow2_{12}$	20,244.81	20,244.46	0.35	0.67	0.7	neg.
$S^{34}O_2F_2$	$1_{11}\rightarrow2_{12}$	20,225.97	20,225.97	—	0.05	0.042	neg.
$S^{32}O_2F_2$	$2_{02}\rightarrow3_{03}$	30,380.22	30,380.71	0.49	0.33	0.36	neg.
	$2_{12}\rightarrow3_{13}$	30,365.10	30,365.29	0.19	(1.0)	(1.0)	neg.
	$2_{11}\rightarrow3_{12}$	30,411.43	30,411.57	0.14	1.33	1.0	neg.

[3] McAfee, Hughes, and Wilson, Jr., Rev. Sci. Instr. **20**, 621–626 (1949).
[4] R. Shulman and C. H. Townes, Phys. Rev. **77**, 500 (1950).
[5] D. H. Baird (to be published).
[6] King, Hainer, and Cross, J. Chem. Phys. **11**, 27–42 (1947). (Hereafter referred to as KHC−I.)
[7] Hainer, Cross, and King, J. Chem. Phys. **17**, 826–836 (1949).

reproduced in the graphs of Figs. 2(A)–(C). These were the simplest transitions observed. The three graphs represent the three possible cases: the dipole moment lying along the least, the middle, or the greatest axis. This fit allows a determination of the value of the parameters $(a-c)$ and (κ), and the identification of the symmetry axis. The latter is a very important point since the moments lie so close to one another that no choice could be made in advance.

The spacing of the 20,000 mc and 30,000 mc groups indicates that these are $J=1\rightarrow2$ and $2\rightarrow3$ transitions respectively. The value of $(a+c)$ is about 5000 mc. Qualitative observations of the Stark effect confirmed this assignment.

For the assignment of individual transitions the graphs of Fig. 2 were studied for all possible fits for the $1\rightarrow2$ group. These are indicated by vertical dotted lines. To choose among these three assignments, parameters were derived from them and the $J=2\rightarrow3$ spectrum calculated and compared with the observed spectrum. As can be seen from Fig. 1(C) only the assignment of the dipole to the least axis is compatible with the observed $2\rightarrow3$ transitions. The qualitative and quantitative study of the Stark effect confirms this assignment as do the relative intensity measurements.

A least squares analysis was made of the data based upon this assignment and it was found possible to fit the six lines of $S^{32}O_2F_2$ with three moments of inertia with a precision (0.10 mc) close to that of the experimental determinations (0.05 mc).

The conventional model has the symmetry C_{2v} with the pair of oxygens and pair of fluorines attached to the central sulfur tetrahedrally (see Fig. 3). This arrangement is confirmed by the agreement between the observed and calculated relative intensities, which include a three-to-one spin weight arising from the pair of equivalent fluorines. The oxygens must therefore also be equivalent or on the two-fold axis, the latter being incompatible with the near-equality of the moments. Finally, the observed moments of inertia are compatible with this structure with reasonable bond distances and would be difficult, if not impossible, to fit with any other reasonable arrangement.

This model would be completely determined by only four parameters, an easily visualized set of which are the S–O distance, the S–F distance, the F–S–F angle, and the O–S–O angle. For the actual computations it was found more convenient to choose a set of difference parameters. Within this set, the four parameters were correction terms based upon an assumed structure derived from the electron-diffraction determination of Stevenson and Russell.[8] Since these corrections could be assumed to be small, terms of second order were ignored and a set of three linear simultaneous equations resulted, one for each moment of inertia. It was therefore necessary to obtain one other relationship.

[8] D. P. Stevenson and H. Russell, J. Am. Chem. Soc. **61**, 3264 (1939).

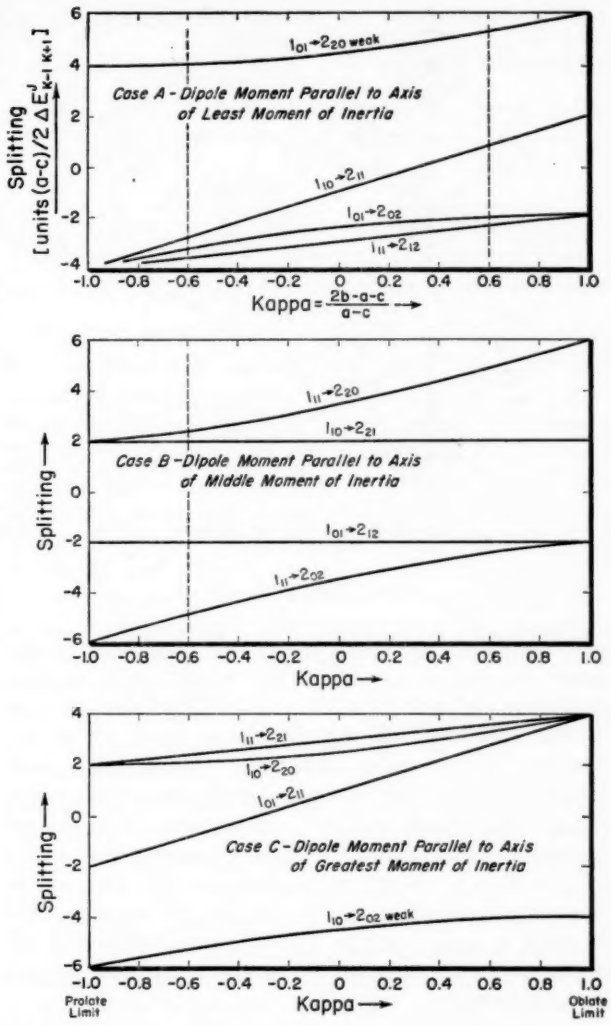

FIG. 2. Asymmetry splitting for $1\rightarrow2$ transitions as a function of Kappa. (Dotted lines mark trial assignments.)

This can be done by measuring lines for another isotopic species of this molecule.

A careful search revealed only one other line (20,225.97) in the twenty thousand megacycle region. It had a relative intensity of 0.05 and a negative temperature coefficient of intensity as would be expected for the $S^{34}O_2F_2$ species. Its location 18.84 mc below the $1_{11}\rightarrow2_{12}$ transition of the S^{32} species made it seem likely that this was the analogous transition of the S^{34} molecule. Calculations based on this assignment indicated that of the other three possible $1\rightarrow2$ transitions, one $(1_{01}\rightarrow2_{20})$ would not have sufficient intensity (0.001) to be observed and the other two $(1_{01}\rightarrow2_{02}, 1_{11}\rightarrow2_{12})$ would be hidden by S^{32} transitions. The other possible assignments of this line would lead to the prediction of other lines of easily discernible intensity in a well-searched frequency region.

This made a sufficient number of lines available to allow a complete determination of the molecular structure, but one further difficulty was encountered in the

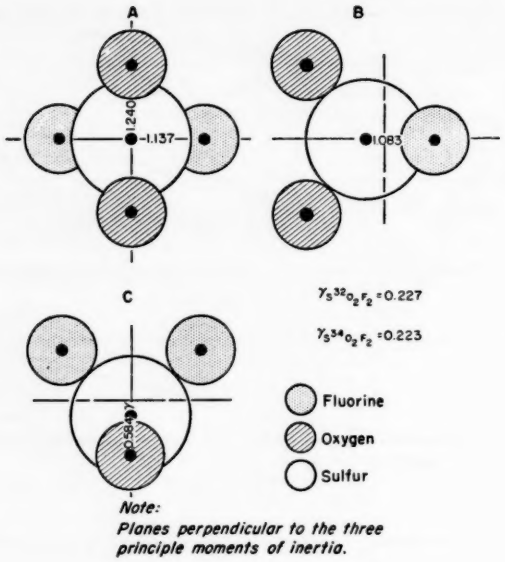

FIG. 3. Sulfuryl fluoride.

structural determination. It was not possible to assign unambiguously the spectroscopic b and c axes to their respective molecular axes. This ambiguity arises because of the smallness of the deviation from sphericity. Reasonable molecular parameters arise from both assignments, and the isotopic substitution of the sulfur atom affects both moments identically. The axis of symmetry along which the dipole moment lies (axis a in Fig. 3) was, of course, unambiguously assigned to the least moment of inertia for the S^{32} isotope. This moment is unchanged by the S^{34} substitution and the dipole moment remains along the least axis in this isotopic species.

Fortunately parameters of reasonable accuracy can be obtained without using this information. It was found that the distances in the plane perpendicular to the symmetry axis were only slightly affected by an interchange of these two axes (b and c). This interchange corresponds to a ten-megacycle shift in frequency and a change of 0.002A in the O−O and F−F distances; therefore these distances were calculated from the assumption that $I_b \cong I_c$. The O−F distance was calculated from this assumption and the value of the I_a moment. These first three parameters were derived from the spectra of $S^{32}O_2F_2$, but the fourth parameter, the location of the sulfur atom along the axis of symmetry, must be obtained from the isotopic shift resulting from the S^{34} substitution. In the case of this line, $1_{11} \rightarrow 2_{12}$, the frequency shift bears a very simple relationship to the molecular parameters, such that

$$d_s \cong \left[\delta f_{32/34} (2/3I_c^{32} + 1/3I_b^{32}) \times \frac{1}{4{,}043{,}592} \right]^{\frac{1}{2}}$$

if the units employed are megacycles, angstrom units, and atomic weight units. This simplification results from the near sphericity of the molecule and smallness of the increase of moments of inertia upon this substitution. $\delta f_{32/34}$ is the isotopic frequency shift and d_s is the distance of the sulfur atom from the center of gravity. Table II gives a compilation of the parameters given by these calculations and compares them with the corresponding electron diffraction data. The values of the fundamental constants given by Dumond and Cohen[9] were used.

DISCUSSION OF ERRORS AND THE RELIABILITY OF STRUCTURAL PARAMETERS

The accuracy of frequency measurement (better than 0.1 mc) and the accuracy of the fundamental constants are not limiting factors in this case. The distances calculated are effective distances for the ground vibrational state and will, therefore, differ somewhat from the equilibrium distances, but this is also true of the electron diffraction values. The limiting factor is probably the change in these effective distances with isotopic substitution. In the calculations this change was assumed to be zero. It is difficult to put reliable limits on this source of uncertainty, but on various grounds it is estimated that it does not exceed 0.01A.

The three parameters determined by the S^{32} lines give self consistent results to 0.2 percent (0.002A) in fitting the spectra. Unfortunately only one S^{34} line is available, so that a direct check of the self consistency of the fourth parameter is not possible. However, if we assume that the two missing lines are hidden by two S^{32} lines, the frequency of the missing lines will lie within the line breadth‡ of the masking S^{32} lines. This determines their frequency to within about four megacycles. These considerations indicate that the self consistency of the isotopically derived parameter is better than two percent.

TABLE II. Molecular parameters of sulfuryl fluoride.

Parameter	Microwave data	Electron diffraction data[8]
O−O	2.48_0A±0.002A	
F−F	2.27_4A±0.002A	
O−O−F−F	1.66_7A±0.002A	
d_s32	0.22_7A±0.01A	
d_s34	0.22_3A±0.01A	
S−O	1.37_0A±0.01A	1.43A±0.02A
S−F	1.57 A±0.01A	1.56A±0.02A
F−C	2.368A±0.002A	2.37A+0.02A
O−S−O	129°38′±30′	130°±10°
F−S−F	92°47′+30′	100°± 8°

Reciprocal moments of inertia:

a_{32}=5139.77 mc	a_{34}=5139.77
b_{32}=5077.81	b_{34}=5073.40
c_{32}=5057.22	c_{34}=5052.51

[9] J. W. M. Dumond and E. R. Cohen, Revs. Modern Phys. **20**, 82 (1948).

‡ At the relatively high pressures necessary to render S^{34} lines visible (approx 0.1 mm of Hg) the line breadth (half width at half height) was about 4 mc.

STARK EFFECTS AND DIPOLE MOMENTS OF SULFURYL FLUORIDE

The Stark effect for the 1→2 transitions was predicted using the perturbation theory results of Golden and Wilson.[10] Because of the smallness of $(a-c)$ the tables of this paper were not used. The equations describing the behavior of the Stark components for the various $J=1\rightarrow2$ transitions are collected in Table III. The six Stark lobes expected were observed, and the standard deviation of the quantitative measurements was two percent. The dipole moment of sulfuryl fluoride is derived from thirty-four Stark measurements including all of the 1→2 transitions.

There are two possible sources of error: the field determination and the frequency determination. The reliability of voltage measurements is primarily determined by the reproducibility of the peak-reading voltmeter between the time of calibration and the time of measurement. This error did not appear to be greater than two percent. Frequency measurements were limited by the ability to locate the peak of the Stark lobe being studied. This depended markedly upon conditions, since these are weak lines, but in general it was of the order of two megacycles or less. The experimental scattering appeared to be random and the dipole moment was determined by the method of least squares.

Dipole moment $=0.228\pm0.004$ Debye units.

DISCUSSION OF THE STRUCTURE AND DIPOLE MOMENT OF SULFURYL FLUORINE

The bond distances and angles reported are normal for sulfur-oxygen-fluorine compounds and check with Russell and Stevenson's electron diffraction work, except in the case of the S—O distance. The probable distance for this link is shorter by 0.06A than that reported by Russell and Stevenson, and is considerably shorter than any other reported sulfur-oxygen distance. This discrepancy with electron diffraction work is unusual and, therefore, deserves careful consideration. It is well outside the sum of the limits of error reported for these measurements. It is interesting to note that their most reliable parameter, O—F, exactly checks the present determination.

[10] S. Golden and E. B. Wilson, Jr., J. Chem. Phys. **16**, 669–685 (1948).

TABLE III. The Stark effect in sulfuryl fluoride $J=1\rightarrow2$ transitions.

Transition		Equation
$1_{01}\rightarrow2_{02}$ $1_{11}\rightarrow2_{12}$ $1_{10}\rightarrow2_{11}$	$M=0$	$\Delta\nu=-14.7_6\times10^{-6}\mu^2E^2$ $\Delta\nu=12.25\times10^{-6}\mu^2E^2$ $\Delta\nu=12.25\times10^{-6}\mu^2E^2$
$1_{01}\rightarrow2_{02}$ $1_{11}\rightarrow2_{12}$ $1_{10}\rightarrow2_{11}$	$M=1$	$\Delta\nu=9.30\times10^{-6}\mu^2E^2$ $\Delta\nu=8.10\times10^{-6}\mu^2E^2+0.33\mu E$ $\Delta\nu=8.10\times10^{-6}\mu^2E^2-0.33\mu E$

The shortening of the S—O bond might be correlated with a decrease in importance of resonance structures involving negative oxygen because of inhibitions introduced by the very electronegative fluorine. This would lead to an increase in importance of the triple bond structure relative to S—O compounds such as SO_3, with a resultant shortening of the bond length of the hybrid. The S—O bond of SOF_2 might also be expected to be abnormal, but present electron diffraction work does not seem to indicate this. Because of the lack of knowledge of the number and structure of the principle resonance forms, it would seem wiser to defer these considerations until more data are available. This could be furnished by a study of the quadrupole splittings of the $S^{33}O_2F_2$ isotopic species.

The dipole moment of sulfuryl fluoride is low (0.228 D.), as would be expected from qualitative considerations of electronegativity. Fluorine and oxygen are both highly electronegative (respectively, 4.0 and 3.5) and occupy equivalent and opposed positions in the molecule, thus tending to cancel the two contributions. It may eventually become possible to combine this dipolar and structural data with nuclear quadrupole splitting data to give a clearer picture of electronic distribution within this molecule.

ACKNOWLEDGMENTS

The author would like to acknowledge: suggestions by Professor M. Kent Wilson on the preparation of sulfuryl fluoride, a check of the Stark effect calculations by Mr. Ray Ferguson, criticism of this manuscript by Drs. D. Mann and C. K. Jen, the considerable interest and assistance of Dr. Marshall H. Sirvetz, and the many helpful suggestions of Professor E. Bright Wilson, Jr., who directed this research.

Diffusion through an Interface—Binary System*

L. H. TUNG AND H. G. DRICKAMER
Department of Chemistry, University of Illinois, Urbana, Illinois
(Received October 4, 1951)

Diffusion measurements have been made between saturated layers in the system SO_2—*n*-heptane, using S^{35} tagged SO_2 as a radioactive tracer. The results are evaluated in terms of the interfacial transfer coefficient α introduced in a previous paper. The resistance in the interface is significant compared with the resistance to ordinary diffusion, even within 4°C of the critical solution temperature.

THE mechanism of molecular motion through an interface is a matter of both theoretical and practical interest. Previous investigations[1] of the situation without the assistance of radioactive tracers have all involved the use of unsaturated solutions. This introduces changes in concentration and in interfacial resistance with time. The use of stirring in one or both phases has further complicated the analysis of the results.

In this paper, results of diffusion measurements for the system SO_2-normal heptane at 0°C and 15°C are presented. Measurements were made between saturated hydrocarbon layers, between saturated SO_2 layers, and from the saturated SO_2 layer to the saturated hydrocarbon layer using S^{35} tagged SO_2 as the tracer. The results were analyzed according to the phenomenological theory presented in a previous paper.[2]

EQUIPMENT AND PROCEDURE

The ordinary SO_2 used was 99.6 percent pure and was obtained from the Matheson Company. The heptane was Phillips Pure grade. The tagged SO_2 was produced by combustion of sulfur containing S^{35} obtained from Oak Ridge National Laboratory.

The saturated layers were obtained in the following manner: Two identical stainless steel storage bombs were each filled with a mixture of heptane and SO_2. The fillings were identical except that one bomb contained some tagged SO_2. The bombs were heated above the critical solution temperature (19°C)[3] and then cooled to the diffusion temperature and allowed to stand for two hours.

Because of the volatility of the SO_2, all subsequent transferring, as well as the diffusion, was carried out under a pressure of 6.8 atmospheres. The pressure was supported by nitrogen and was transmitted to the bombs by mercury U-tubes.

The main features of the diffusion bomb, as shown in Fig. 1, were a cylinder, A, and a piston, B, closely fitted in the cylinder. The cylinder and the piston were lying horizontally. On the upper side of the piston A a hole of $\frac{3}{8}$ inch in diameter was drilled to about $\frac{3}{8}$ inch deep; this hole was the bottom diffusion cell C1. The upper cell C2 was another $\frac{3}{8}$-inch hole on the cylinder. The cell C1 was lined up with the filling lines when the piston was in the filling position and was lined up with the cell C2 when the piston was in the diffusion position. The crystal D of the scintillation counter was

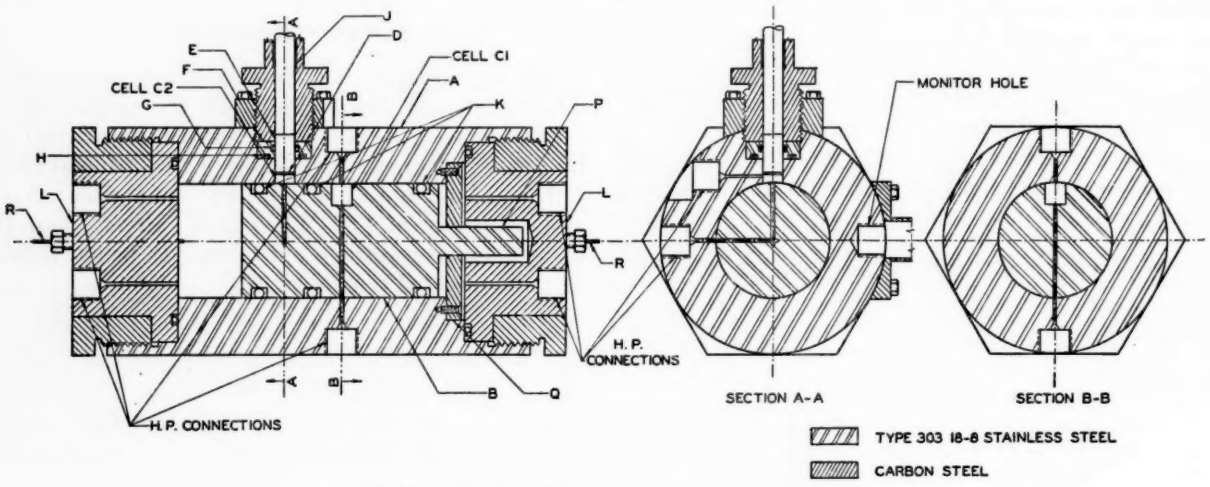

FIG. 1. Diffusion apparatus for volatile liquids.

* This work was supported in part by the AEC.
[1] M. Irwin, Proc. Soc. Exptl. Biol. Med. **26**, 125 (1928); E. Hutchinson, J. Phys. Colloid Chem. **52**, 897 (1948); J. T. Davies, J. Phys. Colloid Chem. **54**, 185 (1950).
[2] Scott, Tung, and Drickamer, J. Chem. Phys. (to be published).
[3] R. T. Leslie, J. Research Natl. Bur. Standards **13**, 589 (1934).

located at the end of the cell C2. The light pulses of the crystal were conducted out of the cell by means of a $\frac{3}{8}$ inch in diameter quartz rod, E. The quartz rod was sealed on a stainless steel ring, F, by means of an "O" ring, G. This stainless steel ring was in turn sealed to the cylinder by another "O" ring, H. The light pulses from the quartz rod were then transmitted through a Lucite rod, J, to the counting circuit. The Lucite rod was provided with a shoulder to keep both the quartz and the Lucite rods in position. The Lucite rod was used because a long quartz rod with a shoulder was too brittle to handle.

The length of the cell C2 could be varied by changing the position of the quartz rod. The length of C1 could be changed by inserting blanks into the bottom of the cell. Both cells were packed tightly with 150-mesh stainless steel screens to prevent convection.

Three "O" rings, K, were used on the piston. The two end "O" rings made the liquid seal of the cells. The middle "O" ring was used to prevent the mixing of the liquids in the two cells while the piston was in the filling position. All the "O" rings were made of compound No. 153–70, a special type of rubber recommended by its manufacturers† for resisting liquid sulfur dioxide and *n*-heptane. Two $\frac{1}{16}$-inch lines were connected to each cell when the piston was in filling position. One of the two $\frac{1}{16}$-inch lines was for the filling and extracting of the cell liquids. The other was for the evacuation of the cell. All these lines were connected to standard $\frac{1}{4}$-inch pressure tubing by means of standard high pressure joints.

The piston was moved from one position to the other position by means of nitrogen pressure. The nitrogen was introduced through the end pieces L of the bomb. Each end piece was provided with two $\frac{1}{16}$-inch lines; one was for the nitrogen inlet, the other for the nitrogen outlet. The piston was prevented from rolling by a guide, P, with a square cross section. The guide fitted snugly in a square hole on a flat plate, Q. One electrical lead, R, was so adjusted that the piston would just come into contact with one of the leads when it was in the diffusion position, and with another lead when it was in the filling position. Thus the position of the piston could be indicated by two pilot lights connected to the electrical leads.

The piston, B, the cylinder, A, and the ring, F, were in direct contact with the diffusing liquids; and they were made of type 303 18–8 stainless steel. The rest of the parts were machined from cold-rolled steel. This bomb was designed to withstand safely 70 atmospheres pressure, though the working pressure for the present system was 6.8 atmospheres. At this working pressure, a nitrogen pressure of 5–6 atmos was required to push the piston from one position to another.

A $\frac{1}{2}$-inch threaded hole was drilled about $\frac{1}{2}$ inch deep on the outside of the cylinder. A γ-ray source monitor could be screwed into the hole when it was desired to check the scintillation counter circuit.

The diffusion bomb and the storage bombs, as well as the transfer lines, were emersed in a bath controlled to ± 0.05°C by conventional methods.

Three measurements were necessary to determine the interfacial transfer coefficient α. First, D_1, the diffusion coefficient of radioactive sulfur dioxide in *n*-heptane saturated sulfur dioxide, and D_2, the diffusion coefficient of radioactive sulfur dioxide in sulfur dioxide saturated *n*-heptane, had to be measured. Then the diffusion of radioactive sulfur dioxide from the *n*-heptane saturated sulfur dioxide layer across the interface into sulfur dioxide saturated *n*-heptane layer was to be measured.

For the *n*-heptane layer measurements, the top layer of both storage bombs were pushed into the cells after the cells were evacuated. As soon as the piston was pushed into the diffusion position, the counting of radioactivity by means of the scintillation counter started, and continued until the change of number of counts per minute became negligible.

When the heavier sulfur dioxide layers in the storage bombs were to be pushed into the diffusion cells, care was taken to remove all the top layer liquid. This was done by pushing the top layer into the recovery system. The location of the interface in the storage bombs was estimated by the amount of liquid introduced to the bombs. Also when any sulfur dioxide layer discharged from the cell to the recovery system, a sudden surge in pressure resulting from the volatility of sulfur dioxide could be observed from the manometer. This was a direct indication that all the *n*-heptane rich layer had been removed from the storage bomb.

For interfacial runs, the bottom layer from one storage bomb and the top layer from the other bomb were pushed into the cells.

PHENOMENOLOGICAL THEORY

The phenomenological theory for diffusion through an interface in an apparatus as considered in the preceding discussion was presented in a previous paper. It was assumed that the rate of transport across the interface is given by the equation:

$$\mathbf{J}=\alpha[c(0-t)-mC(0+,t)]. \tag{1}$$

The general solution of the diffusion equation was

$$J=\frac{Co}{m+1}-\sum_{h=1}^{\alpha}\frac{2\alpha kCo\,\sin\eta_n a\,\cos k\eta_n a(x-a)e^{-D_1\eta_n^2 t}}{\eta_n[\alpha a(k^2m+1)\sin\eta_n a\,\sin k\eta_n a-\alpha ak(m+1)\cos\eta_n a\,\cos k\eta_n a+k(D_1D_2)^{\frac{1}{2}}\{\sin ka\eta_n\,\sin a\eta_n+\eta_n a(k\,\sin\eta_n a\,\cos ka\eta_n+\sin k\eta_n a\,\cos\eta_n a)\}]}, \tag{2}$$

† Precision Rubber Products Corporation, Dayton, Ohio.

for the interval $0<x<a$, with a similar equation for the interval $-a<x<0$. The η_n are roots of

$$k(D_1D_2)^{\frac{1}{2}}\eta \sin k\eta a \sin\eta a - \alpha k m \cos k\eta a \sin\eta a - \alpha \cos\eta a \sin k\eta a = 0. \quad (3)$$

For the case of no resistance (equilibrium) at the interface (2) reduces to

$$C=\frac{Co}{m+1}-\sum_{n-1}^{\infty}\frac{2kCo \sin\eta_n a \cos k\eta_n(x-a)e^{-D_1\eta_n^2 t}}{\eta_n[a(k^2m+1)\sin\eta_n a \sin k\eta_n a - ak(m+1)\cos\eta_n a \cos k\eta_n a]} \quad \text{for } 0<x<a, \quad (4)$$

and (3) becomes

$$km \cos k\eta a \sin\eta a + \cos\eta a \sin k\eta a = 0. \quad (5)$$

For the case of diffusion in a single phase, the result is

$$C=\frac{Co}{2}-\sum_{n=1}^{\infty}\frac{2Co \sin\frac{n\pi}{2}\cos\frac{n\pi}{2a}(x-a)e^{-D(n\pi/2a)^2 t}}{n\pi} \quad \text{for } 0<x<a \quad (6)$$

which is identical with the result given by Barrer.[4]

For weak beta-rays such as those emitted by S^{35}, it can be shown that the intensity of radiation as measured will be proportional to the concentration at the crystal surface.

For the latter part of the run, only the first term of the summation in Eq. (2) need be considered. It then reduces to

$$I=I_f-Be^{-D_1\eta_1^2 t}, \quad (7)$$

where I_f is the final radiation intensity, and B is a constant for any cell and type of radiation.

If I_f is known, then the plot of $\log(I_f-I)$ against t will give a straight line, the slope of which is $-D_1\eta_1^2=-S$.

In the case of diffusion in a single phase $\eta_1=\pi/(2a)$. Knowing the path length $2a$, one can calculate the diffusion coefficient D from the slope which is now $-D[(\pi/2a)]^2=-S$; or knowing D the effective path length $2a$. Also in single phase diffusion the series in equation is relatively simple. A method has been developed by Timmerhaus and Drickamer[5] to calculate D. In their method a ratio $\delta=(I_{t1}-I_{t2})/(I_{t3}-I_{t4})$ was calculated and plotted against S. Sufficient terms were used in the numerical evaluation of δ to make the deviation from the series in Eq. (41) less than 0.1 percent. Therefore, using their method the diffusion coefficient D can be calculated from measurements at any stage of the diffusion. This method has certain advantages: (1) for relatively long runs there is no need to follow the process practically to the equilibrium state; (2) any convection that occurs at the early stage of diffusion can be detected.

In the case of diffusion with an interface, η_1 is a function of D_1, D_2, a, m, and α. D_1, D_2, and a can be determined by the corresponding single phase diffusion measurements. Knowing D_1, one can calculate η_1 from the slope s. Then the transfer coefficient at the interface α can be calculated from Eq. (3).

In order to calculate diffusion coefficients from the experimental results it was necessary to obtain the effective path length ($2a$). The diffusion coefficient of 0.1 M sulfuric acid into pure water at 20°C was used for the calibration. This diffusion coefficient was measured by Öholm[6] to be 1.73×10^{-5} cm²/sec.

The effective path length was found to be 1.49 times the cell length, which corresponds closely to the result obtained by Robb and Drickamer[7] for tightly packed 150-mesh screening.

TABLE I. The experimental results for the system sulfur dioxide $-n$-heptane. The effective path length $2a=1.051$ cm. Pressure $=100$ psig.

Run no.	Type of run	Temp °C	
32	$S^{35}O_2$ in $n-C_7$ saturated with SO_2	0.5	7.86
33	$S^{35}O_2$ in $n-C_7$ saturated with SO_2	0.5	7.66
34	$S^{35}O_2$ in $n-C_7$ saturated with SO_2	0.5	8.07
35	$S^{35}O_2$ across SO_2 and $n-C_7$ interface	0.5	1.82[a]
36	$S^{35}O_2$ across SO_2 and $n-C_7$ interface	0.5	1.69[a]
38	$S^{35}O_2$ in SO_2 saturated with $n-C_7$	0.5	4.32
39	$S^{35}O_2$ in SO_2 saturated with $n-C_7$	0.5	5.34
49	$S^{35}O_2$ in $n-C_7$ saturated with SO_2	15.0	46.2
50	$S^{35}O_2$ in $n-C_7$ saturated with SO_2	15.0	42.7
51	$S^{35}O_2$ in $n-C_7$ saturated with SO_2	15.0	43.0
52	$S^{35}O_2$ in $n-C_7$ saturated with SO_2	15.0	41.7
54	$S^{35}O_2$ across SO_2 and $n-C_7$ interface	15.0	4.90
55	$S^{35}O_2$ across SO_2 and $n-C_7$ interface	15.0	4.68[a]
58	$S^{35}O_2$ in SO_2 saturated with $n-C_7$	15.0	8.18
60	$S^{35}O_2$ in SO_2 saturated with $n-C_7$	15.0	8.26

[a] Apparent diffusion coefficient D_a.

DISCUSSION OF RESULTS

The experimental results are shown in Table I. For runs involved the diffusion across an interface, the values which appear in column "D" are D_a. D_a is the apparent diffusion coefficient obtained by treating the

TABLE II.

Temp °C	$D_1\times10^5$ cm²/sec	D_2+10^5 cm²/sec	$D_a\times10^5$ cm²/sec	m	$\alpha\times10^5$ cm/sec
0.5	4.83	7.85	1.76	8.9	1.10
15.0	8.22	43.4	4.79	5.2	4.33

[4] R. M. Barrer, *Diffusion in and Through Solids* (Macmillan Company, New York, 1941).

[5] K. D. Timmerhaus and H. G. Drickamer, J. Chem. Phys. **19**, 1242 (1951).

[6] J. Öholm, *International Critical Tables* (McGraw-Hill Book Company, Inc., New York, 1926).

[7] W. L. Robb, Ph.D. dissertation (University of Illinois, Urbana, Illinois, 1951).

experimental data in the same manner as treating those of the single phase runs. Since $s=D_1\eta_1^2$ for interfacial runs, then

$$D_A=D_1\left(\frac{2a\eta_1}{\pi}\right)^2.$$

The transfer coefficient for the interface calculated from the experimental results for this system is shown in Table II. D_1 is the diffusion coefficient of $S^{35}O_2$ in the n-heptane saturated sulfur dioxide layer. D_2 is the diffusion coefficient of $S^{35}O_2$ in the sulfur dioxide saturated n-heptane layer. D_a is the apparent diffusion coefficient for the interfacial runs. The values for D_1, D_2, and D_a in Table II were the average values of two or more runs. m is the distribution coefficient. The values of m were calculated from Leslie's data. Two approximations were made in the calculation: (1) the volume of the saturated solution was taken as additive; (2) the effect of pressure on m was neglected. The first approximation was rather bold since the volume for a nonideal solution is not additive and partially miscible liquids certainly do not form ideal solutions. It was used here since an analysis of such a volatile system would be very tedious. The second approximation was justified because the change of mutual solubilities for liquids under such small pressure was probably very small. Also in Leslie's experiments, closed tubes were used. The liquids, confined in the closed tube, exerted pressure probably not greatly different from 6.8 atmos, the pressure used in the present experiment to overcome the volatility of sulfur dioxide. The method used for the calculation of α from D_1, D_2, D_a, and m was described in the section on phenomenological theory.

From the values of α obtained, it can be seen that the interfacial resistance is appreciable and is not negligible in the problem of transport of molecules between phases.

Figure 2 shows the actual curves obtained in the experiments. Curve I is run 58, the diffusion of $S^{35}O_2$ in sulfur dioxide saturated with n-heptane at 15°C. Curve II is run 49, the diffusion of $S^{35}O_2$ in n-heptane saturated with sulfur dioxide at 15°C. Curve III is run 55, the diffusion of $S^{35}O_2$ from the sulfur dioxide rich layer, across the interface into the n-heptane rich layer. Curve III shows a diffusion rate which is definitely slower than either of the runs shown by Curves I and II. Curve IV was calculated from Eqs. (4) and (5). This is the curve the interfacial diffusion would follow if there was no resistance at the interface. The difference between Curves III and IV is quite distinct.

The Curve (V) was calculated from Eqs. (2) and (3) for the interfacial diffusion having the same resistance as the run of Curve III. The dotted curve, calculated from the phenomenological theory agrees perfectly with the actual observed Curve III for the latter part of the diffusional process. This justified the assumption made for the flux at the interface, i.e., Eq. (1), for that part of the diffusional process. There are some discrepancies between the curve for run 55 and the theoretical curve. These discrepancies, however, could be the result of the disturbance made on the interface when the two cells were pushed together at the start of the run.

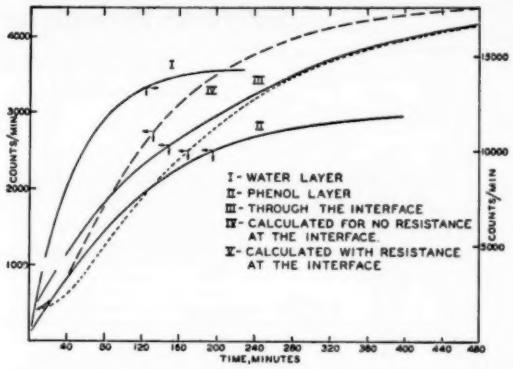

FIG. 2. Curves of concentration *versus* time for diffusion in the system SO_2-n-heptane.

The value of α for 15°C was greater than that for 0.5°C. This meant a decrease of resistance at the interface as temperature increased. However, the diffusion coefficients for both layers increased also. D_1 increased 7-fold, D_2 increased 5.5-fold, while α increased 3.9-fold. Relatively α did not increase any faster than the diffusion coefficients. The 15°C and 0.5°C were 4°C and 18.5°C, respectively, below the critical solution temperature which was 19°C. The interfacial tension should change rapidly where the temperatures were close to the critical solution temperature. Thus, the relative interfacial resistance to diffusion apparently changed little with a decrease of interfacial tension. It is perhaps surprising to note significant interfacial resistance within 4°C of the critical solution temperature, and it indicates that surface tension is not the only important element in this resistance.

NOMENCLATURE

- a half-length of the diffusion cell cm.
- B a constant.
- C concentration.
- Co initial concentration in phase 1.
- D diffusion coefficient.
- D_1 diffusion coefficient in phase 1.
- D_2 diffusion coefficient in phase 2.
- D_a apparent diffusion coefficient.
- I intensity of radiation.
- I_f final intensity of radiation.
- J flux of the diffusing molecules at this interface
- k $(D_1/D_2)^{\frac{1}{2}}$.
- m distribution coefficient of the diffusing component between the phases at equilibrium.
- S $D_1\eta_1^2$; for single phase diffusion $S=D(\pi/2a)^2$.
- t time.
- x distance coordinate of the cell.
- α transfer coefficient at the interface.
- δ the ratio $(I_{t1}-I_{t2})/(I_{t3}-I_{t4})$.

Diffusion through an Interface—Ternary Systems*

L. H. TUNG AND H. G. DRICKAMER
Department of Chemistry, University of Illinois, Urbana, Illinois
(Received October 4, 1951)

Diffusion measurements have been made at 22°C and at 40°C in the system phenol-H_2SO_4-water, using S^{35} tagged H_2SO_4 as a radioactive tracer. Measurements made through the interface indicate that a significant resistance resides in the interface at both temperatures, and that the solution chemistry of the system must be quite complex. The relation of the results to practical mass transfer problems is briefly discussed.

THE work presented in this paper is a continuation of previous work[1] on diffusion through an interface. In this case the system studied was phenol-H_2SO_4-water, using S^{35} tagged H_2SO_4 as a tracer. It was obvious from the first that the system was not simple, and its solution chemistry turned out to be considerably more complex than anticipated. It is difficult, however, to find a satisfactory ternary system involving a reasonably available tracer.

The general method of the present work was the same as that of the previous paper, as diffusion was measured between equilibrium layers, with and without an interface.

EQUIPMENT AND PROCEDURE

The construction of the apparatus for this system was relatively simple as the components were not volatile and no pressure device was needed. The main body of the apparatus into which the cells could be inserted is shown in Fig. 1. A mercury seal cover was provided to make the apparatus light tight and to prevent evaporation of the liquids. The mercury cup, *F*, was welded to the body piece, *A*. Both *F* and *A* were machined from carbon steel. A brass tube, *B*, was soldered to the bottom of the body piece, *A*. The tube *B* was provided with a flange, *G*, through which the piece was fastened to the bottom of the temperature bath. *C* was a short section of Bakelite which served as a heat insulator. *D* was another brass piece directly attached to the photomultiplier tube box. A Lucite rod, *H*, $\frac{3}{8}$ inch in diameter, was used to conduct the light pulses from the crystal in the cell. *J* was a piece of $\frac{3}{8}$-inch diameter quartz rod. This quartz rod was used to protect the polished surface of the Lucite rod. The quartz rod was sealed on a brass ring, *K*, by means of an *"O"* Ring. The brass ring, *K*, was sealed in turn by an *"O"* Ring to the body piece, *A*. Another *"O"* Ring was used to seal the Lucite rod on piece *D*. All these *"O"* Rings served to prevent moisture or any other vapor leaking into the photomultiplier tube box. *E* was the light tight cover. *L* was another lid to prevent mercury droplets falling into *A*.

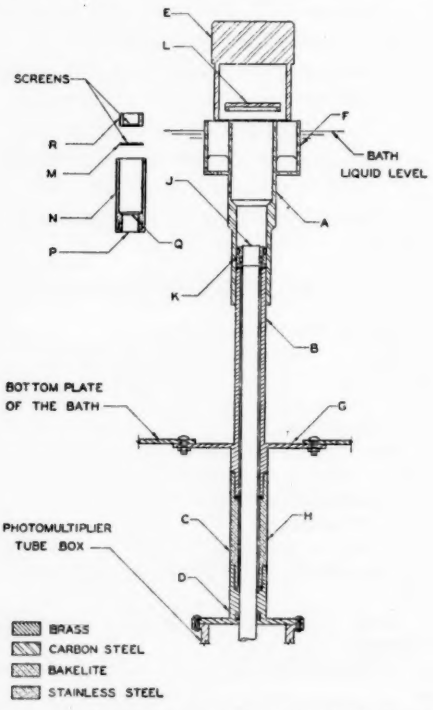

FIG. 1. Diffusion apparatus for nonvolatile liquids.

The diffusion cell consisted of three pieces. The pieces *M* and *N* constituted the bottom cell and *R* was the upper cell. *N* was a stainless steel tube closed from the bottom by a quartz roll, *P*. *P* was sealed to the stainless steel tube by means of fused silver chloride or ceresine wax. *M* was a thin stainless steel ring. Three pieces of 150-mesh stainless steel screen were packed in this ring. *R* was also a stainless steel ring with four pieces of the same mesh stainless steel screen packed at the end of the ring. Rings *R* and *M* could slide easily in and out of the tube *N*. The tube *N* could also slide easily in and out of the narrowed section of the body piece, *A*.

The apparatus was immersed in a constant temperature bath. The bath was 11 inches in diameter and 7 inches deep. The temperature was controlled to 0.1°C with conventional heaters, stircer and mercury thermostatic device.

As in the sulfur dioxide *n*-heptane system, three measurements were necessary to determine the interfacial transfer coefficient α: the diffusion of radioactive

* This work was supported in part by the AEC.
[1] L. H. Tung and H. G. Drickamer, J. Chem. Phys. **20**, 6 (1951).

sulfuric acid in water rich layer, the diffusion of radioactive sulfuric acid in phenol rich layer, and the diffusion of radioactive sulfuric acid from water rich layer across an interface into the phenol rich layer.

In preparing the liquid mixtures, the critical solution composition, which was 44-percent phenol and 56-percent 0.1 N sulfuric acid, was used always. The mixture was put in a test tube, well shaken, and then immersed in the constant temperature bath. After the two layers were formed, the top layer and the lower layer were separated into two other test tubes. The liquids were separated once more to insure a complete separation of the two phases before they were filled into the cells. Both the radioactive and nonradioactive mixtures were treated in the same way.

After the liquids were separated the tube N was inserted into piece A. The diffusion liquid for the bottom cell were dropped in from a Mohr's pipette. Then ring M was slid down the tube N. The amount of liquid in the tube N was just enough to become level with ring M after M was inserted. Then the same amount of radioactive liquid was dropped on the ring R. The stainless steel screens on ring R were immediately wetted. The ring R was then lowered carefully down into the tube N. As soon as the ring R came into contact with the ring M, the lid L and the cover E were put in place and counting was then started. The drop size of the Mohr's pipette was calibrated, so that the volume of the liquid introduced could be calculated by the number of drops dropped in the tube N and on the screens of ring R. In the 40°C runs the pipettes were all warmed above 40°C to prevent a second layer from separating from the saturated liquids.

The effective path length was determined from calibration runs using the diffusion of 0.1 M H_2SO_4 into water as in the previous paper. In this case the screening was loosely packed and was found to add 0.014 cm to the length of each cell. The path length varied from liquid to liquid because of the difference in drop size. This was measured independently and taken into consideration in the calculations.

PHENOMENOLOGICAL THEORY

The phenomenological theory is identical with that of the previous paper[1] and will not be repeated here. All references to equation numbers refer to equations in the previous paper.

DISCUSSION OF RESULTS

The experimental results are shown in Table I. The method of obtaining the effective diffusion coefficient D_a is discussed in reference 1 of the table.

The transfer coefficient for the interface α calculated from the experimental results of this system is shown in Table II.

Here D_1 is the diffusion coefficient of the radioactive sulfuric acid in the water rich layer of the mixture of 44 percent phenol and 56 percent 0.1 N sulfuric acid.

TABLE I. The experimental results for the system water-phenol-sulfuric acid.

Run No.	Type of run[a]	Temp °C	Effective path length $2a$ cm	$D\times10^5$ cm²/sec
94	$H_2S^{35}O_4$ in water rich layer	22.0	0.334	0.352
95	$H_2S^{35}O_4$ in water rich layer	22.0	0.334	0.326
97	$H_2S^{35}O_4$ across the water-phenol interface	22.0	0.320	0.0797[b]
99	$H_2S^{35}O_4$ across the water-phenol interface	22.0	0.320	0.1089[b]
103	$H_2S^{35}O_4$ across the water-phenol interface	22.0	0.320	0.1006[b]
100	$H_2S^{35}O_4$ in phenol rich layer	22.0	0.306	0.137
101	$H_2S^{35}O_4$ in phenol rich layer	22.0	0.306	0.143
115	$H_2S^{35}O_4$ in water rich layer	40.0	0.250	0.0718
116	$H_2S^{35}O_4$ in water rich layer	40.0	0.250	0.0720
124	$H_2S^{35}O_4$ across the water-phenol interface	40.0	0.238	0.0163[b]
127	$H_2S^{35}O_4$ across the water-phenol interface	40.0	0.238	0.0212[b]
104	$H_2S^{35}O_4$ in phenol rich layer	40.0	0.300	0.435
120	$H_2S^{35}O_4$ in phenol rich layer	40.0	0.229	0.454
126	$H_2S^{35}O_4$ in phenol rich layer	40.0	0.229	0.455

[a] Apparent diffusion coefficient D_a.
[b] All the liquids were from the equilibrium mixture of 44 percent phenol and 56 percent 0.1 N H_2SO_4.

D_2 is the diffusion coefficient of the radioactive sulfuric acid in the phenol rich layer of the same mixture. D_a is the apparent diffusion coefficient of radioactive sulfuric acid diffusion from the water rich layer to the phenol rich layer across an interface. The values for D_1 and D_a were also the average of two or more runs. The distribution coefficient m was measured by counting the radioactivity of each layer of a 44 percent phenol and 0.1 N sulfuric acid 56 percent mixture containing radioactive sulfuric acid. The difference of radioactive absorption factor in the two layers was neglected. Thus,

$$m=\frac{\text{(No. of counts in the water rich layer—background)}}{\text{(No. of counts in the phenol rich layer—background)}}.$$

The method used for the calculation of α was the same as that used in reference 1 and is described there.

Figure 2 shows the experimental curves for the 22°C runs. I is the diffusion curve of the radioactive sulfuric acid in the water rich layer. II is the diffusion curve of the radioactive sulfuric acid in the phenol rich layer. III is the curve for the interfacial diffusion. Comparing Curve III with Curve IV, the calculated curve for no resistance at the interface, the presence of interfacial resistance to diffusion is apparent. The calculated curve, V, for the interfacial run from the theory again agrees well with the experimental curve for the latter part of the diffusional process.

In Table II it can be seen that D_1, D_a, m, and α all behave abnormally with the temperature change. D_1 decreased more than could be explained by the increase of phenol concentration in the water rich layer at 40°C, since it was even smaller than the value of D_2 in the phenol rich layer at 20°C and m was also ab-

TABLE II.

Temp °C	$D_1\times10^5$ cm²/sec	$D_2\times10^5$ cm²/sec	$D_a\times10^5$ cm²/sec	m	$\alpha\times10^5$ cm/sec
22.0	0.339	0.140	0.0964	13.6	0.265
40.0	0.0719	0.448	0.0188	14.8	0.0259

normal. The mutual solubility of 0.1 N sulfuric acid and phenol had been measured by Dubrisay and Toquet.[2] From Table II it can be seen that when the mutual solubility of water and phenol increased, the distribution coefficient for sulfuric acid (m) increased, rather than decreased as normally expected. A certain degree of association must, therefore, exist between the sulfuric acid and phenol in the water rich layer. This association would keep the distribution of sulfuric acid in favor of the water layer and also could account for the abnormal decrease of the diffusion coefficient D_1. It is also conceivable that water may play a part in the association. Apparently this association depends more on composition than on temperature since the abnormal change of diffusion coefficient did not occur

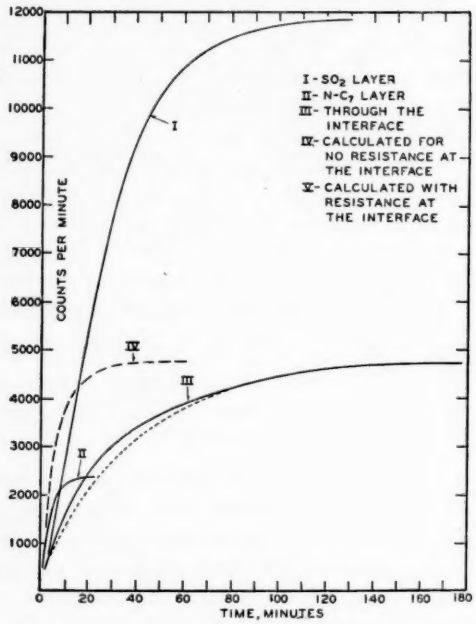

FIG. 2. Curves of concentration *versus* time for diffusion in the system phenol-H_2SO_4-water at 22°C.

in the phenol rich layer where all three components were present.

The value of α decreased even more than D_1. D_1 decreased 4.7-fold, D_2 increased 3.2-fold while α decreased 10.2-fold. This shows that the interfacial resistance to diffusion behaved abnormally also. Since α goes to infinity when the mixture is above its critical solution temperature, a minimum value of α must exist. This minimum value is either between 40°C and 22°C or between 40°C and the critical solution temperature 70.5°C. Analogously a maximum value of m must exist since m equals 1 above the critical solution temperature. This means either that the degree of association in the water rich layer must go down as temperature increases further or that the association in the phenol rich layer must become appreciable as temperature goes up. If the first case is true, a minimum value for D_1, before the system comes to its critical solution temperature, is expected. If the second case is true, abnormal changes of the diffusion coefficient D_2 should occur before the system comes to its critical solution temperature. It is also conceivable that the above mentioned properties of the system maintain their abnormality until the temperature of the system comes very close to its critical solution temperature and then abrupt changes occur.

It is not at present possible to generalize from this and the previous work, except to say that the resistance to motion inherent in the interface must be important in many, if not most, partially miscible systems. It is certainly not safe to assume equilibrium at the interface as is done in many chemical engineering calculations. Since a satisfactory kinetic picture of diffusion in simple liquids is not yet available, it will probably be a long time before these complex phenomena can be completely explained.

It seems certain that the resistance is not a simple function of surface tension. With polar molecules such as these a high degree of orientation is probable at the interface. Molecules approaching the interface with a favorable orientation could then pass through as if there were no resistance. Molecules with less favorable orientation would be retarded unless they had sufficient kinetic energy to overcome the repulsion.

Within the accuracy of the results, the form of the interfacial resistance given in Eq. (1) of reference (1) seems to be a satisfactory method of expressing the results. It should be pointed out that a practical case of mass transfer with changing concentrations in the main body of each phase, and probably also at the interface, would be considerably more difficult to analyze.

[2] Dubrisay and Toquet, Bull. Soc. Chem. France **25**, 354 (1919).

Diffusion in Indium Near the Melting Point*

ROGER E. ECKERT AND H. G. DRICKAMER
Department of Chemistry, University of Illinois, Urbana, Illinois
(Received September 14, 1951)

Diffusion coefficients for the systems Tl^{204}—In and In^{114}—In have been measured in the solid state and in the neighborhood of the melting point. The measurements were made in both polycrystalline masses and in single crystals. For the polycrystalline samples a rapid, but not discontinuous, rise in the diffusion coefficient occurred about 0.5°C below the melting point. For the Tl^{204}—In system in a single crystal the rise in D occurs just below the melting point. This indicates grain boundary melting in the polycrystalline sample. For the In^{114}—In diffusion in a single crystal the rapid rise still occurred well below the melting point, indicating that increasing lattice disorder also contributes to the increase in D.

INTRODUCTION

THERE must be a rapid rise in the diffusion coefficients in the vicinity of the melting point because diffusion coefficients in solids seldom exceed 10^{-9} cm²/sec, while those in liquids are usually greater than 10^{-6} cm²/sec. This 1000-fold change in diffusion must be associated in some manner with the weakening of the forces between molecules as the solid transforms to liquid. According to Frenkel,[1] "The regularity in the arrangement and orientation of the molecules in the crystal begins to fall with the rise of temperature long before the melting point." This leads one to believe that the huge increase in diffusion might be a gradual change starting below the melting point and resulting from the weakening of the molecular binding forces.

In this paper diffusion coefficients are presented for the systems Tl^{204} into polycrystalline indium, Tl^{204} into single crystal indium, In^{114} into polycrystalline indium, In^{114} into single crystal indium. The radioactive chemicals were obtained from the Oak Ridge National Laboratory of the Atomic Energy Commision.

Indium of two purities was used. 99.9 percent indium was used for the thallium-indium measurements, while 99.9975 percent indium was used for the indium self-diffusion measurements.[2]

The diffusion coefficients were obtained in three regions: (1) The solid state up to about one degree below the melting point; (2) The "melting" region, from region 1 to the melting point; (3) The liquid state for 1°–2°C above the melting point.

The radioactive tracer was plated on the face of a cylinder of the inactive metal and held at constant temperature during a definite time of diffusion. The sample was sectioned with a microtome and the diffusion coefficient obtained from the activity profile.

PROCEDURE

The polycrystalline pellets were cast in stainless steel molds lubricated with a film of Apiezon oil B for ease in removal. The indium pellets were 0.250 inch in diameter and approximately ½ inch in length. The grains were 0.10–0.20 cm in diameter. The ends were roughly trimmed with a razor blade and then cut precisely perpendicular to the axis of the cylinder on the microtome.

Single crystals were grown by the method first employed by Bridgman.[3] This method consists of lowering a tube of the liquid metal out of a furnace at a slow uniform rate.

For the thallium-indium runs one long crystal was cut into ½-inch lengths with a razor blade. All diffusion runs were performed on the pellets obtained from this crystal so that the direction of diffusion would always be the same with respect to the crystallographic orientation. Unfortunately, it was not possible to determine this orientation.

It was necessary to polish the cross-sectional surface on which the radioactive material was to be plated. Although electropolishing would probably give the best strain-free surface, no method has been developed for indium. Therefore, the usual metallurgical polishing wheels were used to prepare the surface. An identical procedure was used with a second crystal for the indium-indium runs.

The pellets were etched ten minutes in 50:50 nitric acid, then all but the diffusing surface was coated with glyptal to prevent deposit during plating.

The bath for the electrodeposition of radioactive thallium consisted merely of 5 ml of 1 microcurie/ml of the slightly acid solution of the thallous nitrate tracer added to 35 ml of distilled water. The radioactive indium plating bath contained 6 grams of sodium citrate and 20 ml of 1 microcurie/ml of radioactive indium nitrate solution and was diluted with distilled water to give a total volume of 40 ml.

A current of 1 milliampere was drawn for ten minutes in the plating of the thallium on indium. Indium was plated at 1 milliampere for five minutes followed by 5 milliamperes for ten minutes. The glyptal was removed with acetone, and the pellet was placed in a capsule and immersed into the temperature bath. It remained in the bath a predetermined time which was estimated

* This work was supported in part by the AEC.

[1] J. Frenkel, *Kinetic Theory of Liquids* (Clarendon Press, Oxford, 1946).

[2] The 99.9 percent indium was obtained from the American Smelting and Refining Company, Barber, New Jersey. The 99.9975 percent indium was obtained from the Indium Corporation of America, Utica, New York.

[3] P. W. Bridgman, Proc. Am. Acad. Arts Sci. **60**, 305 (1925).

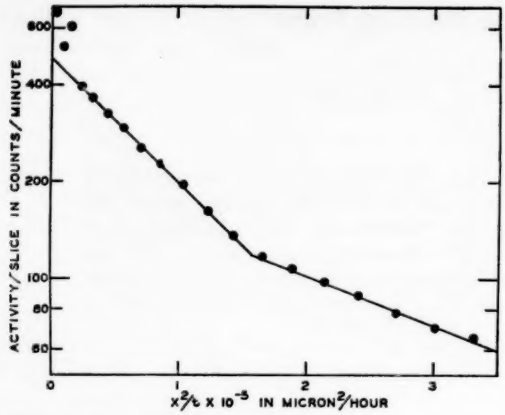

FIG. 1. Typical diffusion curve in the melting region.

so that the distribution of activity would be convenient for analysis. For runs that were shorter than one hour, a preheat period was used. The capsule was immersed in a bath controlled at a temperature about 5°C below the diffusion bath temperature for a period of five minutes. It was then transferred directly to the diffusion bath. The diffusion at the lower temperature had previously been measured, and the penetration resulting from five minutes even at this preheat temperature would have been completely negligible.

The diffusion was very rapid in the liquid, and the times required were so short that the time necessary to heat the pellet from the preheat temperature to that of the diffusion could not be neglected. Therefore, several runs were made at the same temperature but with different times. The results could be analyzed to determine the diffusion coefficient at this temperature as discussed below.

The bath temperature was controlled to ±0.01°C and measured with a Beckmann thermometer calibrated against a totally immersed N.B.S. thermometer.

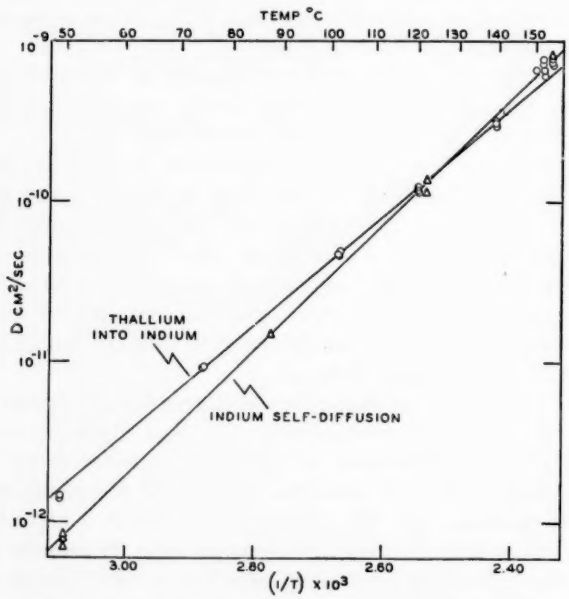

FIG. 2. Solid state diffusion in polycrystalline indium.

The samples were removed from the bath, placed in a holder in the vise of a Leitz Sledge Base Microtome and aligned by means of an optical system. Depending on the depth of penetration, slices from 5–40 microns thick were taken (for any one pellet all slices were the same thickness). The thickness of the first slice was determined by weight. The error in slicing as determined by weighing, was never over 5 percent and was much less for samples over 10 microns thick.

The slices were counted by means of a thin (2 mg/cm²) window Geiger-Mueller tube using a Nuclear Instrument and Chemical Company scaler. Considerable care was taken to maintain constant geometry from slice to slice. Each slice was counted until the probable statistical error was less than one percent, and slices were taken until the net counts per minute approximated background.

The melting points of the pure samples of indium were determined to 0.03°C. A chromel-*p*-alumel thermocouple was immersed in 10 grams of the indium sample contained in a Pyrex tube mounted in the temperature bath. The bath was slowly cooled and the electromotive force of the couple *versus* time recorded until all the metal solidified. The bath was then heated, and the same values determined as the indium melted. This procedure was repeated several times, and the same plateau was obtained each time. The thermocouple was calibrated against a N.B.S. thermometer around this emf to give the melting temperature. The 99.9975 percent indium melted at 156.51°C while the 99.9 percent indium containing tracer qualities of radioactive thallium melted at 156.32°C.

The solution of the diffusion equation with appropriate boundary conditions is given by Barrer.[4]

$$C=\frac{Q}{(\pi Dt)^{\frac{1}{2}}}\exp\left(-\frac{x^2}{4Dt}\right), \tag{1}$$

where Q is the initial surface concentration, x the penetration, t the time, and D the diffusion coefficient. Then,

$$\ln C=\ln K-(x^2/4Dt), \tag{2}$$

and a plot of x^2/t *versus* $\ln C$ has a slope of $1/-4D$.

From these plots the diffusion coefficients were determined.

For runs at high temperature, where the diffusion is very rapid, short times of diffusion were necessary. However, the sample must first be heated to the diffusion temperature and then cooled upon removal. The true diffusion time was calculated by running two or more samples at the same temperature for different lengths of time. The diffusion coefficients can then be determined as can be seen from the following.

Consideration of Eq. (2) shows that a plot of logarithm

[4] R. M. Barrer, *Diffusion in and Through Solids* (Macmillan Company, New York, 1941), Chapter I.

of the counts per minute *versus* x^2 could be used to obtain the diffusion coefficient according to the equation,

$$D=\Delta/Kt, \tag{3}$$

where Δ is the Cartesian distance on a semilogarithm graph corresponding to a change of one logarithmic cycle, and K is a dimensional constant. Let t' refer to the total time that the sample is in the bath. Now, the total time may be divided into equivalent diffusion time, t, and the heat-up time, t_h. If two diffusion samples are run for different times at the same temperature, D's are equal and therefore

$$\frac{\Delta_1}{t_1'-t_h}=\frac{\Delta_2}{t_2'-t_h}. \tag{4}$$

The heat-up time is, of course, the same, provided that the two samples enter the bath at the same initial temperature. The heat-up time can then be calculated

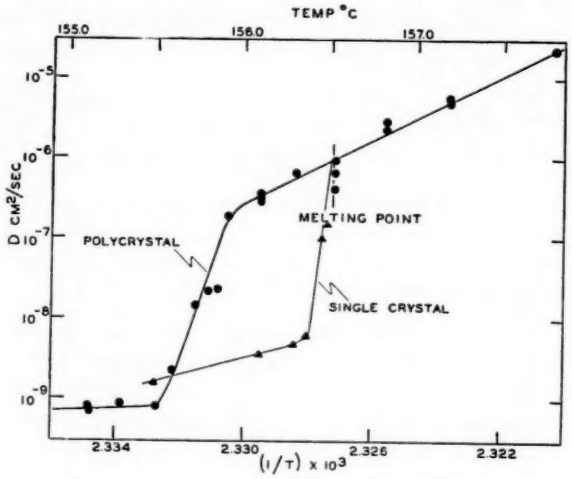

FIG. 3. Diffusion of thallium into indium.

from

$$t_h=\frac{\Delta_2 t_1'-\Delta_1 t_2'}{\Delta_2-\Delta_1}. \tag{5}$$

This calculated heat-up time can be used in the equation for D to obtain a coefficient. The usual procedure was to run three samples and thus calculate three heat-up times to check the consistency of the method. The average heat-up time was used to obtain the diffusion coefficient from each run.

Since there is an expansion of indium on heating and especially on melting and the slices were taken at room temperature, theoretically a correction should be applied. Since this amounted to 7 percent for the melted samples where the accuracy was lowest, and much less elsewhere, it was neglected.

In the solid region good straight lines were obtained. In the melting region and in the liquid, curves such as Fig. 1 were usual, giving two straight lines with a

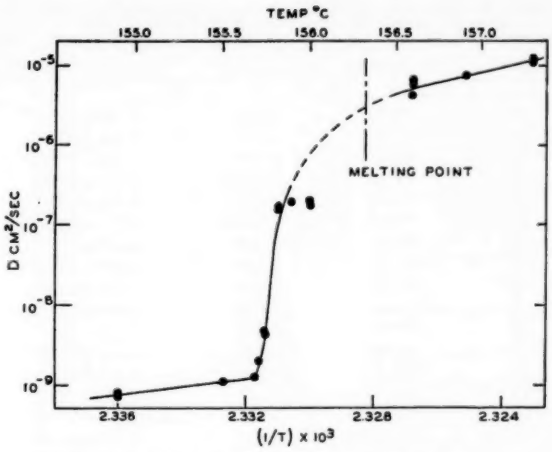

FIG. 4. Self-diffusion in polycrystalline indium.

definite break. This situation was obtained for both systems and for both single and polycrystalline samples. The same results were obtained when the sides of the pellet were scraped after diffusion, and when $\frac{1}{8}$-inch-diameter pellets were substituted for the usual $\frac{1}{4}$-inch-diameter pellets. It is easy to think of several factors which might give faster diffusion near the surface, but it is difficult to account for the steeper slope indicating slower diffusion at the surface. After considerable deliberation and conversations with F. Seitz and D. Lazurus of the Physics Department, it was decided that the flatter slope at deep penetration was more nearly typical of the average material.

In any case the use of the other slope would not change any of the qualitative aspects, nor any of the conclusions, but would merely shift the diffusion coefficients to slightly lower values.

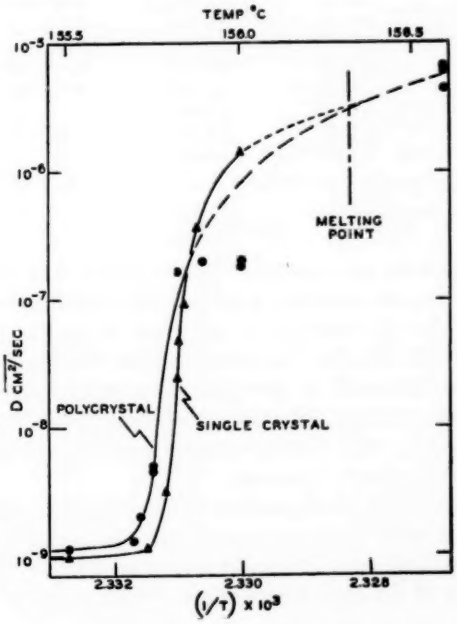

FIG. 5. Indium self-diffusion.

TABLE I. Diffusion of thallium into polycrystalline indium.

Run No.	Temperature (°C)	$1/T\times10^3$ (°K^{-1})	Diffusion coefficient (cm^2/sec)
55	49.27	3.101	1.43×10^{-12}
56	49.27	3.101	1.42×10^{-12}
57	49.27	3.101	1.38×10^{-12}
47	74.19	2.8788	9.24×10^{-12}
48	74.19	2.8788	9.18×10^{-12}
49	74.19	2.8788	9.27×10^{-12}
1	101.55	2.669	4.68×10^{-11}
2	101.55	2.669	4.60×10^{-11}
3	101.55	2.669	4.70×10^{-11}
4	101.55	2.669	4.85×10^{-11}
50	119.89	2.544	1.25×10^{-10}
51	119.89	2.544	1.24×10^{-10}
52	119.89	2.544	1.15×10^{-10}
11	139.16	2.425	2.87×10^{-10}
12	139.16	2.425	3.07×10^{-10}
13	139.16	2.425	3.18×10^{-10}
14	139.16	2.425	2.86×10^{-10}
15	150.25	2.361	6.59×10^{-10}
16	150.25	2.361	6.62×10^{-10}
17	152.85	2.349	7.63×10^{-10}
18	152.85	2.349	7.10×10^{-10}
19	152.85	2.349	7.25×10^{-10}
20	152.85	2.349	7.14×10^{-10}
21	152.85	2.349	6.54×10^{-10}
22	152.85	2.349	6.85×10^{-10}
23	155.12	2.3348	7.59×10^{-10}
26	155.12	2.3348	7.38×10^{-10}
27	155.12	2.3348	7.10×10^{-10}
43	155.30	2.3338	8.52×10^{-10}
42	155.50	2.3327	8.00×10^{-10}
45	155.60	2.3322	2.17×10^{-9}
41	155.72	2.3315	1.40×10^{-8}
44	155.80	2.3311	2.09×10^{-8}
46	155.85	2.3308	2.27×10^{-8}
83	155.85	2.3308	2.18×10^{-8}
40	155.91	2.3305	1.87×10^{-7}
29	156.10	2.3295	3.05×10^{-7}
30	156.10	2.3295	2.94×10^{-7}
31	156.10	2.3295	3.46×10^{-7}
63	156.30	2.3284	6.20×10^{-7}
33	156.53	2.3272	6.90×10^{-7}
53	156.53	2.3272	6.22×10^{-7}
54	156.53	2.3272	9.22×10^{-7}
64	156.82	2.3256	2.83×10^{-6}
65	156.82	2.3256	2.99×10^{-6}
66	156.82	2.3256	2.93×10^{-6}
60	157.19	2.3236	5.41×10^{-6}
61	157.19	2.3236	5.07×10^{-6}
62	157.19	2.3236	4.89×10^{-6}
37	157.80	2.3203	2.27×10^{-5}
38	157.80	2.3203	
39	157.80	2.3203	

RESULTS

The results are given in Tables I–IV and in Figs. 2–5. The reproducibility of the results varied in different regions; in the solid state the coefficients checked to ±5 percent, in the "melting" region they agreed to ±15 percent, and in the liquid phase the agreement was ±40 percent. The limits of error in calculating any one run were almost always less than 15 percent and usually about 5 percent.

The graphs of the logarithm of the diffusion coefficient *versus* reciprocal temperature were the usual straight line relationships in the solid state (see Fig. 2). For the diffusion of thallium into indium the equation is

$$D_{\mathrm{In}}{}^{\mathrm{Tl}}=0.049\exp(-15{,}500/RT)\ \mathrm{cm}^2\ \mathrm{per\ sec}, \quad (6)$$

and for indium self-diffusion,

$$D_{\mathrm{In}}{}^{\mathrm{In}}=1.02\exp(-17{,}900/RT)\ \mathrm{cm}^2\ \mathrm{per\ sec}. \quad (7)$$

The limits of error on the activation energy are ±5 percent. The result is consistent with the previously obtained results, as reported by Seith,[5] that the energy of activation is greater for the self-diffusion process than for heterogenous diffusion into the same metal.

A consideration of Braune's formula[6] (see Table V) shows that the ratio of the energy of activation of self-diffusion to the melting point of indium is in close agreement with this ratio for other metals. It must be pointed out that indium is not a cubic crystal as are the others, and hence this agreement may have no profound significance.

Thallium into Polycrystalline Indium

The melting point of indium for comparison with the diffusion results on the thallium into indium system was determined on the slices removed from the samples after diffusion. Thus, it was the melting point of indium containing tracer quantities of thallium, just as the indium did during diffusion.

A rapid rise in diffusion of thallium into indium (see Fig. 3) started 1.0°C below the melting point. It continued for 0.4°C until beginning to level out at 0.6°C

TABLE II. Self-diffusion in polycrystalline indium.

Run No.	Temperature (°C)	$1/T\times10^3$ (°K^{-1})	Diffusion coefficient (cm^2/sec)
79	49.95	3.0947	7.89×10^{-13}
80	49.95	3.0947	7.04×10^{-13}
81	49.95	3.0947	8.30×10^{-13}
82	49.95	3.0947	7.77×10^{-13}
73	87.25	2.7745	1.49×10^{-11}
74	87.25	2.7745	1.46×10^{-11}
75	87.25	2.7745	1.45×10^{-11}
76	87.25	2.7745	1.47×10^{-11}
71	122.14	2.5296	1.37×10^{-10}
72	122.14	2.5296	1.33×10^{-10}
77	122.14	2.5296	1.38×10^{-10}
78	122.14	2.5296	1.16×10^{-10}
68	154.90	2.3360	8.09×10^{-10}
69	154.90	2.3360	7.18×10^{-10}
70	154.90	2.3360	7.64×10^{-10}
92	155.50	2.3327	1.14×10^{-9}
86	155.70	2.3317	1.30×10^{-9}
89	155.71	2.3316	2.01×10^{-9}
101	155.75	2.3314	4.56×10^{-9}
102	155.75	2.3314	4.95×10^{-9}
87	155.81	2.3310	1.70×10^{-7}
88	155.81	2.3310	1.65×10^{-7}
91	155.90	2.3306	1.97×10^{-7}
85	156.00	2.3300	1.95×10^{-7}
90	156.00	2.3300	1.87×10^{-7}
93	156.60	2.3268	6.52×10^{-6}
94	156.60	2.3268	5.87×10^{-6}
95	156.60	2.3268	5.23×10^{-6}
99	156.90	2.3251	7.5×10^{-6}
100	156.90	2.3251	
96	157.30	2.3230	1.00×10^{-5}
97	157.30	2.3230	1.03×10^{-5}
98	157.30	2.3230	1.23×10^{-5}

[5] W. Seith, Chemie Die **56**, 21 (1943).
[6] H. Braune, Z. physik. Chem. **110**, 147 (1924).

below the melting temperature. A linear rise then continued into the liquid state. This slope must decrease considerably within the next few degrees of increasing temperature since diffusion in a liquid metal could hardly exceed 10^{-4} cm²/sec.

The method used here is not well adapted to diffusion measurement in a liquid and the accuracy was low. The liquid phase runs were used primarily to establish a limit for the solid state diffusion. At each temperature about the melting point three runs of different time length were made and "heat-up" times were calculated as discussed previously. Since the three "heat-ups" calculated from the different pairs usually checked closely, it is felt that the concentration gradients obtained were primarily the result of diffusion. With severe convection the "heat-up" times would have varied significantly.

Thallium into Indium Single Crystal

From Fig. 3 can be seen that the single crystal diffusion gave quite different results for this system. The rapid increase in the diffusion coefficient takes place very near the melting point, but still over a finite range (approximately 0.1°C) of temperature. This appears to be strong evidence that the grain boundaries melt well below the measured melting point. Previous evidence of a different nature[7] has been presented for this viewpoint.

Self-Diffusion in Polycrystalline Indium

For indium self-diffusion (see Fig. 4) this rapid rise in the diffusion coefficient with temperature starts 0.6°C below the melting point. It is a more rapid rise, occurring in roughly half the temperature range of that discussed in the diffusion of thallium into indium. Further, there appears to be a more gradual leveling off into the liquid state diffusion for the self-diffusion process.

Self-Diffusion in Indium (Single Crystal)

The results of the indium single crystal self-diffusion study show that this rise occurs about 0.05°C higher than for polycrystalline diffusion (see Fig. 5). The diffusion coefficient in the solid before the rise is only about 15 percent less than in the polycrystalline metal. Some grain boundary diffusion in the polycrystalline metal would cause such a difference. The two curves must, of course, become identical at the melting point.

[7] B. Chalmers, Proc. Roy. Soc. (London) **A175**, 100 (1940).

TABLE III. Self-diffusion in indium single crystal.

Run No.	Temperature (°C)	$1/T\times10^3$ (°K^{-1})	Diffusion coefficient (cm²/sec)
115	155.50	2.3327	9.91×10^{-10}
118	155.73	2.3315	1.12×10^{-9}
122	155.78	2.3312	3.17×10^{-9}
117	155.81	2.3310	4.67×10^{-8}
120	155.81	2.3310	3.45×10^{-8}
121	155.84	2.3309	9.30×10^{-8}
119	155.88	2.3307	3.61×10^{-7}
116	156.00	2.3300	1.41×10^{-6}

TABLE IV. Diffusion of thallium into indium single crystal.

Run No.	Temperature (°C)	$1/T\times10^3$ (°K^{-1})	Diffusion coefficient (cm²/sec)
126	155.50	2.3327	1.60×10^{-9}
123	156.10	2.3295	3.55×10^{-9}
124	156.30	2.3284	4.77×10^{-9}
127	156.37	2.3280	6.10×10^{-9}
125	156.45	2.3276	1.00×10^{-7}
128	156.49	2.3274	1.62×10^{-7}

TABLE V. Braune's formula comparison for self-diffusion.

	Indium	Copper	Lead	Gold
Activation energy, E	18,080	57,200	27,800	51,000
Melting point, °C	156.32	1,083	327.4	1,063
E/T_s	42.1	42.2	46.3	38.2

The fact that this rapid rise in diffusion occurs 0.5°C below the melting point even for a single crystal indicates that grain boundary melting may not be the major cause of this rise. It appears that the decrease in regularity and arrangement of molecules must occur to a sufficient degree to permit the molecules to move about freely at a temperature below the melting point determined by cooling curves.

In summary it can be said that the rapid rise in the diffusion coefficient in polycrystalline indium occurs about 0.5°C–1.0°C below the melting point. This may be primarily because of grain boundary melting, but probably also involves a high degree of lattice dislocation at this temperature. For both the single crystals and polycrystalline mass the rise occurs over a measurable temperature interval.

The authors wish to acknowledge the assistance of W. P. Krause and D. R. Cova in the work with single crystals.

Dr. W. H. Bruckner of the Mining and Metallurgy Department was very helpful in determining the existence of a single crystal and in recommending and supervising a polishing technique.

Transition Probabilities. II. Calculation of Semi-Theoretical *f*-Numbers for Hydrogen Using the Dipole Velocity Operator*

HARRISON SHULL
Department of Chemistry and Institute for Atomic Research, Iowa State College, Ames, Iowa
(Received August 14, 1951)

The computations of Mulliken and Rieke using the LCAO MO and the AO methods for transition probabilities of the Lyman ($^1\Sigma_g^+ - ^1\Sigma_u^+$) and Werner ($^1\Sigma_g^+ - ^1\Pi_u$) transitions in hydrogen have been repeated using the alternative velocity form of the transition moment operator. It is found that, for an effective Z value of 1.2 for the 1*s* AO (the variation value) and a suitable Rydberg form for the excited state, the transition probabilities calculated from these two operators agree well. In addition there is quite good agreement between the AO and MO methods in each instance and between the calculated and experimental value for the sum of the strengths of the Lyman and Werner transitions.

I. INTRODUCTION

PREVIOUS computations of transition probabilities in diatomic and polyatomic molecules have made use of the dipole moment operator exclusively in its dipole length form.[1] It is well known, however, that the dipole operator may be expressed in other formally equivalent forms, namely, in the velocity and acceleration forms. Calculations using the dipole velocity operator for atoms have been made by Chandrasekhar,[2] Su-Shu Huang,[3] and Bates.[4] If the wave functions for the particular case under consideration are exact, then the three methods for calculation of theoretical *f*-numbers become mathematically identical. On the other hand, since exact wave functions are a rarity in problems of current interest, examination of these alternative forms should prove illuminating as to the validity both of the results of previous *f*-number calculations and as to the validity of the approximate wave functions commonly used.

In this paper we consider the calculation of semi-theoretical *f*-numbers for hydrogen using the dipole velocity operator. Our calculations will parallel closely the treatment of Mulliken and Rieke[1] using the dipole length operator so as to enable close comparison of the results. It is proposed in later papers of this series to consider the calculation of semi-theoretical *f*-numbers for C_2 and N_2^+, paralleling the dipole length calculations of paper I of this series,[5] and to consider the merits of calculation of completely theoretical *f*-numbers, i.e., theoretical calculation of the energy of the transition as well as its dipole strength.

II. GENERAL FORMULATION OF THE METHOD

We first recall the formulas for the dipole length operator method of calculating transition probabilities. Further details may be found in Mulliken and Rieke's review.[1] The dipole strength D for a transition between two electronic states, k and l, is given by

$$D=\sum_i G\mathbf{Q}_i^2 \tag{1}$$

in which

$$\mathbf{Q}_i=\int \psi_k \mathbf{q}_i \psi_l d\tau, \tag{2}$$

$\mathbf{q}_i$ being the vector $\mathbf{x}$, $\mathbf{y}$, or $\mathbf{z}$. We are interested in calculating the oscillator strength for the transition between states k and l (classically, the number of dispersion electrons involved in the transition). This oscillator strength is given by the following formula derived for a single narrow absorption band at wave number ν in the gaseous state.

$$f=(8\pi^2\, mc/3h)\nu D=1.085\times 10^{11}\nu D$$
$$\text{(for } \nu \text{ in cm}^{-1} \text{ and } D \text{ in cm}^2\text{).} \tag{3}$$

Previous practice has made use of this formula, calculating D theoretically by Eqs. (1) and (2), and inserting the *observed* frequency of the transition for ν. This is, then, what may be called a semitheoretical treatment.

The calculation of oscillator strengths making use of the dipole velocity operator uses Eqs. (1) and (3) in the form presented here, but in place of (2) the equivalent integral

$$\mathbf{Q}_i=[2/(E_l-E_k)]\int \psi_k \frac{\partial}{\partial q_i}\psi_l d\tau \tag{4}$$

is employed. It should be noted that the energy difference, E_l-E_k, in Eq. (4) is given in units of Rydbergs. If we absorb the Rydberg constant as well as the conversion factor from cm to atomic units in Eq. (3), we arrive at the following convenient formula for f:

$$f=1.464\times 10^5 G\left[\int \psi_k\left(\sum_i \frac{\partial}{\partial q_i}\right)\psi_l d\tau\right]^2/\nu. \tag{5}$$

In this formula, the energy difference E_l-E_k has been used to cancel the frequency appearing in Eq. (3). The appropriateness of this cancellation with subsequent

* Paper No. 162 from the Institute for Atomic Research, Iowa State College, Ames, Iowa. This work was supported in part by the Ames Laboratory of the AEC.

[1] R. S. Mulliken and C. A. Rieke, Repts. Prog. Phys. **8**, 231 (1941). This review contains extensive references to previous work.
[2] S. Chrandrasekhar, Astrophys. J. **102**, 223, 395 (1945).
[3] Su-Shu Huang, Astrophys. J. **108**, 354 (1948).
[4] D. R. Bates and A. Damgaard, Trans. Roy. Soc. (London) **A242**, 101 (1949).
[5] H. Shull, Astrophys. J. **112**, 352–360 (1950).

use of the observed frequency of the transition will be examined in detail in a later paper. For the purposes of the present calculation, the formula will be used in this form with substitution of the observed frequency. In Eq. (5), ν is in wave numbers and the integral is expressed in atomic units. G is a factor which takes into account the number of independent final states to which transitions are possible from a single initial state. For the calculations presented here, G is one for $\Sigma-\Sigma$ transitions and two for $\Sigma-\Pi$ transitions in hydrogen.

III. LCAO MO AND AO COMPUTATIONS FOR THE N, V TRANSITION

Our first computations are for the ${}^1\Sigma_u^+ \leftarrow {}^1\Sigma_g^+$ transition in hydrogen in which an electron is transferred from a bonding molecular orbital (MO) to the corresponding antibonding MO. This type of transition results in what is called a 'charge-transfer' spectrum and is now commonly labeled, following Mulliken, an N, V transition. In the corresponding terminology for the atomic orbital (AO) approach, one electron is transferred from a state in which both electrons are shared equally between the two nuclei (non-ionic) to a state in which both electrons are found either on one nucleus or on the other (ionic). The transition thus involves effectively a transfer of an electron from one nucleus to the other—hence the term charge-transfer spectrum.

We use for the MO's, a linear combination of atomic orbitals (LCAO), following the usual elementary treatment. For the state N we have the approximate wave function: $\psi_N=\sigma_g(1)\sigma_g(2)$; and for state V, the wave function: $\psi_V=[\sigma_g(1)\sigma_u(2)+\sigma_g(2)\sigma_u(1)]/2^{\frac{1}{2}}$. In the LCAO form, $\sigma_g(1)$ becomes $[1s_a(1)+1s_b(1)]/[2(1+S)]^{\frac{1}{2}}$ in which $1s_a(1)$ is a $1s$ atomic orbital situated at nucleus a, and correspondingly for $1s_b(1)$. S is the overlap integral, $\int 1s_a(1)1s_b(1)d\tau_1$, for which extensive formulas and tables have been computed recently.[6] Correspondingly, $\sigma_u(1)$ is $[1s_a(1)-1s_b(1)]/[2(1-S)]^{\frac{1}{2}}$ where all the symbols are the same as for the $\sigma_g(1)$MO.

The formula for the calculation of the dipole moment of the transition using the dipole velocity operator becomes:

$$\mathbf{Q}=\left(\frac{2}{E_V-E_N}\right)\int \psi_N\left[\frac{\partial}{\partial z_1}+\frac{\partial}{\partial z_2}\right]\psi_V d\tau_1 d\tau_2, \quad (6)$$

in which are substituted the LCAO MO forms given above. Since σ_g is strictly orthogonal to σ_u, and we use normalized functions, Eq. (6) reduces to the simplified form (7),

$$Q=\frac{2\sqrt{2}}{E_V-E_N}\int \sigma_g\frac{\partial}{\partial z}\sigma_u d\tau, \quad (7)$$

where now the integration is over the coordinates of only a single electron. In the above formulations we omit the spin factors since they disappear in the integration over spin coordinates. When the LCAO form is used for σ_g and σ_u, we obtain expressions involving the integrals, $\int 1s_a(\partial/\partial z)1s_a d\tau$, $\int 1s_a(\partial/\partial z)1s_b d\tau$ and similar ones with subscripts a and b interchanged. In the evaluation of these and other similar integrals needed in this paper, it was found convenient to perform the initial differentiation in Cartesian coordinates and to perform the subsequent integration in prolate spheroidal coordinates in which the two-center problem is separable. The resulting formulas may, in certain cases, be expressed as linear combinations of various overlap integrals, but in each case it was found more convenient, faster, and hence more accurate, to compute the values directly rather than use existing tables of overlap integrals. Appendix I summarizes the formulas for the integrals needed in this paper, while Appendix II summarizes the values computed for the parameters used here.

The AO computations for the N, V transition parallel the LCAO MO computations quite closely. For the N state we use

$$\psi_N=[1s_a(1)1s_b(2)+1s_a(2)1s_b(1)]/[2(1+S_{1s}{}^2)]^{\frac{1}{2}} \quad (8)$$

and for the V state:

$$\psi_V=[1s_a(1)1s_a(2)-1s_b(1)1s_b(2)]/[2(1-S_{1s}{}^2)]^{\frac{1}{2}}, \quad (9)$$

where, as before, S_{1s} is the overlap integral between a $1s$ orbital on atom a and a similar orbital on atom b. For both the LCAO MO computations and the AO computations, we have tried Z values of both 1 and 1.2, the latter being the value found by Coulson[7] to give the best results by the variation method for the dissociation energy of the ground state.

In addition to the calculations summarized above, we have considered the analogous calculation in which the upper, V, state is represented in a Rydberg form. That is to say, for the LCAO MO method, we take[8]

$$\psi_V=[2p\sigma_a-2p\sigma_b]/[2(1-S_{2p})]^{\frac{1}{2}}. \quad (10)$$

Correspondingly for the AO approach:

$$\psi_V=[1s_a(1)2p\sigma_b(2)+1s_a(2)2p\sigma_b(1)-1s_b(1)2p\sigma_a(2) -1s_b(2)2p\sigma_a(1)]/2[1-S_{1s}S_{2p}+S_{1s2p}{}^2]^{\frac{1}{2}}, \quad (11)$$

in which

$$S_{1s}=\int 1s_a 1s_b d\tau; \quad S_{2p}=\int 2p\sigma_a 2p\sigma_b d\tau,$$

$$S_{1s2p}=\int 1s_a 2p\sigma_b d\tau.$$

These calculations have also been carried through for the two cases in which μ_{1s} is alternatively 1.0 or 1.2.

[6] Mulliken, Rieke, Orloff, and Orloff, J. Chem. Phys. **17**, 1248 (1949).

[7] C. A. Coulson, Trans. Faraday Soc. **33**, 1484 (1937).

[8] In this paper, as previously, we take each $2p\sigma$ orbital with its positive lobe toward the other atom.

In the AO form, following Mulliken, we have written the Rydberg orbital as non-ionic. Similar calculations were also carried through for the ionic Rydberg orbital, for which one may write the wave function

$$\psi_V=[1s_a(1)2p\sigma_a(2)+1s_a(2)2p\sigma_a(1)-1s_b(1)2p\sigma_b(2) -1s_b(2)2p\sigma_b(1)]/2[1-S_{1s}S_{2p}-S_{1s2p}{}^2]^{\frac{1}{2}}. \quad (12)$$

Because of the large size of the $2p\sigma$ orbitals relative to the dimensions of the molecule, it is to be expected that these two different forms will result in very similar charge distributions (approximately that of a single $2p\sigma$ orbital centered at the midpoint of the molecule). Hence the transition moments should be (and are) nearly the same for these two representations.

IV. LCAO MO AND AO CALCULATIONS FOR THE WERNER BANDS

Paralleling the calculations made by Mulliken and Rieke using the dipole length operator, calculations of oscillator strengths have also been carried through for the perpendicular bands known as the Werner bands. These arise from a transition between a $^1\Pi_u$ excited state and the ground state. The MO formulation represents the transition as being from a $(\sigma_g 1s)^2$ ground state to a $(\sigma_g 1s)(\pi_u 2p\pi)$ excited state. For the $\pi_u 2p\pi$ orbital, we write

$$\pi_u=(2p\pi_a+2p\pi_b)/[2(1+S_{2p\pi})]^{\frac{1}{2}},$$

in which, of course, the axes of the $2p\pi$ orbitals are perpendicular to the internuclear axis. Here $S_{2p\pi}$ represents the usual overlap integral of two $2p\pi$ functions, one on atom a and one on atom b. For the wave function of the excited state in the AO approach, we write

$$\psi_E=[1s_a(1)2p\pi_b(2)+1s_a(2)2p\pi_b(1)+1s_b(1)2p\pi_a(2) +1s_b(2)2p\pi_a(1)]/2(1-S_{1s}S_{2p\pi})^{\frac{1}{2}}.$$

The details of the calculation proceed as before, remembering, however, that for this case of a $\Sigma-\Pi$ transition, the numerical value of G in Eq. (1) is two.

TABLE I. Summary of f-numbers for Lyman and Werner bands of the hydrogen molecule.

Approximation	Dipole velocity operator	Dipole length operator
Lyman bands: $^1\Sigma_g{}^+-{}^1\Sigma_u{}^+$		
MO $\sigma_g(1s)Z=1$; $\sigma_u(1s)Z=1$	0.52	0.68*
AO $1s^2$ (ionic) $Z=1$	0.66	0.49*
MO $\sigma_g(1s)Z=1$; $\sigma_u 2p\sigma Z=1$	0.19	0.44*
MO $\sigma_g(1s)Z=1.2$; $\sigma_u 2p\sigma Z=1$	0.18	0.24*
AO $1s2p\sigma Z_{1s}=1$; $Z_{2p\sigma}=1$	0.19	0.39*
AO $1s2p\sigma Z_{1s}=1.2$; $Z_{2p\sigma}=1$	0.15	0.21*
AO $1s2p\sigma$ (ionic) $Z_{1s}=1$; $Z_{2p\sigma}=1$	0.19	0.46
AO $1s2p\sigma$ (ionic) $Z_{1s}=1.2$; $Z_{2p\sigma}=1$	0.16	0.25
Werner bands: $^1\Sigma_g{}^+-{}^1\Pi_u$		
MO $\sigma_g(1s)Z=1$; $\pi_u(2p)Z=1$	0.45	0.75*
MO $\sigma_g(1s)Z=1.2$; $\pi_u(2p)Z=1$	0.42	0.38*
AO $1s2p\pi Z_{1s}=1$; $Z_{2p\pi}=1$	0.40	0.73*
AO $1s2p\pi Z_{1s}=1.2$; $Z_{2p\pi}=1$	0.38	0.37*

* From R. S. Mulliken and C. A. Rieke, Repts. Prog. Phys. **8**, 231 (1941).

V. DISCUSSION OF RESULTS

Table I presents in tabular form the results of these calculations together with the results of corresponding calculations using the dipole length operator largely from the work of Mulliken and Rieke. Several results emerge from a direct consideration of this table. The dipole velocity results seem to be markedly independent of the Z variation from 1 to 1.2, whereas the dipole length form is very sensitive to this change. On the other hand, the dipole velocity form is much more sensitive to a change from the $\sigma_u(1s)$(MO) or $1s^2$(AO) excited state to the corresponding Rydberg forms involving $2p\sigma$ AO's. These two points taken together produce relatively good agreement of the two methods for Rydberg orbital forms using Z of 1.2 for the bonding σ_g orbital. It seems, then, that the adjustment in Z called for by the variation theorem is just that needed here to make the two methods agree moderately well. This is a promising feature of the present calculations.

Mulliken and Rieke,[1] by reviewing carefully the molecular dispersion data for hydrogen, concluded that an appropriate value for the sum of the oscillator strengths for both the Lyman bands (N, V) and the Werner bands is 0.65. These authors' calculations by the MO dipole length method led to 0.24 and 0.38 for these bands, respectively, a total of 0.62 in essential agreement with the experimental estimate. The corresponding MO dipole velocity computations yield 0.18 and 0.42 for the individual transitions, summing to 0.60. This is still quite satisfactory agreement with the observed sum, since the latter is none too reliably known. Correspondingly, we may compare the results by the AO approach, in which the dipole length sum is 0.58, the dipole velocity 0.53. These, and especially the latter, are distinctly lower than one would like for complete agreement.

It is comforting to note then that these two independent methods give closely similar results by both MO and AO treatments and this tends to strengthen our belief in the approximate methods employed. In view of the number of assumptions, however, it is not clear whether the cancellations in errors which must occur in bringing such approximate methods into agreement will be satisfied in other cases. For this reason, further comparisons will be very desirable from the point of view of testing the validity of these various assumptions. In addition it would be very desirable to obtain an ultimate check upon these values by carrying through similar calculations with functions of the James-Coolidge form for the Lyman band transition.

It has been pointed out by Chandrasekhar[2] that the dipole velocity and dipole length operators tend to emphasize different portions of the wave functions. Namely, the dipole length form is more sensitive to portions of the wave function at relatively large distances from the nucleus. On the other hand, the dipole velocity form emphasizes portions of the wave function in the region of its largest magnitude, but requires

knowledge of the gradient of the function. It is not *a priori* obvious whether one knows more or less about the gradient of the wave function in its region of greatest magnitude than one knows about the wave function itself at larger distances. It is quite possible that, in cases other than the ones treated here, comparison of these two forms may yield new information on suitable approximate wave function forms. Further work is in progress extending these calculations to a larger set of cases.

APPENDIX I

Formulas for dipole velocity integrals used in this paper

$$\int 1s_a\frac{\partial}{\partial z}1s_a d\tau=\int 1s_b\frac{\partial}{\partial z}1s_b d\tau=0$$

$$\int 1s_a\frac{\partial}{\partial z}1s_b d\tau=-\int 1s_b\frac{\partial}{\partial z}1s_a d\tau$$
$$=\mu_{1s}{}^2R(1+\mu_{1s}R)e^{-\mu_{1s}R/3},$$

$$\int 1s_a\frac{\partial}{\partial z}2p\sigma_a' d\tau=-\int 2p\sigma_a'\frac{\partial}{\partial z}1s_a d\tau=\int 2p\sigma_b'\frac{\partial}{\partial z}1s_b d\tau$$
$$=-\int 1s_b\frac{\partial}{\partial z}2p\sigma_b' dt$$
$$=-8\mu_{1s}{}^{5/2}\mu_{2p\sigma}{}^{5/2}/(\mu_{1s}+\mu_{2p\sigma})^4$$

$$\int 1s_a\frac{\partial}{\partial z}2p\sigma_b' d\tau=-\int 2p\sigma_b'\frac{\partial}{\partial z}1s_a d\tau$$
$$=\int 2p\sigma_a'\frac{\partial}{\partial z}1s_b d\tau=-\int 1s_b\frac{\partial}{\partial z}2p\sigma_a' d\tau$$
$$=(\mu_{1s}\mu_{2p\sigma})^{5/2}R^4$$
$$\times[A_2B_3-A_3B_2+A_1B_0-A_0B_1]/8.$$

Argument of A is $\frac{R}{2}(\mu_{1s}+\mu_{2p\sigma})$.

Argument of B is $\frac{R}{2}(\mu_{1s}-\mu_{2p\sigma})$.

$$\int 1s_a\frac{\partial}{\partial x}2p\pi_a' d\tau=\int 1s_a\frac{\partial}{\partial z}2p\sigma_a' d\tau \text{ (see above)},$$

$$\int 1s_a\frac{\partial}{\partial x}2p\pi_b' d\tau=\mu_{1s}{}^{5/2}(\mu_{2p\pi})^{5/2}R^4$$
$$\times[A_3B_0-A_0B_3-A_1B_0+A_0B_1$$
$$-A_3B_2+A_2B_3+A_1B_2-A_2B_1]/16.$$

The argument of A is $R[\mu_{1s}+\mu_{2p\pi}]/2$; that of B is $R(\mu_{1s}-\mu_{2p\pi})/2$.

Notes to Appendix I:

The z direction is taken along the axis of the molecule. The integrals are over the coordinates of a single electron. R is the internuclear distance in atomic units, μ is the Slater effective nuclear charge Z divided by the effective principal quantum number.

$$A_n(\alpha)=\int_1^\infty \mu^n e^{-\alpha\mu}d\mu,$$

$$B_n(\alpha)=\int_{-1}^{+1} \nu^n e^{-\alpha\nu}d\nu.$$

See tables and recursion formulas in Kotani, *et al.** for evaluation of these.

Primes denote differing μ values for the two functions in the integral. The first two equations refer to functions with like μ only. Note that the integrals $\int\phi_1(\partial/\partial z)\phi_2 d\tau$ are not Hermitian. The complete expression

$$[2/(E_2-E_1)]\int\phi_1\frac{\partial}{\partial z}\phi_2 d\tau$$

is, however, Hermitian.

APPENDIX II

Numerical values of integrals used in this paper.

Integral	R	μ_{1s}	μ_{2p}	Value of integral in atomic units	Value of corresponding dipole length integral in atomic units
$\int 1s_a\frac{\partial}{\partial z}1s_a d\tau$	...	1	...	0	−0.6990
$\int 1s_a\frac{\partial}{\partial z}1s_b d\tau$	1.398	1	...	0.2761	0
$\int 1s_a\frac{\partial}{\partial z}2p\sigma_a' d\tau$	...	1	0.5	0.2793	0.7448
$\int 1s_a\frac{\partial}{\partial z}2p\sigma_a' d\tau$	...	1.2	0.5	0.2671	0.5237
$\int 1s_a\frac{\partial}{\partial z}2p\sigma_b' d\tau$	1.398	1	0.5	−0.1830	−0.7943
$\int 1s_a\frac{\partial}{\partial z}2p\sigma_b' d\tau$	1.398	1.2	0.5	−0.1632	−0.5909
$\int 1s_a\frac{\partial}{\partial x}2p\pi_b' d\tau$	1.398	1	0.5	0.2448	0.6795
$\int 1s_a\frac{\partial}{\partial x}2p\pi_b' d\tau$	1.398	1.2	0.5	0.2289	0.4687
$\int 1s_a 1s_b d\tau$	1.398	1	...	0.7535	...
$\int 2p\sigma_a 2p\sigma_b d\tau$	1.398	...	0.5	0.8626	...
$\int 1s_a 1s_b d\tau$	1.398	1.2	...	0.6755	...
$\int 2p\pi_a 2p\pi_b d\tau$	1.398	...	0.5	0.9530	...
$\int 1s_a 2p\sigma_b' d\tau$	1.398	1	0.5	0.3422	...
$\int 1s_a 2p\sigma_b' d\tau$	1.398	1.2	0.5	0.3196	...

* Kotani, Amemiya, and Simose, Proc. Phys.-Math. Soc. Japan **20** extra number 1 (March, 1938); corrections **22** extra number (June, 1940).

Kinetics of Decomposition of Nitric Oxide at Elevated Temperatures. I. Rate Measurements in a Quartz Vessel*

HENRY WISE AND MAURICE F. FRECH
Jet Propulsion Laboratory, California Institute of Technology, Pasadena, California
(Received August 27, 1951)

The rate of thermal decomposition of nitric oxide has been measured in a quartz vessel from 872 to 1275°K. The reaction follows a second-order rate law over the range of temperatures studied. Variations in the surface-to-volume ratio of the reaction vessel indicate the predominance of a heterogeneous mechanism at temperatures below 1000°K, whereas at higher temperatures a homogeneous mechanism prevails. The experimental data are interpreted on the basis of the relative contribution of the heterogeneous and homogeneous mechanisms to the over-all kinetics. Such an analysis explains the variation in effective activation energy with temperature from a value of 21.4 kcal below 1000°K to 82 kcal above 1600°K. An intermediate temperature region exists in which both mechanisms contribute an important part to the over-all rate.

INTRODUCTION

ALTHOUGH the kinetics of decomposition of nitric oxide in the presence of metallic surfaces have previously been investigated,[1–4] the uncatalyzed rate of reaction has not been studied in sufficient detail to permit an evaluation of the underlying reaction mechanism. The results obtained by Jellinek[2] for the rate of thermal decomposition of nitric oxide have been interpreted to exhibit an increase in the energy of activation with temperature. Based on these data, effective activation energies of 24 kcal at 960°K and 71 kcal at 1525°K have been calculated.[5] Furthermore, recent measurements on the rate of formation of nitric oxide in the explosion of combustible gas mixtures composed of hydrogen, nitrogen, and oxygen[6–8] have resulted in an energy of activation of 82±10 kcal for the decomposition at temperatures above 2000°K. It is apparent therefore that the observed reaction is a composite one made up of two or more concurrent reactions differently influenced by temperature.

EXPERIMENTAL METHOD

In the present study a series of measurements was carried out on the decomposition of nitric oxide in a quartz vessel. In order to study more accurately the kinetics of this reaction at temperatures below 1300°K, a static system was chosen in which the residence time of the gas at elevated temperature could be varied over wide limits.

A schematic drawing of the apparatus used in this study is shown in Fig. 1. A sample of nitric oxide[9] (purity in excess of 99.93 percent as determined by infrared spectroscopic analysis) is admitted to the reaction vessel B. It is composed of a quartz cylinder (120 mm in diameter and 150 mm in length) provided with a gas inlet 1 and gas outlet 2 and a thermocouple well which extends the middle of the vessel. The reactor is located in an electrically heated furnace in which the temperature can be adjusted and maintained with a high degree of accuracy (±1°K) during the course of an experimental determination. For temperature measurement a shielded thermocouple (platinum-platinum rhodium 10 percent) is employed.

After a given time interval the hot-gas mixture contained in vessel B (Fig. 1) is rapidly expanded into the evacuated trap C cooled by liquid nitrogen. The section connecting B and C is made relatively short in order to allow fast cooling of the hot gases to a point where the composition of the mixture will not undergo any further change.

In following the progress of the decomposition of NO the rate of formation of products is taken as an index of the reaction rate. The concentration of N_2 formed in the reaction is determined manometrically. The concentration of oxygen produced in the reaction is measured by spectrophotometric analysis for NO_2. This compound is allowed to form at room temperature by reaction of the reaction products composed of O_2 and unreacted NO in vessel E (Fig. 1).

RESULTS

A summary of the experimental data (Table I) indicates that the rate of decomposition of nitric oxide follows a second-order rate law over the range of temperatures studied. However, the temperature coefficient of the specific reaction-rate constant varies with temperature. By means of a graphical analysis of the results, it is found that the energy of activation approaches a limiting value of 21.4 kcal at 900°K, whereas at higher temperature the activation energy rises to 56.6 kcal at 1275°K. It is apparent therefore that the rate-

* This paper presents the results of one phase of research carried out at the Jet Propulsion Laboratory, California Institute of Technology, under Contract No. DA-04-495-ORD 18, sponsored by the Department of the Army Ordnance Corps.

[1] W. Nernst, Z. anorg. u. allgem. Chem. **49**, 213 (1906).
[2] K. Jellinek, Z. anorg. u. allgem. Chem. **49**, 229 (1906).
[3] Green and Hinshelwood, J. Chem. Soc. **1926**, 1909.
[4] Bachman and Taylor, J. Phys. Chem. **33**, 447 (1929).
[5] S. Dushman, J. Am. Chem. Soc. **43**, 411 (1921).
[6] Ya. B. Zeldovich, Acta Physicochim. U. R. S. S. **21**, 577 (1946).
[7] D. Frank-Kamenetzky, Acta Physicochim. **23**, 27 (1947).
[8] Polyakov and Genkina, Acta Physicochim. **11**, 443 (1939).
[9] Johnston and Giauque, J. Am. Chem. Soc. **51**, 3194 (1928). The reactant as obtained from the Matheson Company, Joliet, Illinois, was purified according to the procedure of Johnston and Giauque.

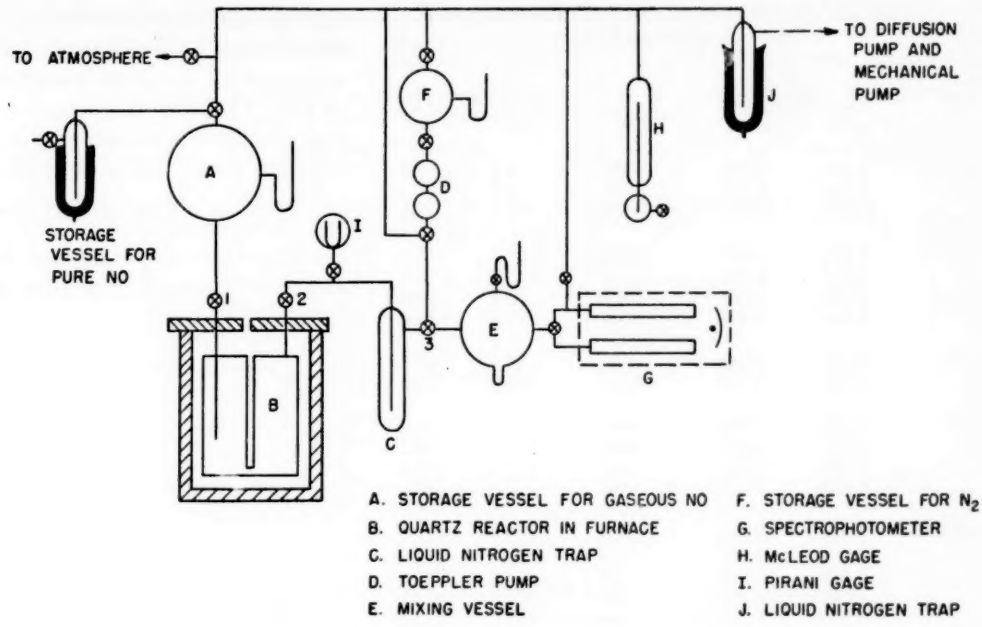

FIG. 1. Apparatus for study of rate of thermal decomposition of nitric oxide.

determining step for this process in the low-temperature range is different from that observed at higher temperatures. Consequently, an intermediate-temperature region would be expected to exist in which both reaction mechanisms contribute to the over-all rate of decomposition.

The reaction rate of 900°K with the smaller value for the energy of activation suggests the predominance of a heterogeneous process. In order to evaluate the contribution of the surface-catalyzed reaction, the surface-to-volume ratio of the quartz reactor was increased by a factor of 2.3 upon the addition of a short section of capillary tubing (120 mm in length, 2 mm inside diameter, 3 mm outside diameter). The experimental measurements in the "packed" reaction vessel (Table II) showed a significant rise in reaction rate as a result of the addition of surface. The catalytic influence of the surface is particularly pronounced at higher concentrations of nitric oxide, for which the ratio of the two rates approaches the quotient of the surface-to-volume ratios between the packed and unpacked vessels. This effect has been correlated with the inhibition in reaction rate caused by the surface adsorption of N_2 produced in the reaction.† The contribution of the heterogeneous reaction diminishes with temperature although it is still apparent at 1270°K the highest temperature studied.

Qualitatively one may conclude therefore that the thermal decomposition of nitric oxide is predominantly heterogeneous at temperatures below 1000°K and that a homogeneous mechanism becomes rate-controlling at higher temperatures. If it may be assumed that the energy of activation observed at temperatures above 2000°K is representative of the homogeneous reaction for which a chain mechanism has been postulated,[6] the contributions of the homogeneous and heterogeneous reactions to the over-all rate may be calculated over a range of temperatures.

At temperatures below 1000°K the experimental measurements presented in Table I may be fitted to the

† These results will be presented in detail in the second paper of this series.

TABLE I. Rate of decomposition of nitric oxide at various temperatures.

Temp. T °K	Reciprocal temperature $1/T \times 10^4$ $(°K)^{-1}$	Concentration of NO mole/cc $\times 10^6$ Initial	Final	Reaction time t (sec)	Specific reaction-rate constant k $(mole/cc)^{-1}$ sec^{-1}
872	11.468	7.330	7.292	10,000	0.07
872	11.468	5.943	5.913	10,500	0.08
872	11.468	4.698	4.681	10,000	0.08
878	11.390	9.207	9.155	10,500	0.06
899	11.123	6.444	6.412	10,000	0.08
901	11.099	10.015	9.951	9,000	0.07
901	11.099	4.282	4.264	12,000	0.08
918	10.893	5.353	5.318	11,020	0.12
951	10.515	4.791	4.761	6,000	0.22
980	10.204	9.677	9.558	6,000	0.21
980	10.204	8.246	8.145	7,000	0.22
1000	10.000	7.310	7.250	5,000	0.23
1001	10.000	3.164	3.145	8,000	0.24
1025	9.750	9.827	9.675	3,000	0.53
1025	9.750	8.141	8.050	3,000	0.46
1025	9.750	4.475	4.428	5,100	0.47
1057	9.461	3.939	3.844	10,000	0.63
1060	9.434	8.286	8.038	6,500	0.57
1080	9.259	5.273	5.194	3,600	0.80
1100	9.091	6.498	6.402	2,000	1.15
1109	9.071	6.228	6.107	3,000	1.06
1135	8.811	3.703	3.662	1,500	2.02
1173	8.525	8.721	6.327	8,000	5.42
1186	8.432	5.051	4.775	1,900	6.02
1186	8.432	4.391	4.291	1,000	5.31
1193	8.382	7.011	5.725	4,000	8.01
1275	7.843	6.825	6.584	200	26.82
1275	7.843	5.785	5.609	200	27.12
1275	7.843	2.775	2.677	500	26.45

TABLE II. Effect of quartz surface on rate of thermal decomposition of NO.

Temp. T °K	Concentration of NO mole $\times cc^{-1} \times 10^6$ Initial	Final	Reaction time t (sec)	Decomposition rate mole $\times cc^{-1} \times sec^{-1} \times 10^{12}$ R_1[a]	R_2[b]
901	6.981	6.942	5000	4.8	7.8
	8.942	8.872	3000	8.0	17.3
	10.612	10.542	2500	12.2	28.0
981	3.491	3.453	10000	3.3	3.8
	4.295	4.261	6000	5.0	5.8
	5.235	5.193	4000	7.4	10.6
	7.972	7.924	2000	17.2	24.0
1051	4.369	4.313	6000	12.3	14.8
	6.357	6.300	2000	17.9	28.6
1151	2.949	2.921	1000	24.5	29.9
	4.377	4.291	1000	54.0	86.5
	6.454	6.320	600	117.3	222.4
	7.681	7.551	200	214.0	414.5
1270	2.214	2.148	600	128.0	110.1
	3.098	3.047	200	252.0	255.0
	4.069	3.941	200	434.0	637.8
	4.690	4.564	150	586.0	842.5
	5.473	5.284	200	784.0	943.0

[a] Surface/volume = 0.49 cm^{-1}.
[b] Surface/volume = 1.12 cm^{-1}.

following rate equation:

$$k_1 = 1.4 \times 10^4 \exp(-21{,}400/RT). \quad (1)$$

On the other hand at 1275°K the specific reaction-rate constant based on Eq. (1) is found to be 3.1 $(M/cc)^{-1}$ sec^{-1}, whereas the experimentally determined value is 26.8 $(M/cc)^{-1}$ sec^{-1} (Table I). It is apparent therefore that the differences in rate constants is a result of the contribution of the high-temperature, homogeneous reaction with an activation energy of 82 kcal to the over-all rate. Thus the rate equation applicable to this high-temperature mechanism may be evaluated by fitting the resulting curve at this point. It is found to be

$$k_2 = 3.1 \times 10^{15} \exp(-82{,}000/RT). \quad (2)$$

Based on these two equations, the values of k_1 and k_2 as a function of temperature may be computed (Table III).

TABLE III. Specific reaction-rate constants calculated for homogeneous and heterogeneous thermal decomposition of nitric oxide.

Temp. T °K	$(1/T) \times 10^4$	k_1	k_2	$k_1/(k_1+k_2)$
800	12.50	0.02	1.3×10^{-7}	1.00
900	11.11	0.09	4.1×10^{-5}	1.00
1000	10.00	0.30	4.0×10^{-3}	1.00
1100	9.08	0.80	0.17	0.83
1200	8.34	1.8	3.8	0.32
1400	7.14	6.5	5.1×10^2	0.01
1600	6.25	16.9	2.0×10^4	0.00
1800	5.55	35.6	3.6×10^5	0.00
2000	5.00	64.8	3.5×10^6	0.00

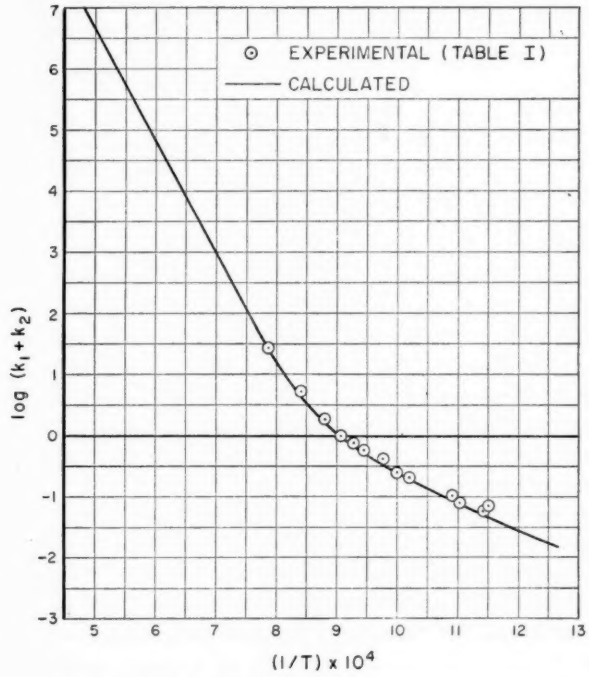

FIG. 2. Rate of thermal decomposition of nitric oxide.

It is of interest to note that in the temperature range from 1100 to 1400°K a transition region is encountered in which both mechanisms play an important part in the over-all reaction kinetics. However, above 1400°K the homogeneous rate of decomposition far exceeds the heterogeneous one; thus the reaction rate is essentially that given by Eq. (2). A graphical analysis of the data (Fig. 2) shows good agreement between the calculated results based on the two rate equations and the experimental measurements listed in Table I.

Decomposition of Di-*t*-butyl Peroxide and Kinetics of the Gas Phase Reaction of *t*-butoxy Radicals in the Presence of Ethylenimine

ROBERT K. BRINTON AND DAVID H. VOLMAN
Department of Chemistry, University of California, Davis, California

(Received August 14, 1951)

The reaction of di-*t*-butyl peroxide with ethylenimine has been studied between 129° and 154°C. The *t*-butoxy radicals formed by the rupture of the O—O bond of the peroxide,

$$(CH_3)_3COOC(CH_3)_3 \xrightarrow{k_1} 2(CH_3)_3CO,$$

are postulated to enter into the following reactions:

$$(CH_3)_3CO \xrightarrow{k_2} CH_3COCH_3+CH_3$$

$$2CH_3 \xrightarrow{k_3} C_2H_6$$

$$CH_3+(CH_2)_2NH \xrightarrow{k_4} (CH_2)_2N+CH_4$$

$$(CH_3)_3CO+(CH_2)_2NH \xrightarrow{k_5} (CH_2)_2N+(CH_3)_3COH.$$

The rate constant for the unimolecular decomposition of the peroxide into *t*-butoxy radicals is found to be in the range $k_1=6\times10^{14}e^{-36,000/RT}$ to $k_1=6\times10^{16}e^{-40,000/RT}$ sec^{-1}. The activation energies $E_4-E_3/2=4.8$ kcal/mole and $E_2-E_5=12$ kcal/mole are calculated from the kinetic data. The complete rate expression for the capture of imine H atom by CH_3 radical,

$$k_4=4.5\times10^{10}e^{-4800/RT} \text{ (moles/cc)}^{-1} \text{ sec}^{-1},$$

is obtained by using Gomer and Kistiakowsky's values for $k_3=4.5\times10^{13}$ (moles/cc)$^{-1}$ sec^{-1} and $E_3=0$. The activation energy for the thermal decomposition of *t*-butoxy radical is about 17 kcal/mole if E_4 and E_5 of similar type H capture mechanisms are assumed equal.

INTRODUCTION

THE thermal decomposition of di-*t*-butyl peroxide in the gas phase has been shown to be a nonchain unimolecular process.[1–3] The results of Raley, Rust and Vaughan[3] show that the reactions

$$(CH_3)_3COOC(CH_3)_3 \xrightarrow{k_1} 2(CH_3)_3CO \quad (1)$$

$$(CH_3)_3CO \xrightarrow{k_2} CH_3COCH_3+CH_3 \quad (2)$$

$$CH_3+CH_3 \xrightarrow{k_3} C_2H_6 \quad (3)$$

lead to acetone and ethane as the reaction products.

In the presence of various organic compounds in the gas phase, reactions of *t*-butoxy radical other than process (2) were not observed.[4–5] Thus at temperatures at which the peroxide decomposes, the *t*-butoxy radical is presumed to decompose very rapidly by (2). However, in the liquid state and in liquid solutions of organic solvents, dehydrogenation reactions attributable to *t*-butoxy radical and leading to the formation of *t*-butyl alcohol were observed.[6–8] Since there is no reason to expect any major qualitative difference in the liquid and gas reactions, the failure to observe *t*-butyl alcohol in the gas phase reactions may be accounted for by the comparatively low concentration of hydrogen donor molecules and the fast rate of reaction of (2) at temperatures necessary to decompose the peroxide. Recently Dorfman and Salsburg[9] reported that in the photochemical gas phase decomposition at about 30°C appreciable quantities of *t*-butyl alcohol are formed. Since the primary photochemical step is almost certainly a split into *t*-butoxy radicals, this observation may be attributed to hydrogen atom abstraction by the radical.

TABLE I. Decomposition of di-*t*-butyl peroxide rate constants.

Temp. °C	Peroxide pressure (mm)	$k\times10^4$ sec^{-1}
129.6	15.6	0.164
140.7	20.2	0.630
141.0	20.6	0.628
145.9	20.8	1.21
152.5	21.0	2.25
153.6	27.4	2.35
166.8	21.5	8.92

[1] N. A. Milas and D. M. Surgenor, J. Am. Chem. Soc. **68**, 205 (1936).
[2] P. George and A. D. Walsh, Trans. Faraday Soc. **42**, 94 (1946).
[3] Raley, Rust, and Vaughan, J. Am. Chem. Soc. **70**, 88 (1948).
[4] Rust, Seubold, and Vaughan, J. Am. Chem. Soc. **70**, 95 (1948).
[5] D. H. Volman, J. Chem. Phys. **19**, 668 (1951).
[6] Raley, Rust, and Vaughan, J. Am. Chem. Soc. **70**, 1336 (1948).
[7] Bell, Rust, and Vaughan, J. Am. Chem. Soc. **72**, 337 (1950).
[8] Rust, Seubold, and Vaughan, J. Am. Chem. Soc. **72**, 338 (1950).
[9] L. M. Dorfman and Z. W. Salsburg, J. Am. Chem. Soc. **73**, 255 (1951).

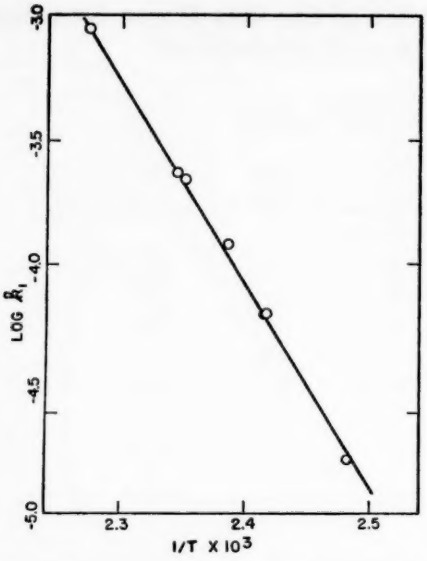

FIG. 1. Effect of temperature on the rate constant for the decomposition of di-*t*-butyl peroxide.

In our experiments it was found that when di-tertiary butyl peroxide was thermally decomposed in the presence of ethylenimine, *t*-butyl alcohol and methane were both formed, presumably because of the relative ease of dehydrogenation of this molecule. From the kinetics of the reactions involved it was possible to make estimates of the activation energies for the removal of a hydrogen atom from the imine by methyl radical and for the decomposition of the *t*-butoxy radical.

EXPERIMENTAL METHOD

Di-*t*-butyl peroxide was kindly supplied by the Shell Development Company; it was further purified by bulb to bulb distillation. Ethylenimine was prepared by the method of Wenker.[10] The product was fractionated in a 20-plate column. The boiling point of the fraction used in the kinetic determinations was 55.2±0.1°C.

The experimental technique is similar to that described previously.[5] Measured pressures of imine and peroxide were mixed in a one-liter flask at room temperature. The mixture was expanded into the one-liter reaction chamber immersed in an oil bath thermostat. The reaction was terminated by expanding the reaction mixture into a sample bulb receiver at room temperature. This aliquot sample was separated by use of a toepler pump into a volatile fraction, noncondensable at −120°C, and a nonvolatile sample, the remainder. Volume of the volatile fraction was determined by a gas microburet. Analyses of both fractions were made by a Consolidated mass spectrometer. Reaction rates were taken as $\Delta C/\Delta t$ over the time interval of each run. For this reason the runs were stopped at small percentage completion so that the $\Delta C/\Delta t$ was essentially the initial reaction rate.

RESULTS AND DISCUSSION

Decomposition of Di-*t*-butyl Peroxide

The kinetics of the thermal decomposition of di-*t*-butyl peroxide reported by Raley, Rust, and Vaughan[3] lead to an activation energy of 39 kcal/mole and to a frequency factor of 3.2×10^{16} sec^{-1}. The high value given for the frequency factor led to a reinvestigation of the kinetics by Murawski, Roberts, and Szwarc.[11] These authors report an activation energy of 36 kcal/mole and a frequency factor of 4×10^{14} sec^{-1}. In view of these differences and the interest in this problem, the data obtained in this study are given in Table I and Fig. 1.

The results obtained lead to a rate constant in the range $k_1=6\times10^{14}e^{-36,000/RT}$ to $k_1=6\times10^{16}e^{-40,000/RT}$ sec^{-1}. These values are just within those given in the two earlier studies.[3,11]

TABLE II. Reaction of di-*t*-butyl peroxide with ethylenimine.

Temp. °C	Initial pressure, mm		Initial rates Volatile products, moles cc^{-1} sec$^{-1}\times10^{12}$			$\frac{R_{(CH_4)}}{R_{C_2H_6}}\times10^6$	$\frac{R_{(CH_3)_3COH}}{R_{(CH_3)_2CO}}$
	Peroxide	Imine	CH_4	C_2H_6	C_2H_4		
129.6	15.5	0	0.32	6.98	0	0.122	0
129.6	15.3	7.5	0.82	2.14	0.17	5.60	0.023
129.6	15.6	14.7	10.9	1.18	0.31	10.1	0.128
129.6	15.4	30.9	11.5	0.45	0.54	17.2	0.291
141.0	20.5	0	1.66	38.1	0	0.269	0.0032
141.0	19.4	6.0	20.9	16.4	0.36	5.16	0.059
141.0	20.4	12.4	34.9	12.1	0.61	9.90	0.105
141.0	20.3	33.9	48.0	4.09	1.43	23.8	0.198
141.0	19.8	77.9	49.3	1.66	1.89	38.4	0.428
141.0	20.8	194.8	47.6	0.90	2.05	50.3	0.570
153.6	16.0	0	3.96	137.1	0	0.338	0
153.6	15.1	5.5	50.3	83.0	0.43	5.53	0.036
153.6	15.6	13.1	94.6	57.3	1.75	12.5	—
153.6	15.8	55.4	156.7	6.88	3.03	59.8	0.234
153.6	16.0	103.6	157.5	3.04	4.30	90.3	0.362

[10] H. Wenker, J. Am. Chem. Soc. **57**, 2328 (1935).
[11] Murawski, Roberts, and Szwarc, J. Chem. Phys. **19**, 698 (1951).

Reactions of Di-*t*-butyl Peroxide and Ethylenimine

Previous studies[3] and experiments reported in the present work indicate that very little methane is formed in the thermal decomposition of pure di-*t*-butyl peroxide. The formation of large amounts of methane when the peroxide decomposes in the presence of ethylenimine indicates that methyl radicals from reaction (2) interact with the imine,

$$CH_3+(CH_2)_2NH\xrightarrow{k_4}CH_4+(CH_2)_2N, \qquad (4)$$

to produce methane. The rate of methane formation is

$$\frac{d[CH_4]}{dt}=R_{CH_4}=k_4[CH_3][(CH_2)_2NH].$$

If ethane formation is attributed solely to Eq. (3)

$$\frac{d[C_2H_6]}{dt}=R_{C_2H_6}=k_3[CH_3]^2.$$

For a steady state of methyl radicals

$$\frac{R_{CH_4}}{R_{C_2H_6}^{\frac{1}{2}}}=\frac{k_4}{k_3^{\frac{1}{2}}}[(CH_2)_2NH],$$

and a plot of $R_{CH_4}/R_{C_2H_6}^{\frac{1}{2}}$ *vs* the imine concentration should yield a straight line. The rate data obtained at three different temperatures for varying imine pressure and about constant peroxide pressure are given in Table II. A plot of the rates in the manner indicated above is shown in Fig. 2. The points given on the graph are confined to the lower imine pressures. A marked deviation from linearity occurs at higher imine pressures indicating that the rate of formation of ethane is too large relative to the rate of methane formation. Inasmuch as the amount of ethane is very small under these conditions, even small amounts of ethane produced from some process other than reaction (3) could easily cause the deviations.

Values for the ratio $k_4/k_3^{\frac{1}{2}}$ obtained from the slopes of the lines in Fig. 2 are plotted on a logarithmic scale *vs* $1/T$ in Fig. 3. The value of $E_4-1/2E_3=4.8$ kcal/moles is obtained from this graph. Since

$$\frac{k_4}{k_3^{\frac{1}{2}}}=\frac{A_4e^{-E_4/RT}}{[A_3e^{-E_3/RT}]^{\frac{1}{2}}}$$

and Gomer and Kistiakowsky[12] give the values of $E_3=0$ and $A_3=4.5\times10^{13}$ for the formation of ethane from methyl radicals, the rate constant for methane production in the peroxide-imine system is

$$k_4=4.5\times10^{10}e^{-4800/RT}\ (\text{moles/cc})^{-1}\ \text{sec}^{-1}.$$

The low value of the pre-exponential factor is in agreement with that predicted for a reaction of this type[12] which generally may be expected to have a steric factor of the order of 10^{-4}.

[12] R. Gomer and G. B. Kistiakowsky, J. Chem. Phys. **19**, 84 (1951).

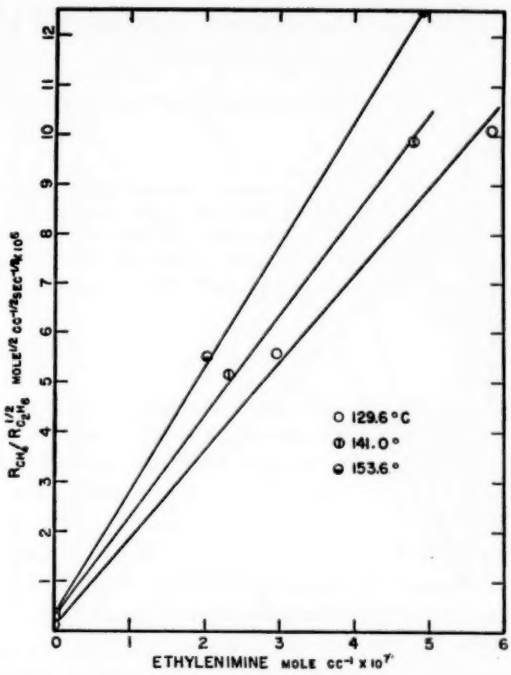

FIG. 2. Ratio of rate of methane production to square root of rate of ethane production *vs* ethylenimine concentration at various temperatures.

The formation of *t*-butyl alcohol may be accounted for by a hydrogen abstraction reaction by the *t*-butoxy radicals,

$$(CH_3)_3CO+(CH_2)_2NH\xrightarrow{k_5}(CH_3)_3COH+(CH_2)_2N. \qquad (5)$$

The rate of formation of *t*-butyl alcohol is then,

$$R_{(CH_3)_3COH}=k_5[(CH_3)_3CO][(CH_2)_2NH].$$

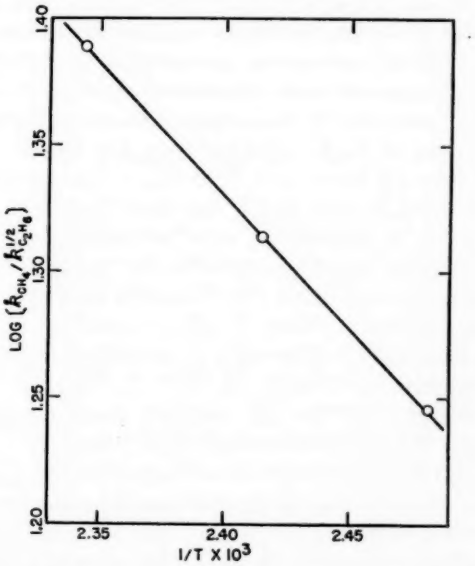

FIG. 3. Effect of temperature on the rate constant ratio, $k_4/k_3^{\frac{1}{2}}$.

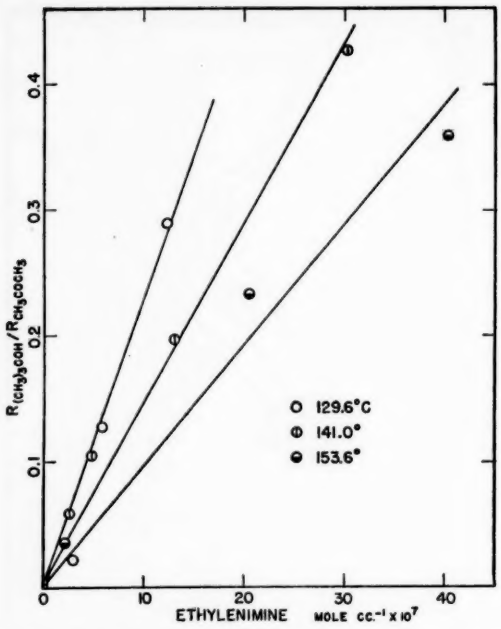

FIG. 4. Ratio of rate of *t*-butyl alcohol production to rate of acetone production *vs* ethylenimine concentration at various temperatures.

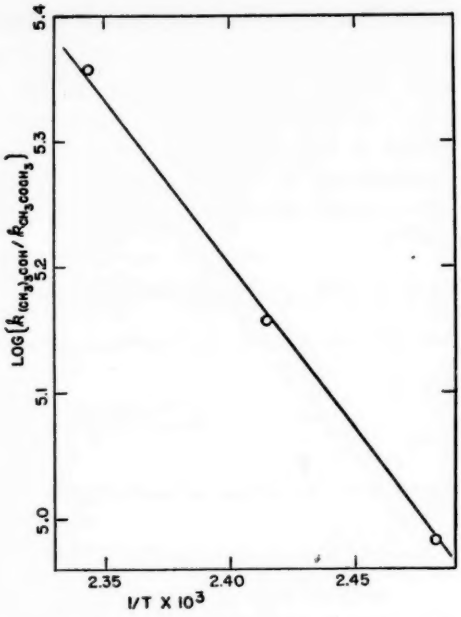

FIG. 5. Effect of temperature on the rate constant ratio, k_5/k_2.

If acetone is formed solely by reaction (2)

$$R_{CH_3COCH_3}=k_2[(CH_3)_3CO]$$

and under a steady state condition of *t*-butoxy radicals

$$\frac{R_{(CH_3)_3COH}}{R_{CH_3COCH_3}}=\frac{k_5}{k_2}[(CH_2)_2NH].$$

The data given in Table II for $R_{(CH_3)_3COH}/R_{CH_3COCH_3}$ is plotted *vs* imine concentration in Fig. 4. The spread of the experimental points from the expected straight lines is wider than in the case of the similar study made on $R_{CH_4}/R_{C_2H_6}$. These deviations are possibly due to the difficulty of making accurate mass spectrometric estimates of small amounts of acetone and *t*-butyl alcohol in the presence of other reaction products and a large excess of unreacted di-*t*-butyl peroxide and ethylenimine. The values of k_5/k_2 obtained from the slopes of the Fig. 4 lines are shown *vs* $1/T$ in Fig. 5. Considering the uncertainties in determining the slopes from Fig. 4, the plot of Fig. 5 is, perhaps, only fortuitously a straight line. However making allowances for the uncertainties the value $E_2-E_5=12\pm2$ kcal/mole is obtained. If the assumption is made that *H* atom abstraction from the imine molecule by either methyl or *t*-butoxy radical has similar activation energy, i.e., $E_5=E_4$, then the activation energy, E_2, for the thermal decomposition of *t*-butoxy radical is about 17 ± 3 kcal/mole.

The products listed in Table II represent the majority of substances formed in the reaction. The absolute rate of formation of *t*-butyl alcohol and acetone was not determined accurately. However, the rates of formation of methane, ethane, acetone, and *t*-butyl alcohol are consistent with those expected on the basis of the known unimolecular rate of decomposition of di-*t*-butyl peroxide at each temperature. Since Eqs. (4) and (8) both yield the $(CH_2)_2N$ radical, reactions to account for the removal of the large amounts of this radical must occur. Two likely removal processes are:

$$2(CH_2)_2N\rightarrow(CH_2)_2NN(CH_2)_2 \quad (6)$$

$$2(CH_2)_2N\rightarrow N_2+2C_2H_4. \quad (7)$$

From Table II it is seen that the relative ethylene formation increases with increasing imine concentration and decreasing temperature. Identification of the small amount of nitrogen to be expected by process (7) was difficult in the mass spectrometric analysis of the rate experiments. Analyses of reactions run almost to completion showed nitrogen to be present in approximately the quantity relative to ethylene which would be expected from Eq. (7). The $m/q=86$ peak was present in the mass spectra of all condensable fractions of the rate experiments. This peak would correspond to the parent peak of the imine radical dimer shown in reaction (6). It is probable that the dimer is a bicyclic molecule resulting from a simple condensation of two cyclic imine radicals.

ACKNOWLEDGMENT

We wish to express our thanks to Dr. Amos Newton and Mr. Laurin Tolman of the Radiation Laboratory and Department of Chemistry, Berkeley, California, for assistance with the mass spectrometric analyses. We also wish to express our appreciation to the Research Corporation for financial aid.

THE JOURNAL OF CHEMICAL PHYSICS VOLUME 20, NUMBER 1 JANUARY, 1952

Bond Orbitals and Bond Energy in Elementary Phosphorus

LINUS PAULING AND MASSIMO SIMONETTA*
Gates and Crellin Laboratories of Chemistry, California Institute of Technology, Pasadena, California†
(Received September 24, 1951)

A discussion of the relative stability of the P_4 molecule and black phosphorus is carried out, with use of hybrid *spd* bond orbitals. The amount of strain in the P_4 molecule, in which the bond angles are 60°, is calculated to be 22.8 kcal mole^{-1}. This value is shown to be compatible with thermochemical data; it corresponds to the value 51.3 kcal mole^{-1} for the bond energy of the normal P—P bond. A structure is proposed for red phosphorus and other allotropic forms of the element, and some of their properties are discussed in relation to their structure.

INTRODUCTION

AN interesting problem in chemical bond theory is offered by the relative stability of the P_4 molecule. In this molecule the four phosphorus atoms are at the corners of a regular tetrahedron, each being bonded to the other three; there are accordingly three 60° P—P—P bond angles per phosphorus atom. The strain associated with these small bond angles might be expected to be rather large: the strain energy for three 60° C—C—C bond angles in cyclopropane is 22 kcal mole^{-1}, and a similar amount of strain energy per phosphorus atom would not be surprising. In fact, however, the strain energy is smaller, the difference in enthalpy[1] of ordinary white phosphorus (PIII) and the stable form, black phosphorus, being 10.3 kcal mole^{-1}. The form of white phosphorus which is stable at temperatures below −77°C, PIV, has enthalpy only 8.9 kcal mole^{-1} greater than that of black phosphorus, and it would be predicted that a still denser form of P_4, with increased van der Waals attraction between the molecules, corresponding to that operating in the denser black phosphorus, would show a still smaller difference in enthalpy from black phosphorus. An argument given below, based on the correction of the enthalpy of black phosphorus for van der Waals attractions and repulsions, leads to the conclusion that the bent-bond strain energy in the P_4 molecule is about 5.7 kcal mole^{-1} per phosphorus atom, or 22.8 kcal mole^{-1} per P_4 molecule.

A theoretical treatment of strain energy in this molecule was carried out by Moffitt,[2] who assumed the bonds in the molecule to be formed with use of pure $3p$ orbitals. Moffitt found the strain energy calculated by his quantum-mechanical treatment to be 11.8 kcal mole^{-1} per P—P bond, or 17.7 kcal mole^{-1} per phosphorus atom. He decreased this value by 40 percent, to 10.6 kcal mole^{-1} per phosphorus atom, by making an empirical correction based on the lack of agreement with experiment given by a similar calculation for cyclopropane. The agreement of his uncorrected value with the experimental strain energy, which we estimate to be 5.7 kcal mole^{-1} per phosphorus atom, is not good.

Arnold[3] has suggested that the phosphorus atoms in the P_4 molecule use pd^2 hybrid orbitals in forming bonds. He pointed out that pd^2 bond orbitals have strength 2.29, and normal bond angles of 66°26′, so that very little strain would be required to distort them to 60°. However, this suggestion cannot be accepted. The energy of promotion of a $3p$ electron to a $3d$ orbital in the phosphorus atom is given by spectroscopic data as about 194 kcal mole^{-1}. In order for a phosphorus atom to form three d^2p bonds, two electrons would need to be promoted in this way, which would confer upon the molecule an instability of 388 kcal mole^{-1} per phosphorus atom.

We have treated the problem by the consideration of *spd* hybrid bond orbitals, the hybridization parameters being selected so as to minimize the energy of the molecule, including the bond energy and the atomic energy. We have obtained for the strain energy of the P_4 molecule, relative to a hypothetical P_4 molecule with normal bonds, the value 22.8 kcal mole^{-1}, or 5.7 kcal mole^{-1} per phosphorus atom. This value seems to be in good agreement with experiment. The hybrid bond orbitals, which have strength 2.0074 in the bond direction (considerably greater than the value 1.6304 for pure p orbitals), are largely p in character, the contribution of the $3s$ orbital amounting to 0.4 percent and that of the $3d$ orbital to 2.2 percent.

HYBRID ORBITALS IN P_4

We assume that the energy of a P—P bond is proportional to the square of the strength of the bond orbital in the bond direction. This postulate for bent bonds was proposed originally by R. Spitzer,[4] and was applied by him in the discussion of cyclopropane, spiropentane, and other molecules,[5,6] for which good agreement with experiment was found. If the bonds formed by the phosphorus atom were pure $3p$ bonds, with $S^2=3$ in the direction of maximum bond strength and $S^2=2.658$ in the direction corresponding to 60° bond

* Present address: Department of General Chemistry, Institute of Technology of Milan, Italy.

† Contribution No. 1500.

[1] Thermochemical data used in this paper are from Selected Values of Chemical Thermodynamic Properties, Nat. Bur. Standards, **1950**.

[2] W. E. Moffitt, Trans. Faraday Soc. **44**, 987 (1948).

[3] J. R. Arnold, J. Chem. Phys. **14**, 351 (1946).

[4] R. Spitzer, Ph.D. thesis, Cal. Inst. tech., **1941**.

[5] J. E. Kilpatrick and R. Spitzer, J. Chem. Phys. **14**, 463 (1946).

[6] G. L. Humphrey and R. Spitzer, J. Chem. Phys. **18**, 902 (1950).

angles (19°28′ from the best bond direction), the calculated strain energy would be about 10 kcal mole^{-1} per phosphorus atom. The calculation is made in the following way. The heat of dissociation of P_4 into 4P corresponds to a P—P average bond energy[7] of 47.5 kcal mole^{-1}. If this is set proportional to S^2 in the bond direction (2.658), and the corresponding value is calculated for $S^2=3$, it is found to be 53.6 kcal mole^{-1}, indicating the strain energy to be about 6.1 kcal mole^{-1} per bond, or 9.2 kcal mole^{-1} per phosphorus atom, there being $1\frac{1}{2}$ bonds per atom in the P_4 molecule.

The calculated strain energy is decreased somewhat by the consideration of *spd* hybridization. Only a small amount of *s* and *d* character would be expected for the bond orbitals, because of the large promotion energy associated with the transfer of an electron from a $3p$ orbital to a $3d$ orbital, or from a $3s$ orbital to a $3p$ orbital. Pure *p* bonds would be formed by an atom in the configuration $3s^23p^3$. The inclusion of $3s$ character in a bond orbital would require a contribution of the configuration $3s3p^4$, and the inclusion of $3d$ character in the bond orbital would require a contribution of the configuration $3s^23p^23d$. We have used the value 194 kcal mole^{-1} for the excitation energy of both configuration $3s3p^4$ and configuration $3s^23p^23d$ of phosphorus.[8] (The lowest states of the configurations $3s3p^4$ and $3s^23p^23d$ lie above the lowest state of $3s^23p^3$ by 170 kcal mole^{-1} and 200 kcal mole^{-1}, respectively, and the estimated valence states is 186 kcal mole^{-1}.) The energy per half of a P—P bond can be expressed approximately by the equation

$$W=-7.13S^2+194(a^2+c^2) \text{ kcal mole}^{-1}. \quad (1)$$

In this equation S is the strength in the bond direction in the P_4 molecule of a hybrid bond orbital $as+bp+cd$. The first term represents the bond energy for the half bond, and the second term the energy of promotion of the electron associated with the *s* and *d* character of the hybrid bond orbital. The factor 7.13 was chosen to lead to essentially the experimental value for the bond energy.

It was found possible to minimize W with respect to the parameters of a general *spd* wave function, of the form

$$\psi=\sum_{i=1}^{9} a_i\psi_i, \quad (2)$$

in which the successive functions $\psi_1\cdots\psi_9$ are s, p_z, d_z, p_x, d_{x+z}, d_{xy}, p_y, d_{y+z}, and d_{x+y}, respectively. Three equivalent bonds of this character related to one another by rotation through 120° around the *z* axis may be formed; the orthogonality and normalization conditions then require the following relations among the coefficients of the orbital for the bond in the *xz* plane:

$$a_1^2+a_2^2+a_3^2=\tfrac{1}{3},$$
$$a_4^2+a_5^2+a_6^2=\tfrac{2}{3},$$
$$a_7=a_8=a_9=0.$$

It was found on solution of this problem that the best bond orbitals have the form

$$\psi_1=0.0622s+0.5694p_z+0.0695d_z +0.8096p_x+0.1230d_{x+z}+0.0435d_{xy} \quad (3)$$

with ψ_2 and ψ_3 similar. The strength of these orbitals in the bond direction for P_4 is 2.0074, and the value of W is -23.75 kcal mole^{-1}.

A similar calculation can be made for arbitrary bond direction. The procedure for finding the best *spd* hybrid bond orbital with promotion energies as given above is that of solving the secular equation for the function $\psi=as+bp_z+cd_z$. This secular equation has the form[9]

$$\begin{vmatrix} Q-W-\alpha & -\sqrt{3}\alpha & -(5)^{\frac{1}{2}}\alpha \\ -\sqrt{3}\alpha & -W-3\alpha & -(15)^{\frac{1}{2}}\alpha \\ -(5)^{\frac{1}{2}}\alpha & -(15)^{\frac{1}{2}}\alpha & Q-W-5\alpha \end{vmatrix}=0 \quad (4)$$

in which $Q=194$ kcal mole^{-1} and $\alpha=7.13$ kcal mole^{-1}. Solution of this equation leads to

$$\psi=0.0685s+0.9858p_z+0.1530d_z$$

with $S=2.118$ and $W=-26.55$ kcal mole^{-1}. The bond angle corresponding to these best *spd* hybrid bond orbitals for phosphorus is 89°55′. The prediction would accordingly be made that the normal bond angles for phosphorus should be close to 90°.

THE NORMAL PHOSPHORUS-PHOSPHORUS BOND

The difference in the values of W found for unstrained bonds and for 60° bond angles is 2.80 kcal mole^{-1} per half-bond, or 8.40 kcal mole^{-1} per phosphorus atom. This value may accordingly be taken as the calculated strain energy per phosphorus atom in P_4, relative to a hypothetical P_4 molecule with unstrained bonds. The calculated strain energy per P_4 molecule is 33.6 kcal mole^{-1}.

We are, however, primarily interested in the energy of the normal P—P bond. A normal P—P bond may be defined as the phosphorus-phosphorus bond in a substance in which the bond angles have normal values. The normal value of the angle between two bonds formed by a phosphorus atom is about 101°; representative values are 99° and 102° in black phosphorus, 100.5° in phosphorus trichloride, 101.5° in phosphorus tribromide, and 102° in phosphorus tri-iodide. The increase over the value 89°55′, at which the strength of the bond orbitals is a maximum, is to be attributed to the van der Waals repulsion of the ligated atoms. (A smaller bond angle, 93°, is observed in phosphine; presumably the van der Waals repulsion of the hydrogen atoms is so

[7] F. S. Dainton, Trans. Faraday Soc. **43**, 244 (1947).
[8] Charlotte E. Moore, Atomic Energy Levels, Circular, Natl. Bur. Standards, 467 (1949).
[9] L. Pauling, Proc. Roy. Soc. (London) **A196**, 343 (1949).

much less than that of larger atoms as to cause only a 3° increase in bond angle.) A calculation similar to that described above for the strain energy for bond angle 60° leads to the value 0.75 kcal mole^{-1} as the strain energy per 101° bond angle. Two phosphorus atoms bonded to a third also experience van der Waals attraction and van der Waals repulsion. The energy quantities per 101° bond angle calculated by use of the equations given in the following section, with the constant α of Eq. (7) (for van der Waals repulsion) chosen so as to lead to equilibrium with the forces of bond angle strain and van der Waals attraction at 101°, have the values −2.29 kcal mole^{-1} and 2.44 kcal mole^{-1}, respectively. The total bond angle strain energy for angle 101° is thus 0.90 kcal mole^{-1} per bond angle, or 2.70 kcal mole^{-1} per phosphorus atom.

We may use this quantity and the calculated strain energy for P_4 to obtain the strain energy of P_4 relative to a molecule containing normal P−P bonds, with the normal amount of strain. This value is 8.40−2.70=5.70 kcal mole^{-1} per phosphorus atom, or 22.8 kcal mole^{-1} per P_4 molecule, and the energy of a normal P−P bond is calculated to be $47.5+\frac{1}{6}\cdot 22.8=51.3$ kcal mole^{-1}.

THE ENTHALPY OF BLACK PHOSPHORUS

Gaseous P_4 has enthalpy 3.12 kcal mole^{-1} per phosphorus atom, relative to white phosphorus III, and it is accordingly greater in enthalpy than black phosphorus by 13.4 kcal mole^{-1}. Black phosphorus is the only modification of phosphorus whose crystal structure is known.[10] Each phosphorus atom is bonded to three other phosphorus atoms, at 2.20A, essentially the same bond distance as in the P_4 molecule. The bonded phosphorus atoms form puckered sheets, with P−P−P bond angles lying between 99° and 102°.

We may use the thermochemical data for black phosphorus as the basis for predicting the energy of a hypothetical P_4 molecule in which there are normal bonds, by correcting for the van der Waals attraction and repulsion in the black phosphorus crystal.

The energy of van der Waals attraction between phosphorus atoms other than those connected directly by bonds can be calculated by use of the London equation. The London equation for van der Waals attraction is

$$E_{\text{att}}=-\frac{3}{2}\frac{\alpha_A\alpha_B I_A I_B}{r_{AB}^6(I_A+I_B)} \qquad (5)$$

in which α_A and α_B are the polarizabilities of atoms A and B, at the distance r_{AB} apart, and I_A and I_B are the average energies of excitation, usually taken as equal to the ionization energies of the neutral atoms. It is found empirically, by consideration of the heats of sublimation of crystals of the noble gases, that this equation gives too small values of the van der Waals attraction, if I_A and I_B are taken as the ionization energies, and that improved agreement with experiment is obtained by multiplying by the factor 1.57. We accordingly make use of the equation

$$E_{\text{att}}=-4.26\frac{R_A R_B I_A I_B}{r_{AB}^6\tfrac{1}{2}(I_A+I_B)}\ \text{kcal mole}^{-1} \qquad (6)$$

in which R_A and R_B are the mole refractions, in cm^3, I_A and I_B are the ionization energies in electron volts, and r_{AB} is the interatomic distance in A. For phosphorus the mole refraction has the value 8.70 cm^3, and the ionization energy the value 11.0 ev. The interatomic distances in black phosphorus according to the structure reported by Hultgren, Gingrich, and Warren,[10] in addition to the bond distances, are 3.31 (2), 3.41 (2), 3.43 (4), 3.68 (2), 3.87 (2), 3.98 (2), 4.14 (1), 4.40 (2), etc. The application of Eq. (6) to these data, with an integration from 4.9A to infinity to give the contributions of the larger distances, leads to −10.2 kcal mole^{-1} as the energy of van der Waals attraction of atoms other than bonded atoms and next-bonded atoms (P ⋯ P) in black phosphorus.

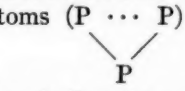

The reason for excluding the next-bonded atoms (2 at 3.31 and 4 at 3.43A) is given below.

Consideration must also be given to the energy of van der Waals repulsion. In general, the energy of van der Waals repulsion between atoms can be expressed approximately by an equation of the form

$$E_{\text{rep}}=\alpha e^{-3.35 r_{AB}}. \qquad (7)$$

In black phosphorus the repulsion between two phosphorus atoms bonded to the same third atom is sufficiently great not only to overcome the van der Waals attraction but also to overcome the tendency of the P−P−P bond angle to assume the normal value 89°55′, the angle being increased to 99° (for one bond angle) and 102° (for the other two). The nonbonded distances that are involved are 3.31A and 3.43A, respectively. It is found that when the constant α is adjusted in such a way as to give equilibrium at these bond angles, with the force of van der Waals repulsion just counterbalancing that of van der Waals attraction and of bond strain, the energy of van der Waals repulsion is 7.32 kcal mole^{-1} and that of van der Waals attraction is −6.87 kcal mole^{-1} per phosphorus atom. These values have been used in a calculation described in the preceding section.

In addition, the puckered layers of phosphorus atoms are superimposed, the atomic contacts between layers being those at 3.68 and 3.87A. Also there are two contacts at 3.41A, for which the force of van der Waals attraction must be counterbalanced by a repulsive force. It is easily shown that the ratio of the energy of the van der Waals repulsion (given by Eq. (7)) to the energy of van der Waals attraction at the equilibrium distance r_{AB} is $-6/3.35 r_{AB}$, and that for these contacts

[10] Hultgren, Gingrich, and Warren, J. Chem. Phys. **3**, 351 (1945).

the van der Waals repulsion energy amounts to 2.4 kcal mole^{-1} per phosphorus atom.

Thus we calculate that there are in black phosphorus a stabilizing energy of van der Waals attraction, other than between bonded and next-bonded atoms, amounting to -10.2 kcal mole^{-1}, and a destabilizing energy of 2.4 kcal mole^{-1} in van der Waals repulsion, resulting in an over-all stabilization of -7.8 kcal mole^{-1} per phosphorus atom. From this calculation the enthalpy of a hypothetical form of phosphorus in which there are normal bonds and the only interactions effective are those between each atom and its three ligates and between these ligates is $-10.3+7.8=-2.5$ kcal mole^{-1} per phosphorus atom, relative to the standard state, white phosphorus. The enthalpy of gaseous P_4 is $+3.3$ kcal mole^{-1} per phosphorus atom, relative to the same standard state, so that the strain energy in P_4, relative to the hypothetical state with unstrained bonds, is given as $2.5+3.3=5.8$ kcal mole^{-1}.

This value corresponds to the value 23.2 kcal mole^{-1} per P_4 molecule for the strain energy relative to a molecule containing normal P—P bonds.

THE HEAT OF HYDROGENATION OF PHOSPHORUS

We may use data for the heat of hydrogenation of phosphorus to phosphine and to solid phosphorus hydride, $(P_2H)_n$, to evaluate the strain energy of the P_4 molecule. Unfortunately the heat of formation of diphosphorus tetrahydride, P_2H_4, has not been determined. If it were known, the strain energy of the P_4 molecule could be calculated simply as the heat evolved by the reaction

$$P_4(g)+8PH_3(g)\rightarrow 6P_2H_4(g) \qquad (8)$$

Since phosphorus and hydrogen have the same electronegativity, we would expect the heat of the reaction

$$P_4(g)+6H_2(g)\rightarrow 4PH_3(g) \qquad (9)$$

to be zero, except for the strain energy of the P_4 molecule. The observed heat of this reaction, 21.7 kcal mole^{-1}, thus provides a value of this strain energy.

It is likely that the hydride $(P_2H)_n$, which is formed (together with phosphine) by photochemical decomposition of diphosphorus tetrahydride and by many other reactions, contains normal P—P bonds. If the van der Waals energy in $(P_2H)_n(c)$ is equal to that in the crystalline elements, the heat of the reaction

$$P_4(c, \text{white})+H_2(c)\rightarrow P_4H_2(c) \qquad (10)$$

would be the strain energy in the P_4 molecule. The observed value is 24.0 kcal mole^{-1}.

A value of the strain energy not dependent on the assumption of zero energy of partial ionic character of the P—H bond is the heat of the reaction

$$P_4(c, \text{white})+\tfrac{4}{5}PH_3(c)\rightarrow(12/5)P_2H(c). \qquad (11)$$

The observed value (involving the estimate 0.6 kcal mole^{-1} for the heat of fusion of phosphine) is 24.6 kcal mole^{-1}.

We may summarize the values of the strain energy of the P_4 molecule relative to a hypothetical molecule with normal P—P bonds as follows:

Bond orbital calculation	22.8 kcal mole^{-1}
Enthalpy of black phosphorus	23.2
Heat of reaction 9	21.7
Heat of reaction 10	24.0
Heat of reaction 11	24.6

None of these values can be considered to have great accuracy; nevertheless, their approximate agreement suggests that they are not in great error. It is gratifying that the average of the thermochemical values is close to the value given by the bond orbital calculation. We accordingly accept 22.8 kcal mole^{-1} as the strain energy of the P_4 molecule, and 51.3 kcal mole^{-1} as the bond energy of a normal P—P bond.

THE ENTHALPY OF WHITE PHOSPHORUS

We may use the expressions for the van der Waals energy of attraction and repulsion to evaluate the enthalpy of white phosphorus. Although the structure of white phosphorus has not been determined, it is likely that it consists of P_4 molecules which in the form stable at room temperature are in essentially free rotation. The density of the crystal is 1.83 g cm^{-3}, which corresponds to a distance between centers of molecules of 5.41A, assuming the molecules to be arranged in cubic closest packing. The energy of van der Waals attraction, using the formula given above and the factor 8.61 for the number of effective contacts, is 19.36 kcal mole^{-1} per P_4 molecule, or 4.84 kcal mole^{-1} per phosphorus atom. The energy of van der Waals repulsion, assumed to be of the form $\alpha e^{-3.35 r_{AB}}$, is 33.2 percent of this, so that the effective energy of stabilization in the crystal is calculated to be 3.23 kcal mole^{-1}. This value is in excellent agreement with the experimental value for the heat of sublimation of phosphorus III, which is 3.28 kcal mole^{-1}.

THE NATURE OF RED PHOSPHORUS AND AMORPHOUS BLACK PHOSPHORUS

The structure of red phosphorus has not been determined. Hultgren, Gingrich, and Warren[10] made x-ray photographs of ordinary "amorphous" red phosphorus, which showed diffuse rings on the powder pattern, and also of crystalline red phosphorus, and prepared radial distribution curves from them. These curves are similar in character to those of black phosphorus, showing that each atom has three bonded ligates at about 2.2A, and several nonbonded neighbors at distances from 3.5 to 4A. There are a smaller number of neighbors at the 101° bond angle distance, 3.4A, in red phosphorus than in black crystalline phosphorus, and a larger number at about 4A.

We suggest that red phosphorus is formed from white phosphorus by the rupture of only one bond in each P_4 tetrahedron. This would permit the P_4 group to open

out into a figure formed by two equilateral triangles with a common base. The two apical phosphorus atoms would then form bonds with similar phosphorus atoms in adjacent P_4 complexes, and presumably long chains of bonded atoms would be formed in this way, with a structure such as

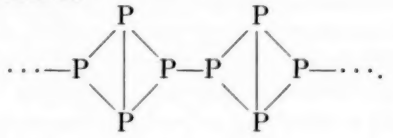

Half of the phosphorus atoms would form bonds with two 60° bond angles and one 101° bond angle, and the other half of the atoms would form bonds with one 60° bond angle and two 101° bond angles. The average number of 60° bond angles would then be $\frac{3}{2}$ per phosphorus atom, rather than 3 as in white phosphorus, and 0 as in black phosphorus. It is obvious that this structure would correspond to an enthalpy value about midway between that of white phosphorus and black phosphorus. The enthalpy of red phosphorus is in fact -4.4, that of black being -10.3 kcal mole^{-1}, relative to white phosphorus. The ease of formation of red phosphorus from white phosphorus, in comparison with the formation of black phosphorus, is explained by the fact that only one bond per P_4 molecule needs to be broken in the formation of red phosphorus, whereas three of the six bonds need to be broken for the formation of black phosphorus. Black phosphorus, although it is the most stable known form of the element at normal conditions, has not been reported to have been made except by application of high pressure.

RATES OF REACTION

A more detailed discussion may be given of the tendency of different forms of phosphorus to occur. The vapor of phosphorus at not too high temperature consists of P_4 molecules. When the vapor is condensed white phosphorus is formed, without change in molecular structure from the vapor. In order for the more stable solid forms of the element to appear, a reaction must take place in which P—P bonds in the P_4 molecules are broken and new bonds are formed. The activation energy for this process is expected to be high, and hence it is not surprising that the conversion of white phosphorus to red phosphorus is slow.

The rate of conversion of white phosphorus to a form containing chains of the type described above (or similar rings) would be predicted to be much faster than the conversion of this form (red phosphorus) to black phosphorus, for the following reason. Let E^* be the activation energy for the conversion of white phosphorus to red phosphorus. This process, as postulated, involves breaking one P—P bond in a tetrahedral P_4 molecule and the conversion of six 60° bond angles into bond angles of about 100°. The strain energy for six 60° bond angles has been evaluated above as about 11.4 kcal mole^{-1}, relative to normal bonds, and this strain energy would be expected to decrease E^* below the value for unstrained bonds. We have estimated the bond energy for an unstrained P—P bond to be 51.3 kcal mole^{-1}, and we would expect this value to be the heat of activation for a reaction involving rupture of such bonds. The heat of activation for the formation of red phosphorus may hence be predicted to be $51.3-11.4=39.9$ kcal mole^{-1}. An experimental value[11] is 38.7 kcal mole^{-1}, in good agreement with the predicted value.

This calculation depends on the assumption that the strain energy of the 60° bond angles in red phosphorus, with the configuration shown above, is the same, per 60° angle, as that of the 60° bond angles in the tetrahedral P_4 molecule. We may check this assumption in the following way. The strain energy per half bond may be taken as a function of the angle between the bond direction and the direction in which the bond orbital would have its maximum strength. For the P_4 molecule this angle is 19°28′, and for a phosphorus atom forming

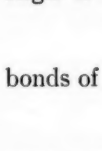

bonds of the type it is 15°. If we assume proportionality of the strain energy to the square of the cosine of this angle (as is true for pure p bonds) the calculated strain energies per 60° bond angle differ by only 15 percent. When the strain energy of the normal bonds is taken into consideration the difference becomes smaller still, and it seems likely that little error is introduced by the assumption that the strain energy can be represented purely as a function of the bond angle values.

To convert red phosphorus into other forms the easiest step can be predicted to be the rupture of the diagonal bond of the P_4 tetrad, to form the square

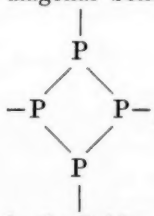

, in which there are four 90° bond angles. In the Bridgman process of making black phosphorus it seems that the temperature rises enough to break other bonds, so that the four-membered rings are not preserved. Crystalline black phosphorus has never been made except by Bridgman's methods,[12] using high pressure (with or without shear) and elevated temperature. It seems likely that the success of the method with pressure around 15,000 atmos and initial temperature around 200°C is due to the heating of the reacting material by the evolved heat of reaction, which for an adiabatic system would cause a temperature increase of

[11] T. W. DeWitt and S. Skolnik, J. Am. Chem. Soc. **68**, 2305 (1946).

[12] P. W. Bridgman, J. Am. Chem. Soc. **36**, 1344 (1914); **38**, 609 (1916).

over 1500°. We can understand why red phosphorus cannot be converted into black phosphorus simply by heating it. At 300°C its rate of conversion into black phosphorus can be predicted to be very slow, the rate constant calculated by assuming the rate to be the same as for the formation of red phosphorus, as observed by DeWitt and Skolnik, except with activation energy 46 kcal mole^{-1} instead of 38.7 kcal mole^{-1} being 1×10^{-5} min^{-1}. Hence months would be required for the conversion into black phosphorus at this temperature, at which, however, the vapor pressure of red phosphorus is appreciable (about 0.06 atmos), so that, unless confined, it would be converted into gas and would escape.

The material called amorphous black phosphorus[13] is formed from white phosphorus at pressures about 12,000 atmos and initial temperatures about 200°C. These pressures and temperatures are somewhat lower than those at which crystalline black phosphorus is formed, and the temperatures are lower than those at which red phosphorus is rapidly made at 1 atmos pressure. The

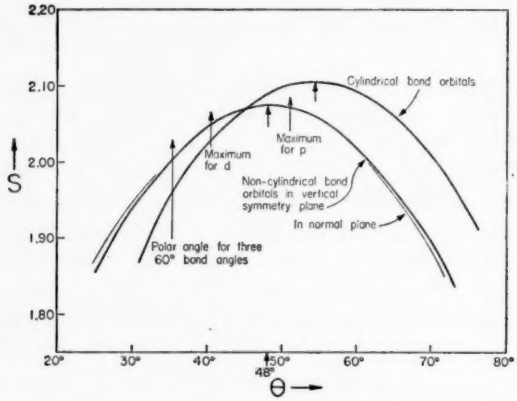

FIG. 1. Strength of bond orbitals for phosphorus as function of polar angle.

reaction is slow to start and evidently speeds up because of the heating of the reacting material.

The density of amorphous black phosphorus is reported to be about 2.25 g cm^{-3}, whereas that of crystalline black phosphorus, which is formed at higher temperatures and pressures, is 2.69 g cm^{-3}, and that of red phosphorus is 2.34 g cm^{-3}. The enthalpy of amorphous black phosphorus is indicated by Jacobs' thermochemical measurements to be near that of red phosphorus. We think that it is likely that Jacobs' amorphous black phosphorus is to be classed with red phosphorus and violet phosphorus, and that its structure involves chains of the same type. In its formation, as in the formation of red phosphorus and violet phosphorus from white phosphorus, only one of the six bonds in the P_4 tetrahedron needs to be broken. Jacobs has reported that by long heating at 125°C amorphous black phosphorus is converted into violet phosphorus.

[13] R. B. Jacobs, J. Chem. Phys. **5**, 945 (1937).

NONCYLINDRICAL *SPD* BOND ORBITALS

In the first discussion of hybrid bond orbitals[14] the *spd* hybrid orbitals that were discussed—the best *spd* orbitals, two equivalent *spd* orbitals involving one *d* orbital, four dsp^2 square orbitals, four best tetrahedral orbitals, and six d^2sp^3 octahedral orbitals—all have cylindrical symmetry about the bond axis, and in his more general discussion of *spd* hybridization Hultgren[15] found it convenient to restrict his treatment to similar cylindrically symmetrical orbitals. In the study of P_4 we first carried out a calculation of strain energy for three equivalent cylindrical bond orbitals, and found the best cylindrical orbitals for a phosphorus atom with 60° bond angles to be of the form $0.070s+0.990p+0.125d$, with $W=-19.59$ kcal mole^{-1}, the calculated strain energy being 11.04 kcal mole^{-1} per phosphorus atom. The calculation was then carried out with noncylindrical orbitals, resulting in a decrease in the calculated strain energy by 33 percent, to 7.38 kcal mole^{-1}. It is evident that in refined calculations the approximation of assuming the bond orbitals to have cylindrical symmetry should not be made without consideration of the magnitude of the error that might be introduced.

It is of interest to consider the reason for the superiority of noncylindrical orbitals over cylindrical orbitals for the problem under discussion. The strength of the best orbital (Eq. 3) in its vertical symmetry plane is shown as a function of the polar angle ϑ in Fig. 1. The value of ϑ at the bond direction is 35°16′, and the maximum strength is at $\vartheta=48°10'$.

The strength at various angles from the direction of the maximum in a plane normal to the vertical symmetry plane is indicated by the two arcs just above (for small ϑ) and below (for large ϑ) the curve for the symmetry plane. It is evident from the proximity of the arcs and the curve that the noncylindrical orbital deviates only slightly from cylindrical symmetry, and that the explanation of its superiority must be elsewhere.

The explanation is to be found by the comparison of the orbital with the cylindrically symmetrical orbital with the same amounts of *s* and *p* character. The three orthogonal orbitals of this type have their maximum strength at $\vartheta=54°25'$, with the strength changing with angle as shown in Fig. 1. It is seen that although the maximum strength ($S=2.1071$) is greater than that of the noncylindrical orbital ($S=2.0744$), the strength in the direction of the P_4 bonds is much less (1.960 instead of 2.0074). The desirable properties of the noncylindrical orbitals are achieved by having the maximum contribution of the *p* part of the orbital at a larger polar angle ($\vartheta=54°53'$) than that of the *d* part ($\vartheta=36°20'$). In this way the three orbitals are kept orthogonal while the strength in the 60°-bond directions is increased.

[14] L. Pauling, J. Am. Chem. Soc. **53**, 1367 (1931).
[15] R. Hultgren, Phys. Rev. **40**, 891 (1932).

Nuclear Quadrupole Effects and Electronic Structure of Molecules in the Solid State*

C. H. TOWNES AND B. P. DAILEY
Columbia Radiation Laboratory, Columbia University, New York, New York
(Received September 15, 1951)

Measured nuclear quadrupole effects in solids are discussed, compared with nuclear quadrupole coupling in gases, and correlated to some extent with molecular structure in the solid state. The iodine crystal affords a good example of intermolecular interactions in the solid state. In this crystal, nuclear quadrupole effects combined with crystallographic information show two intermolecular covalent bonds per atom, each of about 9 percent importance.

INTRODUCTION

A NUCLEAR quadrupole moment represents the deviation of the nuclear charge from a spherical distribution, and this moment can interact with a nonspherical charge distribution outside the nucleus to produce a variation in electrostatic energy of the system with nuclear orientation. Such effects have been extensively observed by microwave techniques as hyperfine structure in the rotational spectra of gas molecules. Quadrupole coupling constants, which are measures of the change in electrostatic energy with nuclear orientation, may be shown to yield useful information on the charge distribution or electronic structure of these isolated gas molecules.[1]

The amount and variety of information to be obtained by the interpretation of nuclear quadrupole coupling data have recently been greatly increased by the observation of a new type of radiofrequency transition in solids.[2] These are transitions directly between energy levels due to the interaction between a nuclear quadrupole moment and electrostatic fields in solids. The electrostatic fields and hence nuclear quadrupole couplings are generally more complex than in isolated gas molecules. However, the major features of present data on quadrupole coupling in solids can be interpreted in a manner similar to that outlined previously[1] for gas molecules. It is our intention to discuss most of these data in a more extended review. Here we shall examine certain cases in which intermolecular effects play a significant role. In the case of crystalline I_2, such an examination seems to show rather clearly the presence of intermolecular bonds of the covalent type. Before discussing the interpretation of electrostatic fields, however, we shall digress into the details of how the fields enter into the measured quadrupole effects in solids.

QUADRUPOLE ENERGY LEVELS IN SOLIDS

The energy of interaction between a nuclear quadrupole moment Q and electric fields in a crystal depends on Q, on the nuclear spin I, and on the tensor or dyadic $\nabla\nabla V$. V is the electrostatic potential caused by all charges in the crystal outside a small sphere surrounding the nucleus of radius only slightly larger than the nuclear radius, and $\nabla\nabla V$ is evaluated at the nucleus. The tensor $\nabla\nabla V$ is symmetric, so that coordinate axes may be chosen in which the only nonzero components are

$$q_{xx}=\partial^2V/\partial x^2,\quad q_{yy}=\partial^2V/\partial y^2,\quad q_{zz}=\partial^2V/\partial z^2. \tag{1}$$

The z axis is usually chosen so that $|q_{zz}|$ is greater than $|q_{xx}|$ or $|q_{yy}|$. If the field is symmetric about the z axis, as frequently happens, then $q_{xx}=q_{yy}=-1/2q_{zz}$. In this case the energy levels are

$$W_M=\frac{eQq_{zz}}{4I(2I-1)}[3M^2-I(I+1)], \tag{2}$$

where e is the proton charge.

M is the projection of I on the z axis. In this case of symmetry about the z axis eQq_{zz} or eQq is called "the" quadrupole coupling constant.

If the field is not symmetric about z, then an asymmetry parameter may be defined:

$$\eta=\left|\frac{q_{xx}-q_{yy}}{q_{zz}}\right|. \tag{3}$$

The energy levels become,†
for I=1

$$W_{M=0}=-\tfrac{1}{2}eQq_{zz},\quad W_{|M|=1}=\left(\tfrac{1}{4}\pm\frac{\eta}{4}\right)eQq_{zz}; \tag{4}$$

for $I=\frac{3}{2}$

$$W_{M=\pm\frac{1}{2}}=-\frac{eQ}{4}q_{zz}\left(1+\frac{\eta^2}{3}\right)^{\frac{1}{2}},\quad W_{M=\pm\frac{3}{2}}=\frac{eQ}{4}q_{zz}\left(1+\frac{\eta^2}{3}\right)^{\frac{1}{2}}; \tag{5}$$

* Work supported jointly by the Signal Corps and ONR.
[1] C. H. Townes and B. P. Dailey, J. Chem. Phys. **17**, 782 (1949).
[2] H. G. Dehmelt and H. Krüger, Naturwiss. **37**, 111 (1950).

† These energies may be derived from the matrix elements given by R. V. Pound, Phys. Rev. **79**, 685 (1950). Pound has pointed out that the element for $(m|F|m\pm2)$ involves an error, however, and should be multiplied by $1/\sqrt{2}$.

TABLE I. Nuclear quadrupole coupling constants obtained from the pure quadrupole spectra of solids.

Molecule	Nucleus	eQq_{zz} in Mc/sec Solid	Gas	η	Reference
trans					
CHI:CHI	I^{127}	1847	···	0.023	a
CH_3I	I^{127}	1753	1931.5	0.027	a
ICN	I^{127}	2549	2420	···	a
ICl	I^{127}	3037	2944	···	a
SnI_4	I^{127}	1363	···	···	a
I_2	I^{127}	2140	···	0.15	a
CH_3Br	Br^{79}	528.9	577.0	···	b
trans					
CHCl:CHCl	Cl^{35}	70.8 (Cl^{35})	···	···	b
$SOCl_2$	Cl^{35}	64.18	···	···	c
		63.78			
$POCl_3$	Cl^{35}	57.96	···	···	c
		57.88			
CH_2Cl_2	Cl^{35}	71.98	78	···	c
$CHCl_3$	Cl^{35}	76.62	···	···	c
		76.50			
C_6H_5Cl	Cl^{35}	69.24	···	···	c
Cl_2	Cl^{35}	108.5	···	···	d
CF_3Cl	Cl^{35}	76.18	78.05	···	d

[a] H. G. Dehmelt, Naturwiss. **17**, 398 (1950).
[b] H. G. Dehmelt and H. Krüger, Z. Physik. **129**, 401 (1951).
[c] R. Livingston, Phys. Rev. **82**, 289 (1951).
[d] R. Livingston, *Symposium on Molecular Structure and Spectroscopy* (Ohio State University, 1951).

for $I=5/2$, if η^4 and higher powers of η are discarded,

$$W_{M=\pm\frac{1}{2}}=-\frac{eQ}{5}q_{zz}[1+4/9\eta^2],$$

$$W_{M=\pm\frac{3}{2}}=-\frac{eQ}{20}q_{zz}[1-\tfrac{3}{2}\eta^2], \qquad (6)$$

$$W_{M=\pm\frac{5}{2}}=\frac{eQ}{4}q_{zz}\left[1+\frac{\eta^2}{18}\right].$$

For nuclei with spin $\frac{3}{2}$ only one energy interval can be measured, so that eQq_{zz} and η cannot be independently determined. For a spin 5/2, however, two frequencies can be obtained, ν_1 corresponding to the transition $M=\pm\frac{1}{2}\rightarrow\pm\frac{3}{2}$ and ν_2 to $M=\pm\frac{3}{2}\rightarrow\pm 5/2$, so that both eQq_{zz} and η can be determined. From Eq. (6) one can obtain, in agreement with Dehmelt[3]

$$\nu_2/\nu_1\approx 2(1-1.30\eta^2). \qquad (7)$$

When the spin is 1, the degeneracy of the $M=\pm 1$ levels is removed by asymmetry, and for the new states M is not a good quantum number, but $|M|=1$.

DISCUSSION OF GENERAL METHOD

Our earlier discussion of quadrupole effects pointed out that $\partial^2V/\partial z^2$ or q_{zz} is primarily dependent on the way in which valence electrons fill the lowest energy p-type orbits. The various arguments for this conclusion will not be repeated here, but we shall take time to mention some new additional evidence for the validity of the approximations. Contributions to q_{zz} come from several different sources:

(1) The valence electrons associated with the nucleus in question.
(2) Other ions, atoms, or charges associated with adjacent atoms.
(3) Distortions of the nonbonding closed shells of electrons around the nucleus.

It was previously pointed out that since $\partial^2V/\partial z^2$ produced by a charge at distance r from the nucleus is proportional to $1/r^3$, the penetrating valence electrons give an effect which generally predominates, being roughly 20×10^{15} esu for Cl, Br, or I. An electronic charge placed 1A from the nucleus gives a contribution of only 1×10^{15} esu assuming the atom is otherwise undisturbed. This shows that effects of type 2 are not very important. However, the effect of such an electronic charge is modified by the changes it produced in the wave functions of other electrons in the atom. In part these are the distortions of the closed electron shells which are contributions of type 3. If the closed shells are completely spherical, they contribute nothing to q at the nucleus, but if there is a nearby negative charge, the atomic electrons including those in closed shells tend to move away from this charge, partially cancelling its effect or shielding the nucleus. Foley[4] has recently calculated the amount of shielding for a charge placed at the atomic radius of chlorine, and finds that its contribution to q is reduced by approximately a factor of 10 because of shielding. Other atoms, he estimates, should not be very different from the chlorine case. This calculation, then, shows that effects of type 2 and 3 cancel to a very considerable extent, and an electronic charge 1A from a chlorine nucleus may be expected to contribute only 0.1×10^{15} esu or $\frac{1}{2}$ percent of the contribution of a valence p electron. Shielding may be considered to produce an even more rapid dependence of $\partial^2V/\partial z^2$ on r than $1/r^3$, since charges close to the nucleus are not shielded, but those outside the atom are almost completely shielded.

If q is primarily dependent on the states of the valence electrons and their bonds, then nonbonding nearby atoms or charges should have very little effect on the quadrupole coupling constants. Some interesting experimental verifications of this expectation are now available. Gwinn and Myers[5] have found that in CH_2Cl_2 the z direction of the tensor $\nabla\nabla V$ at each nucleus concides within experimental error with the C—Cl bond. Furthermore the asymmetry η is no greater than the experimental error of about ±0.02. This shows that the quadrupole coupling is determined by the C—Cl bond, and is very little affected by the adjacent Cl which is 2.9A away.

Livingston has found that the quadrupole coupling increases regularly in the sequence of solid materials[6]

[3] H. G. Dehmelt, Naturwiss. **17**, 398 (1950).

[4] H. M. Foley (private communication).
[5] W. D. Gwinn and R. J. Myers (private communication).
[6] R. Livingston, *Symposium on Molecular Structure and Spectroscopy* (Ohio State University, June, 1951).

CH_2Cl_2, $CHFCl_2$, and CF_2Cl_2, as well as in the sequence CH_2Cl_2, $CHCl_3$, CCl_4, and in $CHCl_3$, $CFCl_3$. This behavior, he points out, may be expected from a change in bonds within the molecule, and indicates that adjacent molecules in the solid state have no very large effect on quadrupole coupling in these compounds. If adjacent molecules did have a large effect, there would be more random behavior in the coupling constants, since the crystalline structures should vary considerably from molecule to molecule.

It is the normal van der Waals interactions which are expected to have little effect on quadrupole coupling. There are at least two types of intermolecular interactions which may be expected to noticeably influence quadrupole couplings in solids: a change in ionic character of the bonds due to electrostatic interactions between neighboring ions, and the occurrence of additional partial bonding of a covalent nature between molecules. The additional covalent bonds are not to be expected in the series of compounds given by Livingston, and evidently do not occur. The effect of the longer-range electrostatic interactions is probably present, but is presumably not widely different for the various compounds.

DISCUSSION OF THE EXPERIMENTAL DATA

All of the nuclear quadrupole coupling constants so far obtained from pure quadrupole spectra in solids together with the comparable values for gas molecules wherever they have been determined, are given in Table I. It is readily seen that there is a good rough agreement between the values measured in the solid and in the vapor. Most of the nuclear quadrupole coupling constants correspond to the values expected for covalent bonds with moderate amounts of ionic character. There is no striking variation of the coupling constant from one molecule to another which would indicate the presence of large effects caused by the presence of neighboring molecules in the crystal lattice. Simple explanations for the small deviations of the values of the coupling constants in solids from those found or expected in the gas phase are given for several of the molecules in the following sections.

I_2

Two features of the pure quadrupole spectrum of solid iodine are of special interest: the nuclear quadrupole coupling constant in the solid is significantly smaller than the value 2500 mc expected for the isolated I_2 molecule, and the asymmetry parameter η is quite large. An isolated I_2 molecule would, of course, be symmetric about its axis (z) and have $\eta=0$. In the solid, η is so large that it corresponds to a change in $\partial^2V/\partial x^2$ or $\partial^2V/\partial y^2$ of 3×10^{15} esu. This is too large to be due to anything but a penetrating valence electron, which means that new bonds must occur in solid I_2, which do not occur in the isolated molecule.

The presence of additional bonds in solid I_2 is made very plausible by an examination of the crystal structure of solid iodine. A typical fragment of a crystal of solid iodine is shown in Fig. 1. Any given iodine atom has two nearest neighbors at a distance of only 3.54A, as well, of course, as its molecular partner at the expected distance of 2.70A. This distance is to be compared with the intramolecular distance of 2.67A obtained from electronic spectral data. No other iodine neighbors are closer than 4.35A.

Two iodine atoms located in different molecules would normally be expected to approach no more closely than a distance corresponding to the sum of the van der Waals radii. Pauling assigns a value of 2.15A to the van der Waals radius of iodine, which is the same as its ionic radius and is considerably larger than the covalent radius of 1.33A. Hence the structural data rather clearly suggest that while only van der Waals forces act between the iodine atoms separated by 4.35A the atoms separated by on 3.54A are held together by stronger interactions.

If the covalent bond from a given iodine atom is assumed to resonate between its molecular partner and the two iodine atoms at a distance of 3.54A, the fractional importance of these bonds and the quadrupole coupling for a normal covalent bond in an isolated I_2 molecule can be uniquely determined from the observed eQq_{zz} and η. All three bonds lie in a plane, the two auxiliary intermolecular bonds making angles of 105°25′ and 169°7′ with the main molecular bond. Since both auxiliary bonds have the same length, they will be given the same fractional importance a, so that the fractional importance of the main bond is $1-2a$. If a covalent bond lies along one particular direction z_0, then it produces a tensor $\nabla\nabla V_0$ which has components

$$\partial^2V/\partial z_0^2=q_{z_0z_0}=q_0 \quad \text{and} \quad \partial^2V/\partial x_0^2=\partial^2V/\partial y_0^2=-q_0/2.$$

This tensor may be referred to any new axes by simple rotation of coordinates in the usual way, but in the new coordinates it may not be diagonal. For the three bonds assumed here, $\nabla\nabla V$ is simply the sum of three contributions each referred to the same chosen set of axes

$$\nabla\nabla V=(1-2a)\nabla\nabla V_1+a\nabla\nabla V_2+a\nabla\nabla V_3, \quad (8)$$

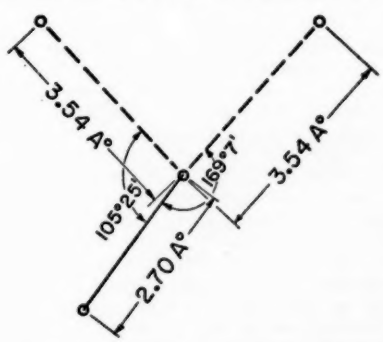

FIG. 1. Relative positions of a group of neighboring atoms in the I_2 crystal. The heavy line joins two atoms in the same I_2 molecule.

where the subscripts refer to the value of $\nabla\nabla V$ produced by a covalent bond along the three different axes, subscript 1 corresponding to the main molecular bond. The tensor $\nabla\nabla V$ may be made diagonal by the proper choice of axes and with respect to these axes the quantities q_{zz}, q_{xx}, and q_{yy} evaluated in terms of the two assumed unknowns, a and q_0. Since there are two quantities determined experimentally, eQq_{zz} and $\eta=|(q_{xx}-q_{yy})/q_{zz}|$, a and eQq_0 may be obtained from the experimental data of Table I. The result is $a=0.091$ and $eQq_0=2480$ Mc. Hence the auxiliary bonds to atoms 2 and 3 have 9 percent importance, and the quadrupole coupling of a covalent iodine bond (as in gaseous I_2) is 2480 Mc in remarkably good agreement with the value 2500 Mc previously obtained.‡

The diagonalized tensor $\nabla\nabla V$ has an axis only 4°9′ from the molecular axis as shown in Fig. 1, since the auxiliary bonds are rather weak. The above calculation of a and q_0 may be checked by observing that the contribution of each bond to the second derivative of the potential with respect to a given direction equals

$$cq_0[(3\cos^2\theta-1)/2],$$

where θ is the angle between the bond and the direction in question, and c is the fractional importance of the bond (in our case a or $1-2a$).

The auxiliary intermolecular bonds are formed at the expense of the main molecular I_2 bond, which is weakened in solid I_2 to 82 percent importance according to the above arguments. This is also indicated by the observed increase in internuclear distance, which is 2.666A in gaseous I_2 and 2.70 in the solid. Although additional bonds in solids sometimes produce very refractory crystals and marked cleavage surfaces, these effects should not be expected in the case of I_2 because the additional bonds are formed at the expense of the main molecular bond, and have a rather small (9 percent) fractional importance.

Pound[7] has observed the quadrupole resonances in solid iodine over a wide range of temperatures. He observes a decrease in η and an increase in q_{zz} with an increase in temperature. Both of these changes would be expected from a loosening (decrease in covalent character) of the intermolecular bonds with increasing temperature. The values given for I_2 in Table I and discussed above are those for room temperature.

ICN

Quadrupole coupling constants are so far known for only six substances in both solid and gas phases, as shown in Table I. There is in each case a small difference between the two values. In all cases except ICN, changes are in the direction of more ionic character in the solid than in the gas. Since Cl, Br, and I are negatively ionic when bonded to carbon, more ionic character decreases their coupling in CH_3I, CH_3Br, CH_2Cl_2, and CF_3Cl. However, more ionic character for I in ICl increases its coupling because it is positively ionic. Unfortunately, the crystal structures of these compounds are unknown. However, it is very reasonable to assume that their crystal structures are partly determined by electrostatic interactions in such a way that the electrostatic energy is decreased and ionic character is favored.

The exceptional case is ICN, where the quadrupole coupling indicates less ionic character in the solid than in the gas. The usually assumed ionic structure $\overset{+}{\mathrm{I}}=\mathrm{C}=\overset{-}{\mathrm{N}}$ has a lower coupling than the covalent structure. $\mathrm{I}-\mathrm{C}\equiv\mathrm{N}$, but the quadrupole coupling is increased on condensation, so that the ionic structure must be suppressed in the crystal. Fortunately the crystal structure of ICN has been determined. Using the known interatomic distances, it can be shown that the electrostatic energy of the structure $\overset{+}{\mathrm{I}}=\mathrm{C}=\overset{-}{\mathrm{N}}$ is actually increased by about 6 kcal/mole when the molecule is located in the solid lattice, assuming that surrounding molecules have 13 percent ionic character as estimated for gaseous ICN. The extra electrostatic energy would tend to suppress this structure and hence increase the quadrupole coupling as observed. Evidently other forces than simple electrostatic ones determine the crystal structure of ICN, and an examination of some of the interatomic distances suggests one of the important contributions.

For most of the atoms in the ICN crystal the distance of closest approach is at least as great as the sum of the van der Waals radii. The ICN molecules in the crystal are aligned in long parallel chains, and the minimum separation of iodine atoms in neighboring chains is 4.40A, which is a little more than twice the ionic radius of iodine, 2.15A. But within the chains the N atom in one molecule is only 2.78A from the I atom in the molecule next in line along the chain. The sum of the nonbonded radii of I and N is 3.65A. Therefore it seems reasonable that one of the significant resonating structures is $-\overset{+}{\mathrm{I}}-\overset{-}{\mathrm{C}}=\mathrm{N}-\overset{+}{\mathrm{I}}-\overset{-}{\mathrm{C}}=\mathrm{N}-$. This structure tends to increase the quadrupole coupling of I rather than decrease it since the π bond of $\overset{+}{\mathrm{I}}=\mathrm{C}$ has been replaced by a σ bond. A reasonable assignment of structures for

‡ The value 2500 Mc is the coupling of a normal covalent iodine bond taken from reference 1. W. Gordy [J. Chem. Phys. **19**, 792 (1951)] has recently suggested that the normal covalent iodine bond has a coupling constant essentially equal to eQq_{zz} in solid I_2. By introducing a new relation between ionic character and electronegativity difference and allowing a certain type of variation of hybridization from bond to bond, he has fitted a series of known quadrupole coupling constants. However, if Gordy's hypotheses are applied to a wider range of data than he discusses, they encounter difficulties. The small dipole moment of ICl and the small difference in dipole moments between BrCl and ICl seem not to allow the combination of a large amount (25 percent) of ionic character and no hybridization which he assumes for ICl. Gordy notes that the large asymmetry in crystalline I_2 is surprising in view of his assumptions. It is also difficult to account for the large quadrupole coupling (2420 mc) in ICN using his value of 1931 mc for the normal single I—C bond.

[7] R. V. Pound, Phys. Rev. **82**, 343 (1951).

this molecule in the solid state is:

Structure	Percent importance
$I-C\equiv N$	88
$\overset{+}{I}=C=\overset{-}{N}$	2
$-\overset{+}{I}-C=\overset{-}{N}-$	10

This assignment gives a quadrupole coupling constant of 2540 mc/sec, very near the observed value. The crystal structure of ICN has a threefold symmetry axis about the I−C bond, and hence η must equal zero.

The shortened I−N distance in ICN and I−I distance in I_2, where auxiliary bonds have been assumed leads one to look for other cases of this type. However, no other pairs of atoms in adjacent molecules lie closer than the sum of their van der Waals radii for the molecules in Table I whose crystal structure is known. Closest distances of approach of halogen atoms in these substances are listed in Table II. A small amount of asymmetry occurs in CH_3I and CHI:CHI. In CH_3I this must be a property of the crystal structure, but in CHI:CHI the small asymmetry may possibly be due to interaction between adjacent atoms in the same molecule, which are separated by only 3.9A, slightly less than the sum of their van der Waals radii.

SnI_4

There are two different types of iodine sites in SnI_4. One of the four Sn−I bonds in every molecule lies along a threefold symmetry axis of the cubic SnI_4 crystal. As pointed out by Dehmelt,[3] these iodines should have $\eta=0$, and undoubtedly are the ones with the very small measured value $\eta<0.005$. The other three iodines have no special symmetry. However, since the distances between these iodines and atoms in adjacent molecules are all close to the van der Waals distances or larger, no strong intermolecular bonds should be expected. The complex structure of the SnI_4 crystal lattice makes exact evaluation of electrostatic energy very tedious. However, rough calculation shows that there is an approximately equal and moderate amount of electrostatic interaction between molecules tending to lower the energy of the ionic form of each Sn−I bond. From this and the absence of intermolecular covalent bonds, the asymmetrically located I atoms should have a quadrupole coupling nearly equal to that of the symmetrically located set of I atoms, and η should be small. Table I shows that these expectations are correct. It would be interesting to know if the higher frequency resonance in SnI_4 is three times more intense than the lower frequency resonance as would be expected from the above identification.

Cl_2 AND Br_2

A comparison of intermolecular bonding in solid Cl_2 and Br_2 with that found in I_2 would be very valuable. Unfortunately not all the necessary information is available. The pure quadrupole spectrum of Br_2 has not yet been measured, and the structure of solid Cl_2 has not been completely and unambiguously determined. Furthermore, since both stable isotopes of Br and of Cl have spins of $\frac{3}{2}$, it will not be possible to determine independently eQq_{zz} and the asymmetry η as pointed out in the section above on energy levels.

The crystal structure of bromine suggests that the same type of intermolecular bonding which occurs in the iodine crystal should exist for bromine as well. Each bromine atom has two intermolecular nearest neighbors at a distance of 3.31A. This is substantially shorter than 3.90A, the sum of the van der Waals radii, and presumably indicates the presence of intermolecular bonds. A rough estimate of the importance of these bonds in comparison to solid iodine may be obtained from some

TABLE II. Closest distances of approach of two halogen atoms in various solids. Distances are listed in order of increasing size. Twice the van der Waals radius for I is 4.30A, for Br 3.90A.
[Data from R. W. G. Wyckoff, *Crystal Structures* (Interscience Publishers, New York, 1948).]

Molecule	Distances of closest approach	
		I−I
trans CHI:CHI	r_1 (intramolecular)	3.94A
	r_2	4.59
I_2	r_1 (intramolecular)	2.70
	r_2	3.54
	r_3	4.35
SnI_4	r_1 (intramolecular)	4.29
	r_2	4.22
	r_3	4.35
	r_4	4.40
	r_5	4.46
ICN	r_1	4.40
		Br−Br
Br_2	r_1 (intramolecular)	2.27
	r_2	3.31
	r_3	4.01

calculations involving Morse potentials. Using an expression for the energy of bonds of varying lengths of the form

$$U(r-r_e)=D\{1-\exp[-\beta(r-r_e)]\}^2,$$
$$\beta=1.22\times10^7\omega_e(\mu/D)^{\frac{1}{2}}$$

with D and ω_e obtained from the table of Herzberg,[8] it has been calculated that the ratio of the energies of the bond to a nearest intermolecular neighbor at the observed distance to the energy of the normal in intramolecular bond is .38 for iodine and .25 for bromine. It would be predicted, therefore, that some intermolecular bonding would occur in solid bromine, but not as much as in iodine. The expected eQq_{zz} for Br should then be slightly less than that for the isolated Br_2 molecule.

[8] G. Herzberg, *Spectra of Diatomic Molecules* (D. Van Nostrand, Inc., New York, 1950).

In determining the structural parameters for solid chlorine Keesom and Taconis[9] made use of rather rough intensity data. One of the assumptions used in deriving the published set of parameters was that the intramolecular Cl−Cl distance should be 1.99A. Through an error, the original calculations were made with an incorrect value of 1.82A for this Cl−Cl distance.§ Although the structure as published gives several intermolecular distances less than twice the van der Waals radii for chlorine, an analysis of the possibilities of intermolecular bonding should probably wait for more exact information on the structure of solid Cl. The existence of intermolecular bonds is not indicated by the observed values 108.5 mc for eQq_{zz} in solid Cl. However, the coupling constants for Br and Cl in BrCl both indicate that the complication of a variable amount of hybridization from bond to bond must be introduced for these atoms. The large quadrupole coupling of Cl in solid chlorine must also be explained as either a reduction in $s-p$ hybridization over what is found for the Cl bond in other known molecules or an increase in hybridization with the d orbital. Solid Br may similarly show an anomolously large quadrupole coupling because of a change in hybridization. Because of these uncertainties, the effect of intermolecular bonding on quadrupole coupling in Cl and Br may remain unknown until some way of measuring the asymmetry η is found.

We are indebted to Miss A. E. Fraebel and Mr. A. Levine for assistance with calculations involved in the above work.

[9] W. H. Keesom and K. W. Taconis, Physica **3**, 237 (1936).

§ We are indebted to Dr. Taconis for advice and information on the nature of this error.

THE JOURNAL OF CHEMICAL PHYSICS VOLUME 20, NUMBER 1 JANUARY, 1952

The Interlayer Binding in Graphite*

ROBERT O. BRENNAN†
Physics Department, The Catholic University of America, Washington, D. C.

(Received June 4, 1951)

The repulsive energy between layers of the graphite crystal has been calculated as an interaction of *LCAO* molecular orbitals in the layers. The van der Waals attractive term was found by setting the energy minimum to fall at 3.37A. When values of the effective nuclear charge and effective quantum number proposed by Kohlrausch were used, the interlayer binding energy was found to be 3.99 kcal/mole. The compressibility, calculated under plausible assumptions, is in satisfactory agreement with the experimental value.

I. INTRODUCTION

THE graphite crystal is made up of layers of closely bound carbon atoms arranged in hexagons.[1] The layers themselves are rather widely separated, the distance between layers being 3.37A, while the distance between atoms within the layers is 1.42A. The relative isolation of the layers makes them models of an idealized two-dimensional metal.[2,3] Although within the layers the crystal is an example of a valence crystal, between layers the binding is the result of long range van der Waals forces.[3,4] From this point of view, graphite serves as an idealized molecular crystal with each layer as a molecule. The object of the present investigation was to calculate the potential energy curve of the interlayer binding.

The van der Waals interaction between two molecules was investigated theoretically by London[5] and by Slater and Kirkwood.[6] It was found to be of a quantum-mechanical nature and a rather straightforward result of a second order perturbation calculation. Physically it is an interaction of "virtual dipoles," that is to say, a correlation of the motion of the electrons in the two molecules brought about by the formation of instantaneous dipoles. This second-order term is of importance at large separations of the molecules and varies as the inverse sixth power of the distance. For molecules or atoms in their normal states the interaction is always attractive.

At very short ranges when the wave functions of the two molecules overlap considerably, the London second-order (and even higher order) terms may be no longer accurate, since this approximation depends on the possibility of developing the classical Coulomb interaction of the two systems of electrical charges in inverse powers of their mutual distance. Fortunately at such

* A dissertation submitted to the Faculty of the Graduate School of Arts and Sciences of The Catholic University of America in partial fulfillment of the requirements for the degree of Doctor of Philosophy.

† Present address: Woodstock College, Woodstock, Maryland.

[1] Doubt has recently been thrown on the regularity of the hexagonal structure. See J. S. Lukesh, Phys. Rev. **80**, 226 (1950). The deviations should not seriously affect the present calculations.

[2] P. R. Wallace, Phys. Rev. **71**, 622 (1947).

[3] C. A. Coulson, Nature **159**, 265 (1947).

[4] J. E. Lennard-Jones, Trans. Faraday Soc. **30**, 58 (1934).

[5] F. London, Z. physik. Chem. (B) **11**, 222 (1930).

[6] J. C. Slater and J. G. Kirkwood, Phys. Rev. **37**, 682 (1931). For a summary of the theory of van der waals forces see H. Margenau, Revs. Modern Phys. **11**, 1 (1939).

separations, if we are dealing with closed-shell ground states, this attractive force is overshadowed by a repulsive force which is also of quantum-mechanical origin.

The repulsive force is a direct consequence of the Pauli exclusion principle. When the wave functions of the two molecular systems overlap sufficiently so that electrons in the same quantum state (including the spin) must occupy the same region of space, there must arise repulsive forces in accord with Pauli's principle. Mathematically this is taken into account by using as the approximate wave function of the system an antisymmetrized product of one-electron wave functions. Such a wave function permits exchanges of electrons between the two molecules and the corresponding "exchange integrals," which occur in the expression for the interaction energy on account of the nonorthogonality of the wave functions belonging to different molecules, are of appropriate size and sign to give rise to short range repulsive forces. In previous calculations[7–9] these have been shown to vary roughly as $\exp(-br)$ where r is the intermolecular separation. In this paper we calculate the repulsive forces *a priori* and adjust the constant in the attractive term to give the proper equilibrium separation between the layers of the graphite crystal.

II. THE REPULSIVE ENERGY

In accordance with the understanding that the interlayer binding is caused by van der Waals forces, each layer was treated as a molecule. Two adjacent layers in the crystal do not have the same orientation, but one is rotated through 60° with respect to the other. The atoms within each layer fall into two classes, depending on their position in a hexagon. The same two classes are also determined by the positions of their neighbors in the adjacent layers. We may conveniently label the atoms which have a first neighbor directly opposite them a atoms in one plane, α atoms in the other; the other atoms will be b and β atoms, respectively (see Fig. 1).

The interaction to be considered is very like that treated by Bleick and Mayer for two neon atoms.[8] However, they considered the interaction of electrons in atomic wave functions, while in the present case the electrons are in molecular orbitals, and hence some knowledge of the molecular orbitals of the single graphite layers is required.

In the formation of C−C bonds, it is well known that one of the $2s$ electrons is promoted so that the atomic orbitals available (if the molecular orbitals are to be linear combinations of atomic orbitals) are $(1s)^2(2s)(2p)^3$. Of these, the two $1s$ orbitals may usually be considered as taking no part in the formation of bonds. The $2s$ and

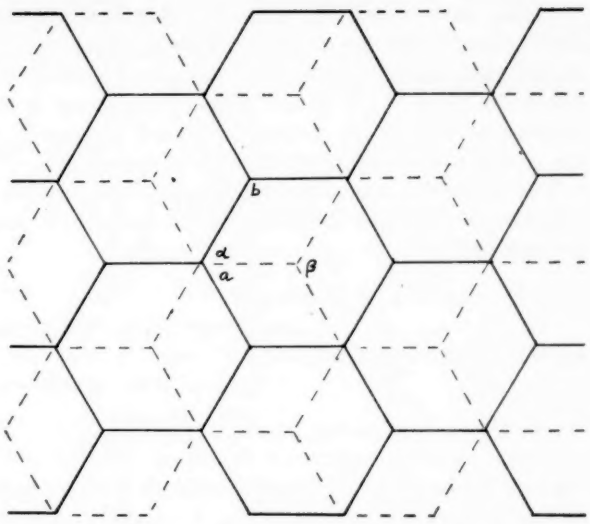

FIG. 1. Two layers of the graphite crystal. a and b are atoms of the unit cell of the upper layer; α and β of the lower layer. The z axis is directed out of the page.

two of the $2p$ orbitals ($2p_x$, $2p_y$) make up the so-called σ or in-plane bonds, while the $2p_z$ orbitals form the molecular orbitals which are responsible for the double-bond character of the C−C bond. Electrons in these last orbitals are usually called π, mobile, or unsaturation electrons. These electrons account for the conductivity of graphite and have been treated from this point of view by Wallace[2] and Coulson.[3] The ionization potential of these electrons in an infinite graphite layer has been calculated by Mulliken.[10] The binding energy contributed by these electrons in small crystallites and in crystallites infinite in one direction has been calculated by Bradburn, Coulson, and Rushbrooke.[11,12]

Since the molecular orbitals of the mobile electrons are formed from atomic orbitals which are perpendicular to the planes of the layers, they will be the first to overlap. It was hoped that the repulsive energy could be accounted for by considering them alone. Preliminary calculations, however, indicated that if one considered these electrons alone, the first-order interaction is strongly attractive. This comes about both because "exchange integrals" between mobile electrons and electrons in other orbitals are almost as important as those between two mobile electrons, and because the asymmetry and orientation of the mobile electron orbitals are such as to cause large Coulomb attractive contributions if considered alone. Hence it was necessary to consider in some detail the molecular orbitals of the $2s$, $2p_x$, and $2p_y$ electrons.

Following Pauling,[13] one usually supposes that the

[7] J. C. Slater, Phys. Rev. **32**, 339 (1928). See also P. Rosen, J. Chem. Phys. **18**, 1182 (1950).
[8] W. E. Bleick and J. E. Mayer, J. Chem. Phys. **2**, 252 (1934).
[9] M. Kunimune, Prog. Theor. Phys. **5**, 412 (1950).
[10] R. S. Mulliken, J. Chim. Phys. **46**, 675 (1949).
[11] Bradburn, Coulson, and Rushbrooke, Proc. Roy. Soc. (Edinburgh) **62**, 336 (1948).
[12] C. A. Coulson and G. S. Rushbrooke, Proc. Roy. Soc. (Edinburgh) **62**, 350 (1948).
[13] L. Pauling, *The Nature of the Chemical Bond* (Cornell University Press, Ithaca, New York, 1948), p. 88.

in-plane wave functions form the so-called trigonal bond: three linear combinations of the $2s$, $2p_x$, and $2p_y$ atomic orbitals, so that the wave functions are directed along the three C—C bonds. Since this picture is not entirely suited to the molecular orbital treatment of the problem, another approach was attempted.

The molecular orbitals which Wallace obtained as a solution of a secular equation for the mobile electron orbitals are:

$$\psi_{1i}=\sum_a \exp(2\pi i\mathbf{k}_i\cdot\mathbf{r}_a)Z(\mathbf{r}-\mathbf{r}_a) -\sum_b \exp(2\pi i\mathbf{k}_i\cdot\mathbf{r}_b)Z(\mathbf{r}-\mathbf{r}_b),$$

$$\psi_{2i}=\sum_a \exp(2\pi i\mathbf{k}_i\cdot\mathbf{r}_a)Z(\mathbf{r}-\mathbf{r}_a) +\sum_b \exp(2\pi i\mathbf{k}_i\cdot\mathbf{r}_b)Z(\mathbf{r}-\mathbf{r}_b),$$

where the $\mathbf{k}_i$ are vectors in the reciprocal lattice; the $Z(\mathbf{r}-\mathbf{r}_a)$ are $2p_z$ atomic wave functions centered at the vector coordinate $\mathbf{r}_a$ (the z axis is chosen perpendicular to the plane of the layer as in Fig. 1); and the sums are over-all atoms of the types a and b in the layer. He suggests that these orbitals might presumably be obtained from considerations of symmetry.

It is well known that the exact solutions of the Schroedinger eigenvalue problem must belong to irreducible representations of the group of operations which leaves the Hamiltonian of the problem invariant.[14] This has not been shown to be true in general for the *LCAO* approximation. However, under the assumption that there is only one set of *LCAO* molecular orbitals which minimizes the energy of the closed-shell ground state, it can be shown that these molecular orbitals must belong to irreducible representations of the group of the Hamiltonian.[15] Here it will be shown that in the case of the infinite graphite layer, the molecular orbitals fall into different symmetry species in such a way that they are completely determined by symmetry.

To avoid difficulties with the group theory, the graphite layer is to be considered as consisting of a finite number of atoms and periodic boundary conditions are supposed in the usual way. Since there are two atoms in the unit cell and four atomic orbitals per atom, we expect $8n$ molecular orbitals, where n is the number of cells in the finite plane.

TABLE I. Symmetry orbitals of infinite graphite layer with symmetry species.

B_{1u}	$\psi_{1i}=\Sigma_a \exp(2\pi i\mathbf{k}_i\cdot\mathbf{r}_a)\,S(\mathbf{r}-\mathbf{r}_a)-\Sigma_b \exp(2\pi i\mathbf{k}_i\cdot\mathbf{r}_b)\,S(\mathbf{r}-\mathbf{r}_b)$
E_{2g}	$\psi_{2i}=\Sigma_a \exp(2\pi i\mathbf{k}_i\cdot\mathbf{r}_a)X(\mathbf{r}-\mathbf{r}_a)-\Sigma_b \exp(2\pi i\mathbf{k}_i\cdot\mathbf{r}_b)X(\mathbf{r}-\mathbf{r}_b)$
	$\psi_{3i}=\Sigma_a \exp(2\pi i\mathbf{k}_i\cdot\mathbf{r}_a)\,Y(\mathbf{r}-\mathbf{r}_a)-\Sigma_b \exp(2\pi i\mathbf{k}_i\cdot\mathbf{r}_b)\,Y(\mathbf{r}-\mathbf{r}_b)$
B_{2g}	$\psi_{4i}=\Sigma_a \exp(2\pi i\mathbf{k}_i\cdot\mathbf{r}_a)\,Z(\mathbf{r}-\mathbf{r}_a)-\Sigma_b \exp(2\pi i\mathbf{k}_i\cdot\mathbf{r}_b)\,Z(\mathbf{r}-\mathbf{r}_b)$
A_{2u}	$\psi_{5i}=\Sigma_a \exp(2\pi i\mathbf{k}_i\cdot\mathbf{r}_a)\,Z(\mathbf{r}-\mathbf{r}_a)+\Sigma_b \exp(2\pi i\mathbf{k}_i\cdot\mathbf{r}_b)\,Z(\mathbf{r}-\mathbf{r}_b)$
A_{1g}	$\psi_{6i}=\Sigma_a \exp(2\pi i\mathbf{k}_i\cdot\mathbf{r}_a)\,S(\mathbf{r}-\mathbf{r}_a)+\Sigma_b \exp(2\pi i\mathbf{k}_i\cdot\mathbf{r}_b)\,S(\mathbf{r}-\mathbf{r}_b)$
E_{1u}	$\psi_{7i}=\Sigma_a \exp(2\pi i\mathbf{k}_i\cdot\mathbf{r}_a)X(\mathbf{r}-\mathbf{r}_a)+\Sigma_b \exp(2\pi i\mathbf{k}_i\cdot\mathbf{r}_b)X(\mathbf{r}-\mathbf{r}_b)$
	$\psi_{8i}=\Sigma_a \exp(2\pi i\mathbf{k}_i\cdot\mathbf{r}_a)\,Y(\mathbf{r}-\mathbf{r}_a)+\Sigma_b \exp(2\pi i\mathbf{k}_i\cdot\mathbf{r}_b)\,Y(\mathbf{r}-\mathbf{r}_b)$

The layer is invariant under the space group made up of its translation group in two dimensions and the point group D_{6h}. Since none of the rotational operators depend on lattice translations, this space group is easily reduced.[16] Functions of the form

$$\exp(i\mathbf{k}\cdot\mathbf{r})\cdot f$$

are invariant under the space group, if the f is invariant under the operations of D_{6h}. Such functions were found partly by inspection and partly by applying the formal methods of representation theory.[17] In Table I are indicated in probable order of energy the functions which fulfill these qualifications together with the symmetry species to which they belong in the (modified) notation of Placzek and Mulliken.[18] The symbol S is used for atomic $2s$ functions; X, Y, and Z are the atomic $2p_x$, $2p_y$, and $2p_z$ wave functions. (The order of the functions in the table is discussed in an appendix.) The influence of the $1s$ electrons will be here simply to reduce the nuclear charge from $6e$ to $4e$.

The orbitals fall into eight bands, each containing n levels. The work of Wallace[2] and Coulson[3] showed that at 0°K the orbitals are doubly occupied up to and including the whole B_{2g} band and that the A_{2u} band is in contact with the B_{2g} band at some points in the Brillouin zone. Electrons thermally excited from the B_{2g} band to the A_{2u} band account for the conductivity of single graphite layers.

The orbitals belonging to one layer form an orthogonal set, but they are not, of course, orthogonal to the orbitals of the adjacent layers. It will be convenient to work with normalized molecular orbitals. Let

$$\psi=\sum_a \exp(2\pi i\mathbf{k}\cdot\mathbf{r}_a)\xi(\mathbf{r}-\mathbf{r}_a) +\lambda\sum_b \exp(2\pi i\mathbf{k}\cdot\mathbf{r}_b)\xi(\mathbf{r}-\mathbf{r}_b)$$

represent any one of the orbitals of Table I, and define the overlap integrals:

$$(\xi_a\xi_b)\equiv\int \xi(\mathbf{r}-\mathbf{r}_a)^*\xi(\mathbf{r}-\mathbf{r}_b)d\tau.$$

Then, with boundary effects neglected so that one summation may be replaced by multiplication by n, we obtain

$$(\psi\psi)^{-1}\equiv\left[\int\psi^*\psi d\tau\right]^{-1}$$

$$=\frac{1}{2n}\{1-\lambda\textstyle\sum_b \cos[2\pi\mathbf{k}\cdot(\mathbf{r}_b-\mathbf{r}_a)](\xi_a\xi_b) -\sum_{a'}{}' \exp[2\pi i\mathbf{k}\cdot(\mathbf{r}_{a'}-\mathbf{r}_a)](\xi_a\xi_{a'})+O[(\xi_a\xi_b)^2]\}.$$

[14] E. Wigner, *Gruppentheorie und ihre Andwendung auf die Quantenmechanik der Atomspektren* (Edwards Brothers, Inc., Ann Arbor, Michigan, 1944), p. 110 ff.

[15] C. C. J. Roothaan, Revs. Modern Phys. **23**, 69 (1951).

[16] F. Seitz, Ann. Math. **37**, 17 (1936).

[17] See Chapter 12 of reference 14.

[18] This notation is conveniently presented by G. Herzberg, *Infrared and Raman Spectra of Polyatomic Molecules* (D. Van Nostrand Company, Inc., New York, 1947), p. 105 and p. 114. The character table of the group D_{6h} may be found on p. 117.

Terms of the second and higher orders in $(\xi_a\xi_b)$ may be neglected. Furthermore, since we will eventually sum over the wave numbers of each of the filled bands, terms containing $\cos[2\pi\mathbf{k}\cdot(\mathbf{r}_b-\mathbf{r}_a)]$ or $\exp[2\pi i\mathbf{k}\cdot(\mathbf{r}_{a'}-\mathbf{r}_a)]$ will disappear, and we may write immediately for use in the following equations

$$(\psi\psi)^{-1}=1/2n. \tag{1}$$

In terms of the molecular orbitals defined above we may write the complete wave function of a single graphite layer. We make the following simple condensation of the notation and introduce at the same time the spin coordinate η, which takes on the two values α and β.

$$\begin{aligned}\chi_i&=(1/2n)^{\frac{1}{2}}\psi_{1i}\alpha && 0<i\leqq n\\ &=(1/2n)^{\frac{1}{2}}\psi_{1i-n}\beta && n<i\leqq 2n\\ &=(1/2n)^{\frac{1}{2}}\psi_{2i-2n}\alpha && 2n<i\leqq 3n\\ &\quad\cdots\cdots\cdots && \cdots\cdots\\ &=(1/2n)^{\frac{1}{2}}\psi_{4i-7n}\beta && 7n<i\leqq 8n.\end{aligned}$$

The complete wave function of a single layer is then

$$(1/8n)^{\frac{1}{2}}\textstyle\sum_\nu P_\nu(-1)^\nu\chi_1(1)\chi_2(2)\cdots\chi_{8n}(8n),$$

where P_ν is the usual permutation operator. With superscripts to indicate the molecular orbitals belonging to different layers, we may write the wave function of two layers in juxtaposition as

$$\Psi=(1/16n)^{\frac{1}{2}}\textstyle\sum_\nu P_\nu(-1)^\nu\chi_1{}^1(1)\chi_2{}^1(2)\cdots \chi_{8n}{}^1(8n)\chi_1{}^2(8n+1)\cdots\chi_{8n}{}^2(16n). \tag{2}$$

This wave function is not normalized. However, in the expression for the energy, the norm will enter in its square which differs from unity only by terms in the square of the overlap integral of atomic wave functions belonging to different layers. Hence to the order of accuracy of these calculations, and certainly near the equilibrium separation of the layers, Ψ may be regarded as normalized.

With neglect of small kinetic terms, the interaction Hamiltonian may be written (in atomic units):[19]

$$H'=\textstyle\sum_{ij}2/r_{ij}-\sum_{iq}8/r_{iq}-\sum_{jp}8/r_{jp}+\sum_{pq}32/r_{pq}, \tag{3}$$

where the subscripts i and p refer to electrons and atomic nuclei, respectively, belonging to the first layer, and j and q to electrons and nuclei of the second layer.

In writing the interaction energy terms to the first order in the molecular overlap integrals will be kept. For this all the permutations of three electrons among themselves must be considered. These permutations introduce the following integrals.

(A) $$(U_\varrho;\ \chi_i{}^1\chi_i{}^1)\equiv\int\chi_i{}^1(m)^*8/r_{m\varrho}\chi_i{}^1(m)d\tau_m.$$

(B) $$(U_\varrho;\ \chi_i{}^1\chi_j{}^2)\equiv\int\chi_i{}^1(m)^*8/r_{m\varrho}\chi_j{}^2(m)d\tau_m.$$

(C) $$(\chi_i{}^1\chi_i{}^1;\ \chi_j{}^2\chi_j{}^2)\equiv\int\int\chi_i{}^1(m)^*\chi_j{}^2(n)^*2/r_{mn}\chi_i{}^1(m)\chi_j{}^2(n)d\tau_m d\tau_n.$$

(D) $$(\chi_i{}^1\chi_j{}^2;\ \chi_i{}^1\chi_j{}^2)\equiv\int\int\chi_i{}^1(m)^*\chi_j{}^2(n)^*2/r_{mn}\chi_j{}^2(m)\chi_i{}^1(n)d\tau_m d\tau_n.$$

(E) $$(\chi_i{}^1\chi_i{}^1;\ \chi_j{}^1\chi_k{}^2)\equiv\int\int\chi_i{}^1(m)^*\chi_j{}^1(n)^*2/r_{mn}\chi_i{}^1(m)\chi_k{}^2(n)d\tau_m d\tau_n.$$

(F) $$(\chi_i{}^1\chi_j{}^1;\ \chi_j{}^1\chi_k{}^2)\equiv\int\int\chi_i{}^1(m)^*\chi_j{}^1(n)^*2/r_{mn}\chi_j{}^1(m)\chi_k{}^2(n)d\tau_m d\tau_n.$$

(G) $$(\chi_i{}^1\chi_j{}^2)\equiv\int\chi_i{}^1(m)^*\chi_j{}^2(m)d\tau_m.$$

The integrals arising from the remaining permutations of three electrons vanish because of the orthogonality of orbitals in the same layer. The hybrid Coulomb-exchange integral under (F) above may be neglected, since it is an order smaller than the other terms. Hence we arrive at the following expression for the interaction energy:

$$\begin{aligned}\int\Psi^*H'\Psi d\tau=&\textstyle\sum_{pq}32/r_{pq}\\ &-2\textstyle\sum_{ijq}[(U_q;\ \chi_i{}^1\chi_i{}^1)-(U_q;\ \chi_i{}^1\chi_j{}^2)(\chi_j{}^2\chi_i{}^1)]\\ &+\textstyle\sum_{ijk}[(\chi_i{}^1\chi_i{}^1;\ \chi_j{}^2\chi_j{}^2)-(\chi_i{}^1\chi_j{}^2;\ \chi_i{}^1\chi_j{}^2)\\ &\qquad-(\chi_k{}^1\chi_k{}^1;\ \chi_i{}^1\chi_j{}^2)(\chi_j{}^2\chi_i{}^1)].\end{aligned} \tag{4}$$

The integrals occurring in Eq. (4) are now to be reduced to atomic integrals. As a general case, the reduction of $\sum_{ij}(\chi_i{}^1\chi_i{}^1;\ \chi_j{}^2\chi_j{}^2)$ may be considered somewhat in detail, where

$$\begin{aligned}\chi_i{}^1&=(\tfrac{1}{2}n)^{\frac{1}{2}}[\textstyle\sum_a\exp(2\pi i\mathbf{k}_i\cdot\mathbf{r}_a)\omega(\mathbf{r}-\mathbf{r}_a)\\ &\qquad-\sum_b\exp(2\pi i\mathbf{k}_i\cdot\mathbf{r}_b)\omega(\mathbf{r}-\mathbf{r}_b)],\\ \chi_j{}^2&=(\tfrac{1}{2}n)^{\frac{1}{2}}[\textstyle\sum_\alpha\exp(2\pi i\mathbf{k}_i\cdot\mathbf{r}_\alpha)\xi(\mathbf{r}-\mathbf{r}_\alpha)\\ &\qquad-\sum_\beta\exp(2\pi i\mathbf{k}_j\cdot\mathbf{r}_\beta)\xi(\mathbf{r}-\mathbf{r}_\beta)].\end{aligned}$$

Straightforward substitution and summation over the wave number lattice leads to

$$\begin{aligned}&\textstyle\sum_{ij}(\chi_i{}^1\chi_i{}^1;\ \chi_j{}^2\chi_j{}^2)\\ &\quad=\textstyle\sum_{ab\alpha\beta}\sum_{\omega\xi}\{(\omega_a\omega_a;\ \xi_\alpha\xi_\alpha)+(\omega_a\omega_a;\ \xi_\beta\xi_\beta)\\ &\qquad+(\omega_b\omega_b;\ \xi_\alpha\xi_\alpha)+(\omega_b\omega_b;\ \xi_\beta\xi_\beta)\},\end{aligned} \tag{5}$$

where in the summation process terms which contained factors $\exp[-2\pi i\mathbf{k}_i\cdot(\mathbf{r}_a-\mathbf{r}_{a'})]$ $(a\neq a')$ have vanished. The summation over ω, ξ is used to indicate a sum over all the atomic orbitals.

The final simplification is carried out under the following conditions:

[19] Distances in units of the first Bohr radius $a_0=0.5292$A; energies in units of $e^2/2a_0=13.60$ ev.

(1) Neglect of boundary effects permits the substitution of a multiplication by n for a summation over atoms of one kind.

(2) By symmetry $\sum_{\omega\xi}(\omega_a\omega_a;\ \xi_\beta\xi_\beta)=\sum_{\omega\xi}(\omega_b\omega_b;\ \xi_a\xi_a)$ for first neighbors, etc. Then

$$\sum_{ij}(\chi_i^1\chi_i^1;\ \chi_j^2\chi_j^2)$$
$$=n\sum_{\omega\xi}\{(\omega_a\omega_a;\ \xi_a\xi_a)+9(\omega_a\omega_a;\ \xi_\beta\xi_\beta)$$
$$+6(\omega_a\omega_a;\ \xi_{a'}\xi_{a'})+9(\omega_a\omega_a;\ \xi_{\beta'}\xi_{\beta'})+\cdots\},\quad(6)$$

where the primes indicate successive neighbors.

The other terms may be reduced in the same way, except that in the hybrid Coulomb-exchange and exchange integrals the spin coordinate reduces the number of integrals by a factor two. Hence in terms of atomic orbitals the energy is:

$$E_R=n\cdot\{E_{a\alpha}+9E_{a\beta}+6E_{a\alpha'}+9E_{a\beta'}+\cdots\},\quad(7)$$

in which

$$E_{a\alpha}=\sum_{\omega\xi\zeta}\{(\omega_a\omega_a;\ \xi_a\xi_a)-2(U_a;\ \omega_a\omega_a)+32/r_{a\alpha}$$
$$-\tfrac{1}{2}(\omega_a\xi_\alpha;\ \omega_a\xi_\alpha)-(\omega_a\omega_a;\ \zeta_a\xi_\alpha)(\xi_a\zeta_a)$$
$$+(U_a;\ \zeta_a\xi_\alpha)(\xi_a\zeta_a)\}.\quad(8)$$

TABLE II. Comparison of overlap integrals for Slater, self-consistent field, and Kohlrausch wave functions. Data from reference 25.

R (at. units)	RZ^*/n^*		(Z_aZ_b)			(X_aX_b)		
	Slater	Kohlrausch	Slater	SCF	Kohlrausch	Slater	SCF	Kohlrausch
5.25	8.55	5.46	0.08	0.16	0.29	0.016	0.06	0.12
7.56	12.3	7.86	0.01	0.05	0.11	0.001	0.01	0.025

The summation over all the atomic orbitals in the terms $E_{a\alpha}$, etc., makes them independent of direction. Hence it is possible to evaluate them directly for one set of neighbors and interpolate for the remaining terms. We shall evaluate the integrals as follows:

The terms

$$\mathfrak{C}=\sum_{\omega\xi}\{(\omega_a\omega_a;\ \xi_a\xi_a)-2(U_a;\ \omega_a\omega_a)+32/r_{a\alpha}\}$$

are the complete Coulomb interaction of two neutral but penetrating carbon atoms. They are most conveniently calculated in terms of the "penetration integrals" introduced by Bleick and Mayer[8] and Sklar and Lyddane.[20,21] In terms of these

$$\mathfrak{C}=-(A_a;Z_aZ_\alpha)-2(A_a;X_\alpha X_\alpha)-(A_a;S_\alpha S_\alpha)+4A_a\quad(9)$$

where $-A_a$ is the potential energy operator for an electron in the field of a neutral carbon atom in the $(1s)^2(2s)(2p)^3$ state. The terms

$$\mathfrak{A}=\sum_{\omega\xi\zeta}\{-(\omega_a\omega_a;\ \zeta_a\xi_\alpha)+(U_a;\ \zeta_a\xi_\alpha)\}(\xi_a\zeta_a)$$

constitute the energy of "exchanged electrons" in the field of the nucleus and the remaining electrons. They may be written

$$\mathfrak{A}=\mathfrak{A}_{ZZ}+2\mathfrak{A}_{XX}+\mathfrak{A}_{SS}+\mathfrak{A}_{SZ}+\mathfrak{A}_{ZS},\quad(10)$$

where

$$\mathfrak{A}_{SZ}=-[(A_a;\ S_aZ_\alpha)+(S_aS_a;\ S_aZ_\alpha)](Z_\alpha S_a).$$

The integrals $(\omega_a\xi_\alpha;\ \omega_a\xi_\alpha)$ must be evaluated individually. The evaluation of these integrals is discussed in the appendix. The numerical results are given in Section IV below.

III. THE ATTRACTIVE ENERGY

The expression derived by London[5,6] for the dipole-dipole interaction of two molecules is

$$\epsilon_{kl}=-\frac{1}{R^6}\frac{3}{2m^2}\left(\frac{he}{2\pi}\right)^4\sum_{k'l'}$$
$$\times\frac{f_{kk'}g_{ll'}}{(E_{k'}-E_k)(F_{l'}-F_l)(E_{k'}+F_{l'}-E_k-F_l)}.\quad(11)$$

Here E_k, $E_{k'}$ designate the energy levels and $f_{kk'}$ the oscillator strength of the transition $E_k\rightarrow E_{k'}$ in one molecule; F_l, $F_{l'}$, and $g_{ll'}$ refer to energy levels and oscillator strengths of the second molecule. Under the assumption that one can write the dispersion formula for each molecule reasonably well as a single term, it is possible to reduce Eq. (11) to

$$\epsilon_{kl}=-\frac{3}{2}\frac{1}{R^6}\frac{I_kI_l\alpha_k\alpha_l}{I_k+I_l},\quad(12)$$

or for a single substance to

$$\epsilon_{kk}=-\frac{3}{4}\frac{1}{R^6}\alpha^2I,\quad(13)$$

in which α is the static polarizability of the molecule and I the energy transition occurring in the one-term dispersion formula.

Since the optical constants of graphite are not known, the attractive interaction between two carbon atoms in the crystal will be written as $-A/R^6$ and A determined so that the minimum of the total energy curve occurs at the known equilibrium separation of the layers in the crystal.

The attractive term falls off somewhat more slowly than the repulsive. It will be necessary, then, to consider more than a single pair of layers. Actual calculation showed that one may replace $\sum_i 1/R_i^6$ summed over a layer by a surface integral with an accuracy of one percent in the neighborhood of equilibrium. Let $F(x)$ be the energy of interaction of a whole layer and a unit cell in a second layer at the distance x. Then (supposing the separation between layers to be the same throughout the crystal) the energy binding the two halves of the crystal together is

$$E_A=n\cdot\sum_{s=1}^{\infty}sF(sx),$$

[20] A. L. Sklar and R. H. Lyddane, J. Chem. Phys. **7**, 374 (1939).

[21] For corrections to reference 20 see R. G. Parr and B. L. Crawford, J. Chem. Phys. **16**, 1049 (1948).

TABLE III. Integrals in repulsive interaction of a single pair of carbon atoms (distances and energies in atomic units).

R	4.79	6.70	7.66	9.58	11.5
RZ^*/n^*	5	7	8	10	12
Coulomb terms					
$-(A_a; Z_\alpha Z_\alpha)$	−0.10607	−0.00908	−0.00235	−0.00013	−0.00001
$-2(A_a; X_\alpha X_\alpha)$	−0.02925	−0.00183	−0.00042	−0.00002	...
$-(A_a; S_\alpha S_\alpha)$	−0.04510	−0.00364	−0.00092	−0.00005	...
$4A_a$	0.02902	0.00092	0.00016	...	...
$\mathcal{C}$	−0.15140	−0.01363	−0.00353	−0.00020	−0.00001
Exchange terms					
$-\mathfrak{A}_{ZZ}$	0.12518	0.02294	0.00802	0.00065	0.00004
$-2\mathfrak{A}_{XY}$	0.04480	0.00267	0.00058	0.00003	...
$-\mathfrak{A}_{SS}$	0.10110	0.00986	0.00271	0.00017	0.00001
$-\mathfrak{A}_{SZ}$	0.08999	0.01110	0.00366	0.00029	0.00001
$-\mathfrak{A}_{ZS}$	0.15902	0.01905	0.00558	0.00038	0.00002
$-\mathfrak{A}$	0.52009	0.06562	0.02055	0.00152	0.00008
$(Z_\alpha Z_\alpha; Z_a Z_\alpha)$	0.11846	0.02536	0.00898	0.00082	0.00005
$4(Z_\alpha X_\alpha; Z_a X_\alpha)$	0.05064	0.00536	0.00148	0.00009	...
$2(Z_\alpha S_\alpha; Z_a S_\alpha)$	0.18602	0.02876	0.00934	0.00076	0.00004
$4(X_\alpha S_\alpha; X_a S_\alpha)$	0.02922	0.00263	0.00069	0.00004	...
$2(X_\alpha X_\alpha; X_a X_\alpha)$	0.03368	0.00235	0.00054	0.00003	...
$2(X_\alpha Y_\alpha; X_a Y_\alpha)$	0.00173	0.00012	0.00003	...	...
$(S_\alpha S_\alpha; S_a S_\alpha)$	0.06303	0.00774	0.00234	0.00017	0.00001
$-\frac{1}{2}\Sigma_{\omega\xi}(\omega_\alpha\xi_\alpha; \omega_a\xi_\alpha)$	−0.24139	−0.03616	−0.01170	−0.00096	−0.00005
$E_{a\alpha}$	0.12727	0.01583	0.00532	0.00036	0.00002
E_{aa}‡	0.12727	0.01582	0.00531	0.00054	0.00005

‡ The last row is calculated from $E_{a\alpha}=13.162\exp(-.88286x-.012861x^2)$.

where

$$F(sx)=-4\pi A\sigma\int_0^\infty\frac{RdR}{[R^2+(sx)^2]^3}=-\frac{4\pi A\sigma}{(sx)^4}.$$

The surface density of atoms is $\sigma=4\cdot3^{-\frac{1}{2}}a^{-2}$. Here a is the interatomic distance in the layers (1.42A). It follows that

$$E_A=-\frac{n\pi\sigma A}{x^4}\sum_{s=1}^{\infty}1/s^3. \tag{14}$$

$\sum_{s=1}^{\infty}1/s^3$ summed with the help of the Euler-Maclaurin sum formula is found to be 1.202.

IV. NUMERICAL RESULTS

The wave functions chosen for the evaluation of the integrals in Eq. (8)–(10) were of the familiar form:

$$S_a=(\delta^5/3\pi)^{\frac{1}{2}}r_a\exp(-\delta r_a),$$
$$X_a=(\delta^5/\pi)^{\frac{1}{2}}x_a\exp(-\delta r_a),$$
$$Y_a=(\delta^5/\pi)^{\frac{1}{2}}y_a\exp(-\delta r_a),$$
$$Z_a=(\delta^5/\pi)^{\frac{1}{2}}z_a\exp(-\delta r_a).$$

The fact that S_a is nodeless should not be significant here where the overlap of the wave functions is small. The choice of $\delta=Z^*/n^*$, however, is critical. The repulsive energy was first calculated with the values of Z^* and n^* proposed by Zener.[22] Zener's values: $Z^*=3.18$, $n^*=2$, differ very little from those of Slater:[23] $Z^*=3.25$, $n^*=2$. The depth of the energy well, calculated with this choice of constants, is too small, and the compressibility calculated from the repulsive energy alone is too great (see Table V).

The depth of the potential well might be improved by including another term (the dipole-quadrupole interaction) in the attractive term.[24] The direction of the error in the compressibility, however, suggests that the repulsive term is the source of the trouble.

From the physical interpretation of the repulsive energy, it should vary as the overlap of the wave functions. Mulliken, Rieke, Orloff, and Orloff[25] have pointed out that in the region 3–4A, the overlap of Slater wave functions is considerably smaller than that of self-consistent-field atomic wave functions. The same authors suggest also that the perturbation of the atomic wave functions in the formation of molecules would tend to increase rather than decrease the overlap.

TABLE IV. Contributions of successive neighbors to interlayer repulsion. (Distances and energies in atomic units.)

R	4.79	6.70	7.66	9.58	11.5
RZ^*/n^*	5	7	8	10	12
$E_{a\alpha}$	0.12727	0.01582	0.00531	0.00054	0.00005
$9E_{a\beta}$	0.24390	0.03834	0.01440	0.00171	0.00018
$6E_{a\alpha'}$	0.01128	0.00264	0.00114	0.00018	...
$9E_{a\beta'}$	0.00558	0.00144	0.00063	0.00009	...
$18E_{a\alpha''}$	0.00054	0.00018	0.00008	...	...
E_R	0.38858	0.05842	0.02156	0.00252	0.00023
E_R§	0.38860	0.05842	0.02156	0.00266	0.00029

§ The last row is calculated from $E_R=24.918\exp(-.78269x-.01794x^2)$.

[22] C. Zener, Phys. Rev. **36**, 51 (1930).
[23] J. C. Slater, Phys. Rev. **36**, 57 (1930).
[24] This term can often be quite important. See article of Margenau cited in reference 6.
[25] Mulliken, Rieke, Orloff, and Orloff, J. Chem. Phys. **17**, 1248 (1949).

Kohlrausch has recently suggested a new system of screening constants and effective quantum numbers.[26,27] In his system the values of Z^* and n^* are chosen to fit empirical ionization potentials and give satisfactory results in the discussion of a number of atomic properties. Since in Kohlrausch's system Z^* and n^* are 2.03 and 1.944, respectively, for carbon, the overlap of the wave functions will be very much greater than with the Zener or Slater choice of Z^* and n^*. The overlap integrals for Slater, self-consistent-field and Kohlrausch wave functions in our region are shown in Table II. The overlap of the Kohlrausch functions is seen to vary in the desired direction, though possibly too much. To recalculate the energy of the new value of Z^*/n^* involves only a change of energy and distance scales.

$E_{a\alpha}$ of Eq. (7) was calculated directly for five distances, and the values thus obtained were fitted by the equation

$$E_{a\alpha}=13.162\cdot\exp(-.88286x-.017861x^2). \quad (15)$$

(See Table III.) The succeeding terms of Eq. (7) were obtained from Eq. (15). (See Table IV.) The total repulsive energy between two layers comes out to be

$$E_R=n\cdot 24.918\exp(-0.78269x-0.01794x^2). \quad (16)$$

The condition that the minimum of $E=E_A+E_R$ shall fall at 6.37 (atomic units) determines A of Eq. (14) to be 546.5. Hence the final expression for the interlayer energy is

$$E=n\cdot\{-221.2/x^4+24.92\exp(-0.7827x-0.01794x^2)\}, \quad (17)$$

where n as before is the number of cells in a layer. Since the unit cell contains two atoms, the energy per mole contributed to the graphite crystal by the interlayer binding is then

$$U=\tfrac{1}{4}N_A(E/n). \quad (18)$$

TABLE V. Contributions of the attractive and repulsive forces to the interlayer binding energy and to the bulk modulus, calculated with Z^*/n^* of Zener and Kohlrausch.

	U_A	U_R	U	$1/\beta_A$	$1/\beta_R$	$1/\beta$
	(kcal/M)			(d/cm$^2\times10^{12}$)		
Zener	−0.36	0.10	−0.27	−0.056	0.163	0.11
Kohlrausch	−10.53	6.54	−3.99	−1.60	1.99	0.39
Experimental	...	...	...	...	...	0.336‖

‖ Extrapolated to atmospheric pressure. From P. W. Bridgman, Proc. Am. Acad. Arts Sci. **76**, 9 (1945).

V. COMPARISON WITH EXPERIMENTAL DATA

There exist no experimental values for the interlayer binding energy. The calculated depth of the energy well is tabulated in Table V for both Zener and Kohlrausch wave functions.[28]

Although the test is not critical, it is of some interest to compare the stability of the actual lattice with one which would occur if the layers were all of the same orientation, one atom lying directly over another, so that every atom would have the same set of neighbors. When the appropriate change is made in the repulsive terms, the actual lattice is found to win out by the narrow margin of 0.36 kcal/M. The minimum falls at 6.79 atomic units.

The relative magnitudes of the binding energies in and between the layers suggests that one may to a reasonable approximation attribute the volume compressibility of graphite, at least at moderate pressures, to a change in one dimension only. On this assumption, one obtains from Eq. (18) and [29] $(\partial^2U/\partial V^2)_{V=V_0}=1/V\beta$ (for $T=0$°K.)

$$\frac{x_0^2}{V_0}\frac{\partial^2U}{\partial x^2}=\frac{N_Ax_0^2}{4V_0}\frac{\partial^2}{\partial x^2}(E/n)=\frac{1}{\beta},$$

where β is the volume compressibility of graphite. The calculated values are compared with Bridgman's experimental value in Table V.

VI. DISCUSSION

Although further experimental checks are to be desired, the agreement of the calculated and experimental compressibilities gives considerable plausibility to Eq. (17).

In dealing with graphite one would not be very sanguine about making the following assumptions:

(1) that it is valid to pass from the exact London equation (Eq. (11)) to the approximation in terms of a single energy transition (Eq. (12) and (13));

(2) that it is legitimate to assume atomic constants from nonconducting states of carbon in order to make use of Eq. (12) and (13). The conclusion of the present work seems to be against the use of either or both of assumptions (1) and (2). Some use of them has been made in the past[30,31] in default of any better procedure. But the values of A which would be deduced from the parameters suggested in previous investigations are of the order of one-tenth of the value found here.

Neither do the results of the present work permit the use of assumption (1) without assumption (2). The use of Eq. (12) requires, together with A of Eq. (14), either I or α of Eq. (13). One might choose $I=4.39$ ev, the experimental value of the work function of graphite.[32]

[26] K. W. F. Kohlrausch, Acta Phys. Austriaca **3**, 452 (1949).

[27] For an interpretation of Kohlrausch's system see O. Theimer, Acta Phys. Austriaca **4**, 1 (1950).

[28] Experimental heats of adsorption cited by London (reference 5) would indicate that a crystal of alternate layers of graphite and CO_2 or CH_4 would be more stable than the graphite crystal itself. Lamb and Ohl [J. Am. Chem. Soc. **60**, 1287 (1938)] have shown that the adsorbed molecules do not occupy interlayer positions. It is to be noted that the heats of adsorption cited by London were measured on charcoal, and in several instances at least are considerably greater than the heats of adsorption on graphite (reference 31).

[29] See, for example, F. Seitz, *The Modern Theory of Solids* (McGraw-Hill Book Company, Inc., New York, 1940), p. 76.

[30] Reference 5, but see also J. H. de Boer and J. F. H. Custers, Z. physik Chem. (B) **25**, 225 (1934).

[31] R. M. Barrer, Proc. Roy. Soc. (London) **A161**, 476 (1937).

[32] A. Braun and G. Busch, Helv. Phys. Acta **20**, 33 (1947).

TABLE VI. Coulomb penetration integrals. $\delta=2Z^*/n^*$. Atomic units.

$R\delta$	10	14	16	20	24	30
$\delta^{-1}(A_a; Z_bZ_b)$	0.05099	0.00436	0.00113	0.00006	...	...
$\delta^{-1}(A_a; X_bX_b)$	0.00703	0.00044	0.00010	...	...	...
$\delta^{-1}(A_a; S_bS_b)$	0.02168	0.00175	0.00044	0.00002	...	...
$\delta^{-1}(A_a; S_bZ_b)$	−0.00061	−0.00015	−0.00005	...	...	...

TABLE VII. Exchange penetration integrals. $\delta=2Z^*/n^*$. Atomic units.

$R\delta$	10	14	16	20	24	30
$\delta^{-1}(A_a; Z_aZ_b)$	−0.07496	−0.01817	−0.00821	−0.00153	−0.00026	−0.00002
$\delta^{-1}(A_a; X_aX_b)$	0.02090	0.00341	0.00122	0.00017	0.00002	...
$\delta^{-1}(A_a; S_aS_b)$	0.07311	0.01542	0.00672	0.00120	0.00020	0.00001
$\delta^{-1}(A_a; S_aZ_b)$	−0.12030	−0.02605	−0.01142	−0.00205	−0.00035	−0.00004
$\delta^{-1}(A_a; Z_aS_b)$	0.04643	0.01082	0.00485	0.00090	0.00015	0.00001

α is then 7.04×10^{-24} cm.[3] Heats of adsorption of H_2, A, and N_2 on graphite, calculated with this choice of constants, were too low when compared with experimental values.[31] A reasonable explanation of this might well be the failure of assumption (1).

The present work further emphasizes the need of investigating the proper choice of atomic wave functions for use in LCAO molecular orbitals. One would not be able to justify Kohlrausch's choice of parameters from a property that is so extrinsic to the molecule as the repulsive forces treated here. It may be that if one is to use atomic orbitals of such a simple functional form, the choice of Z^* and n^* will depend on the problem being investigated.[33]

VII. ACKNOWLEDGMENTS

The writer is greatly indebted to Dr. Karl F. Herzfeld for suggesting the problem and for his competent guidance during the course of the work. He takes this occasion also to express his gratitude to the director and staff of the Watson Scientific Computing Laboratory for making available the facilities of the laboratory for the calculation of hybrid Coulomb-exchange and exchange penetration integrals.

APPENDIX A

The integrals which occur in the above calculations are overlap, coulomb penetration, exchange penetration, hybrid coulomb-exchange, and exchange integrals. The overlap integrals require no comment since both formulas and numerical tables may be found in the work of Mulliken, *et al.*[25] The sources of the other integrals are indicated below together with numerical values which were obtained in the present work.

A. Penetration Integrals

These are of the form $-(A_a; \xi_b\xi_b)$ and $-(A_a; \xi_a\xi_b)$, where $-A_a$ is the potential energy operator for an electron in the field of a neutral carbon atom in the $(1s)^2(2s)(2p)^3$ state:

$$-A_a=H_a=-1/(2r_a)\cdot\exp(-2\delta r_a)\times\{16+24(\delta r_a)+16(\delta r_a)^2+8(\delta r_a)^3\}.$$

Integrals of this kind for π-electrons have been evaluated by Sklar and Lyddane[20] and by Parr and Crawford.[21] The method of these workers was used to evaluate the remainder of the integrals of this type. (See Tables VI and VII.) The integrals which occur in the exchange penetration integrals (and also in the hybrid Coulomb-exchange integrals) are especially tedious. They were evaluated for a number of arguments from their recurrence formulas[20] on IBM machines at the Watson Scientific Computing Laboratory at Columbia University.

B. Hybrid Coulomb-Exchange Integrals

These integrals are of the form $(\xi_a\xi_a; \xi_a\omega_b)$. They have also been evaluated by the authors mentioned in references 20 and 21 and by Kopineck,[34] following Kotani, Amemiya, and Simose,[35] for a number of cases involving $2p$ functions. In the present work, the hybrid Coulomb-exchange integrals were evaluated by the method of Sklar and Lyddane for all cases not given by these authors, and the formulas checked against those of Mulligan.[36] The numerical work was done in great part at the Watson Laboratory and is in satisfactory agreement with the work of Kopineck for the cases he gives.

C. Exchange Integrals

These are of the form $(\xi_a\omega_b; \xi_a\omega_b)$. The best source of these integrals at present is Kopineck's work. Since the whole range of our parameters is not covered there, the formulas of the Japanese physicists[34] were reduced so that no integrals containing $P_n^m(x)$ or $Q_n^m(x)$ with $m\neq0$ remained. The numerical tables necessary could then be developed quite quickly. In this the tables of the Japanese physicists also proved useful.

This way of treating the exchange integrals is based on the work of Rosen,[37] Wheatley and Linnett,[38] and Hirschfelder and Linnett.[39]

---

[33] C. A. Coulson, Trans. Faraday Soc. **33**, 1479 (1937), and C. A. Coulson and W. E. Duncanson, Proc. Roy. Soc. (London) **A181**, 378 (1943) have discussed in some detail the choice of screening constants. Their conclusions lead to an increase rather than a decrease of the Z^*/n^* of the Slater recipe.

[34] H.-J. Kopineck, Z. Naturforsch. **5a**, 420 (1950).

[35] Kotani, Amemiya, and Simose, Proc. Phys.-math. Soc. (Japan) **20**, Extra number 1 (1938); **22**, Extra number 1 (1940).

[36] J. F. Mulligan, J. Chem. Phys. **19**, 347 (1951). The formulas were communicated privately.

[37] N. Rosen, Phys. Rev. **38**, 255, 2099 (1931).

[38] P. J. Wheatley and J. W. Linnett, Trans. Faraday Soc. **45**, 897 (1949).

[39] J. O. Hirschfelder and J. W. Linnett, J. Chem. Phys. **18**, 130 (1950).

TABLE VIII. Hybrid Coulomb-exchange integrals. $\delta=2Z^*/n^*$. Atomic units.

$R\delta$	10	14	16	20	24	30
$\delta^{-1}(Z_aZ_a; Z_aZ_b)$	−0.11373	−0.04618	−0.02775	−0.00752	−0.00178	−0.00016
$\delta^{-1}(X_aX_a; X_aX_b)$	0.04478	0.01055	0.00488	0.00094	0.00018	...
$\delta^{-1}(S_aS_a; S_aS_b)$	0.08760	0.02743	0.01428	0.00351	0.00078	0.00007
$\delta^{-1}(S_aS_a; S_aZ_b)$	−0.10867	−0.03886	−0.02089	−0.00534	−0.00122	−0.00012
$\delta^{-1}(Z_aZ_a; S_aZ_b)$	−0.11406	−0.04118	−0.02191	−0.00565	−0.00129	−0.00013
$\delta^{-1}(Z_aZ_a; Z_aS_b)$	0.09925	0.03865	0.01922	0.00532	0.00118	0.00011
$\delta^{-1}(S_aS_a; Z_aS_b)$	0.09100	0.03282	0.01777	0.00498	0.00108	0.00010
$\delta^{-1}(Z_aX_a; Z_aX_b)$	0.00460	0.00138	0.00052	0.00023	0.00005	...
$\delta^{-1}(X_aX_a; Z_aZ_b)$	−0.09795	−0.03956	−0.02308	−0.00655	−0.00163	−0.00016
$\delta^{-}[(Z_aX_a; Z_aX_b)$	−0.00484	−0.00157	−0.00080	−0.00018	−0.00002	...
$\delta^{-1}(Z_aZ_a; X_aX_b)$	0.04448	0.01065	0.00506	0.00099	0.00019	0.00001

APPENDIX B

The Order of Orbitals in Table I

The calculations show that so long as the wave functions of the form

$$\psi_i=\Sigma_a \exp(2\pi i\mathbf{k}_i\cdot\mathbf{r}_a)\xi(\mathbf{r}-\mathbf{r}_a)\pm\Sigma_b \exp(2\pi i\mathbf{k}_i\cdot\mathbf{r}_b)\xi(\mathbf{r}-\mathbf{r}_b)$$

make up full bands, the interaction energy of any pair of bands is independent of the sign before the second sum. The only thing that matters in our calculations is that ψ_{1i}, ψ_{2i}, ψ_{3i}, and ψ_{4i} (or in each case, the corresponding band with the + sign) are below the other four bands and are therefore filled, while the others are empty. The order among them is unimportant. However, one can attempt to justify the order in Table I as follows.

One expects the perturbation to split the in-plane functions considerably more than the π-functions. Hence the middle place in the table should be occupied by the π bands. Presumably, but here there is room for doubt, the X and Y combinations will be higher than the S bands. It is left to decide which of each pair of functions is lowered and which raised by the perturbation. Wallace has shown by direct calculation that the B_{2g} band lies below the A_{2u}, i.e., for $\xi=Z$, the wave function with the negative sign lies below that with the positive. One sees no reason why this order should be different for $\xi=S$, X, and Y. These were the reasons why the proposed order was chosen.

TABLE IX. Exchange integrals. $\delta=2Z^*/n^*$. Atomic units.

R	16	20	24
$\delta^{-1}(Z_aZ_b; Z_aZ_b)$	0.04318	0.00039	0.00003
$\delta^{-1}(Z_aZ_b; X_aX_b)$	0.00069	0.00005	...
$\delta^{-1}(Z_aX_b; Z_aX_b)$	0.00018	0.00001	...
$\delta^{-1}(Z_aX_b; X_aZ_b)$	0.00014	0.00001	...
$\delta^{-1}(Z_aS_b; Z_aS_b)$	0.00224	0.00018	0.00001
$\delta^{-1}(Z_aS_b; S_aZ_b)$	0.00220	0.00018	0.00001
$\delta^{-1}(Z_aZ_b; S_aS_b)$	0.00218	0.00018	0.00001
$\delta^{-1}(X_aX_b; X_aX_b)$	0.00129	0.00006	...
$\delta^{-1}(X_aX_b; Y_aY_b)$	0.00127	0.00006	...
$\delta^{-1}(X_aY_b; X_aY_b)$	0.00001	...	...
$\delta^{-1}(X_aX_b; S_aS_b)$	0.00037	0.00002	...
$\delta^{-1}(X_aS_b; X_aS_b)$	0.00008	...	...
$\delta^{-1}(X_aS_b; S_aX_b)$	0.00007	...	...
$\delta^{-1}(S_aS_b; S_aS_b)$	0.00113	0.00008	...

It is of interest to consider the relation between the nodal surfaces and the energy. In general, the energy in an eigenvalue problem is an increasing function of the number of nodal surfaces. This has been discussed in detail by Herzfeld[40] as it applies to molecular orbitals. Hence to determine the order of the bands in Table I it is sufficient to consider the number of nodal surfaces in each band. (To discuss the nodes, one must deal with real wave functions. The discussion is possible here, if we replace the exponentials by their real parts.)

The method of comparison offers some difficulty. One would be at first inclined to see which linear combination of a pair is lower if $\mathbf{k}_i$ is set equal to zero. This does not appear just, since one linear combination belongs to the first Brillouin zone, the other to the second, so that $\mathbf{k}_i$ cannot be zero in both bands. Besides, this would lead to setting the A_{2u} band below the B_{2g}, since with $\mathbf{k}_i=0$ in the A_{2u} linear combination there are no nodes perpendicular to the plane of the layers.

The proper way to make the comparison, it seems, is rather to compare the number of nodal surfaces in the two functions at the boundary of the Brillouin zone where they take on the same value of $\mathbf{k}_i$. Wallace has diagrams indicating the position of the nodal surfaces for the π-bands at a point on the zone boundary. The spacing of the nodes does not differ for A_{2u} and B_{2g}, but the signs of the terms in his detailed calculations are such as to determine B_{2g} to be lower. His diagram serves equally well for the S functions (without nodes. If the atomic S function with a node is used, it introduces a nodal surface surrounding each lattice point.) One sees no reason why the same order would not occur in the case of S functions as for the Z functions. In the case of X and Y functions, the nodal spacing changes considerably between the bands.

It follows from this argument that either the rule that the energy increases always with the number of nodes is not generally valid if one compares wave functions in different bands, or one should keep formally the increase by $2\pi i$ in the exponent as one goes from one band to the next higher one.

[40] See Revs. Modern Phys. **21**, 527 (1949) and literature there cited.

Application of the Cell Method to the Statistical Thermodynamics of Solutions

I. PRIGOGINE AND V. MATHOT*
Faculté des Sciences de l'Université libre de Bruxelles, Brussels, Belgium
(Received August 13, 1951)

The cell method for pure liquids in the form used by Lennard-Jones and Devonshire is extended to solutions. It is assumed that (a) the constituents are spherical in shape, with an isotropic field of force, (b) the distance of the maximum interaction for AA, BB, and AB pairs is about the same, and (c) there is random mixing.

For the mean field in the "cage," the complete 6–12 law, the harmonic oscillator, and the smoothed potential model have been studied. The smoothed potential model (potential curve with vertical walls and flat bottom, *both* depth and width depending on concentration) fits the liquid state best. For this model, one obtains important corrections on both the heat of mixing and the excess entropy to the classical, strictly regular solutions. These corrections are related to the volume changes on mixing resulting from the changes of interactions.

According to the value of ϵ_{AB}^*, the excess properties such as volume, entropy, heat of mixing, and free energy present a large variety of shapes, including dissymmetry and inversions which correspond rather nicely to experimental evidence.

This model permits discussion of the severe limitations of Longuet-Higgins's recent theory of conformal solutions.

1. INTRODUCTION

THIS paper continues our previous work[1] on solutions of spherical molecules having the same size but different fields of interaction. Figure 1 gives the potential energy of a pair of particles as a function of the distance apart. It is assumed here that

$$r_{AA}^* \simeq r_{AB}^* \simeq r_{BB}^* \simeq r^*. \tag{1.1}$$

The usual method of statistical treatment of such solutions[2,3,4] is based on several hypotheses which are clearly summarized in Fowler and Guggenheim's *Statistical Thermodynamics*.[3] Besides the quasi-crystalline model of the solutions, it is assumed that there is no excess volume on mixing.

Another hypothesis is that the change of composition does not alter the form of the mean field acting on each molecule.[4] This very restrictive approximation is called the model of *strictly regular solutions*. The crude treatment of this model, assuming random mixing, gives

$$S_e = 0, \tag{1.2}$$

and so

$$G_e \simeq H_e \tag{1.3}$$

where S_e, G_e, H_e are the excess values of the entropy, Gibbs free energy, and enthalpy over the values given by the formulas for perfect solutions.

Therefore all deviations to ideality are here ascribed to the presence of an excess enthalpy, i.e., to the heat of mixing. Experimental determination of the excess functions due to Scatchard and others,[5] clearly invalidate formulas (1.2) and (1.3). In nearly all systems studied, there is an important contribution, either positive or negative, of the entropy excess function to the free energy.

The introduction of the quasi-chemical method by Guggenheim[6] was a considerable improvement in taking into account the non-randomness of mixing. This refined treatment of strictly regular solutions gives a small negative excess entropy. But the experimental excess entropy is by no means always negative; also for many solutions for which the heat of mixing is not large, we still have a non-negligible excess entropy, while the refined treatment gives only in such cases a very small contribution to the excess entropy. (See reference 1 for a numerical example.)

The situation in this whole field of the statistical theory of solutions appears unsatisfactory. For this reason we have tried to apply to this problem the "cell" method which, in the form developed by Lennard-Jones and Devonshire,[7] has proved to be very useful for pure liquids far from the critical point.

In its original form the Lennard-Jones and Devonshire method is a numerical one. In order to apply it to the evaluation of the thermodynamic excess function, it

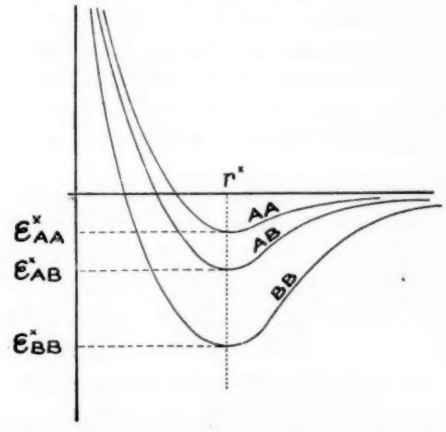

FIG. 1. Schematic representation of the potential energy of a pair of particles AA, AB, BB.

* Chargé de Recherches du Fonds National de la Recherche Scientifique Belge.

[1] I. Prigogine and G. Garikian, Physica **16**, 239 (1950).

[2] Y. H. Hildebrand and R. L. Scott, *Solubility of Non Electrolytes* (Reinhold Publishing Corporation, New York, 1949).

[3] R. H. Fowler and E. A. Guggenheim, *Statistical Thermodynamics* (Cambridge University Press, London, 1939), Sec. 814.

[4] G. S. Rushbrooke, *Introduction to Statistical Mechanics* (Oxford University Press, London, 1948), Chapter XVIII, p. 290.

[5] Scatchard, Wood, and Mockel, J. Phys. Chem. **43**, 119 (1939); J. Am. Chem. Soc. **61**, 3206 (1939); **62**, 712 (1940).

[6] See reference 3, Sec. 819.

[7] J. E. Lennard-Jones and A. F. Devonshire, Proc. Roy. Soc. (London) **A163**, 53 (1937); **165**, 1 (1938).

would be necessary to carry out very extensive numerical computations. Fortunately, we have shown in a previous paper,[8] following a suggestion of Guggenheim, that the results are largely insensitive to simplifications on the law of forces of the mean field because the major error involved is due to the statistical model itself.

Therefore we have considered here two useful approximations of the mean field: (a) harmonic oscillator model which corresponds to the mean field of Fig. 2a, and (b) smoothed potential model (Fig. 2b).

In both approximations we assume that the potential energy between two molecules i and j is given by†

$$\epsilon_{ij}(r)=-\mu_{ij}r^{-6}+\nu_{ij}r^{-12}=\epsilon_{ij}^{*}[(r_{ij}^{*}/r)^{12}-2(r_{ij}^{*}/r)^{6}].$$

So the parameters appearing in the mean field can be expressed in terms of ϵ_{ij}^{*} and r_{ij}^{*}.

No other parameters appear in the present calculations. The potential energy parameters can be determined in the usual way, i.e., measuring the second virial coefficient. Therefore this model permits in principle, a deduction of all the thermodynamic properties of the solution from the study of slightly imperfect gases.

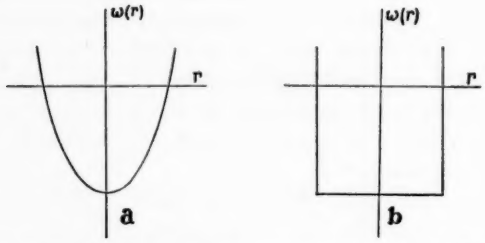

FIG. 2. Approximations on the mean field $\omega(r)$: a. harmonic oscillator model, b. smoothed potential model.

Both limiting cases (a) and (b) give the same qualitative results, with the only difference that for the harmonic oscillator model some effects are associated with the change of the vibration frequency with composition. This effect, of course, does not appear in the smoothed potential model. But in both models the main new effects are related to a change of volume caused by a change of composition at constant pressure. This effect, unduly neglected in the model of strictly regular solutions, can give rise to important entropy and heat effects.

Throughout this paper we have assumed random mixing. Our treatment thus corresponds closely to the crude approximation of strictly regular solutions. We intend to develop in a subsequent paper a more refined treatment taking into account non-randomness of mixing.

2. DEFINITIONS AND NOTATIONS

The cell model of liquids[9] is primarily concerned with the motion of a molecule in a cell formed by its first neighbors. We shall first introduce some general relations.

A. Pure Liquid

Let us call Ψ the *configurational partition function* for the motion of each molecule in its cell, referred to an energy zero with the particle at the center of the cell

$$\Psi=\int_0^{\infty}\exp-\left(\frac{\omega(r)-\omega(0)}{kT}\right)4\pi r^2dr, \qquad (2.1)$$

where $\omega(r)$ is the potential energy, averaged over all angular positions of a particle at a distance r from the center of the cell.

The configurational partition function Q for the whole system of N particles is given by[10]

$$Q=\frac{(N\Psi)^N}{N!}\cdot\exp-\frac{N\omega(0)}{2kT} \qquad (2.2)$$

where $\frac{1}{2}N\omega(0)$ represents the potential energy of the system when each molecule is at the center of its cell.

The free energy (either Gibbs' or Helmholtz', neglecting the pv term)

$$G\simeq F=-NkT\left[1+lg\Psi-\tfrac{1}{2}\frac{\omega(0)}{kT}+lgj(T)\right], \qquad (2.3)$$

where $j(T)$ is the internal partition function for each molecule.

The equation of state will be, using $v=V/N$,

$$p=kT[(\partial lg\Psi/\partial v)-(1/2kT)\{\partial\omega(0)/\partial v\}] \qquad (2.4)$$

or, for vanishing external pressure

$$\partial lg\Psi/\partial v=(1/2kT)\{\partial\omega(0)/\partial v\}. \qquad (2.5)$$

B. Binary Solution

By use of the assumptions stated in Sec. 1, relations (2.1) to (2.5) can easily be extended to a solution of N_A particles of type A and N_B particles of type B.[1]

$$\begin{cases}\Psi_A=\displaystyle\int_0^{\infty}\exp-\{\omega_A(r)-\omega_A(0)/kT\}4\pi r^2dr\\ \Psi_B=\displaystyle\int_0^{\infty}\exp-\{\omega_B(r)-\omega_B(0)/kT\}4\pi r^2dr.\end{cases} \qquad (2.1')$$

$$Q=\frac{(N\Psi_A)^{N_A}}{N_A!}\cdot\frac{(N\Psi_B)^{N_B}}{N_B!}\times\exp-\frac{1}{2kT}[N_A\omega_A(0)+N_B\omega_B(0)]. \qquad (2.2')$$

[8] I. Prigogine and G. Garikian, J. chim. phys. **45**, 273 (1948).

† See also Eq. (1.1).

[9] See reference 3, Sec. 808 ff. The notations used here are largely theirs.

[10] The problem of the "communal entropy" will not be studied here; see P. Janssens and I. Prigogine, Physica **16**, 895 (1950).

$$\frac{G}{NkT}\simeq\frac{F}{NkT}$$

$$=x_A\left\{1-lgx_A+lg\Psi_A-\tfrac{1}{2}\frac{\omega_A(0)}{kT}+lgj_A(T)\right\}$$

$$+x_B\left\{1-lgx_B+lg\Psi_B-\tfrac{1}{2}\frac{\omega_B(0)}{kT}+lgj_B(T)\right\}, \quad (2.3')$$

x_A and x_B are the mole fractions ($x_A+x_B=1$).

The deviations from ideality of the solution are given in terms of the excess free energy of mixing

$$\frac{F_e}{NkT}=\frac{F}{NkT}-\frac{F_A{}^0}{N_AkT}-\frac{F_B{}^0}{N_BkT}-x_Algx_A-x_Blgx_B$$

$$=x_A\left[-lg\frac{\Psi_A}{\Psi_A{}^0}+\frac{1}{2kT}\{\omega_A(0)-\omega_A{}^0(0)\}\right]$$

$$+x_B\left[-lg\frac{\Psi_B}{\Psi_B{}^0}+\frac{1}{2kT}\{\omega_B(0)-\omega_B{}^0(0)\}\right], \quad (2.4')$$

where all properties are considered at the same pressure and temperature.

In Eq. (2.4) all symbols with index ^{0} refer to pure A or B; $\omega_A{}^0(0)$ is the potential at the center of a cell occupied by an A molecule in the pure liquid A.

Every relevant excess thermodynamic property of the solution can be derived from (2.4').

The equation of state for vanishing external pressure becomes here

$$x_A\frac{\partial lg\Psi_A}{\partial v}+x_B\frac{\partial lg\Psi_B}{\partial v}$$

$$=\frac{1}{2kT}\left(x_A\frac{\partial\omega_A(0)}{\partial v}+x_B\frac{\partial\omega_B(0)}{\partial v}\right). \quad (2.5')$$

We shall make use of the excess volume per "mole" of solution, defined by

$$v_e=v-v_A{}^0x_A-v_B{}^0x_B$$

with

$$v=\frac{V}{N_A+N_B}. \quad (2.6)$$

As random distribution is assumed, the interaction parameter $\Lambda=-z\epsilon^*$, which appears in the ω's, is replaced for the solution by

$$\Lambda_A=-z(x_A\epsilon_{AA}{}^*+x_B\epsilon_{AB}{}^*),$$
$$\Lambda_B=-z(x_B\epsilon_{BB}{}^*+x_A\epsilon_{AB}{}^*). \quad (2.7)$$

We shall also make use of the definitions

$$\Lambda_{AA}=-z\epsilon_{AA}{}^*;\quad \Lambda_{AB}=-z\epsilon_{AB},{}^*$$
$$\Lambda_{BB}=-z\epsilon_{BB}{}^*;\qquad \Lambda=x_A\Lambda_A+x_B\Lambda_B, \quad (2.8)$$
$$v^*=\frac{(r^*)^3}{\gamma}.$$

In this last formula, γ is a geometrical parameter ($=\sqrt{2}$ for face-centered cubic lattice) related to the quasi-crystalline lattice of the solution.[7]

3. LENNARD-JONES AND DEVONSHIRE MODEL

The Lennard-Jones and Devonshire refined cell model for a liquid[7] gives the following mean field, assuming the 6–12 interaction law,

$$\omega(r)-\omega(0)=\Lambda\{\alpha^2l(y)-2\alpha m(y)\} \quad (3.1)$$

with

$$\alpha=(v^*/v)^2;\quad v=a^3/\gamma, \quad (3.2)$$

$l(y)$ and $m(y)$ two functions of $y=(r/a)^2$ defined by

$$l(y)=(1+12y+25.2y^2+12y^3+y^4)(1-y)^{-10}-1$$
$$m(y)=(1+y)(1-y)^{-4}-1. \quad (3.3)$$

a is the radius of the cage. The partition function for a molecule in its cell is here

$$\Psi=2\pi a^3g \quad (3.4)$$

with

$$g=\int_0^1 y^{\frac{1}{2}}\exp[-(\Lambda/kT)\{\alpha^2l(y)-2\alpha m(y)\}]dy, \quad (3.5)$$

and $\omega(0)$ is given by

$$\omega(0)=\Lambda(a\alpha^2-b\alpha) \quad (3.6)$$

where a and b are constants related to second and third shell-neighbor interactions,[11]

$$a=1.01095;\quad b=2.4090.$$

Applying Eq. (2.4'), one obtains for a solution

$$\frac{F_e}{NkT}=-lg\left(\frac{g_A}{g_{AA}}\right)^{x_A}\left(\frac{g_B}{g_{BB}}\right)^{x_B}+\tfrac{1}{2}lg\frac{\alpha}{\alpha_A{}^{x_A}\alpha_B{}^{x_B}}$$

$$+\frac{1}{2kT}[\Lambda(a\alpha^2-b\alpha)-x_A\Lambda_{AA}(a\alpha_A{}^2-b\alpha_A)$$

$$-x_B\Lambda_{BB}(a\alpha_B{}^2-b\alpha_B)]. \quad (3.7)$$

From Eq. (3.7) we can deduce immediately the value of the excess entropy and enthalpy. The equation of state becomes

$$\alpha^2\left(2x_A\frac{\Lambda_A}{kT}\frac{g_{lA}}{g_A}+2x_B\frac{\Lambda_B}{kT}\frac{g_{lB}}{g_B}+a\frac{\Lambda}{kT}\right)$$

$$-\alpha\left(2x_A\frac{\Lambda_A}{kT}\frac{g_{mA}}{g_A}+2x_B\frac{\Lambda_B}{kT}\frac{g_{mB}}{g_B}+\frac{b}{2}\frac{\Lambda}{kT}\right)+\tfrac{1}{2}=0 \quad (3.8)$$

[11] Wentorf, Buehler, Hirschfelder, and Curtiss, J. Chem. Phys. **18**, 1484 (1950). See also Lennard-Jones and Ingham, Proc. Roy. Soc. (London) **A107**, 636 (1925).

with g_l and g_m defined as

$$g_l=\int_0^1 y^{\frac{1}{2}}l(y)\exp-\frac{\Lambda}{kT}\{\alpha^2 l(y)-2\alpha m(y)\}dy,$$
$$g_m=\int_0^1 y^{\frac{1}{2}}m(y)\exp-\frac{\Lambda}{kT}\{\alpha^2 l(y)-2\alpha m(y)\}dy. \quad (3.9)$$

In relations (3.7) to (3.9), second and further shell interactions are taken into account in the same way as for pure liquid, i.e., by the constants a and b. As should be easily verified, this is only permissible because random mixing is assumed.

From these relations and numerical tables of the integrals g, g_l, g_m it is possible, in principle, to calculate all excess properties of the solution. For example, the excess volume (2.6) is obtained from a graphical solution of Eq. (3.8) applied successively to the solution and each pure component. However, as Prigogine and Garikian[8] pointed out, the accuracy of such a calculation is rather low because of the form of Eq. (3.8).‡ We have actually calculated the excess volume of a solution with $\Lambda_{AA}/kT=10$, $\Lambda_{BB}/kT=17.143$, and $\Lambda_{AB}=(\Lambda_{AA}\cdot\Lambda_{BB})^{\frac{1}{2}}$. Using the tables of g, g_l, g_m given by Wentorf, Buehler, Hirschfelder, and Curtiss,[11] for $x_A=x_B=0.5$, weo btain $v_e/v^*=-0.10\pm0.05$.

For the excess free energy (3.7), the error in the calculation is greater than the quantity itself, so it is useless to quote the result here.

It may be concluded that the accuracy of the tables of g, g_l, and g_m available at present does not permit explicit calculations for the excess properties of solutions by this method.

Anyway, the "6–12" potential law, combined with $\Lambda_{AB}=(\Lambda_{AA}\cdot\Lambda_{BB})^{\frac{1}{2}}$ corresponds to a contraction on mixing, a result which will be discussed later by the aid of more simplified models.

4. HARMONIC OSCILLATOR MODEL[12]

We shall now consider two simplified models for the mean field which allow explicit calculations.

The potential within a cell (3.2) can be fairly approximated by the expansion[13]

$$[\omega(r)-\omega(0)]/kT=k_1y+k_2y^2+\cdots \quad (4.1)$$

with

$$k_1=(\Lambda/kT)(22\alpha^2-10\alpha),$$
$$k_2=(\Lambda/kT)(357\alpha^2+80\alpha). \quad (4.2)$$

Limiting (4.1) to the square term, we can integrate (2.1) by a series which shows at once the field of validity of the harmonic oscillator model.

The problem is to integrate

$$\Psi=2\pi a^3\int_0^\infty y^{\frac{1}{2}}\exp(-k_1y-k_2y^2)dy. \quad (4.3)$$

Let

$$k_1y=u \quad (4.4)$$

and expand

$$\exp(-k_2y^2)=\exp(-u^2l)$$

(with $l=k_2/k_1^2$) in powers of u^2l. This gives

$$\frac{\Psi}{2\pi a^3}=k_1^{-\frac{3}{2}}\int_0^\infty u^{\frac{1}{2}}\left(1-tu^2+\frac{t^2u^4}{2!}\cdots\right)\exp(-u)du$$

or, with $\Gamma(3/2)=0.88623$

$$\Psi=2\pi a^3k_1^{-\frac{3}{2}}\Gamma(3/2)\times[1-3.75t+29.53t^2-385t^3+\cdots]. \quad (4.5)$$

The first term of this series (4.5) is exactly the Ψ-value used in Prigogine and Garikian's paper (formula 1.5).[1]

The series (4.5) indicates the order of magnitude of the corrections resulting from anharmonicity of the movement of a particle in its cage. It can be reduced to its first term provided the rest of the series does not exceed 0.1. This only occurs at very low temperature. For example, when

$$\Lambda/kT=50;\quad 1-3.75t+29.5t^2=1.11.$$

These Λ/kT values correspond to the solid state, so that the harmonic oscillator model should afford a reasonable approximation for solid solutions.§

The consequences of the harmonic oscillator model together with the assumption $\Lambda_{AB}=(\Lambda_{AA}\cdot\Lambda_{BB})^{\frac{1}{2}}$ have been developed elsewhere.[1]

If second- and third-shell interactions are considered, i.e., if Eq. (3.6) is used, the thermodynamic properties are modified as follows: The equation of state for vanishing external pressure becomes, for pure liquid as for solutions

$$\frac{\Lambda}{kT}=\frac{77\alpha-20}{2\alpha(11\alpha-5)[(b/2a)-\alpha]a}. \quad (4.6)$$

For very low temperature where the model can be reasonably used, α tends to the limiting value $1.1914=b/2a$. If we equate α to 1.1914 everywhere in Eq. (4.6) except in $(b/2a)-\alpha$, Eq. (4.6) becomes

$$\alpha=1.1914-3.6737(kT/\Lambda). \quad (4.7)$$

The excess volume is now

$$\frac{v_e}{v^*}=\left(\frac{kT}{\Lambda}-x_A\frac{kT}{\Lambda_{AA}}-x_B\frac{kT}{\Lambda_{BB}}\right)\cdot1.4125. \quad (4.8)$$

For $\Lambda_{AB}=(\Lambda_{AA}\cdot\Lambda_{BB})^{\frac{1}{2}}$ it is negative, which corresponds

‡ The first two terms of (3.8) are much alike and moreover, the excess volume (2.6) is a difference between the α's obtained graphically from (3.8).

[12] See reference 3, Sec. 802.

[13] I. Prigogine, J. phys. et radium 4, 16 (1943).

§ We are most indebted to Professor E. A. Guggenheim who pointed out this restriction.

to a contraction on mixing. For the same value of Λ_{AB}, the excess free energy, energy, and entropy given by

$$\frac{F_e}{NkT}=+\frac{1}{2kT}[\Lambda(a\alpha^2-b\alpha)-x_A(a\alpha_A{}^2-b\alpha_A)\Lambda_{AA}-x_B(a\alpha_B{}^2-b\alpha_B)\Lambda_{BB}]+\tfrac{3}{4}lg\frac{\Lambda}{\Lambda_{AA}{}^{x_A}\Lambda_{BB}{}^{x_B}}+2lg\frac{\alpha}{\alpha_A{}^{x_A}\alpha_B{}^{x_B}}+\tfrac{3}{2}lg\frac{22\alpha-10}{(22\alpha_A-10)^{x_A}(22\alpha_B-10)^{x_B}}, \quad (4.9)$$

$$\frac{E_e}{NkT}=+\frac{1}{2kT}[\Lambda(a\alpha^2-b\alpha)-x_A(a\alpha_A{}^2-b\alpha_A)\Lambda_{AA}-x_B(a\alpha_B{}^2-b\alpha_B)\Lambda_{BB}], \quad (4.10)$$

$$\frac{S_e}{Nk}=-\tfrac{3}{4}lg\frac{\Lambda}{\Lambda_{AA}{}^{x_A}\Lambda_{BB}{}^{x_B}}-2lg\frac{\alpha}{\alpha_A{}^{x_A}\alpha_B{}^{x_B}}-\tfrac{3}{2}lg\frac{22\alpha-10}{(22\alpha_A-10)^{x_A}(22\alpha_B-10)^{x_B}}, \quad (4.11)$$

can be simplified by use of the equation of state and so become‖

$$\frac{F_e}{NkT}=\tfrac{1}{2}\cdot 1.435x_Ax_B\left[\left(\frac{\Lambda_{AA}}{kT}\right)^{\frac{1}{3}}-\left(\frac{\Lambda_{BB}}{kT}\right)^{\frac{1}{3}}\right]^2+\tfrac{3}{4}lg\frac{\Lambda}{\Lambda_{AA}{}^{x_A}\Lambda_{BB}{}^{x_B}}-4.84\frac{v_e}{v^*}, \quad (4.9')$$

$$\frac{E_e}{NkT}=\tfrac{1}{2}\cdot 1.435\cdot x_Ax_B\times\left[\left(\frac{\Lambda_{AA}}{kT}\right)^{\frac{1}{3}}-\left(\frac{\Lambda_{BB}}{kT}\right)^{\frac{1}{3}}\right]^2+4.83\frac{v_e}{v^*}, \quad (4.10')$$

$$\frac{S_e}{Nk}=-\tfrac{3}{4}lg\frac{\Lambda}{\Lambda_{AA}{}^{x_A}\Lambda_{BB}{}^{x_B}}+9.66\frac{v_e}{v^*}. \quad (4.11')$$

For the energy of mixing, the usual Hildebrand term is corrected here by a term connected with the change of volume due to the solution. This term is negative because of the sign of v_e/v^*. It means that the heat absorption predicted by the regular solution theory is partly compensated by an evolution of heat due to the contraction on mixing. On the other hand, the excess entropy term is entirely new. It consists of (a) a term connected with the change of frequency of each molecule due to the change of composition, and (b) a term determined by the excess volume on mixing.

The corrections introduced by this model are of the same order of magnitude as the deviations from ideality predicted by the crude law of regular solutions. Attention should be drawn to the fact that the excess entropy of mixing does not disappear at very low temperatures.

‖ The first order term $(\Lambda/kT)[3.67(kT/\Lambda)]^2$ which appears in $(\Lambda/kT)(a\alpha^2-b\alpha)$ has been overlooked in our first paper (see reference 1) and should be $4.75(kT/\Lambda)$ for the case there considered.

5. SMOOTHED POTENTIAL MODEL[12]

A. Pure Liquid

We shall now consider a potential well with vertical walls and a flat bottom with both depth and width depending on the composition of the solution.

For a pure liquid as for a solution Ψ is now given by

$$\Psi=\int_0^{\frac{1}{2}(a-D)}4\pi r^2dr=\frac{\pi}{6}(a-D)^3 \quad (5.1)$$

or

$$\Psi=(\pi/6)\gamma v[1-(v_0/v)^{\frac{1}{3}}]^3 \quad (5.2)$$

with

$$v_0=D^3/\gamma;\quad v=a^3/\gamma.$$

In this approximation, the law of forces does not appear explicitly in the integral (5.1), but just fixes its upper limit. The law of forces also determines the value of $\omega(0)$. Moreover, Ψ does no longer depend explicitly on Λ but only on the volume, a situation which is actually observed for the exact 6–12 treatment at sufficiently low dilatation.[14]

In the present case, we shall consider the 6–12 interaction law¶ which corresponds to the $\omega(0)$ given by Eq. (3.6). The radius of the cell $\frac{1}{2}(a-D)$ is defined as the distance at which the interaction energy of a pair of particles becomes zero.[15]

$$D=\frac{r^*}{2^{1/6}}\quad\text{or}\quad v_0=\frac{v^*}{2^{\frac{1}{2}}}. \quad (5.3)$$

The equation of state for the Ψ and $\omega(0)$ values given by Eqs. (5.2) and (3.6) becomes here, for vanishing external pressure,

$$\frac{\Lambda}{kT}=\frac{1}{2\alpha[1-(\alpha/2)^{1/6}][(b/2a)-\alpha]a}. \quad (5.4)$$

Equation (5.4) and the equation of state derived from the Lennard-Jones model (given by Wentorf, Buehler, Hirschfelder, and Curtiss)[11] have been simultaneously plotted, in Fig. 3.

The equation of state of the smoothed potential model is approximately the same as the exact "6–12" one, especially so in the region between $\Lambda/kT=20$ and

[14] See reference 8, p. 278, Fig. 5.

¶ We have also worked out the problem with the $6-\infty$ law as used in paper 8. The results are essentially the same as obtained here.

[15] See reference 8 for details.

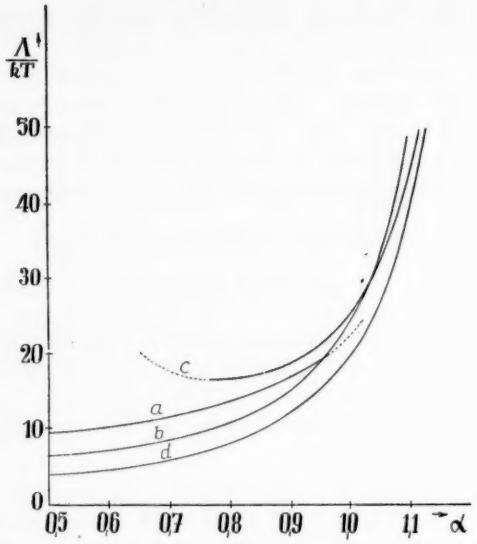

FIG. 3. Equations of state: (a) 6–12 exact model. (See reference 11.) (b) Smoothed potential model (5.4) (the approximate Eq. (5.6) has not been represented: it is almost coincident with (5.4); see Table I). (c) Harmonic oscillator model (4.6). (d) Approximate harmonic oscillator model (4.7).

$\Lambda/kT=15$, where we shall be using it. So we are justified in using the smoothed potential model as a good description for the liquid state.

Relation (5.4) can be easily simplified by a series expansion around the point $\alpha=0.95$ corresponding to $\Lambda/kT=18.5$. If we put

$$\alpha=0.95-\epsilon, \tag{5.5}$$

and if we make Eq. (5.4) linear with respect to ϵ, we obtain easily

$$\alpha=1.1764-4.1833kT/\Lambda. \tag{5.6}$$

Table I gives an idea of the approximation used.

B. Solutions

The preceding equation of state (5.6) can be applied to solutions as well, provided Λ is replaced by its value (2.8). From the simplified expression (5.6), the excess volume (2.6) becomes

$$\frac{v_e}{v^*}\simeq 1.639\left(\frac{kT}{\Lambda}-x_A\frac{kT}{\Lambda_{AA}}-x_B\frac{kT}{\Lambda_{BB}}\right) \tag{5.7}$$

when expanding (5.6) in powers of kT/Λ up to the first order.

The excess free energy, entropy, and heat of mixing appear to be

$$\frac{F_e}{NkT}=\frac{1}{2kT}[\Lambda(a\alpha^2-b\alpha)-x_A\Lambda_{AA}(a\alpha_A{}^2-b\alpha_A)-x_B\Lambda_{BB}(a\alpha_B{}^2-b\alpha_B)]+\tfrac{1}{2}lg\frac{\alpha}{\alpha_A{}^{x_A}\alpha_B{}^{x_B}}-3lg\frac{[1-(\alpha/2)^{1/6}]}{[1-(\alpha_A/2)^{1/6}]^{x_A}[1-(\alpha_B/2)^{1/6}]^{x_B}}, \tag{5.8}$$

$$\frac{E_e}{NkT}=\frac{1}{2kT}[\Lambda(a\alpha^2-b\alpha)-x_A\Lambda_{AA}(a\alpha_A{}^2-b\alpha_A)-x_B\Lambda_{BB}(a\alpha_B{}^2-b\alpha_B)], \tag{5.9}$$

$$\frac{S_e}{Nk}=-\tfrac{1}{2}lg\frac{\alpha}{\alpha_A{}^{x_A}\alpha_B{}^{x_B}}+3lg\frac{[1-(\alpha/2)^{1/6}]}{[1-(\alpha_A/2)^{1/6}]^{x_A}[1-(\alpha_B/2)^{1/6}]^{x_B}}. \tag{5.10}$$

Again, these expressions can be approximated by use of the simplified equation of state (5.6):

$$\frac{E_e}{NkT}=\tfrac{1}{2}\cdot 1.439\left(x_A\frac{\Lambda_{AA}}{kT}+x_B\frac{\Lambda_{BB}}{kT}-\frac{\Lambda}{kT}\right)+8.845\left(\frac{kT}{\Lambda}-x_A\frac{kT}{\Lambda_{AA}}-x_B\frac{kT}{\Lambda_{BB}}\right)$$

$$=\tfrac{1}{2}\cdot 1.439\left(x_A\frac{\Lambda_{AA}}{kT}+x_B\frac{\Lambda_{BB}}{kT}-\frac{\Lambda}{kT}\right)+5.396\frac{v_e}{v^*}, \tag{5.9'}$$

$$\frac{S_e}{Nk}=21.004\left(\frac{kT}{\Lambda}-x_A\frac{kT}{\Lambda_{AA}}-x_B\frac{kT}{\Lambda_{BB}}\right)$$

$$=12.813\frac{v_e}{v^*}. \tag{5.10'}$$

The heat of mixing (5.9) is here the same as for the harmonic oscillator model, a consequence of the choice of $\omega(0)$. Besides the energy difference between AA, BB, and AB couples, a new contribution is obtained, which is connected to the volume change on mixing (as shown by Eq. (5.9′)).

The excess entropy (5.10) is primarily due to volume change on mixing (see Eq. (5.10′)). The disappearance of the term in $lg\Lambda/\Lambda_{AA}{}^{x_A}\Lambda_{BB}{}^{x_B}$ of the corresponding expression (4.11) is explained by the fact that the Ψ functions do not depend explicitly here on the Λ's, but only on the volume.

6. DISCUSSION

So far, we have not discussed the sign or the shape of the actual excess property-curves here obtained. They all depend on the Λ_{AB} value which we will presently discuss. Let us first introduce some notations:

Combining Eqs. (2.7) and (2.8), we can write

$$\Lambda=x_A\Lambda_{AA}+x_B\Lambda_{BB}+2x_Ax_B\delta_{AB} \tag{6.1}$$

with

$$\delta_{AB}=\Lambda_{AB}-(\Lambda_{AA}+\Lambda_{BB})/2.$$

If θ and δ are defined by

$$\delta=(\Lambda_{BB}-\Lambda_{AA})/\Lambda_{AA},\qquad \theta=\delta_{AB}/\Lambda_{AA}, \tag{6.2}$$

all interactions can be "normalized" with respect to Λ_{AA}:

$$\Lambda_{BB}/\Lambda_{AA}=(1+\delta);\quad \Lambda/\Lambda_{AA}=(1+x_B\delta+2x_Ax_B\theta). \quad (6.3)$$

The excess properties can now be expressed in terms of δ and θ. The two parameter-curves so obtained present a large variety of shapes which correspond fairly well to experimental evidence as shown later.

For the sake of clarity, we have based the following discussion on the simplified expressions (5.7), (5.9′), and (5.10′) for the excess volume, the heat of mixing, and the excess entropy of mixing. For actual calculations, it is preferable to make use of the exact expressions (5.4), (2.6), (5.9), and (5.10) rather than (5.7), (5.9′), and (5.10′), which are series expansions. In order to simplify the discussion, we shall consider various characteristic values of δ and θ.

(α) *Dispersion Forces*

It has been shown by London that the upper limit for Λ_{AB} when caused by the dispersion forces is given by

$$\Lambda_{AB}^2=\Lambda_{AA}\Lambda_{BB} \quad \text{or} \quad \theta=-\delta^2/8; \quad (6.4)$$

we shall also consider the case where

$$\Lambda_{AB}=(\Lambda_{AA}+\Lambda_{BB})/2 \quad \text{or} \quad \theta=0. \quad (6.5)$$

(β) *Addition Compound*

We shall call "addition compound" the case where the interactions of pure substances Λ_{AA} and Λ_{BB} are of the same order of magnitude, while the interactions Λ_{AB} differ markedly from the preceding one (example: $CHCl_3-CH_3CO\,CH_3$). This corresponds to

$$\delta=0;\quad \theta\neq 0. \quad (6.6)$$

(γ) *Association in an Inert Solvent*

If the interactions are assumed to be much more important for a BB pair than for an AA or AB pair, we shall picture the case by speaking of association in an inert solvant by analogy with the situation for associated compounds (example: $CH_3OH-CCl_4$). We have here

$$\Lambda_{AA}=\Lambda_{AB} \quad \text{or} \quad \theta=-\delta/2. \quad (6.7)$$

(δ) *Association in an Active Solvent*

If the interactions AB are of the order of the interactions BB, while Λ_{AA} is much smaller, we shall call this case, by analogy, "association in an active solvent" (example: ethanol-dioxan)

$$\Lambda_{BB}=\Lambda_{AB};\quad \theta=+\delta/2. \quad (6.8)$$

The terminology in this classification might be rather misleading. It must be emphasized that the basic idea of the cell theory excludes such energy differences and anisotropic interactions as are usually dealt with in associated substances. The terminology here proposed only aims at expressing the relative values of θ and δ, both of which always have to remain small as compared to unity, in all cases here considered. The situation is best pictured by Fig. 4 where the interactions Λ_{AA}, Λ_{BB}, and Λ_{AB} have been represented on a relative scale.

The various excess properties (5.7), (5.9′), and (5.10′) become, when expressed in terms of θ and δ (expanding in powers of δ and θ up to the second order),

$$\frac{v_e}{v^*}=1.639\frac{kT}{\Lambda_{AA}}(-\delta^2-2\theta+4x_B\delta\theta+4x_Ax_B\theta^2)x_Ax_B, \quad (6.9)$$

$$\frac{E_e}{NkT}=x_Ax_B\Big(-1.439\frac{\Lambda_{AA}}{kT}\theta+8.845\frac{kT}{\Lambda_{AA}} \times[-\delta^2-2\theta+4x_B\delta\theta+4x_Ax_B\theta^2]\Big), \quad (6.10)$$

$$\frac{S_e}{Nk}=21.004\frac{kT}{\Lambda_{AA}}x_Ax_B \times(-\delta^2-2\theta+4x_B\delta\theta+4x_Ax_B\theta^2), \quad (6.11)$$

$$\frac{F_e}{NkT}=x_Ax_B\Big(-1.439\frac{\Lambda_{AA}}{kT}\theta-12.158\frac{kT}{\Lambda_{AA}} \times[-\delta^2-2\theta+4x_B\delta\theta+4x_Ax_B\theta^2]\Big). \quad (6.12)$$

As a consequence of Eq. (5.10′) or Eq. (6.11) there is, in each case, proportionality between excess entropy and excess volume. Therefore, in the following discussion we shall only examine the excess volume, the heat of mixing, and the excess free energy.

(α) *Dispersion Forces*

Let us put $\theta=0$ or $\theta=-\delta^2/8$ in Eqs. (6.9) to (6.12) and neglect third and higher terms in θ or δ. In these conditions, all excess properties begin with a δ^2 term. All the excess curves are parabolas. For the excess volume in both cases there is contraction on mixing since v_e/v^* is always negative. For the carbon tetrachloride-neopentane system (see Sec. 8 following) the excess volume is about $v_e/v^*=-0.0035$.

Whereas the excess volume is rather insensitive to the

TABLE I.

α	Λ/kT from Eq. (5.6)	Λ/kT from Eq. (5.4)
0.5	6.185	6.95
0.8	11.11	11.2
0.90	15.13	15.15
0.925	16.64	16.65
0.95	18.5	18.5
0.975	20.77	20.77
1.0	23.72	23.7
1.05	33.10	32.3
1.1	54.76	51.9

kind of mean chosen for Λ_{AB} (arithmetic or geometric), the heat of mixing and consequently the excess free energy depend strongly on it; when $\theta=0$ there is a small heat evolution corresponding to the contraction studied before; on the contrary, if $\theta=-\delta^2/8$ Hildebrand's term $(1.439/8)(\Lambda_{AA}/kT)\delta^2$ is determinative and gives rise to a considerable heat absorption. Numerically, if $\Lambda_{AA}/kT=15$

$$\frac{E_e}{NkT}\cdot\frac{1}{x_Ax_B}\cdot\frac{1}{\delta^2}=2.26 \quad \text{for} \quad \theta=-\delta^2/8,$$

$$\frac{E_e}{NkT}\cdot\frac{1}{x_Ax_B}\cdot\frac{1}{\delta^2}=-0.59 \quad \text{for} \quad \theta=0.$$

This change is very significant and should provide a valuable test for the validity of the "geometric mean law" usually assumed for the interaction AB.

In both cases, we are very far from a regular solution; if $\Lambda_{AA}/kT=15$, the entropy term is negative and amounts to about one third of the excess free energy when $\theta=-\delta^2/8$ and about twice the excess free energy when $\theta=0$.

(β) *Addition Compound*

When $\delta=0$ and $\theta\neq0$, again all curves are symmetrical in mole fraction. If θ is positive, v_e/v^* is negative: when the interaction AB is larger than ϵ_{AA}^* and ϵ_{BB}^* there is contraction on mixing as expected. When θ is negative, i.e., when ϵ_{AB}^* is abnormally small, there is expansion on mixing. The energy of mixing is negative when $\theta>0$, positive when $\theta<0$.

(γ) *Association in an Inert Solvent*

Figure 5 gives the general feature of the excess volume. It is fairly unsymmetrical and can even present positive and negative deviations. It corresponds to an expansion on mixing, the interaction AB being much smaller than the geometric mean. As for the excess energy or free energy, the curves remain nearly symmetrical, the second-order term being negligible as compared to the first-order term.

(δ) *Association in an Active Solvent*

As shown in Fig. 5, there is a considerable contraction on mixing, beginning with a first-order term in δ (the term in δ^2 is also negative). Again, for the excess energy and free energy, the curves are practically symmetrical in x and, except for second-order terms, these properties

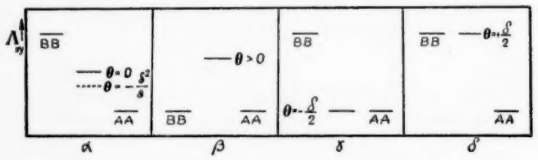

FIG. 4. Λ values in the various cases considered: (α) dispersion forces; (β) "addition compound"; (γ) "association in an inert solvent"; (δ) "association in an active solvent."

are equal to the corresponding expressions for the case γ, with minus in place of plus.

The preceding discussion indicates the relative importance of the various corrections introduced. In the most normal case ($\theta=-\delta^2/8$) the volume changes or entropy changes due to the change in the mean field contribute in a large proportion to the total deviation from ideality. In the other cases, the relative importance of the entropy term remains smaller (10–20 percent).

The dissymmetry of the excess-entropy and -volume for the association cases is in qualitative agreement with experimental evidence.[16]

7. PROPORTIONALITY RELATIONS

If the series expansions (6.9) to (6.12) for the various excess properties are compared, some regularities are observed: (a) As already noted, there is always proportionality between excess volume and excess entropy. (b) For the dispersion forces case, when $\theta=0$, there is proportionality also with the other excess properties, all being proportional to a δ^2 term and symmetrical in mole fraction. Neglecting higher order terms in δ, this also remains true for $\theta=-\delta^2/8$. (c) For the other cases, these proportionality relations are valid only if the second-order terms (δ^2 or θ^2) are negligible as compared to the first-order terms (δ or θ). As easily verified, this is not the case for the excess volume and excess entropy.

8. COMPARISON WITH EXPERIMENT

The assumptions underlying this treatment are very restrictive as regards the choice of experimental systems which could afford a reasonable test for the theory. The system carbon tetrachloride—neopentane is one of the easiest available, fullfilling these requirements.

The vapor pressure and density of this system have been measured at 0°C.** Within the limits of errors, experimental and calculated curves are in good agreement. The "geometric mean law" $\theta=-\delta^2/8$ is roughly obeyed, although there is a slight tendency for ϵ_{AB}^* to be less favorable than this value.

Full details on this question will be published later together with the heat of mixing measurements now in progress.

9. COMPARISON WITH THE THEORY OF CONFORMAL SOLUTIONS

Longuet-Higgins[17] has recently developed another approach to the problem of statistical mechanics of solutions pertaining to the same subject. Using the theory of corresponding states, Longuet-Higgins' treatment is more general in a way, because it does not make any assumption on the structure of the system (no quasi-lattice) and therefore can be applied to liquids and

[16] See for instance, R. Haase, Z. Elektrochem. **55**, 29 (1951).

** The experimental part has been performed by Dr. A. Desmyter.

[17] Longuet-Higgins, Proc. Roy. Soc. (London) **A205**, 247 (1951).

gases as well; on the other hand, it is limited to first-order terms in $(f-1)$.††

The present theory is not restricted to first-order perturbations. Therefore it gives in the simple cases considered here the limitation of the L-H theory. The dispersion forces case, with contraction and heat absorption on mixing, can never be accounted for in the L-H treatment because all excess properties depend here on squared or higher terms. This effect is not at all negligible (see the carbon tetrachloride-neopentane system), and the more important, the higher the δ-value.

Even when both first- and second-order terms contribute to the excess properties, the latter are not necessarily negligible. For example, let us consider the contribution of the δ^2 term in the excess volume of an associated system in an inert solvent,

$$v_e/v^*=1.639(kT/\Lambda_{AA})x_Ax_B(\delta-\delta^2[1+x_B+x_B{}^2]).$$

If $\delta=0.1$, the term between brackets $[\delta-\delta(1+x_B+x_B{}^2)]$ for $x_B=0.5$ is equal to $0.1-0.0175=0.0825$ in place of 0.1, if the δ^2 term is dropped. If $\delta=0.4$, $\delta-\delta^2(1+x_B+x_B{}^2)=0.12$ in place of 0.4. The L-H theory is thus restricted to very particular cases and even the simplest of these cannot be accounted for by this theory.

Apart from these differences, our theory reduces to L-H expressions whenever the first-order terms only are considered. In this approximation the excess free energy (6.12) becomes here

$$\frac{F_e}{RT}=x_Ax_B2\theta\left(-0.719\frac{\Lambda_{AA}}{kT}+12.158\frac{kT}{\Lambda_{AA}}\right). \quad (9.1)$$

This expression is to be compared to the L-H one

$$\frac{F_e}{RT}=x_Ax_Bd_{AB}\frac{E_A}{RT} \quad (9.2)$$

$$=x_Ax_B2\theta\left(-0.719\frac{\Lambda_{AA}}{kT}+8.845\frac{kT}{\Lambda_{AA}}\right). \quad (9.2')‡‡$$

†† L-H's $f-1$ is equal to our δ; d_{rs} is equal to our θ if A is chosen as the reference constituent.

‡‡ It should be noted that, in Longuet-Higgins' theory, $d_{AB}E_A$ corresponds to the energy difference between solution and pure substances, all at the same volume v_A of the reference constituent. This is the origin of (9.2′) which is equal to

$$\frac{E_{AB}(v_A)-x_AE_{AA}(v_A)-x_BE_{BB}(v_A)}{RT}$$

or

$$\frac{1}{2}\left(\frac{\Lambda}{kT}-x_A\frac{\Lambda_{AA}}{kT}-x_B\frac{\Lambda_{BB}}{kT}\right)(a\alpha_A{}^2-b\alpha_A).$$

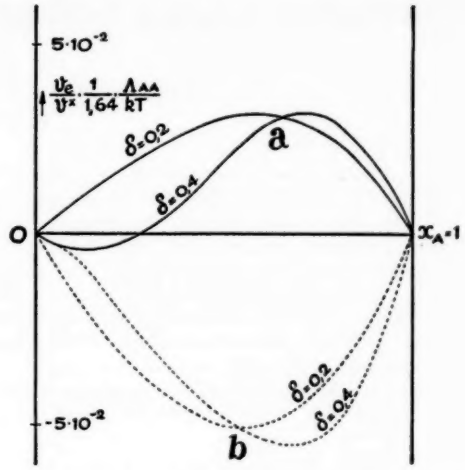

FIG. 5. Excess volume for the "association" cases (a) in an inert solvent and (b) in an active solvent.

The difference between the second terms in the right-hand side of Eqs. (9.2′) and (9.1) is the result of the approximation involved in the series expansion for the excess entropy; since our expressions (5.8) to (5.10) are implicit functions of the interaction parameters, it is necessary to make use of the equation of state and, for the entropy term, of series expansions already considered. If this expansion is pursued up to the second order in kT/Λ, the term $12.158kT/\Lambda_{AA}$ is to be multiplied by $[1-5.968(kT/\Lambda_{AA})]$. So, for $(\Lambda/kT)\simeq 20$, (9.2′) and (9.1) become equal.

We are indebted to Professor E. A. Guggenheim, who made a number of most valuable suggestions concerning the presentation of this paper.

A Study of Selection Rules for Vibrational Spectra of Complex Crystals

THOMAS H. WALNUT
Institute for the Study of Metals, University of Chicago, Chicago, Illinois
(Received August 20, 1951)

Relations are obtained for the expression of the dipole moment and polarizability matrices for a particular transition in a crystal, in terms of corresponding expressions for molecular or ionic groups within the crystal. The results show that, to the degree of approximation used (quadratic terms in the dipole moment or polarizability expansion and cubic terms in the potential energy), the only cause for the appearance of bands which would be forbidden for a given uncoupled complex ionic or molecular group is the alteration of the normal coordinates of these groups by vibrations of neighboring groups. It is also shown that the bands of fully allowed first overtones and binary combinations of frequencies that are not degenerate or near-degenerate in a unit cell have a shape that is approximately given from the distributions of frequencies that arise from lattice coupling.

As an incidental result, the dipole moment matrix elements for the first overtones and binary combinations arising from the cubic terms in the potential energy are given explicitly.

INTRODUCTION

IN order to interpret an observed infrared or Raman spectrum of a crystalline solid, the selection rules must be known. Selection rules for crystals have been derived by Hornig[1] and by Winston and Halford[2] from symmetry considerations alone.

In this paper a further investigation will be made of the relationship between the selection rules of molecular or ionic groups within a crystal and those of the entire crystal. This is achieved by expressing the dipole moment matrix elements of the crystal in terms of those derived from wave functions and normal coordinates of groups of neighboring atoms within a unit cell where coupling with the rest of the crystal is neglected (hereafter called an *uncoupled subcell*).

The explicit assumptions used are that the dipole moment of the crystal can be expressed as the power series,

$$\mu=\mu_0+\sum_p \mu_p r_p+\sum_{pp'}\frac{\mu_{pp'}}{2}r_p r_{p'}\cdots, \tag{1}$$

and that the expansion of the potential energy,

$$V=\sum_K \tfrac{1}{2}\lambda_K Q_K' Q_K'^*+\sum_{pp'p''}\frac{c_{pp'p''}}{6}r_p r_{p'} r_{p''}\cdots, \tag{2}$$

is valid. Here r_p is a normal coordinate of an uncoupled subcell, Q_K' and $Q_K'^*$ represent, respectively, the K-th normal coordinate and its complex conjugate,[3] and λ_K and $c_{pp'p''}$ are constants. When these equations are written in terms of the crystal normal coordinates, the expressions obtained represent standard assumptions in infrared spectroscopy.

INTERACTION WITH RADIATION

The way in which a particular physical system interacts with radiation is determined from the matrix elements of the form,

$$[\mu]_{mn}\equiv\int \Phi_m \mu \Phi_n d\tau, \tag{3}$$

where Φ_m is the wave function of the system in the m-th quantum state and Φ_n is the wave function of the system in the n-th state. This expression will be used to determine the relationship between the matrix elements for the normal coordinates of the entire crystal and those for the uncoupled subcell normal coordinates.

The wave function of the entire crystal can be represented as follows:

$$\Phi_m=\sum_n a_{mn}\prod_j \psi_{jn_j}(Q_j), \tag{4}$$

where a_{mn} is a constant and $\psi_{jn_j(Q_j)}$ is the harmonic oscillator wave function in the state n_j corresponding to a normal coordinate Q_j. However, it can be approximated by

$$\Phi_m\approx\prod_j \psi_{jm_j}(Q_j). \tag{5}$$

In a similar way, the wave functions, ϕ_m, for an uncoupled subcell can be found. Thus

$$\phi_m=\sum_n b_{mn}\prod_j \psi_{jn_j}(r_j)\approx\prod_j \psi_{jm_j}(r_j). \tag{6}$$

In Eq. (2), the normal coordinates of the crystal that were used were, in general, complex. These coordinates are difficult to use in the specifications of the harmonic oscillator eigenfunctions. Consequently, for this discussion, linear combinations of degenerate pairs of complex normal coordinates will be formed so that a set of real normal coordinates are obtained. Thus the coordinates,

$$Q_K=(Q_K'+Q_K'^*)/2 \quad K\leq K^*, \tag{7}$$

and

$$Q_K=(Q_K'-Q_K'^*)/2i \quad K>K^*,$$

are obtained, where K^* is the subscript of Q_K' such that

$$Q_{K^*}'=Q_K'^*. \tag{8}$$

[1] D. F. Hornig, J. Chem. Phys. **16**, 1063 (1948).
[2] H. Winston and R. S. Halford, J. Chem. Phys. **17**, 607 (1949).
[3] F. Seitz, *Modern Theory of Solids* (McGraw-Hill Book Company, Inc., New York, 1940), pp. 131–132.

With these new coordinates the subcell normal coordinates can be expressed as

$$r_p=\sum_K W_{pK}Q_K, \tag{9}$$

where

$$W_{pK}=U_{\mathbf{k}pK_\mathbf{k}}N^{-\frac{1}{2}}\cos 2\pi(l_1k_1/N_1+l_2k_2/N_2+l_3k_3/N_3), \quad K\leq K^* \tag{10}$$

and

$$W_{pK}=U_{\mathbf{k}pK_\mathbf{k}}N^{-\frac{1}{2}}\sin 2\pi(l_1k_1/N_1+l_2k_2/N_2+l_3k_3/N_3), \quad K>K^*. \tag{11}$$

Here the symbol $U_{\mathbf{k}pK_\mathbf{k}}$ denotes an element of a submatrix $\mathbf{U}_\mathbf{k}$ which is associated with the uncoupled subcell normal coordinate r_p and the unit cell normal coordinate of subscript K having the wave number vector $\mathbf{k}$ whose components are the integers, k_1, k_2, and k_3. N_1, N_2, and N_3 are large integers describing the periodicity of the Born-von Karman lattice and N is the product $N_1N_2N_3$. Physically, the matrix $\mathbf{U}_\mathbf{k}$ represents the changes in the uncoupled subcell normal coordinates, r_p, caused by the motions of neighboring uncoupled subcells.

The dipole moment, μ, can now be expressed in terms of the crystal normal coordinates as follows:

$$\mu=\mu_0+\sum_p\sum_K \mu_pW_{pK}Q_K+\sum_{pp'}\sum_{KK'}\frac{\mu_{pp'}}{2}W_{pK}W_{p'K'}Q_KQ_{K'}\cdots \tag{12}$$

or, expressing it directly in terms of Q_K,

$$\mu=\mu_0+\sum_K \mu_KQ_K+\sum_{KK'}\frac{\mu_{KK'}}{2}Q_KQ_{K'}\cdots. \tag{13}$$

Thus,

$$\mu_K=\sum_p \mu_pW_{pK}, \tag{14}$$

and

$$\mu_{KK'}=\sum_{pp'} \mu_{pp'}W_{pK}W_{p'K'}. \tag{15}$$

FUNDAMENTAL ABSORPTION

The above equations will now be used to express the dipole moment matrix for a fundamental absorption of the crystal in terms of fundamental absorptions of the uncoupled subcells. The expression for the dipole moment matrix for a fundamental absorption is

$$[\mu]_{mn}=\int\sum_K \mu_KQ_K\prod_i \psi_{im_i}(Q_i)\psi_{in_i}(Q_i)dQ_i'. \tag{16}$$

On carrying out the integration it is found[4] that $[\mu]_{mn}$ is nonvanishing only when

$$n=m_1\cdots m_j\pm 1\cdots m_{N'},$$

where

$$m=m_1\cdots m_j\cdots m_{N'},$$

(N' being the total number of normal modes of the crystal) in which case

$$[\mu]_{m_jm_j+1}=(\mu_j/2\pi)((m_j+1)h/2\nu_j)^{\frac{1}{2}}, \tag{17a}$$

and

$$[\mu]_{m_jm_j-1}=(\mu_j/2\pi)(m_jh/2\nu_j)^{\frac{1}{2}}, \tag{17b}$$

where ν_j is the frequency associated with the normal coordinate Q_j.

Hornig[1] has shown that the coefficient μ_K is different from zero only for the vibrations of the crystal which are totally symmetric with respect to translation. These are the normal coordinates for which $K=K^*$.

In an analogous way the matrix element for a fundamental absorption of an uncoupled subcell is

$$[\mu]^{(r)}_{m_pm_p+1}=(\mu_p/2\pi)((m_p+1)h/2\nu_p)^{\frac{1}{2}} \tag{18}$$

where ν_p is the frequency corresponding to the p-th subcell normal coordinate.

Equation (17a) can be expressed in terms of the subcell normal coordinate dipole moment coefficients, using Eq. (14), as

$$[\mu]_{m_jm_j+1}=\frac{1}{2\pi}\left(\frac{(m_j+1)h}{2\nu_j}\right)^{\frac{1}{2}}\sum_p \mu_pW_{pj}. \tag{19}$$

This can be written from Eq. (18) as

$$[\mu]_{m_jm_j+1}=\sum_p [\mu]^{(r)}_{m_pm_p+1}W_{pj}(\nu_p/\nu_j)^{\frac{1}{2}} \tag{20}$$

when $m_p=m_j$ is assumed.

This equation can usually be further simplified by considering the relative magnitudes of the elements W_{pj}. These elements are obtained from the equations of motion of the entire crystal.

We have an equation,

$$\ddot{r}_p=\lambda_p{}^0r_p, \tag{21}$$

for each of the uncoupled subcell normal coordinates, r_p, when coupling between neighboring molecular or ionic groups is neglected. On introducing the coupling constants, Eq. (21) becomes

$$\ddot{r}_p=\lambda_p{}^0r_p+\sum_{p'} h_{pp'}W_{p'j}. \tag{22}$$

The determination of the normal coordinates, Q_j, resolves into the familiar problem of solving a secular determinant. Formally, this problem can be expressed as the solution of the set of equations (one for each value of p) represented by

$$\lambda_jW_{pj}=\lambda_p{}^0W_{pj}+\sum_{p'} h_{pp'}W_{p'j}. \tag{23}$$

In cases of molecular and ionic crystals the coupling elements $h_{pp'}$ are small compared to the zero order elements $\lambda_p{}^0$. This should also be usually true for a suitable choice of an uncoupled subcell in other types of crystals. As a result, perturbation theory should be

[4] See, for example, Eyring, Walter, and Kimball, *Quantum Chemistry* (John Wiley and Sons, Inc., New York, 1944), p. 117 ff.

applicable.[5] Thus from the first-order perturbation theory some of the elements W_{pj} connecting coordinates Q_j and r_p associated with equal or nearly equal frequencies, should be much larger than any of the elements where this is not the case. Therefore Eq. (20) can be written as

$$[\mu]_{m_j m_j+1} \approx \sum_p{}' [\mu]^{(r)}_{m_p m_p+1} W_{pj} \tag{24}$$

where the symbol $\sum_p{}'$ represents a sum over all values of p where $\nu_p \approx \nu_j$. In the case of one nondegenerate normal coordinate of a given type per unit cell this equation reduces to

$$[\mu]_{m_j m_j+1} \approx N^{\frac{1}{2}} [\mu]^{(r)}_{m_p m_p+1} \tag{25}$$

when Q_j is totally symmetric with respect to translation. Otherwise it vanishes.

ABSORPTION RESULTING FROM ELECTRICAL ANHARMONICITY

The third term in the dipole moment expansion, Eq. (12), gives rise to first overtones and binary combinations. The wave functions used in this approximation are the same harmonic oscillator functions as were used for fundamental absorption. Thus a dipole moment matrix element arising from the electrical anharmonicity can be written

$$[\mu]_{mn} = \int \sum_{KK'} \frac{\mu_{KK'}}{2} Q_K Q_{K'} \prod_i \psi_{im_i}(Q_i) \psi_{in_i}(Q_i) dQ_i. \tag{26}$$

By an argument analogous to that for fundamentals, it is found that the set of values of m and n where the integral does not vanish are those where

$$n = m_1 \cdots m_j \pm 1 \cdots m_{j'} \pm 1 \cdots m_{N'}$$

or

$$n = m_1 \cdots m_j \pm 2 \cdots m_{N'}. \tag{27}$$

On carrying out the integration the following matrix elements that are involved in absorption are found to be

$$[\mu]_{m_j m_j+1 m_{j'} m_{j'}+1} = \mu_{jj'} (h/4\pi^2)((m_j+1)(m_{j'}+1)/4\nu_j\nu_{j'})^{\frac{1}{2}}, \tag{28a}$$

$$[\mu]_{m_j m_j+1 m_{j'} m_{j'}-1} = \mu_{jj'} (h/4\pi^2)((m_j+1)m_{j'}/4\nu_j\nu_{j'})^{\frac{1}{2}}, \tag{28b}$$

$$[\mu]_{m_j m_j+2} = (\mu_{jj}/2)(h/4\pi^2)((m_j+1)(m_j+2)/4\nu_j^2)^{\frac{1}{2}}. \tag{28c}$$

In an analogous way the matrix elements,

$$[\mu]^{(r)}_{m_p m_p+1 m_{p'} m_{p'}+1} = \mu_{pp'} (h/4\pi^2)((m_p+1)(m_{p'}+1)/4\nu_p\nu_{p'})^{\frac{1}{2}}, \tag{29a}$$

$$[\mu]^{(r)}_{m_p m_p+1 m_{p'} m_{p'}-1} = \mu_{pp'} (h/4\pi^2)((m_p+1)(m_{p'})/4\nu_p\nu_{p'})^{\frac{1}{2}}, \tag{29b}$$

$$[\mu]^{(r)}_{m_p m_p+2} = (\mu_{pp}/2)(h/4\pi^2)((m_p+1)(m_p+2)/4\nu_p^2)^{\frac{1}{2}} \tag{29c}$$

are obtained for the uncoupled subcells.

To find the dipole moment matrix elements for the crystal normal coordinates in terms of those for the subcell coordinates, we shall utilize expression (15) giving $\mu_{KK'}$ in terms of $\mu_{pp'}$, and write, by analogy with Eq. (20) for fundamentals, the equations,

$$[\mu]_{m_j m_j+1,\, m_{j'} m_{j'} \pm 1} = \sum_{pp'} [\mu]^{(r)}_{m_p m_p+1,\, m_{p'} m_{p'} \pm 1} W_{pj} W_{pj'} \left(\frac{\nu_p \nu_{p'}}{\nu_j \nu_{j'}}\right)^{\frac{1}{2}} + \sum_p [\mu]^{(r)}_{m_p m_p+2} \left(\frac{m_{j'}+1}{m_p+2} \frac{\nu_p^2}{\nu_j \nu_{j'}}\right)^{\frac{1}{2}} W_{pj} W_{pj'}, \tag{30a}$$

and

$$[\mu]_{m_j m_j+2} = \sum_p [\mu]^{(r)}_{m_p m_p+2} W_{pj} W_{pj} \nu_p/\nu_j + \sum_{pp',\, p \neq p'} [\mu]^{(r)}_{m_p m_p+1 m_{p'} m_{p'}+1} W_{pj} W_{p'j} \times \left(\frac{m_j+2}{m_{p'}+1} \frac{\nu_p \nu_{p'}}{\nu_j^2}\right)^{\frac{1}{2}}, \tag{30b}$$

where $m_p = m_j$ and $m_{p'} = m_{j'}$ in both cases.

As stated before, an element W_{pj}, connecting the coordinates Q_j and r_p, is usually very small when the frequencies associated with these coordinates are not equal or nearly equal. Consequently, Eqs. (30a) and (30b) can be approximated by

$$[\mu]_{m_j m_j+1 m_{j'} m_{j'} \pm 1} \approx \sum_{pp'}{}'' [\mu]^{(r)}_{m_p m_p+1 m_{p'} \pm 1} W_{pj} W_{p'j'} \tag{31a}$$

and

$$[\mu]_{m_j m_j+2} \approx \sum_p{}'' [\mu]^{(r)}_{m_p m_p+2} W_{pj} W_{pj} + \sum_{pp',\, p \neq p'}{}'' [\mu]^{(r)}_{m_p m_p+1 m_{p'} m_{p'}+1} \times \left(\frac{m_j+2}{m_p+1}\right)^{\frac{1}{2}} W_{pj} W_{p'j}. \tag{31b}$$

The symbol $\sum''$ represents a sum over all values of p where $\nu_p \approx \nu_j$ and $\nu_{p'} \approx \nu_{j'}$. In the first equation ν_p has a widely differing value from $\nu_{p'}$; in the second, $\nu_{p'} \approx \nu_{p}$.

In the case of no degeneracies or near degeneracies corresponding to Q_j or $Q_{j'}$ other than the one arising

[5] The application of perturbation theory analogous to that of quantum mechanics has been used by R. Mecke, Z. Physik **104**, 291 (1937); and T. Y. Wu, *Vibration Spectra and Structure of Polyatomic Molecules* (National University of Peking, 1939), p. 15 to determine the frequency shifts in molecular spectra.

from translational symmetry,

$$[\mu]_{m_jm_j+1m_{j'}m_{j'}\pm1} + [\mu]_{m_j{}^*m_j{}^*+1m_{j'}{}^*m_{j'}{}^*\pm1}(1-\delta(jj^*)\delta(j'j'^*)) \approx [\mu]^{(r)}_{m_pm_p+1m_{p'}m_{p'}\pm1} \quad (32a)$$

and

$$[\mu]_{m_jm_j+2} + [\mu]_{m_j{}^*m_j{}^*+2}(1-\delta(jj^*)\delta(j'j'^*)) \approx [\mu]^{(r)}_{m_pm_p+2} \quad (32b)$$

when Q_j and $Q_{j'}$ have the same translational symmetry and phase.

When the foregoing conditions hold, Eqs. (32a) and (32b) mean that *the shape of a band, that can be described as a combination band between two normal vibrations of an uncoupled subcell, is given by the distribution of the sum of frequencies of crystal normal coordinates that have the same translational symmetry and phase and correspond to the two normal vibrations of the combination band. Thus the shape of a first overtone is given by the distribution of twice the frequencies of the corresponding fundamental vibrations.*[6]

It should be borne in mind that higher order combinations with acoustical lattice modes may obscure the structure described above. Further theoretical and experimental investigation should be necessary on this point.

MECHANICAL ANHARMONICITY

First overtones and binary combinations also arise from the anharmonic terms in the potential energy function. To compute these effects we will utilize the general wave function of the crystal as given in Eq. (4).

When the first-order terms in the dipole moment expansion, Eq. (12), are used the dipole moment matrix $[\mu]_{mn'}$ element is given by

$$[\mu]_{mm'} = \int \sum_n a_{mn}\Big(\prod_i \psi_{in_i}(Q_i)\Big) \sum_K \mu_K Q_K \times \sum_{n'} a_{m'n'}\Big(\prod_i \psi_{in'_i}(Q_i)\Big)dQ_i. \quad (33)$$

This reduces to the expression,

$$[\mu]_{mm'} = \sum_n \sum_{n'} \sum_K a_{mn}a_{m'n'}\mu_K[Q_K]_{nn'}, \quad (34)$$

where

$$[Q_K]_{nn'} = \int Q_K \prod_i \psi_{in_i}(Q_i)\psi_{in'_i}(Q_i)dQ_i. \quad (35)$$

The next step is to determine the values of the coefficients a_{mn}. Since the correct wave functions are close to those of a harmonic oscillator, $a_{mn}\approx 1$ when $m=n$ and, from first-order perturbation theory,

$$a_{mn} = [\Delta V]_{mn}/h(\nu_m-\nu_n), \quad m\neq n \quad (36)$$

where ΔV is the cubic part of the potential function, as expressed in Eq. (2). To compute a coefficient a_{mn}, this expression must be written in terms of the normal coordinates of the crystal as

$$\Delta V = \sum_{KK'K''} \tfrac{1}{6}k_{KK'K''}Q_KQ_{K'}Q_{K''}. \quad (37)$$

From Eq. (37), a_{mn} becomes

$$a_{mn} \approx \frac{1}{h(\nu_m-\nu_n)} \sum_{KK'K''} \tfrac{1}{6}k_{KK'K''}[Q_KQ_{K'}Q_{K''}]_{mn} \quad (38)$$

where

$$[Q_KQ_{K'}Q_{K''}]_{mn} \equiv \int Q_KQ_{K'}Q_{K''}\prod_i \psi_{im_i}(Q_i)\psi_{in_i}(Q_i)dQ_i. \quad (39)$$

Since the coefficients of the form a_{mm} are much larger than any of the others, Eq. (34) can be written

$$[\mu]_{mm'} = \sum_n \sum_K a_{mn}\mu_K[Q_K]_{nm'} + \sum_{n'} \sum_K a_{m'n'}\mu_K[Q_K]_{mn'}. \quad (40)$$

Combining (38) and (40) we obtain the expression,

$$[\mu]_{mm'} = \sum_n \sum_{K_1} \sum_{KK'K''} \frac{1}{h(\nu_m-\nu_n)} \times \tfrac{1}{6}k_{KK'K''}[Q_KQ_{K'}Q_{K''}]_{mn}\mu_{K_1}[Q_{K_1}]_{nm'} + \sum_{n'} \sum_{K_1} \sum_{KK'K''} \frac{1}{h(\nu_m-\nu_n)} \times \tfrac{1}{6}k_{KK'K''}[Q_KQ_{K'}Q_{K''}]_{m'n'}\mu_{K_1}[Q_{K_1}]_{mn'}. \quad (41)$$

When the values of the matrix elements $[Q_KQ_{K'}Q_{K''}]_{mn}$ and $[Q_{K_1}]_{nm'}$, are substituted into Eq. (41), the following expressions are found for the dipole moment matrix:

$$[\mu]_{m_jm_j+1m_{j'}m_{j'}+1} = \sum_{K_0} \frac{\mu_{K_0}k_{jj'K_0}h}{32\pi^4} \times \left(\frac{(m_j+1)(m_{j'}+1)}{\nu_j\nu_{j'}}\right)^{\frac{1}{2}} \Big/ (\nu_{K_0}{}^2-(\nu_j+\nu_{j'})^2), \quad (42a)$$

$$[\mu]_{m_jm_j+2} = \sum_{K_0} \frac{\mu_{K_0}k_{jj'K_0}}{64\pi^4} \times \left(\frac{(m_j+1)(m_j+2)}{\nu_j{}^2}\right)^{\frac{1}{2}} \Big/ (\nu_{K_0}{}^2-4\nu_j{}^2). \quad (42b)$$

[6] These conclusions have previously been derived specifically for the cases of rock salt and diamond, respectively, by Born and Bradburn, Proc. Roy. Soc. (London) **A188**, 181 (1946); and by H. C. Smith, Trans. Roy. Soc. (London) **240A** (1946).

The symbol K_0 in (42ab) represents the subscripts of all those coordinates which are totally symmetric with respect to translation. These relations may be summed up in the expression

$$[\mu]_{mm'}=\sum_{K_0}\mu_{K_0}k_{jj'K_0}A(m_j\nu_j m_{j'}\nu_{j'}\nu_{K_0}). \quad (43)$$

In a similar way we can write the corresponding expression for the uncoupled subcells as

$$[\mu]^{(r)}_{mm'}=\sum_p \mu_p c_{ii'p}A(m_i\nu_i m_{i'}\nu_{i'}\nu_p). \quad (44)$$

We are now in a position to express the crystal dipole moment matrix elements in terms of those of the uncoupled subcells. To do this, the coefficients $k_{KK'K''}$ of Eq. (37) must be expressed in terms of the corresponding coefficients for the subcell coordinates $c_{pp'p''}$. By expressing the coordinates $r_p, r_{p'}r_{p''}$, of Eq. (2) in terms of the normal coordinates $Q_KQ_{K'}Q_{K''}$ using Eq. (9), and then comparing the result with Eq. (37), we obtain the equation,

$$k_{KK'K''}=\sum_{pp'p''} c_{pp'p''}W_{pK}W_{p'K'}W_{p''K''}. \quad (45)$$

On substituting this and (14) in (43), we obtain

$$[\mu]_{mm'}=\sum_{K_0}\sum_{p_1}\mu_{p_1}W_{p_1K_0}$$

$$\times\sum_{pp'p''} c_{pp'p''}W_{pj}W_{p'j'}W_{p''K_0}A(m_j\nu_j m_{j'}\nu_{j'}\nu_{K_0}). \quad (46)$$

Since the elements W_{pj} are small except when connecting coordinates of like frequency,

$$[\mu]_{mm'}\approx\sum''_{p_1pp'p''}\mu_{p_1}Z_{p_1p''}c_{pp'p''}$$

$$\times W_{pj}W_{p'j'}W_{p''K_0}A(m_j\nu_j m_{j'}\nu_{j'}\nu_{p''}) \quad (47)$$

where

$$Z_{p_1p''}\equiv\sum_{K_0}W_{p_1K_0}W_{p''K_0}. \quad (48)$$

The matrix $[W_{pj}]$ converts one normalized set of orthogonal coordinates into another; hence, it must be unitary. Therefore,

$$Z_{p_1p''}=\delta(p_1p''). \quad (49)$$

From this,

$$[\mu]_{mm'}\approx\sum''_{p_1pp'}\mu_{p_1}c_{pp'p_1}W_{pj}W_{p'j'}A(m_p\nu_p m_{p'}\nu_{p'}\nu_{p_1}). \quad (50)$$

Combining (44) and (50), we obtain Eqs. (31a) and (31b). We see that electrical and mechanical anharmonicity lead to approximately the same relations.

These relations for mechanical anharmonicity should not be expected to hold when first-order perturbation theory approximations are no longer valid, i.e., combinations with acoustical lattice vibrations and strong Fermi resonance.

CONCLUSIONS

The mathematical results of the previous sections will now be explained in physical terms. To do this a brief diversion will be made into the dynamics of crystal lattices. From the perturbation method described it is found that the frequency spectrum in the harmonic oscillator approximation is a series of bands, which arise from perturbation of the normal vibrations of the uncoupled subcells by coupling forces between neighboring molecular or ionic groups.

In describing the spectrum of a crystal it is customary to speak of absorption bands of various groups. The discussion of fundamental absorption (*cf* Eqs. (23), (24), and (25)) shows that this point of view is valid in cases where the energy levels of the uncoupled subcells are far apart. For bands due to anharmonic effects this description is subject to the same limitations as for fundamentals. It is quite accurate to describe observed bands of crystals as overtones and combinations of the appropriate vibrations of uncoupled subcells when the component frequencies are not close to any other subcell frequency. The mathematical statement of this is in Eqs. (32a) and (32b). When there are degeneracies or near degeneracies in the subcell frequencies this description loses accuracy. It still can be used but with the additional complication that intensity must be described as being borrowed from one band by another. This can be seen to arise from Eqs. (31a) and (31b).

An interesting example of these effects is the case where the dipole moments matrix element of an uncoupled subcell vanishes because of its site symmetry. As Winston and Halford[2] showed, the site symmetry causes a negligibly small number of the corresponding crystal dipole moment matrix elements to vanish. However, they can only be nonvanishing due to the harmonic borrowing described. Thus an overtone or combination that should be forbidden by the site symmetry has very weak intensity when the component uncoupled subcell frequencies are far from any others. When the component frequencies are degenerate or near degenerate, overtones and combinations that should be forbidden may appear with moderate intensity as a result of borrowing from bands that are allowed under the site symmetry.

The foregoing statements have only been proved for first overtones and binary combinations bands, but are probably true for higher combinations.

These conclusions are equally well adapted to Raman spectra. The only change that must be made is to replace the vectors μ, μ_p, and $\mu_{pp'}$ by the polarizability tensors α, α_p, $\alpha_{pp'}$.

The Structure of the Tetrachloroethylene Molecule

I. L. KARLE AND J. KARLE
U. S. Naval Research Laboratory, Washington, D. C.
(Received September 6, 1951)

The equilibrium distances and average amplitudes of vibration have been determined for the molecule C_2Cl_4 by the analysis of quantitative electron diffraction data. The results are listed in Table II.

PREVIOUS electron diffraction investigations of tetrachloroethylene[1-3] were based on the visual method, and it was felt that more reliable values for the molecular parameters could be obtained with quantitative scattering data. In addition, evaluation of the average vibrational amplitudes between pairs of atoms may be obtained from quantitative data. These average amplitudes may also be derived from spectroscopic data with the use of some assumed force model.[4] Disagreements which occur for the assignment of some of the fundamental frequencies in C_2Cl_4[5] could conceivably be resolved by making spectroscopic computations of the average vibrational amplitudes and by comparing these values to the experimental electron diffraction results. We are planning to perform such computations.

The apparatus and the methods used in obtaining the structure of C_2Cl_4 have been described in previous publications.[6,7] The sample of C_2Cl_4 was obtained from the Eastman Kodak Company and was carefully redistilled. It was heated to $\sim 50°C$ for the electron diffraction exposures. The experimental molecular scattering curve is shown at the top of Fig. 1. From the scattering curve, a radial distribution curve, $f(r)$, was computed using Eq. (1) reference 7, and decomposed into individual peaks for each interatomic distance, Fig. 2. The positions of the maxima indicate the equilibrium interatomic distances, whereas the shapes of the peaks are related to the average amplitudes of vibration between pairs of atoms. The values obtained from the $f(r)$ curve are listed in Table I. The interatomic distances correspond to a planar model with V_h symmetry and a ClCCl angle of 113.5°. An intensity curve, G, computed for this model using Eq. (11), reference 7, and using the vibrational amplitudes already listed, compares very well with the experimental curve in Fig. 1. The s/s_{exp} ratio for eighteen maxima and minima (excluding those below $s=3$) is 1.002 ± 0.0030.

The permissable range of distances and amplitudes of vibration is most conveniently obtained from a study of theoretical intensity curves. Deviations in the theoretical curves in the heights between maxima and adjacent minima of about ten percent from that of the experimental curve are considered borderline. Models are discarded on the basis of a combination of difficulties. Variation of the distance parameters (preserving V_h symmetry) resulted in intensity curves which were not as satisfactory as curve G. Figure 3 is a parameter chart illustrating the planar models which were computed. The dotted or dashed lines denote when particular features in computed intensity curves become sufficiently different from the experimental curve to be considered unacceptable. The solid line concerns the intensity of the two maxima, deep minimum and shelf in the region $s=8-11$. Curves D, S, and P illustrate various difficulties in this region. The dash-dot lines concern the shape of the shelf at $s=6$ as well as the small maximum and the broad maximum at $s=13-16$. Curves D and P illustrate the variations in these regions from the experimental curve. The dashed line is concerned with the shape and intensity of the double maxima at $s=18-20$. Curves S and P show the type

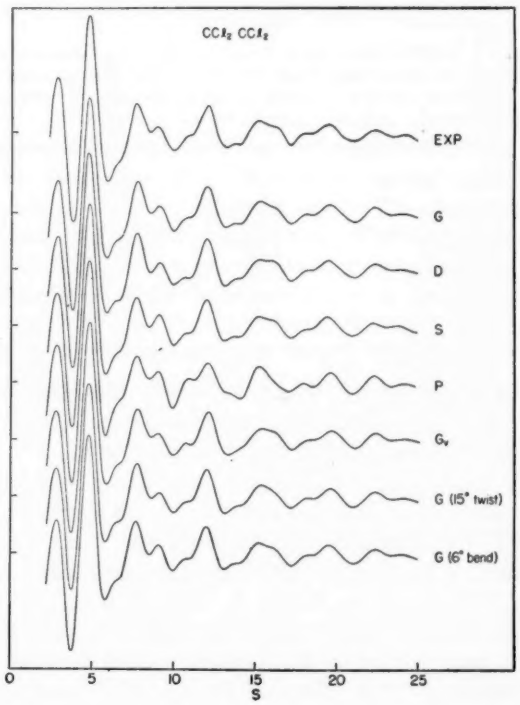

FIG. 1. The experimental and computed intensity curves for C_2Cl_4.

[1] Brockway, Beach, and Pauling, J. Am. Chem. Soc. **57**, 2693 (1935).
[2] R. W. Dornte, J. Chem. Phys. **1**, 566 (1933).
[3] H. de Laszlo, Nature **135**, 474 (1935).
[4] R. W. James, Physik. Z. **33**, 737 (1932).
[5] H. J. Bernstein, J. Chem. Phys. **18**, 478 (1950), and P. Torkington, Trans. Faraday Soc. **45**, 445-7 (1949).
[6] J. Karle and I. L. Karle, J. Chem. Phys. **18**, 957 (1950).
[7] I. L. Karle and J. Karle, J. Chem. Phys. **18**, 963 (1950).

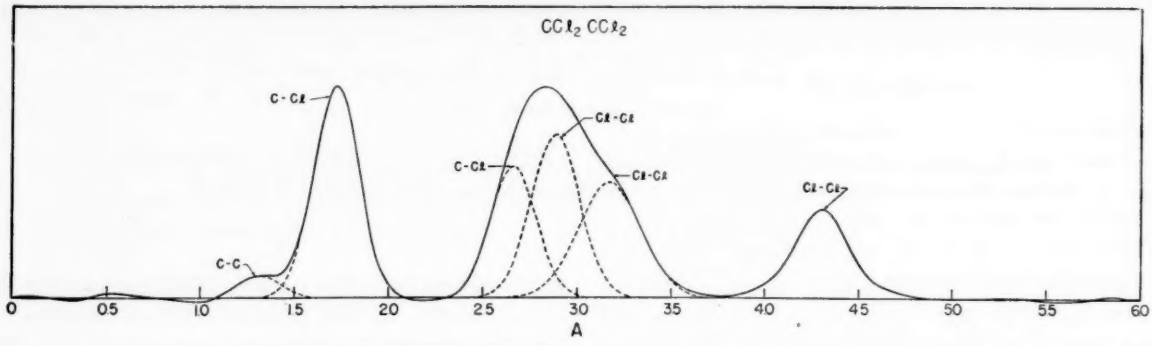

Distance	C−C	C−Cl	C−Cl	Cl−Cl	Cl−Cl	Cl−Cl
nZ_iZ_j	1.06	12	12	17	17	17
Actual area	0.99	12.0	12.0	17.0	16.95	16.8

FIG. 2. The solid line is the computed radial distribution curve, $f(r)$. The dashed lines indicate the individual peaks for each interatomic distance.

of difficulty in this region. Models *F*, *G*, and *N* are all acceptable, however, curve *G* deviates the least from the experimental data.

The data shows that the vibrational amplitude for the *cis* Cl−Cl is greater than that for the *trans* Cl−Cl. Many planar models were computed where the vibrational amplitudes for these two distances were set equal to each other at values ranging from 0.078A to 0.125A. Others were computed with the amplitude of the *trans* Cl−Cl vibration greater than that for the *cis* Cl−Cl. None of these models were satisfactory since the shelf at $s=11$ could not be reproduced properly and the small minimum at $s=14$ disappeared completely. Curve G_v is

TABLE I. Equilibrium distances and average displacements from equilibrium as determined from the radial distribution curve for C_2Cl_4 (without further refinement from the use of computed intensity curves).

	r, A	$\langle l^2\rangle_{Av}^{\frac{1}{2}}$, A
C−C	1.32	
C−Cl	1.72	0.050
C−Cl	2.66	0.061
Cl−Cl	2.885	0.074
Cl−Cl	3.175	0.128
Cl−Cl	4.30	0.093

one of these models where the only difference from curve *G* is that the average vibrational amplitudes for the *cis* and *trans* Cl−Cl distances are 0.103A.

The model for C_2Cl_4 cannot vary from coplanarity very much. A twist about the C−C bond lengthens the *cis* Cl−Cl distances and shortens the *trans* Cl−Cl distance. A twist of 15° which changes the *cis* and *trans* Cl−Cl distances by 0.02A is illustrated in curve *G* (15° twist) which shows the adverse effect of the change on the maximum at $s=16$. A larger twist in the molecule also has an adverse effect on the size of the maximum at $s=8$.

Another change from coplanarity is effected by setting one carbon atom above and the other carbon atom below the plane containing the four chlorine atoms (C_{2h} symmetry). This change lengthens the C−C distance and the nonbonded C−Cl distance relative to the other distances in the molecule. The deviation from coplanarity may be measured by the angle formed between the plane of the chlorine atoms and the ClCCl plane. Curve *G* (6° bend) with C−C=1.33A and C−Cl=2.67A shows the effect of the change on the relative heights of the small maximum and shelf at $s=9-11$. Greater deviations from coplanarity also distort the small maximum at $s=14$.

The structure of C_2Cl_4 as obtained from electron diffraction data is given in Table II. The vibrational amplitudes listed are the root-mean-square amplitudes projected on the lines connecting pairs of atoms at equilibrium.[6] They have been corrected for a finite sample size.[7] The decrease in value of the ideal scattering coefficients as a result of double scattering, causes a

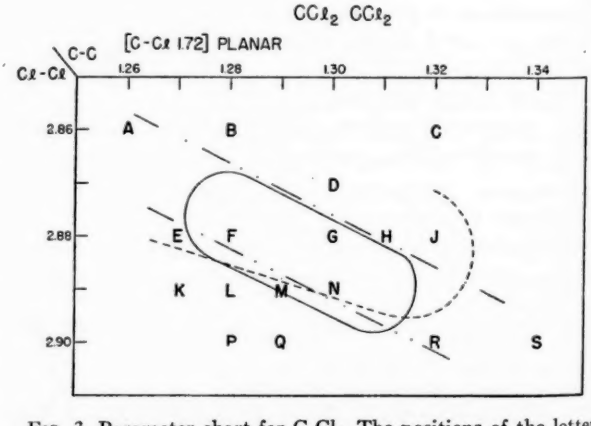

FIG. 3. Parameter chart for C_2Cl_4. The positions of the letters indicate the parameters of the models for which intensity curves were computed. The dashed and dotted lines indicate when particular features of the intensity curves are sufficiently different from the experimental curve to make them unacceptable.

correction in the computed intensity curves of at most three to four percent at the maxima and minima. The effect of double scattering is consequently readily taken into account.[7]

A previous investigation[1] based on the visual[8] method in electron diffraction obtained values for the C−Cl bond (1.73A) and the ClCCl angle (113.5°) which are close to our results. The assumed value (1.38A) for the C−C bond which was used in the previous investigation is seen not to be correct

The C−C bond in C_2Cl_4 is the same (within experimental uncertainty) as in CH_2CF_2 and C_2F_4[7] (1.31A). This value is somewhat smaller than that in C_2H_4 (1.35A).[9] The ClCCl angle in C_2Cl_4 is the same as the FCF angle in C_2F_4. The larger value for the amplitude of the *cis* Cl−Cl vibration as compared to that for the *trans* Cl−Cl vibration may be explained by proposing an important contribution from the modes associated with extension and contraction of the ClCCl angle. This proposal is consistent with spectroscopic information.

TABLE II. Final equilibrium distances and average displacements from equilibrium obtained from the electron diffraction data fo C_2Cl_4.

	r, A	$\langle l^2\rangle_{Av}^{\frac{1}{2}}$, A
C−C	1.30±0.03	0.030 (assumed)
C−Cl	1.72±0.01	0.048±0.005
C−Cl	2.66±0.02	0.058±0.01
Cl−Cl	2.88±0.01	0.070±0.01
Cl−Cl	3.18±0.02	0.125±0.01
Cl−Cl	4.29±0.02	0.086±0.01

ClCC = 113.5°±1.5°.
Possible oscillation about the C−C axis within 10°. Possible bending up to 5°.

[8] W. N. Lipscomb [Ph.D. thesis, California Institute of Technology, 1946] used the visual method and obtained C=C=1.34 ±0.05A, C−Cl=1.71±0.02A, and <CCCl=122¼°±1° for C_2Cl_4.
[9] G. Herzberg, *Infrared and Raman Spectra of Polyatomic Molecules* (D. Van Nostrand Company, Inc., New York, 1945), p. 439.

THE JOURNAL OF CHEMICAL PHYSICS VOLUME 20, NUMBER 1 JANUARY, 1952

An Electron Diffraction Investigation of Cyclooctatetraene and Benzene*

ISABELLA L. KARLE
U. S. Naval Research Laboratory, Washington, D. C.
(Received May 21, 1951)

The interatomic distances and their vibrational amplitudes have been determined for C_8H_8 and C_6H_6 by quantitative analysis of electron diffraction sector photographs. The D_{2d} tub configuration, with the oblique C−C bonds longer than the horizontal ones, has been confirmed for C_8H_8. The interatomic distances involving hydrogen atoms have been evaluated.

THE molecular structure of cyclooctatetraene has aroused considerable interest lately, particularly since three different structures, namely D_{2d}, D_4, and D_{4d}, have been proposed for this substance. Lippincott, Lord, and McDonald[1] interpret their Raman and infrared data of C_8H_8 and C_8D_8 as being consistent with the D_4 structure, a crown model with the C−C bonds alternating in length. Saksena and Narain[2] on the basis of Raman and infrared spectra and Langseth, Bastiansen, and Hassel[3] on the basis of the Raman spectrum and electron diffraction investigation favor the crown model with equal C−C bonds, D_{4d}. The tub configuration with the C−C bonds alternating in length, D_{2d}, is favored by Flett, Cave, Vago, and Thompson[4] on the basis of Raman and infrared spectra, by Kaufman, Fankuchen, and Mark[5] using x-ray diffraction data from the solid, and by Hedberg and Schomaker[6] using electron diffraction data from the vapor. The planar model, a configuration analogous to that of benzene, has been excluded by all the investigators. In this investigation the structure of cyclooctatetraene was studied by the electron diffraction method using the quantitative procedures recently developed in this laboratory.[7] These procedures permit not only the evaluation of the equilibrium interatomic distances in a molecule but also the evaluation of the average displacements between pairs of atoms as a consequence of the molecular vibrations.

The structure of benzene also has been investigated for a comparison with the structure of C_8H_8. Existing

* Presented at the American Crystallographic Society Meeting, New Hampton, New Hampshire, Aug. 21–25, 1950.
[1] (a) E. R. Lippincott and R. C. Lord, J. Am. Chem. Soc. **68**, 1868 (1946). (b) Lippincott, Lord, and McDonald, J. Chem. Phys. **16**, 548 (1948).
[2] B. D. Saksena and H. Narain, Nature **165**, 723 (1950).
[3] (a) Bastiansen, Hassel, and Langseth, Nature **160**, 128 (1947). (b) O. Bastiansen and O. Hassel, Acta. Chem. Scand. **3**, 209 (1949).
[4] Flett, Cave, Vago, and Thompson, Nature **159**, 739 (1947).
[5] Kaufman, Fankuchen, and Mark, Nature **161**, 165 (1948).
[6] K. Hedberg and V. Schomaker, Am. Chem. Soc. Meeting, San Francisco, 1949.
[7] (a) I. L. Karle and J. Karle, J. Chem. Phys. **17**, 1052 (1949). (b) J. Karle and I. L. Karle, J. Chem. Phys. **18**, 957 (1950). (c) I. L. Karle and J. Karle, J. Chem. Phys. **18**, 963 (1950).

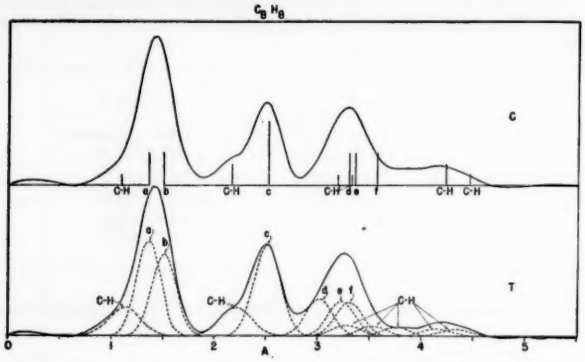

FIG. 1. The solid lines are the computed radial distribution curves, $f(r)$, for C_8H_8 with a crown model inner region for curve C and a tub model inner region for curve T. Crown model interatomic distances are indicated by the vertical lines in curve C. The dashed lines in curve T indicate the individual peaks for each interatomic distance in a tub model.

spectroscopic[8] and diffraction[9] studies of benzene favor the D_{6h} model, a planar regular hexagon, although not unambiguously.

PROCEDURE

Electron diffraction photographs of C_6H_6 and C_8H_8[10] were taken through an s sector with a wavelength near 0.06A and a specimen to plate distance near 11 cm. The photographic plates were rotated rapidly about the center of the diffraction pattern while being scanned by a microphotometer. The microphotometer readings were converted to relative intensities and plotted *vs* the variable s. Several months later, new photographs were taken with new samples and the entire procedure was repeated. The later results were in complete agreement with those of the earlier experiment.

The total intensity of scattering is composed of a steeply falling background as a result of atomic scattering upon which is superimposed an oscillating curve caused by molecular scattering. A smooth background line was drawn through the oscillations and the molecular scattering curve was obtained by dividing the total intensity curve by the background line. To accentuate the oscillations, the total intensity curve was multiplied by another s or s^2 factor.

The function $f(r)$ used for computing the radial distribution curve has been discussed in earlier publications.[7] In practice the peaks of the computed $f(r)$ curves often are composed of peaks for several distances. The two criteria used to decompose composite peaks into individual peaks for each distance are that the peaks should be Gaussian in shape and that the areas under the peaks multiplied by their respective equilibrium distances should be proportional to the scattering powers of the pairs of atoms involved. These criteria are found to be quite restrictive. The permissible range of distances and amplitudes of vibration is most conveniently obtained from a comparison of theoretical intensity curves with the experimental curve. A detailed discussion of the procedure and an evaluation of experimental accuracy can be found in previous papers.[7]

ANALYSIS AND RESULTS

C_8H_8

The radial distribution function, Eq. (1), reference 7(c), requires data from zero scattering angle. Omission of scattering data from the small scattering angle region causes long wavelength oscillations in the radial distribution curve which may cause some of the peaks to be displaced or disappear entirely. In practice, a molecular scattering curve computed from an assumed model is attached to the experimental curve in the small angle region for use in the radial distribution computation. Errors in the computed portion of the scattering curve cause some extraneous oscillations in the radial distribution curve which affect the shapes and areas of the peaks, but the positions of the maxima of the peaks are practically not affected. Successive approximations involving corrections to the inner region and the background line give a good radial distribution curve in a very few steps. The best curve is non-negative and is zero everywhere except in the vicinity of interatomic distances. For C_8H_8 two radial distribution curves are illustrated in Fig. 1. Experimental data was used from $s=4.5-20$[11] and in the region $s=0-4.5$, a scattering curve for the "tub" configuration was used in curve T and a scattering curve for the "crown" configuration was used in curve C. It should be noted that the maxima

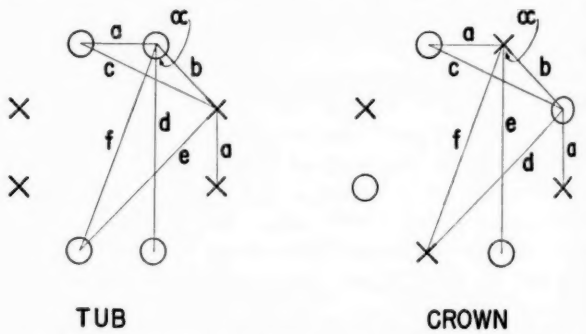

FIG. 2. The tub crown configurations for the carbon skeleton of C_8H_8. All the atoms marked with **O** are in one plane and those marked with **X** are in a parallel plane.

[8] C. K. Ingold, *et al.*, Parts I–VIII, J. Chem. Soc. 912 (1936); Part IX, *ibid.*, 1210 (1936); Part X, *ibid.*, 1728 (1937); Parts XI–XXI, *ibid.*, 222 (1946). See also G. Herzberg, *Infra-Red and Raman Spectra of Polyatomic Molecules* (D. Van Nostrand Company, Inc., New York, 1945), p. 362.

[9] (a) V. Schomaker and L. Pauling, J. Am. Chem. Soc. **61**, 1769 (1939). (b) Archer, Finbak, and Hassel, Tids. Kjemi, Bergveson Met. **2**, 33 (1942).

[10] Two samples of C_8H_8 prepared at different times were obtained from Dr. H. S. Kaufman, Polytechnic Institute of Brooklyn. Soon after preparation electron diffraction exposures were made of these samples heated to ~40°C. The sample of benzene used was prepared by redistilling thiophene-free benzene.

[11] The features beyond $s=20$ are very weak and are not amenable to accurate evaluation. Their small deviation from zero is indicated by the theoretical intensity curves (J) which match the experimental curve in the region $s<20$, Fig. 4.

for both curves are essentially in the same places. Only the area distribution is somewhat different. Hence, the choice of model for the molecule based upon the radial distribution curve is essentially independent of the assumed inner region.

The first problem is to distinguish between the "tub" and "crown" configurations. Figure 2 shows the carbon skeleton for these two models where all the atoms marked with **O** are in one plane and those marked with **X** are in a parallel plane. In the radial distribution curve it is apparent that the second peak is to be attributed to distance c and that it is very close to 2.51A. The first peak is made up of distances a and b which may or may not be equal. However, $(a+b)/2 \sim 1.42$A, hence angle $\alpha \sim 124°$ for a considerable range of a and b. The value of α immediately excludes the planar model which requires an angle of 135°. With the value of the average length, $(a+b)/2$, and the value of angle α known, it is possible to construct a tub or a crown model. The values of the longer distances in each model are essentially independent of the relative values of a and b that are permitted by the radial distribution curve. For $(a+b)/2$ and c the same, the value of $d+e+f$ is much larger for the crown configuration than for the tub. Any combination of a, b, and c (within reason as far as the radial distribution curve is concerned) cannot give values for d, e, and f for the crown model to fit under the third peak of the radial distribution curve. Equilibrium distances for a crown model are indicated in the $f(r)$ curve C, Fig. 1. The interatomic distances should be represented with Gaussian shapes with areas proportional to c_{ij}/r_{ij} and a minimum width derived from the $\exp(-as^2)$ factor in Eq. (1), reference 7(c), plus a spread caused by the interatomic vibration. Distances d, e, and f for a tub configuration, however, account very well for all the area under the third peak of the radial distribution curve T, Fig. 1. All the peaks have proper areas and widths corresponding to reasonable values for the vibrations.

At this point a comparison may be made with the $\sigma(r)/r$ curve for C_8H_8 obtained by Bastiansen and Hassel.[3b] Their $\sigma(r)/r$ curve differs from the $f(r)$ curves of this paper in that their experimental intensity

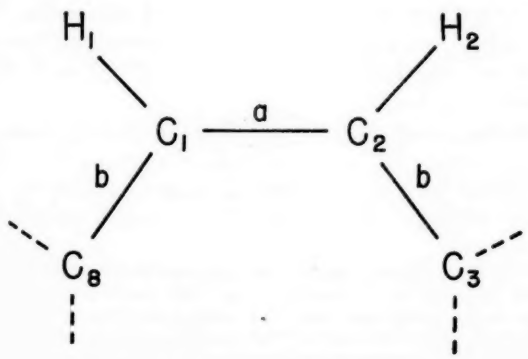

FIG. 3. Each of the above units of a tub model is taken to be co-planar.

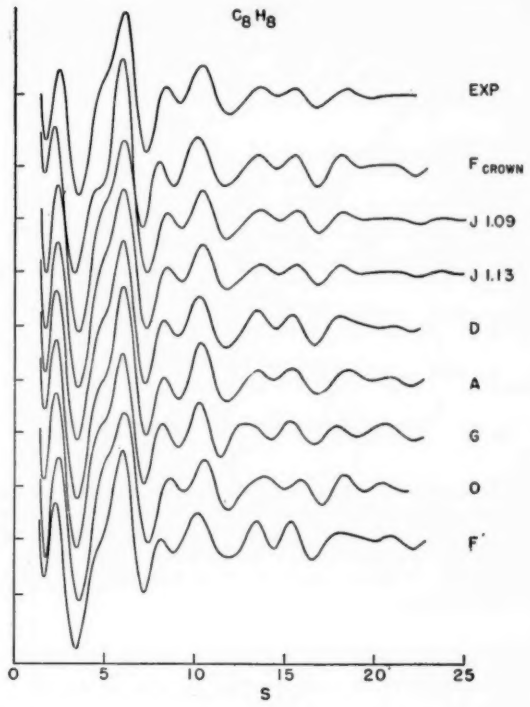

FIG. 4. The experimental and computed molecular intensity curves for C_8H_8.

curve $I_m(s)$ contained scattering factors dependent upon s whereas the intensity curve in this determination has been obtained with essentially constant coefficients, c_{ij}, Eq. (11), reference 7(c). The effect of the variable coefficients on the Fourier transform is to introduce negative values on either side of each maximum corresponding to an interatomic distance. Also scattering data for small scattering angles were left out in the $\sigma(r)/r$ curves which caused extraneous oscillations sometimes referred to as "diffraction effects." These two conditions can affect the positions of the main maxima, especially those where several interatomic distances come under the same peak. Nevertheless, the three main maxima in their $\sigma(r)/r$ curves are at about 1.42, 2.50, and 3.25A which are close to the values obtained in this investigation (1.42, 2.51, 3.25A). It is not clear how they concluded from their radial distribution curve that C_8H_8 has the crown configuration.

The next problem is to establish whether or not distances a and b are equal. The best fit to the first peak of the $f(r)$ curve, Fig. 1, can be obtained with peaks for the C—H distance and two C—C distances with the proper areas as shown. The C—C equilibrium values are 1.35 and 1.50A with average displacements from equilibrium about 0.055 and 0.065A, respectively. Without too large a discrepancy it is possible to bring the C—C peaks closer together if their shapes are compensated with larger vibrational amplitudes. There is still reasonable agreement with the $f(r)$ curve with only one C—C bond distance at 1.42A, however, the average displacement from the equilibrium value because of vibration

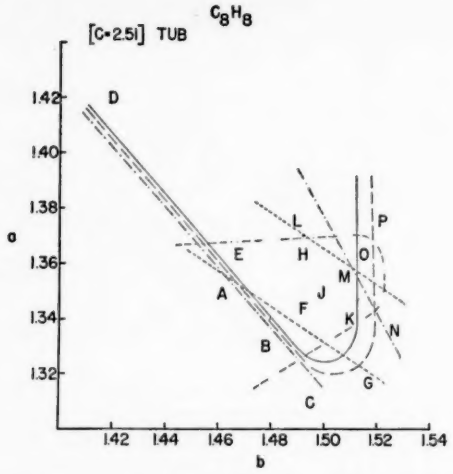

FIG. 5. Parameter chart for C_8H_8. The positions of the letters indicate the parameters of the models for which intensity curves were computed. The dashed and dotted lines indicate the regions which produce features on the theoretical intensity curves that are sufficiently different from the experimental curve to make them unacceptable.

must be at least 0.10A, a value which is larger than that for any other C−C separation in the molecule. The radial distribution curve favors somewhat C−C links which are not all equal in length.

The scattering coefficients and consequently the size of the peaks for the C−H distances are considerably smaller than those for the C−C distances. However, after the Gaussian peaks for the C−C distances are subtracted from the $f(r)$ curve, the remaining area accounts for all the C−H distances in the tub model. All the values of the C−H distances indicate that the C−H bond is longer than 1.09A, preferably about 1.13A. Furthermore, the shape of the second C−H peak shows that C_1-H_2 and C_3-H_2, Fig. 3, are nearly equal.

The values of the equilibrium distances as determined from the radial distribution curve for C_8H_8 correspond almost exactly to the parameters of a tub model with a equal to 1.35A, b equal to 1.50A, the C−C−C angle equal to 124°, and C−H equal to 1.13A.

Molecular intensity curves for assumed models for C_8H_8 were computed using Eq. (11) reference 7(c), and compared with the experimental curve, Fig. 4. The computed intensity curves are used to confirm the conclusions from the radial distribution curve and to establish limits of uncertainty. Crown models corresponding to points A, C, F, L, N, and P of the parameter chart, Fig. 5, were computed with distance c equal to 2.51A and the values of a and b varied as indicated. For these models the C−H distance was assumed to be 1.09A and C_1-H_2 was made equal to C_3-H_2. Values for $\langle l_{ij}^2\rangle_{Av}$ were chosen to be most consistent with the radial distribution curve. All these curves have a common difficulty that is not remedied by a variation in the parameters of the carbon frame or the vibrational amplitudes. The maximum at $s=6$ is much too high and narrow and the minimum at $s=9$ is too deep as is illustrated by curve F_{crown}.[12] In addition, the average deviation from the average s/s_{exp} ratio for the maxima and minima ranges from ±0.013 upward. Thus, the intensity curves confirm the conclusion from the radial distribution curve that C_8H_8 does not have a crown structure.

Tub models were computed for all the points indicated in Fig. 5, with each unit indicated in Fig. 3 kept in a plane with $a<b$. The C−H=1.09A rather than the 1.13A indicated by the radial distribution curve. Some of the intensity curves are shown in Fig. 4. Model J, based on the radial distribution curve, is quite satisfactory, and more satisfactory than any of the others. The solid line of Fig. 5 separates satisfactory from unsatisfactory models according to the shape and height of the particularly sensitive maximum at $s=6$ (too narrow and somewhat too high in A and too wide and too low in O). The −− line concerns the height between the minimum and maximum at $s=7$–8. This height in curve A is more than 10 percent less than in the experimental curve. The − − − − line concerns the depth of the minimum at $s=9$. This feature is too deep in curves A and G and too shallow in curve O. The −·−· line concerns the height of the maximum at $s=10$. The maximum is too high in curve A and too low in curve O. The −−·· line concerns features in the intensity curve from $s=12$ to $s=20$. Curve G is representative of the difficulties encountered in this region.

Models D, E, and F differ mainly in distances a and b. All the other C−C distances are quite similar since $(a+b)/2\sim1.42$ and $\angle CCC\sim124\frac{1}{2}°$ in the three models. The $\langle l_{ij}^2\rangle_{Av}^{\frac{1}{2}}$ values for a and b had to be increased, however, to 0.08A in model E and to 0.10A, a rather large value, in model D to obtain the best possible intensity curves. These curves are satisfactory up to $s=11$, but the maxima at $s=13$ and 15 are too pronounced, especially in curve D. In curve D, the height from the minimum at $s=12$ to the maximum at $s=13$ is ∼25 percent greater than in the experimental curve. Further increases in damping factors would improve this region but would cause discrepancies at lower s values.

It might be expected that the longer C−C bonds would occupy the inclined positions in the tub as was assumed in the models computed above. This assumption is justified since an interchange of distances a and b produces models whose intensity curves are not acceptable, especially in the region $s=13$–15 as is illustrated by curve F′.

All the curves for the tub model, including curve J, have a minimum at $s=12$ which is too deep. This particular feature, however, is quite sensitive to the C−H distance. Shorter C−H distances produce a

[12] The only way to change the shape of the experimental intensity curve to try to conform to a crown model is to put sharp bends in the background line representing the atomic scattering. Such sharp curvatures are at great variance with the shape of the theoretical atomic scattering curve for C plus H. Furthermore, the background line as determined for C_8H_8 corresponds within 2–3 percent of the background line for C_6H_6.

deeper minimum while longer C−H distances produce a shallower minimum. The C−H distances also affect the height of the peak at $s=6$. A C−H bond as small as 1.06A or as large as 1.17A is unsatisfactory. Model J with C−H equal to 1.13A reproduces the intensities of the experimental curve somewhat more closely than model J with C−H=1.09A. The value of 1.13A for the C−H bond is also the value obtained from the radial distribution curve where all the C−H distances are consistent with this value. In curve $J_{1.13}$, the average deviation from the average s/s_{exp} ratio for the maxima and minima is ±0.004. The average deviation from the average s/s_{exp} value for all the acceptable models and for models A and D is of the order of ±0.004–5 while for all the other tub models it is greater than ±0.007.

For a fixed model, the $\langle l_{ij}^2\rangle_{Av}^{\frac{1}{2}}$ values for the stronger contributors to the molecular scattering curve cannot be changed by more than 0.01A without having a measurable effect on the intensity curve. Values of $\langle l_{ij}^2\rangle_{Av}^{\frac{1}{2}}$ for C−H distances, however, usually cannot be obtained accurately from the $f(r)$ curve and must be assumed for computing intensity curves. All $\langle l_{ij}^2\rangle_{Av}^{\frac{1}{2}}$ values which were obtained need a small correction as a result of the spreading of gas about the nozzle during an exposure to an electron beam.[7a] This correction is usually not more than 0.003A and has been taken into account in the reported values.

TABLE I. Equilibrium distances and average displacements from equilibrium obtained from quantitative electron diffraction data.

	C_8H_8 r, A	$\langle l^2\rangle_{Av}^{\frac{1}{2}}$, A
a	$1.35+q\pm0.01$	$0.059+\frac{1}{2}q\pm0.007$
b	$1.50-q\pm0.01$	$0.067+\frac{1}{2}q\pm0.007$
c	2.51 ± 0.02	0.077 ± 0.01
d	3.01 ± 0.03	0.083 ± 0.01
e	3.23 ± 0.02	0.083 ± 0.01
f	3.30 ± 0.03	0.083 ± 0.01
C−H	1.12 ± 0.03	0.072 ± 0.02
C−H	2.19 ± 0.04	0.092 ± 0.02
C−H	3.24	0.116 assumed
C−H	3.55	0.116 assumed
C−H	3.73	0.135 assumed
C−H	4.18	0.135 assumed
C−H	4.29	0.135 assumed
$<CCC=124°\pm1\frac{1}{2}°$		where $0\leqslant q<0.03$
Tub configuration. See Fig. 2.		

	C_8H_8 r, A	$\langle l^2\rangle_{Av}^{\frac{1}{2}}$, A
C−C	$1.393+a\pm0.005$ $1.393-a\pm0.005$	$0.055-\frac{1}{3}a\pm0.007$
C−C	$2.41+b\pm0.015$ $2.41-b\pm0.015$	$0.067-\frac{1}{3}b\pm0.007$
C−C	2.786 ± 0.015	0.075 ± 0.01
C−H	1.08 ± 0.02	0.072 ± 0.015
C−H	2.14 ± 0.03	0.092 ± 0.02
C−H	3.38 ± 0.04	0.116 assumed
C−H	3.86 ± 0.05	0.135 assumed
$<CCC=\begin{cases}120°+80b\\120°-80b\end{cases}$		where $\begin{matrix}0\leqslant a<0.03\\0\leqslant b<0.05\end{matrix}$
z dimension <0.15		

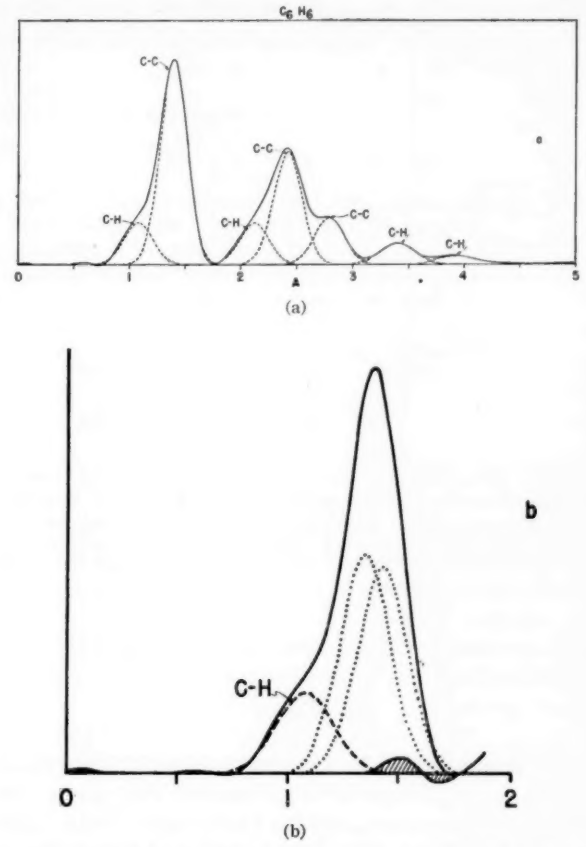

FIG. 6. (a) The solid line is the computed radical distribution curve, $f(r)$, for C_6H_6. The dashed lines indicate the individual peaks for each interatomic distances. (b) The $f(r)$ curve is decomposed into two different ortho C−C distances. The shaded portion is an indication of the error thus introduced.

The structure of C_8H_8 as obtained using quantitative electron diffraction data is given in Table I.

This investigation shows that C_8H_8 has the D_{2d} structure in agreement with the results from x-ray diffraction[5] and electron diffraction[6] based on the *visual* method. In the *visual* method it is usually possible to get fairly reliable measurements of the positions of the maxima and minima. This amount of information is sufficient to distinguish between the tub and crown models of C_8H_8 since the average deviation from the average s/s_{exp} ratio is at least three times larger for the crown than for the tub models. The *visual* method, however, cannot establish the intensities and shapes as as well as an objective procedure. The model proposed by Hedberg and Schomaker is represented by curve A. The deviations from the s/s_{exp} ratio are small for this model and the parameters are fairly close to those obtained in this investigation. However, the shapes and intensities of some of the peaks in the intensity curve are sufficiently different from the experimental intensity curve to make this model less likely than models such as F or J.

It is of interest to note that in tetraphenylene (1,2,3,4,5,6,7,8-tetrabenz-$\Delta^{1,3,5,7}$-cyclooctatetraene) the

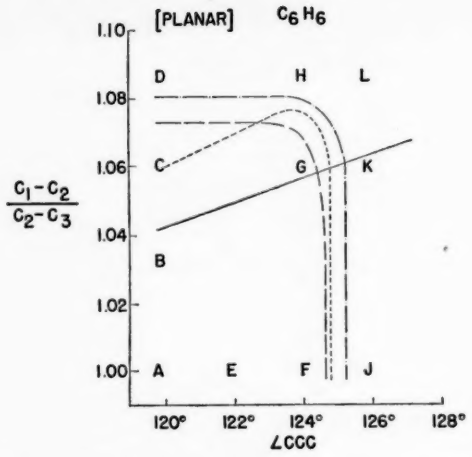

FIG. 7. Parameter chart for C_6H_6. The positions of the letters indicate the parameters of planar models for which intensity curves were computed. The dashed and dotted lines indicate the regions which produce features on the theoretical intensity curves that are sufficiently different from the experimental curve to make them unacceptable.

eight-membered carbon ring also has the tub configuration.[13]

C_6H_6

The radial distribution curve for C_6H_6 is illustrated in Fig. 6(a). The curve was resolved into peaks for three C—C distances, 1.393, 2.410, and 2.786A, and four C—H distances, 1.08, 2.13, 3.40, and 3.89A, which fit a plane regular hexagon. It is possible, however, to split into two the ortho C—C and the meta C—C distances, and fit the curve almost as well if smaller damping constants are used. The dotted curves under the peak at 1.39A, Fig. 6(b), correspond to peaks at 1.35 and 1.43A with $\langle l^2\rangle_{Av}^{\frac{1}{2}}$ equal to 0.04A as compared to an $\langle l^2\rangle_{Av}^{\frac{1}{2}}$ of 0.055A for a single peak at 1.39A. The dashed portion, an indication of the error, is the difference between the dotted curves and the $f(r)$ curve. If the ortho C—C or meta C—C or both distances are split into two, then the molecule possesses a trigonal instead of hexagonal axis of symmetry. No pucker is suggested by the $f(r)$ curve since a puckered ring reduces the length of the meta and para C—C distances relative to the ortho C—C distance.

Intensity curves were computed for the planar models indicated on the parameter map, Fig. 7. The C—H distance used was 1.08A and the distance $C_1—H_2$ was set equal to $C_3—H_2$. Values of $\langle l_{ij}^2\rangle_{Av}^{\frac{1}{2}}$ were chosen to be most consistent with the $f(r)$ curve. Model A is a plane regular hexagon with the C—C bond equal to 1.39A. Its intensity curve reproduces the experimental curve satisfactorily, Fig. 8, and the average s/s_{exp} ratio for the maxima and minima is 1.002 ± 0.003. Curves B, E, and F are also quite acceptable if models with less vibration than in model A are assumed. Curves C, D, L, and J illustrate various unacceptable features encountered in the theoretical intensity curves such as a flat or low maximum at $s=10$ represented by the solid line on the parameter map, Fig. 7, a shallow minimum at $s=12$ (— — line on parameter map), an incorrect shape for the maximum at $s=15$ (— — — line on parameter map) and either too little or too much intensity for the small maximum at $s=21$ (— · — · line on parameter map).

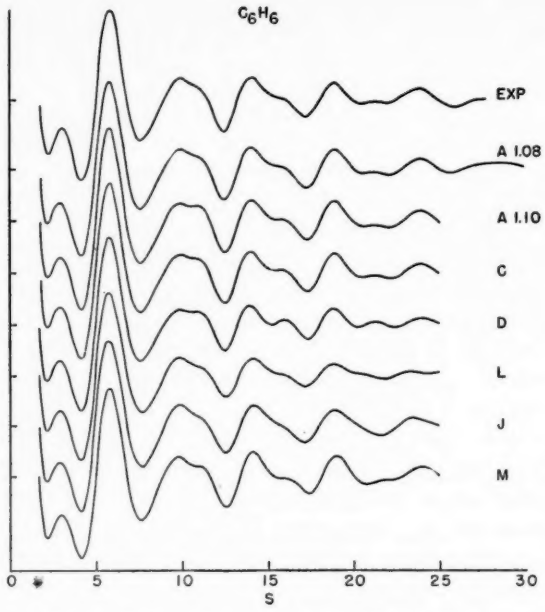

FIG. 8. The experimental and computed molecular intensity curves for C_6H_6.

A crown model computed with C—C bond equal to 1.39A and the z dimension equal to 0.20A ($\angle$CCC $=118°$) is illustrated by curve M. This curve is unsatisfactory in the height and shape of the maximum at $s=15$. A crown model with a z dimension equal to 0.10A ($\angle CCC=119.5°$) is almost indistinguishable from curve A.

The C—H terms affect the height of the maximum at $s=6$ and the shape of the maximum at $s=10$, and C—H values as small as 1.04A or as large as 1.10A lead to poor intensity curves (see $A_{1.10}$).

The electron diffraction data lead to an essentially planar model for C_6H_6, although not unambiguously to the D_{6h} model, as has been shown previously. The mean C—C bond is 1.39A in accordance with earlier investigations.[9] The equilibrium interatomic distances and the average amplitudes of vibration between pairs of atoms for benzene are listed in Table I.

[13] I. L. Karle and L. O. Brockway, J. Am. Chem. Soc. **66**, 1974 (1944).

Collisional Perturbation of Spin-Orbital Coupling and the Mechanism of Fluorescence Quenching. A Visual Demonstration of the Perturbation*

MICHAEL KASHA†
Department of Chemistry, University of Manchester, England
(Received August 13, 1951)

A yellow color is produced when two colorless pure liquids, α-chloronaphthalene and ethyl iodide, are mixed, although no chemical reaction occurs. Spectroscopic examination reveals that the lowest singlet →triplet absorption band of the naphthalene molecule is greatly enhanced in intensity in the presence of the iodide, and that the development of this absorption band is responsible for the color effect. The process is interpreted in terms of a *collisional perturbation of spin-orbital coupling* in the π-electron orbitals of the naphthalene. The significance of this phenomenon in several topics in spectroscopy and chemistry is discussed. In particular, the molecular mechanism of heavy atom quenching of fluorescence by foreign species is resolved. A novel Beer's law anomaly is predicted for intercombinations.

QUENCHING of fluorescence, of, e.g., the aromatic hydrocarbons, by the alkyl halides in solution is well known[1,2] to be in the order of effectiveness $I \gg Br > Cl > F$. The parallel behavior is known for the quenching of fluorescence of molecules in aqueous solution by the halide ions. This is in the natural order of several different physical parameters of the halogen atom, and various ones have been adduced previously to explain the trend in quenching efficiency. Recently it has been shown[3,4] that in *halo*-substituted aromatic hydrocarbons the excited-singlet to triplet ($S' \rightarrow T$) *radiationless* transition probability (see Fig. 1) is enhanced pronouncedly, as shown by the increase in the ratio $\chi = \Phi_P^0/\Phi_F^0$ (quantum yield of phosphorescence to fluorescence, $T \rightarrow S$ *versus* $S' \rightarrow S$). The order of effectiveness of the halogen substituent is the same as that cited above. This latter phenomenon has been interpreted as an external (but intramolecular) perturbation, of the spin-orbital coupling in the π-electron orbitals of the molecule, by the halogen atom. The *atomic number* of the perturbing atom is properly accepted as a fundamental parameter, according to spectroscopic theory.

Consideration of the above results, independently by Dr. H. G. Curme and the present writer, suggested to us that the mechanism of quenching of fluorescence by foreign heavy-atom-containing species might be also through the agency of a spin-orbital perturbation. The loss of fluorescence ($S' \rightarrow S$) as a result of a quenching collision would be explained by an increase in the probability of the $S' \rightarrow T$ radiationless intercombination (see Fig. 1). The molecules in the long-lived metastable (T) state do not radiate in fluid systems. An attempt to observe an increase in the Φ_P^0/Φ_F^0 ratio in the presence of alkyl halide quenchers in the solution was not successful. In the rigid glass solutions required for the observation of the phosphorescence, the *partial* quenching observed initially in the fluid solution was totally recovered in the rigid glass. That the quenching was entirely diffusion-controlled at low concentrations of quencher was demonstrated by its cessation in the high viscosity solution.

Recently, another possibility for demonstrating the quenching mechanism suggested itself. Among the observable intercombinations which can occur between the three chemically most important electronic states of a complex molecule (see Fig. 1)—radiationless $S' \rightarrow T$, radiative $T \rightarrow S$ (emission),[5] and $T \leftarrow S$ absorption[6]—

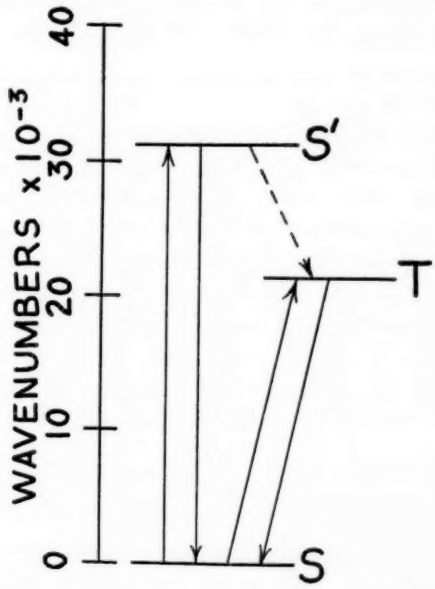

FIG. 1. Energy level scheme for the naphthalene molecule showing the three chemically most important electronic states.

* Presented at the Southwide Chemical Conference of the American Chemical Society, Wilson Dam, Alabama, October 19, 1951.

† John Simon Guggenheim Memorial Fellow, 1950–51. Address after September 1951: Department of Chemistry, Florida State University, Tallahassee, Florida.

[1] P. Pringsheim, *Fluorescence and Phosphorescence* (Interscience Publishers, New York, 1949), p. 328 *ff*.

[2] Th. Förster, *Fluoreszenz Organischer Verbindungen* (Vandenhoeck and Ruprecht, Göttingen, 1951), Chapter 10.

[3] M. Kasha, Faraday Soc. Discussion No. 9, 14 (1950). Also other work in preparation.

[4] See the related papers of (a) P. Yuster and S. I. Weissman, J. Chem. Phys., **17**, 1182 (1949); (b) D. S. McClure, J. Chem. Phys. **17**, 905 (1949).

[5] (a) G. N. Lewis and M. Kasha, J. Am. Chem. Soc. **66**, 2100 (1944); (b) M. Kasha and R. V. Nauman, J. Chem. Phys. **17**, 516 (1949).

[6] G. N. Lewis and M. Kasha, J. Am. Chem. Soc. **67**, 994 (1945).

only the last can be studied under all conditions of physical state. Evidence that any one of these three is increased in probability under some perturbation implies directly that the remaining two are increased in approximately similar proportion,[3,4] even if masked from observation. The following experiment for the study of $T \leftarrow S$ absorption was carried out.

The naphthalene molecule was chosen for the study, because its lowest triplet state[5] has been examined thoroughly and has these favorable characteristics: (a) an unusually large $S'-T$ separation[7] (10,000 cm^{-1}), so that the very weak $T \leftarrow S$ absorption falls in a region clear of the strong $S' \leftarrow S$ normal absorption; (b) the $T \leftarrow S$ absorption alone is in the visible region (between 5000 and 4000A) allowing easy measurement and visual observation of the results; (c) the *energy* of the electronic transition is affected little by halogen substitution, as shown by the small shift in the $T \rightarrow S$ emission spectrum,[5] although the heavy atom strongly influences the *transition probability* of the intercombinations;[3,4] and (d) the very sharp and characteristic pattern of the low-temperature (77°K) $T \rightarrow S$ emission[5] of the halo-naphthalenes is reproduced in the $T \leftarrow S$ absorption, even in warm-solution (298°K) spectra.[8] This latter point will serve as an aid to identification of the transition.

The $T \leftarrow S$ absorption of naphthalene itself is so weak as to be unobservable in optical paths of several centimeters of solid naphthalene. However, its intensity is strong enough in the monohalo-naphthalenes to be measurable in 10 cm absorption cells of strong solutions. In Fig. 2 are given the absorption curves obtained by McClure[8] for solutions of β-chloronaphthalene and β-iodonaphthalene. For the present experiment α-chloronaphthalene was chosen because it is a liquid at 20°C; and because in it the spin-orbital perturbation is weak, yet the $T \leftarrow S$ band is observable in a 5 cm optical path of the pure liquid (Fig. 3, curve A).

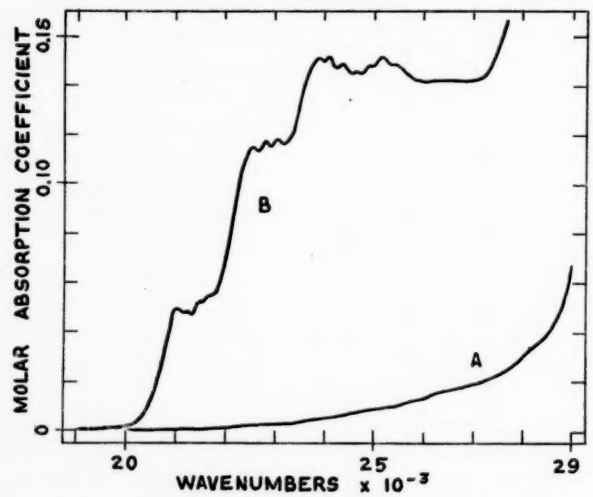

FIG. 2. Visible region singlet-triplet absorption curves at room temperature. Curve A, β-chloronaphthalene; Curve B, β-iodonaphthalene, (after McClure).[8]

To carry out the experiment 20 cc of pure ethyl iodide were pipetted into 10 cc of pure α-chloronaphthalene at 20°C. Upon mixing the two colorless liquids, an easily observable yellow color was produced instantly. Ordinary chemical interpretations could not explain the observed effect: no instantaneous reaction between the two molecules is possible at 20°C, and it is improbable that any strong molecular complex which has color could be formed with such pairs (see below). After the instantaneous development of the color upon mixing, no further change occurred during the experiment time of two hours.

The absorption curve of the yellow solution obtained as the 1:2 volume mixture of α-chloronaphthalene in ethyl iodide at 20°C is given in Fig. 3, curve B. By a comparison with the curve for β-iodonaphthalene, Fig. 2, curve B, it is seen that the curve for the mixture has the correct characteristics to be identified certainly as an enhanced $T \leftarrow S$ absorption of the naphthalene molecule. The two curves are not strictly comparable, since both the 0,0-frequency and the vibrational pattern are slightly different[5] for the intercombinations in β-iodonaphthalene and α-chloronaphthalene. In addition, the alpha-derivatives show a more blurred vibrational structure. It seems quite likely that the ethyl-iodide-induced $T \leftarrow S$ transition in α-chloronaphthalene will have the vibrational structure of the latter molecule, and not of an iodonaphthalene (see below).

Accepting the postulate that a strong molecular complex is not formed, the observed effect may be attributed to a "collisional" spin-orbital perturbation. In the previous studies[3,4] of spin-orbital perturbations in complex molecules only "stationary" perturbations could be observed, i.e., those which varied in magnitude according to the atom substituted. However, not the same parameters are varied in the collisional and stationary perturbations; this will be discussed after the essential experimental details have been described.

The α-chloronaphthalene was an initially colorless sample of cp grade, purified by a careful fractional distillation at 0.1-mm pressure and 70.5°C. Two fractions with very constant boiling point and an equal refractive index $n_D^{19} = 1.6347 \pm 0.0001$ were combined for use in the experiment. The liquid appeared colorless in a 5-cm path.

The ethyl iodide sample was initially of a light pink color. It was purified by distillation over mercury, drying, and then chromatograming through an activated alumina column. The purified liquid appeared colorless in a 5 cm path.

The starting materials were stored in the dark, the iodide at 0°C, until used in the experiment, and all manipulations were carried out in subdued daylight low in ultraviolet, in order to avoid photochemical complications.

As a check against one possible source of error, the color of molecular iodine in each of the pure liquids was examined before plotting the absorption data for the experiment. The colors varied from pink to rose-amber, not a pure yellow. At any rate the absorption curve obtained in the experiment bears no resemblance to the structureless absorption curves of iodine solutions.

[7] M. Kasha, Chem. Revs. 41, 401 (1947); see reference 5(b) above.

[8] D. S. McClure, thesis (University of California, Berkeley, 1948).

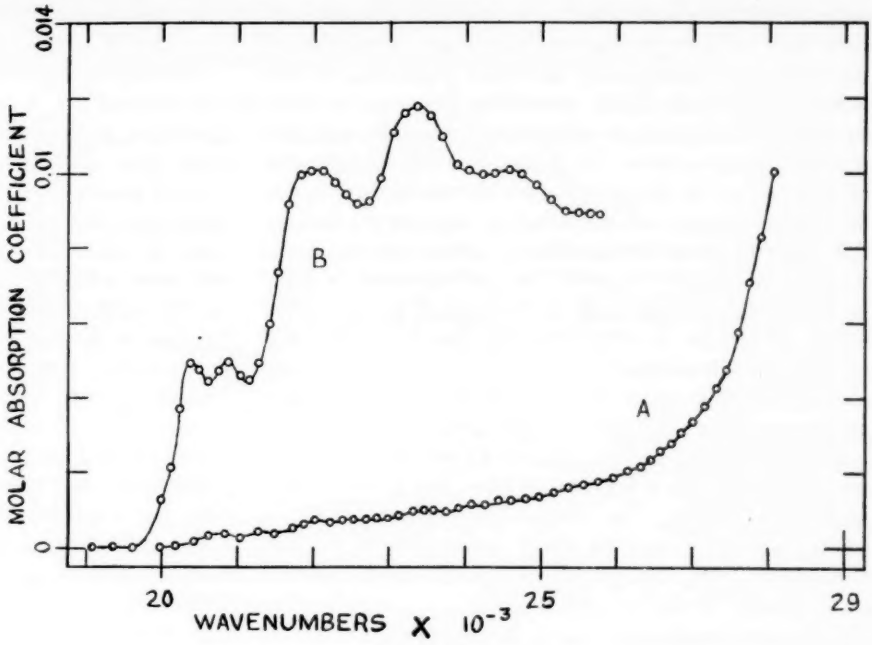

FIG. 3. Visible region singlet-triplet absorption curves at 20°C. Curve A, α-chloronaphthalene; Curve B, the 1:2 volume mixture of α-chloronaphthalene and ethyl iodide.

The absorption curves were measured for the two pure liquids and for the mixture using 5-cm absorption cells in the Beckman Quartz Spectrophotometer. To indicate the absorption magnitudes measured and the corrections applied, the following data will serve as an example.

The absorption coefficients for the 1:2 mixture were calculated by means of the expression $\epsilon=(3D_c-2D_b)/CL$ where D_c is the optical density of (c), the 1:2 mixture, D_b is the optical density of (b) the ethyl iodide, $C=7.35$, the molar concentration of α-chloronaphthalene as a pure liquid (20°C), and $L=5$ cm, the optical path. The absorptions were measured against air as a blank. A constant correction, derived from the nonabsorbing long wavelength region for each sample, was applied to all optical density readings before calculation of the absorption coefficients.

The *stationary* perturbation of spin-orbital coupling in π-electron orbitals, by a substituted heavy atom in the molecule, depends on two main factors—(1) the degree of penetration of the π-electron into the electric field of the nucleus of the perturbing atom, and (2) the strength of this electric field. Thus, the ⟨π-electron orbital, halogen-*p*-orbital⟩ overlap is a limiting parameter for (1), and the atomic number (more accurately, the spin-orbital coupling factor) is a limiting parameter for (2). Evidently, in comparing intercombination probabilities for halogen-substituted aromatics, both parameters are varied simultaneously. In the *collisional* perturbation experiment only the overlap factor is varied as the concentration of the molecule containing the perturbing atom is varied. Since the penetration of the π-electron into the proximity of the nucleus of the perturbing atom is required for strong spin-orbital coupling (the spin-orbital interaction operator for a Coulomb field has an inverse third power dependence on the distance of the "optical" electron from the nucleus),[9] the collisional perturbation cannot be considered as a long-range interaction. Thus, the perturbation can occur only at the time the π-orbital of the naphthalene molecule strongly overlaps with the halogen *p*-orbitals, during the collision.

It is not expected, however, that the concentration of collision-pairs formed in free-space (i.e., the gaseous state) would be great enough to permit their spectroscopic detection by an experiment such as described here. The collision-pairs have too short a lifetime under those conditions. However, in the liquid state the formation of a molecular cage around the fluorescer molecule introduces a complication: the collisions are of two kinds,[10] (a) diffusion-controlled encounter formation, and (b) repeated collisions within the cage. These latter have been described as more of the nature of intermolecular vibrations of the collision pair. The former type of collision leads to the *dynamical* fluorescence quenching phenomenon, whereas the latter leads to *static* quenching.[2] Static quenching has been observed usually as an upward deviation from the linear plot of Φ_F^0/Φ_F (quantum yield ratio) *versus* $[Q]$ (quencher concentration) expected on the basis of the Stern-Volmer quenching law.[1,2] Such deviations are observed

TABLE I. Optical densities ($\log_{10}I_0/I$) for 5 cm path.

	$\bar{\nu}=23{,}358$[a]	$\bar{\nu}=24{,}993$[a]
(a) α-chloronaphthalene	0.036±0.002	0.049±0.002
(b) Ethyl iodide	0.000	0.043
(c) The 1:2 volume mixture, (a:b)	0.144	0.147

[a] 4280 and 4000A, respectively.

[9] Eyring, Walter, and Kimball, *Quantum Chemistry* (John Wiley and Sons, Inc., New York, 1944), p. 152.

[10] E. Rabinowitch and J. Franck, Trans. Faraday Soc. **30**, 120 (1934); E. Rabinowitch and W. C. Wood, *ibid.* **32**, 1381 (1936); E. Rabinowitch, *ibid.* **33**, 1225 (1937).

only at rather high quencher concentrations. Generally,[11] they may be described as resulting from population of the cage, occupied by the fluorescer molecule, by the quencher molecule. Static quenching has been ascribed by some investigators to compound formation, and it is true that in some cases this is the basis for the behavior of the system. In the present case the static component of quenching may be attributed to cage population by the quencher, since as mentioned earlier, a strong compound ("molecular complex") is not expected to form between ethyl iodide and α-chloronaphthalene. This latter contention is supported by the fact that the energy and vibrational pattern of the $T \leftarrow S$ absorption are not anomalous, as they would be if the electronic structure of the naphthalene were greatly affected. No practical distinction can be made between an "encounter complex" such as is postulated here and a very weak molecular complex. The present facts argue against a strong molecular complex (with a measurable heat of formation), but independent physico-chemical evidence on this point would be very valuable.

From the foregoing discussion it is obviously necessary to ascribe the induced $T \leftarrow S$ absorption intensity, observed in the mixture experiment, to the small static component of the quenching phenomenon. The plausibility of this statement may be made clear by comparing the various effects of the stationary and collisional perturbations. For the *stationary* perturbation of spin-orbital coupling by the iodine atom in β-iodonaphthalene, the f-value of the $T \leftarrow S$ absorption[8] is 3.76×10^{-6} (molar absorption coefficient $\epsilon = 0.12$ at 22800 cm^{-1}, see Fig. 2, curve B); the quantum yield of fluorescence, although much less[3] than that of unsubstituted naphthalene, is still measurable and has a value of the order of magnitude $\Phi_F^0 \sim 0.1$. For the *collisional* perturbation, the molar absorption coefficient $\epsilon = 0.01$ at the corresponding frequency of 22000 cm^{-1} (see Fig. 3, curve B). This corresponds to an f-value of only about $\frac{1}{10}$ of that observed in the former case; however, the quantum yield of fluorescence, $\Phi_F = 0$. In fact, a several thousandfold excess of ethyl iodide is present in the mixture experiment over the amount necessary to reduce to 0 (for practical purposes) the intrinsic quantum yield of fluorescence Φ_F^0 of α-chloronaphthalene. Thus, the collisional perturbation observed as an induced $T \leftarrow S$ absorption must represent only a very small fraction of the total perturbation. The main part of the perturbation, associated with the dynamical quenching component, is not measurable by an absorption experiment. It is a somewhat subtle but entirely plausible assumption that the main perturbation is also of a spin-orbital character, just as the small observed perturbation has been proved to be.

The experimental findings of Weiss[12] concerning electron-transfer as a consequence of quenching, to be consistent with these new results, must be taken to mean that electron transfer is sequential to the collisional spin-orbital perturbation. Moreover, it may be noted that if the "electron transfer quencher" cannot cause a collisional spin-orbital perturbation, it may still react with the triplet excited molecules produced by the natural spin-orbital coupling, characteristic of the free molecule. This, however, would not diminish the intrinsic quantum yield of fluorescence. At the present time, a distinction between simple electron transfer photochemistry involving singlet-excited and triplet-excited molecules cannot be made.

An important corollary to the present conclusions may be drawn concerning the electron excitation behaviour of a molecule, as deciphered by experiments *in vitro* in the absence of collisional perturbations. Evidently, quantitative data for the isolated molecule may not be applied tacitly to the interpretation of its performance in complex physical systems (e.g. in organic reaction mixtures), or *in vivo* (i.e., in biological systems).

A second corollary of interest is that a *novel Beer's law anomaly* for intercombinations may be observable in certain cases. Thus, in a pure liquid, the intensity of intercombinations in appropriate cases will consist of the sum of stationary and collisional perturbations, defined as given above. The true or intrinsic oscillator strength of the intercombinational absorption then may be obtained only by extrapolation to infinite dilution.

In conclusion it may be suggested that the collisional perturbation experiment should prove to be a useful general method for the development of $T \leftarrow S$ absorption bands in complex molecules. The method would be particularly effective in the cases where it is most needed, i.e., in extremely large molecules. Here, the effect of the stationary heavy-atom perturbation is very small, whereas their "π-electron surface" becomes comparatively large and the more susceptible to collisional perturbations. For example, it is possible to predict that the *anthracene* molecule should be *blue* under a collisional perturbation, because its induced $T \leftarrow S$ absorption is expected in the red region of the spectrum.[5,6]

It is a pleasure to thank Mr. G. H. Whitham for carrying out the α-chloronaphthalene distillation and Dr. Mark C. Whiting for the very pure ethyl iodide sample.

[11] W. S. Metcalf, dissertation, University College, Oxford, 1950. I am greatly indebted to Dr. E. J. Bowen for a loan of this publication.

[12] J. Weiss, Trans. Faraday Soc. **33**, 48, 219 (1939); Nature **152**, 176 (1943); J. Weiss and H. Fischgold, Z. physik. Chem. B**32**, 135 (1936).

On the Free Energy of a Mixture of Ions: An Extension of Kramers' Theory*

T. H. BERLIN, *Department of Physics, The Johns Hopkins University, Baltimore, Maryland*

AND

E. W. MONTROLL,† *Institute for Fluid Dynamics and Applied Mathematics, University of Maryland, College Park, Maryland*

(Received August 3, 1951)

A theory of electrolytes founded on the principles of statistical mechanics is presented. The primary physical assumptions are: (1) point ions, and (2) small fluctuations. The theory is a modification of Kramers' theory of electrolytes. The modification consists of a more physically accurate development of assumption (2). The main result of the present theory is that a partition function for the electrolyte is obtained for all concentrations, whereas Kramers' theory breaks down beyond a limiting concentration. The deviation from the Debye-Hueckel limiting law is in the direction of the experimental observations.

INTRODUCTION

IN the early days of the development of the theory of strong electrolytes, Kramers[1] showed that the Debye-Hueckel low concentration limiting laws could be derived from the statistical mechanical partition function as well as from the Poisson-Boltzmann differential equation. However, with increasing concentration the Kramers and experimental results diverged in opposite directions from the Debye-Hueckel limiting laws. This can be seen in Fig. 1 where the osmotic coefficient[2] is plotted[3] as a function of the square root of the concentration for a (1–1) salt, a salt of NaCl type.

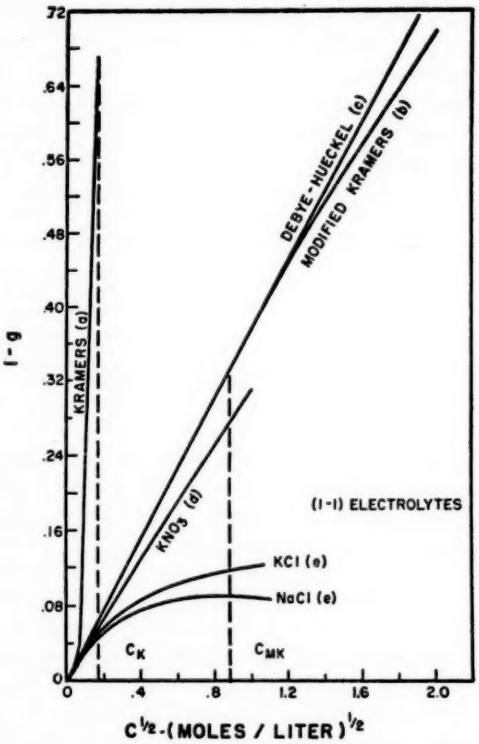

FIG. 1A. The osmotic coefficient, $1-g$, as a function of the square root of the concentration, C for a (1–1) electrolyte. (a) The Kramers theory: $C_K=0.029$ mole/liter. (b) The modified Kramers theory: $C_{MK}=0.78$ mole/liter. (c) The Debye-Hueckel limiting law. (d) Scatchard and Prentiss, J. Am. Chem. Soc. **44**, 2690 (1932). (e) Scatchard and Prentiss, J. Am. Chem. Soc. **55**, 4355 (1933).

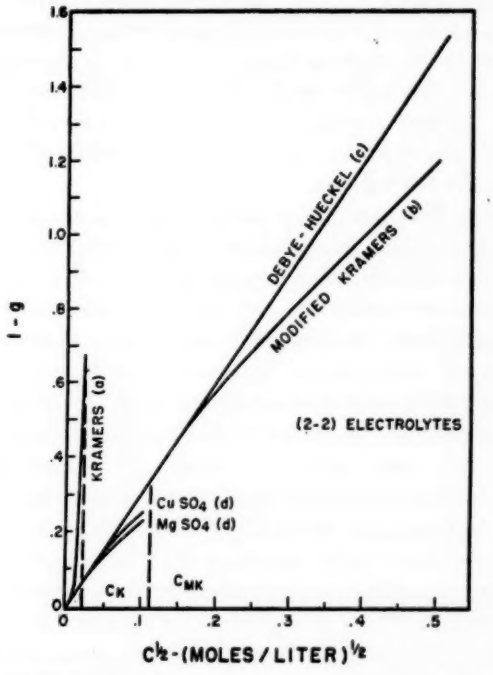

FIG. 1B. The osmotic coefficient, $1-g$, as a function of the square root of the concentration, C, for a (2–2) electrolyte. (a) The Kramers theory: $C_K=0.00048$ mole/liter. (b) The Modified Kramers theory: $C_{MK}=0.013$ mole/liter. (c) The Debye-Hueckel limiting law. (d) Hovorka and Rodebush, J. Am. Chem. Soc. **49**, 647 (1927).

* This work has been partly supported by the ONR.

† Most of this work was done while one of the authors was associated with the Institute for Mathematics and Mechanics at New York University, New York, New York.

[1] H. A. Kramers, Proc. Roy. Acad. (Amsterdam) **XXX**, 145 (1927).

[2] The osmotic coefficient was defined by N. Bjerrum as follows. Let $\bar{P}=NkT$ be the osmotic pressure of a solution of N independent (noninteracting) ions. Also, let $P=gNkT$ be the osmotic pressure of the corresponding real solution in which the ions interact with each other. Here g is the correction factor to $\bar{P}$ for a real solution. The ratio $(\bar{P}-P)/\bar{P}=1-g$ is the osmotic coefficient.

[3] Detailed accounts of the observed behavior of electrolytes and of the consequences of the Debye-Hueckel theory are given in the two treatises: (a) H. Falkenhagen, *Electrolytes* (Oxford University Press, Oxford, England, 1934); (b) H. S. Harned and B. B. Owens, *The Physical Chemistry of Electrolytic Solutions* (Reinhold

An especially interesting feature of Kramers' theory is the existence of a critical concentration above which the partition function becomes a complex number. To understand Kramers' interpretation of this result let us suppose that we have obtained an exact formula for the osmotic coefficient of a system of ions of ionic radius a. A curve such as one of those plotted in Fig. 1 could be drawn for each value of a. In particular there would be a limit curve as $a \to 0$. If the result of Kramers were exact, the critical concentration would be that concentration above which the limit curve would not exist. Physically this might mean that if the concentration of a dilute solution of point ions were gradually increased, a sudden association of oppositely charged ions would occur at the critical concentration with a correspondingly sudden drop in the osmotic coefficient.

The Kramers critical concentration is quite low, and corresponds to 0.03 mole per liter for KCl in water at 15°C and to 0.0005 mole per liter for $MgSO_4$. Even though real ions have nonvanishing ionic radii, one would expect that if the association divergence in the osmotic coefficient for point ions were correct, then some residue of it should still appear in the experimental curves in the neighborhood of the critical concentration. Actually the experimental deviations from the limiting laws for some "small ion" salts (KNO_3) do not become significant until the concentration is considerably higher than the critical one.

Since Kramers' paper contains several mathematical approximations, to which he called attention, we have felt that it would be of interest to see whether or not his qualitative results depend on the mathematical approximations. By replacing what we consider to be Kramers' most severe approximation by one that is physically more reasonable, we shall show that the divergence at the critical concentration disappears and that the new deviations from the Debye-Hueckel limiting laws (for point ions) are in the same direction as the experimental deviations. Inasmuch as we do not include short range repulsive force parameters in the theory, we obtain a single function for thermodynamic quantities of salts of a given ionic type rather than the family of functions that has been observed experimentally.

KRAMERS' THEORY OF ELECTROLYTES

We shall present the main features of Kramers' theory. This is done because Kramers' really elegant analysis is not widely known and because our modification will then be readily understandable.

Let N ions with charges $\epsilon_1, \epsilon_2, \cdots, \epsilon_N$ be located at positions $\mathbf{r}_1, \cdots, \mathbf{r}_N$ in a container of volume V. The thermodynamic properties of this system can be computed from the partition function,

$$Z = V^N \exp[-\Delta\psi/kT]$$

$$= \int_V \cdots \int d\tau_1 \cdots d\tau_N \exp[-U(\mathbf{r}_1, \cdots, \mathbf{r}_N)/kT]. \quad (1)$$

Here $d\tau_j$ is the volume element of the jth ion and $U(\mathbf{r}_1, \cdots, \mathbf{r}_N)$ is the total potential energy of interaction of all the ions. The symbol $\Delta\psi$ denotes the deviation of the free energy of the system of ions from that of a system of N independent point particles.

It was discovered by early workers that if $U(\mathbf{r}_1, \cdots, \mathbf{r}_N)$ represents only Coulomb interactions,

$$U(\mathbf{r}_1, \cdots, \mathbf{r}_N) = D^{-1} \sum_{j<k} \epsilon_j \epsilon_k / r_{jk}, \quad (2)$$

(D = dielectric constant of the solvent and r_{jk} is the distance between the jth and kth ions), then the thermodynamic quantities computed on the basis of (1) diverge. This short range divergence does not really occur because of the existence of short range repulsive forces. In the work of Kramers the divergence is avoided by essentially excluding ionic configurations involving very short distances.

Kramers' analysis is based on a theorem of O. Klein[4] which states that if $U(\mathbf{r}_1, \cdots, \mathbf{r}_N)$ is a homogeneous function of degree μ, that is, $U(\lambda\mathbf{r}_1, \cdots, \lambda\mathbf{r}_N) = \lambda^\mu U(\mathbf{r}_1 \cdots, \mathbf{r}_N)$, then, for N sufficiently large,

$$\exp[-\Delta\psi/kT] = [F(n^{-\mu/3}/kT)]^N,$$

where n is the number of particles per unit volume and F is some function of $(n^{-\mu/3}/kT)$. Klein's theorem cannot be applied if the ionic radius or any of the usual expressions for the repulsive forces is introduced because the homogeneous character of the potential energy function is lost.

The Coulomb interaction as a function of distance is a homogeneous function of degree -1. In order to avoid the short range divergence and preserve the homogeneity of (2), Kramers replaces (2) by

$$U(\mathbf{r}_1, \cdots, \mathbf{r}_N) = D^{-1} \sum_{j<k} \epsilon_j \epsilon_k g_{jk}, \quad (3)$$

where

$$g_{jk} = r_{jk}^{-1}[1 - \exp(-\lambda h_{jk})],$$

$$h_{jk}^2 = r_{jk}^2/4R_{jk}^2 = \frac{(x_j-x_k)^2+(y_j-y_k)^2+(z_j-z_k)^2}{(x_j+x_k)^2+(y_j+y_k)^2+(z_j+z_k)^2}.$$

As $r_{jk} \to 0$, $g_{jk} \to \lambda/2R_{jk}$. However, if λ is chosen to be a very large number, then $g_{jk} = r_{jk}^{-1}$ except when r_{jk} is extremely small. By locating the origin of the coordinate system outside the volume V, R_{jk} is of order $V^{\frac{1}{3}}$. Since the mean distance between ions is of order $n^{-\frac{1}{3}}$, $n = N/V$, h_{jk} is of order $N^{-\frac{1}{3}}$. Hence, by choosing λ to be of order $N^{\frac{1}{3}}$ the potential energy function (3) does not differ

Publishing Corporation, New York, 1950). Very few references to the classical papers will be given here. They can be found in (a) and (b).

[4] O. Klein, Medd. Vetenskapsakad. Nobelinst. **5**, No. 6 (1919).

significantly from the Coulomb function even for r_{jk} considerably smaller than the mean distance between ions. When there is considerable association of oppositely charged ions, i.e., at high concentrations, (3) cannot be expected to give quantitative results. Since the constant λ does not appear in the final results, there is no way of varying the thermodynamic properties with the characteristics of the repulsive forces.

In his detailed calculations, Kramers does not use (1) but a partition function analogous to the Gibbs grand partition function. His generalized ensemble is such that for a given configuration of the centers of the N ions, the charge on a given ion may assume any value which the charge of an arbitrary ion can have. The new partition function is defined by

$$V^N \exp[-\Delta\psi/kT] = \int_V \cdots \int d\tau_1 \cdots d\tau_N N^{-N} \sum \exp[-U/kT], \quad (4)$$

where the summation under the integral extends over all possible arrangements of the charges $\epsilon_1, \epsilon_2, \cdots, \epsilon_N$ on the ions located in the volume elements $d\tau_1, d\tau_2, \cdots, d\tau_N$.[5]

The total potential energy is a quadratic form in the charges $\{\epsilon_j\}$. Kramers diagonalizes this quadratic form by introducing a set of variables $\{y_j\}$ which are linear combinations of the variables $\{\epsilon_j\}$, $y_k = \sum_j \gamma_{kj}\epsilon_j$, and choosing the matrix (γ_{kj}) so that $U = \frac{1}{2}\sum_j b_j y_j^2$. The b's are the characteristic values of the matrix $(D^{-1}g_{kj})$.

In order to take advantage of the diagonalization, Kramers then assumed that the variables $\{y_j\}$ could be regarded as continuous variables and that the distribution of the set $\{y_j\}$ was Gaussian in each variable. The probability that y_k lay in the range dy_k was given by

$$(2\pi\eta)^{-\frac{1}{2}} \exp[-y_k^2/2\eta]dy_k.$$

Here η is a number proportional to the ionic strength, and $\eta^{\frac{1}{2}}$ is the standard deviation from neutrality of a charge chosen at random in a solution.

It was noted by Kramers that the characteristic values $\{b_j\}$, which depend on the ionic configuration, are not all positive for every configuration. This implies that for T sufficiently small integration over y_k, say, would lead to an infinite value. It is the nonpositive definite quadratic form coupled with the assumption of statistically independent y_k's with Gaussian distribution which is responsible for the breakdown of Kramers' theory above a critical concentration. Increasing concentration is equivalent to decreasing temperature because, from Klein's theorem, these two variables are equivalent to the single variable $n^{\frac{1}{2}}/T$.

This concludes our résumé of Kramers' work. Further details involve the evaluation of the partition function (4), and these details will appear below in the evaluation of our modified partition function.

[5] An investigation of thermodynamic fluctuations in this generalized ensemble has been made by S. Levine, Proc. Roy. Soc. (London) **A152**, 529 (1935).

THE MODIFIED KRAMERS THEORY

An important parameter of a system of ions is the reciprocal length κ which is defined by

$$\kappa^2 \equiv (4\pi/DkT)\sum_{i=1}^{s}(N_i/V)e^2z_i^2, \quad (5)$$

where s is the number of ionic species, N_i is the number of ions of the ith species and ez_i is the charge on an ion of the ith species (e being the electron charge).

Let

$$\eta \equiv DkTV\kappa^2/4\pi N. \quad (6)$$

This is a constant proportional to the ionic strength, and we may write, using Eqs. (5) and (6),

$$\sum_{j=1}^{N}\epsilon_j^2 = N\eta. \quad (7)$$

Our modification of Kramers' theory consists of computing thermodynamic averages over the ensemble restricted by Eq. (7) for fixed η. A charge configuration in our ensemble will consist of a set of N ions with the properties:

(a) $-(N\eta)^{\frac{1}{2}} \leqslant \epsilon_j \leqslant (N\eta)^{\frac{1}{2}}$ for all j;

(b) $\sum_{j=1}^{N}\epsilon_j^2 = N\eta$;

the value of the sum in the real physical system of interest. Our complete ensemble will be the set of all systems of N ions with the proper ionic strength (i.e., with the proper value of $N\eta$) which are confined to a container of fixed shape and volume V at constant temperature T.

The average value of a function of position and charge, $F(\{\mathbf{r}_j\}, \{\epsilon_j\})$, will then be

$$\langle F\rangle = Z^{-1}\int\cdots\int_{\sum_{j=1}^{N}\epsilon_j^2 = N\eta}\int_V\cdots\int d\epsilon_1\cdots d\epsilon_N d\tau_1\cdots d\tau_N \times F(\{\mathbf{r}_j\}, \{\epsilon_j\})\exp[-U/kT], \quad (8)$$

where Z is the partition function given by

$$Z = V^N \exp[-\Delta\psi/kT] = A\int\cdots\int_{\sum_{j=1}^{N}\epsilon_j^2 = N\eta}\int_V\cdots\int d\epsilon_1\cdots d\epsilon_N d\tau_1\cdots d\tau_N \times \exp[-U/kT]. \quad (9)$$

The constant A is chosen so that as $T\to\infty$, $\Delta\psi\to 0$. A is the reciprocal of the surface area of an N-dimensional sphere of radius $(N\eta)^{\frac{1}{2}}$.

$$A^{-1} = 2\pi^{N/2}(N\eta)^{(N-1)/2}/\Gamma(N/2). \quad (10)$$

Before attempting to compute the foregoing partition function let us compare the modified ensemble with that of Kramers. Kramers' basic partition function, Eq. (4), may be considered to be correct (to within the limitations inherent in the manner in which the Coulomb divergence is avoided as $r_{jk}\to 0$) at least for symmetrical electrolytes.‡ However, after making his mathematical approximations, Kramers' ensemble becomes one in which the $\{\epsilon_j\}$ are not limited to discrete values $ez_1, \cdots, ez_s$ but are allowed to range between $-\infty$ and $+\infty$ with the probability for ϵ_j to lie between ϵ_j and $\epsilon_j+d\epsilon_j$ given by $(2\pi\eta)^{-\frac{1}{2}}\exp[-\epsilon_j^2/2\eta]d\epsilon_j$. Averages are taken over all ϵ_k's and all $\mathbf{r}_k$'s. Since the $\{\epsilon_j\}$ are independent variables, the ionic strength for the systems in this ensemble ranges from 0 to ∞. The modified ensemble is that part of Kramers' ensemble which contains systems of the correct ionic strength. The ϵ_j's are not independent but connected through the relation,

$$\sum_{j=1}^{N}\epsilon_j^2=N\eta.$$

It is this property which makes the modified ensemble more representative of a real electrolyte than Kramers' ensemble.

To evaluate the partition function, Eq. (9), we (as did Kramers) take advantage of the fact that U is a quadratic form in the charges. Multiplying the integrand of Eq. (9) by the delta function,

$$\delta(\epsilon_1, \cdots, \epsilon_N)=\frac{2(N\eta)^{\frac{1}{2}}}{2\pi}\int_{-\infty}^{\infty}dx\exp[ix(\sum_{j=1}^{N}\epsilon_j^2-N\eta)], \quad (11)$$

normalized to A^{-1} so that $Z\to V^N$ as $T\to\infty$, we have

$$Z=A\int_{-\infty}^{\infty}\cdots\int\int_{V}\cdots\int d\epsilon_1\cdots d\epsilon_N d\tau_1\cdots d\tau_N \times\delta(\epsilon_1, \cdots, \epsilon_N)\exp[-U/kT]. \quad (12)$$

Rearranging the order of integration, we write

$$Z=A\pi^{-1}(N\eta)^{\frac{1}{2}}\int_{ix_0-\infty}^{ix_0+\infty}dx\exp[-ixN\eta] \times\int_{V}\cdots\int d\tau_1\cdots d\tau_N\int_{-\infty}^{\infty}\cdots\int d\epsilon_1\cdots d\epsilon_N \times\exp[ix\sum_{j=1}^{N}\epsilon_j^2-(DkT)^{-1}\sum_{j<k}\epsilon_j\epsilon_k g_{jk}], \quad (13)$$

where the line $ix_0=$constant, x_0 real and positive, is above the singularities of the integrand. The rearrangement is possible because U as defined in (3) is finite for all positional configurations of the ions. Therefore an x-domain will exist for which the quadratic form in the $\{\epsilon_j\}$ is negative definite. Thus, the integration over the $\{\epsilon_j\}$ will be finite. We then have that

$$\int_{-\infty}^{\infty}\cdots\int d\epsilon_1\cdots d\epsilon_N\exp[ix\sum_{j=1}^{N}\epsilon_j^2 -(DkT)^{-1}\sum_{j<k}g_{jk}\epsilon_j\epsilon_k]=\pi^{N/2}/D_N^{\frac{1}{2}}, \quad (14)$$

where D_N is the determinant of the quadratic form in the exponent.

$$D_N\equiv|-ix\delta_{jk}+(2DkT)^{-1}g_{jk}|\,; \quad g_{jj}=0. \quad (15)$$

Therefore,

$$Z=A(N\eta)^{\frac{1}{2}}\pi^{\frac{1}{2}N-1}\int_{ix_0-\infty}^{ix_0+\infty}dx\exp[-ixN\eta] \times\int_{V}\cdots\int D_N^{-\frac{1}{2}}d\tau_1\cdots d\tau_N. \quad (16)$$

We shall briefly digress in order to point out that the condition of electrical neutrality holds in the mean as it does in Kramers' theory. The total charge of a system is

$$Q=\sum_{j=1}^{N}\epsilon_j$$

so that $\langle Q\rangle=N\langle\epsilon_j\rangle$. Now a linear, orthogonal transformation from the variables $\{\epsilon_j\}$ to variables $\{y_j\}$ exists such that the quadratic form in the $\{\epsilon_j\}$ becomes $\frac{1}{2}\sum_j b_j y_j^2$. This means that

$$\langle\epsilon_j\rangle=\sum_{k=1}^{N}\gamma_{jk}\langle y_k\rangle,$$

the γ_{jk}'s being the transformation coefficients. Since the integrand in Eq. (13) becomes an even function of y_j for all j, then $\langle y_j\rangle=0$ for all j and $\langle Q\rangle=0$.

Now we may write

$$\exp[-\Delta\psi/kT]=A(N\eta)^{\frac{1}{2}}\pi^{\frac{1}{2}N-1} \times\int_{ix_0-\infty}^{ix_0+\infty}dx\exp[-ixN\eta]G_N, \quad (17)$$

with

$$G_N\equiv V^{-N}\int_{V}\cdots\int D_N^{-\frac{1}{2}}d\tau_1\cdots d\tau_N\equiv\langle D_N^{-\frac{1}{2}}\rangle_V. \quad (18)$$

Following Kramers, if $\Delta\psi$ is to have thermodynamic sense, G_N would be the most probable value of $D_N^{-\frac{1}{2}}$ as $N\to\infty$, where x would be considered as a parameter of external constraint on the system. Assuming that fluctuations are small, which is valid for not too high concentrations, Eq. (18) can be written as

$$G_N=\langle D_N\rangle_V^{-\frac{1}{2}}. \quad (19)$$

This means that as $N\to\infty$, G_N is the reciprocal square root of the most probable value of D_N.

‡ See reference 5. Apparently in unsymmetrical salts some corrections might have to be made in the free energies.

If we followed Kramers in applying Klein's theorem to Eq. (18), we would have $G_N=[\phi(x, n^{\frac{1}{3}}/T)]^N$ for N sufficiently large, where ϕ is some function of the variables x and $n^{\frac{1}{3}}/T$. This approximation is not sufficiently exact for our purposes because the essential singularity of G_N is not properly characterized by the function ϕ. The essential singularity of G_N can be put in evidence by noting that the transformation from the variables $\{\epsilon_j\}$ to the variables $\{y_j\}$ is such that

$$\sum_{j<k} g_{jk}\epsilon_j\epsilon_k=\tfrac{1}{2}\sum_{j=1}^{N} b_j y_j^2.$$

We can then write

$$D_N=\prod_{j=1}^{N}[-ix+(2DkT)^{-1}b_j]. \tag{20}$$

It is plain that we may write

$$\langle D_N\rangle_V=\prod_{j=1}^{N}[-ix+(2DkT)^{-1}\lambda_j], \tag{21}$$

where $(2DkT)^{-1}\lambda_j$ is one of the N roots of the polynomial $\langle D_N\rangle_V$. Since the matrix (g_{jk}) is real and symmetric, the roots are real, and $|\lambda_j|\leqslant\lambda_m(N)$ where $\lambda_m(N)$ is the magnitude of the maximum root of $\langle D_N\rangle_V$. The maximum root may be independent of N. This also means that in Eq. (17) we must take $x_0>(2DkT)^{-1}\lambda_m(N)$.

Let us put $\alpha^{-1}=-ix2DkT$, and write

$$\langle D_N\rangle_V=(-ix)^N\exp[Ng_N], \tag{22}$$

where

$$g_N(\alpha)=\frac{1}{N}\sum_{j=1}^{N}\ln(1+\alpha\lambda_j).$$

The function $g_N(\alpha)$ is analytic in the region $|\alpha|<1/\lambda_m(N)$.

Thermodynamic arguments require the existence of $g_N(\alpha)$ as $N\to\infty$, that is, $g_\infty(\alpha)$ must exist. Since $\lambda_m(N)$ exists for every N and since the radius of convergence is $1/\lambda_m(N)$ for every N, the existence of the limit function $g_\infty(\alpha)$ implies a nonzero radius of convergence and the consequence that $\lambda_m(N)\to\lambda_m(\infty)\equiv\lambda_m$, where a finite λ_m must exist. Therefore, λ_m may be determined from the radius of convergence of $g_\infty(\alpha)$ if this function can be found.

The existence of a finite λ_m has the following consequence. Since $|\lambda_j|\leqslant\lambda_m(N)$ for all j, the N roots are confined to a finite real interval. In general, the N roots will be all different. Therefore, as $N\to\infty$, the roots will become dense in the limit. It then follows that the behavior of $g_\infty(\alpha)$ as $\alpha\to1/\lambda_m$, that is, the character of the singularity of g_∞ on the radius of convergence, depends on the limiting density of the λ_j. It is then clear that the character of the singularity of g_∞ has little to do with the single term $\ln[1\pm\alpha\lambda_m(N)]$ in the sum g_N which exactly describes the singularity at $\alpha=\mp1/\lambda_m(N)$ for every N. This means that an accurate description of Ng_N as $N\to\infty$ requires us to write

$$Ng_N\to\ln(1-\alpha\lambda_m)+Ng, \quad |\alpha|<1/\lambda_m, \tag{23}$$

where

$$g(\alpha)=\lim_{N\to\infty}\frac{1}{N}\sum_{\substack{j=1\\ \lambda_j\neq-\lambda_m}}^{N}\ln(1+\alpha\lambda_j),$$

and we have supposed that the singularity occurs at $\alpha=+1/\lambda_m$. Because the roots become dense in the limit, $g(\alpha)=g_\infty(\alpha)$. Hence, we are required to write

$$\langle D_N\rangle_V=(1-\alpha\lambda_m)(-ix)^N\exp[Ng] \tag{24}$$

as $N\to\infty$. It should be noted that the previously mentioned $\phi=\exp g$. This more accurate limiting expression for $\langle D_N\rangle_V$ does not influence the result obtained by Kramers.

The application of Klein's theorem implies that g will be a function of the two variables x and $n^{\frac{1}{3}}/T$, or α and $n^{\frac{1}{3}}$, and that λ_m will be proportional to $n^{\frac{1}{3}}$.

Equation (24) is equivalent to stating that for N large, $\langle D_N\rangle_V=O(M^N)$ where M is a function independent of N. We followed Kramers' thermodynamic reasoning to obtain this result. It is implicit in Klein's theorem that the Nth root of the partition function integral be bounded as $N\to\infty$. It is clear, however, that the asymptotic behavior of D_N, and that of $\langle D_N\rangle_V$, depends on the properties of the elements of the determinant. For example, if $D_N=\det a_{ij}$ and if all that was known about the elements a_{ij} was that $|a_{ij}|\leqslant M$ for all i, j with M a positive constant, then the most one could state is the result of Hadamard's theorem,[6] $|D_N|\leqslant N^{\frac{1}{2}N}M^N$. This implies that $|D_N|^{1/N}\leqslant MN^{\frac{1}{2}}\to\infty$ as $N\to\infty$. Thus, we would have no guarantee that a thermodynamic free energy per particle would exist independent of N, and Klein's theorem could not be applied.

A condition on the elements a_{ij} sufficient to insure the existence of the required limit is easily found. The antecedent of Hadamard's inequality is that of Kelvin, Muir, and Hadamard[7] which states that

$$|D_N|^2\leqslant\prod_{j=1}^{N}\Big(\sum_{k=1}^{N}|a_{jk}|^2\Big). \tag{25}$$

Hence, if

$$\sum_{k=1}^{N}|a_{jk}|^2\leqslant M^2$$

for all j, then $|D_N|\leqslant M^N$ so that $D_N=O(M^N)$ if M exists. In our case,

$$\lim_{N\to\infty}\sum_{k=1}^{N}|a_{jk}|^2=x^2+\lim_{N\to\infty}\sum_{\substack{k=1\\ k\neq j}}^{N}(2DkT)^{-2}g_{jk}^2$$

$$\simeq x^2+(2DkT)^{-2}\int_0^\infty f(r)r^{-2}[1-\exp\{-\lambda h(r)\}]^2dr, \tag{26}$$

[6] Whittaker and Watson, *Modern Analysis* (Cambridge University Press, London, 1940), fourth edition, p. 212.

[7] Hardy, Littlewood, and Polya, *Inequalities* (Cambridge University Press, London, 1934), p. 34.

where $f(r)$ is the radial distribution function of ions about a given ion. This is an average value of the required sum. As $r\to\infty$, $h(r)\sim r/V^{\frac{1}{3}}$ and $f(r)\sim r^2$. Thus, the integral does not converge as N, $V\to\infty$, N/V finite. However, we can make the integral converge by introducing a summability factor $\exp[-\mu h(r)]$, μ a small, real, positive constant, into the force law, Eq. (3). Then

$$g_{jk}=r_{jk}^{-1}[1-\exp(-\lambda h_{jk})]\exp(-\mu h_{jk}). \quad (27)$$

Once it is assumed through this factor that $\sum_k|a_{ik}|^2$ is bounded, then $D_N=O(M^N)$, and we are justified in employing Eq. (24) for $\langle D_N\rangle_V$.

Returning to Eq. (19) for G_N, we now have the result that the singularity of G_N is a branch point of order 1, and in the limit $N\to\infty$ occurs at $x=i(2DkT)^{-1}\lambda_m$.

We follow Kramers' method for determining the limiting function $g(x, n^{\frac{1}{3}}/T)$. Let us put

$$\alpha^{-1}=-ix2DkT, \quad \langle D_N\rangle_V=(-ix)^N A_N. \quad (28)$$

Therefore,

$$A_N=\alpha^N\langle|g_{jk}+\alpha^{-1}\delta_{jk}|\rangle_V; \quad g_{jj}=0. \quad (29)$$

Note that A_N depends on x only through α.

Differentiating A_N with respect to α, and noting that the spatial averages of the minors of the diagonal elements of A_N refer to a system of $N-1$ ions and that these averages are all equal, we have

$$\alpha\partial A_N/\partial\alpha=NA_N-NA_{N-1}. \quad (30)$$

Since $\alpha\sim T^{-1}$, and since Klein's theorem shows that A_N depends only on the variables N and $n^{\frac{1}{3}}/T$, let us write

$$A_N=(1-ay^{\frac{1}{3}})[\omega(y)]^N, \quad (31)$$

where

$$y=n\alpha^3, \quad n=N/V, \quad \lambda_m=an^{\frac{1}{3}},$$

with a a numerical constant. Consequently, we are to find the function $\omega(y)$ which satisfies the differential-difference Eq. (30) for N sufficiently large.

Using the form for A_N in Eq. (30), then

$$3y\frac{\partial\omega}{\partial y}-\frac{ay^{\frac{1}{3}}\omega(y)}{N(1-ay^{\frac{1}{3}})}=\omega-\frac{[1-a(y')^{\frac{1}{3}}]}{(1-ay^{\frac{1}{3}})}[\omega(y')/\omega(y)]^{N-1}, \quad (32)$$

where

$$y'=n'\alpha^3=[(N-1)/V]\alpha^3=y-(y/N).$$

However,

$$\omega(y')=\omega(y)-(y/N)(\partial\omega/\partial y)+\cdots. \quad (33)$$

Therefore,

$$[\omega(y')/\omega(y)]^{N-1}=\exp(N-1)[-(y/N\omega)(\partial\omega/\partial y)+\cdots]\cong\exp[-(y/\omega)(\partial\omega/\partial y)], \quad (34)$$

$$1-a(y')^{\frac{1}{3}}=1-ay^{\frac{1}{3}}+ay^{\frac{1}{3}}/3N\cdots.$$

Thus, using Eq. (34), we have in the limit $N\to\infty$,

$$3y(\partial\omega/\partial y)=\omega-\exp[-(y/\omega)(\partial\omega/\partial y)], \quad (35)$$

when $|y|<1/a^3$.

The exact solution of Eq. (35) can be conveniently represented in parametric form. Defining

$$F(y)=-(y/\omega)(\partial\omega/\partial y),$$

we have

$$\omega=e^F/(1+3F), \quad K^2y=F^2/(1+3F)^3, \quad (36)$$

where K is an integration constant. Kramers has neatly determined this constant to be

$$K=\tfrac{1}{3}(4\pi)^{\frac{1}{3}} \quad (37)$$

by finding A_N for small concentrations. It could, of course, be found by fitting the results to the Debye-Hueckel limiting law. Equation (36) differs from Kramers' result in that y, through α, is a function of x.

Consequently, through Eqs. (36), (31), (28), and (24), we find that

$$\exp(g)=(-ix)e^F/(1+3F). \quad (38)$$

This then yields

$$G_N=[1-(-ix2DkT)^{-1}\lambda_m]^{-\frac{1}{3}}\times[(1+3F)e^{-F}/(-ix)]^{N/2}, \quad (39)$$

where λ_m is to be found from the corresponding singularity of g.

Setting

$$z=-ix2\eta, \quad \gamma^3\equiv K^2n(\eta/DkT)^3, \quad (40)$$

F as a function of z is determined by

$$F^2/(1+3F)^3=\gamma^3/z^3. \quad (41)$$

Using the value of A in Eq. (10) for N large, Eq. (17) becomes

$$\exp[-\Delta\psi/kT]=(\pi N)^{\frac{1}{3}}e^{-N/2}I,$$

$$I\equiv(2\pi i)^{-1}\int_{z_0-i\infty}^{z_0+i\infty}dz[1-(\lambda_m\eta/DkTz)]^{-\frac{1}{3}}\times[z^{-1}(1+3F)e^{-F+z}]^{N/2}, \quad (42)$$

where Eq. (39) has been used and the line $z_0=$ constant, z_0 real and positive, is to the right of the singularities of the integrand.

The integral I is evaluated by the method of steepest descent. The details are presented in the appendix and we shall use the result here.

It turns out that I has two forms depending on the value of γ. For N sufficiently large, we obtain

$$-\Delta\psi/NkT=\gamma^3, \quad 0\leqslant\gamma\leqslant\gamma_c, \quad (43)$$

$$-\Delta\psi/NkT=\tfrac{3}{2}(\gamma/\gamma_c)-\tfrac{1}{2}\ln(\gamma/\gamma_c)-\tfrac{5}{6}, \quad \gamma\geqslant\gamma_c, \quad (44)$$

with $\gamma_c=(2/3)^{\frac{1}{3}}$.

DISCUSSION

We are now able, through Eqs. (43) and (44), to calculate all of the thermodynamic properties of the mixture of ions. However, we will restrict ourselves to the more important quantities. It is to be recalled that $\gamma^3=(4\pi/9)n(\eta/DkT)^3$ where η is related to the ionic strength through Eq. (6).

For the decrease $\Delta P=P-\bar{P}$ in the osmotic pressure P we have

$$\Delta P=-\frac{\partial}{\partial v}(\Delta\psi/N)$$
$$=\begin{cases}-(kT/2v)\gamma^3, & \gamma\leqslant\gamma_c\\ -(kT/2v)[(\gamma/\gamma_c)-\frac{1}{3}], & \gamma\geqslant\gamma_c\end{cases} \quad (45)$$

where $v=1/n$. Since $\bar{P}=(kT/v)$, the osmotic coefficient is given by

$$1-g=\begin{cases}\frac{1}{2}\gamma^3, & \gamma\leqslant\gamma_c\\ \frac{1}{2}[(\gamma/\gamma_c)-\frac{1}{3}], & \gamma\geqslant\gamma_c\end{cases}. \quad (46)$$

A plot of the osmotic coefficient against the square root of the concentration is shown in Fig. 1. We obtain the Debye-Hueckel limiting law up to the equivalent concentration γ_c. Deviations from the limiting law in the proper direction set in for concentrations greater than the critical concentration.

For the decrease $\Delta\varphi$ in the thermodynamical potential we have

$$\Delta\varphi/N=\Delta\psi/N+v\Delta P$$
$$=\begin{cases}-(3/2)kT\gamma^3, & \gamma\leqslant\gamma_c\\ -kT[2(\gamma/\gamma_c)-\frac{1}{2}\ln(\gamma/\gamma_c)-1], & \gamma\geqslant\gamma_c\end{cases}. \quad (47)$$

The logarithm of the activity coefficient, f_{ai}, for an ion of the ith species is defined by

$$\ln f_{ai}=(1/kT)\frac{\partial\Delta\psi}{\partial N_i}. \quad (48)$$

We then find

$$\ln f_{ai}=\begin{cases}-(e^2z_i^2/\eta)(\gamma/\gamma_c)^3, & \gamma\leqslant\gamma_c\\ -\frac{1}{2}[(\gamma/\gamma_c)-\ln(\gamma/\gamma_c)-1] & \\ \quad -\frac{1}{2}(e^2z_i^2/\eta)[3(\gamma/\gamma_c)-1], & \gamma\geqslant\gamma_c.\end{cases} \quad (49)$$

The nature of the singularity in $\Delta\psi$ at $\gamma=\gamma_c$ is easily determined to be a discontinuity in $(\partial^3\Delta\psi/\partial\gamma^3)\gamma_c$. This would mean that the osmotic coefficient is continuous with a continuous first derivative at γ_c. It is the specific heat, however, which exhibits the most unusual behavior.

We easily calculate

$$\Delta E/N=\begin{cases}-\frac{3}{2}kT\gamma^3, & \gamma\leqslant\gamma_c\\ -\frac{3}{2}kT[(\gamma/\gamma_c)-\frac{1}{3}], & \gamma\geqslant\gamma_c\end{cases}. \quad (50)$$

Defining the change in specific heat by

$$\Delta C=\frac{\partial}{\partial T}(\Delta E),$$

we find

$$\Delta C/N=\begin{cases}(3k/4)\gamma^3, & \gamma\leqslant\gamma_c\\ k/2, & \gamma\geqslant\gamma_c\end{cases}. \quad (51)$$

Consequently, the modified theory yields a constant change in specific heat above γ_c with a discontinuity in the slope at γ_c.

It is to be emphasized that although the expressions for the common thermodynamic functions change their analytical form at $\gamma=\gamma_c$, they are still continuous through the critical concentration.

The fact that the modified theory yields a limiting partition function for all concentrations of the ions as the ionic radius approaches zero, demands that a revision, and in some aspects a reversal, of Kramers' conclusions be made. The primary assumptions underlying the theory are: (1) point ions, and (2) small fluctuations. Although the same assumptions underly Kramers' theory, the assumption of small fluctuations is not adequately treated in his theory because of the use of the Gaussian charge distribution. The selection in the modified theory of those systems in Kramers' ensemble having a given ionic strength is consistent with the assumption of small fluctuations.

We believe that the existence of the discontinuity in the modified theory is because of the "association" of ions, although we are unable to demonstrate this by a pertinent calculation (except through the behavior of the osmotic coefficient, for example). It is then implied that fluctuations become significant for $\gamma>\gamma_c$. However, the association is not the catastrophe of the Kramers theory. We may then conclude that the thermodynamic functions exist in the limit of zero ionic radius at concentrations greater than the critical concentration. A further implication is that when fluctuations become important it is also required to bring into the theory additional properties inherent in the existence of discrete charges, i.e., that

$$\sum_{i=1}^{s}e^4z_i^4=\text{constant}.$$

Our interpretation of the modified theory is that for concentrations less than the critical concentration fluctuations are unimportant and that deviations from the limiting law are indicative of the effect of finite ionic size and of the approximation of the ion-dipole (solute-solvent) interactions by a macroscopic dielectric constant. For concentrations greater than the critical, association plays an important part and this involves not only the finite ionic size and dielectric constant approximation but also the fluctuations. The modified theory does show the proper direction for the deviation

of the osmotic coefficient from the Debye-Hueckel law for concentrations greater than the critical.

The critical concentration of the modified Kramers theory is 27 times greater than the critical concentration of the Kramers theory (Kramers' results correspond to $z\equiv 1$). For a 1–1 salt, the new critical concentration is approximately 0.8 mole/liter rather than 0.03 mole/liter. The modified theory does not, therefore, allow us to conclude that the association of point ions becomes important at small concentrations.

The result of the work of Bjerrum and Fuoss that association does become important at small concentrations is, of course, in qualitative agreement with the observations. The present theory makes it clear that one cannot avoid the introduction of the finite ionic size if even the qualitative behavior of the small concentration deviations from the Debye-Hueckel law is to be reproduced. The discontinuity at γ_c probably does not actually exist in that a finite ionic size plus fluctuations undoubtedly force association to be gradual rather than sudden, even though the suddenness is not catastrophic.

Recently, J. E. Mayer[8] developed a statistical mechanical theory of strong electrolytes which is based on the Ursell-Mayer cluster integral expansion. His approach is probably more suitable than ours if one wishes to take the detailed ion-dipole interaction and van der Waals forces between ions into account. Since it is practically impossible to evaluate all the required cluster integrals, Mayer limits his main calculation to finding the contribution of the so-called ring clusters (in which each particle interacts with only two others) to various thermodynamic quantities. This contribution seems to be the part of the complete expansion which gives rise to the Debye-Hueckel approximation. Since we obtained similar results, it appears that sphericalization (the condition expressed by Eq. (7)) and the neglect of all cluster integrals except rings give almost equivalent approximations to the partition function.

It has been emphasized by Mayer that the long range Coulomb forces lead to difficulties in the evaluation of the partition function of a system of ions. The difficulties are avoided in his theory by the replacement of the Coulomb law with $(\epsilon_i\epsilon_j/r)\exp(-\mu r)$ where μ is a very small positive number. At short distances this expression reduces to the Coulomb law, but at large distances where electrical neutrality prevents a physical divergence in thermodynamic quantities, the factor $\exp(-\mu r)$ prevents a mathematical divergence in the partition function. Mayer's final results become independent of μ as $\mu\to 0$. The present analysis has also shown the utility of the convergence or summability factor $\exp(-\mu r)$. It was useful not only to prevent a possible divergence but to insure the existence of a limiting free energy per particle which is necessary for the application of Klein's theorem. As in the Mayer theory, if one takes into account the electrical neutrality at every step in the analysis, it should not be necessary to introduce the convergence factor. However, since this requires a much more extensive analysis we have avoided it.

The preceding analysis had its origin in the work of M. Kac on the Gaussian model of a ferromagnet and of M. Kac and the authors on the spherical model of cooperative phenomena.[9]

The authors wish to thank Mr. L. Witten for several discussions and his aid in preparing the figures.

APPENDIX

We shall present here the details of the evaluation by the method of steepest descent of the integral in Eq. (42).

$$I=(2\pi i)^{-1}\int_{z_0-i\infty}^{z_0+i\infty} dz[1-(\lambda_m\eta/DkTz)]^{-\frac{1}{2}} \times[z^{-1}(1+3F)\exp(-F+z)]^{N/2}, \quad \text{(A1)}$$

where

$$F^2/(1+3F)^3=\gamma^3/z^3,$$

and the line $z_0=$ constant, z_0 real and positive, is to the right of the singularities of the integrand.

The function F is a three-valued function of z. We can construct a Riemann surface of three sheets to make F an analytic function of z.

Let $\zeta=(z/3\gamma)^3$. The solutions of the cubic equation for F, are

$$\begin{aligned} F_1(z)&=\tfrac{1}{3}(\zeta-1)-\omega^2L^{\frac{1}{3}}-\omega M^{\frac{1}{3}};\\ F_2(z)&=\tfrac{1}{3}(\zeta-1)-\omega L^{\frac{1}{3}}-\omega^2M^{\frac{1}{3}}; \quad \text{(A2)}\\ F_3(z)&=\tfrac{1}{3}(\zeta-1)-L^{\frac{1}{3}}-M^{\frac{1}{3}}; \end{aligned}$$

the subscripts denoting the different sheets of the Riemann surface, and where

$$\begin{aligned} &\omega=\exp(i2\pi/3),\\ &L=-(\zeta/27)(\zeta^2-2\zeta+\tfrac{3}{2})+i(\zeta/27)(\zeta-9/4)^{\frac{1}{2}}, \quad \text{(A3)}\\ &M=-(\zeta/27)(\zeta^2-2\zeta+\tfrac{3}{2})-i(\zeta/27)(\zeta-9/4)^{\frac{1}{2}}. \end{aligned}$$

The discriminant of the cubic is $(4\zeta^2/27)(\zeta-9/4)$. The branch points occur when the discriminant equals zero and are $\zeta=0, 9/4$, and this means that the cubic has multiple roots. Note that the point at infinity is a branch point since $L\to M$ as $|\zeta|\to\infty$. The values of z at the branch points are $z=0$, $3\gamma(3/2)^{\frac{1}{3}}$, $3\gamma(3/2)^{\frac{1}{3}}\omega$, and $3\gamma(3/2)^{\frac{1}{3}}\omega^2$. Consequently, in the expression (A1) for I, we must take $z_0>3\gamma(3/2)^{\frac{1}{3}}$. Furthermore, λ_m corresponds to this largest, real, and positive singularity, and we conclude that

$$1-(\lambda_m\eta/DkTz)=1-3\gamma(3/2)^{\frac{1}{3}}z^{-1}, \quad \text{(A4)}$$

or

$$\lambda_m=3\pi^{\frac{1}{2}}\eta^{\frac{1}{2}}.$$

By constructing a cut in the z-plane as shown in Fig. 3, F_j is analytic in the cut plane.

[8] J. E. Mayer, J. Chem. Phys. **18**, 1426 (1950).

[9] M. Kac and T. H. Berlin, Phys. Rev. **75**, 1298 (1949). E. Montroll, Nuovo cimento, Supplemento **VI**, 266 (1949).

Let us write

$$e^G=z^{-1}(1+3F)e^{-F+z},$$

or

$$G=z-\ln z-F+\ln(3F+1), \tag{A5}$$

and attempt to find a saddle point. We have

$$dG/dz=z^{-1}(z-1-3F) \tag{A6}$$

and

$$d^2G/dz^2=2(1+3F)^2/z^2(2-3F). \tag{A7}$$

Letting z_s be such that $(dG/dz)_{z_s}=0$, then

$$z_s=1+3F(z_s). \tag{A8}$$

Using the relation between F and z, we obtain

$$F(z_s)=\pm\gamma^{\frac{1}{2}}, \quad z_s=1\pm3\gamma^{\frac{1}{2}}. \tag{A9}$$

Also

$$(d^2G/dz^2)_{z_s}=2/(3-z_s). \tag{A10}$$

We conclude that a saddle point exists for γ in the range $0\leqslant\gamma<\infty$ when $z_s=z_-=1-3\gamma^{\frac{1}{2}}$, and that a saddle point exists for $z_s=z_+=1+3\gamma^{\frac{1}{2}}$ for γ in the range $0\leqslant\gamma<\gamma_c=(2/3)^{\frac{1}{2}}$. When $\gamma=\gamma_c$, $z_+=3$, and the second derivative of G becomes infinite. For $\gamma\simeq0$, $z_s\simeq1$, and since $\zeta=(z/3\gamma)^3$, $|\zeta|\simeq(3\gamma)^{-3}\sim\infty$. It is easily found that when $|\zeta|\to\infty$,

$$\begin{aligned}F_1(z)&=+\tfrac{1}{9}(3/\zeta)^{\frac{1}{2}}+(6\zeta)^{-1}\cdots,\\ F_2(z)&=-\tfrac{1}{9}(3/\zeta)^{\frac{1}{2}}+(6\zeta)^{-1}\cdots,\\ F_3(z)&=\zeta-1-(3\zeta)^{-1}\cdots.\end{aligned} \tag{A11}$$

Therefore, the branch $F_1(z)$ corresponds to $F(z_+)=+\gamma^{\frac{1}{2}}$ and the branch $F_2(z)$ corresponds to $F(z_-)=-\gamma^{\frac{1}{2}}$.

From Eq. (A5),

$$G(z_s)=z_s-F(z_s)=1+2F(z_s),$$

so that

$$G(z_+)=1+2\gamma^{\frac{1}{2}} \quad \text{and} \quad G(z_-)=1-2\gamma^{\frac{1}{2}}. \tag{A12}$$

Since for large N, I is essentially $\exp[NG(z_+)/2]$ or $\exp[NG(z_-)/2]$, it is plain from Eq. (42) of the text, where

$$\exp[-\Delta\psi/kT]=(\pi N)^{\frac{1}{2}}e^{-N/2}I,$$

that the significant contribution to I arises from the saddle point z_+. As a consequence the integral I is to be evaluated on sheet 1 where we require $F(z)\equiv F_1(z)$. This means that we can now write

$$I\simeq(2\pi i)^{-1}\int_{z_+-i\infty}^{z_++i\infty}dz[1-3\gamma(3/2)^{\frac{1}{2}}z^{-1}]^{-\frac{1}{2}}\times\exp\frac{N}{2}[G(z_+)+\tfrac{1}{2}(d^2G/dz^2)_{z_+}(z-z_+)^2\cdots]$$

so that

$$I\simeq[1-3\gamma(3/2)^{\frac{1}{2}}z_+^{-1}]^{-\frac{1}{2}}[\pi N(d^2G/dz^2)_{z_+}]^{-\frac{1}{2}}\times\exp[NG(z_+)/2]. \tag{A13}$$

Hence,

$$\exp[-\Delta\psi/kT]=[1-(3\gamma/z_+\gamma_c)]^{-\frac{1}{2}}\times[1-(\gamma/\gamma_c)^{\frac{1}{2}}]^{\frac{1}{2}}\exp[N\gamma^{\frac{1}{2}}], \tag{A14}$$

and for N very large,

$$-\Delta\psi/NkT=\gamma^{\frac{1}{2}}, \quad \gamma<\gamma_c=(2/3)^{\frac{1}{2}}. \tag{A15}$$

As $\gamma\to\gamma_c$, the saddle point $z_+\to3$, a branch point of F, and the derivative $[d^2G/dz^2]_{z_+}\to\infty$. It would appear that the branch point limits the validity of the integral I because if we use the above saddle point equations for $\gamma>\gamma_c$, then $z_+>3$, the second derivative of G changes sign and the path of steepest descent is along the real axis. This would make I, and $\Delta\psi$ purely imaginary as can be seen by analytically continuing Eq. (A14). The apparent limitation is equivalent to the breakdown found by Kramers. His formulas become meaningless when $\gamma=\gamma_c$ and the branch point is reached, because his equations become undefined for $\gamma>\gamma_c$.

The path along the real axis through the saddle point z_+ is not mathematically legitimate for $\gamma>\gamma_c$ because

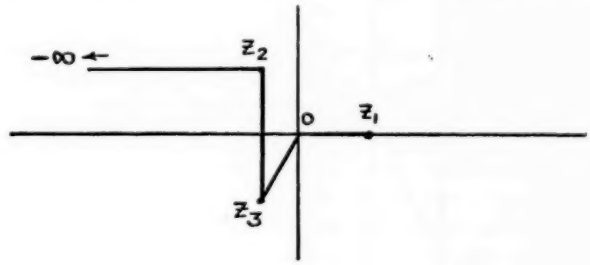

FIG. 3. The branch cuts in the complex z-plane.

the imaginary part of $G(z)$ for this path is identically zero. This path of steepest descent cannot be deformed into the original path, the line for which the real part of z equals z_0. We therefore suppose that $\gamma>\gamma_c$ and investigate in further detail the behavior of the integrand in the neighborhood of the branch point of F, $\zeta=9/4$.

Let us set $\zeta=(9/4)+\epsilon$ with $|\epsilon|$ very small. Then, since $z=3\gamma\zeta^{\frac{1}{2}}$,

$$z=3(\gamma/\gamma_c)[1+(4/27)\epsilon-\cdots].$$

Furthermore,

$$F_1(z)=(2/3)-(4.3^{\frac{1}{2}}/9)\epsilon^{\frac{1}{2}}+(40/81)\epsilon-(592.3^{\frac{1}{2}}/243)\epsilon^{\frac{3}{2}}\cdots. \tag{A16}$$

From the definition of $G(z)$, we then obtain

$$G(z)=G_0+G_0'\epsilon+\alpha\epsilon^{\frac{3}{2}}\cdots, \tag{A17}$$

where

$$\begin{aligned}G_0&=3(\gamma/\gamma_c)-\ln(\gamma/\gamma_c)-\tfrac{2}{3},\\ G_0'&=(4/9)[(\gamma/\gamma_c)-1],\\ \alpha&=32.3^{\frac{1}{2}}/243.\end{aligned} \tag{A18}$$

Now when $\gamma>\gamma_c$, we note that $G_0'>0$. Consequently, for $|\epsilon|$ small and real part of ϵ negative, $G(z)$ has a maximum value, G_0, at $\epsilon=0$, $z=z_1=3(\gamma/\gamma_c)$. The remaining question concerns the possibility of locating a path of steepest descent, imaginary part of $G(z)=0$, which can be deformed into the original path. If we set $\epsilon=re^{i\theta}$ with r small,

$$\text{imaginary part of } G(z)=G_0'r\sin\theta+\alpha r^{\frac{1}{2}}\sin(3\theta/2). \quad \text{(A19)}$$

Setting this equal to zero, we have for the possible path

$$r^{\frac{1}{2}}=-(G_0'/\alpha)\frac{\sin\theta}{\sin(3\theta/2)}. \quad \text{(A20)}$$

The path cannot cross the cut from 0 to $z_1=3(\gamma/\gamma_c)$ in Fig. 3. Therefore, in the upper half plane we take $\theta=\pi-\varphi$ and in the lower half plane we take $\theta=-\pi+\varphi$

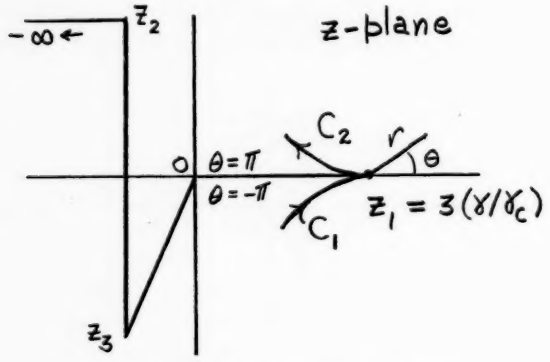

FIG. 4. Path of steepest descent for $\gamma>\gamma_c$.

where φ is positive and small in both cases. Hence

$$r^{\frac{1}{2}}=-(G_0'/\alpha)\frac{\sin\varphi}{-\cos(3\varphi/2)}\simeq(G_0'/\alpha)\varphi, \quad \text{(A21)}$$

and a path not on the real axis exists on both sides of the cut. The path is shown in Fig. 4.

In the neighborhood of z_1, the integrand becomes infinite like

$$[1-(3\gamma/z\gamma_c)]^{-\frac{1}{2}}\simeq(27/4\epsilon)^{\frac{1}{2}},$$

and, as a consequence, the contribution to I from an infinitesimally small path circling z_1 is zero in the limit. The integral may then be written

$$I\simeq(2\pi i)^{-1}\int_{C_1+C_2}(4\gamma/9\gamma_c)d\epsilon(27/4\epsilon)^{\frac{1}{2}}\times\exp[(N/2)(G_0+G_0'\epsilon\cdots)]. \quad \text{(A22)}$$

For N very large the maximum is very sharp and the contributions to I arise from the parts of C_1 and C_2 very near the branch point. Therefore, the contributing parts of C_1 and C_2 may be replaced by integrals along the real axis. In C_1 we may use $\epsilon=re^{-i\pi}$, $\infty>r\geqslant 0$, and in C_2 we may use $\epsilon=re^{i\pi}$, $0\leqslant r<\infty$. Hence,

$$I\simeq(2\pi i)^{-1}(4\gamma/9\gamma_c)(27/4)^{\frac{1}{2}}\times\int_{\infty}^{0}(-dr)r^{-\frac{1}{2}}e^{i\pi/2}\exp[(N/2)(G_0-G_0'r)]+(2\pi i)^{-1}(4\gamma/9\gamma_c)(27/4)^{\frac{1}{2}}\times\int_{0}^{\infty}(-dr)r^{-\frac{1}{2}}e^{-i\pi/2}\exp[(N/2)(G_0-G_0'r)], \quad \text{(A23)}$$

and

$$I\simeq 2(2/3)^{\frac{1}{2}}(\gamma/\gamma_c)(\pi NG_0')^{-\frac{1}{2}}\exp[NG_0/2]. \quad \text{(A24)}$$

Finally,

$$\exp[-\Delta\psi/kT]\simeq 2(3/2)^{\frac{1}{2}}(\gamma/\gamma_c)[(\gamma/\gamma_c)-1]^{-\frac{1}{2}}\times\exp[(N/2)(G_0-1)], \quad \text{(A25)}$$

and for N very large,

$$-\Delta\psi/NkT=\tfrac{3}{2}(\gamma/\gamma_c)-\tfrac{1}{2}\ln(\gamma/\gamma_c)-\tfrac{5}{6},\quad \gamma>\gamma_c=(2/3)^{\frac{3}{2}}. \quad \text{(A26)}$$

We note from Eqs. (A15) and (A26) that $\Delta\psi$ is continuous when $\gamma=\gamma_c$:

$$-\Delta\psi/NkT=\tfrac{2}{3},\quad \gamma=\gamma_c. \quad \text{(A27)}$$

THE JOURNAL OF CHEMICAL PHYSICS VOLUME 20, NUMBER 1 JANUARY, 1952

Macro-Ions. I. Light Scattering Theory and Experiments with Bovine Serum Albumin

PAUL DOTY AND ROBERT F. STEINER*
Gibbs Laboratory, Department of Chemistry, Harvard University, Cambridge, Massachusetts
(Received July 23, 1951)

The theory of light scattering is extended to include solutions of macro-ion salts such as charged proteins and polymeric electrolytes. Equations for the angular intensity distribution are obtained for three types of interaction potential: (1) that of rigid, noninteracting spheres, (2) an electrostatic potential consistent with the Verwey-Overbeek theory, and (3) a simple Gaussian-type repulsion. Because the repulsive forces between the macro-ions are generally strong and long range, the concentration and angular distribution of the scattering may be very pronounced. Two unique and important extremes exist. If the concentration of the macro-ion salt is altered without introducing additional electrolytes, the effective diameter of the macro-ion is inversely proportional to the cube root of the concentration. In this situation the essential features of the scattering are quite novel. First, the reciprocal reduced intensity rises steeply from the intercept at zero concentration, bends over and becomes nearly horizontal at moderate concentrations, and second, the dissymmetry falls sharply from the limiting value at zero concentration, passes through a minimum and rises slowly at higher concentrations. With small particles the dissymmetry is always less than unity. In experiments with bovine serum albumin carrying charges up to 50 protons, all of these features have been found and can be accounted for at least semiquantitatively. The second unique case is that occurring when the concentration is altered by isoionic dilution which keeps the effective diameter of the macro-ion constant. Since it is shown that in the scattering problems the difference between the hard sphere and electrostatic potential is relatively minor, the virial coefficients of Boltzmann can be used to describe the concentration dependence of the absolute intensity of scattering. This procedure permits, in contrast to the previous case, a precise evaluation of the effective ionic diameter. The values so obtained are compared with estimates from the Debye-Huckel theory. As a consequence of these investigations, it appears that both the thermodynamic behavior and diffraction behavior of macro-ion solutions are consistent with a relatively simple electrostatic picture.

THE study of the behavior and interactions of charged colloidal particles in solutions of low electrolyte content has been limited by certain difficulties which beset nearly every physical method of investigation when applied to these systems. In particular there are few thermodynamic data of general interest. This is apparently because of the lack of success in overcoming the effects of membrane hydrolysis in osmotic pressure studies and the inability to achieve sufficient precision with either these measurements or vapor pressure measurements at low concentrations. Moreover, the magnitude and variable character of the electroviscous effect seems to prevent the characterization of size, shape, and interaction from viscosity and sedimentation measurements. In view of this situation we have attempted to extend the theory of light scattering to this area and to examine the light scattering from solutions of typical proteins, polymeric electrolytes, and lyophobic colloids. In several cases it was desirable to obtain other measurements such as those of viscosity and potentiometric titration on the same systems. In this present paper we are concerned chiefly with a summary and extension of the theory and its application to studies of solutions of bovine serum albumin carrying up to fifty protons of charge. Serum albumin was chosen for these initial studies because it is too small in size to give rise to any significant internal interference; that is, its molecules behave as point scatterers. With no internal interference effects one can study the external interference arising from the nonrandom arrangements of the protein molecules without complications that would otherwise be present. In the next paper in this series[1] where studies of polymethacrylic acid are discussed, these complications from internal interference become an essential part of the problem.

In many ways this present paper supplements the light scattering investigations of the same protein by Edsall, Edelhoch, Lontie, and Morrison[2] which were carried out mostly at relatively high ionic strengths where electrostatic effects were considerably suppressed. A preliminary note on some of the interference effects we have observed has appeared previously.[3] Reference to it and a review article[4] will supply the relevant details concerning light scattering procedures and nomenclature.

I. LIGHT SCATTERING THEORY FOR CHARGED PARTICLES

A. Introductory Analysis of the Problem

We wish to consider the problem of deriving the angular variation of the reduced intensity, $R_\theta(=i_\theta r^2/I_0$ where i_θ is the intensity of scattered light at a distance r relative to the incident intensity I_0), of light scattered by a solution of any concentration composed of macro-ions and the corresponding gegenions required for electrical neutrality, with or without additional electrolyte. Taking up the simplest case first we may focus attention on a solution of completely dissociated polyvalent-univalent salt, AX_n, in water, where n is of the order of 10 to 100. The macromolecule exists as the macro-ion, A^{+n}. In general the gegenions, X^-, will

* Present address: Naval Medical Research Institute, Bethesda, Maryland.

[1] A. Oth and P. Doty, J. Phys. Colloid Chem. (January, 1952).
[2] Edsall, Edelhoch, Lontie, and Morrison, J. Am. Chem. Soc. 72, 4641 (1950).
[3] P. Doty and R. F. Steiner, J. Chem. Phys. 17, 743 (1949).
[4] P. Doty and J. T. Edsall, *Advances in Protein Chemistry VI* (Academic Press, New York, 1951), pp. 35–122.

scatter so little in comparison with the macro-ion that their scattering can be neglected. This situation will be assumed for the present. A discussion of the case where gegenion scattering is not negligible will be found in Sec. I-F.

It will be recalled that when scattering centers are randomly distributed, the observed scattering at all angles is equal to that of an isolated particle multiplied by the number of scattering centers. Quantitatively we have

$$R_\theta = KcMP(\theta), \tag{1}$$

where $K = 2\pi^2 n_0^2 (dn/dc)^2 / N_0 \lambda^4$, c represents concentration, M molecular weight, and $P(\theta)$ the particle scattering factor which characterizes the internal interference. For particles as small as serum albumin $P(\theta)$ is unity. In such cases R_θ is independent of θ, provided that the incident light is vertically polarized and any depolarization is corrected for, and c/R_θ is independent of concentration. When a random distribution is replaced by any other arrangement, this independence is lost. In this connection it is important to note two points. First, at $\theta = 0$ the dependence of c/R_0 on c is purely a thermodynamic one equivalent to the dependence of reduced osmotic pressure on concentration and hence its measurement permits a characterization of the system in terms of a set of virial coefficients. The deviations from ideal solution behavior are faithfully reflected in the concentration dependence of c/R_0 as they are in the concentration dependence of π/c because the work required to produce a given fluctuation in concentration will differ from that required in an ideal solution by an amount that is uniquely related to the deviation of π/c from the van't Hoff relation. Second, at all other values of θ the relation of R_θ to θ, assuming $P(\theta) = 1$, depends on the net effect of the external interference and hence upon the details of the mutual arrangement of the scattering centers. In particular the strong repulsions that may be anticipated in solutions of macro-ion salts should lead to very pronounced interference effects. Thus a nonrandom arrangement of particles is reflected in both thermodynamic and diffraction data. It is obvious that a satisfactory characterization of the mutual arrangement (time average) of the scattering centers should permit, in principle at least, a derivation of the functional dependence of c/R_0 on c and R_θ on θ. A sufficiently detailed representation of the mutual arrangement of the particles for this purpose is given by the radial distribution function, $\rho(r)$, which denotes the probability of finding a particle at a distance r from the center of a specified particle. The next four sections deal with the elucidation of the relations outlined here.

Before proceeding it is necessary to emphasize one particular property of electrolyte solutions. After about two decades of vigorous inquiry, it is generally agreed that the interaction of colloidal ions, taking into account their electric double layers, is a repulsive one at nearly all distances.[5] Consequently as a first approximation in characterizing such an interaction, one may employ an effective diameter or a "collision diameter" which is a measure of the distance of closest approach of centers of the macro-ions. Using this approximation the radial distribution function takes on a relatively simple form.

There are two indications that the effective diameter may vary inversely as the cube root rather than the square root. When the ionic strength is not too low and only electrostatic interactions are involved, the requirement of Donnan equilibrium leads to the expression[3,4]

$$Kc/R_0 = 1/M + (Z^2/2M^2 m_3) \tag{2}$$

for a three component system composed of water, a salt and a macro-ion salt. Z represents the charge on the poly-ion and m_3 the molality of the ions of opposite charge because of added electrolyte. As will be pointed out in the next section, the corresponding expression for noninteracting hard spheres of diameter D differs from Eq. (2) only in that the coefficient of c is $4\pi N_0 D^3/3M^2$. Upon equating these coefficients one notes that D is inversely proportional to the cube root of the concentration of ions of the same sign as the gegenions. Although because of the definition of components Eq. (2) does not apply to two component solutions of macro-ion salts the conclusion deduced is probably valid. A second argument is based upon the supposition that at finite concentrations, the distribution of gegenions about the macro-ions will be such as to maintain the excluded volume at a constant value. Support for this view is found in the present experiments (see IV. Conclusion). Consequently the assumption is made here that the effective diameter varies inversely as the cube root of the concentration. Using instead the square root dependence of the Debye-Huckle κ would not greatly affect the treatment which follows.

B. External Interference: Application to Hard Spheres at Extreme Dilution

The importance of the departure from random arrangement in producing diffraction effects was clearly put forward by Debye in 1925[6] in a very important paper on the diffraction of x-rays by gases. Shortly thereafter Zernicke and Prins[7] derived the following general expression for the loss in scattering power per particle because of external interference.

$$\left[1 - \frac{4\pi N}{V} \int_0^\infty \{1 - \rho(r)\} r^2 \frac{\sin hr}{hr} dr\right]. \tag{3}$$

The number of molecules in the volume V is de-

[5] E. J. W. Verwey and J. T. G. Overbeek, *Theory of the Stability of Lyopholic Colloids* (Elsevier Publishing Company, Inc., Amsterdam, 1948).

[6] P. Debye, J. Math. Phys. **4**, 153 (1925); Physik. Z. **28**, 135 (1927).

[7] F. Zernicke and J. A. Prins, Z. Physik **41**, 184 (1927).

noted by N. The symbol h represents the quantity $4\pi(\sin\theta/2)\lambda'$, λ' being the wavelength of light in the medium. In order to incorporate the effects of external interference into light scattering, the right side of Eq. (1) should be multiplied by the foregoing expression. Thus, assuming that $P(\theta)$ is known, our ability to predict the light scattering behavior for a given system is, as in the case of x-ray scattering, completely dependent upon our knowledge of the radial distribution function and, conversely, our interpretation of light scattering data at finite concentrations depends in principle on our ability to obtain information on $\rho(r)$ from the angular intensity distribution. In the case of nonelectrolyte systems at low concentrations, the external interference effects are relatively simple and can be adequately handled in terms of the second and third virial coefficients (see Sec. I-E). However, the larger effects which prevail in solutions containing macro-ions require more elaborate considerations.

The simplest specific case to which the expression (3) can be applied is to noninteracting hard spheres of diameter D. As the first order approximation[3,8] the concentration of scattering particles is limited to very high dilution. Then $\rho(r)=0$ if $r<D$ and has a uniform value, very nearly equal to unity, if $r>D$. Substitution into (3) and combination with (1) leads to

$$R_\theta = KcMP(\theta)\left[1-2B'\frac{c}{M}\Phi(hD)\right], \qquad (4)$$

where $\Phi(x)=(3/x^3)(\sin x - x\cos x)$ and $B'=\frac{2}{3}\pi D^3 N_0$. For values of hD of most common interest $\Phi(hD)$ is a continuously decreasing function. Therefore, the intensity of scattering increases with increasing values of θ. To a good approximation the angular dependence of the intensity can be characterized by the dissymmetry, R_{45}/R_{135}. For this, Eq. (4) yields

$$z=\frac{R_{45}}{R_{135}}=[z]\frac{[1-2B'(c/M)\Phi(\ 4.81D/\lambda')]}{[1-2B'(c/M)\Phi(11.61D/\lambda')]}. \qquad (5)$$

We note that the effect of external interference alone is to produce dissymmetry values of less than unity, the deviation therefrom increasing with D/λ'. However, if this effect were sought in nonelectrolyte solutions where D must be approximately equal to the particle diameter, partial compensation would generally occur because of the intrinsic dissymmetry, $[z]=P(45)/P(135)$, arising from internal interference. With the long range forces available in solutions of macro-ions, this obstacle disappears since it is possible to produce charges on most of the smaller proteins and low molecular weight polymeric electrolytes which give rise to effective diameters that are relatively large, whereas the scattering particle is too small to exhibit any internal interference. Such behavior, in qualitative agreement with Eqs. (4) and (5), has been observed for solutions of charged bovine serum albumin[3] and is reported on further in Part II.

Although the external interference effects produced with larger particles in nonelectrolyte solution are masked by internal interference, it is important to note that the former is concentration-dependent while the latter is not, at least for rigid particles. Consequently the external interference will be manifest by a diminution of the dissymmetry with increasing concentration. This behavior has been clearly recognized in the case of polymers[9] and viruses.[8,10] An extensive analysis of these two types of interference has been carried out for flexible polymer molecules.[11]

C. Second-Order Approximation for Scattering from Hard Surfaces

Although the x-ray counterpart of Eq. (4) has wide applicability in the scattering of x-rays by gases, the use of Eqs. (4) and (5) in light scattering from solutions of macro-ions is limited to extremely dilute solutions. In the case of serum albumin, for example, a typical value of D is 200A. Upon substituting this value into Eq. (4), it is seen that negative values of R_θ are predicted for values of c greater than $0.35g/100$ cc. The failure of Eq. (4) even at such a relatively low concentration is because of the fact that the distribution function assumed is valid for noninteracting hard spheres only at infinite dilution. With increasing concentration the radial distribution function of such a system will necessarily alter in response to the initial stage of formation of nearest neighbor and next nearest neighbor shells.

Consequently it is important to develop an expression similar to Eq. (4) but valid at higher concentrations, and to do this a better approximation to $\rho(r)$ at finite concentrations must be employed. This next step can be taken by following the recent work of Fournet[12] who has pointed out that the essential requirements for this extension are contained in the recent theoretical work of Born and Green.[13] It should be remarked that in order to solve the general equations of their theory, Born and Green are forced to use several approximations. Although these approximations substantially reduce the rigor of the development, they appear to permit at least a second-order approximation to the present problem.

Fournet's development, which is directed toward low angle scattering from gases and liquids, may be summarized as follows. The radial distribution function is written as

$$\rho(r)=e^{-\psi(r)/kT}\{1+f(r)\}, \qquad (6)$$

[3] G. Oster, Rec. trav. chim. **68**, 1123 (1949).

[9] Doty, Affens, and Zimm, Trans. Faraday Soc. **42B**, 66 (1946).

[10] Oster, Doty, and Zimm, J. Am. Chem. Soc. **69**, 1193 (1947).

[11] B. H. Zimm, J. Chem. Phys. **16**, 1093 (1948).

[12] G. Fournet, Compt. rend. **228**, 1421 (1949); Acta Cryst. (to be published).

[13] M. Born and M. Green, Proc. Roy. Soc. (London) **A188**, 10 (1946); **A189**, 103 (1947).

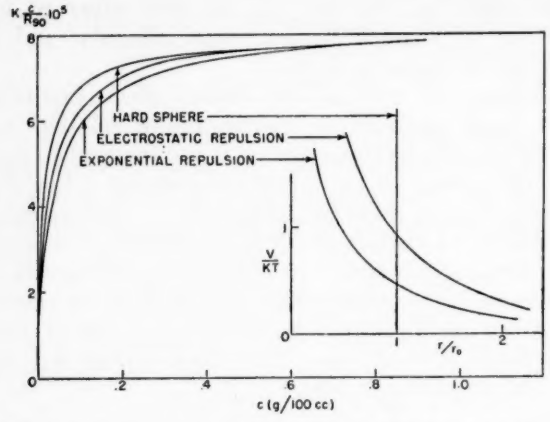

FIG. 1. The concentration dependence of Kc/R_{90} for a typical macro-ion salt solution. The three interaction potentials shown in the inset are compared by requiring the value at 0.9 g/100 cc to be the same in all three cases.

where $\psi(r)$ represents the interparticle potential, and $f(r)$ is a residual quantity, considerably smaller than unity, that is evaluated by solving the integral equations of Born and Green after linearization. If one introduces the function,

$$\alpha(r)=e^{-\psi(r)/kT}-1 \tag{7}$$

and a Fourier transform of $r\cdot\alpha(r)$,

$$h\beta(h)=\frac{1}{(2\pi)^{\frac{1}{2}}}\int_{-\infty}^{\infty} r\alpha(r)\sin hr dr, \tag{8}$$

it can be shown by the use of Born and Green's method that the integral in the Zernicke-Prins expression (3) takes the form,

$$2\int_0^{\infty} r[\epsilon\alpha(r)+f(r)]\sin hr dr, \tag{9}$$

where ϵ is defined by setting $(\epsilon-1)$ equal to the mean value of $f(r)$ near the origin. Carrying out the integration and combining (3) with (1), one obtains for spherically symmetrical particles

$$R_\theta=KcMP(\theta)\frac{1}{1-(2\pi)^{\frac{1}{2}}(\epsilon\beta(h)/v)}, \tag{10}$$

where v is the volume per molecule. The evaluation of ϵ for any specific type of interacting particles is generally quite difficult. For present purposes it may be set equal to unity. This approximation appears to be equivalent to neglecting virial coefficients higher than the second in the equation of state.

For the special case of nonrepelling hard spheres

$$\beta(h)=\frac{-4\pi}{3(2\pi)^{2/3}}D^3\Phi(hD). \tag{11}$$

Substituting into (10) and combining with (2), we have

$$R_\theta=KcMP(\theta)\frac{1}{1+2(B'/M)c\Phi(hD)}, \tag{12}$$

and

$$z=[z]\frac{1+2(B'/M)c\Phi(11.61D/\lambda')}{1+2(B'/M)c\Phi(4.81D/\lambda')}. \tag{13}$$

These expressions represent the second-order approximation to the problem of scattering by hard spheres and are a considerable advance over Eqs. (4) and (5). Thus, according to Eq. (12) R_θ is positive at all concentrations and Kc/R_0 is a linear function of c consistent with the second virial coefficient. Real systems will exhibit positive deviations which increase with concentration. Some of the limitations of Eq. (12) at high concentration have been discussed by Oster and Riley.[14]

For purposes of illustration and comparison with experiments described in a later section, these equations are plotted in Figs. 1 and 2 for a set of conditions corresponding to bovine serum albumin chloride possessing about fifty chloride ions per serum albumin ion, the neutral molecule having a molecular weight assumed to be 77,000. This defines Kc/R_0 at zero concentration. The proportionality constant relating D^3 to c is chosen so that Kc/R_{90} at $c=0.9$ g/cc is six times the value it has at zero concentration. One could estimate the proportionality constant other ways, and this would lead to values similar to that obtained in this manner. This particular choice facilitates later comparison with experiment. Throughout λ' is set equal to 3280A. Kc/R_{90} is plotted in Fig. 1 and the dissymmetry, z, in Fig. 2.

D. Scattering from Particles with Exponential and Electrostatic Repulsion Potentials

While Eqs. (12) and (13) represent a considerable improvement in the treatment of the scattering from a system of noninteracting rigid spheres, it is not clear that this model adequately represents macro-ions between which the potential passes gradually rather than abruptly from low to high values. To investigate this point corresponding equations may be derived using more appropriate potentials.

A relatively "soft" potential which leads to a particularly simple result is the following:

$$\psi(r)/kT=\ln[1-\exp-(r/r_0)^2]^{-1}. \tag{14}$$

Using the transform of the negative exponential of this expression in the manner shown in the previous section, one arrives at the following equations.

$$R_\theta=KcMP(\theta)\frac{1}{1+\pi^{\frac{1}{2}}(N_0/M)r_0^3c\exp(-h^2r_0^2/4)}; \tag{15}$$

$$z=[z]\frac{1+\pi^{\frac{1}{2}}(N_0/M)r_0^3c\exp(-2.86r_0^3/\lambda'^2)}{1+\pi^{\frac{1}{2}}(N_0/M)r_0^3c\exp(-0.58r_0^2/\lambda'^2)}. \tag{16}$$

[14] G. Oster and D. P. Riley, Acta Cryst. (to be published).

These expressions are plotted in Fig. 1 where they can be compared with the results for hard spheres. As before these plots correspond to the conditions that $M=77{,}000$ and that Kc/R_{90} at $c=0.9g/100$ cc$=8.95\times10^{-5}$. We note that in both the reciprocal reduced intensity and the dissymmetry, the effect of the softer potential is to diminish the curvature of the plot. However, the effect is a moderate one.

A more realistic potential may be obtained by applying the results of Verwey and Overbeek[5] to the particular case of serum albumin to which the foregoing conditions apply. This is described in a later section. The result is that the potential can be closely described, except for an additive constant in r, by the equation:

$$\psi(r)/kT=\ln[1-\exp-(r/r_0)^2]^{-2}. \tag{17}$$

Proceeding as before, one obtains for this potential

$$R_\theta=KcMP(\theta)\frac{1}{1+(2\pi)^{\frac{1}{2}}(N_0/M)c(r_0^3/2^{\frac{1}{2}})\exp-(h^2r_0^2/4)-(r_0^3/8)\exp-(h^2r_0^2/8)} \tag{18}$$

and the corresponding expression for the dissymmetry obtained by taking the ratio of R_{45} to R_{135}. Using the conditions employed for the other two cases, these expressions are plotted in Figs. 1 and 2. It is seen from the plot of the potential in the inset of Fig. 1 that this, the electrostatic potential, is intermediate between that of the hard sphere and the exponential repulsion potentials. As is to be expected, therefore, the plots of R_θ and z are situated in between the results for the other two potentials. One can conclude from these results that the concentration dependence of R_θ and z is only moderately sensitive to the form of the potential and that it is unlikely that experimental results on systems of no greater charge than serum albumin could be used to discriminate between alternative forms of reasonable potentials. Such possibilities may exist in the case of particles of higher charge.

E. Scattering from Macro-Ions in Isoionic Solutions: Relation to Exact Equations from Hard Spheres

Thus far we have considered solutions containing only a macro-ion salt and have assumed that the effective ionic diameter of the macro-ion was inversely proportional to the cube root of the concentration. In contrast to this situation in which the number of ions is kept constant as the concentration of the system is varied, another unique condition occurs if the concentration is varied by the addition of an ordinary electrolyte solution in which the ions of charge opposite to the macro-ion are of the same charge-type and exist at a molar concentration equal to that of the gegenions in the macro-ion salt solution. By diluting in this manner, isoionically, the concentration of gegenions with respect to the macro-ions remains constant and in view of our previous discussion the effective diameter should therefore be stabilized. Under these conditions the D and r_0 in the foregoing equations should be independent of concentration, and the form of the plots of these equations will show pronounced alterations in the direction of more orthodox behavior.

If isoionic† dilution does stabilize the size of the ionic diameter, it becomes of interest to examine the applicability of a more precise treatment of the scattering. We have seen that the hard sphere potential is a moderately good approximation for this particular problem with macro-ions but the foregoing equations are limited by neglecting the virial coefficients beyond the second. Since the higher virial coefficients for hard spheres are known, a precise expression for R_0 can be written down. This can be done only at zero degrees since it is only here that the scattering is completely described thermodynamically. However, in practice, it will be seen that by beginning the isoionic dilution at a sufficiently high concentration of macro-ion salt, the angular intensity distribution remains essentially constant and R_{90} is consequently a very good approximation to R_0.

The basic equation of Einstein for scattering resulting from concentration fluctuations is

$$Kc/R_0=(\partial\pi/\partial c)/RT, \tag{19}$$

where π represents the osmotic pressure. The formal equivalence of the osmotic pressure of a solution and the pressure of a gas having been established,[15] one can write for π using the virial coefficients of Boltzmann

$$\pi=RTc[1/M+Bc+0.625(B^2/M)c^2+0.2869(B^3/M^2)c^3+0.928(B^4/M^3)c^4] \tag{20}$$

where $B=2\pi D^3N_0/3M^2$. Substitution of this in (19)

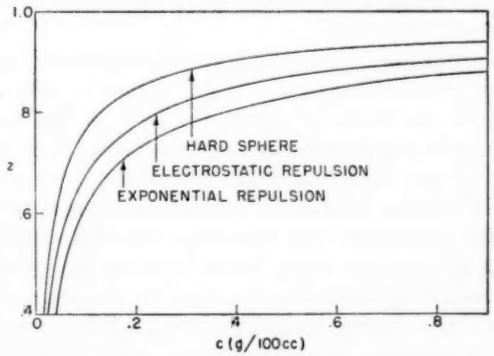

FIG. 2. The concentration dependence of the dissymmetry for the three cases shown in Fig. 1.

† The use of the term isoionic here should not be confused with its more established use to describe a protein solution in which the only nonprotein ions present are OH^- and H^+.

[15] W. G. McMillan and J. E. Mayer, J. Chem. Phys. **13**, 276 (1945).

yields

$$Kc/R_0 = 1/M + 2Bc + 1.875B^2Mc^2 + 1.148B^3M^2c^3 + 0.964B^4M^3c^4. \quad (21)$$

At very high concentrations where still higher virial coefficients may be required, the alternative treatment of Kirkwood, Maun, and Alder[16] may be employed.

The second virial coefficient alone has been used to estimate the effective size of viruses[17] and polymers.[18]

F. The Contribution of Gegenions to the Scattering of a Macro-Ion Salt

In the foregoing discussions it has been assumed that the scattering by the gegenions is negligible. In many cases, particularly when the gegenions are univalent cations, this assumption is justified. Some of the situations which arise when this neglect is not possible have been treated by others.[2,19] We consider here only those aspects that seem to be directly related to experiments that may be designed on the basis of the previous discussions.

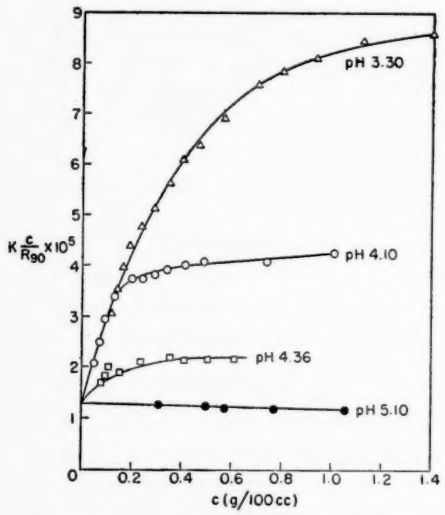

FIG. 3. Kc/R_{90} for solutions of bovine serum albumin in water adjusted to the indicated pH values with hydrochloric acid.

All electrolyte systems and sets of conditions may be divided into three classes: First, those in which the gegenions are entirely within the field of the macro-ions so that the fluctuating unit is a neutral one corresponding to a molecule of the macro-ion salt; second, those in which a fraction of the gegenions are associated with the macro-ion, the remainder forming essentially part of the solvent; third, those in which the gegenions exist completely outside the field of the macro-ions. These three classes roughly correspond to increasing states of dilution of the macro-ion salt solution. The first class includes most commonly occurring cases; further work will be required to see if systems of the second class can be experimentally observed; the third class can apparently exist only at such high dilutions as to be experimentally inaccessible to study and is therefore only of formal interest.

In the first class the situation is relatively simple. Provided that the refractive index increment, dn/dc, required for the evaluation of K, has been determined in the cusomary manner and that the concentration of the macro-ion salt is employed, the molecular weight of the macro-ion salt can be determined from the evaluation of Kc/R_0 at zero concentration. Of course, R_0 cannot be measured directly at higher angles. This determination is easy when the ionic diameter is small but may require measurements at quite small angles if the ionic diameter is large. When the ionic diameter is large, say 1000A, the scattering caused by the gegenions will be greatly diminished because of interference at larger angles such as 90°. However, upon passing to sufficiently small angles this effect will diminish and near 0° the total scattering of the neutral unit will be exhibited. Thus we note that when the gegenions scatter significantly we have a scattering unit of very inhomogeneous structure, and internal interference may arise from the size of the double layer, the size of the macro-ion or both.

In the second class the situation is complicated, and if systems of this type are experimentally accessible, considerable study will be required. If gegenions selected for their high scattering power are used, it may be possible to determine the fraction of gegenions making up double layers and even their radical distribution.

There is a return to simplicity in the third class of systems. Here the scattering would be principally a reflection of the weight average molecular weight of the ion species, each being weighted according to its own value of $(dn/dc)^2$. This quantity can be calculated accurately for ordinary ions, but some uncertainty may attend its estimation for macro-ions. It is interesting to contrast this behavior in the limit of infinite dilution with that of osmotic pressure. In the latter case the corresponding limit at zero concentration would yield the number average molecular weight of the ionic species; this would be very close to the weight of the gegenion. On the other hand, the corresponding light scattering result would be very close to the molecular weight of the macro-ion.

II. EXPERIMENTS WITH SOLUTIONS OF SERUM ALBUMIN CHLORIDE

A. Measurement of the Reduced Intensity

Since the curves shown in Fig. 1 for Kc/R_{90} differ radically from any measurements of light scattering made heretofore, the first test of the theoretical considerations of Part I clearly consists in making measurements on systems which closely approximate the models

[16] Kirkwood, Maun, and Alder, J. Chem. Phys. **18**, 1040 (1950).
[17] G. Oster, J. Gen. Physiol. **31**, 89 (1947).
[18] P. Doty and R. F. Steiner, J. Polymer Sci. **5**, 383 (1950).
[19] J. J. Hermans, Rec. trav. chim. **68**, 1137 (1949).

employed above. Bovine serum albumin solutions do have most of the properties desired in such a system. Its molecules can exist as ions having charges from about +100 to −100 depending upon the pH. In addition the molecules are small enough to behave as symmetrical scatterers, i.e., $P(\theta)=1$. If a thoroughly dialyzed solution of this protein is brought to pH 8 with very dilute NaOH, the protein ion assumes a charge of about −50 and the solution consists of dissociated sodium proteinate, $Na_{50}Pr$. Light scattering measurements on these solutions were not readily reproducible principally because the pH could not be kept constant, especially at the lower concentrations. Consequently the alternative procedure of adding very dilute HCl to bring the dialyzed solution to pH's as low as 3.3 where the charge on the ions reaches −46 was tried. Measurements of these solutions proved to be quite reproducible. Typical data are plotted in Fig. 3 where it is obvious that the general behavior is the same as that displayed in Fig. 1. The magnitude of the decrease of R_{90} with increasing concentration clearly depends on the charge and disappears at pH 5.10 when the protein is isoelectric.

A comparison of the curve obtained at pH 3.3 can be compared with the theoretical curves at once, since the curves in Fig. 1 were drawn so as to coincide with the experimental curve at the intercept and 0.9 g/100 cc. When this and other comparisons are made, it is obvious that the theoretical curves rise much more rapidly from the intercept and then level out more abruptly. These discrepancies can be largely eliminated by taking into account two factors in the experimental system. First the counter-ion concentration is not proportional to the protein concentration as assumed in the equations of Part I. This is because of the presence of chloride ions from the HCl necessary to maintain the pH at 3.3. For example at 0.09 g/100 cc the concentration of chloride ions from the HCl is equal to that from the protein salt. Second, the equations of Part I apply to point particles in that the effective diameter D or r_0 varies with the inverse cube root of c. These two complications can be taken care of in the following way. Since the difference between the hard sphere and electrostatic repulsion potentials with respect to Kc/R_{90} is relatively small, we shall deal only with the hard sphere case. In computing the curves in Fig. 1, it was necessary to put $D=262$A at $c=0.9$ g/100 cc in order to evaluate the proportionality constant between D^3 and $1/c$. If bovine serum albumin were spherical, it would have a molecular diameter of 50A. However, the molecular shape is assymmetrical with the axial ratio being about 4. Consequently a somewhat larger value should be assigned as the "effective particle diameter." In the absence of detailed knowledge of its molecular shape and since we are seeking only to show that the theory and experiment can be brought into semi-quantitative agreement, a value of 62A is taken for this value. Then the effective ionic diameter becomes $D=62+D'$ where D'

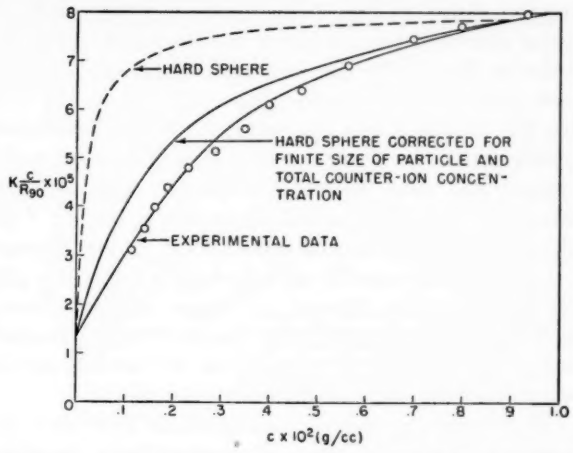
HARD SPHERE
HARD SPHERE CORRECTED FOR FINITE SIZE OF PARTICLE AND TOTAL COUNTER-ION CONCENTRATION
EXPERIMENTAL DATA
$K\frac{c}{R_{90}}\times10^5$
c x 10² (g/cc)

FIG. 4. A comparison of theoretical (hard sphere potential) and experimental behavior of Kc/R_{90} for bovine serum albumin at pH 3.30.

signifies that portion which varies inversely as the cube root of c. Having thus established a relation between D and c, it remains only to employ for c the total chloride ion concentration taking into account the contribution of both the protein salt and the HCl. The result is shown in Fig. 4 together with the data for pH 3.3. The difference remaining between the new curve and the experimental data is now comparable to the difference between the hard sphere and electrostatic repulsion potential curves of Fig. 1. Thus either by using the electrostatic repulsion potential or by choosing the optimal value of the effective particle diameter, the agreement between theory and experiment can be made essentially complete. We shall not pursue this point because approximations in the basic theory, the neglect of virial coefficients beyond the second, do not justify it.

B. Measurement of Dissymmetry

The dissymmetry of bovine serum albumin solutions has been measured under conditions very similar to those described above in order to see to what extent the

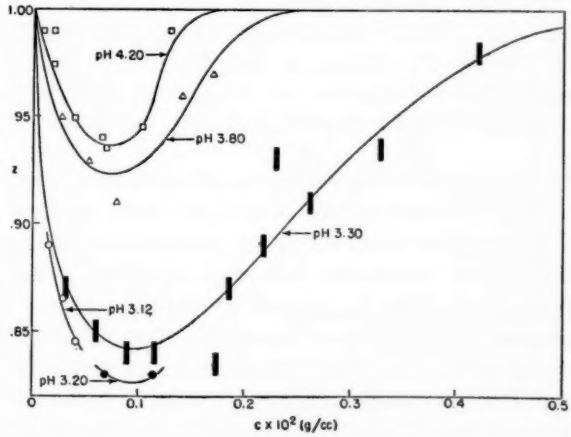

FIG. 5. The dissymmetry (R_{45}/R_{135}) for solutions of bovine serum albumin in water adjusted to the pH values indicated with hydrochloric acid.

behavior shown in Fig. 2 can be found. The results at several values of the pH below the isoelectric point are shown in Fig. 5. At the isoelectric point the dissymmetry was unity. In comparing the data at pH 3.30 with Fig. 2 which was computed for these conditions, we note that in both cases values of z less than unity are obtained and that the values diminish upon dilution down to a concentration of about 0.1 g/100 cc. Two differences are apparent however. First, at low concentrations the dissymmetry goes through a minimum and rises toward unity. Second, at higher concentrations, above 0.6 g/100 cc at pH 3.30, the dissymmetry values have returned to unity whereas the theoretical curves are approaching unity much more gradually.

The differences at low concentrations have two explanations. First and most important is the constant amount of chloride ion as a result of the HCl. Because of this the expansion of the ionic diameters upon dilution is curtailed at low protein concentrations where the

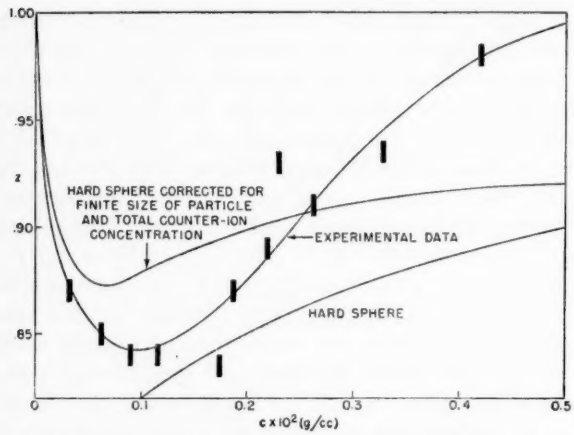

FIG. 6. A comparison of theoretical (hard sphere potential) and experimental values of the dissymmetry for bovine serum albumin at pH 3.30.

concentration of the counter-ions approaches a constant value. Inspection of the dissymmetry equations of Part I shows that the values of z will then increase toward unity as the protein concentration approaches zero. Indeed the minima in Fig. 5 occur at approximately the concentration at which the chloride ion concentrations from the HCl and the protein salt are equal.

In Fig. 6 there is shown the modification of the hard sphere dissymmetry which is brought about by taking into account the finite size of the protein and the total concentration of chloride ions. This calculation, using Eq. (13), was made for the same conditions and in an analogous manner to that for Kc/R_{90} shown in Fig. 4. Here again it will be noted that by making provision for the finite size of the protein and the total concentration of counter-ions, the difference between the hard sphere treatment and the experimental data can be reduced to an amount comparable to the difference between the hard sphere and electrostatic repulsion potential except at relatively high concentrations. Likewise, except at the higher concentrations, it would appear to be unjustified to match precisely the theory and experimental data because of the approximations in the theory. These approximations probably account for most of the discrepancy at the higher concentrations. However, part of this may be the result of the increasing importance in this region of the nonspherical shape of the serum albumin molecule.

C. Experimental Details

Crystalline bovine serum albumin from the Armour Laboratories was used in this work. Solutions were dialyzed and then centrifuged at 20,000 g for 4–12 hours. These solutions were then introduced into a semi-octagonal glass cell in which similarly centrifuged solvent had just been measured. After measuring the scattering of the solution, solvent was added, mixing was achieved by magnetic rotation of a glass encased iron rotor contained in the glass cell, and further dilutions were made in the same manner.

The photometer employed was essentially that described by Brice, *et al.*[20] The calibration employed is discussed by Doty and Steiner.[3] The blue line of mercury (4370A) was used throughout. The particular effects found were less pronounced when green light is employed since they depend upon the ratio, D/λ'. The value used for (dn/dc) was 0.192,[21] thus setting $K=9.85\times10^{-6}$. As seen in Fig. 3 a molecular weight of 77,000 was found at the isoelectric point. This molecular weight was assumed at other pH values since the precision was not sufficient to require consideration of the contribution of the chloride ions. Moreover the possible variation of (dn/dc) with pH was not determined.

A titration curve of bovine serum albumin in the absence of neutral salt was determined using a Beckman pH Meter, Model G. From this it was found that the net charge per molecule was at pH 3.80, 22; pH 3.30, 46; pH 3.20, 54.

III. EXPERIMENTS WITH ISOIONIC SOLUTIONS OF SERUM ALBUMIN CHLORIDE

A. Measurements of R_{90}

The second type of experiments suggested by the discussion in Part I is that in which solutions of the protein salt are diluted with a sodium chloride solution of the same molarity as the chloride ions in the protein salt solution. Consequently solutions of 0.40 and 0.90 g/100 cc of bovine serum albumin were prepared and dialyzed against very dilute HCl until the solution was at pH 3.30. Solutions of 0.0024 M and 0.0054 M NaCl were brought to pH 3.30 with the addition of HCl. After cleaning the values of R_{90} and z were determined for each solution and those obtained by dilution with

[20] Brice, Halwer, and Speiser, J. Opt. Soc. **40**, 768 (1950).
[21] Halwer, Nutting, and Brice, J. Am. Chem. Soc. **73**, 2786 (1951).

the appropriate NaCl solution. The results for R_{90} are shown in Fig. 7 as circles. The dashed line is taken from Fig. 3 and corresponds to dilutions with 0.0005 M HCl. It is clear that the $Kc/R_{90}-c$ relation is now of the orthodox type, and it appears likely that the size of the electric double layer has been stabilized.

To investigate the constancy of the effective ionic diameter one can see if the points in Fig. 7 can be fitted with the virial Eq. (21). This equation applies strictly only to Kc/R_0. However, as measurements recorded below show, the dissymmetry of these solutions is quite small so that R_{90} can be taken as equal to R_0 with a negligible error. The full lines in Fig. 7 are plots of Eq. (21) with the value of D chosen to give the best fit. At 0.4 g/100 cc $D=230$A and at 0.9 g/100 cc $D=180$A. The only discrepancy occurs near 0.9 g/100 cc. To see if this might be caused by the absence of virial coefficients higher than the fifth in Eq. (21), several points were calculated according to the more complete treatment of Kirkwood, Maun, and Adler.[15] Three of these points are shown in Fig. 7 and indicate that although the difference between the two treatments is noticeable at the higher concentrations, it cannot account for the observed discrepancy. It is likely that the remaining difference is the result of the difference between the potentials in the model and in the protein-ion solution. However, the general agreement offers substantial support to the idea that the size of the electric double layer is stabilized in isoionic dilution.

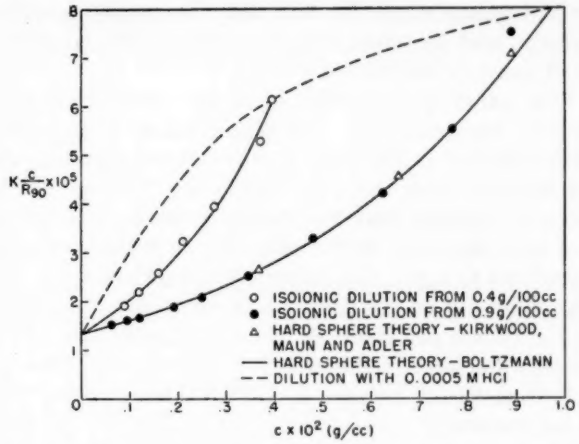
$K\frac{c}{R_{90}}\times10^5$
c x 10² (g/cc)
ISOIONIC DILUTION FROM 0.4 g/100cc
ISOIONIC DILUTION FROM 0.9 g/100cc
HARD SPHERE THEORY – KIRKWOOD, MAUN AND ADLER
HARD SPHERE THEORY – BOLTZMANN
DILUTION WITH 0.0005 M HCl

FIG. 7. The concentration dependence of Kc/R_{90} for isoionic dilutions of bovine serum albumin at pH 3.30. The dashed line is taken from Fig. 3. The full lines are plots of Eq. (21).

B. Measurements of z

Within probable experimental error the dissymmetry was found to be unity when the 0.9 g/100 cc solution was diluted isoionically. The data obtained in the case of 0.4 g/100 cc solution are shown in Fig. 8. It is seen that the dissymmetry changes almost linearly toward unity upon such dilution and does not follow the protein-salt curve through a minimum. This behavior is anticipated from Eq. (13). It is this equation which is plotted in Fig. 8 using values of $D=230$ and 315A. The first value is that found in the fitting of the virial equation and the later from Part II-A. These values are discussed in the following section. Here we note that the experimental points fall between the two plots of Eq. (13) corresponding to these values of D. Thus, although these data are rather poor it is consistent with the foregoing development. In general, it appears that the dilution of any macro-ion salt solution isoionically will cause the dissymmetry to change almost linearly toward the limiting value, this being in accord with an effective ionic diameter of constant size determined by the concentration of the protein salt solution at which the isoionic dilution was begun.

C. A Comparison of Different Estimates of the Size of the Effective Ionic Diameter

On the basis of thermodynamic data using a precise theory it was concluded in Part III-A that upon isoionic dilution from 0.4 g/100 cc $D=230$A and from 0.9 g/100 $D=180$A. On the basis of diffraction data using an approximate theory, we found in Part III-A for the corresponding concentrations values of 315 and 262A for D. The difference between these two sets of results is due principally to the neglect of higher virial coefficients in the diffraction theory. Thus in applying Eq. (13) at high concentrations D takes on the character of a parameter made up of two parts, one corresponding to the real value of D and the other supplying the contribution that would normally have come from the higher virial coefficients in a more complete theory. This may be illustrated by referring to Fig. 7. Plots of Eq. (12) with $D=230$ and 180A would be straight lines having slopes equal to the initial slopes of the curves shown in Fig. 7. On the other hand the use of values of 315 and 262A would lead to straight lines connecting the intercept with the uppermost points of the isoionic curves, that is, at 0.4 and 0.9 g/100 cc. Clearly the former and not the latter curves agree with experiment at low

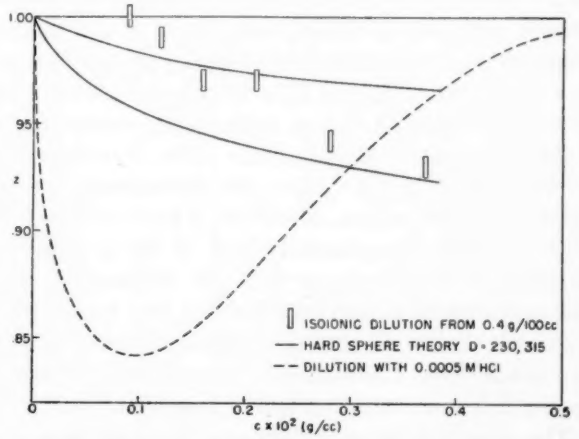

FIG. 8. The concentration dependence of the dissymmetry for isoionic dilution of a 0.4 g/100 cc bovine serum albumin solution at pH 3.30. The two full lines are plots of Eq. (13) for $D=230$ and 315A. The dashed line is taken from Fig. 5.

concentrations where Eq. (12) may be applied quantitatively, and therefore it is the values 230 and 180A which must be considered correct.

Two other possibilities exist for estimating the effective ionic diameter. The simplest is to employ the Debye-Huckel κ. Although it was pointed out in Part I-A that the ionic diameter defined in this way has a different meaning from the one used here a comparison is of interest. The possible objection that the potential is too high to apply this concept is not serious since the charge density on the protein surface is only about one proton charge per 250A^2. If we accept again 62A as an average diameter of the protein molecule, the value of D is then $62+2/\kappa$ where $\kappa=(c'/2)^{\frac{1}{2}}/3.04$, c' being the molar concentration of chloride ions. Thus $D=216$ and 169A at $c=0.4$ and 0.9 g/100 cc, respectively, in reasonable agreement with the values of 230 and 180A.

The other estimate can be made by evaluating the potential of Verwey and Overbeek[5] for a particular set of conditions. The value of r at which $V/kT=1$ should be the value of the effective ionic diameter. In fact, since this quantity has been determined here with some precision, this procedure offers a direct test of the Verwey-Overbeek theory subject principally to the approximation that the serum albumin molecule is spherical.

In summarizing the calculation material contained in reference 5, Chapter 10, is omitted in the interests of brevity. The numerical computations of Verwey and Overbeek are summarized (Fig. 37) by a plot of $V/\epsilon a\psi_0^2$, where V‡ is the potential energy of interaction, ϵ is the dielectric constant, a is the particle radius, and ψ_0 is surface potential, against the reduced distance, r/a, for various ionic strengths expressed as the product κa. Their particular curve for $\kappa a=0.3$ closely approximates the conditions at $c=0.4$ g/100 cc in our experiments. Thus at this value of c, $\kappa=0.012$ and $a=25$A. Using a charge of 46 protons for Q, the quantity $Q^2/\epsilon a=2.40\times10^{-11}$ ergs. The use of this in equation (79) of reference 5 permits the evaluation of $\psi_0^2\epsilon a$ and this in connection with Fig. 37 leads to values of V for various values of r/a. As a result the following values are found: at $r=375$, 282, 225, and 175; $V/kT=0.48$, 1.93, 4.70, 11.6, respectively. A plot of these results shows that at $V/kT=1$, r has a value of about 320A. Alternately at $r=230$A, $V/kT=4.4$. Thus the discrepancy is significant but not serious. Moreover, a part of it may be caused by the non-spherical shape of the protein-ion. However, it would appear that the discrepancy may also arise at least in part from the fact that the Verwey-Overbeek theory is based upon the interaction of only two macro-ions. Undoubtedly some differences would appear if it were extended to an ensemble of ions.

The potential-distance data can be fitted with the following equation:

$$V/kT=2\ln\left[1-\exp-\left(\frac{r}{175}-1\right)^2\right]. \qquad (22)$$

This was the basis of employing Eq. (17) for calculating the scattering from systems with electrostatic potentials.

‡ The V used here is equivalent to the $\psi(r)$ of Eq. 6. The change is made to conform to the nomenclature used in reference 5.

IV. CONCLUSIONS

In view of the confirmation of the theory offered by the experiments just described, it appears that the equilibrium properties of macro-ion solutions as exhibited in light scattering studies can be satisfactorily accounted for by the nonrandom distribution of the macro-ions which results from the relatively large repulsive forces operating among them. These repulsive forces can be characterized by assigning to the macro-ion and its electric double layer an effective diameter or mean distance of approach which can be related to several potential functions. This effective diameter is composed of the diameter of the compact particle which is a constant, and a portion of the electric double layer which changes in size as the inverse cube root of the concentration of gegenions. In dilute macro-ion salt solutions the later contribution predominates. Under these conditions the concentration dependence of the effective diameter requires that the fraction of the solution occupied in this fashion would be nearly constant. In the case of the serum albumin with a charge of +46, it was found that the effective diameter was 180A at 0.9 g/100 cc and 230A at 0.4 g/100 cc. From this it follows that the fraction of the solution occupied by these spheres is 21.4 percent and 19.8 percent, respectively. Thus at this state of charge and at any concentration about 20 percent of the volume of the solution is unavailable for occupancy by any given macro-ion. When it is recalled that in the close packing of spheres only a little more than three times this volume is filled, it is evident that such a solution is well along the way from disorder to order. Certainly in systems of higher charge a closer approach to ordering could be attained.

The stabilization of the effective diameter which is achieved in isoionic solutions makes possible its precise measurement by light scattering. Moreover, it defines a colloidal unit which invites study by other physical methods. It seems unlikely that this information or some of the other results of this investigation could, at present, have been obtained in any other manner. Yet, this having been done, it will be of interest to see if these basic patterns of behavior of macro-ion solutions are adequate to explain the results obtained by other types of investigations on these systems.

ACKNOWLEDGMENT

The authors wish to express their appreciation to the Research Corporation whose financial support was an essential ingredient of this work. In addition they wish to thank Dr. Bruno H. Zimm, Dr. Gerald Oster, and Dr. Gert Ehrlich for helpful discussions.

Rotation-Vibration Spectra of Diatomic and Simple Polyatomic Molecules with Long Absorbing Paths

VII. The Spectrum of Dideuteroacetylene (C_2D_2) in the Photographic Infrared*

B. D. Saksena
Division of Physics, National Research Council, Ottawa, Canada
(Received August 22, 1951)

Twelve absorption bands of C_2D_2 have been observed in the photographic infrared. Eleven of these bands show simple P and R branches with intensity alternation, i.e., they are $\Sigma_u^+-\Sigma_g^+$ bands while one band, without intensity alternation, is a difference band of type $\Pi-\Pi$. From the positions of the bands some of the vibrational constants ω_i^0 and x_{ik} are determined. In addition, from the rotational fine structure, the rotational constants $B_{[v]}$ and $D_{[v]}$ are determined. For $B_{[0]}$ the value 0.8478_7 cm^{-1} is obtained. The α_i values are $\alpha_1=+0.0057_8$, $\alpha_2=+0.0030_2$, $\alpha_3=+0.0045_5$, $\alpha_4=-0.0012_0$, $\alpha_5=-0.0026$ cm^{-1}. From the α_i and $B_{[0]}$ one obtains $B_e=0.8507_5$ cm^{-1}. Combining $B_e(C_2D_2)$ with $B_e(C_2H_2)$ yields, for the internuclear distances in the acetylene molecule, $r_e(C\equiv C)=1.201_0\times10^{-8}$ and $r_e(C-H)=1.063_7\times10^{-8}$ cm in very satisfactory agreement with the values previously obtained from $B_e(C_2HD)$ and $B_e(C_2H_2)$. Evidence for l-type doubling in C_2D_2 is given and approximate values for the l-type doubling constants q_4 and q_5 are obtained.

A. INTRODUCTION

THE absorption spectrum of acetylene (C_2H_2) and monodeuteroacetylene (C_2HD) in the photographic infrared region has been investigated by a number of workers.[1] Until now there are no data available on the absorption spectrum of C_2D_2 in this region. From the unsuccessful attempts of earlier workers,[2,3] it appears that in this region the absorption of C_2D_2 is very much weaker than that of C_2H_2, and therefore long absorbing paths are very essential for its study. In the present work path-lengths of the order of 500 m were used by employing the method due to White, a full description of which may be found in the first paper[4] of this series. Twelve C_2D_2 bands were observed and analyzed, and accurate values of some of the vibrational and rotational constants have been obtained.

B. EXPERIMENTAL

The dideuteroacetylene used in this investigation was prepared by the action of heavy water on CaC_2 which had previously been heated for several hours at 900°C. Seventeen liters of gas were prepared in two batches and were examined on a mass spectrograph for the ratio of C_2D_2 to C_2HD. The first sample of six liters had 8 percent of C_2HD while the second sample had only 4 percent which gave an average of 5.5 percent of C_2HD in the entire volume. Even this small fraction of C_2HD present in the tube gave rise to absorption bands, the strongest of which were almost as intense as the strong C_2D_2 bands. The bands of C_2D_2 can be distinguished from those of C_2HD by the phenomenon of alternating intensities which is present only in the former. The amount of C_2H_2 in the sample was entirely negligible, and correspondingly, no C_2H_2 bands were found in the spectrum.

The gas was first collected in a gasometer, and then condensed in a glass tube dipped in liquid nitrogen. It was transferred to the absorption tube by replacing the bath of liquid nitrogen by one of solid CO_2. This served to purify the gas still further and remove traces of water vapor. The absorption tube which was 5 meters long was filled to a pressure of 320 mm. The continuous background was provided by a Western Union concentrated arc. The light traversed the tube up to 120 times, giving an absorbing path of up to 600 meters. The spectra were photographed in the first order of a 21 ft grating spectrograph, and iron lines of the second and third order were used as standards. Kodak 1 N, 4 N, 1 M, and 1 Z plates were used for photographing the spectra in the region 7500A to 11800A. The more intense bands were measured eight times and the weaker ones four times. The measurements of the relative positions of the unblended lines in the stronger bands are probably correct to 0.02 cm^{-1}, although the absolute accuracy may be somewhat less.

Twelve bands were observed, all of which are of the parallel type. They are listed in the first column of

TABLE I. Observed C_2D_2 bands.

ν_0(obs)	Int.	Assignment	ν_0(calc)	Obs-Calc
8550.12	s.	$\nu_1+2\nu_2+\nu_3$	8549.12	+1.00
8952.89	v.s.	$\nu_2+3\nu_3$	8950.53	+2.36
9444.51	s.	$2\nu_1+\nu_2+\nu_3$	9439.11	+5.40
9794.06	s.	$\nu_1+3\nu_3$	9794.44	−0.38
10347.92	m.	$3\nu_1+\nu_3$	10350.94	−3.02
11146.0	v.w.	$2\nu_1+2\nu_2+\nu_3$	11143.94	+2.06
11455.79	v.w.	$\nu_1+\nu_2+3\nu_3+\nu_4-\nu_4$	...	...
11492.66	v.s.	$\nu_1+\nu_2+3\nu_3$	11492.30	+0.36
11905.3$_4$	w.	$5\nu_3$	11905.30	+0.04
12036.8$_7$	w.	$3\nu_1+\nu_2+\nu_3$	12036.88	−0.01
12344.5$_0$	w.	$2\nu_1+3\nu_3$	12339.16	+5.34
13181.9	v.w.	$\nu_1+2\nu_2+3\nu_3$	13187.82	−5.92
cm^{-1}			cm^{-1}	cm^{-1}

* Contribution No. 2586 from the National Research Council, Ottawa, Canada.

[1] For bibliography see G. Herzberg, *Infrared and Raman Spectra of Polyatomic Molecules* (D. Van Nostrand, Inc., New York, 1945), p. 289.

[2] Herzberg, Patat, and Spinks, Z. Physik **92**, 87 (1934).

[3] C. A. Bradley and A. McKellar, Phys. Rev. **47**, 914 (1935).

[4] H. J. Bernstein and G. Herzberg, J. Chem. Phys. **16**, 30 (1948).

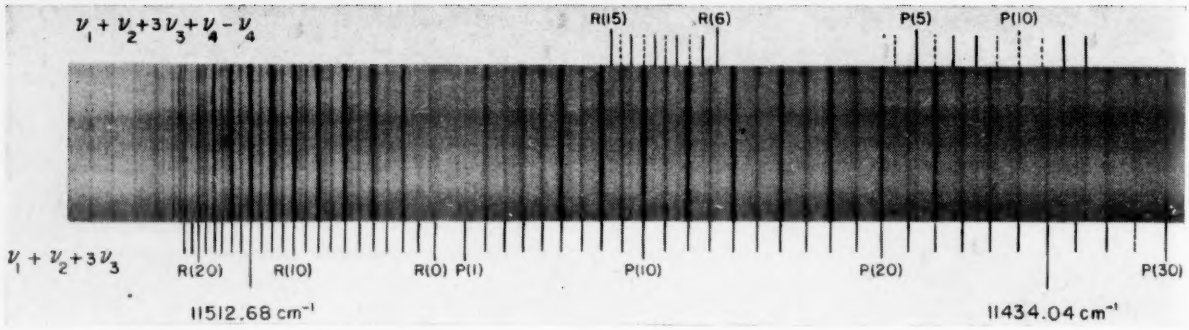

FIG. 1. C_2D_2 bands at 8700A. The lines of the main band, $\nu_1+\nu_2+3\nu_3$, are indicated below, the lines of the weak "hot" band, $\nu_1+\nu_2+3\nu_3+\nu_4-\nu_4$, above the spectrogram. The unmarked lines at the left are due to the C_2HD band 8670A. A few unassigned lines at the right may be the result of the second "hot" band, $\nu_1+\nu_2+3\nu_3+\nu_5-\nu_5$.

Table I. Six bands are fairly strong; three of the remaining bands are weak and the other three very weak. There are a few cases in which lines of the H_2O and C_2HD bands overlap those of the C_2D_2 bands, but these cases can be easily recognized. In Fig. 1 a spectrogram is reproduced which shows one of the stronger C_2D_2 bands, at 8700°A, as well as the very weak band at 8727A. In the strong band the intensity alternation si immediately recognizable, the lines with even J being the stronger. In the weak band no intensity alternation occurs indicating that it is of the $\Pi-\Pi$ type rather than $\Sigma-\Sigma$ as are all the other observed bands.

The wave numbers of the individual lines of the bands are given in Table II. In the weaker bands the first few lines near the zero gap were too weak to be measured. A few other gaps in the table are caused by the presence of strong emission lines in the spectrum of the source.

C. VIBRATIONAL ANALYSIS

A linear four-atomic molecule has five fundamentals ν_1, ν_2, ν_3, ν_4, ν_5, of which the first three correspond to nondegenerate modes and the remaining two to doubly-degenerate ones.[1] To a first approximation the vibrational energy of such molecule referred to the lowest level ($v_1=v_2\cdots=v_5=0$) is given by

$$G_0(v_1, v_2\cdots v_5, l_4, l_5) = \sum_i \omega_i^0 v_i + \sum_i \sum_{j>i} x_{ij}^0 v_i v_j + \sum_i g_{ii} l_i^2.$$

Here, if higher powers are neglected, the anharmonicity constants x_{ik}^0 are identical with the usual x_{ik}; the ω_i^0 are related to the zero-order frequencies ω_i by

$$\omega_i^0 = \omega_i + x_{ii} d_i + \tfrac{1}{2} \sum_{j\neq i} x_{ij} d_j + \cdots,$$

(where d_i and d_j are the degrees of degeneracy of vibrations ν_i and ν_j) and related to the fundamental frequencies by

$$\nu_i = \omega_i^0 + x_{ii}^0 + g_{ii};$$

l_i is the quantum number of vibrational angular momentum which is zero for $i=1$, 2, 3 and has the values v_i, v_i-2, $\cdots 1$ or 0 for $i=4$, 5; g_{ii} is different from zero for $i=4$, 5 only.

The assignment of the observed bands to particular vibrational quantum numbers was made on the basis of a comparison of the relative intensities of the bands as observed in C_2D_2 to those observed in C_2H_2. An additional criterion was the approximate agreement of the observed band-origins with those predicted from the known fundamentals neglecting anharmonicity. The assignments obtained in this way are included in Table I. It is uncertain whether the "hot" band 11455.79 cm^{-1} involves the excitation of ν_4 or of ν_5 in the upper and lower state of the main band 11492.66 cm^{-1}. The assignment $\nu_1+\nu_2+3\nu_3+\nu_4-\nu_4$ is very slightly preferable to $\nu_1+\nu_2+3\nu_3+\nu_5-\nu_5$ because ν_4 is smaller than ν_5.

Revised values of the five fundamentals have recently been given by Talley and Nielsen.[5] They are

$$\nu_1(\sigma_g^+)=2701.84, \quad \nu_2(\sigma_g^+)=1764.9, \quad \nu_3(\sigma_u^+)=2439.1,$$
$$\nu_4(\pi_g)=511.38, \quad \nu_5(\pi_u)=538.66 \text{ cm}^{-1}.$$

The present data are unfortunately not sufficient to determine all the vibrational constants (ω_i^0 and x_{ij}^0) of C_2D_2. But, assuming the correctness of the fundamental frequencies and of the assignments of the overtone and combination bands given in Table I, some of the vibrational constants have been obtained. They are listed in the second column of Table III and compared in the third and fourth columns with the corresponding constants of C_2H_2 as obtained by Herzberg and Spinks[6] and Nordin and Haslam,[7] respectively.

In the case of the progression v_3v_3 of C_2H_2 it is necessary to introduce a cubic term $y_{333}^0 v_3^3$ in the energy formula. This has also been done for C_2D_2, although the term is much smaller and possibly zero within the accuracy of the determination.

The fourth column of Table I gives the positions of

[5] R. M. Talley and A. H. Nielsen, Phys. Rev. **82**, 338 (1951); J. Chem. Phys. **19**, 805 (1951).

[6] G. Herzberg and J. W. T. Spinks, Z. Physik **91**, 386 (1934).

[7] N. H. Nordin and R. N. H. Haslam, Can. J. Research **A26**, 279 (1948).

TABLE II. Wave numbers of the lines in the C_2D_2 bands (ν_{vac}, cm^{-1}).

	$\nu_1+2\nu_2+\nu_3$ $\nu_0=8550.12$		$\nu_2+3\nu_3$ $\nu_0=8952.89$		$2\nu_1+\nu_2+\nu_3$ $\nu_0=9444.51$		$\nu_1+3\nu_3$ $\nu_0=9794.06$		$3\nu_1+\nu_3$ $\nu_0=10347.92$		$\nu_1+\nu_2+3\nu_3$ $\nu_0=11492.66$	
J	R(J)	P(J)	R(J)	P(J)	R(J)	P(J)	R(J)	P(J)	R(J)	P(J)	R(J)	P(J)
0	...	...	8954.58†	...	...	...	...	...	...	...	11494.76†	...
1	...	...	56.29	8951.01†	...	...	...	...	...	...	96.06†	11491.26†
2	8554.98	8546.68	57.76†	49.46	9449.40	9441.06	9798.94	9790.63†	10352.74	10344.52	97.47	89.28†
3	56.58	44.94	59.31	47.69	50.91	39.37	800.46	88.85	54.28	...†	99.01	87.44†
4	58.12	43.12	60.86	45.86	52.42	37.51	01.96	87.07	55.75	40.89	500.47	85.62
5	59.60	41.31	62.36	44.08†	53.87	35.64	03.42	85.16†	57.18	38.98†	01.89	83.75
6	61.08	39.47	63.85	42.20	55.32	33.78	04.82	83.30	58.57	37.09	03.29	81.83
7	62.50	37.56	65.25	40.33	56.70	31.87†	06.21	81.38	59.91	35.14	04.63	79.87
8	63.89	35.65	66.63	38.40	58.04	29.89	07.56	79.42†	61.22	33.12	05.91	77.85
9	65.27	33.69	68.05	36.39†	59.36	27.88	08.85	77.40	62.49	31.11	07.16	75.79
10	66.60	31.66	69.37	34.44†	60.63	25.83	10.10	75.35	63.66	29.02	08.36	73.69
11	67.88	29.64	70.66	32.45	61.86	23.76	11.34	73.26	64.88	26.88	09.50	71.54
12	69.15	27.59	71.93	30.36	63.08	21.64	12.54	71.12	65.98	24.70	10.62	69.35
13	70.37	25.51	73.16	28.37†	64.23	19.49	13.67	68.93†	67.06	22.47	11.68	67.11
14	71.59	23.36	74.36	26.13	65.35	17.31	14.77	66.75	68.11	20.22	12.68	64.85
15	72.76	21.21	75.53	23.99	66.42	15.06	15.85	64.52	69.10	17.93	13.67	62.52
16	73.87	19.03	76.66	21.81	67.47	12.82	16.87	62.25	70.04	15.57	14.59	60.16
17	74.98	16.81	77.77†	19.61	68.47	10.48	17.84	59.93	70.97	13.21	15.49	57.73
18	76.06	14.57	78.82	17.37	69.46	08.14	18.79	57.54	71.83	10.74	16.32	55.30
19	77.10	12.29	79.86	15.02	70.38	05.79	19.69	55.16	72.62	08.29	17.23†	52.78
20	78.09	09.98	80.87	12.87†	71.26	03.33	20.54	52.71	73.41†	05.73†	17.86	50.23
21	79.03	07.61	81.83	10.36	72.12	00.89	21.39	...	74.15	03.16	18.61	47.65
22	79.97	05.23	82.78	07.98	72.92	398.37	22.18	...	74.82	00.58	19.22	45.01
23	80.88	02.82	83.69	05.58	73.70	95.88	...	...	75.48	297.88†	19.76†	42.35
24	81.77	00.35	84.56†	03.07†	74.42	93.26	...	...	76.04	95.22	20.40	39.61
25	82.62	497.98†	85.36	00.71	75.16	90.66†	...	...	76.59	...†	20.93	36.85†
26	83.41	95.36	86.17	898.18	75.77	88.04	...	...	77.13	89.66	21.43	34.04
27	84.81	...	86.94	95.62	...	85.31†	...	...	...	...	...	31.20
28	85.53	...	87.69	93.04	...	82.61	...	...	...	...	...	28.29
29	...	...	...	90.46	...	...	...	...	...	...	...	...
30	...	...	...	87.79	...	...	...	...	...	...	...	...

	$2\nu_1+2\nu_2+\nu_3$ $\nu_0=11146.0$		$\nu_1+\nu_2+3\nu_3+\nu_4-\nu_4$ $\nu_0=11455.79$		$5\nu_3$ $\nu_0=11905.3_4$		$3\nu_1+\nu_2+\nu_3$ $\nu_0=12036.8_7$		$2\nu_1+3\nu_3$ $\nu_0=12344.5_0$		$\nu_1+2\nu_2+3\nu_3$ $\nu_0=13181.9$	
J	R(J)	P(J)	R(J)	P(J)	R(J)	P(J)	R(J)	P(J)	R(J)	P(J)	R(J)	P(J)
0	...	...	...	...	...	...	...	...	...	...	...	...
1	...	...	...	...	...	...	...	...	...	...	...	...
2	...	...	...	...	...	...	12041.68	...	12349.26	...	...	...
3	...	...	...	...	...	...	43.07	...	50.76	...	...	...
4	...	11139.00	...	...	11913.09	11898.22	44.65	12029.88	52.20	...	13189.75	13174.98
5	...	37.22	...	11446.83	14.48	...	46.05	27.75	53.62	...	...	...
6	11156.66	35.21	11466.41	45.01†	15.94	94.50	47.44	25.98	54.89	12333.59	92.38	71.15
7	58.02	33.18	67.77	42.98	17.27	...	48.74	23.96	56.25	31.58	93.64	68.93
8	59.30	31.25	69.35†	40.96	18.54	90.51	49.97	22.01	57.43	29.50	94.93	66.93
9	60.54	29.21	70.35	...	19.87	...	51.16	19.92	58.64	27.38	96.06	...
10	61.75	27.06	71.55†	...	20.95	86.30	52.33	17.75	59.79	25.23	97.18	...
11	62.92	...	72.72	...	22.16	84.21	53.33†	15.58	60.87	22.99	98.32	...
12	63.98	22.74	73.69†	32.46	23.27	82.00	54.54	13.50†	61.84	20.61	99.36	...
13	65.12	...	75.00	30.27	24.32	79.71	55.55	11.10	62.85	...	200.30	...
14	66.16	...	75.79†	...	25.30	77.42	56.50	08.76	63.80	16.18†	01.27	...
15	67.17	...	76.90	...	26.28	75.18	...	06.39	64.65	13.72	02.14	...
16	68.13	...	77.85†	...	27.19	72.73	58.32	03.99	65.50	11.22	03.03	...
17	69.01	...	...	...	...	...	...	...	66.26	08.73	...	...
18	69.89	...	...	...	28.91	67.89†	...	199.16†	66.96	06.14	...	...
19	70.67	...	...	...	29.68	...	...	...	...	03.52	...	...
20	71.46	...	...	...	30.42	62.85†	...	...	...	300.91†	...	...
21	...	...	...	...	...	60.23†	...	...	...	...	...	...
22	72.95	...	...	...	...	57.55†	...	...	...	...	...	...

†Lines marked by † are either blends with other C_2D_2 lines or H_2O lines, or very faint and therefore not very accurately measured.

the band origins calculated from the vibrational constants of Table III, and the last column gives the deviations of the observed from the calculated values. These deviations are for most bands much larger than would be expected from the accuracy of the measurements. This fact should not be considered as an indication of incorrect assignments since similar deviations have been found for other molecules where also the assignments appear quite certain (e.g., N_2O, see paper VI of this series).[8] Other assignments have been tried, but lead to no better agreement unless one introduces the excitation of ν_4 and ν_5 in many of the photographic bands and admits rather large values of x_{i4} and x_{i5}.

The present assignment is quite satisfactory from the

[8] G. Herzberg and L. Herzberg, J. Chem. Phys. 18, 1551 (1950).

point of view of the relative intensities of the bands. Thus the band $2\nu_1+2\nu_2+\nu_3$ is weaker than both $2\nu_1+\nu_2+\nu_3$ and $\nu_1+2\nu_2+\nu_3$; the bands $3\nu_1+\nu_2+\nu_3$ and $2\nu_1+3\nu_3$ are, respectively, weaker than $3\nu_1+\nu_3$ and $\nu_1+3\nu_3$, while the bands $\nu_2+3\nu_3$, $\nu_1+3\nu_3$, and $\nu_1+\nu_2+3\nu_3$ are all strong. Further confirmation of this assignment is obtained from the rotational analysis which follows.

An attempt has been made to improve the agreement between observed and calculated ν_0 values by introducing the resonance between levels $v_1\nu_1+v_2\nu_2+v_3\nu_3$ and $(v_1+2)\nu_1+v_2\nu_2+(v_3-2)\nu_3$ as was done by Nordin and Haslam[7] for C_2H_2; but no improvement was found.

D. ROTATIONAL ANALYSIS

As mentioned in Sec. B all but one of the observed photographic bands are of the $\Sigma_u^+-\Sigma_g^+$ type. The rotational numbering in these bands is immediately obvious. In each case it is found that the even rotational lines are the strong ones in agreement with expectation (the D nuclei follow Bose statistics) and opposite to the behavior of C_2H_2. The rotational constants have been determined in the usual way. In order to give an idea of the accuracy obtained Table IV lists the combination differences $\Delta_2F''(J)=R(J-1)-P(J+1)$ for the six strongest bands as well as the mean for each J value.[9] In Fig. 2 the mean values of $\Delta_2F''(J)/(J+\frac{1}{2})$ are plotted against $(J+\frac{1}{2})^2$. The intercept of the straight line thus formed with the ordinate axis is $4B_{[0]}$ and its slope is $8D_{[0]}$. In this way one obtains

$$B_{[0]}=0.8478_7\pm0.0001_5 \text{ cm}^{-1}$$

and

$$D_{[0]}=8.0\times10^{-7}\pm0.7\times10^{-7}.$$

The same $B_{[0]}$ value is obtained by taking the mean of the six B'' values obtained from each band independently.

The observed value of $D_{[0]}$ agrees very satisfactorily with that obtained theoretically from the relation $D_{[0]}=4B_{[0]}{}^3\omega^2$, if one substitutes for ω the wave number of ν_2 (1764.9 cm^{-1}). One finds $D_{[0]}{}^{(\text{calc})}=7.8\times10^{-7}$ cm^{-1}. A similar agreement, although not quite as close, was found by Herzberg and Spinks[6] for C_2H_2. It may be noted that strictly speaking a combination of ω_2 and ω_1 enters the formula for D_0, but the effect of ω_1 is quite small in this case.[1]

Talley and Nielsen[5] have recently reported the value of $B_{[0]}$ as 0.8482_7 cm^{-1} which is slightly greater than our value (0.8478_7). It may be seen from Fig. 2 that their $B_{[0]}$ value (i.e., an intercept at 3.3931 cm^{-1}) would yield a straight line that does not represent the observed points as well as the one chosen here. Further, in none of the six separate $\Delta_2F''(J)/(J+\frac{1}{2})$ plots for the six strong bands has it been possible to obtain an intercept as high as 3.3931.

The rotational constants $B_{[v]}$ for the upper states of most of the $\Sigma_u^+-\Sigma_g^+$ bands were obtained by first determining $B'-B''$ from the combination sums $R(J-1)+P(J)$ [see Herzberg[1]], and then using the $B_{[0]}$ value obtained above. In the case of the two very weak bands, $2\nu_1+2\nu_2+\nu_3$ and $\nu_1+2\nu_2+3\nu_3$, for which the R branch is better developed than the P branch, the value of $B'-B''$ was derived from the relation,

$$R(J-1)+R(J-2)-4(J-\tfrac{1}{2})B''=2\nu_0+2(B'-B'')J^2.$$

The single $\Pi-\Pi$ band required special treatment particularly since, in addition to the R branch, only a few lines of its P branch have been observed. The numbering was uniquely obtained by the requirement that B'' for this band must be close to $B_{[0]}$ even though it is not equal to it. $B'-B''$ was then determined from $R(J-1)+P(J)$ while $B'+B''$ was determined by plotting the left hand side of the relation (see Herzberg[1])

$$\nu+(B''-B')m^2=\nu_0+(B'+B'')m$$

against m ($m=-J$ for the P branch and $m=J+1$ for the R branch). The very weak Q branch of this band should occur at $\nu_0=11455.79$ but is hidden by the strong line $P(18)$ of the main band. It should be noted that all lines of a $\Pi-\Pi$ band are double on account of l-type doubling, the two branches having opposite intensity alternation so that if, as here, the doubling is unresolved, no intensity alternation is noticeable.

In Table V all the $B_{[v]}$ values obtained in the above described ways are collected. The $B_{[v]}$ values for the upper and lower states of the $\Pi-\Pi$ band refer to the average of the two l-type doubling components.

As long as there are no perturbations, the $B_{[v]}$ values should follow the relation,

$$B_{[v]}=B_e-\alpha_1(v_1+\tfrac{1}{2})-\alpha_2(v_2+\tfrac{1}{2})-\alpha_3(v_3+\tfrac{1}{2})-\alpha_4(v_4+1)-\alpha_5(v_5+1),$$

or

$$B_{[0]}-B_{[v]}=\alpha_1v_1+\alpha_2v_2+\alpha_3v_3+\alpha_4v_4+\alpha_5v_5.$$

From the observed $B_{[v]}$ values the following α_i values are obtained:

$$\alpha_1=0.0057_8,\quad \alpha_2=0.0030_2,$$
$$\alpha_3=0.0045_5,\quad \alpha_4=-0.0012_0 \text{ cm}^{-1}.$$

The $B_{[v]}$ values calculated with these α_i values are given

TABLE III. Vibrational constants of C_2D_2 and C_2H_2.

	C_2D_2	C_2H_2[6]	C_2H_2[7]
$\omega_1{}^0$	2710.98	3358.4	3366.2
$\omega_2{}^0$	1766.07	$1974-x_{11}$	1981
$\omega_3{}^0$	2453.11	3318.4	3323.87
$x_{11}{}^0$	−9.14	13.6	7.5
$x_{22}{}^0$	−1.17	...	−7.2
$x_{33}{}^0$	−13.91	−28.10	−36.87
$x_{13}{}^0$	−46.28	−112.10	−107.15
$x_{23}{}^0$	−15.27	−4.9	−4.5
$x_{12}{}^0$	−21.23	−4.9	−10.75
$y_{333}{}^0$	−0.1	−2.3	...
	cm^{-1}	cm^{-1}	cm^{-1}

[9] The combination differences were evaluated to 0.001 cm^{-1} before the wave numbers of the band lines were rounded off to 0.01 for Table II.

TABLE IV. Combination differences for the strong C_2D_2 bands.

	$\Delta_2F(J)=R(J-1)-P(J+1)$						
J	$\nu_1+2\nu_2+\nu_3$	$\nu_2+3\nu_3$	$2\nu_1+\nu_2+\nu_3$	$\nu_1+3\nu_3$	$3\nu_1+\nu_3$	$\nu_1+\nu_2+3\nu_3$	Mean
1	...	5.127†	...	...	...	5.481†	5.304†
2	...	8.593†	...	...	...	8.611†	8.602†
3	11.859	11.900†	11.897	11.870	11.847	11.856	11.866
4	15.268	15.230†	15.271	15.297†	15.297†	15.256	15.265
5	18.655	18.655	18.638	18.660	18.658	18.638	18.651
6	22.038	22.033	22.001†	22.034	22.038	22.018†	22.033
7	25.434	25.445	25.429	25.401†	25.455	25.439	25.440
8	28.810	28.859†	28.821	28.812	28.796†	28.836	28.820
9	32.225	32.188†	32.212	32.209	32.198	32.222	32.213
10	35.620	35.597	35.596	35.594	35.611	35.610	35.605
11	39.012	39.004	38.993	38.978	38.963	39.006	38.993
12	42.374	42.292†	42.365	42.414	42.405	42.395	42.391
13	45.789	45.805†	45.766	45.787	45.761	45.764	45.778
14	49.162	49.171	49.170	49.152	49.130	49.153	49.156
15	52.554	52.549	52.532	52.517	52.542	52.527	52.537
16	55.952	55.926	55.942	55.923	55.892	55.942	55.930
17	59.299	59.299	59.329	59.336	59.300	59.293	59.309
18	62.686	62.755†	62.684	62.677	62.680	62.709	62.687
19	66.079	65.955†	66.126	66.075	66.116†	66.085	66.091
20	69.491	69.498	69.485	...	69.458	69.580†	69.483
21	72.865	72.888	72.891	...	72.828†	72.847	72.864
22	76.212	76.250	76.238	...	76.276†	76.260	76.240
23	79.617	79.714†	79.661	...	79.608	79.612	79.624
24	82.898†	82.974	83.034	...	...	82.910†	83.004
25	86.403	86.377	86.388	...	86.374	86.356	86.379
26	...	89.745	89.841†	...	...	89.736	89.740
27	...	93.133	93.169	...	...	93.134	93.145
28	...	96.479	...	...	...	...	96.479
29	...	99.900	...	...	...	...	99.900

† Values with † involve blended or very weak lines. They have been disregarded in the averaging.

in the third column of Table V. It may be seen that in most cases the differences between the observed and calculated B' values are quite small and within the limits of experimental error, but in a few cases the deviations are slightly larger than the estimated accuracy of the particular observed $B_{[v]}$ value. This is again similar to the situation for N_2O.[8] On the whole, the agreement of observed and calculated $B_{[v]}$ supports the vibrational assignments of the observed bands.

Talley and Nielsen[5] have derived $\alpha_5=-0.0001$ from the fine structure of the fundamental ν_5, and $\alpha_4=-0.0037$ from the fine structure of the band $\nu_4+\nu_5$, while several difference bands involving ν_4 yield $\alpha_4=+0.0004$ cm^{-1}. None of these values agrees with the α value (-0.0012_0 cm^{-1}) here obtained from the $\Pi-\Pi$ band, which is most probably α_4 but may also be α_5. The explanation of these discrepancies would appear to lie in the effect of l-type doubling not considered by Talley and Nielsen. The value of α_5 obtained from the fundamental ν_5 refers to one l-type doubling component only and may be designated $\alpha_5{}^{PR}$ since it corresponds to the upper states of the P and R branches which are different from those of the Q branch. The band $\nu_4+\nu_5$ which is a $\Sigma_u\leftarrow\Sigma_g$ transition[10] yields $\alpha_4+\alpha_5$, while the difference bands $\nu_i-\nu_4$ yield $\alpha_4{}^{PR}$. One cannot expect $\alpha_4{}^{PR}+\alpha_5{}^{PR}$ to check with $\alpha_4+\alpha_5$. From the $\alpha_4+\alpha_5$ value of Talley and Nielsen (-0.0038) together with the α_4 value determined previously, one finds

$$\alpha_5=-0.0026$$

(or if the assignment of the hot band has to be changed, $\alpha_4=-0.0026$, $\alpha_5=-0.0012$).

From these α_4 and α_5 values and the $\alpha_4{}^{PR}$ and $\alpha_5{}^{PR}$ values obtained by Talley and Nielsen ($+0.0004$ and -0.0001 cm^{-1}, respectively) one finds for the l-type doubling constants

$$q_4=2(\alpha_4{}^{PR}-\alpha_4)=0.0032,$$
$$q_5=2(\alpha_5{}^{PR}-\alpha_5)=0.0050 \text{ cm}^{-1}.$$

The corresponding values for C_2H_2 are $q_4=0.0038$, $q_5=0.0059$ cm^{-1} (see Herzberg[11]). In agreement with expectation the PR levels of ν_4 and ν_5 lie below the Q levels.

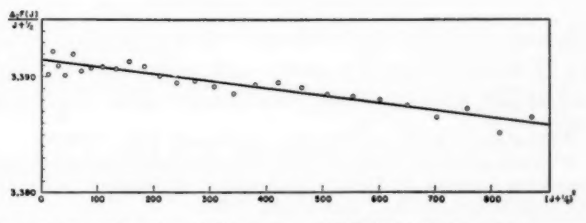

FIG. 2. Combination differences $\Delta_2F(J)/(J+\frac{1}{2})$ for the ground state of C_2D_2.

[10] In addition to $\Sigma_u{}^+$ the combination $\nu_4+\nu_5$ gives rise to the states $\Sigma_u{}^-$ and Δ_u which do not combine with the ground state. On the basis of present theory all three levels would be expected to have the same $B_{[v]}$ value. Higher order interactions may, however, lead to small differences not taken into account here.

[11] G. Herzberg, Revs. Modern Phys. **14**, 219 (1942).

TABLE V. Rotational constants $B_{[v]}$ of the C_2D_2 molecule.

v_1	v_2	v_3	v_4	v_5	$B_{[v]}^{(obs)}$	$B_{[v]}^{(calc)}$	Obs-Calc
0	0	0	0	0	0.8478_7	...	...
0	0	0	1	0	0.8490_7	0.84907	0.0000_0
1	2	1	0	0	0.8313_9	0.8315_0	-0.0001_1
0	1	3	0	0	0.8314_1	0.83120	$+0.0002_1$
2	1	1	0	0	0.8287_5	0.82874	$+0.0000_1$
1	0	3	0	0	0.8282_3	0.82844	-0.0002_1
3	0	1	0	0	0.8260_7	0.82597	$+0.0001_0$
2	2	1	0	0	0.8259	0.82572	$+0.0001_8$
1	1	3	0	0	0.8254_2	0.82542	0.0000_0
1	1	3	1	0	0.8268_2	0.82677	$+0.0000_5$
0	0	5	0	0	0.8252	0.82512	+0.0001
3	1	1	0	0	0.8238	0.82296	+0.0008
2	0	3	0	0	0.8223	0.82266	−0.0004
1	2	3	0	0	0.8226	0.82240	+0.0002
					cm^{-1}	cm^{-1}	cm^{-1}

It may be interesting to compare the values of the various α_i in C_2D_2 with those in C_2HD and C_2H_2. This is done in Table VI.

From the α_i values of C_2D_2 and the $B_{[0]}$ value previously given one finds for B_e,

$$B_e=0.8507_5 \text{ cm}^{-1}.$$

This value is independent of the individual values of α_4 and α_5, and depends only on the sum $\alpha_4+\alpha_5$ which follows directly from the band $\nu_4+\nu_5$ analyzed by Talley and Nielsen.

E. INTERNUCLEAR DISTANCES

In isotopic molecules the potential function remains unaltered, and therefore the internuclear distances are the same. This equality exists rigorously only for the equilibrium internuclear distances r_e, and not for the effective internuclear distances r_0 which involve the zero point energy of the vibrations. In the case of C_2H_2 there are two internuclear distances. These can be determined if we know the moment of inertia I_e of both C_2H_2 and an isotopic molecule. Herzberg, Patat, and Verleger[12] determined the moment of inertia I_e of C_2HD and comparing with I_e of C_2H_2 obtained $r_e(C-C)=1.202_6$ and $r_e(C-H)=1.059_7\times10^{-8}$ cm.[13]

If $I_e(C_2D_2)$ and $I_e(C_2H_2)$ represent the moments of inertia of C_2D_2 and C_2H_2, we have

$$I_e(C_2D_2)=2m_Ca_e^2+2m_Db_e^2$$

and

$$I_e(C_2H_2)=2m_Ca_e^2+2m_Hb_e^2$$

where $a_e=\frac{1}{2}r_e(C-C)$, $b_e=\frac{1}{2}r_e(C-C)+r_e(C-H)$. Using $I=27.9830\times10^{-40}/B$ g/cm^2, and $m_H=1.00813$, $m_D=2.01472$, $m_C=12.00386$, one obtains from $B_e(C_2D_2)$

[12] Herzberg, Patat, and Verleger, Z. Physik **102**, 1 (1936).

[13] These are revised values using the values of the fundamental constants adopted by Herzberg in *Spectra of Diatomic Molecules* (D. Van Nostrand, Inc., New York, 1950).

TABLE VI. α_i values.

	C_2D_2	C_2HD[a]	C_2H_2[a]
α_1	0.0057_8	$0.00633(\alpha_{C-D})$	0.00647
α_2	0.0030_2	$0.00427(\alpha_{C-C})$	0.00617
α_3	0.0045_5	$0.00499(\alpha_{C-H})$	0.00613
α_4	-0.0012_0	...	-0.0012^{16}
α_5	−0.0026	...	-0.0015^{16}

[a] See reference 12.

$=0.8507_5$ and $B_e(C_2H_2)=1.1838$ cm^{-1},

$r_e(C-C)=1.201_0$ and $r_e(C-H)=1.063_7\times10^{-8}$ cm.

These values are in very satisfactory agreement with those obtained by combination of $I_e(C_2H_2)$ and $I_e(C_2HD)$ [see above]. The very slight difference is probably due to the fact that for C_2HD, $\alpha_4+\alpha_5$ was not independently determined, but taken over from C_2H_2 (see reference 12). For this reason and because of the larger isotope effect, the present values appear to be preferable and should represent the internuclear distances in acetylene to $\pm0.001\times10^{-8}$ cm.

If instead of the equilibrium B values we use the effective B values referring to the lowest vibrational level ($B_{[0]}$), that is $B_{[0]}(C_2D_2)=0.8478_7$ and $B_{[0]}(C_2H_2)=1.1769_2$ cm^{-1}, we find

$r_0(C-C)=1.208_0$ and $r_0(C-H)=1.057_8\times10^{-8}$ cm.

These values are surprisingly close to the values obtained from C_2HD and C_2H_2, namely,[12,13]

$r_0(C-C)=1.207_4$ and $r_0(C-H)=1.059_4$A.

This close agreement is probably not very significant as can be judged from the fact that while $r_0(C-C)$ shows the expected increase over $r_e(C-C)$, $r_0(C-H)$ comes out smaller than $r_e(C-H)$ and can therefore not be a true mean internuclear distance in the lowest vibrational level. Microwave investigations of different pairs of isotopic species of N_2O (see Coles and Hughes)[14] have indeed given rather conflicting values of the internuclear distances on account of the use of r_0 rather than r_e values.

ACKNOWLEDGMENTS

In conclusion the author wishes to thank Dr. G. Herzberg for suggesting the problem and for several helpful discussions. He is also deeply grateful to him for the opportunity afforded to come and work in his laboratory, and for the great kindness shown to him during his stay. Thanks are also due to Dr. A. E. Douglas for his considerable help, to Dr. L. C. Leitch for help in preparing heavy acetylene, and to Dr. F. P. Lossing for the analysis of C_2D_2 on the mass spectrograph.

[14] D. K. Coles and R. H. Hughes, Phys. Rev. **76**, 178 (1949).

l-Type Doubling in Energy Levels of Carbon Dioxide Coupled by Fermi Resonance*

J. DE HEER AND HARALD H. NIELSEN
Department of Physics and Astronomy, The Ohio State University, Columbus, Ohio
(Received September 5, 1951)

In this paper we discuss the l-type doubling in levels of linear molecules which are coupled by Fermi resonance; in particular we consider here a triad of such levels in carbon dioxide. In principle, it becomes necessary to consider *simultaneously* the perturbations related to both anharmonic resonance interaction *and* l-type doubling. A further analysis reveals, however, that we are justified in carrying out an approximate solution, in which we first consider the resonance interaction as if l-type doubling did not occur and subsequently find the energy levels associated with $+l$ and $-l$ as a result of small perturbations on the twofold degenerate levels involved. It appears that the applicability of the well-known formula $\Delta\nu=qJ(J+1)$, in which q is the l-type doubling constant, is inherent to this approximation. The agreement between q values computed by our method and those obtained experimentally is very satisfactory indeed.

I. INTRODUCTION

IT is well known that in instances where two or more vibration frequencies of polyatomic molecules are accidentally degenerate, resonance interaction may take place because of the presence of certain terms in either the anharmonic portion of the potential energy or the Coriolis operator. It is also well known that in linear and axially symmetric molecules the correction terms to the moments of inertia in the rotation vibration Hamiltonian may in second order remove the degeneracy of levels associated with the quantum number l of internal angular momentum, arising from a doubly degenerate perpendicular mode of oscillation ("l-type doubling"). Measurements have recently been made on certain energy levels of CO_2,[1] where anharmonic resonance interaction and l-type doubling manifest themselves simultaneously. We refer to the bands measured by Goldberg, *et al.*[2] arising from the transition from a $(0\ 1_1\ 0)$ ground level to the upper triad

$$\begin{Bmatrix} 0 & 5_1 & 1 \\ 1 & 3_1 & 1 \\ 2 & 1_1 & 1 \end{Bmatrix}.$$

The observed band centers were successfully calculated by Goldberg, *et al.*[2] from formulas derived by Adel and Dennison,[3] neglecting rotational motion, l-type doubling, etc. The experiments further indicated that here as in earlier examples[4–6] the l-type doubling can be written in the form:

$$\Delta\nu=qJ(J+1). \tag{1}$$

Values for the l-type doubling constants q of the ground level and two upper levels (transitions to the third one have not been observed) were obtained from an analysis of the observed bands.

In the present paper we shall give a theoretical computation of the constants q. To accomplish this for the triad under consideration, it becomes necessary to consider the perturbations related to both anharmonic resonance interaction and l-type doubling simultaneously. Since each component of the triad is a double level, this involves solving a sixth-order secular determinant. From the nature of this determinant, it is not at all self-evident that a formula of the type (1) will hold at all and it appears at first sight that $\Delta\nu$ might be a much more complicated function of the rotational quantum number J. A close inspection of the magnitude of the quantities involved, however, reveals that one is justified in carrying out an approximate solution, to which the validity of Eq. (1) is inherent. In fact our analysis will show that this equation will be valid to all practical purposes, hence confirming the experimental results referred to above. A numerical calculation of the l-type doubling constants q will be presented. Taking into account the approximate character of the entire theoretical approach and allowing for probable errors in the experimental values, the agreement appears satisfactory.

II. THE SECULAR EQUATION

The diagonal elements in the secular determinant can be written in the form (neglect centrifugal stretching):

$$W_{v_1v_2v_3}=T_{v_1v_2v_3}+[J(J+1)-l_2^2]B_{v_1v_2v_3}, \tag{2}$$

where the total energy of vibration, $T_{v_1v_2v_3}$, is given by

$$T_{v_1v_2v_3}=\sum_{i=1}^{3}\omega_i\left(V_i+\frac{d_i}{2}\right)$$

$$+\sum_{i=1}^{3}\sum_{k\leqslant i}X_{ik}\left(V_i+\frac{d_i}{2}\right)\left(V_k+\frac{d_k}{2}\right)+X_{l_2l_2}\cdot l_2^2. \tag{3}$$

* Presented at the Symposium on Molecular Structure and Spectroscopy at the Ohio State University, June, 1951.
[1] Throughout this paper we are exclusively dealing with the isotope $C^{12}O_2^{16}$.
[2] Goldberg, Mohler, McMath, and Pierce, Phys. Rev. **76**, 1848 (1949).
[3] See D. M. Dennison, Revs. Modern Phys. **12**, 175 (1940).
[4] G. Herzberg, Revs. Modern Phys. **14**, 219 (1942).
[5] H. H. Nielsen and W. H. Shaffer, J. Chem. Phys. **11**, 140 (1943).
[6] H. H. Nielsen, Phys. Rev. **77**, 130 (1950).

Since we are dealing exclusively with the triad

$$\begin{Bmatrix} 0 & 5_{\pm} & 1 \\ 1 & 3_{\pm 1} & 1 \\ 2 & 1_{\pm 1} & 1 \end{Bmatrix},$$

we can label its levels uniquely by means of the parameter V_2. Hence we shall write W_5 for $W_{0\ 5_{\pm 1}\ 1}$, T_3 for $T_{1\ 3_{\pm 1}\ 1}$, B_1 for $B_{2\ 1_{\pm 1}\ 1}$, etc. Moreover, since only with V_2 can we associate an internal angular momentum, we shall simply write l instead of l_2. After the hamiltonian has undergone the usual contact transformation, it contributes the following off-diagonal matrix elements, which are not zero.

(a) Resonance interaction elements:[3,7]

$$(V_1, V_2, V_3, l|H'/hc|V_1-1, V_2+2, V_3, l)$$
$$=(V_1-1, V_2+2, V_3, l|H'/hc|V_1, V_2, V_3, l)$$
$$=-(b/2)[(V_2+2)^2-l^2]^{\frac{1}{2}}(V_1/2)^{\frac{1}{2}}, \quad (4)$$

where b is the appropriate anharmonicity constant;

(b) l-type doubling elements:[5,6]

$$(V_1V_2V_3, l|H'/hc|V_1V_2V_3, l\pm 2)$$
$$=(q_0/4)[(V_2+l)(V_2-l+2)]^{\frac{1}{2}}\cdot J(J+1), \quad (5)$$

where

$$q_0=(2B_e^2/\omega_2)[1+4\omega_2^2/(\omega_3^2-\omega_2^2)], \quad (6)$$

the l-type doubling constant for the level $(0\ 1_1\ 0)$. This gives rise to the following secular determinant:

$$\Delta=\begin{vmatrix} T_5+[J(J+1)-1]B_5-W & -b\sqrt{3} & 0 & 0 & 0 & \frac{3}{2}q_0J(J+1) \\ -b\sqrt{3} & T_3+[J(J+1)-1]B_3-W & -b\sqrt{2} & 0 & q_0J(J+1) & 0 \\ 0 & -b\sqrt{2} & T_1+[J(J+1)-1]B_1-W & \frac{1}{2}q_0J(J+1) & 0 & 0 \\ 0 & 0 & \frac{1}{2}q_0J(J+1) & T_1+[J(J+1)-1]B_1-W & -b\sqrt{2} & 0 \\ 0 & q_0J(J+1) & 0 & -b\sqrt{2} & T_3+[J(J+1)-1]B_3-W & -b\sqrt{3} \\ \frac{3}{2}q_0J(J+1) & 0 & 0 & 0 & -b\sqrt{3} & T_5+[J(J+1)-1]B_5-W \end{vmatrix}=0. \quad (7)$$

This determinental equation can be factorized into the following two:

$$\Delta_{\pm}=\begin{vmatrix} T_5+[J(J+1)-1]B_5\pm\frac{3}{2}q_0J(J+1)-W_{\pm} & -b\sqrt{3} & 0 \\ -b\sqrt{3} & T_3+[J(J+1)-1]B_3 \pm q_0J(J+1)-W_{\pm} & -b\sqrt{2} \\ 0 & -b\sqrt{2} & T_1+[J(J+1)-1]B_1\pm\frac{1}{2}q_0J(J+1)-W_{\pm} \end{vmatrix}=0. \quad (8)$$

If the roots of these equations are $W_{\pm}^0$, then we find the l-type doubling as the difference between a W_+^0, and a corresponding W_-^0. It is not at all obvious from the form of the determinant (8) that this difference will have the form embodied in Eq. (1), i.e., be equal to a constant (independent of J) times $J(J+1)$.

III. SOLUTION BY MEANS OF A SERIES EXPANSION

We make the following assumptions (for a justification, see Sec. V):

(a) $B_1\simeq B_3\simeq B_5\simeq B$,

(b) q_0 is so small that terms in q_0^2 and q_0^3 may be neglected. For brevity we set

$$W_j=T_j+[J(J+1)-1]B, \quad (9)$$

where j takes the values 1, 3, and 5. We then obtain on expansion of the determinants (8):

$$W_{\pm}^3-W_{\pm}^2(W_1+W_3+W_5)$$
$$+W_{\pm}(W_1W_3+W_1W_5+W_3W_5-5b^2)$$
$$+3b^2W_1+2b^2W_5-W_1W_3W_5$$
$$\mp(q_0/2)J(J+1)[6W_{\pm}^2-W_{\pm}(5W_1+4W_3+3W_5)$$
$$+3W_1W_3+2W_1W_5+W_3W_5-9b^2]=0. \quad (10)$$

If there were no l-type doubling, the two equations (1) would reduce to only one equation for W:

$$f(W)=W^3-W^2(W_1+W_3+W_5)$$
$$+W(W_1W_3+W_1W_5+W_3W_5-5b^2)$$
$$+3b^2W_1+2b^2W_5-W_1W_3W_5=0, \quad (11)$$

the solution of which we shall call W^0. Equation (11) originates from the secular determinant:

$$\Delta_0=\begin{vmatrix} W_5-W & -b\sqrt{3} & 0 \\ -b\sqrt{3} & W_3-W & -b\sqrt{2} \\ 0 & -b\sqrt{2} & W_1-W \end{vmatrix}=0, \quad (12)$$

which enables us to calculate the resonance interactions, neglecting l-type doubling. For the particular case

[7] H. H. Nielsen, Phys. Rev. **68**, 181 (1945).

$J=0$ ($l=0$) Eq. (12) reduces to the one solved by Goldberg, *et al.*[2] (see the previous introduction). Now call

$$g(W)=6W^2-W(5W_1+4W_3+3W_5)+3W_1W_3+2W_1W_5+W_3W_5-9b^2. \quad (13)$$

We then can write the Eq. (10) in the form:

$$z_\pm(W_\pm)=f(W_\pm)\mp(q_0/2)J(J+1)g(W_\pm)=0. \quad (14)$$

Since q_0 is very small, we may expect the solutions of these two equations, $W_+{}^0$ and $W_-{}^0$ to differ very little from the corresponding solutions W^0. We can, therefore, expand $z_\pm(W_\pm{}^0)$ in a Taylor series with respect to W^0, neglecting terms in $(W_\pm{}^0-W^0)$ and q_0 of powers higher than one. This yields the following solution of Eq. (14) and hence of the Eq. (10):

$$W_\pm{}^0-W^0=\pm(q_0/2)\frac{g(W^0)}{(df(W)/dW)_{W=W^0}}J(J+1). \quad (15)$$

Remembering that the l-type doubling $\Delta\nu$ is given by $W_+{}^0-W_-{}^0$, we obtain from (1), (15), (13) and (11):

$$q=q_0\frac{[6(W^0)^2-W^0(5W_1+4W_3+3W_5)+3W_1W_3+2W_1W_5+W_3W_5-9b^2]}{[3(W^0)^2-2W^0(W_1+W_3+W_5)+W_1W_3+W_1W_5+W_3W_5-5b^2]}. \quad (16)$$

In the following way we can easily see why the q's thus computed are independent of the magnitude of J. First consider $f(W)$ as originating from the determinant (12). If we change J, then, according to (9), W_1, W_3, and W_5 all change by the same amount $\delta(J)$. This merely implies a change of origin and hence the new W^0's are obtained from the old ones simply by adding this amount $\delta(J)$. Moreover, since this change in J has merely shifted $f(W)$ with respect to the origin, the values of $[df(W)/dW]_{W=W^0}$, as occurring in the denominator of (15), are completely unchanged.

Finally by substituting in Eq. (13) $[W^0+\delta(J)]$ for W and $[W_1+\delta(J)]$ for W_1, etc., we readily obtain that $g[W^0+\delta(J)]=g(W^0)$. Hence also the numerator of (15) is unchanged, and we may finally conclude that the q's as given by Eq. (16) are indeed constants, independent of the magnitude of J. The validity of the assumptions which led to this equation will be discussed in Sec. V.

IV. NUMERICAL CALCULATIONS

The total vibrational energies T are obtained from Eq. (3) with the aid of the following constants:[3]

$\omega_1=1351.2$	$X_{11}=-0.3$	$X_{12}=5.7$
$\omega_2=672.2$	$X_{22}=-1.3$	$X_{13}=-21.9$
$\omega_3=2396.4$	$X_{33}=-12.5$	$X_{23}=-11.0$
	$l^2=1$	
$b^2=5081$	$X_{ll}=1.7$	

We get:

$$T_1=8196.9\ \text{cm}^{-1}$$
$$T_3=8181.2\ \text{cm}^{-1}$$
$$T_5=8131.8\ \text{cm}^{-1}.$$

We shall solve Eqs. (11) and (16) numerically for the case $J=1$. We take:[2,3]

$$B=B_e=0.39,$$

and obtain from Eq. (9):

$$W_1=8197.3\ \text{cm}^{-1}$$
$$W_3=8181.6\ \text{cm}^{-1}$$
$$W_5=8132.2\ \text{cm}^{-1}$$

Now by (11):

$$f(W)=W^3-24{,}511W^2+200{,}238{,}115.26W-545{,}194{,}907{,}903.4=0.$$

The solutions are found to be:

$$W^0=8332.53\ \text{cm}^{-1},$$
$$8171.97\ \text{cm}^{-1},$$
$$8006.60\ \text{cm}^{-1}.$$

Finally, by Eqs. (6) and (16):

$$q=0.00061\frac{[6(W^0)^2-98{,}109.5W^0+401{,}013{,}933.68]}{[3(W^0)^2-49{,}022.2W^0+200{,}238{,}115.26]}, \quad (17)$$

which yields: For

$$W^0=8332.53:\ q=11.6\times10^{-4}$$
$$=8171.97:\ =10.9\times10^{-4}$$
$$=8006.60:\ =14.1\times10^{-4}.$$

An alternative way of arriving at these same results will be discussed in an appendix to this paper.

V. DISCUSSION

Before comparing the results just obtained with the corresponding observed values, we shall discuss the approximations inherent to our method of calculation. With $J=1$ and $q_0=6.1\times10^{-4}$, Eq. (14) takes the form:

$$z_\pm(W_\pm)=f(W_\pm)\mp0.00061g(W_\pm).$$

It is clear that the constant multiplying $g(W_\pm)$ is so small, that the solution (11)–(16) can be expected to be a very good approximation. It can easily be seen that the result of obtaining q-values independent of the magnitude of J is not a consequence of replacing the solution (10) by the solution (11)–(16), but a consequence of the fact that we have chosen

$$B_1=B_3=B_5=B,$$

and of the fact that q_0 is as small as it is, i.e., of the order B^2/ω. To see this, we refer back to the determinantal Eq. (8). If we change from $J=1$ to $J=10$, the

change in $[J(J+1)-1]B$ will be 42.12. Since this amount will be added to all T's, it simply changes the roots of $\Delta_\pm$ by this amount. The *difference* between $\frac{3}{2}q_0J(J+1)$ and $\frac{1}{2}q_0J(J+1)$ changes by an amount 0.066 when J takes the values $J=1$ and $J=10$, respectively. This is certainly negligible compared to the figure 42.12 given above. Under these conditions, if a change in J is made, the roots of $\Delta_\pm$ may be expected to change by amounts proportional to $J(J+1)$.

Accurate values of B_1, B_3, and B_5 are not known yet, but it seems probable that these constants will not differ more than about 0.002. These differences will only become important at very high J values. It is clear that for large values of J a change in J will not in general make the roots of Eq. (8) change by an amount proportional to $J(J+1)$. Also for high J values the approximation (11)–(16) breaks down on account of the fact that $(q_0/2)J(J+1)$ is no longer small. Finally, if J takes on such high values, we may expect many more complications; e.g., centrifugal stretching may no longer be neglected.

Thus we may conclude that, *in accordance with the experimental observations*, Eq. (1) holds in good approximation for J values of, let us say, 1 to 10. On the other hand, our analysis shows that, contrary to current beliefs on account of qualitative considerations,[4] the validity of Eq. (1) is by no means universal and has to be tested in each particular case. In fact, if J were large enough and B_1, B_3, and B_5 sufficiently different, q would become a function of J.

TABLE I. l-type doubling constants
(q_0 calculated: 6.1×10^{-4}; average q_0 observed[2]: 5.05×10^{-4}).

q calculated		q observed[2,8]
With $q_0=6.1\times10^{-4}$	With $q_0=5.05\times10^{-4}$	$\left(q_0=\begin{matrix}4.9\\5.1\end{matrix}\right)\times10^{-4}$
11.6×10^{-4}	9.6×10^{-4}	
10.9×10^{-4}	9.0×10^{-4}	8×10^{-4}
14.1×10^{-4}	11.6×10^{-4}	13×10^{-4}

In Table I we have collected our results together with the values observed by Goldberg, *et al.*[2] For the "ground level" (0 1_1 0) q_0 as calculated is somewhat too high, although the agreement with Goldberg's value is much better than that with one of the values (3.4×10^{-4}) as suggested by Herzberg.[4] In the first column of Table I we have listed the q values as computed in Section IV of this paper. They agree with the observed values in their sequence and in predicting a doubling appreciably higher than in the "ground level." In the second column we have listed the q values obtained by using the average observed value for q_0 instead of the calculated one (replace 0.00061 by 0.000505 in Eq. (17)). Now the agreement with the observed values for the upper states is still better.

We conclude that, taking into account the approximate character of the theory and the accuracy of the experimental determinations[8] the agreement is quite gratifying. On account of the figures given in Table I we would predict the l-type doubling constant, which has not been observed hitherto to be $(9.5\pm1)\times10^{-4}$.

ACKNOWLEDGMENT

One of us (J. de Heer) wishes to acknowledge the award of a postdoctoral scholarship of the Graduate School of the Ohio State University, which has enabled him to cooperate in carrying out the investigation reported in this paper.

APPENDIX. AN ALTERNATIVE METHOD FOR CALCULATING THE q-CONSTANTS

We have shown that for values of J which are not too large, it is legitimate to replace Eqs. (8) or (10) by the approximate solution (11)–(16). Thus, in Eq. (11), we first considered the twofold degenerate resonance interaction levels as if l-type doubling did not occur. Subsequently, the energy levels associated with $+l$ and $-l$ were found as a result of small perturbations of the degenerate levels. This procedure suggests that there must be an alternative method, which ultimately yields the same numerical results.

With each of the solutions W^0 of Eq. (11) we can associate two degenerate wave functions:

$$\Phi_\pm=[c_1\Phi_1+c_3\Phi_3+c_5\Phi_5]e^{\pm i\varphi}$$

where Φ_1, Φ_3, and Φ_5 refer to the component states (2 1_1 1), (1 3_1 1), and (0 5_1 1). Subsequently the matrix elements which cause the l-type doubling are:

$$((c_1\Phi_1+c_3\Phi_3+c_5\Phi_5)e^{i\varphi}|H'/hc|(c_1\Phi_1+c_3\Phi_3+c_5\Phi_5)e^{-i\varphi}). \quad (17)$$

Since the portion of H' we are interested in connects only states which differ in the sign of the quantum number l only, we obtain from (17):

$$c_1^2(\Phi_1e^{i\varphi}|H'/hc|\Phi_1e^{-i\varphi})+c_3^2(\Phi_3e^{i\varphi}|H'/hc|\Phi_3e^{-i\varphi}) +c_5^2(\Phi_5e^{i\varphi}|H'/hc|\Phi_5e^{-i\varphi}). \quad (18)$$

Each of the three terms in the expression (18) is the product of the weight factor of the wave function of one of the component levels in the Φ function under consideration times the matrix element for the l-type doubling in that component level. In other words, remembering the validity of Eq. (1) for the component levels, we find for the l-type doubling constant q associated with the Fermi resonance level Φ:

$$q=c_1^2q_1+c_3^2q_3+c_5^2q_5.$$

Using Eq. (5) to express q_1, q_3, and q_5 in terms of q_0, we derive:

$$q=q_0(c_1^2+2c_3^2+3c_5^2). \quad (19)$$

The constants c_1, c_3, and c_5 are readily obtained from the minors of the determinant (12) in which W has been replaced by W^0. Finally, numerical calculations show that Eq. (19) does indeed lead to the results reported in Table I.

The procedure outlined in this appendix seems an "obvious" one and perhaps appeals more than the equivalent solution by means of Eq. (16). The value of the complete analysis is, however, that it shows that under certain conditions, either approximation breaks down. In such cases one must proceed by solving the Eqs. (8) for W_+ and W_- exactly.

[8] According to Goldberg (private communication) the observed q values[2] are not more accurate than to about 10 percent.

THE JOURNAL OF CHEMICAL PHYSICS VOLUME 20, NUMBER 1 JANUARY, 1952

The Kinetics of Coordinate Bond Formation

DAVID GARVIN* AND G. B. KISTIAKOWSKY
Gibbs Chemical Laboratory, Harvard University, Cambridge, Massachusetts
(Received August 2, 1951)

A novel method has been developed for determining the rates of very fast gas-phase bimolecular reactions, which is based on interpretation of the temperature gradients in a flow system similar to that used for the study of the reactions of sodium vapor and alkyl halides. The kinetics of the reactions between boron trifluoride and tri-, di-, and monomethylamine to form the corresponding coordinately bonded compounds have been studied. These reactions appear to have negligibly small activation energies, and their rates show a pressure dependence consistent with a mechanism:

$$y+z \rightleftharpoons yz^*$$
$$yz^*+m \rightarrow yz+m^*$$

in which the long-lived intermediate yz^* must be stabilized by loss of energy in a collision. The random scatter of individual rate constants is about 20 percent.

INTRODUCTION

COORDINATELY bonded compounds of such type as results from the reaction,

$$BX_3+NR_3 \rightarrow X_3B:NR_3,$$

where X may be H, alkyl or halogen, and R be H or alkyl, have been studied rather extensively, the emphasis being on physical properties of the adducts and the thermodynamics of these processes.[1–4] The factors controlling the stability of the coordinate compounds have been interpreted in terms of the generalized acid-base theory and steric interactions in the reactant and product molecules.[5–7]

From the point of view of kinetics as well, these reactions are of considerable interest. They are intermediate to radical recombinations and to association reactions in which existing bonds must be broken.[8] Here, as in the former, no bonds need be broken, nor are any rearrangements other than bending and stretching of bonds necessary. As in the latter, the reactants are in general relatively unreactive molecules in singlet electronic states. The only kinetic evidence available on these reactions is that of Lewis and Seaborg, who found that the activation energy must be slight.[9]

The simplicity of these reactions and the likelihood that their kinetics could be treated in an unambiguous manner invited quantitative study, the results of which on boron trifluoride and the three methylamines are reported below. A qualitative study of the boron trifluoride-ammonia reaction has also been made.

A technique suitable for measurement of rates of the magnitude expected here, the "diffusion flame," was developed by Polanyi[10–11] for the study of the reactions of sodium vapor. This is a flow method in which a stream of one reagent diluted with an inert "carrier" gas is fed through a nozzle into a low pressure, slowly moving, atmosphere (0.1- to 10-mm Hg) containing an excess of the other reagent, also diluted with carrier gas. With proper choice of experimental conditions, the nozzle reagent penetrates the atmosphere mainly by diffusion, reacting with the atmospheric reagent at a rate determined by their local concentrations. A steady state reaction pattern, substantially spherically symmetrical, is established, and some characteristic property of the steady state is then measured.

As used previously, this method has been limited chiefly to the reactions of alkali metals, since the method of measurement relied upon strong light absorption or emission by one reactant. This limitation has been removed here by determining the steady state temperature pattern set up by the balance of heat production due to reaction and heat conduction. For this purpose a fine wire thermocouple probe has been introduced into the system and used to search the reaction region to determine local temperatures. This method was explored in this laboratory two years ago by Dr. V. P. Guinn, and was shown by him to be applicable to these reactions.[12] As developed to date, the method is suitable for the study of any very fast, exothermic, gaseous bimolecular reaction.

---

* Standard Brands Predoctoral Fellow 1949–1950, Monsanto Predoctoral Fellow 1950–1951. Present address: Department of Chemistry, Princeton University, Princeton, New Jersey.

[1] Bauer, Finlay, and Laubengayer, J. Am. Chem. Soc. **65**, 889 (1943).

[2] A. W. Laubengayer and G. R. Finlay, J. Am. Chem. Soc. **65**, 884 (1943).

[3] A. W. Laubengayer and G. F. Condike, J. Am. Chem. Soc. **70**, 2274 (1948).

[4] A. B. Burg and A. A. Green, J. Am. Chem. Soc. **65**, 1838 (1943).

[5] Brown, Schlessinger, and Cardon, J. Am. Chem. Soc. **64**, 325 (1942).

[6] Brown, Bartholomay, Jr., and Taylor, J. Am. Chem. Soc. **66**, 435 (1944).

[7] H. C. Brown, J. Am. Chem. Soc. **67**, 378, 1452 (1945).

[8] A. Wassermann, Trans. Faraday Soc. **34**, 128 (1938).

[9] G. N. Lewis and G. T. Seaborg, J. Am. Chem. Soc. **61**, 1886, 1894 (1939).

[10] M. Polanyi, *Atomic Reactions* (Williams and Norgate, London, 1932).

[11] L. Frommer and M. Polanyi, Trans. Faraday Soc. **30**, 519 (1934).

[12] V. P. Guinn, "A new method for the measurement of the rates of fast gas reactions" (Doctoral dissertation, Harvard University, Cambridge, 1949).

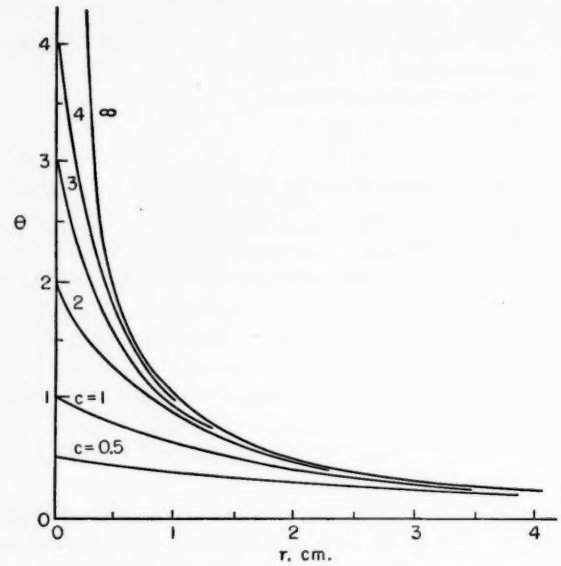

FIG. 1. Theoretical temperature profiles in a stationary spherically symmetric diffusion of one reaction partner of a bimolecular reaction into another. c is a rate parameter in cm, θ is temperature rise on a relative scale.

THEORY

Following the treatment used by Polanyi, the system has been considered as a strictly diffusional problem, ignoring the mass flow of gases. An expression relating the temperature pattern to the rate constant and diffusion coefficient is derived below by first obtaining a formula expressing the steady state concentration of the nozzle reagent, and then using this to solve the temperature problem.

A convenient mathematical model is an infinitely large sphere with a point source of one reagent (nozzle) located at the origin, from which the reagent diffuses outward symmetrically into the atmosphere of the other reagent, (assumed to be at the same concentration everywhere) reacting with it at a rate determined by the local reagent concentrations, i.e., $dy/dt=-kyz$. Mathematically, the steady state condition is defined by Poisson's equation, which in this case becomes

$$\frac{d^2y}{dr^2}+\frac{2}{r}\frac{dy}{dr}-\left(\frac{k}{D}z\right)y=0\begin{cases}y(r\to\infty)\to 0\\ b=\int_0^\infty 4\pi kyzr^2dr.\end{cases} \tag{1}$$

The symbols used previously and later in this section have the meanings y=concentration of nozzle reagent, moles/cm³, z=concentration of atmosphere reagent, moles/cm³, r=distance from origin, cm, k=rate constant, cm³/mole sec, D=diffusion coefficient, cm²/sec, b=nozzle flow rate, moles of y/sec, T=temperature, °K, Q'=heat of reaction $(-\Delta H)$, cal/mole, and κ=coefficient of thermal conductivity, cal/cm deg sec. The general integral of Eq. (1) is

$$y(r)=A_1\frac{e^{cr}}{r}+A_2\frac{e^{-cr}}{r},\quad c^2\equiv\frac{kz}{D}, \tag{2}$$

where A_1 and A_2 are constants of integration. The boundary conditions for (1) require that all y be consumed within the system, and that the rate of consumption per unit time be equal to the source strength. Applying them to (2), the expression for the concentration of the nozzle reagent is

$$y=\frac{b}{4\pi D}\frac{e^{-cr}}{r}. \tag{3}$$

The thermal steady state is defined by an equation similar to (1). Using the expression for y given by (3) in the heat production term, this equation is

$$\frac{d^2T}{dr^2}+\frac{2}{r}\frac{dT}{dr}+\frac{Q'kzb}{4\pi\kappa D}\cdot\frac{e^{-cr}}{r}=0,\quad \lim_{r\to\infty}(-r^2\nabla T)=\frac{Q'b}{4\pi\kappa}. \tag{4}$$

For small temperature rises, such that Q', k, and D are constant, Eq. (4) may be integrated directly to yield

$$T(r)=\frac{A_3}{r}-\frac{Q'b}{4\pi\kappa}\cdot\frac{e^{-cr}}{r}+A_4. \tag{5}$$

The boundary condition requires that, at great distances, reaction be unimportant, and there (4) reduces to Laplace's equation for heat conduction. Applying this condition to evaluate A_3, and then taking the difference in temperature between that at r and a fixed point r_2, (5) becomes

$$\Delta T=T(r)-T(r_2)=\frac{Q'b}{4\pi\kappa}\left[\frac{1}{r}(1-e^{-cr})-\frac{1}{r_2}(1-e^{-cr_2})\right]. \tag{6}$$

Equation (6) is the basis upon which the rate determinations were made. Experimental temperature profiles were fitted to this equation to determine the appropriate value of c, which according to Eq. (2), is a ratio involving the rate and diffusion constants. It may be noted that Eq. (6), for a given r_2, is determined by two parameters, a scale factor, $Q'b/4\pi\kappa$, and a shape factor, c. It is the latter with which we are primarily concerned. Figure 1 shows a family of theoretical temperature profiles derived from (6) for the case that r_2 is infinite.

EXPERIMENTAL

The practical analog of the model treated in the preceding section is a flow system in which the linear rate of gas flow is negligible compared to the diffusion flow rate of the nozzle reagent. With the exception of the temperature measuring device, the equipment was modeled on that used for sodium diffusion flames.

The reactor, shown schematically in Fig. 2, was a Pyrex cylinder 40 cm long and 10 cm in diameter, one

end of which was drawn down to take a coaxially mounted nozzle and the inlet tubes for the atmospheric gas and a McLeod gage. The other end was ground flat and closed by a $\frac{1}{8}$-in. brass plate, sealed to the glass with Apiezon Q putty. This plate served as the main support for the thermocouple assembly and contained the exit tube for the spent gases. Premixed reagents flowed into the reactor through capillaries from high pressure reservoirs of sufficient size to assure a nearly constant rate of flow. The flow rates were determined from the pressure changes in these reservoirs during an experiment. The pressure in the reactor was controlled by a one-inch gate valve in the exit line. This line terminated in a Kinney CVD 556 mechanical vacuum pump.

Two nozzles were used in the experiments, both much smaller than those used for sodium diffusion flames. They were mounted in the reactor through a standard-taper ground glass joint to facilitate adjustment and removal. The nozzles extended 11 cm above the bottom of the reactor and were drawn down from 6 mm o.d. Pyrex tubing to form a 4–5-cm length of narrow thin-walled capillary ending in the orifice. One nozzle was 0.093 cm i.d., the other 0.0566 cm i.d., providing a variation in mass flow by a factor of 2.7 at the same linear gas velocity.

The thermocouple probe was affixed to the bottom of a long thin-walled metal tube, which passed through the brass plate closing the top of the reactor. The tube contained the lead-in wires for the couple, and had affixed to its upper end the necessary positioning equipment. Several couples were used in these experiments. They differed principally in the length of the wires and their geometry relative to the reaction zone. They consisted of two-mil diameter iron and constantan wires, 4.5 to 5 cm long, soldered to a silver foil heat collector ($0.01\times0.05\times0.05$ cm). The wires were soldered to the lead-ins at the surface of a hard rubber cap covering the bottom of the support tube. These connections formed the cold junction, which was, therefore, at the temperature of the metal of the tube. So that heat conduction along this metal tube would not influence the cold junction temperature, the support tube passed through a bearing fastened to the wall of the reactor a few centimeters above the height of the orifice. The couple wires were held in a position roughly perpendicular to the nozzle axis by means of a Pyrex fiber glued to the tube and the wires. A Leeds and Northrup Low Range Wenner Potentiometer was used to determine the thermal emf's. Readings were made directly to 0.1 microvolt.

The thermocouple probe could be moved in a plane perpendicular to the nozzle axis by rotating the support tube. This motion was made and measured by a dial, which was fastened rigidly to the support tube. Vertical motion was achieved by means of a knurled knob through which passed a threaded portion of the support tube. A steel scale served both for measuring vertical displacement and as an index for the angular dial. This arrangement permitted the couple to be swept through an arc, usually including the nozzle axis, from wall to wall, and to be moved vertically a distance of 95 mm, its position being known to better than ±0.5 mm.

In practice, a search of the reaction zone was made to locate that plane perpendicular to the nozzle axis which passed through the origin of the pattern; then the temperature profile of this plane was taken and was used in the rate determinations. Individual temperatures in any run could be reproduced to about 0.1 microvolt, being subject only to long term drifts in flow rates and reactor pressures. These were slight and were averaged out in drawing the profile through the individual points. Such a profile, with both experimental points and the theoretical curve, is shown in Fig. 3. Tests made with gas flow through the nozzle alone showed a slight (about 2 microvolt) lowering of temperature near the nozzle, probably because of expansion of the gas. This zero point correction profile was added to the experimental pattern for all runs with methylamine and dimethylamine prior to making the rate calculations. Its effect was slight in most cases. All experiments, except one, were made at room temperature. For temperature control, the reactor was immersed in a large Dewar flask filled with water.

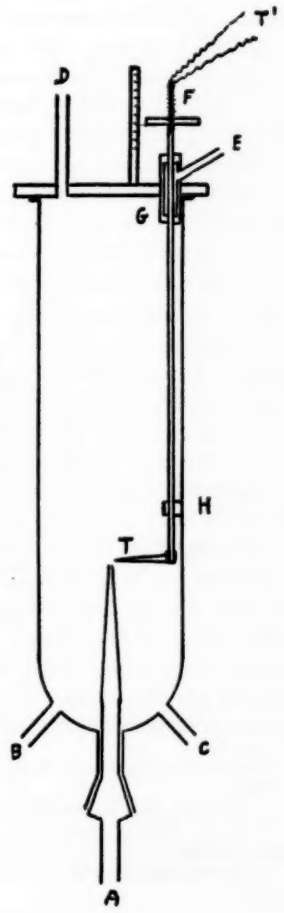

FIG. 2. A schematic diagram of the reactor. A—inlet of the nozzle reagent. B—inlet of the atmospheric reagent. C—connection to a McLeod gage. D—outlet to the main pump. E—outlet to an auxiliary pump. F—positioning device for the thermocouple. G—main bearings of the thermocouple lead-in tubing. H—auxiliary bearing of the thermocouple tubing. T—thermocouple. T'—thermocouple lead-in wires.

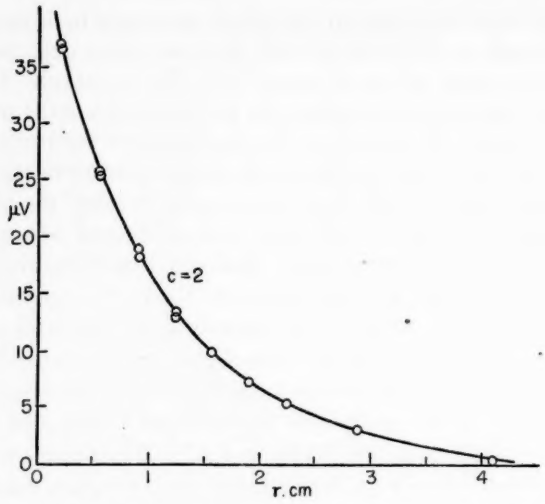

FIG. 3. The fit of experimental temperature measurements to a theoretical curve.

REAGENTS

Nitrogen: Air Reduction Company "Prepurified" (dry) Nitrogen, supplied in a cylinder was used without purification except to pass it through a column of "Anhydrone" during admission to the system.

Helium, boron trifluoride, and *ammonia* (anhydrous): These gases were supplied by the Matheson Company in cylinders and were used without purification.

Trimethylamine: All amines were purified using methods based upon procedures described by Swift[13,14] and Felsing.[15,16] Eastman Kodak Company "White Label" anhydrous trimethylamine was distilled under vacuum from an equal volume of acetic anhydride through a one-meter column packed with glass helicies using a reflux rate which kept the entire column wet and collected in an ampule cooled in liquid nitrogen. The ampule was sealed onto the reactor system, and was stored in dry ice-acetone.

Dimethylamine:[13] Eastman Kodak Company "White Label" dimethylamine hydrochloride was converted to the *N*-dimethyl *p*-toluene sulfonamide by treatment with an alkaline solution of technical *p*-toluene sulfonylchloride. The sulfonamide was filtered hot and recrystalized twice from a 70 percent ethanol-water mixture, Mp. 82–84°C. The crystals were refluxed with an excess of HCl in a minimum amount of water until the solution was homogeneous, reforming the amine hydrochloride. This mixture was treated with a two-fold excess of 50 percent KOH solution to release the amine which was then dried by passing over KOH pellets and by contact with sodium wire before distillation under vacuum into a storage ampule. The apparatus for liberating the amine was modeled on that used by Felsing.[12]

Methylamine:[13] Eastman Kodak Company "White Label" methylamine hydrochloride was refluxed with chloroform for 30 hours to extract higher amine hydrochlorides, then recrystalized from absolute ethanol. The hydrochloride was split in the same manner as was the dimethylamine salt, a drying tube containing yellow mercuric oxide being added to the gas train in order to remove ammonia.

RESULTS

The quantities needed for determination of a rate constant are the temperature profile, the total reactor pressure and the composition and flow rates of gas mixtures into the reactor. In addition the diffusion coefficient of the nozzle reagent into the atmospheric gas mixture must be known.

The last was calculated from the kinetic theory formula:[17]

$$D_{1,2}=\frac{3}{4}\left(\frac{2}{\pi}\right)^{\frac{1}{2}}\frac{(RT)^{\frac{1}{2}}}{N_A P(\sigma_1+\sigma_2)^2}\left[\frac{M_1+M_2}{M_1M_2}\right]^{\frac{1}{2}}, \qquad (7)$$

where M=molecular weight, g/mole, σ=molecular cross section, cm$\times 10^{-8}$, P=pressure, dynes/cm^2, and N_A=Avogadro's number. For this purpose, the atmospheric gas was assumed to be a single species whose molecular weight and molecular diameter were the mole fraction average of those of the atmospheric reagent and the carrier gas. Some uncertainty in the absolute value of the rate constant is introduced by the use of this approximation for a complex gas mixture, but is felt to be a minor factor. The molecular diameters used in calculating diffusion coefficients were as follows:

N_2:3.1A;[18] He:2.0;[18] BF_3:4.2;[19] NH_3:3.6;[18]

$MeNH_2$:4.4; Me_2NH:5.0 and Me_3N:5.3.[19]

The values for methylamine and dimethylamine were calculated from viscosities which were interpolated in the amine series by comparison to the hydrocarbon series: methane, ethane, propane, isobutane, whose viscosities were obtained from standard references.[20]

The concentration of the atmospheric reagent in the reactor was calculated from its mole fraction in its reservoir and the flow rates of the mixtures into the reactor. The mole fraction of atmospheric reagent, on this basis, is

$$X_z=\frac{\text{reservoir } X_z\times\text{flow from } z \text{ reservoir}}{\text{total gas flow into reactor}}.$$

[13] E. Swift, Jr., and C. R. Calkins, J. Am. Chem. Soc. **65**, 2415 (1943).
[14] E. Swift, Jr., J. Am. Chem. Soc. **64**, 115 (1942).
[15] W. A. Felsing and P. H. Wohlford, J. Am. Chem. Soc. **54**, 1442 (1932).
[16] E. A. Kelso and W. A. Felsing, J. Am. Chem. Soc. **60**, 1949 (1938).
[17] E. H. Kennard, *Kinetic Theory of Gases* (McGraw Hill, Book Company, Inc., New York, 1938), p. 194.
[18] E. H. Kennard, reference 17, p. 149.
[19] V. P. Guinn, reference 12, p. 51.
[20] *International Critical Tables* (McGraw-Hill Book Company, Inc., New York, 1929), V, 1 ff.; *Landolt Bornstein Tables* (Julius Springer, Berlin, 1923), Hw I, 172, Eg 11a 137, 140.

The reactor pressure was measured directly on a McLeod gage connected to the former near the gas inlets.

The temperature profiles were interpreted in terms of Eq. (6) which may, for this purpose, be written in the form,

$$\Delta_{\mu V}=A_5\left[\frac{1}{r}(1-e^{-cr})-\frac{1}{r_2}(1-e^{-cr_2})\right]. \tag{8}$$

A value of r_2 was chosen for the profile and the emf values adjusted to this standard. Then, by trial, values of c (determined only to two significant figures) and A_5 were found which reproduced the profile. The rate constant was then determined from the definition of c, which, rewritten in terms of the experimental variables, is

$$k=\left(\frac{c}{p}\right)^2\frac{D'RT}{X_z}, \tag{9}$$

where p=pressure, mm Hg, D'=pressure independent factor of the diffusion coefficient, cm² mm Hg/sec, R=gas constant, mm Hg cm³/mole °K, and X_z=mole fraction of z in atmosphere of reactor.

For this procedure to be applicable to experimental reaction zones, the assumptions that they be spherically symmetrical, the temperature rise be small, diffusion alone control the mixing and the concentration of z be everywhere the same, must be met. Only the establishment of the last two proved to be difficult to assess. The problem is basically to prevent depletion of z because of its inability to diffuse rapidly enough into the reaction zone to counteract consumption by reaction and against the mass flow from the nozzle. The latter problem was studied by Heller in a comprehensive analysis of sodium diffusion flames.[21] He concluded that the assumptions were not seriously violated for flames of 1.5 cm radius or greater when the linear nozzle velocity, v, was within the limits $5\leqslant v/D\leqslant 12$ cm^{-1}. These recommendations have been followed in general, with some runs having a v/D ratio above the upper limit. However, the mass flows in the present experiments were all much below those studied by Heller because smaller nozzles were used. The use of small nozzles is believed to be a very important factor in the design of experiments which approach the conditions assumed in the theory. As will be mentioned later, little dependence of rate upon depletion was found.

The parameter c is also a measure of reciprocal reaction zone size. Only zones having c in the range $1<c<3.5$ cm^{-1} have been used. These limits are equivalent to selecting zones of 90 percent completion of reaction with radii from 3.9 to 1.1 cm ($r_{90\%}=3.9/c$). As may be seen from Fig. 1, values of c above 3.5 define temperature profiles too similar to those for point source heat conduction over most of the range to be useful in the determination of c to 10 percent or better.

[21] W. Heller, Trans. Faraday Soc. **33**, 1566 (1937).

The boron trifluoride-trimethylamine reaction: The data on experiments with this system are collected in Table I. The values center about 3×10^{12} cm³/mole sec, and, as Fig. 4 shows, exhibit considerable random spread. This reaction was studied in some detail to test the feasibility and reliability of the temperature gradient method. Extensive searches of the three dimensional temperature pattern were made in two runs which differed considerably in experimental conditions. In both cases the isotherms were spheres whose centers were 1–3 mm ahead of the orifice, justifying the assumption of spherical symmetry. Equation (6) predicts that the temperature rise will be proportional to the nozzle reagent flow rate, c and r_2 being constant. This was found to be true for the three sets of points examined, c=1.1, 1.5, and 2. No apparent drift with the mass flow-diffusion ratio v/D could be found, nor any appreciable dependence upon the extent of reaction, except possibly where this was above 20 percent consumption of z. In order to test the stoichiometry of the reaction, runs were made with boron trifluoride as well as trimethylamine as the atmospheric reagent. The lack of trends in the rate constant shows the reaction to be first order in each reagent. These runs, as well as the ones with added helium in the gas mixtures also show the expected dependence upon the diffusion coefficient. Although the latter varied from 84 to 118 cm²/sec at one mm Hg, the calculated rate constants all fell within the spread of data for the large series made with trimethylamine as the atmospheric reagent. The runs with added helium also indicate that there is no important lag in thermal equilibration between the product molecules and the atmospheric gas, since they are virtually indistinguishable from runs in nitrogen.

Minor differences between these sets may be attributed to the uncertainty introduced by using approximate diffusion coefficients calculated from Eq. (7). In order to test whether or not a catalytic reaction on

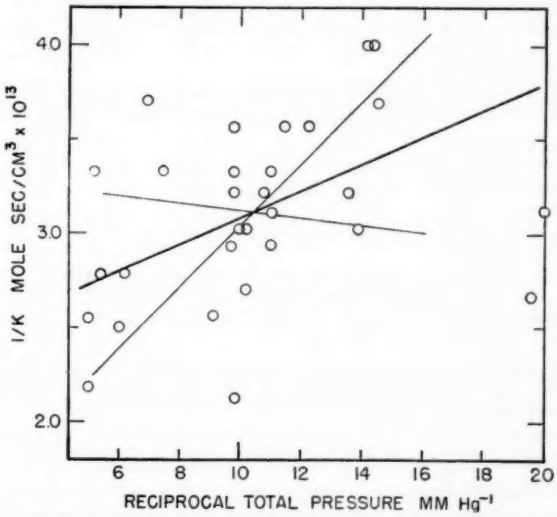

FIG. 4. Reciprocal plot of the rate constants of the boron trifluoride-trimethylamine reaction against inverse total pressure.

TABLE I. Experimental data for the reaction $BF_3+(CH_3)_3N \rightarrow F_3BN(CH_3)_3$ 296.6±1°K.

Total flow moles/sec ×10⁶	Atmospheric reagent (z) Reactor mole fraction ×10²	Fraction consumed ×10²	v/D_y cm⁻¹	Pressure mm Hg ×10	c cm⁻¹	k cm³/mole-sec ×10⁻¹²
A. $(CH_3)_3N=z$, 0.093-cm nozzle, straight uncoated thermocouple, nitrogen carrier gas.						
2.6	16.4	5.2	10.5	1.1	2.0	3.9
2.5	17.4	3.6	8.0	0.91	1.6	3.4
3.25	16.8	3.6	10.2	0.68	1.0	2.5
3.25	16.8	3.6	10.2	0.91	1.5	3.2
3.0	17.8	3.3	9.0	0.91	1.5	3.0
3.0	20.8	3.1	4.7	1.0	1.9	3.3
2.8	18.3	3.2	12.2	0.93	1.6	3.1
3.3	19.5	2.1	10.2	0.98	1.8	3.3
2.7	20.6	1.1	4.5	1.02	1.5	2.8
2.0	19.6	4.8	16.5	0.69	1.15	2.7
1.6	21.4	3.6	16.5	0.71	1.2	2.5
1.4	24.0	2.2	6.6	0.72	1.5	3.3
1.32	23.4	2.4	6.6	1.02	2.0	3.0
1.28	24.1	1.9	6.8	0.74	1.5	3.1
1.28	8.57	8.6	6.4	1.9	2.3	3.6
1.28	8.57	8.6	6.4	1.02	1.15	3.1
2.4	8.5	2.9	6.4	2.0	2.5	3.9
2.6	4.3	10.5	10.0	2.0	1.95	4.6
2.6	4.3	10.5	10.0	4.0	3.0	2.8[a]
1.4	26.7	6.3	8.7	0.50	1.1	3.2
1.4	26.7	6.3	8.7	0.98	2.3	3.7
B. $(CH_3)_3N=z$, 0.093-cm nozzle, straight, fluorocarbon-coated thermocouple, nitrogen carrier gas.						
1.6	14.8	7.6	8.5	1.33	2.0	3.0
1.4	8.34	20.1	10.7	1.0	1.0	2.52[a]
1.4	8.34	20.1	10.7	1.45	1.5	2.7
C. $(CH_3)_3N=z$, 0.093-cm nozzle, fluorocarbon-coated, bent thermocouple, nitrogen carrier gas.						
1.7	9.65	7.8	6.1	1.03	1.3	3.4
1.7	9.65	7.8	6.1	1.63	2.1	3.6
2.16	10.0	5.9	6.1	1.02	1.5	4.7
2.16	10.0	5.9	6.1	1.68	2.3	4.0
D. $(CH_3)_3N=z$, 0.0566-cm nozzle, uncoated straight thermocouple, nitrogen carrier gas.						
1.33	26.5	5.0	9.3	0.51	1.2	3.75
1.7	18.6	11.5	8.7	0.92	2.1	5.4[a]
1.57	14.0	20.4	19.6	0.97	1.3	2.55[a]
2.13	11.4	6.7	9.8	1.92	2.5	3.0
2.13	11.4	6.7	9.8	0.88	1.1	2.8
1.78	17.4	8.2	8.0	0.82	1.3	2.8
E. $BF_3=z$, 0.093-cm nozzle, uncoated straight thermocouple, nitrogen carrier gas.						
2.44	17.4	4.5	12	0.84	2.0	5.1[b]
1.99	16.5	5.8	12	0.85	1.7	3.6
2.48	9.56	7.4	10.5	1.83	3.0	4.6
0.74	17.5	10.4	7.5	0.63	1.3	3.8
3.12	12.9	5.2	11.5	1.40	2.6	4.5
F. $BF_3=Z$, 0.0566-cm nozzle, uncoated, straight thermocouple, nitrogen carrier gas.						
2.06	14.4	16.9	25.6	0.79	1.45	3.7
G. $BF_3=z$, 0.093-cm nozzle, uncoated straight thermocouple, carrier gas mole fractions: nozzle gas: He=0.189, N_2=0.832, atmospheric gas mixture: He=0.164, N_2=0.624.						
1.51	15.8	21.0	7.3	1.52	3.1	4.4
1.69	14.1	7.2	12.8	0.67	1.2	3.8

[a] Omitted from Fig. 4 and the calculation of the pressure dependence of the rate because of high (0.2) fractional consumption of the atmospheric reagent.
[b] Temperature profile of this run shown in Fig. 2.

TABLE II. Experimental data for the reaction $BF_3+(CH_3)_2NH \rightarrow F_3BNH(CH_3)_2$ 298±1°K.

Total flow moles/sec ×10⁶	Atmospheric reagent (z) Reactor mole fraction ×10²	Fraction consumed ×10²	v/D_y cm⁻¹	Pressure mm Hg ×10	c cm⁻¹	k cm³/mole-sec ×10⁻¹²
$(CH_3)_2NH=z$, 0.093-cm nozzle, uncoated straight thermocouple, nitrogen carier gas.						
1.82	12.7	18	16	1.56	2.3	3.6
1.82	12.7	18	16	1.09	1.45	2.9
2.48	7.46	9.9	12	2.15	2.2	3.0
2.48	7.46	9.9	12	1.44	1.3	2.3
1.64	18.1	8.3	15	1.02	1.6	2.8
2.46	11.4	8.7	14	1.55	2.0	3.0
2.36	3.8	15	11	3.36	3.1	5.0
2.36	3.8	15	11	2.22	2.3	6.3
2.36	3.8	15	11	3.2	3.5	7.1
2.60	1.11	26	16	5.7	3.5	7.7[a]
2.60	1.11	26	16	3.55	2.1	7.1[a]
1.21	0.89	51	9.7	4.7	1.7	3.4[a]
1.21	0.90	51	9.7	5.5	2.4	4.8[a]
1.91	16.4	4.8	15	0.92	1.05	1.6
1.91	16.4	4.8	15	1.82	2.6	2.5
2.50	3.8	19	16	3.05	3.4	7.3
2.50	4.0	16	13	1.99	2.1	6.2

[a] Omitted from Fig. 5 and the calculation of the pressure dependence of the rate because of high (0.2) fractional consumption of the atmospheric reagent.

the couple perturbed the homogeneous reaction temperature pattern, the couple was coated with a perfluorinated hydrocarbon (DuPont FCX 409A) for several runs, without noticeable effect. An attempt was made to assess the importance of heat conduction along the couple wires by bending the wires parallel to the nozzle axis about 5 mm from the hot junction. Such an arrangement places this length essentially along an isotherm throughout most of the reaction zone, and should reduce markedly any heat drain from the hot

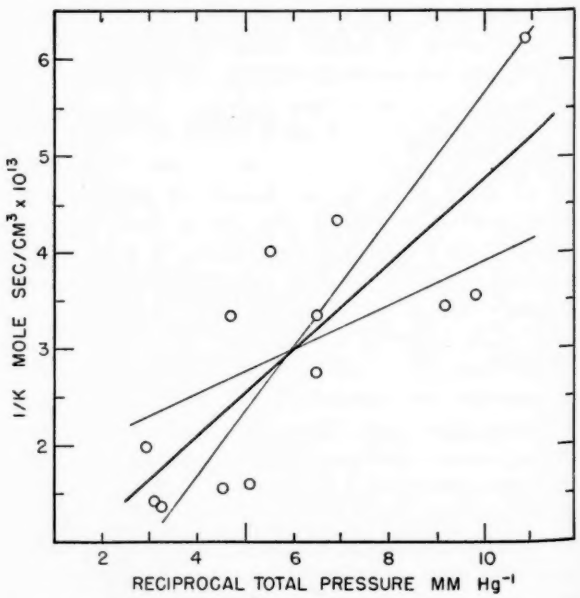

FIG. 5. Reciprocal plot of rate constants of the boron trifluoride dimethylamine reaction against inverse total pressure.

junction. No appreciable change in the pattern was observed. Slight drifts of rate constants with total pressure, but not the partial pressure of the atmospheric reagent and with zone size were observed. We shall return to these in a later section.

The boron trifluoride-dimethylamine reaction: The data for this reaction are collected in Table II. The same general remarks may be made for this reaction as for the reaction with trimethylamine. In this case the drifts with total pressure and with zone size were much more pronounced as shown in Fig. 5. The rate was again of the order of 10^{12} cm³/mole sec.

TABLE III. Experimental data for the reaction $BF_3+CH_3NH_2 \rightarrow F_3BNH_2CH_3$ 298.6±1.5°K.

Total flow moles/sec ×10⁸	Atmospheric reagent (z) Reactor mole fraction ×10²	Fraction consumed ×10²	v/D_y cm⁻¹	Pressure mm Hg ×10	c cm⁻¹	k cm³/mole-sec ×10⁻¹²
A. $CH_3NH_2=z$, 0.093-cm nozzle, uncoated straight thermocouple, nitrogen carrier gas.						
2.27	16.8	7.1	11.3	2.12	1.3	4.9
1.51	6.0	34	13.0	3.25	1.0	3.5[a]
2.23	21.5	3.8	11.7	3.05	2.8	8.2
2.23	21.5	3.8	11.7	2.27	1.9	6.8
2.79	30.2	2.4	13.6	2.46	2.1	5.0
2.79	30.2	2.4	13.6	1.33	1.0	3.9
2.79	30.2	2.4	13.6	2.33	2.3	6.6
2.22	8.4	12.7	14.7	3.75	1.9	6.4
2.22	8.4	12.7	14.7	3.11	1.5	5.8
2.22	8.4	12.7	14.7	5.2	2.7	6.7
2.59	26.3	3.1	14.6	1.77	1.6	6.4
2.59	26.3	3.1	14.6	1.36	1.1	5.1
2.33	26.0	3.3	13.7	1.39	1.1	4.9
2.33	26.0	3.3	13.7	1.73	1.3	4.4
2.51	7.7	13	16.1	1.40	1.6	5.6
1.69	25.3	5.3	14.1	1.68	1.1	3.5
1.69	25.3	5.3	14.1	2.42	2.0	5.6
1.69	25.3	5.3	14.1	1.6	1.3	5.4
2.65	15.5	5.3	14.3	2.69	1.7	5.5
2.65	15.5	5.3	14.3	2.17	1.4	5.7
2.34	3.8	24	13.5	5.2	1.5	5.0[a]
2.34	3.8	24	13.5	4.2	1.15	4.6[a]
2.34	3.8	24	13.5	5.2	1.7	6.4[a]
2.34	3.8	24	13.5	6.1	2.0	6.4[a]
B. $CH_3NH_2=z$, 0.093-cm nozzle, straight uncoated thermocouple, nozzle gas mole fractions: He=0.369, N_2=0.607, atmospheric gas mixture mole fractions: He=0.43, N_2=0.468.						
2.68	7.05	9.9	14.7	3.25	1.2	4.0
2.68	7.05	9.9	14.7	4.3	1.9	5.6
C. $CH_3NH_2=z$, 0.093-cm nozzle, straight uncoated thermocouple, nitrogen carrier gas, temperature 314.5°K.						
2.65	15.5	5.3	13.2	2.98	1.6	4.6
D. $CH_3NH_2=z$, 0.093-cm nozzle, bent thermocouple, nitrogen carrier gas.						
2.08	8.9	5.4	10.9	3.1	2.0	10.4[b]
2.08	8.9	5.4	10.9	4.96	2.6	6.8
2.08	8.9	5.4	10.9	2.75	1.3	5.5
6.68	3.88	3.96	11	3.1	1.1	7.2
5.65	3.83	4.74	11	3.75	1.3	7.0
4.36	3.72	6.36	11	3.9	1.3	6.7
3.32	7.37	0.58	9.5	0.97	1.4	4.9
3.32	7.37	0.58	9.5	2.0	3.3	6.4
3.32	7.37	0.58	9.5	2.20	3.5	5.9
3.32	7.37	0.58	9.5	1.72	2.5	4.9

[a] Omitted from Fig. 6 and the calculation of the pressure dependence of the rate because of high (0.2) fractional consumption of the atmospheric reagent.

[b] Omitted from Fig. 6 and the calculations because of large deviation from the other values. The reason for this deviation is unknown.

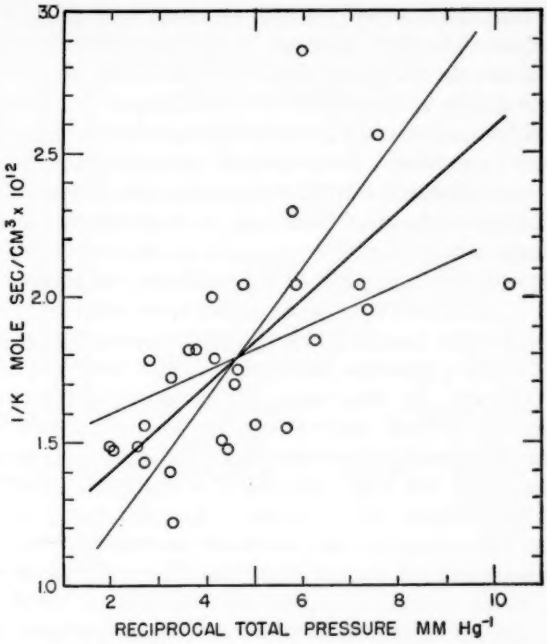

FIG. 6. Reciprocal plot of the rate constants of the boron trifluoride-methylamine reaction against inverse total pressure.

The reaction boron trifluoride-methylamine: The data for this reaction are collected in Table III. The rate constant is less than that for the two preceeding reactions, being of the order of 5×10^{11} cm³/mole sec. The total pressure and zone size drifts were of similar magnitude as those for the dimethylamine reaction and are shown in Fig. 6. A number of runs were made on this system using a bent thermocouple similar to that described. Again, heat conduction along the wires appeared to be unimportant.

The reaction boron trifluoride-ammonia: No quantitative results were obtained for this reaction because deposits of solid product formed on the nozzle and the thermocouple, making the temperature measurements uncertain. It appears, however, that the rate is slower than that of the methylamine reaction by an order of magnitude.

DISCUSSION

Reliability of the Method

The various tests described above show that the conditions assumed in deriving Eq. (6) have been met by experiment, and indeed, the random spread of rate constants show that these approximations are not the limiting factor in the application of the method. Exceptions to this statement appear in two marked drifts of rate constants. The general increase in rate constant with total pressure shown by the methyl- and dimethylamine reactions may be explained satisfactorily by postulating the participation of a third body in the

reaction. The *decrease* in rate constant with increasing reaction zone size, however, is not amenable to interpretation. In fact, any drift with zone size should be attributable in large part to depletion of the atmospheric reagent within the reaction zone. Such depletion would be expected to be greater in small zones, hence the rate constants calculated ignoring this phenomenon should be *less* in small zones than in larger ones, whereas experimentally just the opposite is observed. Unfortunately, the interplay of experimental variables was such that most of the runs at higher pressures were made with smaller reaction zones, and it appeared possible that either a pressure effect was faking a zone size drift or *vice versa*. In fact, when the pressure drift was assumed to be real, and all rates were corrected to the same pressure, the zone size drift disappeared. If, on the other hand, the latter was taken as real, and corrected for, the pressure effect vanished. In order to solve this dilemma, a series of runs was made on the methylamine system using as large zones as possible at high pressures and small zones at low pressures. These runs broke up the apparent zone size drift, and substantiated the pressure effect.

Figures 4–6 show that there is a considerable random spread of rate constants for the same experimental conditions. Some of this is probably due to uncertainties in pressures, flow rates and gas compositions, which can be reduced by further refinement of technique. But, the major cause of the spread is due to the necessity of determining the rate constant from the *shape* of the temperature pattern. Slight variations in local temperatures from run to run change substantially the shape parameter c, which is a sensitive function of the temperature profile, and an uncertainty in c is then further magnified in the calculation of the rate constant. Even so, the reproducibility of the method must be considered good for rates of these magnitudes.

Kinetics of Reactions

The observed increase of rate constant with total pressure is consistent with a kinetic mechanism requiring the participation of a third molecule in the addition process. The molecularity of the reactions indicates that the role of such a third molecule is physical, that of an energy absorber, rather than chemical. The high speed of these reactions, the slowest of which occurs once every 360 collisions at 0.2 mm Hg, rules out the possibility of a true three body collision; there are not enough such collisions by several orders of magnitude.

However, postulating a mechanism which corresponds to that proposed by Lindemann for unimolecular reactions:

$$y+z \underset{k_{-1}}{\overset{k_1}{\rightleftharpoons}} yz^*$$

$$yz^*+M \xrightarrow{k_2} yz+M^*,$$

where M represents any molecule, permits a reasonable explanation of the rate data for these three reactions.[22–24] If a steady state is assumed for the species yz^*, the experimental rate constant may be expressed as a function of total gas concentration thus,

$$\frac{1}{k_e}=\frac{1}{k_1}+\frac{k_{-1}}{k_1k_2M}. \tag{10}$$

Figures 4–6 show analyses of the rate data in accord with Eq. (10). The best straight lines were fitted to the data by the least squares method. The accuracy limits shown are the 95 percent confidence level values for the slopes. The rate constant expressions are summarized as follows:

$$BF_3-MeNH_2;\ 10^{13}/k=12.6\ +1.16/P,$$
$$BF_3-Me_2NH;\ 10^{13}/k=\ 0.31+0.444/P,$$
$$BF_3-Me_3N;\quad 10^{13}/k=\ 2.68+0.041/P,$$

where k is in cm³/mole sec and P in mm Hg. The limiting high pressure association rate constants are, therefore, 0.08×10^{13}, 3.2×10^{13}, and 0.37×10^{13} in the series monomethylamine, dimethylamine, trimethylamine. Surprising is that dimethylamine, rather than monomethylamine, has the highest rate because simple geometric considerations, at least, would suggest that in the latter the steric hindrances should be least. Also in the lifetimes of the initially formed "hot" adduct molecules, there appears to be no regular progression with the extent of substitution on ammonia. If one assumes that the rate constants of the stabilizing collisions, k_2, are the same in the three reactions, previous equations give for relative lifetimes 10.8, 0.7, and 65, whereas it would be reasonable to suppose that the lifetime is increased by an increase in the number of internal degrees of freedom in the adduct molecule. Since the data on dimethylamine reaction, which is out of line, are many fewer than for the other two reactions and the pressure range studied shorter, the possibility remains that experimental errors have obscured the regular progression of kinetic constants, in the amine series. Such errors, however, would have to be considerably larger than is suggested by the statistical analysis of the data and therefore we are inclined to consider the observed deviations from regular progression as real.

The great speeds of these reactions, which in two cases are comparable to the recombination rate of methyl radicals[25] and are close to the classical collision number, makes it highly improbable that there is any activation energy involved. As the Eyring treatment of

[22] F. A. Lindemann, Trans. Faraday Soc. **17**, 598 (1922).
[23] L. S. Kassel, *The Kinetics of Homogeneous Gas Reactions* (Chemical Catalog Company, New York, 1932), p. 38 ff.
[24] C. E. H. Bawn and A. G. Evans, Trans. Faraday Soc. **33**, 1571, 1580 (1937).
[25] R. Gomer and G. B. Kistiakowsky, J. Chem. Phys. **19**, 85 (1951).

radical recombination gives maximum rates almost exactly the same as the collision treatment, both for methyl radicals and for these addition reactions,[26,27] we feel confident that the order of magnitude of the maximum possible rate is $2\text{–}3\times10^{14}$ cm³/mole sec leaving room for at most 1–3 Kcal activation energy.

This negligible activation energy leads to the conclusion that the transition state must be relatively loose, i.e., the B—N distance must be large enough so that steric repulsions of substituent groups are still unimportant. It would appear that the type of steric effects suggested by Brown[5] comes into play only at shorter distances and controls the depth of the potential energy minimum of the stable adduct rather than produce an activation energy hump in the reaction coordinate.

[26] Glasstone, Laidler, and Eyring, *The Theory of Rate Processes* (McGraw Hill, Book Company, Inc., New York, 1941), p. 131, 220, 260.
[27] T. L. Hill, J. Chem. Phys. **17**, 503 (1949).

THE JOURNAL OF CHEMICAL PHYSICS VOLUME 20, NUMBER 1 JANUARY, 1952

The Heat of Formation of Nitric Oxide and Phosphorus Trioxide*

WILLIAM E. KOERNER† AND FARRINGTON DANIELS
Department of Chemistry, University of Wisconsin, Madison, Wisconsin
(Received October 8, 1951)

The heat of formation of nitric oxide has been redetermined by burning samples of red phosphorus in nitric oxide and in an equimolecular mixture of nitrogen and oxygen. A varying fraction of the phosphorus consumed by reaction with nitric oxide was converted to phosphorus trioxide; the remainder being converted to the pentoxide. A value of 21.8 kcal per mole was obtained for the heat of formation of nitric oxide at 25°C. A value of −270 kcal per mole was chosen as the best value for the heat of formation of phosphorus trioxide at 25°C.

INTRODUCTION

THE heat of dissociation of nitrogen, oxygen, and nitric oxide molecules into neutral atoms of oxygen and nitrogen can be studied using band spectroscopy, electron impact, and photochemical methods. The set of values chosen for the three molecules, NO, N_2, and O_2, is subject to the restriction that the sum of the heats of dissociation of nitrogen and oxygen minus twice the value for the heat of dissociation nitric oxide must give the experimentally determined heat of reaction for the reaction:

$$N_2+O_2\rightarrow 2NO.$$

The presently accepted value of ΔH for this reaction is Berthelot's value of 43.2 kcal at 25°C,[1] giving a value for the heat of formation of nitric oxide of 21.6 kcal per mole. His value was obtained by burning samples of either cyanogen or ethylene in nitric oxide and in oxygen. This value is also supported by equilibrium constant measurements at different temperatures.[2]

Schmid and Gero,[3] according to Zeise,[4] have suggested a value of 35.1 kcal. This conflicting value and the present controversy about the heats of dissociation of nitrogen and nitric oxide[5–13] into neutral atoms made it desirable to check Berthelot's value for the reaction.

In the present investigation red phosphorus was burned in a 50–50 mixture of pure oxygen and nitrogen and also in nitric oxide. When the same amount of phosphorus is burned and the products are the same, the difference between the heat evolved in oxygen and the larger amount evolved in nitric oxide is a measure of the heat released by the decomposing nitric oxide.

EXPERIMENTAL PROCEDURE

A flow calorimeter utilizing the combustion chamber illustrated in Fig. 1 was used for all experiments. The chamber and attached spiral heat exchanger were made of Pyrex glass, and the sample dish was made of fused quartz. The brass calorimeter held about 1400 g of water. An electrical resistance heater was used to measure the heat capacity of the calorimeter which was found to be 239 cal/°C.

* More complete details may be obtained from a part of a Ph.D. thesis of William E. Koerner filed in the library of the University of Wisconsin in August, 1949.
† DuPont graduate fellow in chemistry (1948–1949). Present address: Monsanto Chemical Company, St. Louis, Missouri.
[1] M. Berthelot, Ann. chim. et phys. (5) **6**, 178 (1875); (5) **20**, 255 (1880).
[2] G. N. Lewis and M. Randall, *Thermodynamics and the Free Energy of Chemical Substances* (McGraw-Hill Book Company, Inc., New York, 1923).
[3] R. Schmid and L. Gero, Math. naturwiss. Anz. ungar Akad. Wiss. **62**, 408 (1942) (Chem. Abstracts **41**, 7262 (1947)).
[4] H. Zeise, Physik. Z. **45**, 53 (1944).
[5] A. G. Gaydon, Nature **153**, 407 (1944).
[6] A. G. Gaydon and W. G. Penney, Proc. Roy. Soc. (London) **A183**, 374 (1945).
[7] P. J. Flory and H. L. Johnston, J. Chem. Phys. **14**, 212 (1946).
[8] J. G. Valatin, J. Chem. Phys. **14**, 568 (1946).
[9] A. G. Gaydon, *Dissociation Energies and Spectra of Diatomic Molecules* (John Wiley and Sons, Inc., New York, 1947).
[10] G. Glockler, J. Chem. Phys. **16**, 602, 604 (1948).
[11] H. D. Hagstrum, J. Chem. Phys. **16**, 848 (1948).
[12] J. Kaplan, Phys. Rev. **78**, 93 (1950).
[13] A. E. Douglas and G. Herzberg, Can. J. Research **29**, 294 (1951).

Pellets made from Eimer and Amend special "micro" amorphous phosphorus were ignited by the spark from a 4000-volt transformer. Matheson nitric oxide (~93 percent NO −7 percent N_2) was used. A calibrated Beckman thermometer having divisions of 0.01°C was used to measure the temperature rise. A small Cottrell precipitator in the exit line from the calorimeter was used to remove the last traces of finely divided phosphorus pentoxide smoke.

The determination of the amount of red phosphorus burned was straightforward in the experiments in which the nitrogen-oxygen mixture was used. The red phosphorus pellet was weighed before ignition, and the residue was collected and weighed on a tared Gooch crucible. To check this result the phosphorus pentoxide produced was dissolved in water and either titrated with sodium hydroxide or determined gravimetrically as magnesium pyrophosphate.

Combustion of red phosphorus in nitric oxide is analogous to combustion in a limited supply of oxygen, and a mixture of phosphorus trioxide and phosphorus pentoxide is obtained. Solution of the mixed oxides was effected by carefully hydrating the solids, using nitrogen gas saturated with water vapor. The mixture of phosphoric and phosphorous acids was titrated with sodium hydroxide solution to determine the total phosphorus consumed. The phosphite ion was determined iodometrically using the method of Wolf and Jung.[14] The small amount of nearly pure phosphorus pentoxide recovered from the Cottrell precipitator and other parts of the exit line was determined by precipitation and weighing as ammonium phosphomolybdate.

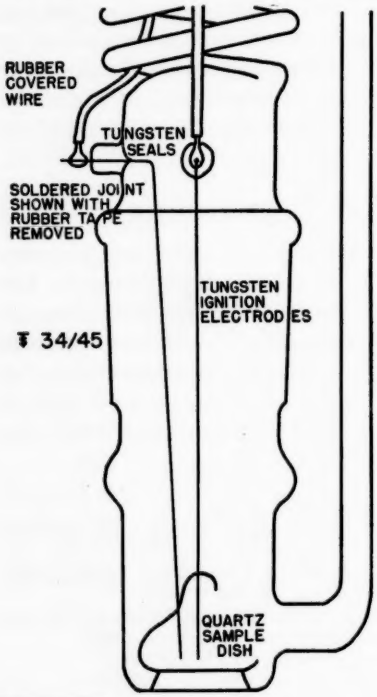

FIG. 1. Lower portion of calorimeter combustion chamber.

[14] L. Wolf and W. Jung, Z. anorg. u allgem. Chem. **201**, 337 (1931).

In all of the nitric oxide experiments a small amount of the oxygen, produced from the nitric oxide by the high temperature flame, failed to combine with the phosphorus. Instead, nitrogen dioxide was produced by combination with the excess of nitric oxide. The magnitude of this heating effect, 14 kcal per mole of nitric oxide, was determined by absorbing the nitrogen dioxide in a 0.1N solution of sodium hydroxide and titrating the resulting nitrite ions with a solution of 0.02N potassium permanganate according to the method of Laird and Simpson.[15]

Appropriate corrections were made in the calculations for the heat produced by the ignition arc, the stirrer, and formation of nitrogen dioxide and the heat lost by radiation and convection.

RESULTS

Eight experiments were made in which red phosphorus samples were burned in an equimolecular mixture of nitrogen and oxygen. The product of combustion was pure phosphorus pentoxide. An average value of −355 kcal per mole was obtained for the heat of formation of phosphorus pentoxide with a mean deviation of ±2 kcal per mole. The heat of formation of phosphorus pentoxide from red phosphorus is −351.6 kcal per mole for the macrocrystalline form and −358.6 kcal per mole for the amorphous form according to Bichowsky and Rossini.[16] Thus it appears that a mixture of the two forms of phosphorus pentoxide was obtained in the experiments described here and that the calorimeter had been correctly calibrated.

Because no reliable data for the heat of formation of phosphorus trioxide were available, a different method of calculation was used for the experiments in which red phosphorus was burned in nitric oxide. An arbitrary value for the heat of formation of phosphorus trioxide, −180 kcal per mole, was used to calculate an apparent heat of formation of nitric oxide from each of seven experiments. These results together with the mole fraction of phosphorus converted to phosphorus trioxide are shown in Table I. A sample calculation for the last experiment follows.

Duration of experiment = 520 sec. Corrected temperature rise = 1.716°.
Calories evolved = 2824.
Arc heating = 12 cal.
Heat loss from gas flow = 2 cal.
Heat of chemical reactions = 2824 + 2 − 12 = 2814 cal.
Phosphorus titrated as H_3PO_4 and H_3PO_3: 0.4037 g.
Phosphorus titrated as phosphite ion: 0.1407 g.
NO_2 produced in side reaction: 6.2×10^{-4} mole.
Calories from P_2O_5 formation = $0.00444\times355{,}000 = 1575$.
Calories from P_2O_3 = $0.00227\times180{,}000$ (assumed) = 409.
Calories from $2NO+O_2\rightarrow2NO_2$ = $0.00062\times14{,}000 = 9$.
Calories from NO dissociation = 2814 − (1575 + 409 + 9) = 821 cal.

[15] J. S. Laird and T. C. Simpson, J. Am. Chem. Soc. **41**, 524 (1919).

[16] F. R. Bichowsky and F. D. Rossini, *The Thermochemistry of the Chemical Substances* (Reinhold Publishing Corporation, New York, 1936).

Moles of NO dissociated in forming $P_2O_5 = 0.00444 \times 5 = 0.0222$.
Moles of NO dissociated in forming $P_2O_3 = 0.00227 \times 3 = 0.0068$.
Moles of NO dissociated into O_2 which combined with excess NO: 0.0006.
Moles of NO dissociated $= 0.0222 + 0.0068 + 0.0006 = 0.0296$.
Kcal apparently released when one mole of NO dissociates into N_2 and O_2 at 25°C assuming the heat of formation of P_2O_3 is -180 kcal/mole $= 0.821/0.0296 = 27.7$.

When the value of ΔH_{NO} is plotted against the mole fraction of phosphorus burned to phosphorus trioxide as given in Table I and the best straight line is drawn through the points, this straight line extrapolates out to about 21.6 for a value of ΔH_{NO} at zero mole fraction of phosphorus burned to phosphorus trioxide. In other words, a rather unsatisfactory extrapolation gives 21.6 as the value for the heat of formation under conditions where all the phosphorus is burned to phosphorus pentoxide and there is no correction for incomplete combustion to phosphorus trioxide.

By using the method of least squares to determine the best straight line for the extrapolation, a value of 21.8 kcal per mole was obtained. If a different arbitrary value for the heat of formation of phosphorus trioxide is used, the value for the heat of formation of nitric oxide will vary by at most 0.3 kcal per mole.

By using the value of 21.6 kcal per mole for the heat of formation of nitric oxide a value for the heat of formation of phosphorus trioxide was calculated from each experiment. The mean of these seven values was -262 kcal per mole with a mean deviation of ± 4 kcal per mole.

DISCUSSION

The value of -262 kcal per mole for the heat of formation of phosphorus trioxide from red phosphorus becomes -270 kcal per mole for white phosphorus. Ogier[17] reported -244 kcal in fair agreement with the present value but Berthelot[16] reports a value of only -78 kcal. Accurate measurements on these products of incomplete combustion are very difficult.

[17] J. Ogier, Compt. rend. **87**, 210 (1878).

TABLE I. The relationship between the apparent heat of formation of nitric oxide and the mole fraction of phosphorus burned to phosphorus trioxide.

Mole fraction P_2O_3	0.221	0.225	0.268	0.268	0.299	0.303	0.338
ΔH_{NO} (apparent)	25.6	25.5	26.5	26.8	26.7	27.2	27.7

The value obtained for the heat of formation of nitric oxide in this research is 21.8 ± 0.3 kcal per mole. It is more reliable than the values for the phosphorus oxides since the conditions after suitable corrections are the same for the nitric oxide as for the equimolecular mixture of nitrogen and oxygen. Under these conditions the only difference lies in the heat of dissociation of the nitric oxide.

This value of 21.8 kcal is in excellent agreement with old, accepted value of Berthelot, 21.6 kcal. Whatever the values that are accepted for the heat of dissociation of nitric oxide, oxygen and nitrogen gases into atoms the present investigation indicates that they should meet the requirement that the sum of the heat required to dissociate the nitrogen molecule into atoms plus the heat required to dissociate the oxygen molecule into atoms should be 43.6 kcal greater than the heat required to dissociate two molecules of nitric oxide into oxygen and nitrogen atoms.

ACKNOWLEDGMENTS

The authors wish to thank Mr. L. Henke and Mr. L. Lincoln for their assistance in building the calorimeter, Mr. J. Davis for blowing the experimental models of the combustion chamber, and Dr. G. Furukawa and Dr. J. Hyndman for their help in calibrating the Beckmann thermometer and the standard resistances.

The Catalytic Conversion of Parahydrogen by Paramagnetic Complex Ions in Aqueous Solution*†

W. K. WILMARTH AND C. F. BAES, JR.
Department of Chemistry, University of Southern California, Los Angeles 7, California

(Received June 19, 1951)

Rates of conversion of parahydrogen by paramagnetic complex ions of copper (II) and chromium (III) in aqueous solution have been measured at 25°C. The results are discussed in terms of the Wigner theory, which predicts the effects of magnetic moment and collision distance. Owing to the planar configuration of the copper (II) complexes, only a qualitative test of theoretical predictions is possible. The rate effects produced by various symmetrical octahedral complexes of chromium (III) can be explained in terms of the theory if one evaluates the various collision distances for H_2 from a detailed examination of the complex structure in each case.

I. INTRODUCTION

L. FARKAS and H. Sachsse reported in 1933[1,2] that parahydrogen is converted to normal hydrogen with considerable rapidity at room temperature by paramagnetic molecules in the gas phase or paramagnetic ions in solution. In both cases the conversion was found to be a homogeneous second-order process, being first order with respect to both the hydrogen concentration and the concentration of the paramagnetic molecule or ion. As studied in the gas phase, the reaction has a surprisingly small temperature coefficient.

E. Wigner was the first to treat this process theoretically.[3] By the use of the perturbation theory he derived an expression for the collision efficiency Z_{p-O},[4] as a function of the interaction between the nuclear spin magnetic dipole of H_2 and the magnetic dipole of the paramagnetic molecule or ion. The resulting expression was

$$Z_{p\to 0}=\frac{8\mu_a^2\mu_b^2 I\pi^2}{9h^2r^6kT}(\mathrm{S}), \qquad (1)$$

wherein μ_a and μ_b are, respectively, the magnetic moment of the paramagnetic species and of the proton; (I) is the moment of inertia of the hydrogen molecule; r is the collision distance; (S) represents a temperature dependent distribution function which takes into account the contribution of transitions between various rotational (ortho and para) states. The collision time is taken as $r/3v$ (v being the velocity of the H_2 molecule).

Calculations based upon this theory lead to a correct order of magnitude for the rate of the gas phase reaction, and to an approximately correct temperature coefficient. No temperature coefficients were reported by Farkas and Sachsse[1,2] for the solution reaction. Further, while the data established, more or less, the effect of magnetic moment, the radius effect predicted by the theory was not conclusively demonstrated because of the uncertainty of the collision diameters for the simple hydrated ions studied.

The present work was planned to test more carefully the Wigner relationship. In particular, it should be possible to effect variations in the catalytic efficiency of a given ion in solution by changing its collision size through the use of various complexing agents. Though the theory was developed for the gas phase reaction, there are data[5] which indicate that the same process occurs in the liquid phase reaction. In addition, the rates of conversion by dissolved ions are comparable with those observed in the gas phase. Ultimately, it is hoped that such studies will provide a greater knowledge of collision processes in solution.

Copper-amine complexes were chosen for the preliminary work because they are readily prepared by the addition of the complexing agent to aqueous cupric ion, and because the resulting complexes have one unpaired electron per metal atom, regardless of bond type. However, since copper (II) complexes are known to be planar, it is difficult to define a collision distance, and so, effectively, test theoretical predictions. Hence, having established that the rate effects for the copper (II) complexes were small, we subsequently directed our attention to the more symmetrical octahedral complexes of chromium (III).

II. EXPERIMENTAL

Para-rich Hydrogen

Parahydrogen was prepared in the usual way, by means of low temperature catalysis on charcoal. Electrolytic hydrogen, which had been freed of traces of oxygen by passage through a Deoxo catalytic purifier and drying tubes, was passed over charcoal at the temperature of liquid nitrogen. Under these conditions the maximum parahydrogen content obtainable is 50.2 percent.

* A large portion of this investigation was carried out under Task Order IV, Contract No. N6onr-238, with the ONR.

† Based on a dissertation submitted by C. F. Baes, Jr., in partial fulfillment of the requirements for the degree of Doctor of Philosophy at the University of Southern California.

[1] L. Farkas and H. Sachsse, Z. physik. Chem. **B23**, 1, 19 (1933).

[2] H. Sachsse, Z. physik. Chem. **B24**, 429 (1933).

[3] E. Wigner, Z. physik. Chem. **B23**, 28 (1933).

[4] Defined as the fraction of the total number of collisions between H_2 and the catalyzing species resulting in conversion.

[5] L. Farkas, and U. Garbatski, Trans. Faraday Soc. **35**, 263 (1939).

The Analysis of Ortho-parahydrogen Mixtures

A modification of the spiral-filament Pirani gauge described by Bolland and Melville[6] was used in the analysis of hydrogen mixtures. The gauge found most suitable employed an unused filament manufactured for a 6-watt, 120-volt incandescent lamp. The customary constant-voltage method of measurement was used. The resistance of the filament at the optimum temperature (*ca* −100°C) was about 140 ohms, and the maximum difference in resistance obtainable with para-rich hydrogen prepared at the liquid nitrogen temperature was found to be approximately 3.5 ohms. A constant pressure of about 50 mm, reproduced by means of an electric contact manometer, was maintained in all measurements. The accuracy of analysis was limited by the variability of the wire resistance to an uncertainty of about 2 percent.

Rate Measurements

In the investigation of the Cu(II) complexes and in the preliminary work on the symmetrical Cr(III) complexes, the conversions were carried out in a spherical, thermostatted vessel of about 110-ml capacity, partially filled with a solution of the paramagnetic complex. This vessel was agitated by a mechanical shaker.

Studies conducted in this laboratory on the conversion of parahydrogen by sodium in liquid ammonia solutions[7] have shown that agitation of the reaction mixture by means of a magnetic stirrer arrangement is feasible. This method has the advantage that no error in time measurement is incurred upon the extraction of hydrogen samples. In later measurements on the Cr(III) complexes this stirrer arrangement was used (Fig. 1).

The experimental procedure may be outlined as follows. A measured volume of the solution to be studied was pipetted into the reaction vessel and subsequently, degassed by alternate boiling under vacuum and saturation with hydrogen gas. Parahydrogen was then introduced to a pressure of 500–700 mm. Zero time was taken at the moment agitation began. Water, thermostatted to 25±0.1°C, was passed through the outer jacket of the vessel. The gas samples subsequently taken were dried for at least twenty minutes in a liquid nitrogen trap. Some four or five samples were taken during each run, the results plotted in the conventional manner for a first order reaction, and the observed rate constant evaluated from the slope of the best straight-line fit of the experimental points. In every case this fit was within the uncertainty of the individual analyses.

Gas Solubility Measurements

In order to evaluate the rate constant k_s for the liquid phase reaction, it is necessary to determine the solubility of hydrogen in the liquid phase. In his work on solutions of the sulfates of bivalent, first transition series metal ions, Sachsse noted a more or less linear decrease in the rate constant with increasing salt concentration. He assumed, reasonably, that this effect was caused by a corresponding decrease in the hydrogen solubility in these solutions. The limited data for the solubility of hydrogen in various aqueous solutions[8] indicate that this is the case. Some later work by Calvin lends further support to this view.[9] In this manner, the first-order character of the parahydrogen conversation with respect to the concentration of the paramagnetic ion in solution was first demonstrated.

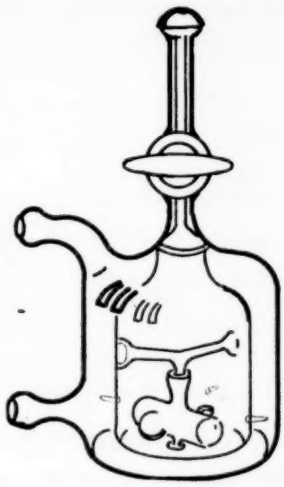

FIG. 1. Magnetically stirred reaction vessel.

It was not necessary to measure the solubility of hydrogen in the various Cu(II) solutions studied in the present investigation since simple salt solutions are not involved, but rather, liquid systems sufficiently complex so that it is not possible to predict the various hydrogen solubilities with any certainty. The method employed was developed to yield results of sufficient accuracy (2–3 percent) without the expenditure of an excessive amount of time. It consisted of shaking the solution under measurement with hydrogen and then draining it into an evacuated bulb, maintaining a nearly constant gas pressure. The dissolved gas was then extracted by repeated cycling of a Topler pump, passed through a liquid nitrogen trap, and thence to a gas burette. The Ostwald solubilities a, measured in this way, appear in Table I. It is interesting to note that for each case in which the ratio of Cu(II) to amine group is 1:4, the gas solubility falls within 3 percent of the value one would predict from the results of Sachsse.

The values of a used in calculating the chromium data (Table II) were estimated assuming in all cases a solubility *vs* salt concentration curve similar to that for $AlCl_3$.[10] Since these solutions are fairly dilute, only slight errors can be introduced by this procedure.

[6] J. L. Bolland and H. W. Melville, Trans. Faraday Soc. **33**, 1318 (1937).

[7] Claeys, Baes, and Wilmarth, J. Chem. Phys. **16**, 425 (1948).

[8] A. Seidell, *Solubilities of Inorganic and Metal-organic Compounds* (D. Van Nostrand Company, Inc., New York, 1940), third edition, Vol. I, pp. 554–561.

[9] Melvin Calvin, J. Am. Chem. Soc. **60**, 2003 (1938).

[10] M. Randall and C. F. Failey, Chem. Revs. **4**, 271 (1927).

TABLE I. Rate data for Cu(II)-amine complexes at 25°C.

Complex		$\frac{\Sigma[CuII]}{\Sigma[R]}$	Σ[CuII] moles, l^{-1}	k^0 min^{-1}
$Cu-NH_3$	(f)	1/5	0.272	1.15
		1/14.8	0.237	1.34
$Cu-H_2O$		···	0.1813	1.12
$Cu-H_2NC_2H_4OH$	(c)	1/5	0.272	0.92
		1/4	0.287	0.93
Cu−en	(a)	1/2.5	0.272	0.73
		1/2	0.287	0.87
$Cu-HN(C_2H_4OH)_2$	(d)	1/5	0.272	0.77
		1/4	0.287	0.66
$Cu-N(C_2H_4OH)_3$	(e)	1/5	0.272	0.60
Cu−(py)	(b)	1/5	0.272	0.50
		1/4	0.287	0.61

Magnetic Susceptibilities

Solutions of the Cr(III) complexes were measured by means of the Gouy technique, the concentrations being the same as in the rate measurements. The values of μ appearing in Table II were calculated in the usual way, assuming the Curie law. No diamagnetic correction was made. The results indicate three unpaired electrons per Cr atom in every case.

Preparation of Complexes

Rate measurements were made on standardized solutions of Reagent grade $Cu(NO_3)_2 \cdot 3H_2O$, to which the following amines had been added: (a) ethylenediamine (en);[11] (b) pyridine (py);[11] (c) monoethanolamine; (d) diethanolamine; (e) triethanolamine; (f) ammonia. The organic amines were purified by fractional distillation through a packed column.

References to the procedures followed in the preparation of the various Cr(III) complexes follow:

(g) A solution of reagent grade $[Cr(H_2O)_6](NO_3)_3$ was standardized by iodimetric analysis.

(h) $[Cr(NH_3)_6](NO_3)_3$; Jorgensen, J. prakt. Chem. **30**, 1 (1884).

(i) $[Cr(en)_3]Cl_3 \cdot 3H_2O$;[11] J. C. Bailar, Jr., and J. B. Work, J. Am. Chem. Soc. **67**, 176 (1945).

(j) $[Cr(pn)_3]I_3 \cdot H_2O$;[11] (This complex was first prepared as the very soluble chloride by the same method used for the trisethylenediamine complex (i) and then converted to the iodide by the addition of saturated KI solution.)

(k) $[Cr(urea)_6]Cl_3 \cdot 3H_2O$; King, *Inorganic Preparations* (D. Van Nostrand Company, Inc., New York, 1936), p. 106.

(l) $[Cr(antipyrene)_6](ClO_3)_3$; E. Wilke-Dörfürt and H. G. Mureck, Z. anorg. u. allgem. Chem. **184**, 132 (1929).

(m) $K_3[Cr(CN)_6]$; H. S. Booth and W. C. Fernelius, *Inorganic Synthesis* (McGraw-Hill Book Company, Inc., New York, 1946), first edition, Vol. 2, p. 203.

(n) $K_3[Cr(SCN)_6] \cdot 4H_2O$; King, *Inorganic Preparations* (D. Van Nostrand Company, Inc., New York, 1936), p. 109.

(o) $K_3[Cr(C_2O_4)_3] \cdot 3H_2O$; H. S. Booth and W. C. Fernelius, *Inorganic Synthesis* (McGraw-Hill Book Company, Inc., New York, 1939) first edition, Vol. 1, p. 37.

(p) $(NH_4)_3[CrF_6]$; this complex was prepared simply by warming $Cr_2(SO_4)_3$ with an excess of NH_4F in aqueous solution. The precipitated product was then recrystallized from NH_4F solution; R. Wagner, Ber. deut. Chem. Ges. **19**, 896 (1886).

[11] The abbreviations py, en, and pn are commonly used to represent a molecule of pyridine, ethylenediamine, and propylenediamine.

These compounds were all analyzed for Cr by means of a perchloric acid oxidation method adapted from G. Frederick Smith.[12] The results were in agreement with the calculated values within a relative error of 1 percent.

Stability of Cu (II) Complexes

Whereas many Cr(III) complexes appear to undergo irreversible decomposition in aqueous solution, it is known, in general, that Cu(II) complexes are formed reversibly. The stability constants for the various complexes of cupric ion with en, py,[11] and ammonia have been reported by Bjerrum.[13] These values are listed in Table III. Here K_n is given by $[Cu(R)_n]/[Cu(R)_{n-1}][R]$, wherein R is a molecule of complexing amine. The value of the over-all stability constant of $Cu(en)_2^{++}(K_1 \cdot K_2)$ recently reported by Laitinen, Onstatt, Bailar, and Swann[14] is in good agreement with the results of Bjerrum.

Reduction of Cu(II) to metallic copper was observed to occur in triethanolamine solution upon long standing (several days). Since only fresh solutions were used in the rate measurements, and since no systematic deviation from first-order behavior was observed in the experimental points, it appears that no appreciable reduction occurred during the run.

Stability of Cr(III) Complexes

The luteo-amine complexes of Cr(III) (en, pn, NH_3) undergo slow, irreversible decompositions to Cr_2O_3 in aqueous solution. Spectral studies carried out with a Beckmann spectrophotometer revealed that $Cr(SCN)_6^{3-}$ and $Cr(urea)_6^{3+}$ [15] decompose appreciably within a day. Only $Cr(C_2O_4)_3^{3-}$ and $Cr(antipyrine)_6^{3+}$ appear not to change over long periods in solution.

Crude conductivity, precipitation, and titration ex-

TABLE II. Rate data for the symmetrical Cr(III) complexes at 25°C.

Complex		Σ[CrIII] mole, l^{-1}	k^0 min^{-1}	μ Bohr mag.	k^0/μ^2
$Cr(SCN)_6^{3-}$	(n)	0.0382	6.6	3.73	0.475
$Cr(C_2O_4)_3^{3-}$	(o)	0.0398	6.8	3.81	0.469
$Cr(CN)_6^{3-}$	(m)	0.0516	4.54	3.79	0.315
$Cr(urea)_6^{3+}$	(k)	0.0500	3.22	3.82	0.220
$Cr(H_2O)_6^{3+}$	(g)	0.145	2.28	3.83	0.155
$Cr(antip.)_6^{3+}$	(l)	0.0234	1.52	3.73	0.109
$Cr(NH_3)_6^{3+}$	(h)	0.0533	1.16	3.74	0.083
$Cr(en)_3^{3+}$	(i)	0.0589	0.78	3.77	0.0549
$Cr(pn)_3^{3+}$	(j)	0.0494	0.88	3.89	0.0582

[12] G. Frederick Smith, *Mixed Perchloric, Sulfuric, and Phosphoric Acids and their Applications to Analysis*, 1942.

[13] J. Bjerrum, *Kgl. Danske Videnskab Selskab Methfys. Med.* **11**, No. 5 (1931). J. Bjerrum and E. J. Nielsen, Acta Chem. Scand. **2**, 298 (1948).

[14] Laitinen, Onstatt, Bailar, Jr., and Swann, Jr., J. Am. Chem. Soc. **71**, 1550 (1949).

[15] N. Bjerrum [Z. anorg. u. allgem. Chem. **118**, 131 (1921)] has examined the stabilities of the various chromic-thiocyanate complexes in solution. A kinetic study of the decomposition of $Cr(urea)_6^{+++}$ has been reported by Martin Kilpatrick, Jr. [J. Am. Chem. Soc. **50**, 358 (1928)].

periments carried out on solutions of $(NH_4)_3CrF_6$ revealed that immediate hydrolysis of perhaps two or three fluoride ions per chromium atom occurs. Further hydrolysis is slow, requiring weeks to reach equilibrium. Scheffer and Hammaker[16] conclude, on the basis of spectral measurements, that CrF^{++} is formed when chromic nitrate and sodium fluoride are mixed in acid solution. Our conductivity measurements on such solutions tend to confirm that only a small amount of complexing occurs. In addition, however, it is clear simply from visual evidence that these solutions are quite different from a fresh solution of $(NH_4)_3CrF_6$. In view of these results the parahydrogen rate data for $(NH_4)_3CrF_6$ will be but briefly noted in the discussion.

Freshly prepared solutions of all the complexes were used in the rate measurements. The spectroscopic data, as well as conductimetric data, failed to indicate appreciable decomposition within the first eight hours, the usual time required to complete a run. The observed conversion rates were all first order within the uncertainty of the measurements.

Recently, it has been reported[17] that $Cr(NO_3)_3$ solutions change slowly on aging, the $Cr(H_2O)_6^{3+}$ ion being partially transformed to polynuclear, oxygen bridged cations. A large number of measurements have been made upon freshly prepared as well as aged solutions of $Cr(H_2O)_6(NO_3)_3$ with the result that no significant change in catalytic efficiency has been noted.

III. RESULTS

The paramagnetic conversion of parahydrogen proceeds as follows:

$$p\text{-}H_2+C\underset{k_2}{\overset{k_1}{\rightleftharpoons}}o\text{-}H_2+C, \tag{2}$$

wherein C is a paramagnetic molecule or ion. Accordingly, if the conversion were followed directly in the liquid phase, the gaseous phase being absent, we have

$$-[d(P_{p\text{-}H_2})/dt]=k_1(C)(P_{p\text{-}H_2})-k_2(C)(P_{o\text{-}H_2}), \tag{3}$$

in which the concentrations of $p\text{-}H_2$ and $o\text{-}H_2$ have been replaced by the percentages $P_{p\text{-}H_2}$ and $P_{o\text{-}H_2}$ of each in the dissolved H_2 mixture. Since it is easily shown that $k_1=3k_2$,[18] we have, taking $k^0=k_1+k_2$,

$$-[d(P_{p\text{-}H_2})/dt]=k^0(C)(P_{p\text{-}H_2}-25). \tag{4}$$

The constant k^0 is the one usually tabulated, by convention of the earlier workers.

When the conversion in the liquid phase is followed by extraction of samples from the gas phase, it is necessary, of course, that the rate of shaking or stirring be sufficiently rapid so that it is not the rate-determining factor. The results of a series of runs indicated that for observed half-lives greater than 150 min a shaking speed of 400 strokes/min was adequate. In the case of stirring, no decrease in observed rate was noted for stirring speeds as low as 800 rpm. Under these conditions a rate constant k is defined by the equation,

$$\frac{R_\infty-R_t}{R_\infty-R_0}=\frac{P_t-P_\infty}{P_0-P_\infty}=e^{-k(C)t}, \tag{5}$$

wherein R_0, R_t, and R_∞ denote measured wire resistances for hydrogen samples taken at time $t=0$, t, and infinity, respectively. The corresponding P values denote the percentage of parahydrogen in the samples.

It can be shown that k^0 for the solution phase reaction will be related to the k, by

$$k=\left[k^0+k_{H_2O}\frac{(H_2O)}{(C)}\right]\left(\frac{aV_1}{V_g+aV_1}\right), \tag{6}$$

wherein k_{H_2O} is the molal rate constant for pure water (which is small, but appreciable);[19] a is the Ostwald solubility of H_2 in the solution; V_g and V_1 are, respectively, the volume of gas and of solution in the reaction vessel.

Listed in Table I are the data for the various copper (II) complexes studied. The mole ratios of copper (II) to amine, $\Sigma(Cu(II))/\Sigma(R)$ are given in column 2. Table II contains the chromium (III) data. In the last two columns of this table are listed values of μ and k^0/μ^2, significant in the Wigner theory of the conversion process.

A systematic consideration of the possible error introduced by the interruption of shaking, in order that samples might be extracted, indicates that it is not as large as the uncertainty introduced in analysis, and the rate constants are not in error by more than ± 2 percent when all sources of error are considered.

TABLE III. Stability constants of Cu(II)-amine complexes (see reference 13).

$K_n=$	K_1	K_2	K_3	K_4	K_5
$Cu(en)_n$	$5\cdot10^{10}$	$2\cdot10^9$	0.1	...	...
$Cu(NH_3)_n$	$14.6\cdot10^3$	$3.3\cdot10^3$	780	143	0.261
$Cu(py)_n$	257	76	13.8	4.0	...

IV. DISCUSSION

The preliminary studies with the Cu(II) complex ions indicate that, while differences in rate constants do exist and can readily be measured, no very spectacular effects can be achieved using only the amine ligands. Qualitatively, an increase in size of the complexing group generally seems to lower the catalytic efficiency, but any attempt to consider the data in a more quantitative fashion is complicated by the planar nature of the

[16] E. R. Scheffer and E. M. Hammaker, J. Am. Chem. Soc. **72**, 2575 (1950).

[17] H. Tracy Hall and Henry Eyring, J. Am. Chem. Soc. **72**, 782 (1950).

[18] At equilibrium, at room temperature, $P_{p\text{-}H_2}=25$, and $P_{o\text{-}H_2}=75$.

[19] The value $k_{H_2O}=6.8\times10^{-5}$ l, mole^{-1}, min^{-1}, reported by L. Farkas and L. Sandler, Trans. Faraday Soc. **35**, 337 (1939), was used.

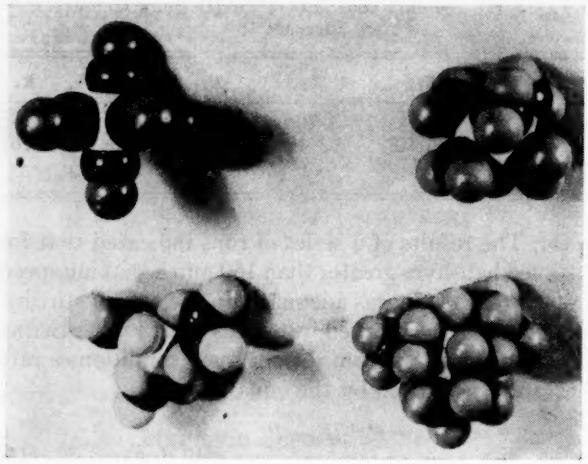

FIG. 2. Fischer-Hirschfelder-Taylor models of
$Cr(CN)_6^{3-}$ $Cr(H_2O)_6^{3+}$
$Cr(C_2O_4)_3^{3-}$ $Cr(en)_3^{3+}$.

complexes and the uncertainty as to the degree of association with the various amines. After establishing the fact that the rate of conversion was not strongly viscosity dependent, we decided to study a number of symmetrical chromic complexes since they permit a greater variation in the nature of the complexing group and total charge of the complex ion.

Upon examination of the Cr(III) data it is immediately apparent that the value of k/μ^2 does not decrease with an inverse high power of any reasonable collision distance based upon the size of the complexing group. In fact, there is often a reversal of order; e.g., $Cr(SCN)_6^{3-}$ is more efficient than $Cr(CN)_6^{3-}$. The urea complex is more efficient than the simple hydrated ion, and perhaps most surprising of all, the enormous $Cr(antipyrine)_6^{3+}$ [20] is more efficient than $Cr(NH_3)_6^{3+}$. If one assumes that the collision time is constant for each member of this series of complexes, it is obvious that one must either discard the notion of correlating the rate with molecular size, or look for some new criteria of collision size.

One can hardly discard the idea that efficiency of conversion increases with closeness of approach, and further, even the idea that it must be some fairly high power of this distance, since in reasonably accurate experiments, over a 600-fold range in concentration,[2] the conversion has been shown to be first order with respect to the paramagnetic ion concentration. In addition, the extreme variation of almost tenfold in rate constant must arise through a difference in collision efficiency, since it is unlikely that replacement of one ligand by another in the complexing sphere would result in long-range catalytic effects. Thus, we are compelled to retain a collision mechanism; i.e., one in which the probability of conversion rapidly increases as the distance between H_2 and the complex decreases.

In examining the remaining alternatives we were led to construct Fisher-Hershfelder-Taylor models of the various complexes studied. Features immediately evident were: (1) Branching at the atom directly attached to the metal ion permits the most efficient coverages Thus, while oxalate and ethylenediamine complexes appear not to be greatly different in size, a glance at Fig. 2 clearly reveals the greater closeness of packing caused by the amino hydrogens on ethylenediamine. (2) When branching does not occur at the atom directly attached to the metal atom, coverage is not complete enough to prevent considerable penetration of the first complexing sphere. This is true even in the case of the large sulfur atom of $Cr(SCN)_6^{3-}$. (3) The presence of a large outer structure in the complex such as in the case of $Cr(antipyrine)_6^{3+}$, Fig. 3, is not important in determining the minimum distance of approach, since this structure is relatively an open one.

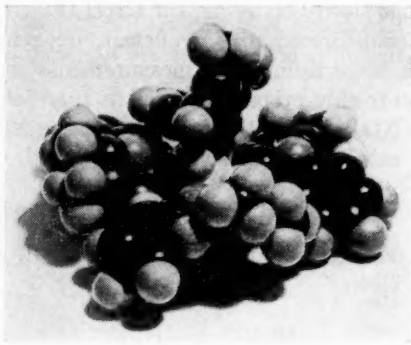

FIG. 3. Fischer-Hirschfelder-Taylor model of $Cr(antipyrine)_6^{3+}$.

If one is willing to assume that H_2 can penetrate these complexes to the extent that is indicated by the models, one can then better understand why there appears to be so little correlation between catalytic efficiency and the size of the complexing groups. A semiquantitative test of this postulate is presented in Table V. The fourth column of the table contains values of the minimum collision distance r, which were evaluated from the geometry of each $Cr(A)_6$ octahedron using the conventional values of covalent and van der Waals' radii and an average radius of 1.3 A for the hydrogen molecule. In this model a sphere of 1.3 A radius is allowed to approach the face of the octahedron at the angle most favorable for closest approach to the chromium atom. In all cases except for the $Cr(NH_3)_6^{3+}$ ion it has been assumed, on the basis of models, that the atom bonded directly to chromium determines the collision distance;

[20] Antipyrine has the structure

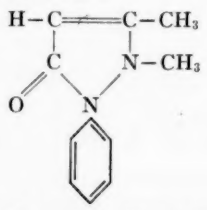

Coordination is sterically possible only at the oxygen atom.

here the hydrogen atoms effectively shield the nitrogen atom and a consideration of their van der Waals radii leads to a somewhat larger value of r.

This minimum collision distance of column four is to be compared with a collision distance $r'=2.9(\mu^2/k^0)^{1/6}$, based upon the assumption that the Wigner theory predicts the correct dependence of rate upon r and u. The agreement shown by $Cr(C_2O_4)_3^{3-}$, $Cr(CN)_6^{3-}$, and $Cr(NH_3)_6^{3+}$ is almost within the accuracy of the experimental data and, while the value of r has not been calculated for the two remaining amines, the direct comparison with the $Cr(NH_3)_6^{3+}$ ion is not too unfavorable since one might expect a trend toward larger values of r'. The greater discrepancy for the thiocyanate complex suggests that its structure may be $Cr(NCS)_6^{3-}$ although a fairly large amount of chemical evidence favors the chromium to sulfur bonding. Since the CrF_6^{3-} ion rapidly loses several fluoride ions through hydrolysis the deviation here is also in the anticipated direction. Values of r have not been calculated for the remaining three ions involving chromium to oxygen bonds since either the oxygen atoms are only partially shielded or the details of their structure are less clearly understood

TABLE IV. The effect of viscosity.

Comp'n. of solvent vol. %	$[Cu^{++}]$ mole, l^{-1}	$\frac{\eta_s}{\eta_{H_2O}}$	$a\cdot10^2$ [a] ml, ml^{-1}	k 1, $mole^{-1}$, min^{-1}
50% Ethylene Glycol	0.181	4.2	1.33	1.2
75% Glycerol	0.173	*ca* 50	0.56	1.1

[a] The value of a for the ethylene glycol solution was obtained by direct measurement, and is uncertain because of experimental difficulties resulting from the viscosity of the solution. The second value of a was estimated from literature data [Seidell, *Solubilities of Inorganic and Metal Organic Compounds* (D. Van Nostrand Company, Inc., New York, 1940), third edition, Vol. 1, p. 561].

than in the other cases. However, their catalytic efficiencies are, as one might predict, somewhat less than that of the $Cr(C_2O_4)_3^{3-}$ ion.

In general, the over-all agreement is all one can expect from so naive a model. A variety of unpublished data confirms that the rate varies linearly with μ^2 but one has no assurance that the other features of the Wigner expression are applicable, even to a first approximation, under these experimental conditions. It is possible that further studies may change the picture considerably but the present data are probably extensive enough to clarify the type of corrections which must be made if one is to predict conversion rates from the conventional atomic radii.

TABLE V. The effect of collision distance.

Complex	Bond	Bond length A	Coll. dist., r A	$r'=2.9\left(\frac{\mu^2}{k^0}\right)^{1/6}$
$Cr(CN)_6^{3-}$	Cr—C	2.02	3.6	3.5
$Cr(NH_3)_6^{3+}$	Cr—N	1.95	3.5	4.4
	$Cr-NH_3$	1.95	4.2	4.4
$Cr(en)_3^{3+}$	...	...	...	4.7
$Cr(pn)_3^{3+}$	...	...	...	4.7
$Cr(C_2O_4)_3^{3-}$	Cr—O	1.91	3.3	3.3
$Cr(urea)_6^{3+}$	...	...	...	3.8
$Cr(H_2O)_6^{3+}$	...	...	...	4.0
$Cr(antip.)_6^{3+}$	...	...	...	4.2
$Cr(SCN)_6^{3+}$	Cr—S	2.29	3.9	3.3
$Cr(F)_6^{3-}$	Cr—F	1.89	3.3	3.8

In discussing the catalytic behavior of these complex ions, we have pictured them as unassociated whereas on the basis of recent work,[21] bivalent and trivalent ions, in the concentration region of our results ($0.02-0.3M$), may form an appreciable number of ion pairs with the oppositely charged ions. However, it is not apparent at this time that the above interpretation of the data would be altered by consideration of the presence of such ion pairs; thus it is known that, in general, the rates of bimolecular reactions involving an uncharged molecule are little affected by ionic strength. In addition, the work of Sachsse[2] and Calvin[9] has established the absence of any important effect of ionic strength upon conversion rate.

It is felt that further discussion of the detailed mechanism of this process can be profitably postponed until the completion of more varied studies which are now in progress. These include a separate comparison of the effects of ionic charge and magnetic moment as well as temperature coefficient studies. A similar series of experiments involving the conversion of ortho-deuterium will also be reported.

ACKNOWLEDGMENTS

We wish to thank Dr. S. S. Dharmatti, who carried out the magnetic measurements contained in this paper, and the ONR for financial support of a large part of this investigation.

[21] Cecil W. Davis, J. Chem. Soc. **137**, 2421 (1930); Martin Linhard, Z. Elektrochem. **50**, 224 (1944); Laitinen, Bailar, Jr., Holtzclaw, Jr., and Quagliano, J. Am. Chem. Soc. **70**, 2999 (1948); A. R. Olson and T. R. Simonson, J. Chem. Phys. **17**, 1167 (1949); E. R. Katzenellenbogen, private communication.

The Microwave Spectra of the Deuterated Methyl Halides*

JAMES W. SIMMONS, *Department of Physics,*

AND

J. H. GOLDSTEIN, *Department of Chemistry, Emory University, Emory University, Georgia*

(Received October 2, 1951)

The hyperfine structure lines of the pure rotational absorption transitions $J=0\rightarrow1$ for CD_3Cl and $J=1\rightarrow2$ for CD_3Br and CD_3I, all in the ground vibrational state, have been measured in frequency and yield the following values of ν_0 in Mc/sec and I_B in g cm$^2\times10^{-40}$, respectively: for CD_3Cl^{35}, 21683.75 and 77.3764; for CD_3Cl^{37}, 21316.86 and 78.7081; for CD_3Br^{79}, 30858.29 and 108.743; for CD_3Br^{81}, 30724.93 and 109.215; for CD_3I, 24161.13 and 138.885. The quadrupole coupling coefficient, eqQ, has been determined for each of these molecules and its variation from eqQ for the corresponding normal methyl halide compound is considered.

I. INTRODUCTION

PRELIMINARY measurements of the pure rotational absorption spectra of CD_3Cl and CD_3I have been reported.[1] The work has been extended to include CD_3Br and absorption line frequencies of all these molecules have been measured with a frequency standard. The study of the series of deuterated methyl halides was begun in the hope that the resulting data could be combined with data already obtained for the normal methyl halides[2] to yield molecular structural parameters without a need for inclusion of less accurate results of infrared studies of these molecules. However, the substitution of deuterium results in a marked difference in the effective length and position of the C—H bond due primarily to the zero-point vibrational energy so that a reliable determination of the H position could not be made. Moreover, determinations of the eqQ values for these deuterated molecules have shown that in all cases this quadrupole coupling coefficient is less than for the corresponding normal methyl halide. The significance of this effect is considered in Sec. IV.

TABLE I. Hyperfine structure of the $J=0$ to $J=1$, $K=0$, rotational transition of CD_3Cl in the ground vibrational state.

F Transition	Frequency (Mc/sec) Observed	Calculated[a]	Relative intensity Observed	Theoretical
	For CD_3Cl^{35}			
$3/2\rightarrow1/2$	21702.36±0.08	21702.35	40	33
$3/2\rightarrow3/2$	21668.88	21668.87	65	67
$3/2\rightarrow5/2$	21687.46	21687.47	100	100
	For CD_3Cl^{37}			
$3/2\rightarrow1/2$	21331.51	21331.51	9	11
$3/2\rightarrow3/2$	21305.15	21305.14	20	22
$3/2\rightarrow5/2$	21319.79	21319.79	34	33

[a] Using values of ν_0 and eqQ as given in Tables IV and V, respectively. Second order quadrupole effects are negligible here.

* Research assisted by a Frederick Gardner Cottrell grant and a grant-in-aid from the University Center in Georgia. The deuterium compounds were obtained from the Texas Research Foundation on allocation from the Isotopes Division, AEC.

[1] J. W. Simmons, Phys. Rev. **76**, 686 (1949).

[2] Gordy, Simmons, and Smith, Phys. Rev. **74**, 243 (1948).

II. APPARATUS

Measurements of the absorption line frequencies were made for each molecule with the gas at a pressure of approximately 10^{-3} mm Hg in an absorption cell composed of 100 feet of coin silver K-band wave guide. The single-crystal detection system was used with low frequency sweeping of the klystron oscillator and low frequency filtering to eliminate the klystron mode contour and reflections in the wave-guide cell. Frequencies were determined with a secondary frequency standard constructed by R. H. Rohrer and W. O. Swan, Jr.,

TABLE II. Hyperfine structure of the $J=1$ to $J=2$ rotational transition of CD_3Br in the ground vibrational state.

F Transition	Frequency (Mc/sec) Observed	Calculated[a]	Relative intensity Observed	Theoretical[b]
	For CD_3Br^{79}			
	$K=0\rightarrow K=0$			
$1/2\rightarrow1/2$	30858.24±.10	30858.29	16	14
$1/2\rightarrow3/2$	31002.43	31002.39	12	14
$3/2\rightarrow3/2$	30743.99	30743.91	13	18
$3/2\rightarrow5/2$	30846.00	30845.98	100	100
$5/2\rightarrow7/2$	30846.00	30846.06		
$5/2\rightarrow5/2$	30898.82	30989.80	13	15
	$K=1\rightarrow K=1$			
$3/2\rightarrow3/2$	30916.21	30916.28	10	14
$3/2\rightarrow5/2$	30967.53	30967.47	27	28
$5/2\rightarrow5/2$	30895.58	30895.59	13	12
$5/2\rightarrow7/2$	30823.44	30823.41	61	54
	For CD_3Br^{81}			
	$K=0\rightarrow K=0$			
$1/2\rightarrow1/2$	30724.89	30724.93	18	14
$3/2\rightarrow3/2$	30629.28	30629.35	25	18
$3/2\rightarrow5/2$	30714.74	30714.71	92	100
$5/2\rightarrow7/2$	30714.74	30714.65		
$5/2\rightarrow5/2$	30834.73	30834.72	12	15
	$K=1\rightarrow K=1$			
$1/2\rightarrow3/2$	30665.35	30665.40	9	11
$3/2\rightarrow3/2$	30773.17	30773.24	10	14
$3/2\rightarrow5/2$	30815.96	30816.01	17	28
$5/2\rightarrow5/2$	30756.12	30755.99	15	12
$5/2\rightarrow7/2$	30695.83	30695.76	65	54

[a] Using values of ν_0 and eqQ as given in Tables IV and V, respectively. Both first- and second-order nuclear effects are included as well as a stretching term $-2D_{JK}(J+1)K^2$ with $D_{JK}=39$ kc/sec.

[b] The factor $\nu\exp(-E_r/kT)$ is neglected in the calculations.

which employed electronic tube multipliers to convert the output of a 1 Mc/sec crystal controlled oscillator to 810 Mc/sec and a silicon crystal to furnish harmonics in the desired frequency region. The base oscillator was continuously monitored against WWV and interpolation between standard markers spaced 54 Mc/sec apart was accomplished with a calibrated radio receiver. An electronic switch allowed the absorption lines and standard markers to be displayed on an oscilloscope on separate traces, thus making possible more accurate marker settings. Relative intensities of the absorption lines for each molecule were determined by visual comparisons of line heights.

III. RESULTS

As was the case with the normal methyl halides, the shifts of the hyperfine structure absorption lines from the undisplaced rotational absorption line frequency, ν_0, include both first-[3] and second-order[4] quadrupole effects in CD_3Br and CD_3I. The second-order effects are negligible in CD_3Cl. Table I lists the frequencies and relative intensities of the hyperfine structure components for the $J=0$ to $J=1$ rotational transition for CD_3Cl while Tables II and III give the same data for CD_3Br and CD_3I, respectively. A comparison of observed with calculated line frequencies shows that use of the second-order theory of Bardeen and Townes[4] results in good agreement. For each case the relative intensities of the lines for $K=0$ and for $K=1$ agree well with the values predicted using Dennison's equations[5] with the value $I=1$ for the spin of deuterium.

TABLE III. Hyperfine structure of the $J=1$ to $J=2$ rotational transition of CD_3I in the ground vibrational state.

F Transition	Frequency (Mc/sec) Observed	Calculated[a]	Relative intensity Observed	Theoretical[b]
		$K=0\rightarrow K=0$		
3/2→1/2	24277.13±0.08	24277.17	25	18
3/2→3/2	24029.16	24029.10	31	26
5/2→3/2	24608.61	24608.60	8	11
5/2→5/2	24336.26	24336.27	25	34
5/2→7/2	24235.67	24235.68	50	47
7/2→7/2	23831.16	23831.20	31	26
7/2→9/2	24203.19	24203.13	95	92
		$K=1\rightarrow K=1$		
3/2→1/2	24493.36	24493.35	13	20
3/2→3/2	24373.36	24373.40	19	28
3/2→5/2	24232.16	24232.16	25	19
5/2→3/2	24081.25	24081.30	18	12
5/2→5/2	23940.01	23940.05	36	37
5/2→7/2	23893.51	23893.45	50	51
7/2→7/2	24097.49	24097.49	36	29
7/2→9/2	24279.89	24279.89	100	100

[a] Calculated using $\nu_0=24161.13$ Mc/sec and $eqQ=-1929$ Mc/sec. Both first- and second-order nuclear effects are included as well as a stretching term $-2D_{JK}(J+1)K^2$ with $D_{JK}=47$ kc/sec.
[b] The factor $\nu\exp(-E_r/kT)$ is neglected in the calculations.

TABLE IV. Values of ν_0, B_0, and I_B for the deuterated methyl halides.

Molecule	J Transition	ν_0 (Mc/sec)	B_0[a] (Mc/sec)	I_B[b] ($\times10^{-40}$ g cm^2)
CD_3F[c]	0→1	40899.54	20449.83	41.0226
CD_3Cl^{35}	0→1	21683.75	10841.88	77.3764
CD_3Cl^{37}	0→1	21316.86	10658.43	78.7081
CD_3Br^{79}	1→2	30858.29	7714.57	108.743
CD_3Br^{81}	1→2	30724.93	7681.23	109.215
CD_3I	1→2	24161.13	6040.28	138.885

[a] Calculated by using as a first approximation to the centrifugal distortion constant D_{JK} the values listed under Tables II and III.
[b] Calculated using $h=6.62373\times10^{-27}$ erg sec.
[c] Private communication from Johnson, Trambarulo, and Gordy.

In Table IV are listed the ν_0, B_0, and I_B values for each of the molecules. In each case B_0 and the resulting I_B have been calculated without making any correction for the centrifugal distortion constant D_J. The estimated D_{JK} values used are listed under Tables II and III. Judging from the preliminary and final determinations of the centrifugal distortion constants for the normal methyl halides[2,6] it might be expected that the values used here are too low and that the B_0 values are, consequently, too low. Work is now in progress to determine the distortion constants accurately for all the d-methyl halides listed here.† The effect of the zero-point vibrational energy is demonstrated in each molecule by the observed value of ν_0 being of the order of 90 Mc/sec higher than the value calculated from structural parameters for the corresponding normal methyl halide.

IV. QUADRUPOLE COUPLING CONSTANTS

The quadrupole coupling constants of the d-methyl halides are presented in Table V together with values for the normal methyl halides for purposes of comparison. For I and the two Br isotopes identical values of eqQ were obtained from the K=0 and K=1 multiplets separately. All observed hyperfine structure lines agreed with the frequencies calculated from the tabulated values of eqQ to within the estimated experimental error of 0.09 Mc/sec.

The most striking feature of these results is that in all cases the eqQ value is less for the deuterated compound

TABLE V. Comparison of values of eqQ for the methyl halides and d-methyl halides.

X	eqQ(Mc/sec) CD_3X	CH_3X[2]	δ(eqQ) (Mc/sec)	δ(eqQ)/eqQ
Cl^{35}	−74.41	−75.13	0.72	0.97%
Cl^{37}	−58.58	−59.03	0.45	0.77
Br^{79}	574.6	577.0	2.4	0.42
Br^{81}	479.8	482.0	2.2	0.46
I^{127}	−1929	−1934	5	0.26

[3] J. Bardeen and C. H. Townes, Phys. Rev. **73**, 97 (1948).
[4] J. Bardeen and C. H. Townes, Phys. Rev. **73**, 627 (1948).
[5] D. M. Dennison, Revs. Modern Phys. **3**, 280 (1931).
[6] J. W. Simmons and W. E. Anderson, Phys. Rev. **80**, 338 (1950).
† Preliminary measurements of the $J=5$ to $J=6$ rotational transition of CD_3I yield values for D_J and D_{JK} of approximately 6.0 kc/sec and 66.0 kc/sec, respectively.

than for the corresponding normal methyl halide and, moreover, the percentage decrease diminishes with increasing weight of the halogen. In the case of the Br and I compounds the effect is considerably outside the estimated experimental error, based on a maximum error of 0.1 Mc/sec per measurement of hyperfine structure frequencies. In the case of Cl, the probable error in eqQ is somewhat smaller than the observed decrease.

A reasonable qualitative explanation of the observed effects is that substitution of deuterium for hydrogen in the methyl halides alters their normal vibrations and hence changes the averaging of q over the ground vibrational states of these molecules. Because of the anharmonicity of the carbon-halogen motions the substitution of deuterium decreases the effective carbon-halogen separation with the probable result that the asymmetry of the charge distribution at the nucleus is reduced. In addition, because of the lower zero-point energy of the heavier compounds the amplitude of the nuclear vibrations is decreased, which affects the averaging of q in a complicated manner. Both of these effects are difficult to estimate quantitatively but such an explanation is supported by the fact that the percentage change in eqQ decreases with increasing weight of the halogen. This is consistent with the fact that the change in reduced mass decreases with increasing weight of the halogen. Work is being continued on the quantitative estimation of these effects and the results will be reported later.

The authors wish to express their appreciation to Professor E. B. Wilson, Jr., and to Dr. J. K. Bragg for valuable discussions in connection with the interpretation of the quadrupole coupling data and to Mr. W. O. Swan, Jr., for assistance with some of the measurements.

THE JOURNAL OF CHEMICAL PHYSICS VOLUME 20, NUMBER 1 JANUARY, 1952

Energy Levels and Rate Processes in the Thallium Activated Potassium Chloride Phosphor

PETER D. JOHNSON AND FERD E. WILLIAMS
General Electric Research Laboratory, Schenectady, New York

(Received August 3, 1951)

The dependence of spectral distribution and intensity of emission of KCl: Tl on temperature and excitation wavelength are correlated with absorption data and theoretical calculations to provide a detailed picture of the energy relationships in this phosphor. The two principal excited states are the $^1P_1^0$ and $^3P_1^0$ states of Tl^+ and are found to be approximately in thermal equilibrium with each other. The equilibrium is disturbed by emission, and the 4750A emission is favored by 1960A excitation and the 3050A emission is favored by 2470A excitation. The former processes are attributed to $^1P_1^0 \leftrightarrow {}^1S_0$ transitions; the latter, to $^3P_1^0 \leftrightarrow {}^1S_0$ transitions. The rate processes are formulated and the specific rate constants deduced. The presence of Tl^+ or Cd^{++} adjacent to the activator induces additional excitation and emission bands. The activation energy for radiationless de-excitation has been computed theoretically and found to be in accord with experiment.

I. INTRODUCTION

THALLIUM activated potassium chloride has two principal emission bands[1] with peaks at 3050A and 4750A and a less prominent one in evidence at high activator concentrations and low temperatures at 3775A. It has two principal absorption bands[2] at 2470A and 1960A with a subsidiary one at 2060A. In addition, at high activator concentrations, evidence will be presented for a weak absorption band near 2575A. The relative intensities of the emission bands depend on temperature and to some extent on the wavelength of excitation; and the relative intensities of both absorption[3] and emission bands depend on activator concentration. It is our purpose to establish the quantitative energy and rate process relationships among the ground and excited states which govern the luminescent properties of this phosphor. The problems to be considered include the assignment of absorption and emission bands to transitions between the known states of the thallous ion and the determination of the principles which govern the transitions between various states.

The previously available information on this problem is limited. The 3775A emission peak it has been shown[1] is probably due to interaction between nearby activators. On theoretical grounds[4] the 2470A absorption and 3050A emission have been assigned to transitions between the $^1S_0$ ground state and the $^3P_1^0$ excited state; and the energy-configuration relations for these two states are known in detail from the fundamental calculations.

The results of measurements of excitation dependence

[1] P. D. Johnson and F. E. Williams, J. Chem. Phys. **18**, 1477 (1950).
[2] R. Hilsch, Z. Phys. **44**, 860 (1927).
[3] W. Koch, Z. Phys. **57**, 638 (1929).
[4] F. E. Williams, J. Chem. Phys. **19**, 457 (1951).

of emission spectrum, temperature dependence of emission intensity of the 3050 and 4750A emission bands at low temperatures and the efficiency of the 3050A emission as a function of temperature at high temperatures will be reported. These results will be correlated with previously known absorption and emission data and the theoretical conclusions to give a detailed quantitative treatment of the relationships among the energy levels of the thallous ion in potassium chloride.

II. EXPERIMENTAL

Measurements of emission intensity as a function of temperature were obtained by integrating the emission curves obtained with a G. E. recording grating spectroradiometer. A G. E. 4-watt germicidal lamp, yielding predominantly 2537A radiation, was used for excitation. For emission measurements above 298°K, a thin layer of the powdered phosphor and a thermocouple were clamped between two 1-mm thick quartz plates and heated by a 300-watt calrod unit. For measurements from 77 to 298°K the sample and thermocouple were held in place against a copper block by a quartz disk and metal retaining ring. The chamber containing the sample and thermocouple was evacuated and the copper block which extended into this chamber through a Fernico seal was cooled from the outside by liquid nitrogen. Excitation and emission radiation passed through a quartz window in the vacuum chamber. The heat capacity of the copper block was such that several hours were required for it to warm up to 298°K. This permitted the measurement of emission spectra at all temperatures from 77°K to 298°K. As a check on the accuracy of this procedure, the emission at 195°K was obtained using dry ice-acetone as a coolant, giving excellent agreement with the spectrum at this temperature obtained during the warm-up from 77°K. In all cases at least 1.5 cm of the 5-mil thermocouples were exposed to the temperature at the surface of the phosphor. A check of these measurements was obtained in an entirely different apparatus in which filters, rather than the spectroradiometer, were used to separate the emission peaks. Good agreement was obtained.

Emission spectra at 77°K of KCl:Tl containing amounts of Ca^{++}, Ba^{++}, Sr^{++} or Cd^{++} and $O^{=}$, varying from 0.0001 to 0.01 mole fraction in the melt, were recorded to determine the effect of cation and anion vacancies. The oxide was introduced as KNO_3, which decomposed to oxide on fusing in KCl. All samples were prepared by fusing the ingredients.

The excitation dependence of the emission spectrum of KCl:Tl was obtained by irradiating the sample with U.V. at 2470A, 2060A and 1960A and measuring the ratio of intensities of 3050A and 4750A emission using Corning filters 9863 and 3080 to separate the two bands and 1 mm of Pyrex to keep the excitation U.V. from reaching the photomultiplier. Over limited ranges of wavelength excitation spectra were obtained. The quantum output of the monochromator used as the source of excitation was measured as a function of wavelength with a Cs–Sb photocell previously calibrated against a thermocouple for spectral sensitivity.

The monochromator is a vacuum instrument employing a one meter concave reflecting grating used near normal incidence with geometry similar to the instrument described by Parkinson and Williams[5] and a low voltage hydrogen discharge lamp, with no window, clamped directly to the entrance slit. Proper pressures of hydrogen for operation of the lamp (~2 mm) are maintained in the system by leaking hydrogen in continuously through an electrically heated palladium tube and pumping it out through a capillary 2 mm in diameter and 10 cm long. Since this instrument furnishes usable intensities down to 1050A, quartz or other appropriate filters are placed at the exit slit when measurements at wavelengths longer than 2100A are being made. A 5819 photomultiplier sensitized with a mixture of $ZnSiO_4$:Mn and $CaSiO_4$:Mn is used to measure radiation shorter than 3000A. ZnS:Mn is used for radiation in the neighborhood of 3000A and the unsensitized photomultiplier for wavelengths longer than 4000A.

The purity of the KCl and TlCl used in the preparation of the phosphors has been ascertained spectroscopically. In addition, crystals of the pure KCl have been prepared, like the phosphor crystals used in the absorption and excitation measurements, in a furnace described elsewhere[6] similar to the design of Strong.[7] Optical absorption was determined. Both absorption and spectroscopic examination indicate negligible impurities in the KCl. The TlCl has less than 0.1 percent of Pb, barely detectable Cu and no Ag, Hg or transition elements.

III. RESULTS AND DISCUSSION

A. Effect of Vacancies and Divalent Ions

Although previous work[1,4] indicates that all of the emission bands of KCl:Tl are due to the presence of Tl^+ and that the 3050A peak is due to transitions between energy levels characteristic of the isolated Tl^+ ion, the precise origin of the 3775A and 4750A emitting levels and their relation to the 3050A emitting and unexcited states has not been completely understood. In order to determine whether lattice vacancies have any role in the longer wavelength emission processes, the emission spectra of phosphors in which both cation and anion vacancies were introduced, by deliberate addition of divalent cations and anions, were obtained at 77°K. At divalent anion and cation concentration of 0.01 mole percent there is no effect on the luminescent properties of KCl:0.004Tl or KCl:0.0004Tl although this corresponds to increase of several orders of magni-

[5] W. W. Parkinson, Jr., and F. E. Williams, J. Opt. Soc. Am. **39**, 705 (1949).
[6] P. D. Johnson, Ceramic Age **58**, 32 (1951).
[7] J. Strong, Phys. Rev. **36**, 1663 (1930).

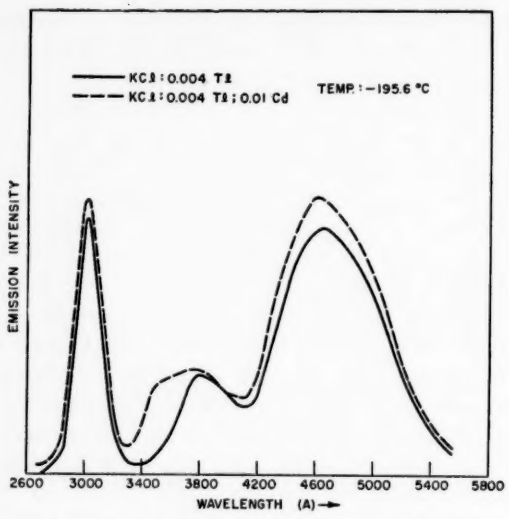

FIG. 1. Emission spectrum of KCl:0.004Tl with and without Cd^{++}.

tude in vacancy concentration. This is in agreement with the interpretation[1] that the 3050A and 4750A emission arise from isolated Tl^+ and that the 3775A emission results from increasing the transition probability for a forbidden emission process in Tl^+ by interaction with nearby Tl^+ ions.

At higher Cd^{++} concentration in KCl:0.004 Tl an additional weak emission on the short wavelength side of the 3775A emission was discovered as shown in Fig. 1. This was attributed to a $Tl^+ - Cd^{++}$ interaction increasing the transition probability for the same process responsible for the 3775A emission but with modification of the transition energy by coulomb interaction effects, and it was predicted that decreasing the Tl^+ concentration would yield enhancement of the new emission band relative to the 3775A band. This is demonstrated experimentally in Fig. 2.

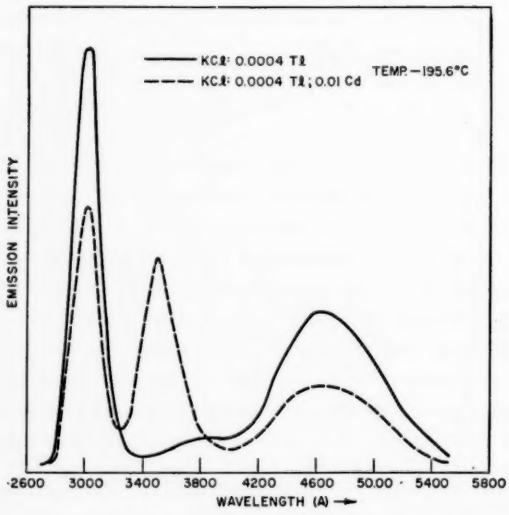

FIG. 2. Emission spectrum of KCl:0.0004Tl with and without Cd^{++}.

B. Identification of Energy Levels

It is important for the complete understanding of KCl:Tl to identify the states responsible for the absorption and emission bands. From theoretical considerations[4] the 2470A absorption and 3050A emission have been assigned to transitions between $^1S_0$ and $^3P_1^0$ levels of Tl^+. The dependence of spectral distribution of emission on excitation wavelength confirm this conclusion. The 3050A emission is favored by excitation in the 2470A absorption band; and conversely the 4750A emission is favored by either of the shorter wavelength bands. Since the 1960 and 2060A absorption overlap as shown in Fig. 3, it is not possible to identify from excitation data precisely which of these are directly related to the 4750A emission. Defining R_λ as the ratio of 4750A to 3050A emission intensity with excitation by wavelength λ, R_{1960}/R_{2470} is found experimentally to be 1.10 at 298°K.

From the selection rules, the 2470A absorption is attributed to the $^1S_0 \rightarrow {}^3P_1^0$ transition and the strong

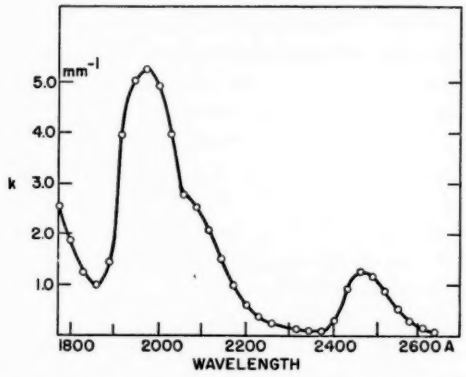

FIG. 3. Optical absorption of KCl:0.00002Tl at 298°K.

1960A absorption is attributed to the $^1S_0 \rightarrow {}^1P_1^0$ transition. The 3050A and 4750A emission are associated with $^3P_1^0 \rightarrow {}^1S_0$ and $^1P_1^0 \rightarrow {}^1S_0$ transitions, respectively, because of the dependence of emission distribution on excitation wavelength.

The 3775A and 5800A emission[1,8] with high Tl^+ concentration and the 3500A emission are believed to arise from $^3P_2^0 \rightarrow {}^1S_0$ and $^3P_0^0 \rightarrow {}^1S_0$. There is weak absorption at 2060A as shown in Fig. 3. Also, Fig. 4 shows evidence in the excitation spectrum for the existence of another weak absorption band at 2575A. The width of the 2470A absorption band at 298°K for concentrations of Tl^+ less than 0.02 mole percent, in accord with previous work,[2,3,9] is about 110A. At higher concentrations, there is a broadening to 170A suggesting an additional absorption band. The existence of this band is confirmed by the excitation spectra of Fig. 4. Normalized values of I_{3050} and I_{4750} are given for constant excitation intensity over a spectral region where the quantum output

[8] P. Pringsheim, Revs. Modern Phys. **14**, 132 (1942).
[9] P. D. Johnson and F. J. Studer, Phys. Rev. **82**, 976 (1951).

of the monochromator is known. Excitation at 2575A becomes even more pronounced at higher activator concentration, however, b of Fig. 4 shows most clearly the coexistence of the two excitation bands. The $^1S_0 \rightarrow {}^3P_2{}^0$ and $^1S_0 \rightarrow {}^3P_0{}^0$ transitions probably account for the 2060 and 2575A absorption bands.

C. Temperature Dependence of Emission

Excitation in any of the four absorption bands results in emission in all the emission bands of KCl:Tl. The relative intensities of the emission bands depend on temperature as well as on excitation wavelength and activator concentration. Figure 5 shows the dependence of the ratio of intensities of the two principal emission bands on temperature, with 2537A excitation. Assuming thermal equilibrium between the $^3P_1{}^0$ and $^1P_1{}^0$ states, the average slope of the function corresponds to an energy difference of 0.021 ev and the ratio of transition probabilities for 3050A to 4750A, A_2/A_1, is approximately 6. The knowledge of this energy difference

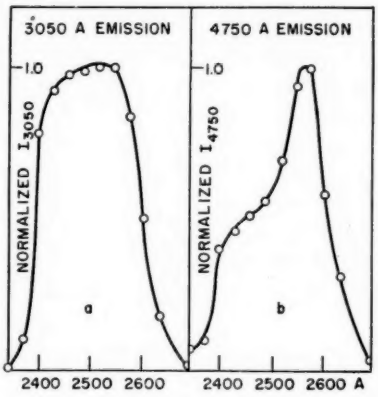

FIG. 4. Excitation spectra of KCl:0.00027Tl.

along with the theoretical energy-configuration diagram[4] of these states and the assignment of energy levels indicated leads to the arrangement of energy levels shown in Fig. 6. The total energy of the system is plotted against the activator-nearest neighbor distance for the $^1S_0$, $^3P_1{}^0$ and $^1P_1{}^0$ states. All ions outside of the nearest neighbors rearrange to positions of minimum energy. The $^1S_0$ and $^3P_1{}^0$ are the calculated curves modified so as to coincide as nearly as possible with experimental absorption and emission. The $^1P_1{}^0$ is constructed from the position of the absorption and emission peak, and the difference in minimum energy of the $^3P_1{}^0$ and $^1P_1{}^0$ as determined from the data of Fig. 5.

Although thermal equilibrium has been assumed in the calculation of the energy difference of the emitting states, a dependence of emission distribution on excitation wavelength demonstrates a small departure from equilibrium. This arises from transition probabilities for emission A_1 and A_2 not being negligible compared to the rate constants k_1 and k_2 for transfer from one excited state to another.

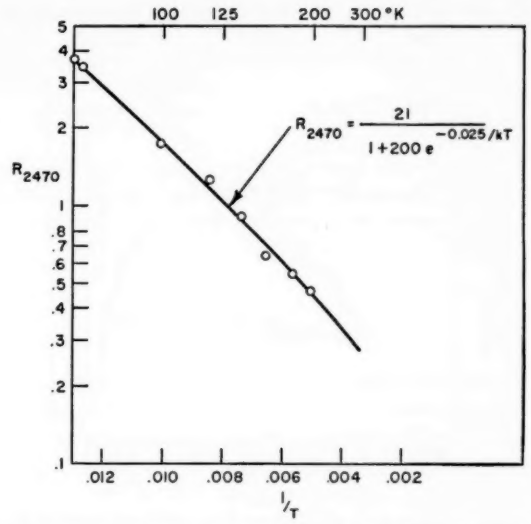

FIG. 5. Ratio of 4750A and 3050A emission intensities with 2537A excitation as a function of temperature.

In order to evaluate quantitatively the dependence of the relative emission intensities on temperature and excitation band, an investigation of the rates of the various processes involved is necessary. With excitation by 1960A radiation to the $^1P_1{}^0$ state, the rate of change of occupation with no radiationless de-excitation is:

$$dn_1/dt = J_1N + k_2n_2 - k_1n_1 - A_1n_1 \qquad (1)$$

where J_1 is the excitation intensity, N the number of absorbing centers per unit volume, n_2 the number of occupied $^3P_1{}^0$ states, n_1 the number of occupied $^1P_1{}^0$ states and A_1 the transition probability for emission from $^1P_1{}^0$. Similarly:

$$dn_2/dt = k_1n_1 - k_2n_2 - A_2n_2. \qquad (2)$$

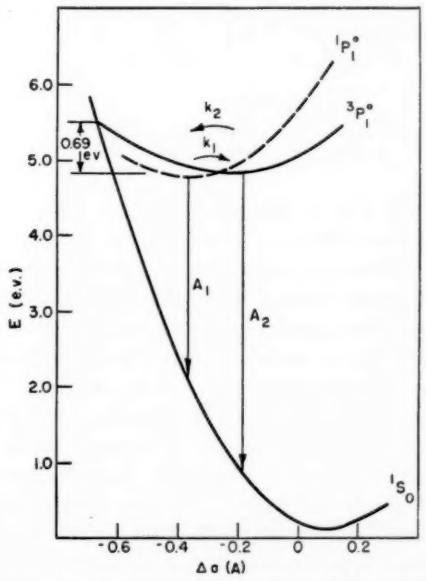

FIG. 6. Potential energy *versus* change in Tl^+ nearest Cl^- neighbor distance for states of Tl^+ in KCl:Tl.

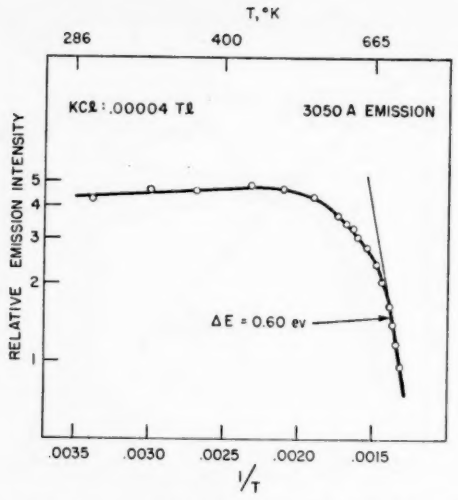

FIG. 7. Efficiency of 3050A emission of KCl:0.00004Tl as a function of temperature.

A_1n_1 and A_2n_2 are the intensities of emission, I_{4750} and I_{3050}, from the $^1P_1^0$ and $^3P_1^0$ states, respectively. Under steady-state conditions, Eqs. (1) and (2) yield

$$(I_{4750}/I_{3050})_{1960}=R_{1960}=A_1(A_2+k_2)/A_2k_1. \quad (3)$$

Similarly, under 2470A excitation:

$$(I_{4750}/I_{3050})_{2470}=R_{2470}=A_1k_2/A_2(A_1+k_1). \quad (4)$$

The rate constants k_1 and k_2 have the form:

$$k_i=s_ie^{-\epsilon_i/kT}, \quad (5)$$

where s_1 and s_2 are the frequency factors for passage from state 1 to state 2 and the reverse process, respectively; and ϵ_1 and ϵ_2 are the corresponding activation energies. Equations (3) and (4) become

$$R_{1960}=\left(\frac{A_1}{s_1}\right)e^{\epsilon_1/kT}+\left(\frac{A_1}{s_1}\right)\left(\frac{s_2}{A_2}\right)e^{-(\epsilon_2-\epsilon_1)/kT}, \quad (6)$$

$$R_{2470}=\frac{(s_2/A_2)e^{-\epsilon_2/kT}}{1+(s_1/A_1)e^{-\epsilon_1/kT}}. \quad (7)$$

The data of Fig. 5 show a departure from a straight line. From the difference in energies of the $^3P_1^0$ and $^1P_1^0$ states and the ratio of transition probabilities for emission calculated on the basis of thermal equilibrium it is possible by successive approximations to determine the values of s_1/A_1, s_2/A_2, ϵ_1, and ϵ_2 in Eq. (7) which fit the data within the experimental error. These are 200, 21, 0.025 ev and 0 ev, respectively. Confirmation of the validity of these quantities is obtained by using them in Eq. (6) and (7) at 298°K to determine $R_{1960}/R_{2470}=1.07$ as compared with the experimentally determined 1.10. From a consideration of these values, it is evident that true thermal equilibrium is not established, but is a good approximation. This formulation has not included the effects of the $^3P_2^0$ and $^3P_0^0$ levels. Its extension to include these levels is obvious.

D. Radiationless De-Excitation

Corresponding to the thermal accessibility of each excited state from the others, there is at high temperatures the possibility of reaching the ground state from the excited levels thermally with no optical transition. Figure 6 shows the way in which the analytical expressions obtained from fundamental calculations[4] for the energy of the $^1S_0$ and $^3P_1^0$ states of Tl^+ in KCl as a function of activator nearest neighbor distance intersect. By solving the two simultaneous equations for the common point, one can calculate the height of the energy barrier for going by a radiationless process from the $^3P_1^0$ to the $^1S_0$ state. From the equations given in reference 4, a value of 0.69 ev is obtained.

By measuring the efficiency of the 3050A emission as a function of temperature at elevated temperatures, this activation energy can be determined experimentally. The results of this measurement are shown in Fig. 7. The high temperature portion of the curve of intensity on a logarithmic scale *vs* $1/T$ corresponds to an activation energy of 0.60 ev in good agreement with the theoretical value. An error of 10 percent could be expected in either the theoretical calculation or the experimental result. The frequency factor for this process is of the order of 10^{12} sec^{-1} or greater, as contrasted to approximately 10^7 sec^{-1} for the frequency factors for transfer from one excited state to the other. An interesting feature is the gradual realization of the high temperature slope. This may be explained by the approach of the other excited states to points lower on the ground-state curve.

IV. CONCLUSIONS

It is concluded that the 1960A absorption and the 4750A emission arise from $^1P_1^0 \leftrightarrow {}^1S_0$ transitions and the 2470A absorption and 3050A emission, from $^3P_1^0 \leftrightarrow {}^1S_0$ transitions in Tl^+ isolated from impurities in KCl. A tendency toward equilibrium between the two principal states of the excited system is modified by emission.

It is confirmed that the 3775A emission arises from Tl^+ interacting with other Tl^+. A new emission band at 3500A is attributed to Tl^+ interacting with Cd^{++}.

The quantitative agreement of the experimental and theoretical activation energies for radiationless de-excitation demonstrates the process is localized to Tl^+ and extends the applicability of the configuration coordinate model.

V. ACKNOWLEDGMENTS

The authors are indebted to Dr. F. J. Studer and Miss G. Lloyd for emission spectra measurements, and to Mr. L. Harris and Mr. M. Zucker for preparation of many of the phosphors.

The Diamagnetism of Ammonium Ion

MATA PRASAD, C. R. KANEKAR, D. D. KHANOLKAR, AND M. G. DATAR
Chemical Laboratories, Institute of Science, Bombay, India

(Received October 1, 1951)

A linear relation between the molar susceptibilities of inorganic and organic salts of Li, NH_4, and K containing a common anion and the number of electrons in the cations has been established. This relation has been used to deduce susceptibilities of ammonium ion and inorganic and organic anions in combination with it.

THE NH_4 radical, though composed of five atoms, behaves as a single unit in its physical and chemical properties and the ammonium salts resemble the salts of alkali metals in isomorphism, solubility, and hydroscopic nature. Since the chemical properties of elements are the result of the electrons in the ultimate and penultimate shells, the similarity between ammonium salts and the salts of the alkali metals is because of the fact that the ammonium radical contains nine electrons in the outermost shell, one more than required to make the stable group of eight. This electron is, therefore, given up in the formation of a compound, leaving the ammonium ion with a single positive charge and electronic configuration similar to that of sodium ion.

Kido,[1] Trew,[2,3] and Gray and Farquharson[4] have reported the susceptibilities of some ammonium salts. The work of Kido and Trew aimed at finding out the susceptibility of ammonium ion, while Gray and Farquharson attempted to establish the molecular structure of ammonium halides and some substituted ammonium salts. The authors have measured the magnetic susceptibilities of a large number of ammonium salts of inorganic and organic acids with a view to examine the behavior of ammonium ion in these salts.

TABLE I.

Compounds	x_a	x_m
Ammonium chloride	0.605	32.37
Ammonium bromide	0.435	42.59
Ammonium iodide	0.413	59.84
Ammonium nitrate	0.343	27.45
Ammonium sulfate	0.429	56.63
Ammonium carbonate	0.443	42.53
Ammonium formate	0.413	26.02
Ammonium acetate	0.534	41.13
Ammonium propionate	0.567	51.60
Ammonium butyrate	0.604	63.42
Ammonium oxalate, H_2O	0.452	64.18
		51.22 (anhydrous)
Ammonium malonate	0.454	62.65
Ammonium succinate	0.504	76.61
Ammonium benzoate	0.561	77.98
Ammonium salicylate	0.558	86.49
Ammonium citrate	0.451	109.5
Ammonium cinnamate	0.597	98.51

[1] K. Kido, Sci. Repts. Tohoku Imp. Univ. **21**, 149 (1932).
[2] V. C. G. Trew, Trans. Faraday Soc. **32**, 1658 (1936).
[3] V. C. G. Trew, Trans. Faraday Soc. **37**, 476 (1941).
[4] F. W. Gray and J. Farquharson, Phil. Mag. **10**, 191 (1930).

EXPERIMENTAL

Some of the ammonium salts studied in this investigation were obtained as Merck's extra pure compounds. Those which were pure products of Merck were crystallized out three times from distilled water. The others were prepared in the laboratory and were used only after ascertaining their purity. The magnetic susceptibilities were measured on a modified form of Gouy's balance, details of which have been described by Prasad, Dharmatti, and Gokale.[5] The susceptibilities of the hygroscopic salts were measured in solution at four different concentrations, and the values of the solid salts were obtained by plotting the susceptibilities of the solutions (x_{sol}) against the concentrations (C_s), assuming the validity of the mixture law ($x_{sol}=x_{solute}C_s+(1-C_s)x_{H_2O}$) in these cases. All the measurements were made relative to KCl ($x_a=-0.516\times10^{-6}$) in the case of solids and conductivity water ($x_{H_2O}=-0.72$

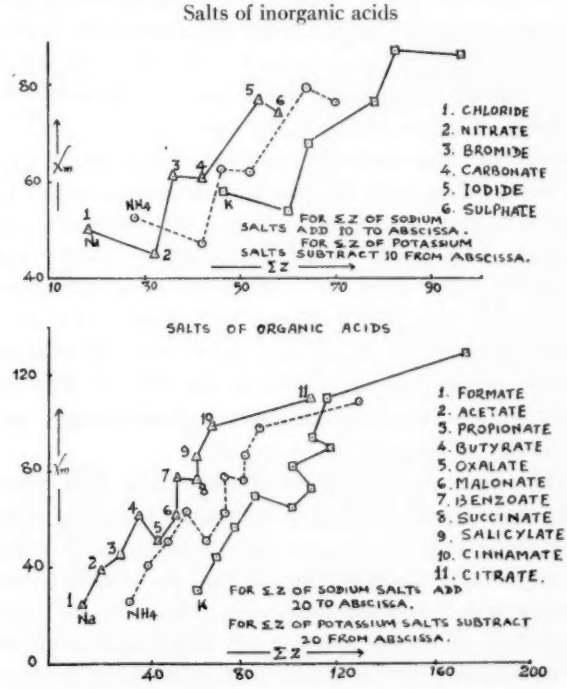

FIG. 1. Values of molar susceptibilities plotted against total number of electrons.

[5] Prasad, Dharmatti, and Gokhale, Proc. Indian Acad. Sci. **20**, 224 (1944).

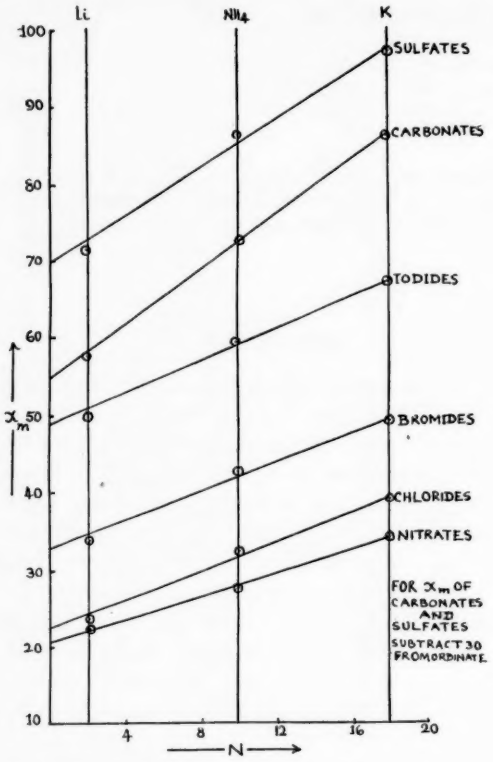

FIG. 2. Values of molar susceptibilities plotted against number of electrons in the cation.

$\times 10^{-6}$) in the case of solutions. All the necessary precautions such as (1) placing the specimen tube always in the same position and in such a way that one end of it lay exactly at the center of the field and the other end in a region where the field was negligible, (2) packing the substance as uniformly and as tightly as possible for every filling, and (3) keeping the field constant by having a rigorous check on the current feeding the magnet, were taken in the measurement of the susceptibilities. In order to average the error caused by packing, if any, measurements were made with three fillings of the same substance, and an average of three closely agreeing values of the susceptibility thus obtained was taken as the final value of the specific susceptibility of the substance.

The values of the susceptibilities of the ammonium salts are given in Table I in which the following notations have been used: x_a = specific susceptibility and x_m = molecular susceptibility. In the case of ammonium oxalate which is a hydrated salt, the molecular susceptibility of the anhydrous salt has been calculated by subtracting the molecular susceptibility of water of crystallization ($x_{H_2O} = -12.96 \times 10^{-6}$) from the molecular susceptibility of the hydrate, assuming strict additivity. All the susceptibility values have been expressed in terms of -1×10^{-6} cgs unit.

DISCUSSION OF RESULTS

Prasad and co-workers[6,7] have shown that in the case of salts of (1) Ca, Sr, Ba, and (2) Mg, Zn, Cd, and Hg, with inorganic and organic acids, the patterns obtained by plotting x_m of these salts against $\sum Z$ are characteristic of the group or subgroup of the periodic table to which the cations belong. Since ammonium salts closely resemble salts of alkali metals in their chemical behavior, the graphs of x_m against $\sum Z$ have been drawn for ammonium and alkali salts of organic and inorganic acids and are shown in Fig. 1.

It will be seen that the patterns obtained for the alkali salts of inorganic and organic acids are strikingly similar to those obtained by joining the corresponding points for the ammonium salts of these acids.

SUSCEPTIBILITIES OF INORGANIC AND ORGANIC ANIONS AND AMMONIUM ION

Prasad and co-workers[7] have shown that a series of straight lines are obtained on plotting the molecular susceptibilities (x_m) of the salts of alkali and alkaline

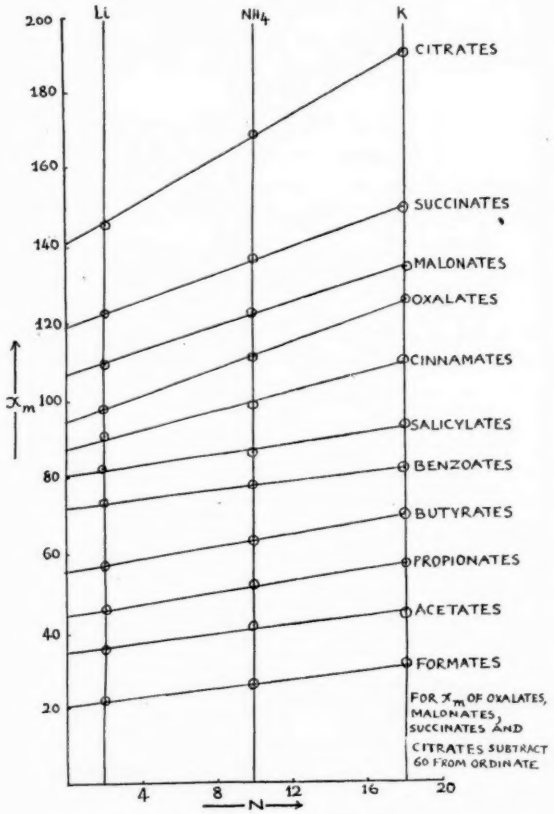

FIG. 3. Values of molar susceptibilities plotted against number of electrons in the cation.

[6] Prasad, Dharmatti, and Kanekar, Proc. Indian Acad. Sci. **16**, 301 (1942); Prasad, Dharmatti, and Gokhale **20**, 224 (1944); Prasad, Dharmatti, and Amin **26**, 312 (1947); Prasad, Dharmatti, Kanekar, and Bhobe **31**, 289 (1950).

[7] Prasad, Dharmatti, and Ghose, J. Chem. Phys. **17**, 819 (1949); Prasad, Kanekar, Walvekar, and Khanolkar **18**, 936 (1950); Prasad, Dharmatti, Kanekar, and Khanolkar **18**, 941 (1950).

earth metals with inorganic and organic acids, containing a common anion, against the total number of electrons (N) in the cation. It has been shown earlier that the magnetic behavior of ammonium salts is similar to that of alkali salts. Moreover, ammonium and sodium ions are electronic isomers. As the x_{m-N} relation holds for the salts of chemically related cations, it was thought that it would also hold for the salts of lithium, ammonium, and potassium ions. For this purpose it is necessary to have reliable data on the susceptibilities of the corresponding salts of lithium and potassium. A set of widely divergent values of the susceptibilities of the alkali salts of inorganic acids has been reported in the literature. According to Trew the values of the lithium halides reported by Brindley and Hoare[8] are more reliable than those of any other worker. The authors have, therefore, chosen these values. As the susceptibilities of Li_2CO_3, $LiNO_3$, and Li_2SO_4 have not been measured by Brindley and Hoare, Kido's[1] values for these salts have been used. Values of potassium salts have also been taken from Kido[1] as it is necessary that for a comparative study values reported by the same author should, as far as possible, be chosen. The susceptibilities of the salts of lithium and potassium with organic acids have been taken from Prasad and co-workers.[7] The graphs between x_m- and N are shown in Figs. 2 and 3.

It is evident from the graphs that the plotted points do lie on straight lines. These lines have been extrapolated to meet the x_m axis, and the values of the slopes and the intercepts on the x_m axis have been measured.

TABLE IIA. Salts of inorganic acids.

Anion	$x$anion Li–NH_4–K	Li–Na–K[a]	Mg–Zn–Cd	Ca–Sr–Ba[a]
Nitrate	20.60	21.00	...	18.50
Chloride	22.10	22.50	23.00	23.00
Bromide	32.50	32.50	33.00	31.50
Iodide	49.00	49.00	44.00	49.00
Sulphate	39.50	39.00	38.00	38.00
Carbonate	24.60	26.00	26.50	27.00

TABLE IIB. Salts of organic acids.

Anion	$x$anion Li–NH_4–K	Li–Na–K	Mg–Zn–Cd	Ca–Sr–Ba
Formate	20.50	20.50	20.00	15.00
Acetate	34.00	34.00	29.50	25.00
Propionate	43.50	44.00	39.75	44.00
Butyrate	54.50	55.50	52.50	52.50
Benzoate	72.80	72.50	70.00	68.50
Salicylate	81.00	81.00	75.50	74.50
Cinnamate	87.10	89.00	...	...
Oxalate	34.50	34.40	38.00	34.00
Malonate	45.10	45.50	52.00	53.00
Succinate	58.80	58.80	60.00	36.00
Citrate	82.00	79.50	...	...

[a] Prasad and co-workers (unpublished work).

[8] G. W. Brindley and F. E. Hoare, Proc. Roy. Soc. (London) 152A, 342 (1935).

TABLE IIIA. Salts of inorganic acids.

Series	$x(NH_4^+)$
Nitrates	7.45
Chlorides	9.45
Bromides	9.45
Iodides	10.30
Sulphates	8.05
Carbonates	9.00

TABLE IIIB. Salts of organic acids.

Series	$x(NH_4^+)$
Formates	6.14
Acetates	6.50
Propionates	7.64
Butyrates	8.33
Benzoates	5.50
Salicylates	6.00
Cinnamates	12.25
Oxalates	8.93
Malonates	8.50
Succinates	8.85
Citrates	9.02

SUSCEPTIBILITIES OF ANIONS

The susceptibilities of the inorganic and organic anions have been deduced from the intercepts on the x_m axis. These values are given in Tables IIA and IIB. In the same table the values obtained by Prasad and co-workers[6,7] for these ions in combination with (1) Li–Na–K, (2) Mg–Zn–Cd, and (3) Ca–Sr–Ba are given for the sake of comparison.

It will be seen from the table that (1) the authors' values for the susceptibilities of the inorganic and organic anions in combination with Li–NH_4–K are in good agreement with those obtained from Li–Na–K salts as it should be and (2) the values for organic anions obtained from salts of Li–Na–K and Li–NH_4–K are different from those obtained from the salts of Ca–Sr–Ba and Mg–Zn–Cd. This observation is in line with the previous findings of Prasad and co-workers[7] that the susceptibility of an organic anion is a fixed quantity in combination with a particular cation belonging to a group or a subgroup in the periodic table.

SUSCEPTIBILITY OF THE AMMONIUM ION

The susceptibility of the ammonium ion has been calculated in the following two ways as done by Prasad and co-workers:[7] (1) by subtracting the value of the susceptibility of an anion from the molecular susceptibility of the salt containing the anion and (2) by multiplying the value of the slope by the number of electrons in the cation. Since the values obtained by the second method are more reliable only these values are given in Tables IIIA and IIIB.

It will be seen that the susceptibility value of the ammonium ion is not a fixed quantity but is different in combination with different anions. The divergence is

much more marked for the values deduced from salts with organic anions than those with inorganic anions.

A close examination of the values of the ammonium ion deduced from formates, acetates, propionates, and butyrates shows that they increase with the increase in the size of the anion.

SUMMARY

Magnetic susceptibilities of some pure ammonium compounds of inorganic and organic acids have been determined on a modified form of Gouy's balance.

The graphs obtained by plotting molecular susceptibilities (x_m) of ammonium salts against $\sum Z$ are definitely nonlinear. The $x_m - \sum Z$ patterns for corresponding salts of ammonium and alkali ions are strikingly similar.

A linear relation is obtained on plotting x_m of salts of Li, NH_4, and K containing a common anion against the number of electrons in the cation. The susceptibilities of (1) inorganic and organic anions and (2) ammonium ion have been calculated by using the linear relation. It has been found that the susceptibility of an anion in combination with chemically related cations is a fixed quantity. The susceptibility of the ammonium ion is different in combination with different anions.

THE JOURNAL OF CHEMICAL PHYSICS VOLUME 20, NUMBER 1 JANUARY, 1952

Electron Deficient Compounds. VI. The Structure of Beryllium Chloride*

R. E. RUNDLE AND PAUL H. LEWIS
Institute for Atomic Research, Iowa State College, Ames, Iowa

(Received August 20, 1951)

The simple compound, beryllium chloride, offers an opportunity to study halogen bridge bonding. Beryllium chloride is isomorphous with dimethylberyllium and silicon disulfide. The orthorhombic unit, $a_0=9.86$, $b_0=5.36$, $c_0=5.26$A contains four beryllium chloride molecules. The structure consists of continuous chains:

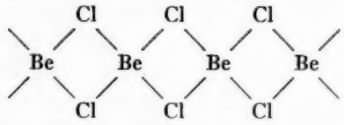

with an essentially tetrahedral configuration about beryllium. The Cl−Be−Cl bond angle within the four membered rings is 98.2° which is less than the tetrahedral angle, as is found in SiS_2, instead of more, as in dimethylberyllium. The bond angles indicate that all bonds in beryllium chloride contain an electron pair, so that chlorine uses an unshared pair in forming bridge bonds. Hence, chlorides isomorphous with electron deficient metal alkyls are not to be classified as electron deficient compounds.

INTRODUCTION

BRIDGE bonds in Al_2Cl_6 vapor[1] and $[(CH_3)_3PtCl]_4$[2] seem to be analogous to those in $Al_2(CH_3)_6$ and $[(CH_3)_4Pt]_4$,[2] although the structure of the trimethyl aluminum dimer is still somewhat uncertain. In certain other cases, e.g., $PdCl_2$[3] and $[R_2AuBr]_2$,[4] halogen atoms bridge metal atoms together in cases where it seems appropriate to assign considerable covalent character to the metal-halogen interatomic link.

Knowing that in the case of methyl bridges, bonding must be electron deficient in the sense that there are more interatomic links than there are electron pairs for forming bonds, the question arises whether analogous halogen bridges are to be regarded as electron deficient, or whether halogen atoms use an unshared pair of electrons to provide each interatomic link with an electron pair. One could try to decide this question on the basis of existing data, using bond distances, but the only rule relating bond type to bond distance is that of Pauling,[5] and the reliability of the rule in unusual cases is not known. Moreover, the electron diffraction results on aluminum compounds lack the accuracy required for a decision.

In the discussion we show that one should be able, in some circumstances, to decide whether there are one or two electron pairs in the M−X−M bridge bonds on the basis of bond angles without any appeal to rules relating bond number to bond lengths. The basis of this is a comparison of the structure of $BeCl_2$ with dimethylberyllium, which is an electron deficient bridge-type compound,[6] and silicon disulfide,[7] which contains normal electron-pair bonds; the three compounds are isomorphous.

* Contribution No. 166 from the Institute for Atomic Research and Department of Chemistry, Iowa State College, Ames, Iowa. Work performed in the Ames Laboratory of the AEC.

[1] K. J. Palmer and N. Elliot, J. Am. Chem. Soc. **60**, 1852 (1938).
[2] R. E. Rundle and J. H. Sturdivant, J. Am. Chem. Soc. **69**, 1561 (1947).
[3] A. F. Wells, Z. Krist. **100**, 189 (1938).
[4] Burawoy, Gibson, Hampson, and Powell, J. Chem. Soc. **1937**, 1690–3.
[5] L. Pauling, J. Am. Chem. Soc. **69**, 542–553 (1947).
[6] R. E. Rundle and A. I. Snow, J. Chem. Phys. **18**, 1125 (1950).
[7] Büssem, Fischer, and Gruner, Naturwiss. **23**, 740 (1935).

STRUCTURE DETERMINATION

Preparation of Compounds

Anhydrous beryllium chloride, prepared by the action of dry hydrogen chloride on beryllium oxide, was furnished to us by the metallurgy group of the Ames Laboratory of the AEC. Single crystals of satisfactory size were found in the preparation, and though anhydrous beryllium chloride is very hygroscopic, it was found possible to mount these crystals in thin-walled glass capillaries by manipulating them in a dry box or under thoroughly dried mineral oil. Because of the needle-like character of the crystals the needle axis was parallel to the capillary in all cases. Data, other than that about the needle axis, were found by use of a precession camera, or by mounting the capillary so that the needle axis was perpendicular to a glass fiber, an orthorhombic axis perpendicular to the x-ray beam, and using the Weissenberg technique over short oscillation ranges.

X-Ray Data

Weissenberg data, ($hk0$), were obtained using CuKα radiation, $\lambda=1.542$A, and the multiple film technique. The zones [100] and [010] were examined by means of a precession camera, MoKα radiation, $\lambda=0.7107$A, a precession angle of 25°, and timed exposures using G. E. XRD-3 unit with stabilized current and voltage. To obtain ($00l$) data with l greater than 6, MoKα radiation, Weissenberg camera and timed exposures were used. Intensities were judged visually using the multiple films or timed exposures.

Unit Cell and Space Group

Beryllium chloride is orthorhombic with $a_0=9.86$, $b_0=5.36$, $c_0=5.26$A. Reflections (hkl) are present only if $h+k+l=2n$; ($hk0$), only with $h+k=2n$; ($h0l$) only with $h=2n$ and $l=2n$; ($0kl$), only with $k=2n$ and $l=2n$. The space group is, then, either $D_{2h}^{26}-Ibam$ or $C_{2v}^{21}-Iba$. Lattice constants of isomorphous dimethylberyllium are $a_0=11.53$, $b_0=5.65$, and $c_0=5.54$A.

The handbook specific gravity of anhydrous beryllium chloride is 1.899 25°/4, in good agreement with a calculated density of 1.91 g/cm^3, using the cell dimensions aforementioned, and assuming four $BeCl_2$ molecules per body-centered unit cell.

Atomic Positions

In either space group the chlorine atom positions are $\pm(xy0,\ x\bar{y}\tfrac{1}{2})+000,\ \tfrac{1}{2}\tfrac{1}{2}\tfrac{1}{2}$, and the beryllium positions are $(00z,\ 00\tfrac{1}{2}+z)+000,\ \tfrac{1}{2}\tfrac{1}{2}\tfrac{1}{2}$, where $z\equiv\tfrac{1}{4}$ if the space group is *Ibam*. The structure, in the latter case, is isomorphous with SiS_2.

Chlorine parameters were determined roughly from a Patterson projection onto the (001) plane. These parameters were refined by a two-dimensional Fourier and the electron density peaks located by the method of Donohue and Carpenter.[8] A second Fourier was run correcting some signs as demanded by the result of the first Fourier. The series termination correction, obtained by Booth's method,[9] was less than 0.001 parameter units in y and 0.001 in x. Final parameters were $x_{Cl}=0.109\pm0.001$, $y_{Cl}=0.203\pm0.002$. Errors were estimated by the method of Cruickshank.[10]

Calculated and observed structure factors are compared in Table I, where observed values include a temperature factor of the form $\exp-(B\sin^2\theta/\lambda^2)$, with $B=7.5$A^2, and an absorption factor as given by Bradley,[11] assuming a circular cross section for the crystal. The temperature factor is probably asymmetric since ($00l$) data can be obtained at somewhat higher $\sin\theta/\lambda$ values than ($hk0$) data. However, for the ($hk0$), ($hk1$), and ($hk2$) data of Table I, this causes only a minor effect. The over-all R factor is 0.19, where $R\equiv$

$$\frac{\sum\big||F_{obs}|-|F_{calc}|\big|}{\sum|F_{obs}|}.$$

Precession data, ($h0l$) and ($0kl$), did not produce reflections with sufficiently high l to establish the beryllium z parameter with any accuracy. Consequently, the Weissenberg camera and MoKα radiation were used to determine z, regarding z_{Cl} and y_{Cl} as fixed. Data were obtained to $l=8$, with (0·0·10) barely perceptible, from which we found that $z_{Be}=0.25\pm0.02$ parameter units, and that in all probability the correct space group is *Ibam*.

DISCUSSION OF THE STRUCTURE

Anhydrous beryllium chloride is isomorphous with SiS_2 and dimethylberyllium. The continuous chains

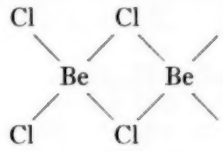

run parallel with c_0. The chains pack rather like circular cylinders, with Cl−Cl distances between chains of 3.85A, somewhat larger, but near previously observed values which range from 3.6 to 3.8A.

The Be−Cl distance is 2.02A *vs* 2.05A given by the sum of the covalent radii of Pauling.[12] If Pauling's newer metallic radius[5] for Be is adopted the sum is 1.883A. The discrepancy makes it difficult to determine reliably the bond number of the Be−Cl bond from distances, even if Pauling's rule is accepted.

Though similar to dimethylberyllium in many respects, the angles within the four-membered rings show

[8] G. B. Carpenter and J. Donohue, J. Am. Chem. Soc. **72**, 2315 (1950).
[9] A. D. Booth, Proc. Roy. Soc. (London) **A188**, 77–92 (1946).
[10] D. W. J. Cruickshank, Acta Cryst. **2**, 65 (1949).
[11] A. J. Bradley, Proc. Phys. Soc. (London) **47**, 879 (1935).
[12] L. Pauling, *Nature of the Chemical Bond* (Cornell University Press, Ithaca, New York, 1942), p. 179.

TABLE I. Comparison of observed and calculated structure factors for beryllium chloride.

Indexes	F_{obs}	F_{calc}	Indexes	F_{obs}	F_{calc}
200	60	+42	811	46	+43
400	74	−72	10·1·1	47	−29
600	31	−31	121	32	−31
800	51	+52	321	37	−40
10·0·0	46	+56	521	14	+11
12·0·0	25	−13	721	33	+36
020	86	−67	921	0	+ 4
040	29	+33	11·2·1	55	+29
110	58	+45	231	45	+46
310	7	− 1	431	24	+17
510	9	−12	631	35	−33
710	12	+10	831	30	−26
910	22	+24	141	35	+39
220	8	− 3	341	43	+53
420	65	+69	541	23	−16
620	36	+40	741	68	−53
820	19	−27	251	0	− 1
10·2·0	41	−33	451	0	− 2
12·2·0	26	+22	161	33	−33
130	37	−35	361	46	−56
330	35	+34	561	21	+14
530	50	+57	202	24	+11
730	0	− 3	402	76	−78
930	51	−37	602	31	−46
11·3·0	14	− 8	802	35	+37
240	13	+13	10·0·2	35	+40
440	14	−14	12·0·2	35	−23
640	16	− 6	112	13	+ 3
10·4·0	18	+23	312	21	−13
150	46	+54	512	22	−27
350	16	−21	022	69	−73
550	46	−51	222	21	−20
211	110	−92	422	44	+46
411	25	−31	622	18	+25
611	50	+55	822	39	−40
10·2·2	44	−48			
132	44	−48			
332	18	+17			
532	29	+40			
732	0	− 3			
932	47	−46			
042	30	+18			
242	17	− 2			
442	17	−27			
152	37	+38			
352	20	−34			
552	44	−58			

interesting differences. In dimethylberyllium the ∠C−Be−C is 114°, greater than tetrahedral, whereas the corresponding ∠Cl−Be−Cl is only 98.2°, very much less than tetrahedral. The angles Be−C−Be and Be−Cl−Be are, accordingly, 66° and 81.8°, respectively. It was suggested that the very small Be−C−Be angle arises because one tetrahedral carbon orbital is directed between two Be atoms in dimethylberyllium.[6] To achieve maximum overlap, both Be atoms tend to move together, toward the direction of greatest electron concentration in this orbital. We suggest that very different angles arise in beryllium chloride because two electron pairs are used in the two Be−Cl−Be bonds. One would expect that the chlorine bonds would be nearly pure *p*-bonds, and that the ideal bond angle for chlorine would be about 90°. However, a 90° Be−Cl−Be bond angle would require a 90° Cl−Be−Cl bond angle which would be, ideally, 109°28′. The compromise reached is thus very reasonable, since the Cl−Be−Cl angle is about 10° less than tetrahedral, and the Be−Cl−Be angle is about 10° less than 90°. The bond angles in $BeCl_2$ are very similar to those in SiS_2, where there is little reason to doubt that electron-pair bonds occur.

An alternative explanation for the small Be−C−Be angle in dimethylberyllium is a considerable contribution of Be−Be bonding. The Be−Be distance along the chain is 2.09A in dimethylberyllium, while it is 2.63A in beryllium chloride. In this interpretation the Be−Be distance increases enormously as the electron density in the four-membered ring is increased, which seems unreasonable. Since all distances and angles are very reasonable in both compounds without considering Be−Be bonding, its significance appears to be of a secondary nature in both compounds, and we regard the short Be−Be distance in dimethylberyllium to be a result of the acute Be−C−Be angle, not a cause, though the possibility of some extra stabilization as a result of Be−Be bonding cannot be eliminated in dimethylberyllium.

It is interesting to note that electron diffraction results required a very sharp Al−C−Al angle of about 55° in $(CH_3)_6Al_2$ if a bridge bond model were adopted,[13] and at the time such an acute angle seemed unreasonable, so the bridge model was discarded. It is also noteworthy that the Al−Cl−Al angle of the bridge in Al_2Cl_6 vapor has been estimated to be about 80°[1] by electron diffraction. It seems likely that the bridge angles in trimethylaluminum and aluminum trichloride dimers are very close to those found in the corresponding beryllium compounds, so the angles found in the beryllium compounds may well be typical of tetrahedral metal atoms in electron deficient and electron-pair-bond bridges, respectively.

[13] L. O. Brockway and N. Davidson, J. Am. Chem. Soc. 63, 3287–97 (1941).

Force Constants and Calculated Thermodynamic Properties of Nitrosyl Fluoride*

C. V. STEPHENSON AND E. A. JONES
Department of Physics, Vanderbilt University, Nashville, Tennessee
(Received October 2, 1951)

The force constants for NOF were calculated using the Wilson FG Matrix method. Unique values could not be calculated, since the number of force constants exceeded the number of fundamental vibrations. However, upper and lower limits have been set for the force constants. The thermodynamic functions for NOF were calculated for temperatures ranging from 273.16°K to 1500°K, using the rigid rotator, harmonic oscillator approximation.

INTRODUCTION

NITROSYL fluoride was first prepared by Ruff and Stauber[1] by passing NOCl over AgF at 200°C in a platinum tube. It was later prepared by Ruff, Menzel, and Neumann[2] by the direct addition of fluorine to nitric oxide in a copper tube. A refinement to this process has been recently reported by Faloon and Kenna.[3]

The infrared spectrum of NOF was first reported by Jones and Woltz[4] and grating work in the infrared region was recently done by Magnuson.[5] The moments of inertia and molecular dimensions determined from microwave data have also been reported by Magnuson.[6] Since no force constants or thermodynamic properties have been reported for this compound it was considered advisable to calculate them and tabulate them in the usual manner.

FORCE CONSTANTS

The force constants for NOF were calculated using a valence potential function containing an interaction term. The assumption of a simple valence force field using the equations of Lechner[7] did not give real values for the force constants. Likewise the assumption of a simple central force field using the equations of Radakovic[8] did not give real results, although Burns and Bernstein[9] have reported force constants for NOCl and NOBr using this method. This is probably attributable to the presence of the fluorine atom, an effect which has been noted by other observers in other compounds.

The following potential function for NOF was used:

$$2V = f_{d_1}(\Delta d_1)^2 + f_{d_2}(\Delta d_2)^2 + f_\alpha(d\Delta\alpha)^2 + 2f_{d_1d_2}\Delta d_1\Delta d_2,$$

where Δd_1 and Δd_2 are the changes in the N—O and N—F bond distances d_1 and d_2, $\Delta\alpha$ is the change in the O—N—F angle α, and $d=(d_1d_2)^{\frac{1}{2}}$. Although this is not the most general second degree potential function, there are more force constants than can be solved for uniquely since NOF has only three fundamental frequencies. In order to make the calculations it was necessary to assume various ratios of $f_{d_1d_2}$ to f_{d_2}. It was found that for ratios less than about 0.53, imaginary results were obtained. The calculations were made using the Wilson FG matrix method.[10] The molecular

TABLE I. Molecular constants for NOF.

Fundamental frequencies	Moments of inertia	Molecular dimensions
$\nu_1=1844.03\ cm^{-1}$	$I_a=\ 8.8135\times10^{-40}\ g\ cm^2$	$R_{N-O}=\ 1.13A$
$\nu_2=\ 521$	$I_b=70.8354\times10^{-40}\ g\ cm^2$	$R_{N-F}=\ 1.52A$
$\nu_3=\ 765.85$	$I_c=79.8375\times10^{-40}\ g\ cm^2$	$\alpha=110.2°$

TABLE II. Force constants of the NOF molecule (dynes/cm).

$f_{d_1d_2}/f_{d_2}$	$f_{d_1}\times10^{-5}$	$f_{d_2}\times10^{-5}$	$f_\alpha\times10^{-5}$	$f_{d_1d_2}\times10^{-5}$
0.55	15.000	2.036	0.9400	1.1198
0.65	14.979	1.8250	1.0443	1.1863
0.75	14.961	1.6727	1.1224	1.2545
0.85	14.958	1.5950	1.1635	1.3558

TABLE III. Thermodynamic functions of NOF (cal mole^{-1} deg^{-1}).

T(°K)	C_p^0	$H^0-H_0^0/T$	$(F^0-E_0^0)/T$	S^0
273.16	9.651	8.467	49.93	58.40
298.16	9.881	8.567	50.67	59.24
300	9.897	8.585	50.72	59.31
400	10.650	9.011	53.26	62.27
500	11.226	9.400	55.30	64.70
600	11.682	9.743	57.05	66.80
700	12.052	10.049	58.57	68.62
800	12.349	10.318	59.93	70.25
900	12.587	10.555	61.15	71.71
1000	12.779	10.768	62.29	73.06
1100	12.938	10.957	63.32	74.28
1200	13.065	11.131	64.28	75.41
1300	13.170	11.282	65.16	76.45
1400	13.260	11.420	66.02	77.44
1500	13.331	11.547	66.82	78.37

* This document is based in part on work performed under Contract No. AT(40-1)-1087 for the AEC.

[1] Ruff and Stauber, Z. anorg. u. allgem. Chem. **47**, 190 (1905).
[2] Ruff, Menzel, and Neumann, Z. anorg. u. allgem. Chem. **208**, 293 (1932).
[3] Faloon and Kenna, J. Am. Chem. Soc. **73**, 2937 (1951).
[4] E. A. Jones and P. J. H. Woltz, J. Chem. Phys. **18**, 1516 (1950).
[5] Presented at the Symposium on Molecular Structure and Spectra at Ohio State University, 1951.
[6] Presented at the meeting of the Southeastern section of the American Physical Society, Chattanooga, Tennessee (April 5, 1951). [Phys. Rev. **83**, 485 (1951)].
[7] F. Lechner, Wien. Ber. **141**, 291, 633 (1932).
[8] M. Radakovic, Monatsh. Chem., **56**, 447 (1930).
[9] W. G. Burns and H. J. Bernstein, J. Chem. Phys. **18**, 1669 (1950).
[10] E. B. Wilson, Jr., J. Chem. Phys. **7**, 1047 (1939); **9**, 76 (1941).

constants used are given in Table I. The results of the calculations are given in Table II. The extreme values given are thought to constitute the upper and lower limits of the force constants. In addition, for each value of the ratio $f_{d_1d_2}/f_{d_2}$, the calculations yielded a second set of values which were discarded since they gave values of f_{d_2} in excess of 6.5×10^5 dynes/cm, a value which is too large. Each set of values will reproduce the fundamental frequencies to within 2 cm^{-1}.

THERMODYNAMIC PROPERTIES

The heat capacity, entropy, heat content, and free energy function were calculated at 273.16°K, 298.16°K, and at 100°K intervals from 300°K to 1500°K. The calculations were made using the usual rigid rotator, harmonic oscillator assumption. The physical constants were those of Birge.[11] The molecule belongs to the point group C_s and has a symmetry number $\sigma=1$. The values of the functions are listed in Table III. Electronic and spin contribution have been neglected and the pressure was assumed to be one atmosphere.

ACKNOWLEDGMENT

We wish to thank Dr. D. Magnuson for discussion of the microwave data prior to publication.

[11] R. T. Birge, Revs. Modern Phys. **13**, 233 (1941).

THE JOURNAL OF CHEMICAL PHYSICS VOLUME 20, NUMBER 1 JANUARY, 1952

On the Infrared Spectrum of Hydrazine

PAUL A. GIGUÈRE AND I. D. LIU
Department of Chemistry, Laval University, Québec, Canada

(Received September 5, 1951)

The absorption spectrum of hydrazine was reexamined in the region 1.5—25μ with a prism instrument. In the vapor some twenty bands were found of which a few are appreciably different from previous data. The low frequency fundamentals showed enough structural details to make possible a rough calculation of the rotational constants of the molecule. Because of extensive overlapping the identification and assignment of certain bands remain doubtful. The absorption spectrum of the liquid and that of the solid at −70° were also measured over a limited range.

IN spite of several investigations the vibrational spectrum of hydrazine is not yet completely elucidated. If the model suggested by Penney and Sutherland[1] is correct, the molecule should belong to the point group C_2 and, therefore, should have twelve nondegenerate fundamental modes as follows: four N—H stretching and six NH bending in addition to the N—N stretching and the torsional oscillation. The frequencies of some of these modes fall close together; this coupled with the possibility of accidental resonance and inversion doubling results in a spectrum fairly confused in parts.

The Raman spectrum of hydrazine has been studied successively by Sutherland,[2] Imanishi,[3] Kahovec and Kohlrausch,[4] and Goubeau.[5] Like the Raman, the infrared spectrum of hydrazine shows many strong bands. In the photographic region the work of Freymann[6,7] has confirmed existence of strong molecular association in the liquid. Krivich,[8] using a manual instrument with quartz and fluorite prisms, measured the absorption of both liquid and vapor from 1 to 14μ. Finally Fresenius and Karweil[9] in an extensive investigation have covered what they thought to be the entire vibrational spectrum. Their assignments of the observed frequencies (Table I) have been revised in some cases by Scott *et al.*[10] who calculated the thermodynamic functions of hydrazine. In particular it was pointed out that the two NH_2 wagging modes, ν_6 and ν_{12}, (Fig. 1) should appear as doublets in the spectra because of the possibility of inversion doubling. The two pairs of infrared bands at 815 and 850 cm^{-1} and at 930 and 965 cm^{-1} were, therefore, assigned to these vibrations. Also, the frequency 749 cm^{-1} is certainly much too high for a torsional oscillation. Lately a casual observation of the spectrum of a sample of anhydrous hydrazine made in this laboratory revealed a few discrepancies with that of the German authors and much more detail than reported by them.

EXPERIMENTAL

The infrared spectrometer was a Perkin-Elmer (Model 12C) with automatic recording on a Leeds and Northrup "Speedomax." Prisms of lithium fluoride, rock

[1] W. G. Penney and G. B. B. M. Sutherland, Trans. Faraday Soc. **30**, 898 (1934); J. Chem. Phys. **2**, 492 (1934).
[2] G. B. B. M. Sutherland, Nature **126**, 916 (1930).
[3] S. Imanishi, Nature **127**, 782 (1931). Sci. Papers Inst. Phys. Chem. Research Tokio **16**, 1 (1931).
[4] L. Kahovec and K. W. F. Kohlrausch, Z. physik. Chem. (*B*) **38**, 96 (1938).
[5] J. Goubeau, Z. physik. Chem. (*B*) **45**, 237 (1940).
[6] M. Freymann and R. Freymann, Compt. rend. **200**, 1043 (1935); **205**, 852 (1937).
[7] M. Freymann, Ann. chim. (11) **11**, 11 (1939).
[8] S. S. Krivich, Compt. rend. Acad. Sci U.R.S.S. **23**, 36 (1939); J. Phys. Chem. (U.S.S.R.) **15**, 739 (1941).
[9] W. Fresenius and J. Karweil, Z. physik. Chem. (*B*) **44**, 1 (1939).
[10] Scott, Oliver, Gross, Hubbard, and Huffman, J. Am. Chem. Soc. **71**, 2293 (1949).

TABLE I. Previous data on vibrational spectrum of hydrazine.[a]

Raman			Infrared			
				Vapor		
Ref. 3 $\Delta\nu$(cm^{-1})	Ref. 4 $\Delta\nu$(cm^{-1})	Ref. 5 $\Delta\nu$(cm^{-1})	Liquid Ref. 8[c] ν(cm^{-1})	Ref. 8[c] ν(cm^{-1})	Ref. 9 ν(cm^{-1})	Assignment[b]
	174 (0)	101 (1)				
	583 (0)	513 (1)				
	702 (0)	749 (0)				ν_7
		802 (2)			815 (2)	ν_6
	876 (4)	876 (6)	885 (s.)		850 (2)	ν_5
914 (0)		943 (1)			930 (10)	ν_{12}
		995 (1)			965 (10)	ν_{11}
1130 (2)	1108 (5)	1108 (8)	1097 (s.)		1082 (1)	ν_4
		1199 (0)			1165 (0)	
		1316 (1)	1324 (w.)		1282 (3)	ν_3
	1620 (3)	1618 (5)	1613 (s.)		1585 (7)	ν_{10}
			1818 (w.)	1923 (w.)		
			2000 (m.)	2008 (s.)		
			2200 (m.)	2240 (w.)	2215 (2)	$\nu_3+\nu_{12}$
			2380 (w.)	2380 (w.)		
			2562 (v.w.)	2585 (w.)		
		2848 (00)				
		2885 (00)		2900 (w.)		
		2971 (0)				
		2994 (1)				
		3044 (00)				
		3078 (1)				
	3181 (10)	3182 (10)			3160 (1)	ν_2
3210 (3)		3241 (6)	3195 (v.s.)		3255 (10)	ν_9
3289 (3)	3263 (7)	3265 (10)	3268 (v.s.)	3280 (v.s.)	3285 (10)	ν_8
3339 (2)	3332 (7)	3328 (9)		3350 (v.s.)	3360 (2)	ν_1
				3900 (v.w.)		
			4387 (v.w.)	4387 (w.)		
			4566 (v.w.)			
			4830 (v.w.)	4950 (w.)		
			6370 (v.w.)	6500 (v.w.)		
				8333 (v.w.)		
				9800 (v.w.)		

[a] Sutherland (see reference 2) reported three Raman shifts at 3196, 3270, and 3344 cm^{-1}.
[b] Assignments of Fresenius and Karweil (see reference 9) on the basis of their results and those of Goubeau (see reference 5). The vibrations are designated as in Fig. 1.
[c] Relative intensities estimated by present authors from tracings published by Krivich (see reference 8).

salt, fluorite, and potassium bromide were used, and a cut-off grating filter served to eliminate most of the scattered radiation beyond 6μ. For the vapor two cells were used, one 10 cm long, made of Pyrex, and the other, of metal, with multiple reflection[11] giving a one-meter path length. The salt windows were held tight against the cells by means of plastic gaskets (Polythene). No fogging of the salt plates by hydrazine vapor occured as long as condensation was prevented. To that effect the cells were heated by Nichrome windings so that they were at least 10° above the temperature of the liquid sample (usually at 25°). For studying the liquid and the solid the salt windows were protected with a thin film of an appropriate plastic (polythene or Teflon). No suitable material could be found for the range 5–8μ. The low temperature cell was of the type described by Wagner and Hornig,[12] the Housekeeper seal being replaced by a Kovar joint.

The sample of anhydrous hydrazine obtained from Mathieson Chemical Company was slightly over 98 percent pure from analysis by the iodate or the direct acid method.[13] After standing at room temperature for a number of months it contained some dissolved ammonia which could be removed completely by repeated de-

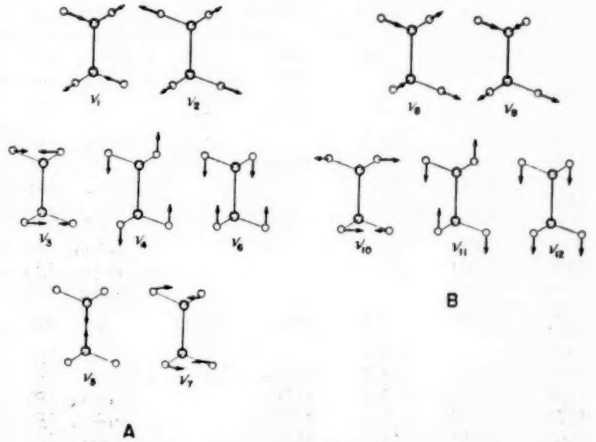

FIG. 1. Fundamental vibrations of the hydrazine molecule.

[11] J. U. White, J. Opt. Soc. Am. **32**, 285 (1942).
[12] E. L. Wagner and D. F. Hornig, J. Chem. Phys. **18**, 296 (1950).
[13] L. F. Audrieth and B. A. Ogg, *The Chemistry of Hydrazine* (John Wiley and Sons, Inc., New York, 1951).

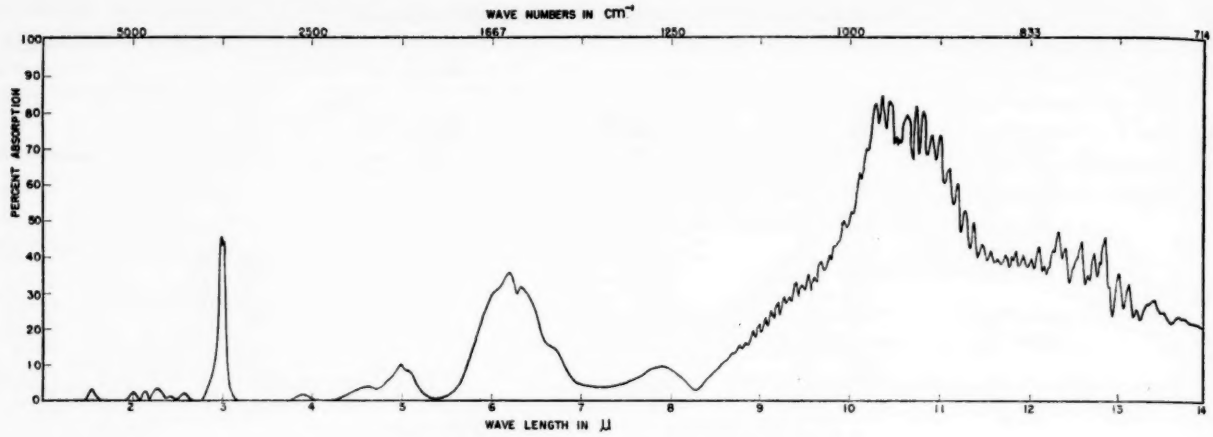

FIG. 2. Infrared spectrum of hydrazine vapor.

gassing in vacuum; then it was recrystallized a number of times.

DISCUSSION OF RESULTS

The spectrum of the vapor is shown in Fig. 2 and that of the condensed phases in Fig. 3. The list of frequencies at the center of the various bands is given in Table II together with the proposed assignments.

N–H Stretching

Three fairly strong peaks were observed in the 3μ region (Fig. 4) along with a fourth, very weak one at 3325 cm^{-1}. In as much as the latter is real it must correspond to a fundamental vibration as it does not fit any possible combination or overtone; it is therefore assigned tentatively to ν_1. The other symmetric frequency ν_2 is probably overlapped by the much stronger asymmetric vibrations. The 3350 cm^{-1} band undoubtedly corresponds to ν_8; the Raman shift of nearly equal frequency (3328 cm^{-1}) seems rather strong for an asymmetric mode. Indeed, the assignment of the four intense Raman bands at 3μ to each of the four N–H stretching fundamentals[9] is questionable as it does not take into account the possibility of Fermi resonance with the overtone of the bending frequencies at 6μ. In infrared such resonance could occur only with the symmetric vibrations, but these are weak as expected.

Since the two maxima of equal intensity at 3280 and 3314 cm^{-1} show the same separation as some other hydrazine bands they are believed to be the two branches of ν_9; this vibration has a strong parallel component and should, therefore, give rise to a hybrid band. This is also confirmed by the fact that only two strong bands were found at 3μ in the spectrum of the liquid and the solid. Clearly, further investigation of this region with a grating instrument will be needed before definite assignments can be made.

TABLE II. Infrared spectrum of hydrazine.

ν(cm^{-1})	Vapor α[a]	Slit width (cm^{-1})	Liquid ν(cm^{-1})	Solid ν(cm^{-1})	Assignment
780	0.60	1.8	800	795	ν_6 (a)
			873	885	ν_5 (a)
933				1072	
966	1.15	2.5	1038	1078	ν_{12} (b)
1098	0.22	2.8		1124	ν_4 (a)
1275	0.08	3.5	1280	1320	ν_{11} (b)
1493	0.01				ν_3 (a)
1587					
1628	0.30				ν_{10} (b)
2000	0.045				$\nu_4+\nu_{12}$ (B)
2250	0.021				$\nu_3+\nu_6$ (A)
2526	0.012				$\nu_{10}+\nu_{12}$ (B)
3280	0.24	4.5	3200	3204	ν_9 (b)
3314					
3325		4.6			ν_1 (a)
3350	0.27	4.8	3338	3315	ν_8 (b)
4125	0.005	8.3	4136		$\nu_6+\nu_8$ (B)
4370	0.013	9.8	4390		$\nu_4+\nu_9$ (B)
4660	0.011	11.0	4632		$\nu_3+\nu_9$ (B)
4954	0.012	12.7	4902		$\nu_5+\nu_{10}$ (B)
6500	0.013		6383		

[a] $\alpha=(1/pl)\log I_0/I$, with p in atmos and l in cm.

NH Bending

The region of strong absorption from 6 to 14μ must include the N–N stretching and the six NH bending vibrations. Of these the two NH_2 bending modes ν_3 and ν_{10} are expected to have the higher frequencies, somewhere around 1600 cm^{-1}, as observed in primary amines[14]

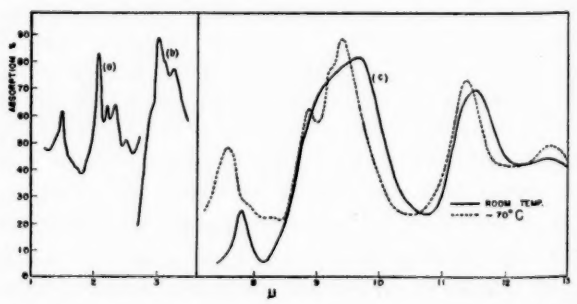

FIG. 3. Absorption spectrum of hydrazine in condensed phases: (a) liquid at 20°C, $l=10$ mm. (b) liquid at 20° and solid at −70°, $l=0.14$ mm. (c) $l=0.002-0.004$ mm.

[14] A. P. Cleaves and E. K. Plyler, J. Chem. Phys. 7, 563 (1939).

and in substituted hydrazine.[15] Because of appreciable absorption by atmospheric water vapor the outline of the strong band at 6μ was not very clear. Roughly it seemed to consist of a double peak of almost equal intensity and about 35 cm^{-1} apart, which must be the P and R branches of ν_{10} since the change of electric moment associated with this vibration has a component along the minor axis of the molecule. The slight shoulder on the low frequency side of the 6μ band is of suitable frequency (1493 cm^{-1}) and intensity for ν_3 the symmetric bending vibration.

Next in order of decreasing frequency are the two rocking vibrations ν_4 and ν_{11}. Neither is expected to be very intense in infrared and so the two weak bands at 1098 and 1275 cm^{-1} seem suitable. That the former is the symmetric mode is indicated by the relative in-

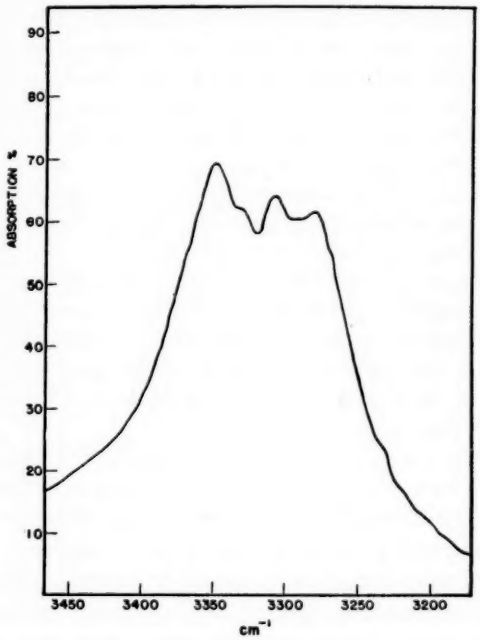

FIG. 4. Absorption spectrum of hydrazine vapor in the 3μ region.

tensity of the corresponding Raman lines at 1108 and 1316 cm^{-1}. The change in frequency on going from vapor to liquid is in the right direction for bending vibrations. In that region the resolution was sufficient to reveal some of the coarse rotational structure. Thus the band at 1275 cm^{-1} exhibited the contour of a hybrid band (Fig. 5), which is unexpected as vibration ν_{11}, to which it is assigned here, should be purely perpendicular. The presence of a minimum instead of a maximum of intensity near the center may be due to the fact that the hydrazine molecule is a slightly asymmetric top. A similar situation has been observed in the photographic bands of methylamine.[16] At any rate the various maxima in that region show the same spacing and they lead to values of the rotational constants of the molecule

[15] Axford, Janz, and Russell, J. Chem. Phys. **19**, 704 (1951).
[16] H. W. Thompson, J. Chem. Phys. **7**, 448 (1939).

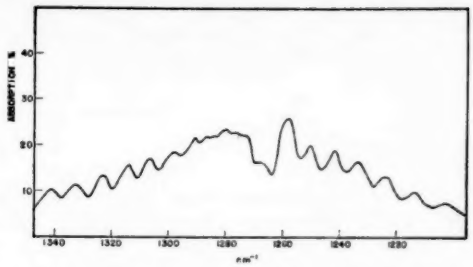

FIG. 5. Coarse rotational structure of the hydrazine band at 7.8μ.

(Table III) which are in agreement with the moments of inertia calculated from the most probable structural parameters.[10] The exact center of the weak perpendicular band near 1100 cm^{-1} could not be ascertained because of its location on the sloping background of the much more intense doublet at 933–966 cm^{-1}. The latter belongs certainly to the asymmetric wagging mode ν_{12}, while the symmetric one ν_6 very likely corresponds to the band of medium intensity near 800 cm^{-1}. These two wagging vibrations should be double minima because of the possibility of inversion as in ammonia.

A propos of inversion doubling it may be noted that the situation in hydrazine is somewhat different since the two H atoms in one amino group must oscillate through a greater angle (about 20 percent) than in ammonia, and on that account, the potential barrier should be higher. Also, in order to revert to the normal configuration, inversion in one NH_2 group must be

TABLE III. Frequency of principal maxima in the hydrazine bands at 950, 1098, and 1275 cm^{-1}.

K	$^{P}Q_K$ ν(cm^{-1})	$^{R}Q_K$ ν(cm^{-1})	$\frac{^{R}Q_K - {}^{P}Q_K}{4K}$	$\frac{^{R}Q_{(K-1)} - {}^{P}Q_{(K+1)}}{4K}$
0		950		
1	942	958.8	4.2	4.2
2	933.1	966.5	4.2	4.2
3	925.2	973.8	4.1	4.1
4	917.5	983.1	4.1	4.0
5	910.4	991.3	4.1	4.1
6	902.0	999.0	4.0	4.0
7	895.2	1008	4.0	4.0
8	888.0			
9	880.3			
0		1097.8		
1	1089.5	1105.0	3.9	4.1
2	1081.3	1113.5	4.0	3.9
3	1073.5	1122.3	4.0	4.0
4	1065.5	1130.3	4.1	4.0
5	1057.8	1137.2	4.0	4.0
6	1049.6	1144	3.9	4.0
7	1041.4	1152	4.0	4.0
8	1033.5			
0		1275		
1	1266	1282	4.0	4.1
2	1258.5	1292	4.2	4.0
3	1250	1300	4.2	4.2
4	1241	1309	4.2	4.2
5	1233.5	1318	4.2	4.2
6	1225	1327	4.3	4.2
7	1218	1336	4.2	4.3
8	1207.5			

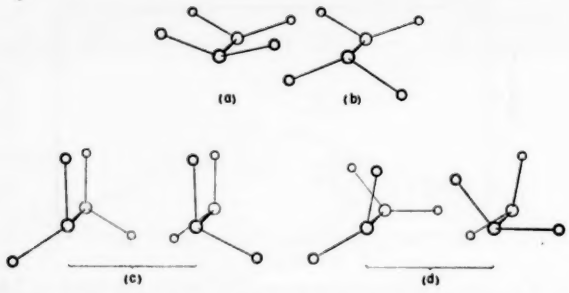

FIG. 6. Possible configurations for the hydrazine molecule.

accompanied by a similar motion in the other group or else, by an internal rotation about the N—N bond, leading possibly to the isomeric form of the molecule. The pair of weak Raman lines at 943 and 995 cm^{-1} have been assigned by Scott *et al.*[10] to the doublet of ν_{12}; in view of what has been said above this splitting seems rather large. In infrared any features arising from inversion doubling must be submerged in the extensive overlapping for the strong doublet at 933–966 cm^{-1} shows the same separation as the other hybrid bands and the coarse rotational structure leads to the same rotational constants for the molecule. There exists another possibility of inversion doubling in hydrazine, namely that associated with the torsional mode ν_7, as in the case of hydrogen peroxide.[17] It has not been possible to observe this oscillation no doubt because its frequency is beyond the range of KBr optics. Scott *et al.*[10] have pointed out that a value of 360 cm^{-1} for the torsional frequency would explain two weak Raman bands at 513 and 749 cm^{-1} as difference-combinations.

Finally the N—N fundamental vibration ν_5 is expected to be weak in infrared since it involves an essentially nonpolar bond. In addition, it falls in a region of strong absorption from the NH wagging modes. No definite evidence of it was observed in the spectrum of the vapor, but in the liquid a remarkably strong maximum at 873 cm^{-1} corresponds to a Raman line of moderate intensity at 876 cm^{-1}. This frequency seems a little low compared to the O—O vibration in hydrogen peroxide[17] (877 cm^{-1}) and the C—N vibration in methylamine[14] (1045 cm^{-1}). From electron diffraction[18,19] and x-ray data[20] the N—N bond length in hydrazine is known to be 1.46A; application of Badger's rule yields about 960 cm^{-1} for the corresponding frequency. Values of 816 and 801 cm^{-1}, respectively, have been found for it in methylhydrazine and sym-dimethylhydrazine,[15] the gradual decrease in frequency being caused by an increase in the reduced mass of the vibrating groups.

Although the above data have been interpreted in terms of the model of Penney and Sutherland,[1] (d) Fig. 6, it cannot be said that other models are excluded on purely spectroscopic grounds. The *cis* or eclipsed configuration (a) seems less likely *a priori*, at least for the free molecule, because of the opposed position of the hydrogen atoms. A case in point is the ethane molecule. The same would apply to a lesser extent to the semi-eclipsed configuration (c). True, the crystal structure of hydrazine suggests the eclipsed configuration for the molecule but, as has been pointed out,[20] the potential barrier between the *cis* and the staggered configurations may be low enough to be overcome by packing constraints in the solid phase. As for the *trans*-configuration (b), it is ruled out by the large dipole moment of hydrazine,[21] 1.83*D*, and the coincidence of a number of infrared and Raman bands.

Recently some preliminary results have been reported[22] indicating that the infrared and Raman spectra of anhydrous hydrazine and deuterohydrazine show appreciable temperature dependence. From this it was concluded that liquid and gaseous hydrazine must consist of an equilibrium mixture of the *trans*- and one pair of the *gauche*-isomers having either the staggered (d) or the semi-eclipsed (c) configuration. However, the appearance or nonappearance of some N—H frequencies at various temperatures could well have to do with formation or breaking of hydrogen bonds in condensed phases. At any rate no significant difference was noted in the present work between the spectrum of the liquid at 20°C and that of the solid at −70° in the 3μ region, Fig. 3 (b).

Of the various overtone and combination bands reported here some are capable of unique assignment whereas others, and particularly that at 6500 cm^{-1}, can fit a number of combinations. A high dispersion study of the region from 1 to 3μ would be valuable, although extensive overlapping may be expected if the case of hydrogen peroxide is any indication. As in the photographic bands[23] no evidence whatsoever could be detected for the existence of a monohydrate in the vapor from aqueous solutions of hydrazine. This is in agreement with the results of recent vapor density measurements.[24]

ACKNOWLEDGMENT

The authors are grateful to the National Research Council of Canada for a generous grant towards the purchase of an infrared spectrometer.

[17] P. A. Giguère, J. Chem. Phys. **18**, 88 (1950).
[18] P. A. Giguère and V. Schomaker, J. Am. Chem. Soc. **65**, 2025 (1943).
[19] W. Beamer, J. Am. Chem. Soc. **70**, 2979 (1948).
[20] R. L. Collin and W. N. Lipscomb, Acta Cryst. **4**, 10 (1951).
[21] Audrieth, Nespital, and Ulich, J. Am. Chem. Soc. **55**, 673 (1933).
[22] E. L. Wagner and E. L. Bulgozdy, J. Chem. Phys. **19**, 1210 (1951).
[23] E. Eyster, Ph.D. thesis, Cal. Inst. Tech., Pasadena, (1938).
[24] L. V. Coulter, J. Am. Chem. Soc. **73**, 3505 (1951).

Statistical Thermodynamics of the Transition Region between Two Phases. II. One Component System with a Plane Interface

TERRELL L. HILL
Naval Medical Research Institute, Bethesda, Maryland
(Received September 24, 1951)

An approximate statistical theory is used to investigate the nature of the density transition curve in passing from a one component liquid phase to the equilibrium vapor phase. This density curve is related thermodynamically to the surface tension, the surface energy, the location of the surface of tension, and to the dependence of surface tension on curvature.

I. INTRODUCTION

We have indicated in earlier communications[1-3] the general approach being used in the present series. We have discussed the thermodynamics and quasi-thermodynamics of the problem and now turn to an approximate statistical treatment. Kirkwood and Buff[4] have given a general statistical mechanical theory for a plane surface, and Buff[5] has extended the theory to the curved surface case, but numerical calculations based on these theories are not possible in their rigorous form and still very formidable using, say, a superposition approximation. The aim here is to obtain a complete set of numerical results from a very approximate model, with the expectation of gaining a semi-quantitative picture of the nature of the liquid-vapor transition region. The much simpler computational problem encountered here is still serious, as will be seen. As far as we are aware, an analysis of the type given here has not been carried out before, on any model, however simple, which treats the density transition in the interfacial region as continuous.

II. THE STATISTICAL MODEL

In passing through the transition region, from the liquid phase to the gas phase, the mean local density varies, but the chemical potential, or local Gibbs free energy per molecule, stays constant. This is the condition for equilibrium and follows from minimizing the Helmholtz free energy A of the entire system (liquid phase+gas phase+transition region) at constant N, V, T. The general technique used here to obtain the density transition curve is therefore to solve the nonlinear integral equation (see below) expressing the constancy of the chemical potential in passing from one phase to the other.

Perhaps the simplest possible model of any value is that on which van der Waals' equation for a bulk fluid is based; that is, a "smoothed potential" model with both the potential energy per molecule and the free volume per molecule functions of density only. Specifically, the chemical potential μ is given by the well known expression,

$$\begin{aligned} &\nu=\ln[\theta/(1-\theta)]+[\theta/(1-\theta)]-\alpha\theta \\ &\theta=Nb/V=\rho b, \quad \alpha=2a/bkT \\ &a=\epsilon b, \quad b=2\pi r^{*3}/3 \\ &\nu\equiv[\mu-\mu^0(T)-kT\ln(kT/b)]/kT, \end{aligned} \tag{1}$$

where $\mu^0(T)$ is a function of T only. The quantity $-\alpha\theta kT$ is the potential energy of interaction of a molecule with all the rest of the fluid, taking the potential of intermolecular force as

$$\begin{aligned} u(r)&=-\epsilon(r^*/r)^6 \quad r\geqslant r^* \\ &=+\infty \qquad\quad r<r^* \end{aligned} \tag{2}$$

and the radial distribution function as

$$\begin{aligned} g(r)&=1 \quad r\geqslant r^* \\ &=0 \quad r<r^*. \end{aligned} \tag{3}$$

The other ("entropy") terms in Eq. (1) are supposed to represent the behavior of a fluid of hard spheres, if $\epsilon=0$.

In writing down an equation, analogous to Eq. (1), but applicable to the transition region, we should expect to have to correct both the potential energy and entropy terms to take into account the fact that ρ is no longer constant. Retaining Eq. (3), this is easy to do (see Eq. (4)) for the potential energy. It is, however, a much more involved problem for the entropy terms and we make the additional simplification here of assuming that it is the *local* density at each point which determines the *entropy* contribution to the chemical potential at the point. Since the density is higher on the liquid side of the point of interest and lower on the gas side, the error made will partially cancel. One way in which this local density assumption for the entropy can be improved is considered in the Appendix.

Let $\Phi(z)kT$ be the potential energy of interaction of a molecule at z with the rest of the fluid (take the z-axis perpendicular to the interfacial plane, with z increasing toward the liquid phase). Let θ', φ', r' and x', y', z' be spherical and Cartesian coordinates, respectively, with origin at z. Then

$$\Phi(z)kT=\int_{r^*}^{\infty}\int_0^{\pi}\int_0^{2\pi} u(r')\rho(z+z')r'^2\sin\theta'd\varphi'd\theta'dr'. \tag{4}$$

[1] T. L. Hill, J. Chem. Phys. **19**, 261 (1951).
[2] T. L. Hill, J. Chem. Phys. **19**, 1203 (1951).
[3] T. L. Hill, J. Phys. Chem. (to be published).
[4] J. G. Kirkwood and F. P. Buff, J. Chem. Phys. **17**, 338 (1949).
[5] F. B. Buff, Phys. Rev. **82**, 773(T) (1951).

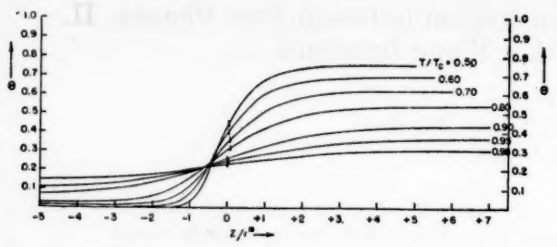

FIG. 1. Density transition curves in the interfacial region.

We integrate over φ', change variables from θ' and r' to z' and r', and then integrate over r' (using Eq. (2)). The result is

$$\Phi(s)=-3\alpha/8\left[\int_{-\infty}^{-1}\theta(s+t)t^{-4}dt+\int_{-1}^{+1}\theta(s+t)dt+\int_{+1}^{+\infty}\theta(s+t)t^{-4}dt\right] \quad (5)$$
$$s=z/r^*, \quad t=z'/r^*.$$

If, in Eq. (1), we now replace θ by $\theta(s)$ in the entropy terms, in accordance with the discussion above, and $-\alpha\theta$ by $\Phi(s)$, we have the desired (nonlinear) integral equation for the van der Waals model, taking ν as a constant determined[1] by the bulk equilibrium between gas and liquid at the temperature of interest.

We can now make a considerable improvement in the theory by replacing the van der Waals hard sphere (or entropy) terms in Eq. (1) by an analogous expression derived from Tonks' much more realistic equation of state for a gas of hard spheres,[6] but still handling the potential energy in the same way. We have van der Waals' ($\epsilon=0$)

$$pb/kT=\theta/(1-\theta), \quad \theta=\rho b, \quad b=2\pi r^{*3}/3, \quad (6)$$

and Tonks'

$$pb'/kT=\frac{\theta(1+2.9619\theta+5.483\theta^2)}{1-0.8517\theta^3-0.1483\theta^4}, \theta=\rho b', b'=r^{*3}/\sqrt{2}. \quad (7)$$

Note that θ is different in the two cases. Tonks' equation is exact in the limit $\theta\to 0$, since the numerator contains the correct second and third virial coefficients. Also

$$pb'/kT\to\theta/(1-\theta^1) \quad \text{as} \quad \theta\to 1. \quad (8)$$

Rice[7] and Kirkwood, Maun, and Alder[8] have also discussed the gas of hard spheres.

With the van der Waals potential energy (Eqs. (2) and (3)) superimposed, the equation of state for the bulk phases is then taken as

$$\frac{pb'}{kT}=\frac{\theta(1+2.9619\theta+5.483\theta^2)}{1-0.8517\theta^3-0.1483\theta^4}-\frac{\alpha'}{2}\theta^2 \quad \alpha'=2.9619\alpha. \quad (9)$$

[6] L. Tonks, Phys. Rev. **50**, 955 (1936).
[7] O. K. Rice, J. Chem. Phys. **12**, 1 (1943).
[8] Kirkwood, Maun, and Alder, J. Chem. Phys. **18**, 1040 (1950).

Even if Eq. (7) were exact for hard spheres without attraction, Eq. (9) would be a serious approximation for hard spheres *with* attraction because of the use of Eq. (3) and a lack of self-consistency between the entropy and potential energy terms. The obvious next step in improving Eq. (3), incidentally, would be to use

$$g(r)=\exp[-u(r)/kT].$$

The critical properties of Eq. (9) are found to be

$$\begin{aligned}\theta_c&\cong 0.220\\ p_cb'/kT_c&=0.754\\ \alpha_c'/2&=7.238\end{aligned} \quad (10)$$

or

$$\begin{aligned}\epsilon/kT_c&=2.44 & p_cv_c/kT_c&\cong 0.342\\ v_c/v^*&\cong 4.54 & v^*&=r^{*3}/\sqrt{2}\\ p_cv^*/\epsilon&=0.0309\end{aligned} \quad (11)$$

all of which are improvements (on comparing with experiment) over van der Waals' equation.[9] The chemical potential is found from Eq. (9) in the standard way:

$$N\mu=A+pV$$
$$A=-\int pdV. \quad (12)$$

The result is

$$\begin{aligned}\nu'&\equiv[\mu-\mu^0(T)-kT\ln(kT/b')]/kT\\ &=f(\theta)-\alpha'\theta\end{aligned} \quad (13)$$
$$\begin{aligned}f(\theta)\equiv&\ln[\theta/(1-\theta)^3]-0.99195\ln(1+0.173069\theta)\\ &+1.49597\ln(1+0.826931\theta+0.856884\theta^2)\\ &-1.33238\tan^{-1}(1.03462\theta+0.49923)\\ &+\frac{1+2.9619\theta+5.483\theta^2}{1-0.8517\theta^3-0.1483\theta^4}-0.38307.\end{aligned}$$

The integral equation in the transition problem is then

$$\nu'=f(\theta(s))+\Phi'(s), \quad (14)$$

where Φ' is given by Eq. (5) with α' in place of α.

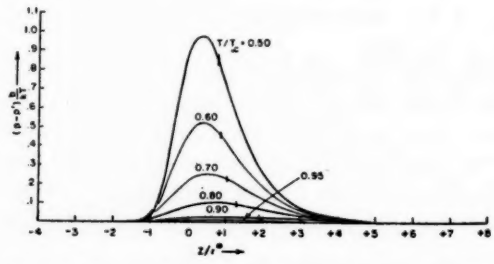

FIG. 2. Curves determining the surface tension and location of the surface of tension.

[9] T. L. Hill, J. Chem. Phys. **18**, 1252 (1950).

III. CALCULATIONS

The only extensive calculations were carried out on the hard sphere integral equation (Eq. (14)) rather than the van der Waals integral equation. The computations were done at the National Bureau of Standards on an I.B.M. punched card machine using an iterative procedure.[1] Convergence in $\theta(s)$ to 0.001 or better was obtained after 8–11 iterations. Numerical integration was used with interval $s=0.25$ and range $s=\pm 10$ (the origin is determined by the initial step function[1] for $\theta(s)$). The solutions $\theta(s)$ of Eq. (14) for seven temperatures are shown in Fig. 1. It is seen that the density transition at $T/T_c=0.5$ is essentially complete in a range of about four molecular diameters, and that this range increases as $T/T_c\rightarrow 1$. The marks on the curves near the origin indicate the location of the Gibbs dividing surface $\Gamma=0$ as determined from $\theta(s)$ by numerical integration.

Adam[10] summarizes the experimental evidence indicating a transition region of only one or two molecules in thickness. The argument does not appear to be final, and applies only to water. The spherically symmetrical molecules considered in the present theory may behave rather differently. However, the present approximation could lead to a slightly too diffuse transition region because nearest neighbor interactions are not sufficiently emphasized (Eq. (3)).

The surface tension is given by[3,11]

$$\gamma=\int_{-\infty}^{+\infty}[p-p'(z)]dz \tag{15}$$

$$p'(z)=\rho(z)[\mu-A(z)] \tag{16}$$

where $A(z)$ is the local Helmholtz free energy per molecule. In the present theory (see Eqs. (9), (12), and (13))

$$\frac{p'(s)b'}{kT}=\theta(s)\left[\frac{1+2.9619\theta(s)+5.483\theta(s)^2}{1-0.8517\theta(s)^3-0.1483\theta(s)^4}\right]+\tfrac{1}{2}\Phi'(s)\theta(s). \tag{17}$$

The function $(p-p')b'/kT$ is plotted in Fig. 2 for different temperatures. The value of this function at each z indicates the relative contribution to γ of molecules in dz, and the area under the curve is $\gamma b'/kT$ (Eq. (15)). Values of $\gamma r^{*2}/\epsilon$ obtained by numerical integration are given in Table I.

Guggenheim[12] has shown that the experimental values of the surface tension for argon, nitrogen, and oxygen, over the combined range $T/T_c=0.45$ to 0.71, obey the empirical equation

$$\gamma=\gamma_0[1-(T/T_c)]^r, \quad r=11/9, \tag{18}$$

with $\gamma_0 v_c^{\frac{2}{3}}/T_c=4.4$ ergs deg^{-1} mole$^{-\frac{2}{3}}$. Values of $\gamma_0 r^{*2}/\epsilon$ from the present theory and Eq. (18) are shown in Table I. There is about a 10 percent variation in γ_0 from $T/T_c=0.5$ to 0.7. The theoretical value (using Eq. (11)) of $\gamma_0 v_c^{\frac{2}{3}}/T_c$ is 6.7 ergs deg^{-1} mole$^{-\frac{2}{3}}$ at $T/T_c=0.6$. Actually, the surface tension in Table I follows closely an equation analogous to Eq. (18) but with $r=13/9$, from $T/T_c=0.5$ to 0.9. But $r>13/9$ for $T/T_c>0.9$. This naturally raises the question as to whether Guggenheim's equation (Eq. (18)) is actually valid all the way to $T=T_c$ for molecules obeying the law corresponding states.

TABLE I.

T/T_c	$\gamma r^{*2}/\epsilon$	$\gamma v^{*2}/\epsilon$	δ/r^*	$r^{*2}\Gamma_{S.T.}$	$E_s r^{*2}/\epsilon$ ($\Gamma=0$)
0.50	0.574	1.34	0.740	0.792	1.401
0.60	0.420	1.29	0.825	0.808	1.339
0.70	0.276	1.20	0.967	0.840	1.232
0.80	0.152	1.08	1.225	0.891	1.077
0.90	0.0565	0.94	1.880	0.986	0.766
0.95	0.015	0.59	~1.9	~0.70	0.413
0.98	0.002	0.25	~2	~0.5	0.180
1.00	0.000	...	...	0.000	0.000

The function $p-p'(z)$ may also be used to locate the Gibbs dividing surface known as the surface of tension,[3,11] located at an origin $z=0$ such that

$$0=\int_{-\infty}^{+\infty}z[p-p'(z)]dz. \tag{19}$$

The marks on the curves in Fig. 2 indicate the location of the surface of tension, found by numerical integration. The distance δ between the surface of tension and the dividing surface $\Gamma=0$,

$$\delta=z_{S.T.}-z_{\Gamma=0} \tag{20}$$

is important in that it determines the dependence of surface tension on curvature according to the rigorous thermodynamic Gibbs-Tolman[11] equation,

$$\frac{d\ln\gamma}{d\ln r}=\frac{(2\delta/r)[1+(\delta/r)+\frac{1}{3}(\delta^2/r^2)]}{1+(2\delta/r)[1+(\delta/r)+\frac{1}{3}(\delta^2/r^2)]}, \tag{21}$$

where r is the radius of the (spherical) surface of tension and γ is the surface tension referred to the surface of tension.[3,11] As seen in Table I, δ is positive and of the order of magnitude of a molecular diameter, and increases with temperature. This is in agreement with the results of Tolman[11] based on a less satisfactory model[13] (van der Waals' equation was used in such a

[10] N. K. Adam, *Physics and Chemistry of Surfaces* (Oxford University Press, London, 1941), pp. 5–6.

[11] R. C. Tolman, J. Chem. Phys. **16**, 758 (1948); **17**, 118, 333 (1949). See also F. O. Koenig, J. Chem. Phys. **18**, 449 (1950).

[12] E. A. Guggenheim, *Thermodynamics* (North Holland Publishing Company, Amsterdam, 1949); J. Chem. Phys. **13**, 259 (1945).

[13] We should also remark that the present theory is much more satisfactory than that used in an earlier paper (T. L. Hill, J. Am. Chem. Soc. **72**, 3923 (1950)) in which a rather crude picture was employed not only for the molecular theory but *also* in the thermodynamics. The thermodynamics of the present approach is rigorous,

TABLE II. Argon, 90°K ($T/T_c=0.60$).

	This paper	Kirkwood and Buff[a]	Experiment[a]
γ(ergs/cm²)	6.0	14.9	11.9
$E_s(\Gamma=0)$(ergs/cm²)	19.0	27.2	35
δ(A)	2.81	3.63	···
$\Gamma_{S.T.}$(g/cm²)	4.61×10^{-8}	4.99×10^{-8}	···

[a] See reference 4.

way that a finite discontinuity in density existed in the transition region). Since $\delta>0$, γ decreases with decreasing r. Of course δ is a function of r as well as T, but the dependence on r must be slight until one reaches rather small drops.

Incidentally the occurrence of the maxima in the $p-p'(z)$ curves on the liquid side of the $\Gamma=0$ dividing surface and the asymmetry of these curves with the relatively long tail on the liquid side are together responsible for δ being positive.

The superficial density of matter at the surface of tension, $\Gamma_{S.T.}$, is also given in Table I, as calculated from

$$\Gamma_{S.T.}=\delta(\rho_{\text{liquid}}-\rho_{\text{gas}}) \tag{22}$$

The Gibbs surface density of internal energy E_s referred to a dividing surface at $s=s'$ is given by

$$\frac{2E_sb'}{r^*kT}=\int_{-\infty}^{s'}[\Phi'(s)\theta(s)+\alpha'\theta_G^2]ds + \int_{s'}^{+\infty}[\Phi'(s)\theta(s)+\alpha'\theta_L^2]ds \tag{23}$$

where θ_G and θ_L are the bulk values of θ. The important choice of s' is at the surface $\Gamma=0$ since only when referred to this surface is E_s related to γ by

$$d(\gamma/T)/dT=-E_s/T^2. \tag{24}$$

Table I includes E_sr^{*2}/ϵ, calculated from Eq. (23), for the dividing surface $\Gamma=0$. As a check, Eq. (24) has been used to calculate $\gamma r^{*2}/\epsilon$ at $T/T_c=0.5$ and 0.7 by integration of E_s (after drawing a smooth curve) from $T/T_c=1$ to T/T_c. The results are 0.576 and 0.271, respectively, in satisfactory agreement with Table I.

Finally, numerical values have been computed for argon at 90°K ($T/T_c=0.6$), using[14] $r^*=3.41$A and $\epsilon=16.5\times10^{-15}$ erg. These are compared in Table II with the calculations of Kirkwood and Buff[4] and with experiment.[4] For the purpose of these latter calculations (not to be confused with the more extensive calculations—not yet carried out—mentioned in Section I), Kirkwood and Buff employed essentially the experimental bulk liquid radial distribution function, a considerable improvement over Eq. (3), but used a step function for $\rho(z)$. The Kirkwood and Buff values of γ and E_s are in better agreement with experiment than those obtained here (though our ratio γ/E_s is better). δ and $\Gamma_{S.T.}$ are of the same order of magnitude in the two calculations. While Eq. (14) leads to a value of γ too small by a factor of two (Table II), it might be remarked that solution of the van der Waals integral equation leads to a value of γ too small by a factor of about ten.

These calculations are being extended to spherical surfaces and to physical adsorption.

APPENDIX

A continuous theory for $\rho(z)$ (i.e., avoiding a lattice[15]) can also be set up based on the Lennard-Jones and Devonshire[16] theory of liquids. The dependence of the local entropy on the density gradient would be included in this type of approach.*

We merely sketch the method here. We use the LJD theory with $Z=12$ nearest neighbors and take account of nearest neighbor interactions only. Consider a cell with center at z. Because ρ is not constant, nearest neighbors on the liquid side will be nearer the cell center than those on the gas side. We assume that the Z nearest neighbors are still distributed isotropically over the cell surface as far as *solid angle* is concerned.† Using the same coordinate system as in Eq. (4), there will then be $(Z/2)\sin\theta'd\theta'$ nearest neighbors between θ' and $\theta'+d\theta'$. These molecules will be at a distance a from the cell center, where

$$a=z'/\cos\theta'$$

and z' is the root of

$$(z'/\cos\theta')^3=\sqrt{2}/\rho(z+z')$$

for given $\rho(z)$ and θ'. This completely determines the shape of the cell surface and hence the potential field in which the central molecule moves inside the cell. It is then straightforward to write down an expression for the contribution A of a molecule in this cell to the Helmholtz free energy of the system, in terms of the phase integral for motion in the cell, and including the communal entropy. If the position of minimum potential energy inside the cell is at z'', the central molecule is counted as "belonging" to z'' in writing down the expression for the Helmholtz free energy of the entire system,

$$A=\mathfrak{A}\int_{-z_G}^{+z_L}\mathrm{A}(z'')\rho(z'')dz''$$

where the cross-sectional area $\mathfrak{A}$ and the location of the top and bottom of the container at $-z_G$ and z_L are constant. The remaining problem is then to find that function $\rho(z)$ which minimizes A at constant z_G, z_L, $\mathfrak{A}$, T, and N, where

$$N=\mathfrak{A}\int_{-z_G}^{+z_L}\rho(z'')dz''.$$

[14] This value of r^* is taken as the value of r such that $u(r)=0$, using the Lennard-Jones 6-12 potential, as given by Fowler and Guggenheim, *Statistical Thermodynamics* (Cambridge University Press, London, 1939).

[15] J. E. Lennard-Jones and J. Corner, Trans. Faraday Soc. **36**, 1156 (1940); J. Corner, **44**, 1036 (1948); J. W. Belton and M. G. Evans, **37**, 1 (1941).

[16] J. E. Lennard-Jones and A. F. Devonshire, Proc. Roy. Soc. (London) **163A**, 53 (1937); **165A**, 1 (1938); hereafter referred to as LJD.

* Incidentally, we recognize that the concepts of "local entropy" and "local Helmholtz free energy" are properties of approximate theories and need not arise in a rigorous theory such as that of Kirkwood and Buff. (See reference 4.)

† A more general approach would be, for a given curve $\rho(z)$, to make the distribution in solid angle nonisotropic in such a way as to minimize the local Helmholtz free energy A of a molecule in the cell.

The NH Stretching Vibration and NH—N Hydrogen Bonding in Several Aromatic Compounds*

NELSON FUSON, MARIE-LOUISE JOSIEN, ROBERT L. POWELL, AND EMERY UTTERBACK
Infrared Spectrometry Laboratory, Fisk University, Nashville, Tennessee
(Received July 27, 1951)

The three-micron infrared absorption bands assigned to the NH stretching vibration have been studied in pyrrole, indole, carbazole, diphenylamine, and aniline. Spectra have been obtained in solution in carbon tetrachloride, carbon disulfide, chloroform, and benzene over a wide range of concentrations. In pyrrole and indole with increasing concentration the sharp NH band fades out and a broader band to lower frequencies appears. While the results are not as clearcut for diphenylamine and aniline, for these four compounds hydrogen bonding satisfactorily explains the observed data. This conclusion, for pyrrole and indole, sets aside the infrared spectroscopic basis for Pauling's hypothesis of two species of molecules. Carbazole was not soluble enough to make association studies possible. The relation of both the solvent and the solute molecular structure to the position of the associated and unassociated frequencies is discussed.

INTRODUCTION

IN recent years correlations between the infrared spectrum of a compound and its chemical properties have been increasingly investigated. In 1945, Linnett[1] summarized the relation between the force constants of NH, CH, and other X—H bonds and the frequency of the stretching vibrations of these groups. A few years later Richards,[2] from known values of frequencies, calculated force constants for about thirty OH and NH compounds, suggesting a relationship between the latter and acidity for carboxylic acids. By a study of reaction rates Flett[3] was able to add weight to the hypothesis that small variations in the frequency of bands of several different stretching vibrations were predominately related to changes in the force constants of these bonds. The latter writer also suggested infrared spectroscopy as a means of gaining information about electron distribution in the molecule. Recently Sutherland[4] stated that shifts in hydrogenic stretching frequencies and changes in their intensities can both arise from variations in the intramolecular field caused by changes in charge distribution on the bond.

In 1947, Longuet-Higgins and Coulson[5] calculated the distribution of electrons in pyrrole, indole and carbazole by the method of molecular orbitals in order to see if there would be any correlation between electron density and some of the properties of these molecules. These authors concentrated their attention on the carbon atoms. The following year Berthier and Pullman[6] noticed that the increasing value of electronic density on the N atom with increasing size of the molecule in the pyrrole, indole, carbazole series was in disagreement with conclusions drawn by Wheland[7] from the theory of resonance. However a similar molecular orbital calculation of electron density for aniline, diphenylamine, and triphenylamine by Berthier and Pullman[6] gave results in agreement with resonance theory.

Since extensive theoretical work on these NH containing molecules has been made, we thought it would be of value to make a comparative study of the infrared spectrum of the NH stretching vibration frequency in these compounds to see whether further light could be thrown on this disagreement. For this purpose the free vibration frequencies are needed, so the possibility of hydrogen bonding had to be taken into consideration. Sutherland,[8] for example, in 1940 stated that, in comparison with the situation for the OH group, the results of studies of hydrogen bonding in NH containing compounds are not clearcut, though there are strong indications that such bonding can occur in certain cases. A literature survey and some preliminary experiments[9] showed that it would be necessary to make a thorough study of the effect of solution concentration upon the position of the NH frequency before being able to draw any conclusions.

EQUIPMENT

The infrared spectrometer used was a single beam, automatic recorder which has been described briefly elsewhere.[10] A large lithium fluoride prism was used throughout the work. Its calibration in the 3600–1500 cm^{-1} region (2.8–6.5μ) was based[11] on the 6μ water vapor band, the carbon dioxide band at 4μ, and the ammonia and methane bands in the 3μ region. From 3900–3500 cm^{-1} (2.6–2.8μ) lines of the 2.7μ water vapor

* This paper has been reported in part at the Symposium on Molecular Structure and Spectroscopy, Ohio State University, June 11–15, 1951, and at the international meeting on infrared spectroscopy held in Basel, Switzerland, June 28–30, 1951. Some preliminary results form the thesis which was submitted by E. Utterback to the Graduate Faculty of Fisk University in partial fulfillment of the requirements for the degree of Master of Arts, May, 1951.

[1] J. W. Linnett, Trans. Faraday Soc. **41**, 223 (1945).
[2] R. E. Richards, Trans. Faraday Soc. **44**, 40 (1948).
[3] M. St. C. Flett, Trans. Faraday Soc. **44**, 767 (1948).
[4] G. B. B. M. Sutherland, Disc. Faraday Soc. **9**, 274 (1950).
[5] H. C. Longuet-Higgins and C. A. Coulson, Trans. Faraday Soc. **43**, 87 (1947).
[6] G. Berthier and B. Pullman, Compt. rend. **226**, 1725 (1948).
[7] G. W. Wheland, *The Theory of Resonance* (John Wiley and Sons, Inc., New York, 1944), p. 167.
[8] G. B. B. M. Sutherland, Trans. Faraday Soc. **38**, 889 (1940).
[9] M. L. Josien and N. Fuson, Compt. rend. **232**, 658 (1951).
[10] Josien, Fuson, and Cary, J. Am. Chem. Soc. **73**, 4445 (1951).
[11] Oetjen, Kao, and Randall, Rev. Sci. Instr. **13**, 515 (1942).

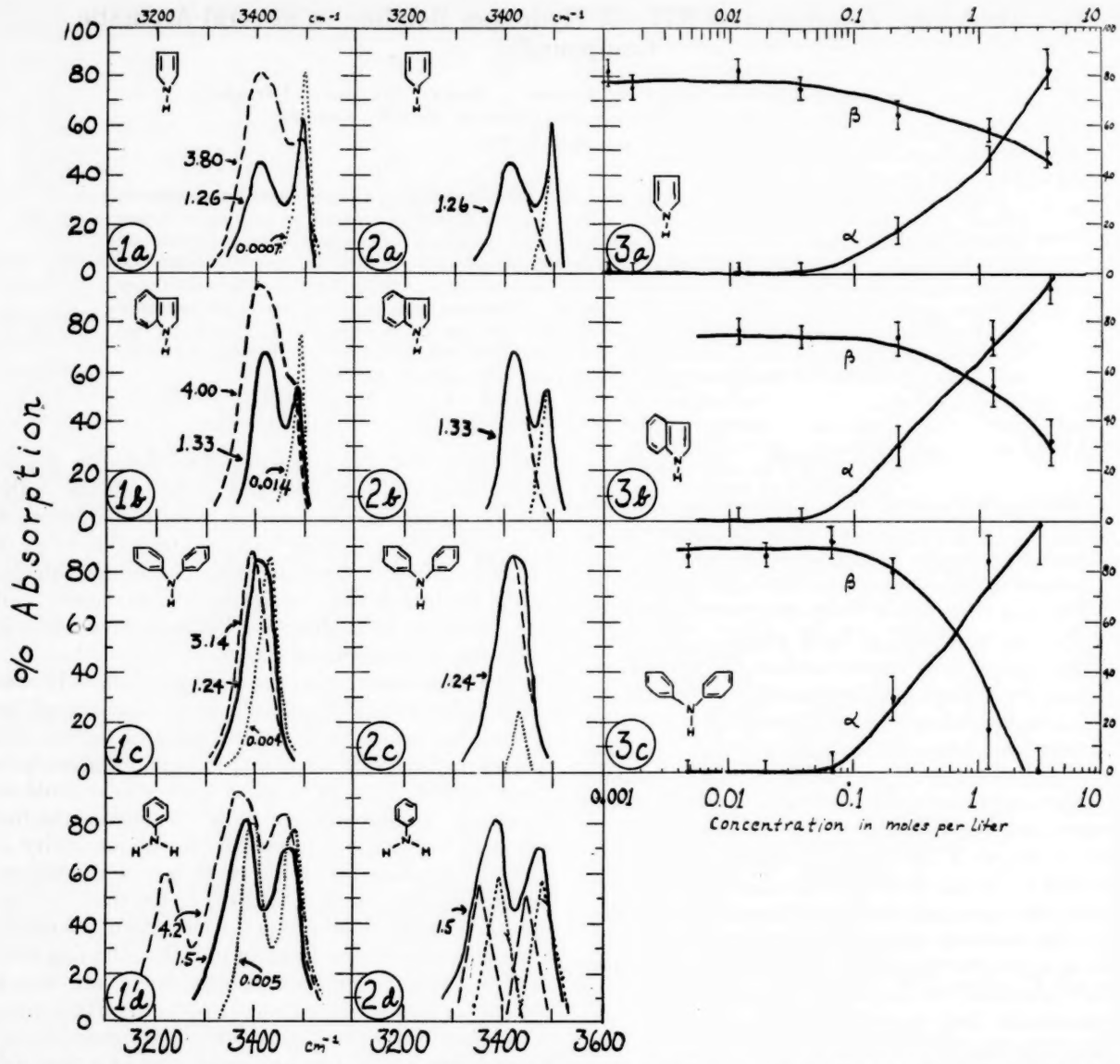

FIG. 1. Superposition of absorption spectra of the NH stretching vibration at different concentrations in carbon tetrachloride solution (path length times concentration held constant). (a) pyrrole: 3.80, 1.26, and 0.0007 mole/liter; (b) indole: 4.00, 1.33, and 0.014 mole/liter; (c) diphenylamine: 3.14, 1.24 and 0.004 mole/liter; and (d) aniline: 4.20, 1.50, and 0.005 mole/liter.

FIG. 2. Examples of graphical resolution of medium concentration spectra (taken from Fig. 1) to show overlapping contributions of the associated and unassociated NH bands (shown by dashed and dotted lines, respectively). (a) pyrrole, 1.26 molar; (b) indole, 1.33 molar; (c) diphenylamine, 1.24 molar; and (d) aniline, 1.50 molar.

FIG. 3. Effect of concentration upon the intensity of associated (α) and unassociated (β) NH bands (the vertical lines indicated the uncertainty). (a) pyrrole; (b) indole; and (c) diphenylamine.

band under medium grating dispersion[12] were used for the calibration.

The performance of the spectrometer in the 3μ region with the lithium fluoride prism is such that a single record enables the location of a sharp band to within ± 2 cm^{-1}. The average of three records of the same spectrum reduces the uncertainty to ± 1 cm^{-1}. The spectral slitwidth of the spectrometer was approximately 10 cm^{-1} in the 3000–3600 cm^{-1} region.

Cell lengths used ranged from 0.001 cm to 5.2 cm. All the absorption cells were made with rock salt windows. For the thinner cells, spacers of aluminum foil, tin foil, and lead sheet were used; the walls of the larger cells were constructed from glass tubing.

[12] W. W. Sleator, Astrophys. J. 48, 125 (1918).

EXPERIMENTAL RESULTS

The following compounds have been studied in solution in the 3700–3000 cm^{-1} region: pyrrole, indole, carbazole, diphenylamine and aniline. The results are given in Tables I through V. These compounds were of the highest purity obtainable from the Eastman and the Eimer and Amend Catalogue listings.

Carbon tetrachloride was the standard solvent used.

TABLE I. Effect of concentration upon the carbon tetrachloride solution spectra of the NH stretching vibration band of pyrrole, indole, carbazole, and diphenylamine.

Compound	Molar concentration	Path length (cm)	Conc. ×path length	Unassociated band Frequency (cm^{-1})[e]	Unassociated band Intensity (% abs.)[f]	Associated band Frequency (cm^{-1})[e]	Associated band Intensity (% abs.)[f]
Pyrrole	14.4[a]	cap. film	( )[c]	...	0	3395	60
	3.80	0.0010	0.0038	3487	50	3408	82
	1.26	0.0030	0.0038	3494	57	3411	46
	0.225	0.0165	0.0038	3494	63	3420	17
	0.039	0.10	0.0038	3497	73	...	0
	0.013	0.29	0.0038	3496	85	...	0
	0.0018	2.13	0.0038	3498	76	...	0
	0.0007	5.12	0.0038	3496	82	...	0
Indole	...	solid	...	...	0	3401	100
	4.00	0.0010	0.0040	3480	30	3417	96
	1.33	0.0030	0.0040	3487	53	3422	70
	0.24	0.0165	0.0040	3491	74	3430	33
	0.040	0.10	0.0040	3491	73	...	0
	0.014	0.29	0.0040	3491	76	...	0
Carbazole	...	solid	...	...	0	3413	80
	0.0008	5.12	0.0041	3483	79	...	0
Diphenylamine	3.14[b]	0.0030	0.0105[d]	...	0	3400	93
	1.24	0.0165	0.0205	3427	15	3405	84
	0.21	0.10	0.0205	3432	80	3400	30
	0.07	0.29	0.0205	3431	93	...	0
	0.010	2.13	0.0205	3434	87	...	0
	0.004	5.12	0.0205	3433	87	...	0

[a] Pure liquid pyrrole.
[b] Approximately saturated solution.
[c] Not measured.
[d] Not in the same product series.
[e] Frequencies as read before graphical resolution, e.g., from Fig. 1(a).
[f] Intensities as read after graphical resolution, e.g., from Fig. 2(a).

Supplementary solution studies were made in carbon disulfide, chloroform, and benzene. The series of concentrations investigated ranged from about 0.001 molar to about 10 molar for each compound with the exception of carbazole, whose maximum solubility was about 0.006 molar. In some of the series the number of molecules per unit area in the optical path was kept constant by maintaining a constant product of concentration and sample cell path length. The largest uncertainty in the value of this product was introduced in those cases involving the two thinnest cells whose thickness was measured to an accuracy of 10 percent.

A spectral background was obtained with the appropriate cell filled with pure solvent immediately before each solution spectrum in this cell was recorded. With the aid of these backgrounds percentage absorption plots of each sample spectrum were made. Some of these are shown superposed upon each other in Fig. 1.

COMPARISON WITH PREVIOUS RESULTS

We have elected to summarize the literature on each compound immediately preceeding the discussion of our results in order to make comparisons more easily. All the work described in this section, unless specified otherwise, was done in carbon tetrachloride solution.

Pyrrole

In 1935, Wulf and Liddell,[13] in the course of a spectroscopic study of the second NH vibration harmonic, found for pyrrole in dilute solution a "definite evidence of a small subsidiary maximum" on the low frequency side of the main absorption peak. They interpreted both peaks as resulting from characteristic vibrations of the molecule and attributed this complex structure to mechanical resonances with neighboring CH groups. Pauling,[14] in analyzing their results a year later, suggested that the doubling of the NH band might be explained by simultaneous existence of "two molecular species in a solution of pyrrole" consisting of "coplanar and non-coplanar molecules." M. Freymann and R. Freymann, in 1936, studied the third harmonic in solution[15,16] and as a vapor.[17] They concluded that their observations were in agreement with Wulf's results and Pauling's analysis. In 1939, Buswell and coworkers[18,19] in their studies of hydrogen bonding mention, without further detail, that the NH vibration in liquid pyrrole is at 3410 cm^{-1} while in dilute solution it is at 3510 cm^{-1}, and state that this compound does not show "any appreciable tendency to associate." Gordy,[20] whose curves, published in 1940, show a shift from *ca*

[13] O. R. Wulf and U. Liddel, J. Am. Chem. Soc. **57**, 1464 (1935).
[14] L. Pauling, J. Am. Chem. Soc. **58**, 94 (1936).
[15] M. Freymann and R. Freymann, J. phys. et radium **7**, 476 (1936).
[16] M. Freymann, Ann. chim. (11) **11**, 11 (1939).
[17] M. Freymann, Compt. rend. **205**, 852 (1937).
[18] Buswell, Downing, and Rodebush, J. Am. Chem. Soc. **61**, 3252 (1939).
[19] Buswell, Downing, and Rodebush, J. Am. Chem. Soc. **62**, 2759 (1940).
[20] W. Gordy and S. C. Stanford, J. Am. Chem. Soc. **62**, 497 (1940).

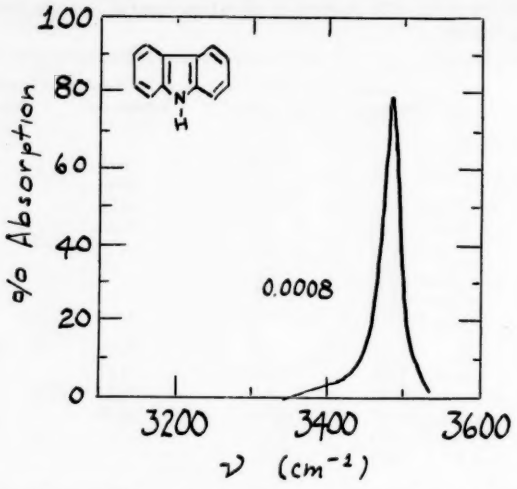

FIG. 4. The NH vibration band spectrum of carbazole in 0.0008 molar carbon tetrachloride solution.

3425 cm^{-1} to *ca* 3590 cm^{-1} in going from pure liquid to 0.1 molar solution, decided that there was reason to believe association was present in the pure liquid.

Examination of the spectral data for pyrrole in Table I and Fig. 1(a) shows immediately that, even though the total number of molecules in the optical path remains constant, two peaks are present for higher concentrations while for the lower concentrations only one simple sharp absorption remains. These results do not contradict the observations of Buswell and Gordy; their work being made with rock salt prism spectrometers, the dispersion available to them was not sufficient to resolve the two peaks, so they observed only a single band which shifted with change in concentration.

Figure 1(a) is qualitatively very similar to the spectra of hydroxy compounds, for example to the curves for phenol in solution published by Fox and Martin.[21] For sufficiently high concentrations a broad band appears on the low frequency side of a sharp band, the former being assigned to the OH stretching vibration of the associated molecules, the latter to that of the free or unassociated molecules. The frequency difference between the peaks in pyrrole is much smaller than in the case of phenol. To show more clearly that the low frequency band in pyrrole is an associated band, curves such as Fig. 2(a) were drawn to resolve, graphically, the two overlapping bands. From the intensities obtained by this method a plot of percentage absorption against molar concentration could be made for each peak. The resulting curve, Fig. 3(a), while approximate, as is indicated by the vertical line "error" ranges, shows conclusively that the associated band disappears at a molar concentration between 0.01 and 0.1 while at the same time the unassociated band intensity increases and levels off at its maximum value. The high frequency peak, which is always the sharper peak, remains almost unchanged in position as the concentration changes. Its small shift, which occurs for very concentrated solutions, may be attributed to the overlapping interference of the associated band. The associated band peak shifts to lower frequencies as the concentration increases, in a manner similar to that for phenol,[21] although the shift is much less, being about 12 cm^{-1}.

Whatever the reason for the complexity of the band found by Wulf and Liddell and by the Freymanns in the overtone spectra of the NH vibration for pyrrole, we are satisfied that our high dispersion study of the fundamental frequency over a wide range of concentrations removes the infrared spectroscopic basis for Pauling's hypothesis of two types of molecules and for Wulf's suggestion of coupling with neighboring CH groups. It should be mentioned that there are additional reasons for believing both that pyrrole is associated,[22] and that it consists of only one species of molecule.[23]

Indole

The statements made by Wulf[13] and Pauling[14] on indole are very similar to theirs already summarized for pyrrole. Gordy[24] observed no shift in frequency for indole in studying 0.1 molar and 1.63 molar solution. He suggested that the lack of a shift as compared to that which he found for pyrrole could be explained by steric hindrance.

The present study, in Table I and Fig. 1(b), shows that the behavior of indole is very similar to that of pyrrole. Going through the same procedure of graphical resolution of the overlapping curves (Fig. 2(b)), it is possible to show (Fig. 3(b)) the effect of concentration upon band intensity and to conclude that, here again, association is responsible for the appearance of the lower wave number band and the disappearance of the higher frequency band with increasing concentration. Thus our results are not only in disagreement with those of Gordy, but also they remove the infrared spectroscopic basis for Pauling's and Wulf's hypotheses.

Carbazole

Our results on carbazole (Table I and Fig. 4) are in agreement with those of Wulf[13] who found only a single sharp band for the 2nd harmonic. The low solubility of carbazole made it impossible to carry through the same series of experiments as for pyrrole and indole, though the trend of our results for these latter two would indicate that at high concentrations the former might show bonding.[25]

[21] J. J. Fox and A. E. Martin, Proc. Roy. Soc. (London) **A162** 419 (1937).

[22] J. M. Robertson, J. Chem. Soc. 615 (1935); 1195 (1936).

[23] J. Lecomte, Bull. soc. chim. France (5) **13**, 415 (1946).

[24] W. Gordy, J. Am. Chem. Soc. **59**, 464 (1937).

[25] While no concentrated solution study of the spectrum of carbazole could be made, it was possible to compare the spectra of both carbazole and indole as solids as well as in dilute solution. The results are given in Table I. Note that the difference between the NH stretching frequency for the dilute solution and the solid sample for carbazole is 70 cm^{-1}, for indole, 90 cm^{-1}. These being approximately the same, this is indirect evidence that carbazole and indole might also behave in the same fashion in concentrated solution.

Diphenylamine

A number of studies of diphenylamine in solution are available in the literature. Wulf[13] found a single sharp peak for the second harmonic of the NH vibration. Buswell[19] found the fundamental to lie at 3460 cm^{-1} and states that this compound does not have any appreciable tendency to associate. Gordy's curves[20] show a shift from *ca* 3500 cm^{-1} to *ca* 3425 cm^{-1} in going from 0.1 to 1.63 molar solution; this he interpreted as evidence of association. Richards[2] lists, from his unpublished data, the value 3445 cm^{-1}.

From the present results on diphenylamine shown in Table I and Fig. 1(c), it may be seen that the effect of concentration upon the appearance of the band is somewhat like that of pyrrole and indole. This is true in spite of the difficulty in resolution, the separation between the two bands for diphenylamine being only about onehalf as great as in the spectra of indole and pyrrole. In several cases, one of which is illustrated in Fig. 5, better resolution was obtained than in the set of records included in Fig. 1(c). Therefore it appears justifiable to make a graphical resolution of the two peaks in the absorption bands at different concentrations (Fig. 2(c)) and to draw the graph of intensity *vs* concentration (Fig. 3(c)) which, while less accurate, still gives much the same result as that obtained for pyrrole and indole.

Our results differ numerically, in varying amounts, from those of the previous workers but do not contradict them. However again, rather than a band shift, we believe that for increasing concentration we observe the simultaneous appearance of an associated band at one point in the spectrum as the unassociated band close by grows weaker.

Aniline

The spectral region for the pair of stretching vibrations in the NH_2 group in aniline has been widely studied. In 1933, R. Freymann[26] made a preliminary study of the effect of dilution upon the unresolved third harmonic. A few years later, M. Freymann[16] resolved the third harmonic of the pure liquid and of the 0.5 normal solution, obtaining frequencies of 10,001 cm^{-1} and 9719 cm^{-1} in the former case and 10,086 cm^{-1} and 9792 cm^{-1} in the latter. Noticing such a shift both with dilution and with elevation of temperature, she interpreted this as being due to van der Waal's forces of molecular interaction rather than hydrogen bonding. Wulf[13] observed two well separated peaks *ca* 6900 and 6700 cm^{-1} in the spectrum of the second harmonic, the latter being much the stronger. He observed that "from dilute solution through very concentrated solutions even to pure liquid aniline, the absorption bands though undergoing some changes still had about the same position and had roughly the same absorption." Kinsey and Ellis,[27] who repeated Wulf's work, found only one additional feature, a diminution in intensity of the higher frequency band such that in the pure liquid it became but a shoulder of the band. Yaroslavskii[28] reports that the second harmonic at 6620 cm^{-1} in the solid shifts 60 cm^{-1} to higher frequency in solution.

Buswell, *et al*,[17,18] observed the two peaks in dilute solution at 3485 cm^{-1} and 3415 cm^{-1}. For the pure liquid they found "a fairly narrow single (unresolved) peak" at 3365 cm^{-1}. They suggested that the shifting could be due to changes in dielectric constant rather than hydrogen bonding. In 1937, Gordy[24] found one band which did not shift in going from pure liquid to a 1:1 solution. In a later study[29] in benzene solution he again observed but one band which shifted from 3450 cm^{-1} in the pure compound to 3540 cm^{-1} in 1.0 molar and 0.5 molar solutions, and postulated weak hydrogen bonds between the molecules as being the cause of this shift. Williams, Hofstadter, and Herman[30] also suggest hydrogen bonding of the pure liquid. Richards[2] lists, from his unpublished data, 3410 cm^{-1} and 3480 cm^{-1} as the positions of the two NH peaks. Flett[3] gives 3410 cm^{-1} and 3489 cm^{-1} in a 0.05 percent solution.

A study of our results in Table II and Fig. 1(d) shows that the change in position of each of the two bands for aniline is about the same as that for diphenylamine (Fig. 1(c)). Because of this and because of slight shoulders and other asymmetries present at various stages of concentration this change does not seem to be a true shift but the resultant effect of an appearance of an associated band and the simultaneous disappearance of the unassociated band. An attempt made to resolve graphically each of the two bands (Fig. 2(d)) made it clear that the uncertainty in both position and intensity would be so great that a plot of percentage absorption

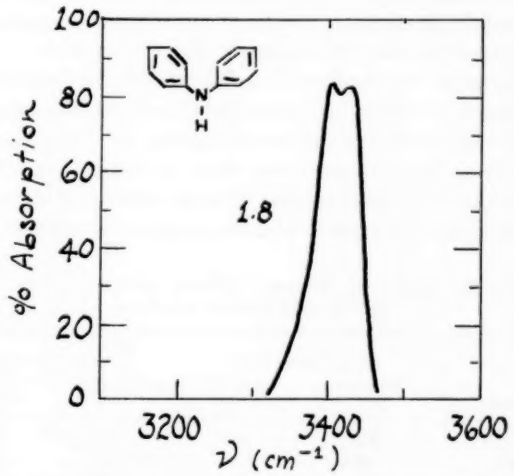

FIG. 5. Sample of the spectrum of diphenylamine in 1.8 molar carbon tetrachloride solution showing partial resolution of associated and nonassociated bands.

[26] R. Freymann, Ann. phys. (10) **20**, 243 (1933).
[27] E. L. Kinsey and J. W. Ellis, J. Chem. Phys. **5**, 399 (1937).
[28] N. G. Yaroslavskii, J. Phys. Chem. U. S. S. R. **22**, 265 (1948).
[29] W. Gordy, J. Chem. Phys. **7**, 167 (1939).
[30] Williams, Hofstadter, and Herman, J. Chem. Phys. **7**, 802 (1939).

TABLE II. Effect of concentration upon the CCl_4 solution spectrum of the two NH_2 stretching vibration bands of aniline.

Molar concentration	Path length (cm)	Conc. ×path length	Asymmetrical Frequency (cm^{-1})	Asymmetrical Intensity (% abs.)	Symmetrical Frequency (cm^{-1})	Symmetrical Intensity (% abs.)
11.0[a]	cap. film	( )[b]	3432	30	3353	50
8.35	0.0030	0.025	3437	82	3355	95
4.20	0.0060	0.025	3458	84	3364	93
1.54	0.0165	0.025	3456	84	3366	93
0.25	0.10	0.025	3472	71	3385	82
0.086	0.29	0.025	3480	82	3395	84
0.0116	2.13	0.025	3479	74	3393	78
0.0048	5.12	0.025	3481	78	3395	82

[a] Pure liquid aniline.
[b] Not measured.

versus concentration for aniline would not contribute any real objective information.

In this case again, we suggest that a true hydrogen bonding takes place rather than van der Waal's force interaction or dielectric constant changes. It is interesting to note that Gordy's intuition led him to a hydrogen bonding interpretation in spite of the lack of resolution of his spectrometer.

GENERAL DISCUSSION

In the following paragraphs the influence both of the solvent and of the particular solute molecule upon the NH frequencies will be summarized.

Effect of the Solvent upon Hydrogen Bonding

Analysis of the experimental results previously presented showed that for all the compounds studied in sufficiently concentrated carbon tetrachloride solution, the NH group engaged in hydrogen bonding with like molecules.[31] The previous uncertainty already referred to[8,32] with regard to hydrogen bonding in NH containing compounds may be attributed, at least for the compounds here studied, to lack of instrument resolution or sufficient number and range of concentrations.

In order to study the influence of the solvent on hydrogen bonding, additional solution spectra of pyrrole were obtained in carbon disulfide, chloroform, and benzene. The concentration effect in these solvents was found to be similar to that already described in carbon tetrachloride. Of particular interest is the comparative result at rather high concentration (Table III and Fig. 6) which shows that while the frequency of the unassociated band depends upon the solvent, the position of the associated band is practically independent of solvent. A possible explanation would be that when a molecule of the solute is hydrogen bonded to another like molecule (N—H···N) it becomes almost totally unaffected by the solvent. We have not found any similar phenomenon reported in the literature. It should be noted, too, that at the concentration shown in Fig. 6, the ratio of intensities of the two bands differs from solvent to solvent, the unassociated band being the stronger for benzene and chloroform, the opposite being true for the two less polar solvents. This indicates that in the case of NH hydrogen bonding the percentage of molecules associated is a function both of the solvent and of the concentration, as has been shown by Mecke[33] for hydrogen bonding involving OH.

TABLE III. Effect of different solvents upon the spectrum of pyrrole in 2.0 molar solution.[a]

Solvent	Unassociated band Frequency (cm^{-1})	Unassociated band Intensity (% abs.)	Associated band Frequency (cm^{-1})	Associated band Intensity (% abs.)
CCl_4	3491	38	3406	43
$CHCl_3$	3484	53	3411	34
CS_2	3476	50	3401	69
C_6H_6	3453	64	3400	40

[a] Path length approximately 0.001 cm.

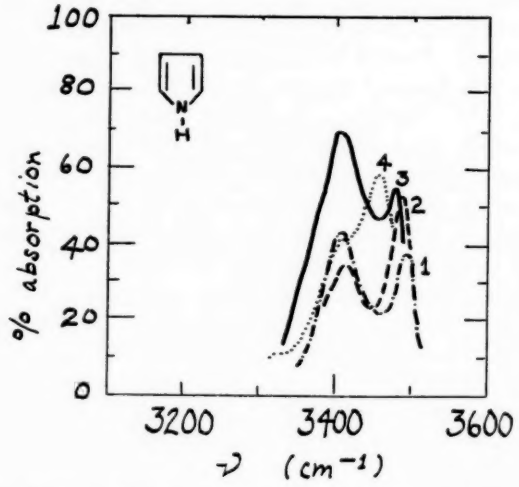

FIG. 6. Effect of different solvents upon the 2.0 molar solution of pyrrole. A comparison of the relative intensities of the associated and the unassociated bands for each particular solvent is significant. Because the pathlength was not very constant (0.01 mm±20 percent) no significance should be attached to differences in associated (or for unassociated) band intensities as the solvent is changed. (1) carbon tetrachloride; (2) chloroform; (3) carbon disulfide; and (4) benzene.

The Effect of Solvent upon the Free NH Vibration

The results of a preliminary study of the effect of solvent upon the unassociated NH vibration are summarized in Table IV. The extinction coefficients for pyrrole, indole and carbazole are approximately four times those for aniline and diphenylamine. For each of the five compounds the carbon tetrachloride solution frequency is the highest. With one exception, that of the higher frequency member of the pair of aniline bands, the decreasing frequency sequence is in the following solvent order: carbon tetrachloride, chloroform, carbon disulfide, benzene. The frequency shift due to solvent

[31] Skatole (methylindole) also shows this hydrogen bonding, its NH vibration spectrum being almost identical to that for indole (E. Utterback, thesis, Fisk University, May, 1951).
[32] P. Rumpf, Bull. soc. chim. France 211 (1948).
[33] R. Mecke, Disc. Faraday Soc. 9, 161 (1950).

TABLE IV. Effect of different solvents upon the spectrum of the unassociated NH vibration.

Compound	Molar concentration	Path length cm	Solvent	Unassociated NH absorption band: Frequency (cm^{-1})	Freq. dif.[a] (cm^{-1})	Intensity[b] % abs.	Intensity[b] E_a^{10}	Half-width[c] (cm^{-1})
Pyrrole	0.12	0.0165	CCl_4	3497	0	50	150	23
			$CHCl_3$	3486	11	53	160	27
			CS_2	3481	16	51	150	24
			C_6H_6	3458	39	57	180	43
Indole	0.12	0.0165	CCl_4	3491	0	43	140	21
			$CHCl_3$	3482	9	42	140	27
			CS_2	3478	13	42	140	26
			C_6H_6	3447	44	48	165	37
Carbazole	0.006[d]	0.10	CCl_4	3483	0	20	165	16
			$CHCl_3$	3473	10	25	205	25
			CS_2	3466	17	17	135	25
			C_6H_6	3433	50	25	205	25
Diphenylamine	0.10	0.10	CCl_4	3434	0	60	40	38
			$CHCl_3$	3431	3	60	40	40
			CS_2	3423	11	70	55	38
			C_6H_6	3409	25	85	85	45
Aniline (asymm. vib.)	0.10	0.10	CCl_4	3481	0	50	30	60
			$CHCl_3$	3454	27	40	23	70
			CS_2	3473	8	58	40	40
			C_6H_6	3470	11	50	30	50
Aniline (sym. vib.)	0.10	0.10	CCl_4	3394	0	60	40	45
			$CHCl_3$	3388	6	50	30	70
			CS_2	3385	9	65	45	35
			C_6H_6	3382	12	68	50	40

[a] Difference between frequency for CCl_4 solution and the solution frequency for the solvent listed in the same row.
[b] The apparent extinction coefficient $E_a' = (1/cl) \log_{10}(T_0/T)$ is chosen as the absolute intensity comparison. The spectral slit width, (s) is 10 cm^{-1}. The uncertainty range for these coefficients is 20 percent. See Marion, Ramsay, and Jones, J. Am. Chem. Soc. **73**, 305 (1951) for discussion of this coefficient.
[c] Width at half of peak intensity: uncertainty = ± 3 cm^{-1}.
[d] Probably 10 to 20 percent less concentrated in case of CCl_4 and CS_2 (some solid particles were observed to be suspended in the solution.)

was largest for pyrrole, indole, and carbazole in benzene; diphenylamine and aniline were somewhat less affected.

For each compound, with the exception of aniline, we found that the width of the unassociated band tended to increase as the frequency decreased, in agreement with the findings of Mecke on phenol.[33] However within the limit of accuracy of our intensity measurements, the particular solvent used appeared to have little effect upon the extinction coefficients. In other words, we did not observe any significant change in intensity as Mecke did.

Effect of Intramolecular Environment upon NH Association

We will confine our discussion of the effect of intramolecular environment upon the NH bond to carbon tetrachloride solution values since this solvent has the least interaction with the molecules of the solute. The percentage of molecules remaining in the monomeric form at any particular solution concentration may be calculated from the ratio of the extinction coefficient of the unassociated band at that concentration to the extinction coefficient at infinite dilution.[32] From the data in Table I it is possible to make this calculation in a very approximate manner. The results for pyrrole, indole, and diphenylamine are shown in Fig. 7. Mecke's results for phenol[33] are included for comparison purposes. In general it appears that the association at any particular concentration is less for the NH compounds than for the phenol.

In order to compare the hydrogen bonding in the different molecules in another way, the frequencies and frequency separations of the NH associated and unassociated bands in carbon tetrachloride solution are listed in Table V. Both of the two groups of compounds studied contain a trivalent nitrogen atom. The acidity of some of these compounds, which have been measured

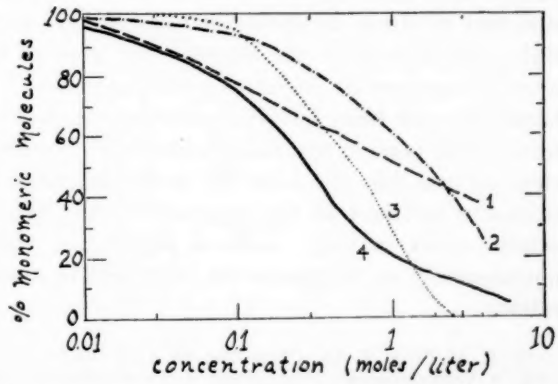

FIG. 7. Effect of concentration upon the proportion of unassociated or monomeric molecules present in the solution. (1) pyrrole; (2) indole; (3) diphenylamine; and (4) phenol (data taken from Mecke's work (reference 33)).

TABLE V. Comparison of NH valence vibration frequencies and frequency differences with electron density and acidity.

Compound	Electron density[a] (electron units)	Acidity[b] (pK)	Unassociated band frequency[c] (cm^{-1})	Associated band frequency (cm^{-1})	Frequency difference (cm^{-1})	
Pyrrole	1.692	16.5	3497[d]	~3410	~90	3%
Indole	1.742	···	3491[d]	~3420	~70	2%
Carbazole	1.782	···	3483[d]	···	···	
Diphenylamine	1.822	23.0	3433	~3400	~35	1%
Aniline	1.909	27.0	3436[e] (3481, 3395)	~3440, ~3360	~35	1%

[a] Values of electron density obtained from references 5 and 6.
[b] Acidities taken from reference 34; none available for indole and carbazole.
[c] These frequencies were obtained from CCl_4 solution samples.
[d] As a result of more accurate instrument calibration these values differ slightly from and supercede those previously published (see reference 9).
[e] This average frequency computed by the method described in reference 1. (In this simple case the average wavelength is just the arithmetical average of the two wavelengths of the experimentally observed bands.)

by McEwen,[34] are also included in Table V. This table recalls Venkateswaran's work[35] on the weak associated band in the Raman spectra of OH compounds although this present infrared study enables the simultaneous observations of both the associated and the unassociated frequencies of the NH vibration.

The separation, $\Delta\nu$, between the free and the associated band maxima increases with acidity. This is related to the comment of Bernal[36] that "high acidity means strong hydrogen bonding and corresponding increase in breadth and displacement of the band." Even for OH compounds a direct proportionality between $\Delta\nu/\nu$ and the energy of hydrogen bonding[21,37] is in question;[8] nevertheless, it seems possible to say qualitatively that while hydrogen bonding for all these compounds is weak, the bonding for pyrrole, indole, and carbazole is stronger than that for aniline and diphenylamine.

Sutherland[8] has suggested that hydrogen bonding is to be considered only for band shifts in which $\Delta\nu/\nu > 3$ percent. Because of the size of $\Delta\nu$ for these compounds, it being two to four times as small as, for example, that of phenol,[21] the question may thus arise as to whether or not hydrogen bonding is involved at all. We feel it is important to stress, in answering this question in the affirmative, that all of the experimental work of this paper was performed on compounds in solution,[38] no change of state being involved. Furthermore, as has already been pointed out, the $\Delta\nu$ discussed throughout refers *not* to a shift of a band but to the difference between the locations of the unassociated and the associated band maxima, both of which are visible simultaneously in the spectra for intermediate concentrations.

[34] W. K. McEwen, J. Am. Chem. Soc. **58**, 1124 (1936).
[35] C. S. Venkateswaran, Proc. Indian Acad. Sci. **7A**, 13 (1938).
[36] J. D. Bernal, Trans. Faraday Soc. **38**, 912 (1940).
[37] R. M. Badger, J. Chem. Phys. **5**, 839 (1937); **8**, 288 (1940).
[38] With one exception, for which see reference 25.

Effect of the Intramolecular Environment upon the Absolute Values of Unassociated NH Frequencies

In addition to being useful in the study of association, Table V is helpful in a comparison of the unassociated NH stretching vibration frequencies, the corresponding acidities, and the electron densities calculated by the method of molecular orbitals.[5,6] For aniline the symmetric and antisymmetric frequencies of the NH_2 group have been combined using Linnett's formulas.[1] The N atom is in such a different environment in pyrrole, indole, and carbazole than in aniline and diphenylamine that variable factors other than electrostatic binding may be dominant in affecting the NH frequency.[39] We will, therefore, consider these two sets of molecules separately.

The theory of resonance applied to these molecules by Wheland[7] leads to the conclusion that pyrrole is a weaker acid than indole and carbazole, and aniline, than diphenylamine. For these two groups the infrared frequencies, even though the frequency differences are very small, agree with this conclusion, for, other factors being unchanged, weaker acidity implies a stronger binding of the H atom to the N atom and, correspondingly, a higher NH stretching vibration frequency. McEwen's measurements of acidity[34] on aniline and diphenylamine also agree with Wheland's conclusions. For the other three compounds no comparable acidity measurements are available.

In order to evaluate the comparison of frequencies with electron densities it should be stated that the smaller the electron density on the N atom the smaller the electrostatic contribution to the strength of the bond, and thus, other things being equal, the smaller the force constant of the bond. We would therefore expect the frequency to become correspondingly smaller. This is true for the aniline group, and for this case the infrared data agrees with both the energy of resonance method and the electron density calculation. The frequency does not become correspondingly smaller, however, in the case of the pyrrole group. Here the infrared data, while contradicting the electron density results, continues to agree with the resonance energy method. This suggests that in the electron density calculations for the pyrrole series by means of the molecular orbital method some important secondary effects may have been neglected.

ACKNOWLEDGMENT

This investigation has been supported by a grant from the National Cancer Institute, U. S. Public Health Service.

[39] One might expect a decrease in the free NH frequency with increase in acidity (see reference 2), but a study of Table V indicates just the opposite for these two groups of compounds. This would indicate that the different position of the N atom, in one case in an aromatic 5-membered ring and, in the other case, attached to a phenyl ring, has more effect upon the NH band frequency than does the acidity.

Nonisotropic Propagation of Combustion Waves in Explosive Gas Mixtures and the Development of Cellular Flames*

JOHN MANTON,† GUENTHER VON ELBE,‡ AND BERNARD LEWIS§
Central Experiment Station, U. S. Bureau of Mines, Pittsburgh, Pennsylvania

(Received August 13, 1951)

The phenomenon of nonisotropic propagation consists in the spontaneous development of blisters or cells on the surface of a combustion wave. The present experiments on spherical flames and the experiments of Markstein on flames in wide tubes show that the phenomenon is characteristic of nonstoichiometric explosive mixtures in which the deficient reactant constituent is also the constituent of largest diffusivity. This suggests that the phenomenon is primarily caused by the effect of diffusion processes on the burning velocity. It is proposed that in curved areas of the wave that are convex with respect to the burned gas, the burning velocity is reduced because the lines of diffusion diverge, and hence the concentration of the faster diffusing constituent decreases; whereas in concave areas the lines of diffusion converge, and hence the concentration of the faster diffusing constituent increases. In rich mixtures of hydrocarbon and oxygen, additional evidence for the effect is furnished by the emergence of carbon streamers and by characteristic changes of light emission from convex wave areas, showing that the oxygen concentration, and probably therefore the burning velocity, is decreased in these areas below the average for the mixture.

1. DISTURBANCE OF COMBUSTION WAVES BY HYDRODYNAMIC AND DIFFUSION PROCESSES

It has been shown by numerous observations that combustion waves in explosive gas mixtures are often broken or folded in various ways even when no apparent external conditions interfere with the establishment of a smooth, unbroken wave surface. Among the observed phenomena, we mention polyhedral and open-tipped burner flames, flame filaments on grid burners, rising isolated flamelets in tubes,[1] and particularly the cellular flames that have been studied in detail by Markstein.[2] In explanation of the effect, two possible causes have been considered, namely, (1) hydrodynamic instability of a plane combustion wave as described in substantially identical theories by Landau[3] and Darrieus,[4] and (2) diffusional change of mixture composition in curved regions of the wave, with attendant change of burning velocity and flame temperature.[1]

The principle of hydrodynamic instability of a combustion wave may be visualized with the aid of Fig. 1a. Thermal expansion of the gas passing through the wave generates mass acceleration, which subjects the wave surface to a thrust in the direction of the unburned gas. If a ripple is formed in the wave surface with a curvature concave toward the burned gas, the lines of mass flow in the indented area converge, and hence the thrust is locally increased above that acting on the plane portions of the wave surface. The indentation should therefore grow in depth. Conversely, if the ripple has a convex curvature, the lines of mass flow diverge, and the thrust is locally decreased below that acting on the plane portions of the wave surface. Such indentation should therefore also grow in depth. Landau and Darrieus have formalized this concept by developing the first-order solutions of the equations of momentum perturbation for an idealized model of the combustion wave. It is noted that the first-order solutions are inherently incapable of predicting the amplitude that is ultimately attained by the perturbations; on the other hand, a simple supplementary consideration shows that the perturbations cannot grow indefinitely, but their amplitude is limited by the process of wave propagation. This consideration, which bears some similarity to Huyghen's construction of isochronous wave surfaces, has originally been advanced by Karlovitz to demonstrate the behavior of a combustion wave in turbulent flow.[5] For the present purpose, the principle that is involved here may be illustrated by a construction such

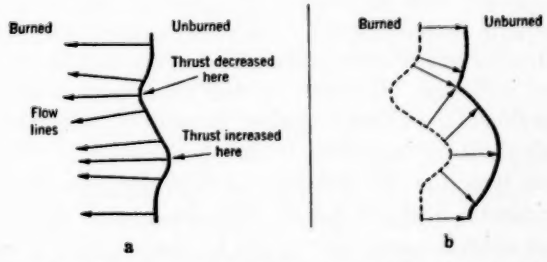

FIG. 1. Illustrating (a) the principle of hydrodynamic instability and (b) the stabilizing effect of wave propagation.

* This research is a part of the work being done at the Bureau of Mines on Contract NA onr 25-47, NR 090 117, (33-038) 51-4151, supported by the ONR and the Department of the Air Force.

† Physicist, Flame Research Section, Explosives and Physical Sciences Division, Bureau of Mines, Pittsburgh, Pennsylvania.
‡ Physical Chemist, Chief, Combustion Research Branch, Explosives and Physical Sciences Division, Bureau of Mines, Pittsburgh, Pennsylvania.
§ Physical Chemist, Chief, Explosives and Physical Sciences Division, Bureau of Mines, Pittsburgh, Pennsylvania.

[1] B. Lewis and G. von Elbe, *Combustion, Flames, and Explosions of Gases* (Academic Press, Inc., New York, 1951); also G. H. Markstein, reference 2.

[2] G. H. Markstein, J. Chem. Phys. **17**, 428 (1949); Cornell Aeronaut. Lab. Tech. Rep. 24 (Project SQUID), October 1, 1950; J. Aeronaut. Sci. **18**, 199 (1951).

[3] L. Landau, Acta Physicochim. U.R.S.S. **19**, 77 (1944).

[4] G. Darrieus, La Technique Moderne **30**, No. 18 (1938); **31** Nos. 15, 16 (1939); **33**, Nos. 21, 22 (1941).

[5] Karlovitz, Denniston, and Wells, J. Chem. Phys. **19**, 541 (1951).

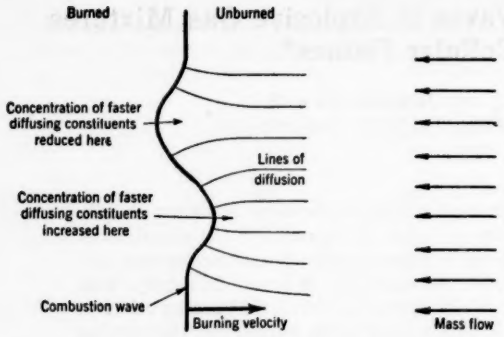

FIG. 2. Illustrating the principle of diffusional change of mixture composition.

as shown in Fig. 1b. If the wave were merely a surface of discontinuous momentum change as depicted in Fig. 1a, the indentations would, after some element of time, have grown to the size indicated by the dotted line. Actually, the wave has been propagating during this time element, and, assuming that the rate of propagation normal to the surface—the burning velocity—is constant, the wave now assumes the shape shown by the solid line. One sees that in the process of wave propagation a convex indentation tends to vanish because opposite surfaces approach each other until they merge; whereas a concave indentation tends to become flatter because its base is widening while its height of protrusion above the wave average changes little or not at all. In consequence, the wave should attain a steady state in which the surface is not smooth but broken into cells that are concave toward the burned gas and form sharp ridges along the lines of contact with neighboring cells; the steady state is maintained by equality between the rate of increase of cell curvature (because of hydrodynamic thrust) and the rate of decrease of cell curvature (because of propagation). This concept of cellular wave structure bears a striking similarity to the observations of Markstein[2] on actual combustion waves. This author reports that the cells have indeed a characteristic size depending on the explosive mixture, and photographs of the cells—showing concave surfaces bounded by sharp ridges—conform to the theoretical picture. If one thus accepts hydrodynamic instability as the cause of break-up of combustion waves into cells, it appears that first-order perturbation theory is inadequate to describe the actual phenomenon and that, instead, a steady-state treatment is demanded along the lines indicated. However, we feel that there is strong experimental evidence against a predominant role of hydrodynamic instability in the phenomenon of cellular wave structure. We point to the fact, supported by experimental evidence below, that combustion waves of large unbroken area are the rule for slow-burning as well as for fast-burning mixtures, and that the broken or folded variety is characteristic of nonstoichiometric explosive mixtures in which the deficient component is also the component of largest diffusivity. Hence, it seems to us that the stabilizing effect of wave propagation normally so much overshadows the disturbance created by hydrodynamic instability that the wave has practically a smooth noncellular surface, and that the primary cause of cellular break-up must be attributed to another effect, namely, diffusional change of mixture composition in curved regions of a combustion wave.

In a combustion wave, the mixture is changed not only by chemical reaction but also by interdiffusion of reactants and reaction products. A mass element moving along a stream tube through the wave exchanges molecules not only with preceding and succeeding elements of its own stream tube, but also with elements in adjacent stream tubes. When the wave is plane, all concentration gradients are normal to the wave, and all lines of mass flow are parallel to each other, though they may be inclined against the wave. It follows that the exchange of molecules between adjacent stream tubes causes no change of concentration of any molecular species. When the wave is convex toward the burned gas, the concentration gradients of the reactant species diverge; when the wave is concave, they converge. This is shown schematically in Fig. 2, in which the "lines of diffusion" indicate the direction of the concentration gradients. The lines of mass flow (indicated only by arrows in front of the wave) are much less diverging or converging. It follows that a stream tube passing through a convex indentation loses molecules of reactants to the adjacent stream tubes, and a stream tube passing through a concave indentation similarly gains molecules of reactants. If the diffusivities of fuel and oxygen are approximately equal, it is reasonable to expect that the fuel-oxygen ratio is not appreciably changed, but in a convex indentation the convergence of the flow of heat and chain carriers from the burned to the unburned gas causes the burning velocity to

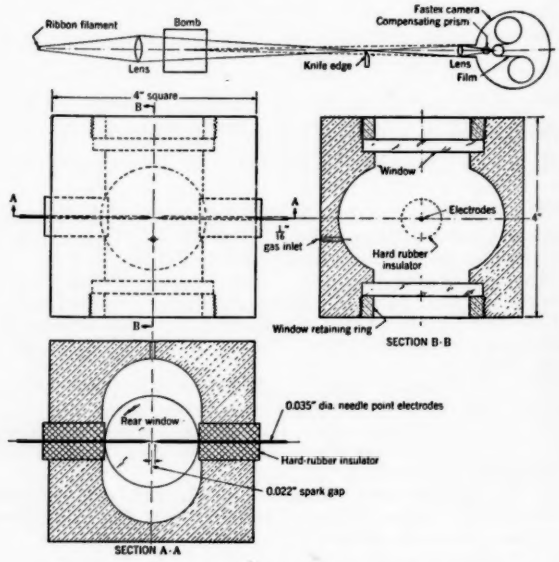

FIG. 3. Schlieren camera and test bomb for observing flame development from sparks.

increase; this corresponds to the usual situation at the tip of a Bunsen burner flame. The reverse applies to a concave indentation, and the two effects thus enhance the stability of the combustion wave against fortuitous ripples. If the diffusivities of fuel and oxygen are greatly different, the fuel-oxygen ratio may be expected to be changed significantly by such ripples. The effect of such change on combustion-wave stability should be critically dependent on the stoichiometry of the reactant mixture. If the more rapidly diffusing constituent is present in excess, its loss from a convex indentation should increase the burning velocity and its gain in a concave indentation should decrease the burning velocity; hence, the diffusion process should assist in eliminating any ripples. If the more rapidly diffusing constituent is present in a ratio below stoichiometric, its loss should render the mixture in a convex indentation slower-burning or even noninflammable, whereas in a concave indentation the burning velocity is increased. In this case the indentations do not straighten themselves, and an initially smooth wave surface may be expected to become spontaneously rippled by fortuitous fluctuations during the process of propagation.

2. EXPERIMENTAL OBSERVATIONS

A test of the relative importance of hydrodynamic instability and diffusional change of mixture composition is afforded by experiments with fuel-oxygen mixtures of various diffusivities and stoichiometric ratios. Whereas hydrodynamic instability would tend to induce cellular structure of the combustion wave in any mixture, the diffusion effect leads to the expectation that cellular structure is largely confined to mixtures in which the stoichiometrically deficient constituent also possesses the largest diffusivity. The authors have made such tests by taking high speed schlieren photographs of combustion waves developing from electric sparks. Depending on mixture composition, the wave either developed isotropically in the shape of a smooth sphere, or nonisotropically with a markedly irregular contour that shows the development of "blisters" or "cells" reminiscent of the observations reported by Markstein.[2] Figure 3 is a diagram of the schlieren camera and test bomb used in these experiments; the dimensions and shape of the bomb are also shown for a better understanding of some of the following photographs. Figure 4 shows eight examples of wave development, each comprising a series of snapshots during a stage of growth when the flame begins to fill the field of vision afforded by the circular bomb window, but the pressure of the bomb has not greatly increased. Attention is called to the fact that the four cases of nonisotropic propagation in the upper part of the figure comprise rich mixtures of butane and propane with air and lean mixtures of methane and hydrogen with air, whereas the four cases of isotropic propagation in the lower part comprise lean mixtures of butane and propane and rich mixtures of methane and hydrogen. This result is fully consistent with the diffusion theory. In the former group the stoichiometrically deficient constituent also possesses the largest diffusivity, and in the latter group the situation is reversed. Figure 5 shows isotropic propagation for both lean and rich mixtures of carbon monoxide and air and ethylene and air. As the diffusivities of carbon monoxide and air are approximately equal, the propagation of flame in mixtures of these gases conforms to expectations. Ethylene,

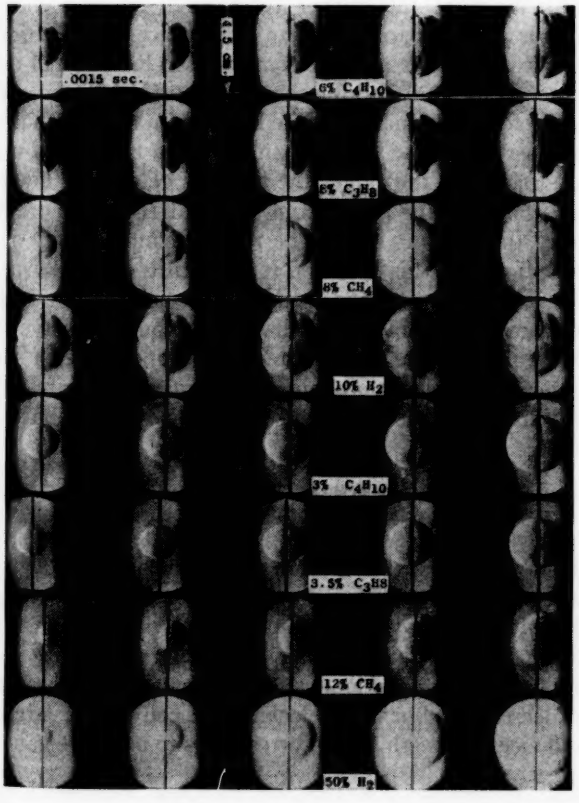

FIG. 4. Propagation of spark-ignited combustion waves in fuel-air mixtures. Upper four series, nonisotropic; lower four series, isotropic.

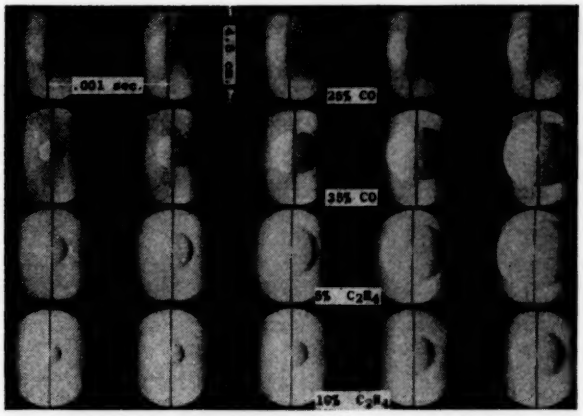

FIG. 5. Isotropic propagation of spark-ignited combustion waves in lean and rich fuel-air mixtures when molecular weight of fuel is approximately equal to the molecular weight of air.

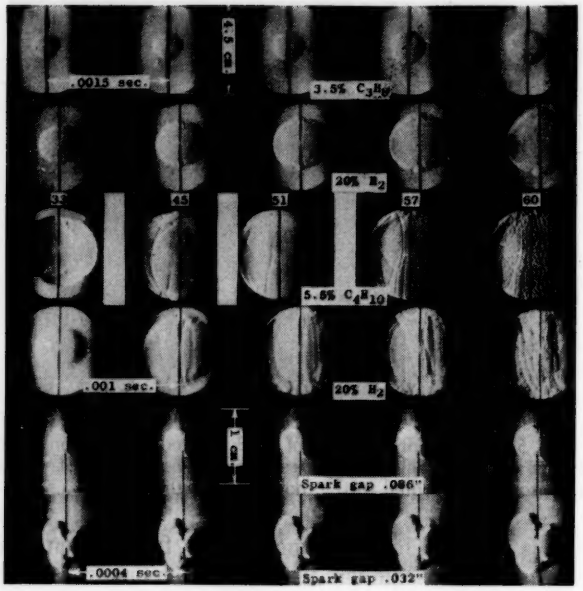

FIG. 6. Propagation of spark-ignited combustion waves in various fuel-air mixtures under various conditions.

however, has a somewhat lower diffusivity, as judged from data on kinematic viscosities, and supplemental observations in a much larger bomb (12-inch diameter) have indeed shown that blisters develop in rich mixtures.

In Fig. 6, the top row shows that in a mixture that is expected to sustain isotropic propagation (lean mixture of propane and air), the wave develops from an initially irregular contour to a smooth sphere. In the second row, an initially spherical wave in a lean hydrogen-air mixture becomes spontaneously indented. The latter mixture belongs to the group in which propagation is expected to be nonisotropic. The third and fourth series show that such mixtures develop numerous small cells as the pressure increases. In these pictures the flame grows beyond the field of vision but does not come in contact with the glass window of the bomb until a later stage not shown here. The last two series show an effect of length of spark gap on the initial flame shape in lean methane-air mixtures. A narrow gap produced three separate flame centers, which appear to be fairly regularly spaced. A wider gap resulted in a more regular flame outline with indentations corresponding to the penetration of the wave by the electrode wires.

The results of these and many other observations on nonisotropic propagation are summarized in Table I. They correspond closely with Markstein's observations on cell structure of combustion waves in wide tubes. One notes from Markstein's work that rich ethylene or ethane mixtures do produce cells[2] in agreement with the fact that these gases have lower diffusivities than oxygen, although very similar molecular weights; but the cell size is so large that in a small test bomb such as shown in Fig. 3 the propagation appears to be isotropic. The cell size decreases with increasing molecular weight

TABLE I. Nonisotropic (+) and isotropic (−) propagation in fuel-air mixtures.

Fuel-air mixture	H_2	CH_4	CO	Larger fuel molecules
Lean	+	+	−	−
Rich	−	−	−	+

and hence with decreasing diffusivity of the hydrocarbon; it also decreases with increasing pressure.[2] These effects appear consistent with the fact that with decreasing diffusivity of the hydrocarbon, separation of the reactants is enhanced, and that with increasing pressure the width of the combustion wave decreases, the cells being scaled accordingly.

Direct evidence for the change of mixture composition in the region of convexity is furnished by the observation that in rich mixtures of the heavier organic fuels, such as propane, benzene, etc., carbon streamers emerge from the ridges that point toward the burned gas. This has been the experience not only of Markstein[2] but was previously noted on polyhedral flames by Smith and Pickering[6] and by Leason.[7] In mixtures that did not produce carbon streamers, the latter investigator noticed changes of color of the light emission indicative of a shift to richer mixtures. The phenomenon of regular polyhedral flames can now be explained as caused by cells that are regularly spaced along the circumference of the burner tube. Such spacing corresponds to a critical cell size and hence to a critical adjustment of the mixture composition. Rotation of the structure around the burner axis is probably arrested in the following manner: The burner rim receives much less heat from the ridges than from the troughs of the cells, as along the ridges the burning velocity is lower, and therefore the combustion wave at the ridge draws away (up and out) from the rim, as confirmed by observation.[6] In this way the temperature of the burner rim is higher below the troughs than below the ridges. As the distance of approach of a combustion wave to the rim decreases with increasing temperature of the latter, it is seen that such temperature distribution stabilizes the troughs at the hotter zones of the burner rim.

3. REMARKS ON MARKSTEIN'S THEORY

Markstein[2] has modified Landau's development of the first-order perturbation equations by introducing additional terms representing assumptions concerning the effect of curvature on burning velocity. The formal conclusions of this treatment may be summarized as follows: All combustion waves are unstable. In the case of decrease of burning velocity with convex curvature, and vice versa—this case corresponds to negative values

[6] F. A. Smith and S. F. Pickering, U. S. Bur. Standards J. Research 3, 65 (1929).

[7] D. B. Leason, Engines Note 132 (1949), Aeronautical Laboratory, Austrailian Department of Supply and Development, Melbourne.

of the parameter μ in Markstein's treatment—cells of all sizes are possible, and the probability of occurrence increases with decreasing size. In the opposite case of increasing of burning velocity with convex curvature, and *vice versa*—this case corresponds to positive values of μ—the range of cell sizes is limited, and a size of maximum probability exists. Assuming the latter case to be universally applicable, all combustion waves should break up into cells of definite size. Noncellular flames presumably are merely flames of such large cell size that over the observed wave area no cell structure is noticeable. In addition, Markstein shows that in flames traveling down a vertical tube a levelling effect of gravity exists which might inhibit cell formation altogether. We find it difficult to accept these views. The rule that cells appear whenever the stoichiometrically deficient component is also the component of largest diffusivity strongly suggests that the parameter μ is negative in cellular flames, that is, the burning velocity decreases in regions of convex curvature as discussed previously. The formation of carbon streamers along the cell ridges, corresponding to a mixture shift from rich to over-rich, leaves little room for doubt in this respect. The fact that spherically propagating flames behave in a same manner as flames traveling down a tube refutes the theory that gravity plays a significant role. We believe therefore that either the first-order perturbation treatment does not carry the development far enough to obtain results applicable to actual combustion waves, or that the model underlying Markstein's treatment is basically deficient. This is a difficult question to answer at present and must be left to future development.

THE JOURNAL OF CHEMICAL PHYSICS VOLUME 20, NUMBER 1 JANUARY, 1952

Adsorption Studies on Clay Minerals. I. Chromatography on Clays

JOSEPH A. FAUCHER, JR., RAYMOND W. SOUTHWORTH, AND HENRY C. THOMAS
Sterling Chemistry Laboratory, Yale University, New Haven, Connecticut

(Received August 20, 1951)

With the aid of chromatographic columns containing a clay mineral dispersed on asbestos, ion-exchange processes on this mineral have been studied. The results of isotopic exchanges show that the columns do not run under equilibrium conditions. These isotopic exchanges do make possible a correction procedure which serves to produce isotherms for cases of true ion-exchange. The details of the correction procedure are given together with some results for a cesium-sodium exchange on a montmorillonite from Chambers, Arizona.

FOR a variety of reasons the subject of base exchange on clay minerals has received much attention. Important parts of the chemistry of the earth's crust are dependent on the phenomenon.[1] The process is also of importance in various biological connections, the best known of which is plant nutrition.[2] The matter is of very considerable scientific interest for its own sake. A montmorillonite clay may be considered as a peculiar type of polyelectrolyte, or as a concentrated electrolytic solution in which the negative portion of the ion atmosphere is held in a nearly fixed configuration. The study of these minerals and their equilibrium relations with solutions of salts is not an insignificant part of the theory of solutions as a whole. Very recently there has appeared another and cogent reason for prosecuting the study of these relations. As a by-product of nuclear fission large quantities of radioactive wastes are collecting and await disposal. The possibility of fixing these wastes in clay minerals—which are plentiful and relatively cheap ion-exchangers—deserves careful attention.

For whatever reason one may be interested in the clay minerals, it is fundamental that there be available accurate knowledge of the isothermal surfaces which represent the equilibria between these minerals and mixed salt solutions. The present paper reports developments in a method for the determination of these surfaces. Only a little consideration is needed to realize that a nearly prohibitive amount of chemical analysis would be necessary to map the simplest of these isothermal surfaces. The application of the technique of ion-exchange chromatography is indicated. The possibility of determining adsorption isotherms from chromatographic experiments was apparently first noticed by de Vault.[3] The method has been developed by Glückauf.[4] In principle, at least, the procedure is a simple one. The equation of conservation in a chromatographic column may be written

$$dF = qdx - cdy. \tag{1}$$

F is the total amount of substance of interest in the column, adsorbed (measured here as q millimoles per gram of exchanger) and in solution (c millimoles per milliliter). Distances from the input of the column are

[1] See, for example, K. Rankama and Th. G. Sahama, *Geochemistry* (The University of Chicago Press, Chicago, Illinois, 1950), p. 210 *ff*.
[2] Walter P. Kelley, *Cation Exchange in Soils* (Reinhold Publishing Company, New York, 1948), p. 100 *ff*.
[3] Don de Vault, J. Am. Chem. Soc. **65**, 532 (1943).
[4] E. Glückauf, J. Chem. Soc. **1949**, 3280.

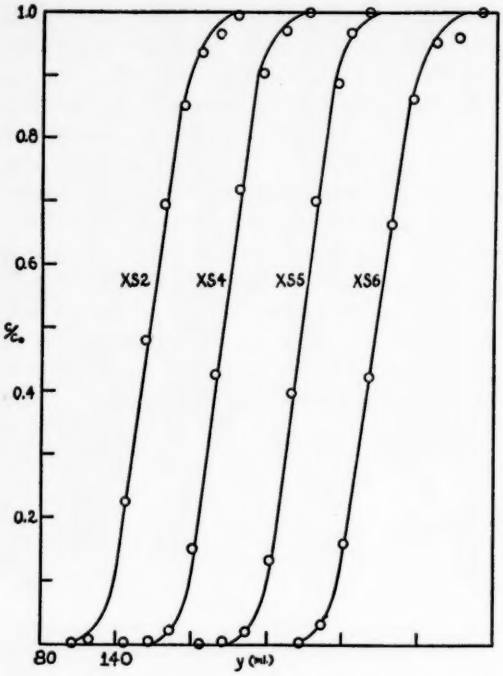

FIG. 1. Isotopic exchanges on the clay API 23. Curves from Eq. (4). (The curves are arbitrarily displaced along the volume axis.)

measured in terms of mass of exchanger, x grams. In most applications of (1) it is supposed that the column is packed to uniform density. The natural choice for the "time" variable, y, is the volume (milliliters) of solution downstream from the point x. This differential equation is valid under any operating conditions. If, in particular, the equation is integrated for an elution process ($c=0$ for $x=0$) we get

$$F=xq-\int(xdq+cdy)$$

or under conditions near equilibrium, for which $q=f(c)$,

$$f=(F+yc)/x, \tag{2}$$

where f is the isotherm wanted.[5] In exchange adsorption, of course, the elution of one ion from a column corresponds to saturation with another. If it can be shown that the exchange of only two ions is the process measured, then the f determined by Eq. (2) corresponds to the intersection of a definite plane with the isothermal surface $q=f(c_1, c_2)$. The process of mapping the f surface is reduced to a series of elution experiments, each at different total concentration. When radioactive tracers are applicable, much of the work can be relegated to automatic machinery. Perhaps the most important advantage of the method is the exact control over the position of the isotherm measured. The chief disadvantage of the method is the necessity of working under conditions which at best can only approximate equilibrium. As has been shown,[4] however, this difficulty is not so serious as might appear at first sight. One must choose as his eluting substance the less strongly adsorbed species. (He measures the diffuse front for the saturation with this species.) The fundamental principle of chromatography then insures that small deviations from ideality are largely corrected in the column. The elution curve, therefore, has nearly its equilibrium shape, and differences can be taken into account by methods of approximation.[4]

TABLE I.

Expt	$\dot{V}$ ml/min	Δ	$\Delta/\dot{V}$
XS2	0.39	1.54	3.9
XS4	0.25	1.40	5.6
XS5	0.20	1.34	6.7
XS6	0.083	1.75	21

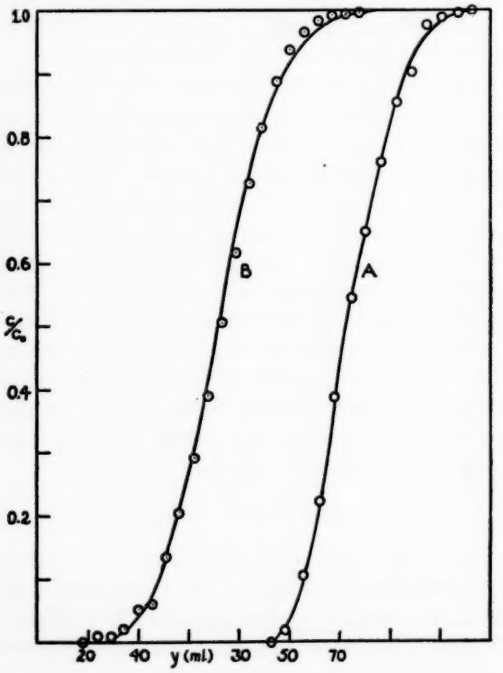

FIG. 2. Initial elution of clay API 23 by cesium, (A). Isotopic cesium exchange, (B).

In the present work with clays there are indications that the rate determining factor can be taken as diffusion in the solid clay substance, although undoubtedly other disturbances are present. Our experiments have been carried out in a very simple fashion. The raw clay, a montmorillonite from Chambers, Arizona, API 23,* was ground to pass a 100-mesh screen. Weighed portions of the clay (of definite but unknown water

[5] Eq. (2) was first given by Glückauf, Nature **156**, 784 (1945).

* The designation of API 23 refers to the sample number of the American Petroleum Institute, Research Project No. 49. The properties of this and many other clays can be found in the invaluable reports of this organization. Samples of the clays are obtainable from Ward's Natural Science Establishment, Rochester, New York.

content) were mixed with finely divided Gooch asbestos, and a glass tube was packed with this mixture. A preliminary experiment showed that the absorption of cesium by the asbestos itself amounted to less than one percent of the total exchange adsorption of the columns here reported. The clay in the column was converted to the cesium form by elution with cesium chloride solution. The total capacities of the columns were determined by graphical integration of the breakthrough curves. Many successive isotopic exchanges on a single column gave the same capacity to within one percent, showing that we are dealing with a true ion-exchange and that the flow of solution did not wash the clay into the eluate. In Fig. 1 is given a series of these curves for the isotopic exchange of cesium. The

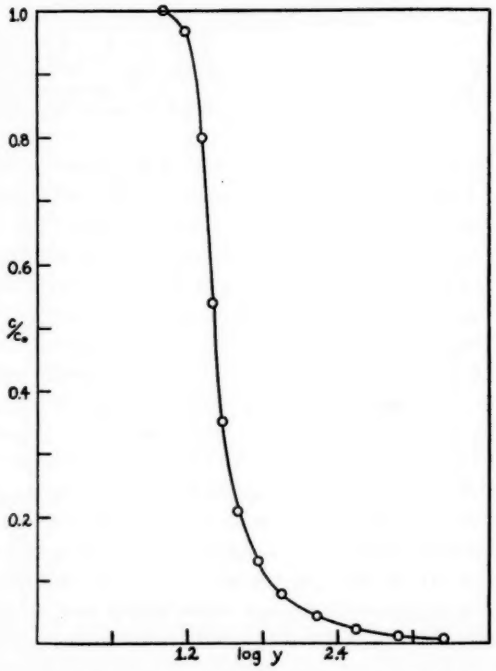

FIG. 3. Displacement of cesium from the clay API 23 by sodium ($c_0 = 0.0627_4$M NaCl).

circles represent the experimental points, and the solid lines have been calculated as follows.

If solid diffusion is the rate limiting factor, we must perforce use an approximate form for the rate law:[6]

$$(\partial q/\partial y) = (D/\dot{V}S)(f(c) - q) \qquad (3)$$

or

$$\Delta(\partial q/\partial y) = ac - q \quad \text{for isotopic exchange.} \qquad (3a)$$

For convenient comparison with Glückauf's equations we have put $\Delta = \dot{V}S/D$; $\dot{V}$ is the volume rate of flow through the column; S, a shape factor depending on the character of the packing; and D is the diffusion

[6] Even for a linear isotherm the exact theory is at present not in condition to permit of detailed numerical computations. See, in this connection, Henry C. Thomas, J. Chem. Phys. **19**, 1213 (1951).

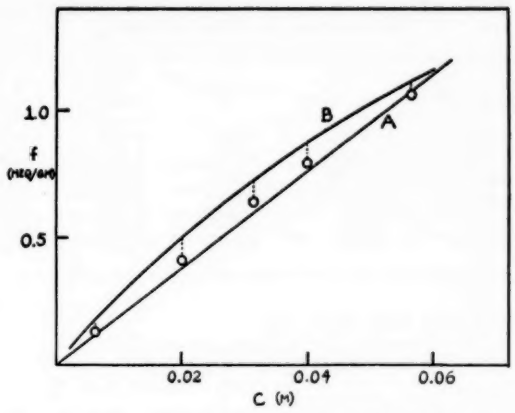

FIG. 4. Computation of linear isotherm from data for isotopic elution.

constant in the solid. In any single column experiment Δ is to be maintained constant throughout the column. For these kinetics we have[7]

$$(c/c_0) = e^{-(ax/\Delta)-(y/\Delta)}\varphi[(ax/\Delta), (y/\Delta)]. \qquad (4)$$

An extensive table of the function $g(u, v) = \varphi(u, v) \times \exp(-u-v)$ is now extant.[8] Using this table the curves of Fig. 1 have been constructed. In Table I are given the values of Δ so obtained as well as the values of $\Delta/\dot{V}$. Certainly the variation of $\Delta/\dot{V}$ indicates that the process is not one of pure solid diffusion (although this variation might be due in part to inadequacies in the theory), but as a semi-empirical method of representing the elution curves the procedure leaves little to be desired. It is possible that this variation in $\Delta/\dot{V}$ is in part due to minor channeling in the column. However, in view of the method of packing the columns, channeling could not have been a major factor.

Now that the value of Δ for a column is available from a study of isotopic exchange, we may proceed to develop a correction procedure applicable to the determination of nonlinear isotherms from elution data. It is convenient to obtain an equation in c corresponding to the rate process (3). Using the conservation condition,

TABLE II. Calculation of linear isotherm from isotopic elution. $\Delta = 2.58$, $x = 3.800$ g.

c (M)	$-\partial c/\partial y$	$-\Delta[y(\partial c/\partial y)/c]$	f ideal	f corr	f true
0.00627	0.000625	0.045	0.172	0.127	0.119
0.0200	0.00126	0.083	0.495	0.412	0.380
0.0314	0.00124	0.082	0.725	0.643	0.597
0.0400	0.00120	0.080	0.875	0.795	0.760
0.0565	0.000603	0.058	1.119	1.061	1.074

[7] Henry C. Thomas, Ann. N. Y. Acad. Sci. **XLIX**, 170 (1948). The properties of the function φ, which may be called the Laplace function, are also to be found here, as well as in F. C. Nachod, *Ion Exchange* (Academic Press, Inc., New York, 1949), pp. 40, 41.

[8] This table, at present available only in a limited edition reproduced from the original computation sheets, is due to Dr. S. R. Brinkley, Jr., of the laboratory of the Bureau of Mines at Pittsburgh, Pennsylvania.

TABLE III. Calculation of cesium-sodium isotherm from elution data. $\Delta=2.58$, $x=3.800$ g.

c, [Cs] (M)	$-\partial c/\partial y$	$-\Delta[y(\partial c/\partial y)-c]$	f ideal	f corr
0.0031	0.0002	0.004	1.009	1.005
0.0063	0.00011	0.008	1.070	1.062
0.0125	0.00040	0.015	1.125	1.110
0.0188	0.0011	0.024	1.160	1.136
0.0251	0.0019	0.029	1.180	1.151
0.0376	0.0031	0.035	1.200	1.165

derivable at once from (1)

$$(\partial q/\partial y)=-(\partial c/\partial x) \tag{5}$$

we find[9]

$$\Delta(\partial^2 c/\partial x\partial y)+(\partial c/\partial x)+(\partial f/\partial y)=0. \tag{6}$$

If now we apply the ingenious trick due to Glückauf,[4] Eq. (6) can be integrated at constant y, and we find the approximation,

$$f\simeq(1/x)\{F+yc+\Delta[y(\partial c/\partial y)-c]\}. \tag{7}$$

In the application of (7) to an elution curve, F is determined by graphical or other approximate integration, combined, if necessary, with a knowledge of the capacity of the column under the conditions of the experiment. The correction term is easily determined with adequate accuracy. We must make the assumption that the coefficient of the correction, Δ, is the same as determined in the isotopic exchange. Better guesses could be made if isotopic exchanges for both species were available.

In Figs. 2 and 3 are given the curves for an experiment serving to determine a cesium-sodium isotherm on the montmorillonite API 23. Curve A of Fig. 2 represents the displacement by cesium of the original ions of the clay. The circles on curve B are the experimental points for an isotopic cesium exchange carried out at the same concentration and flow rate as the elution of Fig. 3, the latter being a displacement of cesium by sodium. (In this curve the concentration ratio has been plotted against $\log V$ to compress the long tail of the elution.) In Fig. 4 is given the known linear isotherm, A, for the clay under the conditions of the isotopic exchanges. In Table II and in Fig. 4 are given the results of the calculation of this isotherm by means of the approximate equation (7). Curve B (Fig. 4) represents the results obtained on the assumption of equilibrium; the corrected points are indicated. It is to be noticed that the correction is here being applied under the most adverse possible circumstances, i.e., with a non-self-sharpening chromatographic boundary.

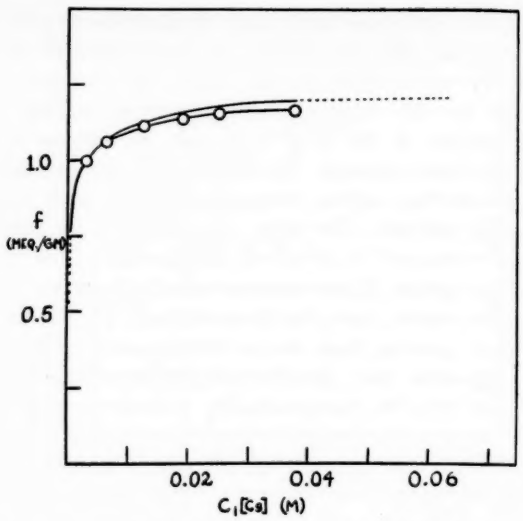

FIG. 5. Cesium-sodium isotherm on the clay API 23. The circles represent points corrected by Eq. (7) from the upper curve, which was calculated without the non-equilibrium correction.

In Table III and in Fig. 5 are given the results of the computation of the cesium-sodium isotherm. As is seen, the correction amounts to one percent or less in the sharply curved part of the isotherm. The correction is larger along the flat portion; however, for this particular case there was some uncertainty as to the hold-up volume of the column, and our results for the isotherm itself cannot be considered accurate in this region.

This work has been supported by a contract between Yale University and Brookhaven National Laboratory, Upton, Long Island, New York. We want to express our indebtedness to Mr. L. P. Hatch of Brookhaven Laboratory, without whose continued interest and support this work would not have been done.

[9] Equation (6) is entirely similar to that given by Glückauf, Barker, and Kitt, Discussions of the Faraday Society **VII**, 199 (1949) although it does not involve, as does their equation, an unnecessary (and usually insignificant) mathematical approximation.

On the Measurement of Vapor Pressures by Effusion

CHARLES I. WHITMAN
Chemical Laboratories of New York University, New York, New York
(Received July 27, 1951)

The effect of apparatus dimensions on the accuracy of vapor pressure measurements by Knudsen's effusion method is discussed for the usual type of experimental arrangement. It is shown that the total surface area of a condensed solid phase is not fundamentally related to the pressure of the effusing vapor. Equations are derived which may be used to check the pressure of the effusing vapor for saturation. Two cases in the literature are discussed.

INTRODUCTION

IN the course of some recent work on the vapor pressure of zinc with another[1] the author became interested in the "free molecule" flow which occurs at the vapor pressures measureable by Knudsen's effusion method.[2] A prime condition for the success of this method is that the vapor entering the effusion aperture be effectively at the vapor pressure of the substance. It is conceivable the design of the effusion cell may be such that relatively slow molecular flow from the vaporizing material to the aperture will reduce the effusion rate below the maximum, saturation pressure, value. It has been found possible to estimate with reasonable accuracy any such effect for the customary design of effusion cell. The development which follows is sufficiently general to permit application in other cases where free molecule flow can be important, such as high vacuum work.

DERIVATION

Consider two circularly cylindrical tubes A and B of arbitrary lengths, L_A and L_B, and radii, r_A and r_B, joined together as in Fig. 1. The tube A, of larger diameter, is connected to a reservoir R_A at pressure p_A. Tube B is connected to reservoir R_B at pressure p_B. The entire system is assumed to be at a constant temperature. The pressures p_A and p_B are low enough for "free molecule" flow to occur, i.e., the gas molecules make collisions only with the walls of the pipes.

Let $p_B=0$ and consider the gas flow from R_A to R_B. Of the molecules which enter the larger tube A, not all will reach R_B, but some will be reflected at the walls and eventually find their way back to R_A. Let W_A be the probability that molecule entering tube A will reach the pipe junction, and W_B the probability that a molecule entering tube B will reach reservoir R_B. Let $f=\pi r_B^2/\pi r_A^2=(r_B/r_A)^2$.

If N is the number of molecules which enter A from R_A in unit time, then W_AN will reach the junction and $(1-W_A)N$ will be reflected back into R_A. Of these W_AN, the fraction f will enter B, the remaining fraction, $(1-f)$, will be reflected at the junction. Of the fW_AN which enter B, fW_AW_BN will enter R_B and $fW_A(1-W_B)N$ will be returned to A.

Summing the molecules reflected at the junction and by B,

$$S=(1-f)W_AN+fW_A(1-W_B)N=W_AN(1-fW_B) \quad (1)$$

molecules will be at the junction heading toward R_A. Assuming W_A to be the same for the returning molecules, which is not strictly true, W_AS will return to R_A but $(1-W_A)S$ will once again be reflected and return to the junction. The reasoning then repeats itself. The result is a series for the number of molecules which reach R_B.

$$N'=fW_AW_BN+fW_AW_BN(1-fW_B)(1-W_A)+fW_AW_BN(1-fW_B)^2(1-W_A)^2+\cdots, \quad (2)$$

or

$$N'=fW_AW_BN[1+(1-fW_B)(1-W_A)+(1-fW_B)^2(1-W_A)^2+\cdots], \quad (3)$$

which has the functional form,

$$N'=fW_AW_BN/[1-(1-fW_B)(1-W_A)]=fKN, \quad (4)$$

where

$$K=W_AW_B/[1-(1-fW_B)(1-W_A)]. \quad (5)$$

This flow is independent of p_B if the flow is of the free molecule type, and because when $p_B=p_A$ there can be no net flow of gas, Eq. (4) also holds for flow from R_B to R_A.

In terms convenient for use in vacuum work Eq.

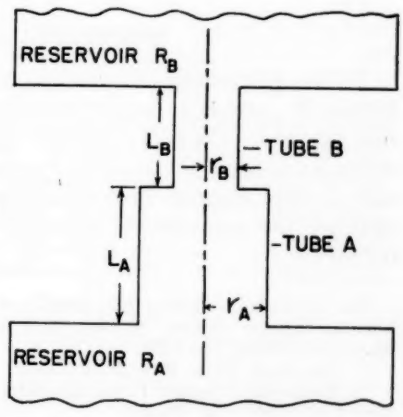

FIG. 1. Vertical cross section of tubes and reservoirs.

[1] J. E. Vance and C. I. Whitman, J. Chem. Phys. **19**, 744 (1951).
[2] M. Knudsen, Ann. Physik **29**, 179 (1909).

(4) can be written in the form,

$$Q=pV'=fK[RT/2\pi M]^{\frac{1}{2}}(\pi r_A^2)(p_A-p_B), \quad (6)$$

where Q is the net flow of gas pV' from R_A to R_B, p is the pressure at a plane in the system, V' is the volume of gas flowing across this plane in unit time, M is the molecular weight and the other constants have their usual meaning.[3]

The form useful when applying to vapor pressure work is

$$p_A=(\mu/KAt)(2\pi RT/M)^{\frac{1}{2}}, \quad (7)$$

where μ is the mass of gas effusing through the area A (here πr_B^2) into R_B in time t, M is the molecular weight of the gas, and the other symbols have their usual meaning. Here p_B is taken as zero.

For this case reservoir R_A of Fig. 1 is replaced by a flat layer of vaporizing material. The accommodation coefficient, α, is assumed unity. In the case of a solid, the state of subdivision (chunks, powder, turnings, etc.) is then immaterial. This arrangement is exactly equivalent to a reservoir R_A at the vapor pressure p_A of the substance.[4] and therefore Eq. (7) applies. Tube A is the effusion cell and tube B is the effusion orifice (probably with small L/r). This resembles the usual type of apparatus used experimentally.

If α is not unity the state of subdivision of the condensate may be important. For a liquid, or a solid effectively in one piece, the fraction $1-\alpha$ of the molecules returning to the surface of the vaporizing material will be reflected back toward R_B and have another chance to contribute to the total flow. Including these extra terms in an expression analagous to (3), Eq. (7) becomes

$$p_A=\mu(\alpha KAt)(2\pi RT/M)^{\frac{1}{2}}(1-b), \quad (8)$$

where

$$b=(1-\alpha)[1-W_A+KW_A(1-fW_B)/W_B]. \quad (9)$$

However, for a loosely packed solid such as coarse turnings, some molecules returning to the "surface" may not be reflected but instead pass through spaces between the turnings. For such molecules the effective α will be closer to unity, and the true p_A will be somewhere between the values given by (7) and (8).

DISCUSSION

To use (8) requires knowledge of α and the probabilities W_A and W_B. Accurate values of α are generally not available. Plausible reasons for α to be close to unity have been advanced,[4,5] but it would only seem safe to say, judging from the experimental evidence, that for the majority of cases α is probably between 0.7 and 1.

Further, the b term in (8) does not reduce to zero, as it should, for W_A and $W_B=1$, unless $f=1$. The reasons for this are discussed in the appendix. In view of the preceding statements, (8) should not be relied on to give more than an indication of the effect of α.

Theoretical values for probabilities such as W_A and W_B have been calculated for various ratios of the tube length to radius L/r by Clausing.[6] However, the validity of these calculations is dependent on four fundamental conditions:

(1) The molecules collide only with the walls of the tube (free molecule flow).

(2) The reflection of molecules after such collisions is diffuse.

(3) The molecules enter the tube with the usual cosine distribution of directions. The probability will obviously depend on the directional distribution of entering molecules.

(4) The molecules enter uniformly over the face of the tube. This is required because the probability, $W(r)$, for an individual molecule depends on *where* it enters the tube. $W(r)$ is greatest at the axis and least at the wall, and, for a given L/r, is a function only of the radial distance from the axis. W is related to $W(r)$ through the relation,

$$W=\int_0^{r_0} W(r)2\pi r dr/\pi r_0^2, \quad (10)$$

where r_0 is the radius of the tube.

Condition (1) requires the mean free path (MFP) of the molecules to be at least ten times the order of the dimensions of the apparatus.[7]

It is this requirement for the effusion orifice (tube B) which effectively limits the effusion method to the measurement of vapor pressures of less than 10^{-2} mm. In case of practical interest free molecule flow will also occur in the effusion cell (tube A). For example, at a pressure of 10^{-3} mm, with $T=600°$K, and taking 3.0×10^{-8} cm as a typical "molecular diameter" the MFP will be 15 cm. Under these conditions, free molecule flow will occur if the effusion cell diameter is less than 1.5 cm.[8]

Available discussions of condition (2) offer plausible arguments in its support,[1,2] but experimental evidence is not extensive enough to give it general validity. To the extent that reflection is not diffuse, some uncertainty will be introduced into calculated values of K and b.

Condition (3) will not be fulfilled at the entrance to tube B because of distortion of the cosine distribution by tube A.[9]

[3] R. Loevenger, *Vacuum Equipment and Techniques* (National Nuclear Energy Series, McGraw-Hill Book Company, Inc., New York, 1949), pp. 1–58.

[4] I. Langmuir, Phys. Rev. **2**, 329 (1913).

[5] S. Dushman, *Vacuum Technique* (John Wiley and Sons, Inc., New York, 1949), pp. 20, 442.

[6] P. Clausing, Ann. Physik **12**, 961 (1932).

[7] S. Dushman, reference 5, p. 93.

[8] The effect of condensate surface on v.p. measurements when the diameter of tube A is tenfold less than the MFP has been discussed by (a) R. Speiser and H. L. Johnston, Trans. Am. Soc. Metals **42**, 283 (1950); (b) C. I. Whitman, Ph.D. thesis, Yale University (1949).

[9] P. Clausing, Z. Physik **66**, 471 (1930).

Condition (4) will obviously not be fulfilled by those molecules returning along tube A after reflection at the annular region determined by the tube junction. This effect will be partly compensated by the molecules returning to A after reflection in B.

The error in K resulting from these last two effects is estimated to be less than 10 percent. It may be much less. For instance, with $W_A=0.6720$ ($L/r=1.0$), $W_B=1$ and $f=0.1$, the error is less than 2 percent. It is worth noting that the K calculated by (5) will always be less than the "true" K. The method of estimation is described in the appendix.

APPLICATION

As Eq. (7) is generally employed to calculate vapor pressures, K is assumed, with or without some justification, to be unity. If the effusion oriffice (tube B) has a finite thickness K is sometimes taken as W_B.[1] As can be seen from (5), K will approach W_B either as $W_A\rightarrow 1$ or as $f\rightarrow 0$. If $\alpha=1$ the vapor effusing into tube B under these conditions will be at the vapor pressure of the substance. Thus contrary to what is sometimes said, the *total* surface area of the condensate is not fundamentally related to the pressure of the effusing vapor. Only the surface bordering the vapor volume (here πr_A^2) is important. In the case of a solid a fine state of subdivision, such as a powder, will not contribute any more molecules per unit time to the vapor than a solid piece. Clearly, the minimum area required for vapor saturation (if $\alpha=1$) is just πr_B^2, provided it is placed at the entrance to pipe B ($W_A=1$). This arrangement then becomes essentially Langmuir's method.[4]

The effect of α on p_A, as given by (8) and (9), is dependent for the most part on f. For $\alpha=0.7$, and $f=0.1$, the error caused by neglecting α would be 5 percent at most. For $f=0.01$ this error becomes 0.5 percent. The effect of α can therefore be made negligible by use of a small f provided W_A is not so near unity that the arrangement is effectively that of a single tube B with $f=1$ (see Appendix).

In measuring the vapor pressure of zinc,[1] the author filled the effusion cell ($f=0.002$) nearly completely with *loosely packed* helical coils of zinc. Although $W_A\cong 0.95$, it is believed because of the loose packing of the zinc, and for an additional reason presented in the appendix, that the effusing vapor was saturated, even if α for zinc is not close to unity.

As another example Cogin and Kimball[10] used a cell 0.9 cm in diameter and 4 cm in length to measure alkali halide vapor pressures by a modification of Knudsen's method. For their cell $W_A=0.23$, $W_B=1$, and $f=0.012$. The result is $K=0.96^+$. In practice W_A would be greater than 0.23 because vaporizing material occupies some of the length, and K would be even closer to the desired value of unity.

[10] G. E. Cogin and G. E. Kimball, J. Chem. Phys. **16**, 1035 (1948).

On the other hand, Rudberg[11] has measured the vapor pressure of calcium using a cell consisting only of a cylindrical tube 9.5 mm deep, 2.15 mm in diameter. For a cell of this type $W_B=1$, $f=1$, and K reduces to W_A, here equal to 0.22.

The total effusion rate would thus be only about $\frac{1}{5}$ that for saturated vapor, (less if $\alpha\neq 1$) although, because Rudberg collected only in a solid angle containing the more intense portion of the beam, the collimating effect of the tube would compensate to some undetermined extent for the large decrease in total intensity.[9,12] Also, the calcium in the cell will decrease the length L and increase K.

Some earlier measurements of Pilling,[13] using Langmuir's method, are 10 times the values reported by Rudberg. Vapor pressure measurements by effusion are subject to numerous errors,[14] which make it very difficult to assign definite reasons for differences in measurements by independent investigators. At the very least, however, it is apparent from the discussion in this paper that the use of a cell of Rudberg's type in a vapor pressure measurement is undesirable.

APPENDIX

The error in K can be considered as resulting from two nearly independent effects, (a) an error in the use of W_B because condition (3) is not fulfilled, and (b) an error in the use of W_A because condition (4) is not fulfilled.

The net effect on K in each case depends on the factor f. In (a), the error will be largest when $f=1$ and will become smaller as $f\rightarrow 0$ and $K\rightarrow W_B$, the effect of tube A on the flow becoming small. In (b) the error in K will be small for $f\cong 1$ and $f\cong 0$, becoming larger at intermediate values of f. The error is small for $f\cong 1$ because only a small percentage of the molecules are reflected at the junction and small for $f\cong 0$, because condition (4) is then nearly fulfilled.

These errors can be estimated as follows. In (a) the maximum error occurs for $f=1$, i.e., when tubes A and B have the same radius. A comparison of K with Clausing's calculated values for the over-all tube length, L_A+L_B gives directly the maximum error. For example, with $W_A=0.3589$ ($L_A/r_A=4.0$) and $W_B=0.5136$ ($L_B/r_B=2.0$), $K=0.2678$, whereas $W_{A+B}(L/r=6.0)$ is 0.2807. The error is -4.6 percent.

In estimating the error from (b) it is necessary to obtain some knowledge as to how $W_A(r)$ varies across the face of the tube. It is convenient to write $W_A(r)$ as

$$W_A(r)=W_A'(r)+W_A''(r), \qquad \text{(A1)}$$

where $W_A'(r)$ is the probability of a molecule traversing the tube directly without reflection by the tube wall at any point and $W_A''(r)$ is the probability of traversing the tube only after one or more such reflections.

It follows from the laws of kinetic theory that $W_A'(r)$ is proportional to the area of a sphere determined by the intersection of this sphere (of arbitrary radius) tangent to the face of the tube at the point for which $W_A'(r)$ is desired, and a cone whose generating line always intersects the point of interest and the circle described by the other end of the tube. This solid angle can be calculated readily by graphical integration. When the value of f is known, an

[11] E. Rudberg, Phys. Rev. **40**, 763 (1934).
[12] Phipps, Sears, Seifert, and Simpson, J. Chem. Phys. **18**, 713 (1950).
[13] N. B. Pilling, Phys. Rev. **18**, 366 (1921).
[14] R. W. Ditchbourn and J. C. Gilmour, Revs. Modern Phys. **13**, 310 (1941).

average value of $W_A'(r)$, $\langle W_A'r\rangle_{Av}$, can be calculated for the annular region of reflection at the junction by an equation analogous to (10).

It is necessary to estimate $\langle W_A''(r)\rangle_{Av}$ by referring to the corresponding W_A'' for W_A. Clausing[6] gives a very simple equation for calculating W_A' from which W_A'' follows from an equation analogous to A1. One then assumes that the ratio of the number of molecules which traverse the tube after one or more reflections to the total number of molecules which undergo reflection is the same over the face of the tube. This will be approximately true because the previous history of the molecule is wiped out after reflection. $\langle W_A''(r)\rangle_{Av}$ then follows immediately from $\langle W_A'(r)\rangle_{Av}$.

The sum $\langle W_A'(r)\rangle+\langle W_A''(r)\rangle_{Av}$ gives a value for $\langle W_A(r)\rangle_{Av}$ [$\langle W_A(r)\rangle_{Av}$ is always $\leq W_A$] for the region of interest. Substitution into this series expression for K,

$$W_A[1+(1-f)(1-\langle W_A(r)\rangle_{Av})+(1-f)^2(1-\langle W_A(r)^2\rangle_{Av}+\cdots] \quad (A2)$$

gives a more exact value for K. W_B is taken as unity here to obtain the maximum percent error in K because as $W_B\rightarrow 0$, $\langle W_A(r)\rangle_{Av}\rightarrow W_A$ because molecules are now returning to tube A from tube B.

The accuracy of K has been estimated in this manner over a wide range of values for the variables. The largest error calculated under any circumstances was 7 percent. The estimate of 10 percent maximum error is believed to be a generous one.

It has been noted earlier that (9) does not reduce properly as $W_A\rightarrow 1$, while (5) does. Now as $W_A\rightarrow 1$, the assumption that condition (4) is fulfilled for molecules reflected at the condensate becomes less accurate. In (5) this introduces no error because $\alpha=1$ and no molecules are reflected at the condensate. However, when $\alpha\neq 1$ then molecules which are reflected at the condensate can account for a considerable fraction of the total flow into tube B as is indicated by (8) and (9). If W_A is close enough to unity, the arrangement will be effectively that of a single tube B with $f=1$, i.e., most of the molecules entering B will come directly from a small region of the condensate, say of area πr_B^2 directly below B. However if f is small, W_A can be quite close to unity without affecting greatly the validity of condition (4). In the measurements of zinc,[1] $f=0.002$, $W_A\cong 0.95$ and only about 5 percent of the molecules entering B would come from the area πr_B^2 directly below B. For $W_A=1$, 100 percent would come from this area.

THE JOURNAL OF CHEMICAL PHYSICS VOLUME 20, NUMBER 1 JANUARY, 1952

Microwave Spectra and Molecular Structures of POF_3, PSF_3, $POCl_3$, and $PSCl_3$*

QUITMAN WILLIAMS,† JOHN SHERIDAN,‡ AND WALTER GORDY
Department of Physics, Duke University, Durham, North Carolina

(Received August 13, 1951)

From measurements of pure rotational transitions in the microwave region the following B_0 values in Mc/sec were determined: 4594.25±0.04 for $PO^{16}F_3$, 4395.27±0.20 for $PO^{18}F_3$, 2657.63±0.04 for $PS^{32}F_3$, 2614.73±0.04 for $PS^{33}F_3$, 2579.77±0.04 for $PS^{34}F_3$, 2015.20±0.05 for $PO^{16}Cl_3^{35}$, 1932.38±0.08 for $PO^{16}Cl_3^{37}$, 1402.64±0.05 for $PS^{32}Cl_2^{35}$, 1355.72±0.05 for $PS^{32}Cl_3^{37}$, 1370.13±0.05 for $PS^{34}Cl_3^{35}$. With the aid of electron diffraction results the molecular structures have been determined as follows: for POF_3, $d_{PO}=1.45\pm0.03$A, $d_{PF}=1.52\pm0.02$A and $\angle FPF=102.5°\pm2°$; for PSF_3, $d_{PS}=1.87\pm0.03$A, $d_{PF}=1.53\pm0.02$A and $\angle FPF=100.3°\pm2°$; for $POCl_3$, $d_{PO}=1.45\pm0.03$A, $d_{PCl}=1.99\pm0.02$A and $\angle ClPCl=103.6°\pm2°$. The structure of $PSCl_3$, determined entirely from microwave data is: $d_{PS}=1.85\pm0.02$, $d_{PCl}=2.02\pm0.01$ and $\angle ClPCl=100.5°\pm1°$.

PREVIOUS investigations of the structures of phosphoryl fluoride[1] and chloride[1] and thiophosphoryl fluoride[2] and chloride[3] have been made with electron diffraction. Because of the large contribution of the three P−Hal combinations to the electron diffraction pattern, the P−Hal distances were determined with a reasonable accuracy in all four compounds. The lack of consistency with the present microwave data indicates that the previous electron diffraction values for some of the other dimensions are badly in error. Only for $PSCl_3$, however, have we been able to obtain sufficient microwave data for a complete structural determination. For the others we have obtained complete structural determinations by combining our data with the most accurately evaluated parameters from electron diffraction. The molecule, POF_3, has been previously studied with microwaves.[4] Although there is approximate agreement of this spectral measurement with the one reported here, there is a marked difference in the two structural evaluations. Also two transitions, $J=3\rightarrow 4$ and $J=4\rightarrow 5$, for the most abundant isotopic form of PSF_3 have been previously measured.[4a] The results are in harmony with the measurements of other transitions reported here.

EXPERIMENTAL

Phosphoryl fluoride was prepared by the method of Booth and Dutton[5] and purified by vacuum fractionation in combination with measurements of gas density. Thiophosphoryl fluoride was made as described by

* The research reported in this paper has been made possible through sponsorship extended by the Geophysical Research Directorate of Air Force Cambridge Research Laboratories under Contract No. W19-122-ac-35. It will be submitted by Quitman Williams in partial fulfilment for the requirements of the Ph.D. degree.

† Texas Company Fellow. Present address: School of Physics, Georgia Institute of Technology, Atlanta, Georgia.

‡ Present address: Department of Chemistry, University of Birmingham, England.

[1] L. O. Brockway and J. Y. Beach, J. Am. Chem. Soc. **60**, 1836 (1938).

[2] D. P. Stevenson and H. Russell, Jr., J. Am. Chem. Soc. **61**, 3264 (1939).

[3] J. Y. Beach and D. P. Stevenson, J. Chem. Phys. **6**, 75 (1938).

[4] S. J. Senatore, Phys. Rev. **78**, 293 (1950).

[4a] A. Roberts, private communication to Kisliuk and Townes, (J. Research Natl. Bur. Standards **44**, 611 (1950)).

[5] H. S. Booth and F. B. Dutton, J. Am. Chem. Soc. **61**, 2937 (1939).

Booth and Seabright[6] and was purified as was phosphoryl fluoride. Thiophosphoryl chloride was prepared by Thorpe's method[7] and was distilled in a vacuum, the center fraction being used.

All frequencies were measured with a precision frequency standard monitored by station WWV. The rotational lines of POF_3 and PSF_3 were detected with the simple video method and those of $POCl_3$ and $PSCl_3$ with the Stark modulation method.

RESULTS

POF_3

The isotopic combinations $PO^{16}F_3$ and $PO^{18}F_3$ were measured for POF_3. The $PO^{18}F_3$ lines were measured with O^{18} in its natural abundance of 0.204 percent. The frequencies of the transitions measured are listed in Table I and the spectral constants in Table II. The B_0 value 4593.50±0.02 Mc/sec given by Senatore[4] lies outside our estimated limits of error. Because of the remarkably small centrifugal distortion constants, the lines of different K were not resolved. For this reason and because there is no nuclear hyperfine structure, the rotational lines are exceptionally strong for a symmetric-top molecule.

TABLE I. Observed frequencies.

	Transition	Frequency Mc/sec
$PO^{16}F_3$	$J=2\rightarrow3$	27565.43±0.05
	$J=3\rightarrow4$	36753.83±0.05
$PO^{18}F_3$	$J=2\rightarrow3$	26,371.7 ±0.06
	$J=3\rightarrow4$	35,162.0 ±0.5
$PS^{32}F_3$	$J=5\rightarrow6$	
	$K=0, 1, 2$	31,891.62±0.05
	$K=3$	31,891.45±0.05
	$K=4$	31,891.27±0.05
	$K=5$	31,891.13±0.05
	$J=6\rightarrow7$	
	$K=0, 1$	37,206.77±0.05
	$K=2$	37,206.67±0.05
	$K=3$	37,206.55±0.05
	$K=4$	37,206.36±0.05
	$K=5$	37,206.13±0.05
	$K=6$	37,205.84±0.05
$PS^{33}F_3$	$J=5\rightarrow6$	31,412.7 ±0.3
$PS^{34}F_3$	$J=6\rightarrow7$	
	$K=0, 1, 2$	36,116.72±0.05
	$K=3$	36,116.47±0.05
	$K=6$	36,115.78±0.05
$POCl_3^{35}$	$J=6\rightarrow7$	28,212.8 ±0.5
	$J=7\rightarrow8$	32,242.9 ±0.5
	$J=8\rightarrow9$	36,273.5 ±0.5
$POCl_3^{37}$	$J=6\rightarrow7$	27,052.0 ±0.5
	$J=7\rightarrow8$	30,918.4 ±0.5
	$J=8\rightarrow9$	34,783.0 ±0.5
	$J=9\rightarrow10$	38,648.6 ±0.5
$PS^{32}Cl_3^{35}$	$J=9\rightarrow10$	28,053.1 ±0.5
	$J=10\rightarrow11$	30,857.9 ±0.5
	$J=11\rightarrow12$	33,662.9 ±0.5
$PS^{32}Cl_3^{37}$	$J=10\rightarrow11$	29,825.5 ±1.0
	$J=11\rightarrow12$	32,537.4 ±1.0
$PS^{34}Cl_3^{35}$	$J=10\rightarrow11$	30,143.2 ±1.0
	$J=11\rightarrow12$	32,882.4 ±1.0

TABLE II. Spectral constants.

	B_0 (Mc/sec)	D_J (Kc/sec)	D_{JK} (Kc/sec)	I_B($\times10^{-40}$ g/cm^2)[a]
$PO^{16}F_3$	4594.25±0.04	~1	<|2|	182.59_{59}
$PO^{18}F_3$	4395.27±0.20			190.86_{25}
$PS^{32}F_3$	2657.63±0.04	~0.3	1.8	315.65_{39}
$PS^{33}F_3$	2614.73±0.04			320.46_{58}
$PS^{34}F_3$	2579.77±0.04			325.18_{06}
$PO^{16}Cl_3^{35}$	2015.20+0.05			416.28_{32}
$PO^{16}Cl^{37}$	1932.38±0.08			434.12_{41}
$PS^{32}Cl_3^{35}$	1402.64±0.05			598.08_{30}
$PS^{32}Cl_3^{37}$	1355.72±0.05			618.78_{14}
$PS^{34}Cl_3^{35}$	1370.13±0.05			612.27_{45}

[a] Value of h equals 6.62363×10^{-27} erg sec (J. A. Bearden and H. M. Watts, Phys. Rev. **81**, 73 (1951).

Since the structural parameters determined from electron diffraction by Brockway and Beach,[1] $d_{PF}=1.52\pm0.02$A, $d_{PO}=1.56\pm0.03$A, and $\angle FPF=107°\pm2°$, yield a moment of inertia, I_B, which differs widely from the observed value, and since insufficient microwave data are available for an independent determination, we have sought to find parameters which would be consistent with both measurements. The parameters finally chosen are listed in Table III. Figure 1 shows how these parameters, which yield the observed moment of inertia, agree with the electron diffraction radial distribution curve of Brockway and Beach.[1] The agreement is gratifying. Indeed, it is much better than that for the parameters chosen by Brockway and Beach. Furthermore, the P=O distance, as expected, is close to that found for $POCl_3$, and the PF distance is close to that in PSF_3. The largest disagreement with the results of Brockway and Beach is in the P=O distance, which is understandable because it corresponds to the term having the lowest electron scattering power.

PSF_3

Rotational lines of three different isotopic combinations were measured for PSF_3. The frequencies and spectral constants are given in Tables I and II. To determine the structure it is still necessary to assume one dimension. Fortunately, one dimension, d_{PF}, is determined rather closely from electron diffraction because of the large scattering of the P−F combination. Also, the P−F distance has been found to have the same value in a number of molecules similar to PSF_3. For this reason it can be estimated rather accurately. Assuming $d_{PF}=1.53$A, which agrees within the error limits with the value 1.51±0.02A given by Stevenson and Russell,[2] the values $d_{PS}=1.87$A and $\angle FPF=100.3°$ are obtained from the microwave data. These also agree within the limits of error with the values 1.85±0.02A and 99.5±2° given by Stevenson and Russell. If, however, a lower value is assumed for d_{PF}, the values obtained for the

[6] H. S. Booth and C. H. Seabright, J. Am. Chem. Soc. **65**, 1834 (1943).
[7] T. E. Thorpe, Trans. Chem. Soc. **37**, 341 (1880).

TABLE III. Molecular dimensions.

	d_{P-S}	d_{P-O}	d_{P-Cl}	d_{P-F}	∠Hal−P−Hal
$PSCl_3$	1.85±0.02A		2.02±0.01A		100.5°±1.0°
$POCl_3$		1.45±0.03A	1.99±0.02A		103.6°±2.0°
POF_3		1.45±0.03A		1.52±0.02A	102.5°±2.0°
PSF_3	1.87±0.03A			1.53±0.02A	100.3°±2.0°

other two parameters lie outside the error limits of Stevenson and Russell. Thus, the values listed in Table III are the only ones which are consistent with both the microwave and electron diffraction data. Figure 2 shows how the parameters assigned here fit the electron diffraction radial distribution curve.

$POCl_3$

Two symmetric-top configurations of phosphoryl chloride, $POCl_3^{37}$ and $POCl_3^{35}$, were measured. Tables I and II show the results. The asymmetric combinations $POCl_2^{35}Cl^{37}$ and $POCl^{35}Cl_2^{37}$ were also measured but were not very useful because the rotational transitions observed consisted of a group of incompletely resolved lines which could not be assigned with certainty.

The rotational lines of the chlorides cannot be measured with the same accuracy as those of the fluorides because the unresolved Cl quadrupole hyperfine structure broadens the lines. Fortunately, at the high transitions observed, the rotational lines of $POCl_3^{35}$ and $POCl_3^{37}$ are so widely spaced and the hyperfine splitting so small that the separations of the rotational lines can be measured to an accuracy of a fraction of a percent. The measurements do not, therefore, limit the accuracy of the structural determination.

To determine the structure it was necessary to assume one parameter. The P−Cl distance was chosen because it is the one which can be determined most accurately from electron diffraction.[1] However, in order to obtain the closest approach to the other parameters obtained by Brockway and Beach,[1] $d_{PO}=1.58$A (assumed) and ∠ClPCl=106±1°, it was found necessary to take the smallest value for d_{PCl}, 1.99A, which is allowed by their limits of error, 2.02±0.03A. The d_{PO} assumed by Brockway and Beach appears to be much too long. The assumption of their 2.02A as the P−Cl distance would make the disagreement with the P=O distance even greater and, in fact, would make d_{PO} absurdly short, 1.36A.

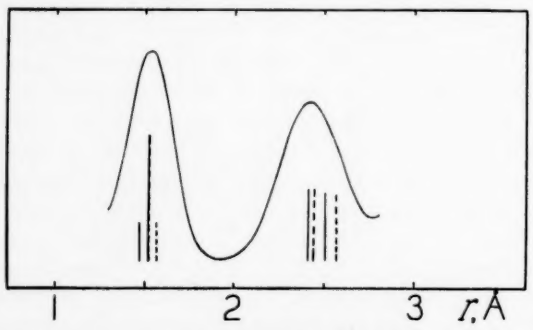

FIG. 1. Electron diffraction radial distribution curve for POF_3 by Brockway and Beach (see reference 1). The dotted lines represent the parameters chosen by Brockway and Beach, the solid lines those determined in the present study.

$PSCl_3$

The spectral constants for the different isotopic combinations are given in Tables I and II, and the molecular structure is given in Table III. A complete structural determination for this molecule was made from the microwave data alone. Except for d_{PCl} the structural parameters obtained do not agree with those from electron diffraction measurements by Beach and Stevenson:[3] $d_{PS}=1.94\pm0.03$A, $d_{PCl}=2.01\pm0.02$A, and ∠ClPCl=107°±3°. This was at first a bit disturbing since Beach and Stevenson were able to obtain measurements of six maxima and six minima on their electron diffraction pattern. However, upon plotting their electron diffraction measurements with the theoretical diffraction curve for the model determined from microwaves, we found the agreement to be better than for any other models tried by Beach and Stevenson. This agreement was apparently overlooked by Beach and Stevenson. The plot is shown in Fig. 3. The agreement is seen to be very good for the outer lines which are the only ones particularly sensitive to variations in the structural parameters.

DISCUSSION OF THE STRUCTURES

From the conventional valencies of the atoms one would write the structure of these molecules as

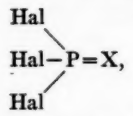

where X is O or S. To provide a starting basis for the discussion, we have calculated for comparison with the observed distances the lengths of the single bonds P−F and P−Cl with the Schomaker-Stevenson rule[8] and the lengths of the double bonds P=O and P=S from this rule as adapted to double bonds by Gordy.[9] The revised

TABLE IV. Comparison of observed and calculated bond lengths.

Molecule	d_{P-F} Obs	d_{P-F} Calc[a]	d_{P-Cl} Obs	d_{P-Cl} Calc[a]	d_{P-O} Obs	d_{P-O} Calc[a]	d_{P-S} Obs	d_{P-S} Calc[a]
POF_3	1.52	1.64	···	···	1.45	1.52	···	···
PSF_3	1.53	1.64	···	···	···	···	1.87	1.93
$POCl_3$	···	···	1.99	2.01	1.45	1.52	···	···
$PSCl_3$	···	···	2.02	2.01	···	···	1.85	1.93

[a] Calculated with the Schomaker-Stevenson rule (see reference 8). $d=r_1+r_2-\beta|x_A-x_B|$, where $\beta=0.09$ for single bonds (see reference 8) and 0.06 for double bonds. (See reference 9.)

[8] V. Schomaker and D. P. Stevenson, J. Am. Chem. Soc. **63**, 37 (1941).

[9] W. Gordy, J. Chem. Phys. **15**, 81 (1947).

TABLE V. Comparison of structures of phosphorus compounds.

	d_{P-F}	∠FPF
PF_3	1.53_5[a]	(100°)[c]
PSF_3	1.53	100.3°
POF_3	1.52	102.5°
	d_{P-Cl}	∠ClPCl
PCl_3	2.04_4[b]	99.9°[b]
$PSCl_3$	2.02	100.5°
$POCl_3$	1.99	103.6°

[a] Calculated from B values given in reference 15.
[b] From reference 12.
[c] Assumed.

radii[8,9] were used except that the radius used for F is one-half the length 1.418A in F_2 as determined recently by Andrychuk.[10] The comparisons are given in Table IV. Only for the PCl distances are the calculated and observed distances in good agreement. In POF_3 the observed P−F distance is 0.12A shorter, and the P=O distance 0.07A shorter, while in PSF_3 the PF distance is 0.11A shorter and the PS distance 0.06 shorter than the calculated values. These large decrements are in addition to the corrections already included for shortening caused by ionic resonance. If the straight additivity rule is used with the Pauling radii,[11] the deviations are much greater. A part of this additional shortening may be caused by resonance of structure I with structures of Types II and III

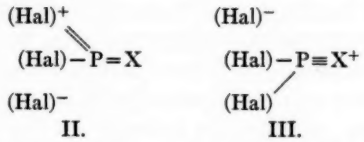

and a part by a shrinkage of the P radius caused by its positive formal charge in the contributing structures of Type IV and V.

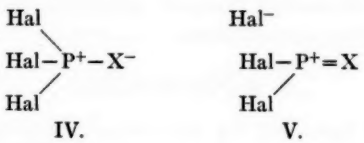

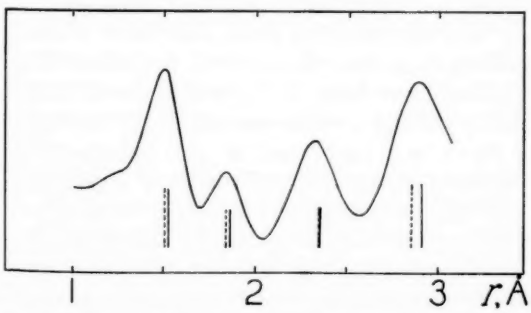

FIG. 2. Electron diffraction curve of PSF_3 by Stevenson and Russell (see reference 2). The dotted lines represent the parameters chosen by Stevenson and Russell, and the solid lines those determined in the present work.

[10] D. Andrychuk, Can. J. Phys. **29**, 151 (1951).
[11] L. Pauling, *The Nature of the Chemical Bond* (Cornell University Press, Ithaca, New York, 1940), p. 164.

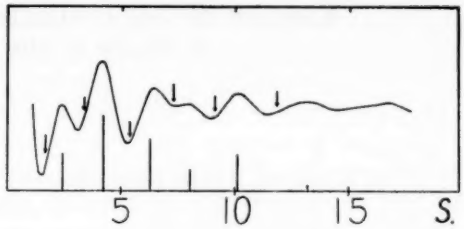

FIG. 3. Theoretical electron diffraction pattern of $PSCl_3$ for the model given in Table III with bars indicating the measured intensities and positions of the maxima and arrows indicating the position of the minima as measured by Beach and Stevenson (see reference 3).

In addition to the multiple bond shortening, there is a coulomb attraction of the nonbonded plus and minus atoms in II and III. Since the plus and minus charges are constantly shifting among the corner atoms, the Coulomb force acts somewhat as a surface tension to pull the nonbonded atoms toward the center of an approximately spherical-top molecule such as POF_3.

It is interesting to compare the bond angles and bond lengths formed by trivalent and pentavalent phosphorus (see Table V). The most accurate comparisons available are for PCl_3 and $PSCl_3$, both structures of which have been completely determined from microwave spectroscopy. For PCl_3 Townes and Kisliuk[12] give $d_{PCl}=2.04_4 \pm 0.01$A and ∠ClPCl = 99.9°±1°. The P−Cl distance is slightly shorter and the ClPCl angle slightly larger for the $PSCl_3$. In view of this result, and by comparison with PSF_3, it appears that ∠FPF in PF_3 should be near the lowest limit allowed by the electron diffraction measurements,[13] 104°±4°, or about 100°. This lower value is more nearly in accord[14] with ∠FNF, 102°9′, in NF_3 which should not be smaller than ∠FPF in PF_3. With the latter value the microwave results on PF_3 lead to a value of 1.535A for the P−F distance. The value, obtained by Gilliam, Edwards, and Gordy[15] assuming 104° for ∠FPF, is 1.546A.

The difference in angle FPF in POF_3 and PSF_3, about 2°, and the similar difference, 3°, for $POCl_3$ and $PSCl_3$ are probably caused by the greater contribution from structures of Type IV in the oxygen compounds. In ionic structures of this type there are four covalent bonds to P, and the bonding orbitals of P would tend to be equivalent sp^3 hybrids like those of C. Thus, large contributions from structure IV should increase the angles toward the tetrahedral value of 109°28′. The possible importance of four equivalent covalent bonds in similar ionic structures in PF_5 has been noted by Pauling.[16]

We wish to thank Mr. John Cox, who assisted with some of the measurements.

[12] P. Kisliuk and C. H. Townes, Phys. Rev. **78**, 347 (1950).
[13] L. O. Brockway and F. T. Wall, J. Am. Chem. Soc. **56**, 2373 (1934).
[14] J. Sheridan and W. Gordy, Phys. Rev. **79**, 513 (1950).
[15] Gilliam, Edwards, and Gordy, Phys. Rev. **75**, 1014 (1949).
[16] L. Pauling, reference 11, p. 90.

Kinetics of OH Radicals from Flame Emission Spectra. IV. A Study of the Hydrogen-Oxygen Flame

H. P. Broida, *National Bureau of Standards,* Washington, D. C.*

AND

K. E. Shuler, *Applied Physics Laboratory,† The Johns Hopkins University, Silver Spring, Maryland*

(Received September 28, 1951)

The inner and outer cones of hydrogen-oxygen flames burning lean (1:1), stoichiometric (2:1), and rich (4:1, 6:1) at atmospheric pressure have been studied spectroscopically with the object of gaining some information as to the elementary processes occurring in this flame. The rotational, vibrational, and electronic distribution of $OH(^2\Sigma^+)$ has been determined for both the inner and outer cone of each fuel mixture. A thermal equilibrium distribution of the internal degrees of freedom was found for $OH(^2\Sigma^+)$ in the outer cones for all fuel ratios; in the inner cones there was a vibrational nonequilibrium distribution indicated by an excess population of the levels $v'=2$ and 3. It is suggested that this nonequilibrium may be due to a radiationless transition reaction involving H or O atoms in excess of their thermal concentrations. This assumes, in agreement with the suggestion of Gaydon and Wolfhard, that the $^2\Sigma^+$ state of OH is weakly predissociated between the levels $v'=2$ and 3 by a $^2\Sigma^-$ state. The possible significance of this excess atomic concentration for the active particle diffusion theory of flame propagation is indicated briefly. It is concluded that the radiation of $OH(^2\Sigma^+)$ in the oxy-hydrogen flame is predominantly thermal.

A. INTRODUCTION

In the preceding papers of this series[1] the determination, from spectroscopic studies, of the rotational and vibrational distribution of $OH(^2\Sigma^+)$ and of the relative concentration of $OH(^2\Sigma^+)$ and $O_2(^3\Sigma_u^-)$ in flames has been discussed in some detail. It is the purpose of this paper to apply the methods and calculations of I, II, and III to a spectroscopic study of the hydrogen-oxygen flame to see whether it is possible to gain some information as to the elementary reactions in this flame from the energy distribution of the electronically excited $OH(^2\Sigma^+)$. This study has been carried out under a wide variety of experimental conditions, i.e., for both the inner and outer cones of hydrogen-oxygen flames burning lean, stoichiometric, and rich at atmospheric pressure.

The hydrogen-oxygen flame was chosen for two reasons. In the first place, this system has only two atomic constituents, O and H, so that the elucidation of the elementary processes should prove to be simpler than for a hydrocarbon flame where one has an additional atomic component and thus is faced with a much greater variety of possible reactions. Secondly, previous spectroscopic work on the hydrogen-oxygen flame has indicated that there are abnormal, i.e., nonthermal, intensity distributions of $OH(^2\Sigma^+)$[2,3] so that a further and more detailed study of this system promised to give valuable information relevant to the elementary processes occurring in this flame.

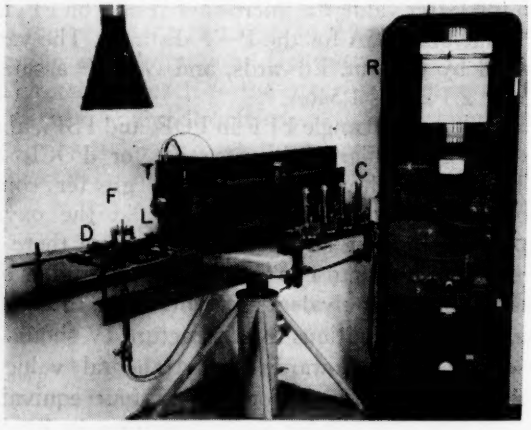

Fig. 1. High resolution monochromator and recording unit. F=flame, L=lens, S=entrance slit, M=monochromator, D=rack and pinion, T=photomultiplier tube, P=power supply, A=amplifier, and R=pen recorder.

B. EXPERIMENTAL

The arrangements for the experiments reported in this paper are illustrated in Fig. 1. A complete description of this equipment is given here since it has never been adequately described before. Radiation from the hydrogen-oxygen flame, F, is focused on the slit, S, of the direct-reading monochromator, M, by a quartz lens, L, of 3-inch focal length and $2\frac{1}{4}$-inch diameter. Vertical and horizontal positioning of the flame is possible with the rack and pinion devices, D. Initial focusing is made visually and the final adjustments are made with the aid of the photoelectric response, the maximum intensity being used as a criterion for correct positioning. After traversing the dispersing system, the light falls upon the cathode of a 1P28 photomultiplier tube, T. A

* This work was done under sponsorship of the Navy Bureau of Aeronautics.

† The work described in this paper was supported by the Bureau of Ordnance, U. S. Navy under Contract NOrd-7386.

[1] K. E. Shuler, J. Chem. Phys. **18**, 1221, 1466 (1950); **19**, 888 (1951) hereafter referred to as I, II, and III.

[2] V. Kondratjew and M. Ziskin, Acta Physichochim. U.R.S.S. **7**, 65 (1937).

[3] A. G. Gaydon and H. G. Wolfhard, Rev. inst. Franc., petrole et ann. combustibles liquides IV, No. 8, 405 (1949).

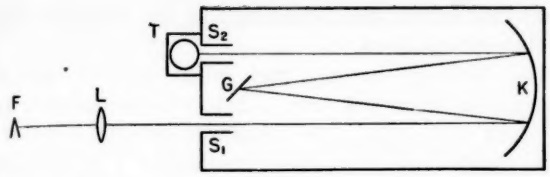

FIG. 2. Schematic diagram of light path. F=flame, L=lens, S_1=entrance slit of monochromator, K=concave spherical mirror, G=grating, S_2=exit slit to photomultiplier tube, and T=photomultiplier tube.

continuous variation of the dynode voltages from 45 to 129 volts can be made with the power supply, P. The current from the anode of the phototube is fed into the dc amplifier, A, with a range from 1×10^{-11} to 4×10^{-6} ampere and a response time of 3 seconds to within 1 percent of the final reading. The zero reading of the amplifier is stable to better than 1 percent of full scale reading. The electrical output from the amplifier goes into the pen recorder, R, with a response time of approximately 2 seconds for full scale travel. Linear intensity is recorded along the horizontal axis of the chart and wavelength along the vertical axis.

An ordinary acetylene burner of 1.5 mm diameter was adapted for the burner, F, by straightening the tube to make it more convenient for positioning. With the rack and pinion, D, it is possible to set the location of the burner to within 0.2 mm both vertically and horizontally. Tank gases were used and controlled at 5 lb/in.^{2} gauge pressure by regulators on the tanks. Hydrogen was specified by the supplier to be 99.8 percent pure and oxygen, 99.7 percent pure. Needle valves controlled the flow. Calibrated flowmeters, C, of the floating ball type were used for flow measurement to an accuracy of the order of 5 to 10 percent.

The spectral dispersing system, M, is an experimental, high resolution grating monochromator[4] which was constructed by the Research Department of Leeds and Northrup Company and loaned to the Heat and Power Division at the National Bureau of Standards on a field trial arrangement. This equipment is a special adaptation for laboratory use of a more general instrument designed for industrial metallographic analysis. It includes the optical and mechanical parts, the housing of the monochromator, and the appropriate electronics for the photoelectric detection and recording of light intensities.

A schematic diagram of the light path is shown in Fig. 2. Light from a selected portion of the flame, F, is focused by the quartz lens, L, on the entrance slit, S_1, of the monochromator. The light passes through the slit to part of the 8-inch diameter concave spherical mirror, K, at the focal distance (30 inches) from the slit and is reflected in a parallel beam to the grating, G. G is a flat reflection grating, 3×3 inches, ruled with 30,480 lines per inch on aluminum coated glass. It is blazed for strong second-order diffraction in the region of 3000A. The intensity of the first Rowland ghost is less than 1/200 of the parent line in the second order. The diffracted beam is refocused by another portion of the mirror, K, to the exit slit, S_2, and then to the photomultiplier tube, T. The aperture of the system is f:10. Since the exit beam uses the off-axis section of the spherical mirror in the reverse sense to that which the entrance beam uses the opposite portion of the mirror, aberration errors, normally encountered in off-axis use of spherical mirrors, are partially compensated.

The slit widths are continuously variable from about 0.001 to 0.150 mm, and by means of diaphragms one can use a range of slit heights from 0.3 mm to the maximum of 6 mm. It is thus possible to observe a section of the flame only 0.01 mm wide by 0.3 mm high.

A motor drive rotates the grating for scanning the spectrum at 1.2 or 5.9A per minute in the second order. There is also a rapid drive for changing wavelength regions and a provision for manual operation of the scanning. The grating is so mounted that it is possible to scan continuously from 1800 to 3550A in the second order and 3575 to 7100A in the first order. The entire monochromator, exclusive of the electronics, is contained in a rugged tubular housing of cast iron and with its dust cover has a dimension of only 34×14×12 inches. This conveniently small size and its ruggedness contribute to the usefulness of the equipment.

Figure 3(A) shows the stability of the flame over a one minute interval. This tracing was obtained by setting the grating of the monochromator *on the peak* of a line emitted by the flame. The small fluctuations of intensity are probably caused by the random emission from the photoelectric surface. Figure 3(B) records the intensity of the same line scanned repeatedly first in the direction of increasing wavelength and then in the opposite direc-

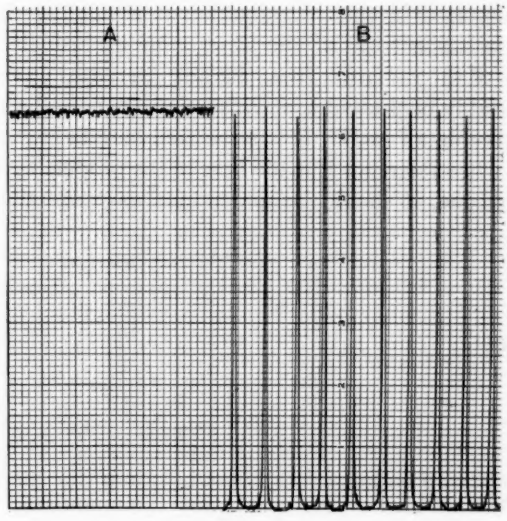

FIG. 3. Tracing showing response of monochromator. (A) Monochromator set on peak of line over 1.5-min interval. (B) Monochromator scanning one line in forward and reverse direction for 2-min interval.

[4] W. G. Fastie, J. Opt. Soc. Am. **40**, 800 (A) (1950).

tion. The reproducibility in intensities shown in Fig. 3(B) is characteristic of the reproducibility obtained over much longer times.

Although this equipment is still in the process of development, it has been possible to separate lines of 0.054A wavelength difference in the second order of the OH spectrum at 3100A. This indicates a resolving power, $\lambda/\Delta\lambda$, of the order of 55,000, which is about 30 percent of the theoretical value.

As an example of the usefulness of the monochromator for studies of flames, Fig. 4 shows a 9A region of the (0,0) band of OH which includes low and high K transitions of the R_2 branch.

The resolution is distinct and the noise level is low, so that a quantitative comparison of relative intensities is not difficult. Owing to the linear intensity response of phototubes, it is of great advantage in making intensity measurements to use photoelectric detection rather than photographic. There are none of the difficulties of processing and calibrating photographic plates, and continuous background is not a source of error with the direct reading monochromator since intensities are measured directly as heights above the background. Of course, for very weak sources or for instantaneous surveys over a wide wavelength range photographic exposures are still necessary.

The data were taken in the second order at a scanning rate of 5.9A per minute using the entire slit height of 6 mm. Two different slit widths were used: 0.010 mm (0.1A in the first order) for the scan of the (0,0) band of OH between 3060 and 3090A and 0.025 mm for the scan of the other regions listed below. The measurements on the inner cone were made with the base of the nozzle at the top of the slit in such a manner that the inner cone filled the slit at all times. The outer cone measurements were taken 2 cm above the base of the nozzle. With the burner used in this investigation it is not possible to obtain a spectrum of the inner cone exclusively, and some of the radiation from the hot interconal gases will invariably be present too. This point has been discussed in more detail in III. It is reiterated here to emphasize that when reference is made here to the properties of the inner cone, it should be understood as predominantly inner cone with some admixture of the radiation from the interconal gases.

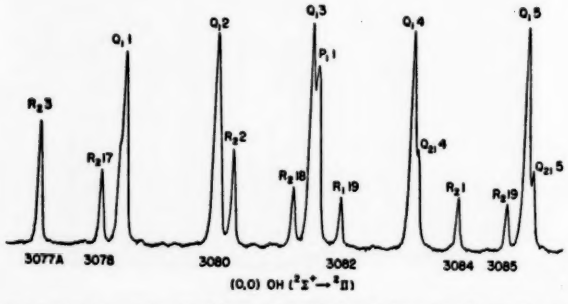

FIG. 4. Part of the (0,0) band of OH including the lines $K=1$, 2, 3, 17, 18, and 19 of the R_2 branch in the inner cone of a stoichiometric H_2-O_2 flame taken with the Leeds and Northrup monochromator. (Slow scanning rate, 1.2A per minute.)

The hydrogen-oxygen fuel ratios used in this investigation were 1:1 (lean), 2:1 (stoichiometric), and 4:1 and 6:1 (rich); the measurements thus cover a rather wide range of burning conditions. The total flow rate was adjusted to 200 cm³/sec at *NTP* for all fuel ratios in order to eliminate any possible effect of variable flow rates on the geometry and kinetic behavior of the flame.

C. ANALYSIS OF DATA

The wavelength regions analyzed were as follows:

(1) 3060–3090A,
(2) 3275–3285A,
(3) 3420–3435A.

1. Region (1) contains the (0,0) band of OH($^2\Sigma^+-{}^2\Pi$) from R_21 to R_220.[5] This band was used to determine the rotational temperature of OH by the modified iso-intensity method outlined in II. The main advantage of this method is that it gets around the difficulties caused by self-absorption by utilizing only lines of equal intensity. Doubt has recently been expressed regarding the applicability of the iso-intensity method when the emitting and absorbing layers of gas are at different temperatures.[6] While the question raised by Dieke and Crosswhite is of importance in case the iso-intensity method shows an apparent nonequilibrium distribution, it does not appear to seriously affect the validity of the method when a rotational equilibrium distribution is indicated as is the case in our investigation where we have found a rotational equilibrium distribution for 18 different combinations of fuel ratios and flame positions using 7 pairs of rotational lines for each determination. One may say in general that if the *modified* iso-intensity method[1] shows a rotational equilibrium distribution, the possibility that this is due to canceling errors is extremely slight, and an actual rotational equilibrium distribution in the flame is most strongly indicated. An example of the type of plot obtained in the analysis for rotational equilibrium is shown in the next section.

2. Region (2) covers part of the overlap region of the (0,0), (1,1), (2,2), and (3,3) bands of the $^2\Sigma^+\rightarrow{}^2\Pi$ system of OH. The lines studied were P_126 (0,0), P_226 (0,0), Q_127 (1,1), P_121 (1,1), Q_219 (2,2), P_114 (2,2), Q_25 (3,3), Q_18 (3,3), and Q_27 (3,3). These lines are weak enough not to be seriously affected by self-absorption, are free of blends and satellites and could easily be resolved by our spectrograph. By choosing such a small wavelength interval ($\sim$10A) one can carry out the analysis without

[5] The spectroscopic notation of this paper corresponds to that of the report of G. H. Dieke and H. M. Crosswhite, *The Ultraviolet Bands of OH*, Bumblebee Series Report No. 87, 1948, The Johns Hopkins University. This report also contains the wavelengths of the various transitions and the rotational transition probabilities used in the present study.

[6] G. H. Dieke and H. M. Crosswhite, Quarter Report NOrd-8036, JHB-3, Problem *A*, January 1–March 31, 1951.

TABLE I. "Temperature" and energy distributions of $OH(^2\Sigma^+)$ in the hydrogen-oxygen flame.

	$H_2/O_2=1/1$ (Lean) [a] $T_{adiab}=2920°K$		$H_2/O_2=2/1$ (Stoichio) $T_{adiab}=3100°K$		$H_2/O_2=4/1$ (Rich) $T_{adiab}=2850°K$		$H_2/O_2=6/1$ (Rich) $T_{adiab}=2450°K$
	Inner cone	Outer cone	Inner cone	Outer cone	Inner cone	Outer cone	Inner cone
T_{rot} (°K)	2830°K	2530°K	2875°K	2650°K	2800°K	2730°K	2670°K
T_{vibr} (°K)	Nonequilibrium	2440°K	Nonequilibrium	2550°K	Nonequilibrium	2640°K	Nonequilibrium
$v'=0$–1	2600		2400		2600		2600
$v'=1$–2	3300		2800		3200		3000
$v'=2$–3	5000		3400		4000		5000
$I_{OH^*}/I_{O_2^*}$ (calc)	0.5	0.5	2.6	2.5	53	80	120
$I_{OH^*}/I_{O_2^*}$ (exp)	0.9	1.4	2.5	3.9	~30	[b] $>10^2$	[b] $>10^2$

[a] The adiabatic flame temperatures have been calculated from the tables of Hottel, Williams, and Satterfield, *Thermodynamic Charts for Combustion Processes* (John Wiley and Sons, Inc., New York, 1949).
[b] No $O_2(^3\Sigma_u^- \rightarrow {}^3\Sigma_g^-)$ Schumann-Runge bands could be detected under these burning conditions. This makes $I_{O_2^*}$ less than ~0.1 on our recorder scale.

the necessity of standardizing the phototube for change of response with wavelength.

The determination of the vibrational energy distribution of OH in the levels $v'=0$ to 3 was based essentially on the method outlined in II. The intensity $I_{K,v}$ of a rotational line K with (upper) vibrational state v is given for the case of a rotational-vibrational equilibrium distribution by

$$I_{K,v}=CA_rA_v \exp(-E_r/kT_r) \exp(-E_v/kT_v)h\nu_{K,v}, \quad (1)$$

where C is a numerical factor which contains the electronic transition probability, A_r and A_v are the rotational and vibrational transition probabilities, E_r is the rotational energy which also contains the rotation-vibration interaction term, E_v is the vibrational energy, and T_r and T_v are the rotational and vibrational "temperatures," respectively. Equation (1) can be transformed into

$$L\equiv \log I_{K,v}-\log A_r-\log A_v+0.4343E_r/kT_r = -0.4343E_v/kT_v+C' \quad (2)$$

where the $h\nu_{K,v}$ of Eq. (1) has been taken into C' since $\nu_{K,v}\sim$constant over the small wavelength region investigated. In this equation, all the terms except T_v are known. $I_{K,v}$ is obtained from the monochromator tracing, E_r, E_v, A_r, and A_v have been calculated and tabulated[1,5] and the rotational "temperature" T_r is obtained independently by the modified iso-intensity method. By plotting the left-hand side of Eq. (2) against E_v one can then obtain some information in regard to the vibrational energy distribution. If this plot gives a straight line, then one is dealing with a vibrational equilibrium (Boltzmann) distribution and the vibrational "temperature" T_v can be obtained from the slope. When $T_v=T_r$ one has an equilibrium-equipartition distribution in the rotational and vibrational energy levels; when $T_v\neq T_r$, and both T_v and T_r are well defined through the appropriate straight line relationships, one has vibrational and rotational equilibrium but a nonequipartition of energies. If the plot of L *vs* E_v does not lead to a straight line relationship, one is dealing with a vibrational nonequilibrium distribution and a vibrational "temperature" is of course not defined. Examples of these different types of distributions are shown in Section D.

3. Region (3) covers part of the overlap region of the (0,1) band of $OH(^2\Sigma^+\rightarrow{}^2\Pi)$ and of the (0,14) band of $O_2(^3\Sigma_u^-\rightarrow{}^3\Sigma_g^-)$. This region was used to determine the relative concentration of $OH(^2\Sigma^+)$ to $O_2(^3\Sigma_u^-)$ as described in detail in III. The principle of this method is to compare the experimental intensity ratio of $OH[R_110;\ (0,1)](^2\Sigma^+)$ and $O_2[P(31)+R(35);\ (0,14)](^3\Sigma_u^-)$ with the calculated equilibrium intensity ratio using T_r as the equilibrium temperature. Possible deviations from a thermal distribution will then be indicated by the nonequality of the experimental and the calculated equilibrium intensity ratios. It would of course be possible to calculate an electronic "temperature" from the experimental intensity ratios using Eq. (15) of III and then compare this T_{el} with the rotational and vibrational "temperatures" T_r and T_v. This procedure, however, is not as sensitive to the trend of the data as comparing the calculated and experimental intensity ratios. The temperature enters Eq. (15) of III both explicitly in the exponential factor and implicitly in the term N_{OH}/N_{O_2} and experience has

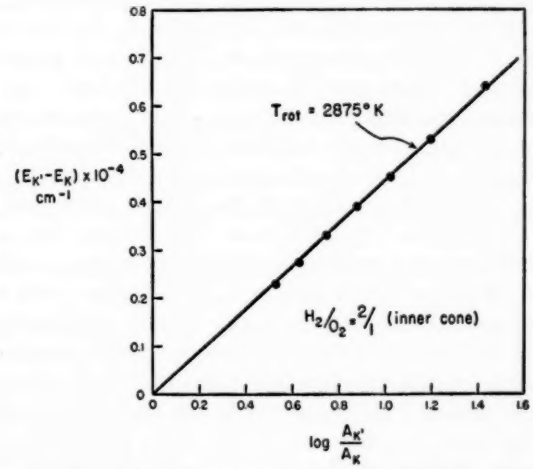

FIG. 5. A plot of $E_{K'}-E_K$ *vs* $\log(A_{K'}/A_K)$ for the R_2 branch of the (0,0) band of $OH(^2\Sigma^+\rightarrow{}^2\Pi)$ in the inner cone of a stoichiometric H_2-O_2 flame. The rotational temperature, T_r, is determined from the slope of the graph.

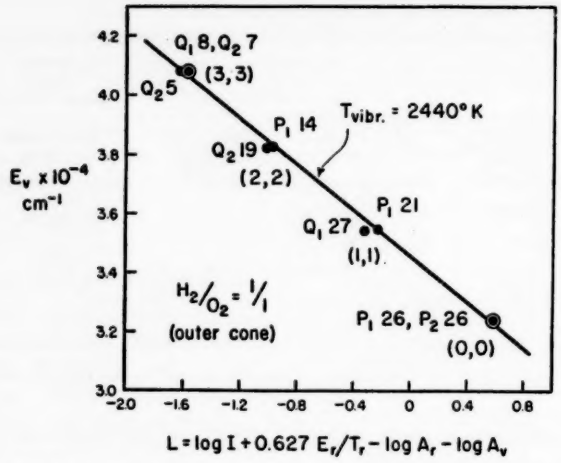

FIG. 6. A plot of L *vs* E_v for the outer cone of a lean (1/1) H_2-O_2 flame for several lines in the vibrational levels $v'=0$, 1, 2, and 3 of the $OH(^2\Sigma^+ \rightarrow {}^2\Pi)$ transition. The vibrational temperature, T_v, is determined from the slope of the graph.

shown that a rather large variation of the experimental I_{OH}/I_{O_2} will have only a small effect on the "temperatures" calculated in this manner.

D. EXPERIMENTAL RESULTS

The over-all results of this study are presented in Table I. A rotational equilibrium distribution of $OH(^2\Sigma^+)$ was found for all fuel ratios in both the inner and outer cone. Figure 5, which can serve as a representative example of the type of relationship obtained, shows the analysis for the inner cone of the stoichiometric ($H_2/O_2=2/1$) hydrogen-oxygen flame. The plots for the other fuel mixtures in both the inner and outer cone are very similar and are therefore not reproduced here. In all cases, the good straight line relationship between $\log(A_{K'}/A_K)$ and $E_{K'}-E_K$ and the 0,0 intercept are indicative of a rotational equilibrium distribution.[1]

The rotational "temperatures" T_r determined from the slopes of the lines are in fair agreement with the calculated adiabatic flame temperatures. In the inner cone, T_{rot} follows the trend of T_{adiab} but is generally somewhat lower, possibly reflecting the heat loss by radiation, which is of course not taken into account in adiabatic flame temperature calculations. The rotational "temperature" in the outer cone is less than that for the inner cone corresponding to the cooling undergone by the hot gases as they move away from the reaction zone. It may be noted incidentally that while there is a difference of about 300°K between T_{rot} for the inner and outer cones for both the lean (1/1) and stoichiometric (2/1) fuel mixture, there is a much smaller amount of cooling (~70°K) for the hydrogen rich (4/1) mixture. While this may be due partly to the changed geometry of the flame, (so that one is not really observing comparable regions of the outer cone) one contributing reason for this apparent anomaly may well be the burning of excess hydrogen with the oxygen from the surrounding air.

A vibrational equilibrium distribution of $OH(^2\Sigma^+)$ was found in the *outer cone* for all fuel mixtures. An example of the graph obtained from Eq. (2) is shown in Fig. 6 which refers to the outer cone of the lean (1/1) hydrogen-oxygen flame. The rather good straight line which can be drawn through the experimental points indicates the vibrational equilibrium. The graphs of L *vs* E_v for the outer cones of the other fuel ratios are very similar and are therefore not shown here. The vibrational "temperatures" T_v which may be obtained from the slopes of the lines are in good agreement with the corresponding rotational "temperatures" in the outer cones, the discrepancy of about 100°K being attributable largely to the various approximations introduced in the calculation of the vibrational matrix elements.[1]

The analysis for the vibrational distribution of $OH(^2\Sigma^+)$ in the *inner cones* indicates a distinct non-equilibrium distribution for all the fuel ratios examined. This is pointed up in Figs. 7 to 9 which clearly show that no straight line, indicative of an equilibrium distribution, can be drawn through the experimental points. The curvature is particularly pronounced for the lean and rich mixtures, while the plot for the stoichiometric one approaches more closely to that of a straight line. An analysis of these curves carried out by determining the vibrational "temperatures" from straight line segments drawn between $v'=0$ and 1, $v'=1$ and 2, and $v'=2$ and 3 shows that the vibrational levels $v'=2$ and 3 are over-populated as compared to a Boltzmann distribution with $T_{equil}=T_r$. This is particularly true of the level $v'=3$. A calculation for the inner cone of a (1/1) fuel mixture shows that the population of $OH(^2\Sigma^+)$ in the level $v'=3$ is about 8.0 times its equilibrium value. The values obtained for the vibrational "temperatures" in the above manner are listed in Table I; the figures there quoted indicate that the deviation from the vibra-

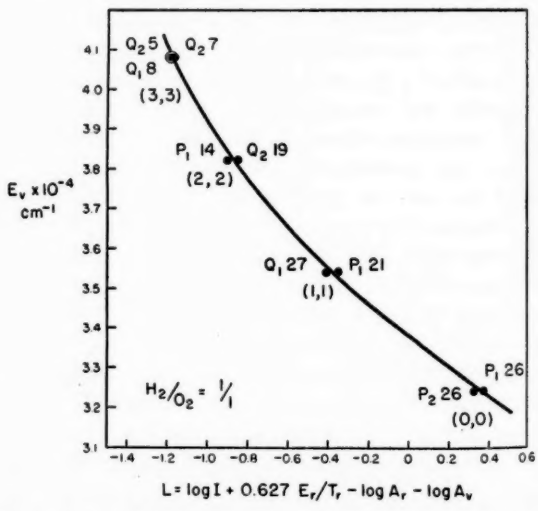

FIG. 7. A plot of L *vs* E_v for the $OH(^2\Sigma^+ \rightarrow {}^2\Pi)$ transition in the inner cone of a lean (1/1) H_2-O_2 flame. The curvature of the line connecting the experimental points indicates the vibrational non-equilibrium distribution of $OH(^2\Sigma^+)$.

tional equilibrium distribution is most pronounced for the nonstoichiometric fuel mixtures.

The experimental values for the relative intensities of excited OH to $O_2(^3\Sigma_u^-)$ are in agreement with the calculated equilibrium intensity ratios for both the inner and outer cones as shown in Table I. The agreement is comparable with that noted in III, and an equilibrium distribution of excited OH to O_2 in the hydrogen-oxygen flame is indicated. Owing to the various approximations in the theoretical treatment and to the somewhat uncertain experimental data (f values, heat of formation of OH) entering into the calculation of the equilibrium intensity ratios, not too much significance should be attached to the differences between $I_{OH^*}/I_{O_2^*}$ calculated and experimental in any one column. In particular, attempts to draw any conclusion as to the finer details of the $OH(^2\Sigma^+)/O_2(^3\Sigma_u^-)$ distribution in the various fuel mixtures in both inner and outer cones would not seem to be warranted by the accuracy of the data or by that of the calculations.

The reproducibility of the data is very good. Several runs were made on some of the fuel mixtures, for both inner and outer cone, by different personnel and at different times. All these runs gave concordant results as to the equilibrium or nonequilibrium distributions and temperatures (±3 percent). Furthermore, the data reported here for T_{rot} of the inner cones and the $OH(^2\Sigma^+)/O_2(^3\Sigma_u^-)$ distribution for the various fuel ratios are in good agreement with those obtained previously (III) on a Jarrell-Ash spectrograph with the conventional photographic technique.

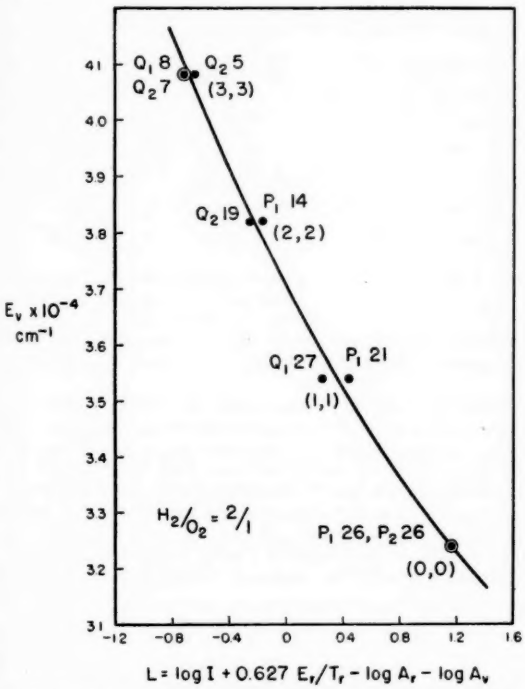

FIG. 8. A plot of L *vs* E_v for the $OH(^2\Sigma^+ \rightarrow {}^2\Pi)$ transition in the inner cone of a stoichiometric (2/1) H_2-O_2 flame. The curvature of the line connecting the experimental points indicates the vibrational nonequilibrium distribution of $OH(^2\Sigma^+)$.

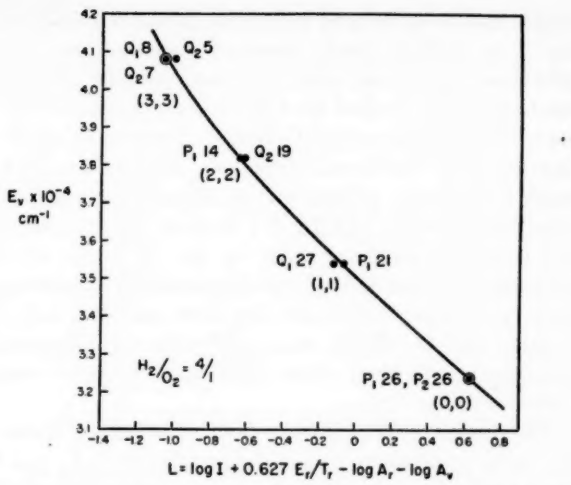

FIG. 9. A plot of L *vs* E_v for the $OH(^2\Sigma^+ \rightarrow {}^2\Pi)$ transition in the inner cone of a rich (4/1) H_2-O_2 flame. The curvature of the line connecting the experimental points indicates the vibrational nonequilibrium distribution of $OH(^2\Sigma^+)$.

E. INTERPRETATION OF DATA

The finding of rotational, vibrational, and electronic equilibrium in the outer cone of all these flames is not very surprising since one is dealing here mostly with the hot gases streaming away from the reaction zone. In flames burning at atmospheric pressure there will probably have been a sufficient number of equilibrizing collisions by the time the radiating species reaches the outer cone for a Boltzmann distribution among the various energy levels to be established, even if these species should have been formed in a nonequilibrium distribution in the inner cone reaction zone. The approximate equality of T_{vibr} and T_{rot} in the outer cones indicates that the vibrational transition probabilities calculated in I are essentially correct. In the inner cone one finds a rotational temperature in good agreement with the adiabatic flame temperature and Na line reversal temperatures;[7] furthermore, the measurements of the relative intensities in the $OH(^2\Sigma^+ - {}^2\Pi)$ and $O_2(^3\Sigma_u^- - {}^3\Sigma_g^-)$ systems indicate that these electronic states are in thermal equilibrium. Considering all these facts one would be inclined to conclude that the radiation due to $OH(^2\Sigma^+)$ in the hydrogen-oxygen flame is of a purely thermal nature were it not for the observed nonequilibrium distribution among the vibrational levels in the inner cone.

A vibrational nonequilibrium distribution of $OH(^2\Sigma^+)$ in hydrogen-oxygen flames has been reported previously, both for low pressure[2,3] and atmospheric pressure[8] burning. In particular, Gaydon and Wolfhard noted a selective excitation to the $v'=2$ and 3 levels of $OH(^2\Sigma^+)$ in a hydrogen-air flame at atmospheric pressure; our

[7] H. H. Lurie and G. W. Sherman, Ind. Eng. Chem. **25**, 404 (1933).

[8] A. G. Gaydon and H. G. Wolfhard, Proc. Roy. Soc. (London) **208A**, 63 (1951). One of us (K.E.S.) is greatly indebted to Professor Gaydon for furnishing him with a manuscript of this paper prior to publication.

results are in agreement with this. It was attempted at first[2,3] to explain these observed nonequilibrium distributions as being due to some specific chemical reactions which excited the OH radicals preferentially to the $v'=2$ and 3 levels of $OH(^2\Sigma^+)$. The recent work of Gaydon and Wolfhard,[8] however, has shown that a much more likely explanation for the anomalous vibrational distribution of $OH(^2\Sigma^+)$ is that the $^2\Sigma^+$ state of OH is weakly predissociated by the $^2\Sigma^-$ state of OH between $v'=2$ and 3. The experimental evidence for such a postulated predissociation has been set forth fully by Gaydon and Wolfhard, and since we are in substantial agreement with their views there is no need to repeat their discussion here.

The preferential excitation to the $v'=2$ and 3 levels in the inner cones of hydrogen-oxygen flames may now be attributed to a radiationless transition involving $OH(^2\Sigma^+)$ and $OH(^2\Sigma^-)$. Such a process may be written *schematically* as[8]

$$O(^3P)+H(^2S)\rightarrow OH(^2\Sigma^-)\rightarrow OH(^2\Sigma^+). \qquad (3)$$

The interaction between $OH(^2\Sigma^-)$ and $OH(^2\Sigma^+)$ is, however, so weak[9] that reaction (3) probably would not be very efficient in producing $OH(^2\Sigma^+)$. The detailed process leading to $OH(^2\Sigma^+)$ in the hydrogen-oxygen flame probably involves the reactions $H+O_2\rightarrow OH+O$ and $O+H_2\rightarrow OH+H$, and the radiationless transition will then be between intersecting, nonlinear[10] HO_2 or H_2O surfaces. It can be shown that these interactions are somewhat stronger than the direct interaction between $OH(^2\Sigma^+)$ and $OH(^2\Sigma^-)$ and thus provide a more efficient path for the production of $OH(^2\Sigma^+)$. This will be discussed in more detail in a subsequent communication.

Regardless of the detailed path of the radiationless transition reaction leading eventually to $OH(^2\Sigma^+)$, one of the prerequisites for the observed nonequilibrium distribution in the vibrational levels is that the atoms entering into the reaction are present in excess of their thermal equilibrium concentration.[11] Such an abnormally high concentration of atoms (and radicals) in the reaction zone of flames would not be surprising.[12] In flames, the absence of any walls on which atoms can be removed facilitates the build-up of these atoms formed in chain propagating and chain branching steps to a much higher steady-state concentration than corresponds to equilibrium. The main removal processes must be gas phase reactions and diffusion out of the reaction zone.

The gas phase recombination and removal processes of atoms involve most probably three-body collisions, and the effectiveness of these processes will thus depend upon the ability of the third body to carry away some of the energy of reaction. The most efficient third body in the hydrogen-oxygen flame is undoubtedly H_2O whose efficiency in the removal of excess energy is well known from sound dispersion studies.[13] This property of H_2O would then explain the less pronounced vibrational nonequilibrium distribution in the stoichiometric fuel mixture: there is a larger concentration of H_2O in the stoichiometric flame which will serve to reduce the excess concentration of atoms via three-body collisions. As the combustion intermediates, such as H and O atoms, move out of the reaction zone toward the outer cone, they will continuously undergo collisions leading to recombination and to formation of OH and H_2O so that by the time the surviving atoms have reached the outer cone they will be in their thermal equilibrium concentration and give rise to a Boltzmann distribution of $OH(^2\Sigma^+)$ in its vibrational energy levels.[14]

The suggestion advanced in this paper that there may be a concentration of atoms in excess of their equilibrium thermal value in the reaction zone of the hydrogen-oxygen flame would seem to have an interesting bearing on the active particle diffusion theory of flame propagation advanced by Lewis and von Elbe[15] and by Tanford and Pease.[16] This excess atomic concentration in the reaction zone increases the concentration gradient along which the atoms will diffuse into the unburned gas and may thus facilitate the propagation of the flame. It may be of interest to follow up this point in more detail.

[9] The interaction of the $^2\Sigma^+$ and $^2\Sigma^-$ states is caused by only a very small spin-internuclear axis coupling term in the Hamiltonian of the perturbation matrix. The interaction is thus so weak that it should not affect the calculated values (reference 1) of the vibrational matrix elements to any large extent. This may also be seen from the fact that in the outer cone, where equilibrium might be presumed to exist, a vibrational-rotational equilibrium distribution with $T_{vibr}=T_{rot}$ is always found in the hydrogen-oxygen flame.

[10] K. J. Laidler and K. E. Shuler, Chem. Revs. **48**, 153 (1951).

[11] In the case of complete thermal equilibrium, a radiationless transition cannot lead to a nonequilibrium distribution since it will, by the principle of detailed balancing, be exactly balanced by the inverse radiationless transition.

[12] K. J. Laidler and K. E. Shuler, paper delivered at the Am. Chem. Soc. Symposium on Combustion Chemistry, Cleveland, April 9–12, 1951, Ind. Eng. Chem. **43**, 2758 (1951).

[13] A. Eucken and R. Becker, Z. phys. Chem. **20B**, 467 (1933); **27B**, 219 (1934); I. M. Metter, Physik. Z. Sowjetunion **12**, 232 (1937).

[14] The rotational and electronic energy distributions determined as outlined in section *C* of this paper are not affected by the predissociation and preassociation discussed above since the relevant data for their analysis were obtained from the $v'=0$ level of $OH(^2\Sigma^+)$ which for the low K values ($K\leq 20$) used in this work is too far removed from the region of intersection of the potential curves to be affected by it (see reference 8).

[15] B. Lewis and G. von Elbe, J. Chem. Phys. **2**, 537 (1934).

[16] C. Tanford and R. N. Pease, J. Chem. Phys. **15**, 431, 861 (1947).

Precise Measurements in the Infrared Spectrum of Carbon Monoxide*

EARLE K. PLYLER AND W. S. BENEDICT,
National Bureau of Standards, Washington, D. C.

AND

SHIRLEIGH SILVERMAN
Applied Physics Laboratory, The Johns Hopkins University, Silver Spring, Maryland

(Received August 23, 1951)

New measurements have been made in the CO infrared spectrum in both emission and absorption, using a 15,000-line/inch grating spectrograph and a 7200-line/inch vacuum grating spectrograph. High precision in wavelength determinations was obtained by superimposing on the spectra emission lines in higher order of Hg, Kr, and A discharges. The measurements are believed accurate to ± 0.02 cm^{-1}. The observed lines in absorption are those of the 2−0 and 3−0 bands of $C^{12}O^{16}$, between R 30–P 29 and R 9–P 16, respectively; 27 lines of $C^{13}O^{16}$ and 10 lines of $C^{12}O^{18}$ have also been measured. In emission from oxy-acetylene and CO−O_2 flames, over 300 lines in the 2−0, 3−1, 4−2, and 5−3 bands have been identified between 4360 and 4000 cm^{-1}. The emission bands form heads in the R branch near $J=50$, and the 2−0 band shows resolved lines out to $J=46$ in both P and R branches.

The new measurements are in good agreement with earlier results at low quantum numbers, but show discrepancies at high numbers which result in slightly different values for the molecular constants, especially in y_e and D_e. Our constants are in cm^{-1}

ω_e	$x_e\omega_e$	$y_e\omega_e$	B_e
2169.81	13.284	0.010	1.93130

α	γ	D_e	β
0.017543	4.5×10^{-6}	5.95×10^{-6}	0

The observed isotope shifts of the 2−0 band origin for $C^{12}-C^{13}$ and $O^{16}-O^{18}$ are, respectively, 93.27 ± 0.02 cm^{-1} and 101.03 ± 0.05 cm^{-1}, in good agreement with the calculated values.

The emission spectra permit the determination of rotational "temperatures" with an accuracy of ±5 percent and vibrational "temperatures" with an accuracy of ±10 percent. Thermal equilibrium between the two modes is observed in the outer cone of the flames, but in the region just above the reaction zone, the rotational temperatures are several hundred degrees higher than the vibrational values or the calculated equilibrium values.

INTRODUCTION

WITH the development of infrared detectors of increased sensitivity, permitting the construction of grating spectrometers of high resolving power, it has become both desirable and possible to increase the precision by which the wavelengths of absorption or emission lines are known. The conventional method of fixing wavelengths has been to make use of the grating constant, which is empirically determined by measuring the angle at which one or two standard lines appear at the higher orders. This method, although satisfactory when extreme precision is not required, demands an instrument of great mechanical and optical perfection if systematic or random errors are not to be introduced.

In the photographic region of the spectrum, the optical principles are the same, but because of the greater simplicity of recording, the conventional method of fixing wavelength has been to superimpose on the desired unknown spectrum a comparison spectrum of known standard lines, which ultimately go back to the international primary standards. For this purpose iron-arc or rare-gas discharges are commonly used. By this means it has been possible to measure a number of molecular spectra with high accuracy, and thereby to obtain knowledge of the frequencies at which other transitions in the same molecule must appear in the infrared region. These calculated frequencies are, however, often not in agreement.

A case in point is the vibration-rotation spectrum of CO. The fundamental and first overtone have been measured several times in the infrared, most recently by Lagemann, Nielsen, and Dickey.[1] The third overtone has been measured photographically by Herzberg and Rao.[2] The ground state of the molecule appears in several electronic transitions, and recently quite accurate measurements in the Cameron system ($^3\Pi-{}^1\Sigma$), including bands involving the five lowest vibrational levels, have been reported by Rao.[3] He has also pointed out[4] that a discrepancy exists between the photographic and infrared data, and has suggested that the frequencies computed from the photographic data be used as standards for the infrared region.

In the course of a study of infrared flame spectra under high resolution,[5] we have been able to observe the vibration-rotation spectrum of CO in emission. Because of the high temperatures involved (of the order of 2500°K) lines of high rotational and vibrational quantum numbers appear. Their wavelengths were in agreement neither with the earlier infrared measurements nor with values calculated by the constants suggested by Rao.[4] Accordingly, we have endeavored to remeasure as precisely as possible the spectrum, both in absorption and in emission. For wavelength standards we have used higher order atomic lines, superimposed directly on the spectra. The measurements include absorption measurements of the 2−0 and 3−0

* This work was supported by the U. S. Navy, Bureau of Ordnance and ONR.

[1] Lagemann, Nielsen, and Dickey, Phys. Rev. **72**, 284 (1947).
[2] G. Herzberg and K. N. Rao, J. Chem. Phys. **17**, 1099 (1949).
[3] K. N. Rao, Astrophys. J. **110**, 304 (1949).
[4] K. N. Rao, J. Chem. Phys. **18**, 213 (1950).
[5] S. Silverman and W. S. Benedict, Phys. Rev. **82**, 337 (1951).

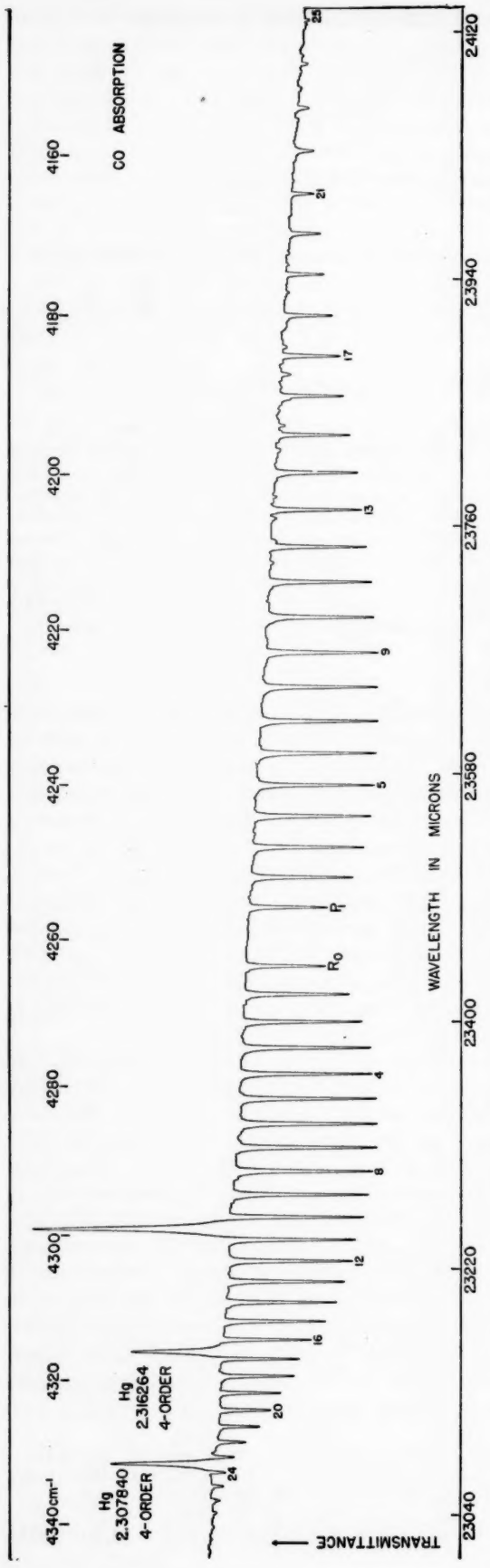

FIG. 1. The absorption spectrum of carbon monoxide in the 2—0 band. Three emission lines of mercury are superimposed on the record. The cell length is 60 cm and the pressure 20 cm of Hg.

bands of $C^{12}O^{16}$; in the former region a number of lines of the isotope bands $C^{13}O^{16}$ and $C^{12}O^{18}$ also have been recognized. The emission measurements were confined to the first overtone region, where nearly 300 lines of the 2—0, 3—1, 4—2, and 5—3 bands have been measured between 4360 and 4000 cm^{-1}. The present measurements are in quite good agreement with the data calculated by Herzberg and Rao for the lower energy levels observed by them, but yield somewhat different centrifugal-stretching and higher order anharmonic constants.

EXPERIMENTAL METHODS AND RESULTS

In the measurements of the CO spectrum two grating spectrometers were used. The spectrometer which was constructed at the National Bureau of Standards contains a 15,000 lines-per-inch grating ruled at Johns Hopkins University. An off-axis paraboloidal mirror of 1 meter focus is used as the collimator. The detector is a PbS cell. The impulses from the photoconducting cell are amplified by a Wilson-type ac amplifier of narrow band pass. The amplifier is fed into a Leeds and Northrup Speedomax recorder. In absorption measurements a tungsten ribbon filament lamp is used as the source of radiation. When the lamp is operated at 40 amperes very narrow slits may be used. The spectral slit width was about 0.15 cm^{-1} in the regions of 1.6 and 2.4μ.

The other spectrometer used in these measurements was a vacuum spectrograph. It was constructed at the Applied Physics Laboratory of The Johns Hopkins University and employs a 7200 line/inch grating at aperture f:6. The optics are the conventional Pfund perforated plane mirror type, using on-axis parabolic mirrors of 72 cm focal length. Ahead of the spectrometer is a monochromator employing a 20° KBr Littrow foreprism. The working pressure is approximately 0.1 mm, and the total outside air path from flame source to entrance window is 6 cm. The detector used in these experiments was a PbS cell. The signals were amplified by a 1000 cycle high gain narrow-band pass phase-gating amplifier designed and built at the Applied Physics Laboratory.

The emission spectrum of CO was obtained from a variety of flames produced by burning C_2H_2—O_2 and CO—O_2 mixtures. For the oxy-acetylene flame a welding torch was employed. Various fuel-oxygen ratios were used; the strongest lines were obtained when the ratio was about $2C_2H_2$:$1O_2$. A region of the flame about 1 inch above the inner cone was focused on the slit. A mirror was placed back of the flame so that an image was formed inverted and superimposed on the flame. This resulted in very nearly doubling the intensity of the CO lines. For the best runs the effective slit width was 0.3 cm^{-1}. When comparison wavelengths were desired the mirror was used to focus the light of a rare-gas lamp through the flame and onto the slit.

The CO-oxygen flame spectra were obtained by burning premixed gases in the ratio of 5 CO to 1 of

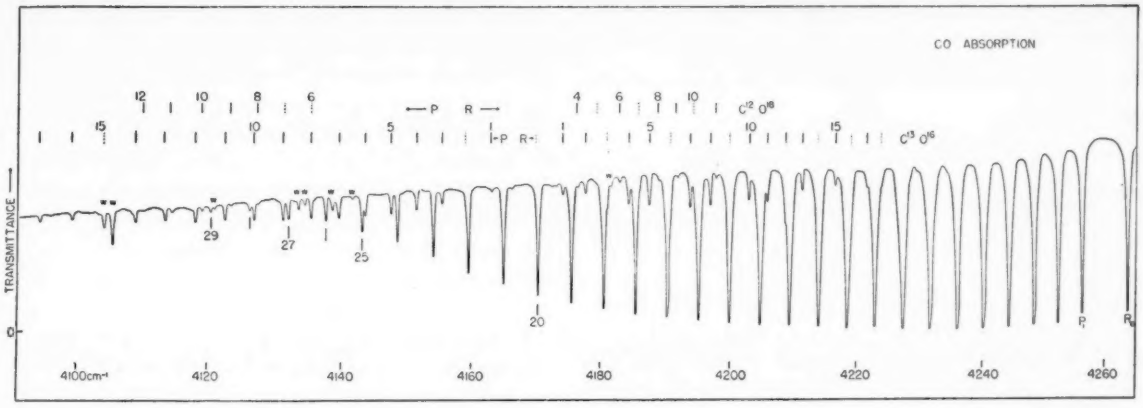

FIG. 2. A part of the 2—0 band showing some lines of the $C^{13}O^{16}$ and the $C^{12}O^{18}$ molecules. The cell length was 105 cm and the pressure 76 cm. A few absorption lines of H_2O, marked *w*, appear.

oxygen. Commercial grade CO containing approximately 1.5 percent of H_2 as principal impurity and ordinary, tank O_2 were used in these experiments. Iron carbonyl was removed from the CO by passing the gas over a train of porcelain chips heated at 275°C. The gases were carefully metered through calibrated flowmeters, and burned from the end of a rectangular channel of 30×0.5 mm cross section and 60 mm high. The 30-mm dimension of the burner was parallel to the optic axis of the instrument. To further increase the signal, a mirror was placed behind the flame, thus forming an image on the flame. The flames as described above with a total flow of 6 liters per minute burned with a stability such that the noise in the system was mainly electrical. Slits of 60 microns were used, which at this dispersion and frequency are equivalent to about 0.5 cm^{-1} for the vacuum spectrometer.

In the absorption measurements two cells were used. One absorption cell was 60 cm in length, and the pressure of the carbon monoxide was 20 cm. The other cell was of the multiple reflection type and had a total path length of 1.05 meters. The pressure of the gas was 76 cm.

The 2—0 band, as obtained with the smaller amount of gas, is shown in Fig. 1. A portion of the same band, with the larger quantity of gas, is shown in Fig. 2; a number of lines due to the isotopic molecules $C^{13}O^{16}$ and $C^{12}O^{18}$ may be observed. At the longest wavelengths, a few absorption lines due to the H_2O also appear, and are identified by the symbol *w*. With the same quantity of gas the 3—0 band also appears weakly in the region of 1.58μ; it is illustrated in Fig. 3.

In the emission spectra, the lines of the 2—0 band extend to much higher *J* values. A head is formed near $J=50$ in the *R* branch, and is a prominent feature of the spectra. Additional heads due to the higher state bands 3—1, 4—2, and 5—3 also appear. Figure 4 is a reproduction of the region from 4360–4180 cm^{-1} from an oxy-acetylene flame. Figure 5 shows the same region for a CO—O_2 flame from the slit burner. The region of the flame represented was one-inch high starting just above the inner cone. As may be seen by comparing the figures, the heads and resolved lines of the 5—3 and 4—2 bands are much more prominent in the oxy-acetylene flames, because of the higher temperature. A further discussion of the relative intensities of the lines is given later. The emission lines of CO, corresponding to the *P* branches of the bands, extend to longer wavelengths than illustrated. Emission lines due to H_2O are a complicating factor beyond 4200 cm^{-1}, particularly in the oxy-acetylene flames. These may be recognized by comparing the spectra taken under different conditions with oxy-hydrogen flame spectra; a few such lines are indicated in Fig. 4. Between 4050–4000 cm^{-1} the H_2O emission lines are very strong compared with the lines of CO, even when relatively hydrogen-free CO is burned, and beyond 4000 cm^{-1}, few if any CO lines can be recognized.

In order to measure the wavelengths of the absorption lines to a high accuracy, higher orders of atomic spectra were superimposed on the absorption trace. This was accomplished in several ways. For the absorption measurements there were available lamps with electrodes which become hot when the enclosed gas is excited. These provided a continuum for the absorption and calibration standards at the same position. The *S*-1 mercury lamp is of this type and was used in obtaining the record shown in Fig. 1. The figure is made

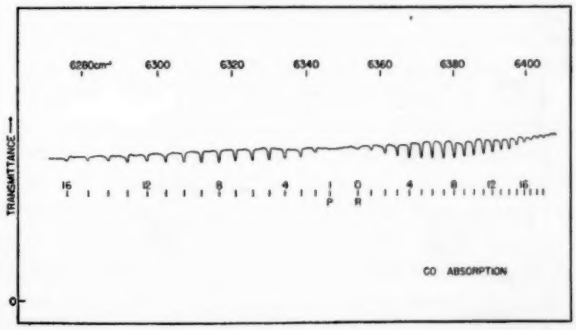

FIG. 3. The absorption of CO in the 3—0 band. The cell length was 105 cm and the pressure 76 cm of Hg.

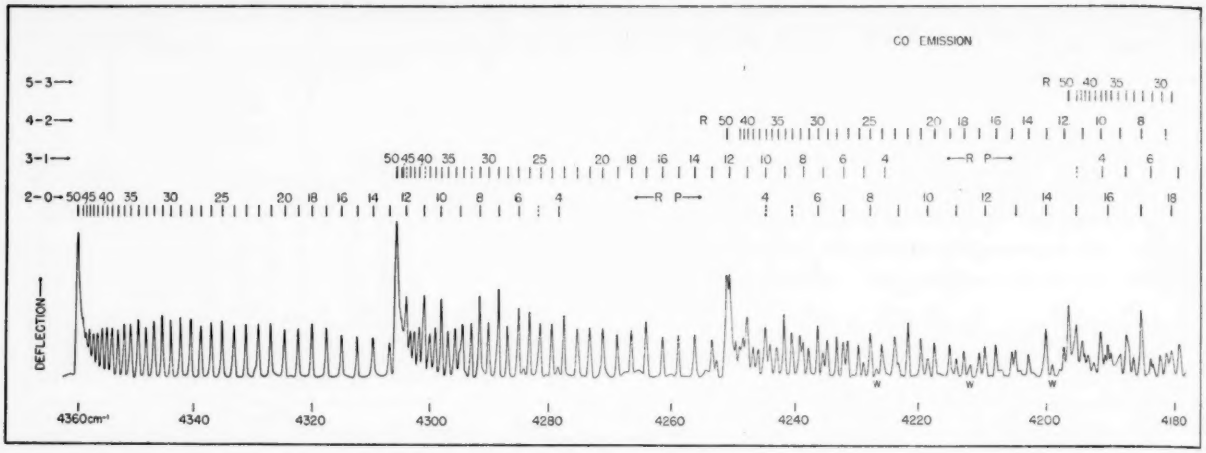

FIG. 4. The emission spectrum of CO in the 2.4μ region as observed in the outer cone of a near-stoichiometric oxyacetylene flame.

from an original record on unruled recorder paper. Alternately, the low pressure *H*-11 mercury lamp could be placed in the beam which originated at the tungsten source so that the yellow mercury lines in the fourth order were recorded on the absorption curve. No difference in the wavelengths of the CO lines was found by comparison with the two sources. Other rare-gas discharge tubes were similarly used and gave consistent results, both with the absorption and emission measurements.

The higher order lines of Hg, A, and Kr obtained in this way served as standards throughout the region from 2.30 to 2.50μ. They were particularly useful when pairs of atomic lines fell so closely together that a linear dispersion curve could be assumed without introducing appreciable error. The yellow mercury doublet illustrated in Fig. 1 is one such pair; others may be recognized in Table I, which lists the atomic lines used. These are given to 0.01A, which is sufficient for our measurements. They are, however, known to eight significant figures. Other atomic lines appear on the traces; for example, the third line shown in Fig. 1 is a first-order Hg line at 23,254A. Since it has not been previously measured with high accuracy it was not used in the CO reduction.

By making use of close pairs of atomic lines it was possible to measure 23 CO lines with the highest accuracy. These include lines near both ends of the 2–0 absorption band and near the center. Lines were determined on nine different absorption curves, taken at different recording speeds, and with different standards. They were measured and reduced independently by three different observers. In the measurement the distances between the centers of the standard and CO lines were measured with a steel ruler, graduated to 0.01 inch. The agreement between the several reductions was such that the greatest deviation of an individual value from the mean was 0.55A, and the probable error of the mean less than 0.1A. As a further example of the consistency of the measurements, Table II lists a comparison of the average wavelengths of eight lines of the *R* branch, as obtained in absorption using fourth-order Hg lines as standards, with the values obtained in emission using third-order Kr lines as standards.

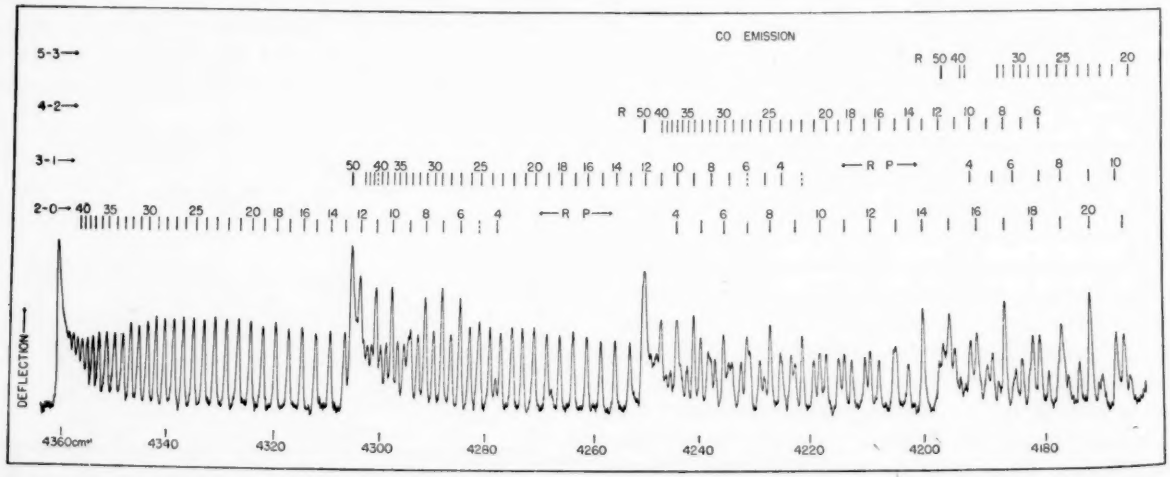

FIG. 5. Emission spectrum of CO in the 2.4μ region as observed just above the inner cone of a fuel-rich CO–O_2 flame.

The same method, using Kr standards in the second order, was used to obtain wavelengths of the 3−0 band in the region of 1.6μ. Because of the weaker absorption, the lines could not be measured with quite such accuracy, but the error is believed not to exceed 0.1A.

The wavelengths, measured in air, were reduced to wave numbers in vacuum by inverting Kayer's "Tabelle der Schwingungszahlen" and applying Babcock's correction[6] which incorporates the extrapolated value for the index of refraction in the infrared. An experimental verification that the refractive-index correction is not far in error was obtained by making measurements with the vacuum grating spectrometer, both evacuated and filled with air. No shift of the CO absorption lines relative to the fourth-order Hg standards could be detected. According to the Babcock correction, the shift should amount to +0.018 cm^{-1}; the sharpness of the lines was such that a shift of 0.03 cm^{-1} would have been noted.

As was mentioned in the introduction, it was not possible to obtain measurements of such accuracy on lines distant from the standards. While the average of a number of runs may yield fairly reliable values, individual readings, if based on a dispersion curve fitted to the standards, either in terms of linear distance on the chart, or in terms of the fiducial marks impressed on the chart at equal angular displacements, may vary by 1A or more. These effects are apparently random, and occur to about the same extent in both spectrometers.

Accordingly it was believed that in order to establish the wavelength scale between the atomic standard lines, recourse should be made to the known regularities which the CO lines must follow. To a high accuracy, the equation

$$\nu=\nu_0+(B'+B'')m+(B'-B'')m^2 -2(D'+D'')m^3+2(D'-D'')m^4, \quad (1)$$

where $m=(J''+1)$ for the R branch and $m=-J''$ for the P branch, must represent the line positions. The lines listed as observed in Table III, which include a number in both branches from $J=17$ to 27, as well as a few near the band center, were used to determine the

TABLE I. List of atomic lines used as standards.

Mercury	
5769.60A	5790.66A
Argon	
7948.18A	8014.79A
8006.16	
Krypton	
7601.55A	8112.90A
7685.25	8190.06
7694.54	8263.24
7854.82	8281.06
8059.51	8298.11
8104.37	

[6] H. D. Babcock, Phys. Rev. **46**, 382 (1934).

TABLE II. Comparison of absorption and emission measurements.

Line	Absorption	Emission
R	λ_{air}	λ_{air}
17	23157.16A	23157.04A
18	23143.86	23143.80
19	23130.90	23130.69
20	23118.38	23118.32
21	23106.04	23106.20
22	23094.51	23094.67
23	23083.05	23083.10
24	23072.34	23072.23

constants of Eq. (1). This was done with a slight variation of the usual manner, by obtaining $\Delta_2F''/(J+\frac{1}{2})$ and $\Delta_2F'/(J+\frac{1}{2})$ and plotting against $J(J+1)$. The results are displayed in Fig. 6. For the state $v=0$, our results are in excellent agreement with the values, at lower J, derived from the measurements on the 4−0 band.[2] Also included in the figure is the highly accurate value, at $J(J+1)=0$, derived from the microwave determination of the 0−1 line.[7] Our points, since they extend to higher J values, permit a more reliable determination of the slope of the lines which yield the constants D. The points of highest $J(J+1)$ are derived from emission lines in the P branch which fall close to atomic standards. The corresponding R-branch lines require a longer interpolation, and may be in error by ±0.1 cm^{-1}, but at $J=40$ this introduces very little uncertainty in the determination of the constants. A further check on the constants is the position of the band head, which should also be measurable to ±0.1 cm^{-1}. Any slight uncertainty in the constants D cannot affect the calculated position of the lines of low J. These are given in Table III. The average deviation from the twenty-three accurately observed lines is 0.09A, or 0.016 cm^{-1}, the greatest deviation being 0.29A. It may be noted that our values are about 0.07 cm^{-1} lower than those calculated by Rao. It is believed that the calculated wavelengths listed in Table III should provide good wavelength standards in the region 23,000–24,300A.

Using the lines of the 2−0 band as standards, together with atomic comparison lines when they occur, it is now possible to obtain measurements of the other emission lines of CO, with an accuracy of ±0.05 cm^{-1}, except where blended. Values, averaged from a number of measurements of both oxy-acetylene and CO-oxygen flames, are listed in Table IV. They are compared with values calculated from equations of the form (1) for each band. The constants used are listed in Table V. Combination differences for the various vibrational states are included in Fig. 6. The observed lines in Table IV that are italicized are those obtained directly from the atomic standards, and are presumably the most accurate. No "observed" values are given for a number of 2−0 lines that appear since the calculated values were used in establishing the wavelength scale.

The lines of the CO isotopes were measured on a

[7] Gilliam, Johnson, and Gordy, Phys. Rev. **78**, 140 (1950).

TABLE III. A list of the observed and calculated wavelengths in air and calculated wave numbers in vacuum for the 2−0 CO absorption band.

Line	ν_{vac}(calc)	λ_{air}(calc)	λ_{air}(obs)
R 33	4348.14 cm^{-1}	22992.07A	
32	4346.76	22999.39	
31	4345.30	23007.09	
30	4343.77	23015.20	
29	4342.16	23023.71	
28	4340.48	23032.62	
27	4338.73	23041.93	
26	4336.90	23051.63	23051.53A
25	4335.00	23061.74	23061.64
24	4333.03	23072.25	23072.34
23	4330.98	23083.17	23083.05
22	4328.85	23094.50	23094.51
21	4326.66	23106.21	23106.04
20	4324.39	23118.34	23118.38
19	4322.05	23130.89	23130.90
18	4319.63	23143.80	23143.86
17	4317.14	23157.14	23157.16
16	4314.59	23170.87	
15	4311.95	23185.03	
14	4309.24	23199.60	
13	4306.47	23214.56	
12	4303.62	23229.93	
11	4300.69	23245.72	
10	4297.70	23261.92	
9	4294.63	23278.52	
8	4291.50	23295.54	
7	4288.29	23312.93	
6	4285.01	23330.75	
5	4281.66	23349.02	
4	4278.23	23367.76	
3	4274.74	23386.85	
2	4271.18	23406.37	
1	4267.54	23426.30	
0	4263.84	23446.65	
P 1	4256.22	23488.43	
2	4252.30	23510.25	
3	4248.32	23532.31	
4	4244.26	23554.79	23554.90
5	4240.14	23577.70	23577.68
6	4235.95	23601.04	
7	4231.68	23624.81	
8	4227.35	23649.01	
9	4222.95	23673.67	
10	4218.48	23698.75	
11	4213.94	23724.27	
12	4209.33	23750.23	
13	4204.66	23776.65	
14	4199.92	23803.51	
15	4195.10	23830.81	23830.64
16	4190.23	23858.55	23858.40
17	4185.28	23886.76	23886.82
18	4180.26	23915.41	23915.38
19	4175.18	23944.54	23944.69
20	4170.03	23974.10	23973.88
21	4164.81	24004.13	24003.84
22	4159.53	24034.63	24034.66
23	4154.18	24065.59	24065.55
24	4148.76	24097.03	
25	4143.27	24128.94	
26	4137.72	24161.30	24161.20
27	4132.10	24194.15	24194.17
28	4126.42	24227.47	
29	4120.67	24261.29	
30	4114.85	24295.54	
31	4108.97	24330.36	
32	4103.02	24365.62	

number of tracings similar to Fig. 2, using the $C^{12}O^{16}$ lines as standards. In the region beyond 4130 cm^{-1}, where $C^{12}O^{16}$ lines become too weak to measure, the pairs of Kr and A lines furnished standards, by which the $C^{13}O^{16}$ *P* 13 and *P* 14 lines could be measured with the highest accuracy. The results are given in Table VI, which lists the observed wave number and the wave number difference from the corresponding line in $C^{12}O^{16}$.

The 3−0 band, as shown in Fig. 3, is relatively weak. Second-order Kr lines served as standards to locate a few lines in each branch with an accuracy of ±0.05 cm^{-1}; the known Δ_2F'' values, as obtained from the constants of the 2−0 band, fixed the remainder of the dispersion curve. The results are given in Table VII.

DISCUSSION

The band constants given in Table V are in essential agreement with earlier accurate data. The sum of ν_0 for the 2−0 and 4−2 bands, 8414.44 cm^{-1}, may be compared with ν_0 for 4−0, 8414.46 cm^{-1}, and with the sum of the first four vibrational intervals for the Cameron bands, 8414.40 cm^{-1}. If we fit our data for the 2−0, 3−1, 4−2, and 5−3 origins to the vibrational formula,

$$G_{vib}=\omega_e(v+\tfrac{1}{2})-x_e\omega_e(v+\tfrac{1}{2})^2+y_e\omega_e(v+\tfrac{1}{2})^3, \qquad (2)$$

we obtain the constants and results listed in Table VIII. The fit with our results is excellent. Agreement with the 1−0 difference obtained from the Cameron bands is less good, but may be within the error of the measurements. The constants we obtain differ from those of Rao principally in $\omega_e y_e$, which is very sensitive to small changes in the data; it may be noted that our constants give good agreement with the levels up to $v=20$ determined (with less accuracy) from observations of the fourth positive system.[8]

The rotational constants we obtain are also in good agreement with the other accurate results, as may be seen from the plots of Δ_2F in Fig. 6. Our value of D_e, 5.95×10^{-6} cm^{-1}, is probably accurate to ±3 percent; it agrees within this limit with the theoretically calculated value, $4B_e^3/\omega_e^2=6.12\times10^{-6}$ cm^{-1}. Even at the high *J* values observed, the determination of *D* would not be affected by the sixth-power rotational constant, whose theoretical value is $H_e=5.8\cdot10^{-12}$ cm^{-1}. There is no observable regular trend in *D* with vibrational state; we have therefore arbitrarily taken $\beta=0$; the theoretically calculated value is -1.8×10^{-9} cm^{-1}. The recommended value of B_0, 1.92253 cm^{-1}, which fits our data well, is based on the microwave value, using our *D*, and $c=2.99790\cdot10^{10}$ cm/sec. The B_v values have been smoothed to fit an equation of the form $B_v=B_e-\alpha(v+\frac{1}{2})+\gamma(v+\frac{1}{2})^2$, with $B_e=1.93130$ cm^{-1}, $\alpha=0.017543$ cm^{-1}, and $\gamma=4.5\times10^{-6}$ cm^{-1}.

It may be noted that although the changes in the constants y_e, *D*, α, β, and γ that we propose are relatively minor, so far as any effect on the lines of $J\lesssim20$ is concerned, they are needed to account for the observed position of the band heads. A comparison of the heads, as calculated from our constants and from those of Rao[4] is given in Table IX.

[8] D. N. Read, Phys. Rev. 46, 571 (1934).

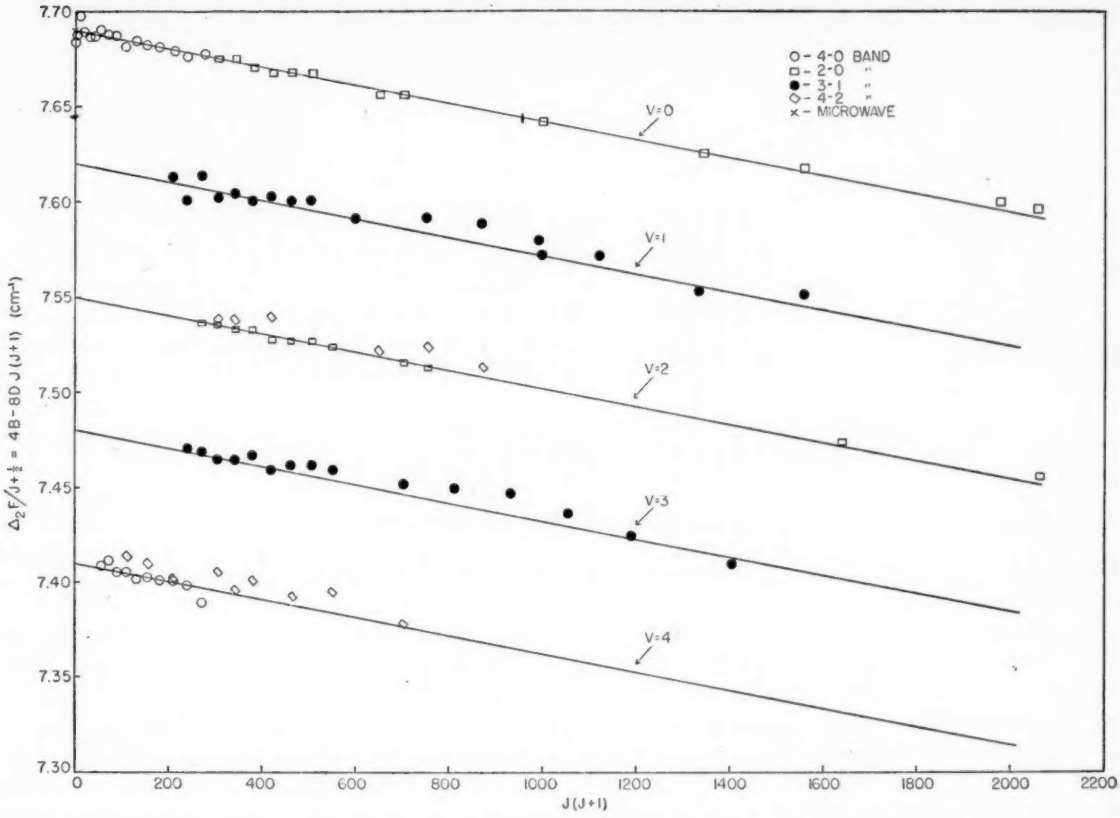

FIG. 6. Determination of the rotational constants of CO from combination differences, for the states $v=0$, 1, 2, 3, and 4.

The observed isotopic shifts are compared in Table VI with values calculated from our molecular constants and the accepted values of the nuclear masses,[9] $C^{12}=12.00382$, $C^{13}=13.00751$, $O^{16}=16$, and $O^{18}=18.0049$. The constants for the isotopic molecules were obtained by multiplying the corresponding constants for $C^{12}O^{16}$ by the ratio of the reduced masses, taken to the appropriate power. The agreement with observation is quite good. There appears to be a consistent discrepancy in the $C^{13}O-C^{12}O$ shift; the average difference (obs–calc) for 26 lines is $+0.03\pm0.02$ cm^{-1}. If our results are used to obtain the $C^{13}-C^{12}$ mass difference, they yield 1.00404 ± 0.0002 amu compared with the mass spectroscopic value, 1.00369 ± 0.00002. Although our results appear to be among the more precise determinations of mass differences by spectroscopic methods, they are not comparable in accuracy with nuclear or mass-spectroscopic methods. It may be of interest to point out that they are nearly as accurate, however, as the microwave determination. Gilliam, Johnson, and Gordy found a frequency shift of 5069.5 ±0.5 mc between the $J=0-1$ lines in $C^{12}O$ and $C^{13}O$; using our values for the constants D and α, this corresponds to a mass difference of 1.00343 ± 0.0001 amu. Our measurements of the $CO^{16}-CO^{18}$ isotope shift are less accurate, since the lines are weaker; the agreement with the calculated positions is fortuitously nearly perfect, the average deviation of the 8 lines that are not overlapped being -0.02 ± 0.03 cm^{-1}.

The good general agreement of our frequency measurements with other accurate data, and the internal consistency of our results, lends support to our belief that the use of comparison standards in higher orders has resulted in an accuracy of ±0.02 cm^{-1} for the lines listed in Table III.

INTENSITIES AND TEMPERATURE DETERMINATIONS

The intensities of the CO absorption lines in the 2−0 band are in good agreement with a recent determination. Penner and Weber[10] have determined, from low resolution studies of the pressure-broadened band, a value of the integrated absorption coefficient, namely 1.64 cm^{-2} atmos^{-1}. They have also computed from this datum the integrated absorption coefficients of the individual lines. In our experiments with the gas at 1 atmos pressure, the spectral slit width of 0.15 cm^{-1} appears to be of the same order as the line width. The integrated absorption coefficient of a weak line, such as P 26, which shows a peak absorption of 15 percent, would then be about 0.055 cm^{-1}. According to Penner and Weber's tables, for a path of 105 cm atmos, the value should be

[9] Hornyak, Lauritsen, Morrison, and Fowler, Revs. Modern Phys. **22**, 291 (1950).

[10] S. S. Penner and D. Weber, J. Chem. Phys. **19**, 807, 817 (1951).

TABLE IV. Observed and calculated frequencies of CO lines from emission measurements.

Band	2−0				3−1				4−2				5−3			
	R(J)		P(J)		R(J)		P(J)		R(J)		P(J)		R(J)		P(J)	
J″	ν_{obs}	ν_{calc}	ν_{obs}	ν_{calc}	ν_{obs}	ν_{calc}	ν_{obs}	ν_{calc}	ν_{obs}	ν_{calc}	ν_{obs}	ν_{calc}	ν_{obs}	ν_{calc}	ν_{obs}	ν_{calc}
0	a	4263.84	...	...	...	...	...	...	...	...	...	...	...	...	...	...
1	a	4267.54	a	4256.22	...	...	...	...	...	...	...	...	...	...	...	...
2	a	4271.18	a	4252.30	...	...	...	...	...	...	...	...	...	...	...	...
3	a	4274.74	a	4248.32	...	...	...	...	...	...	...	...	...	...	...	...
4	a	4278.23	*4244.24*	4244.26	4225.08	4225.17	...	...	...	...	...	...	...	...	...	...
5	a	4281.66	*4240.14*	4240.14	4228.55	4228.56	4187.39	4188.42	...	...	...	...	...	...	...	...
6	a	4285.01	a	4235.95	(4231.75)	4231.87	4183.20	4183.27	...	...	...	...	...	...	...	...
7	a	4288.29	a	4231.68	4235.04	4235.11	4179.09	4179.04	4182.05	4182.05	...	...	...	...	...	...
8	a	4291.50	a	4227.35	4238.29	4238.29	(4174.68)	4174.71	(4185.28)	4185.20	4122.27	4122.18	...	...	...	...
9	a	4294.63	a	4222.95	4241.43	4241.39	(4170.03)	4170.39	4188.27	4188.25	(4117.89)	4117.89	...	...	...	...
10	a	4297.70	a	4218.48	4244.44	4244.42	4165.90	4165.94	4191.34	4191.25	4113.50	4113.50	...	...	...	...
11	a	4300.69	a	4213.94	4247.32	4247.39	4161.53	4161.44	4194.13	4194.18	(4108.97)	4109.03	...	...	...	...
12	a	4303.62	a	4209.32	4250.38	4250.28	4156.91	4156.85	4197.03	4197.04	4104.41	4104.48	4143.95	4143.95	(4052.04)	4052.28
13	4306.47	4306.47	a	4204.66	4253.13	4253.09	4152.13	4152.22	(4199.92)	4199.82	4099.83	4099.89	4146.69	4146.69	...	4047.71
14	4309.27	4309.24	a	4199.92	4255.84	4255.83	4147.45	4147.52	4202.53	4202.52	4095.21	4095.22	4149.38	4149.35	...	4043.07
15	4312.02	4311.95	*4195.13*	4195.10	4258.53	4258.51	4142.74	4142.74	(4204.9)	4205.17	(4090.6)	4090.48	(4151.8)	4151.94	...	4038.36
16	*4314.59*	4314.59	*4190.25*	4190.23	4261.05	4261.11	(4137.72)	4137.90	4207.79	4207.74	(4085.76)	4085.68	(4154.18)	4154.48	...	4033.58
17	*4317.15*	4317.15	*4185.26*	4185.28	4263.60	4263.63	(*4132.90*)	4132.98	4210.28	4210.23	4080.69	4080.80	(4156.91)	4156.94	...	4028.74
18	*4319.63*	4319.63	*4180.27*	4180.26	4266.10	4266.09	4128.01	4128.01	4212.59	4212.65	*4075.87*	4075.87	(4159.53)	4159.32	4023.82	4023.84
19	*4322.04*	4322.05	*4175.15*	4175.18	4268.51	4268.47	4122.91	4122.96	4215.03	4215.00	*4070.72*	4070.83	(4161.53)	4161.63	...	...
20	*4324.38*	4324.39	*4170.06*	4170.03	4270.80	4270.77	*4117.89*	4117.84	4217.30	4217.26	(4065.71)	4065.76	4163.86	4163.88	...	...
21	*4326.69*	4326.66	*4164.86*	4164.81	4273.07	4273.01	4112.65	4112.66	4219.45	4219.46	4060.47	4060.61	(4165.90)	4166.05	...	...
22	*4328.84*	4328.86	*4159.52*	4159.53	4275.27	4275.16	4107.39	4107.41	4221.60	4221.58	(4055.04)	4055.41	4168.00	4168.13	...	...
23	*4330.98*	4330.98	4154.18	4154.18	4277.33	4277.26	4102.05	4102.10	4223.61	4223.65	4049.85	4050.16	(4170.03)	4170.16	...	...
24	*4333.00*	4333.03	4148.76	4148.78	4279.34	4279.27	(4096.80)	4096.72	4225.65	4225.63	(4044.85)	4044.80	4171.99	4172.10	...	...
25	*4334.99*	4335.00	4143.25	4143.27	(4281.37)	4281.21	(4091.06)	4091.26	(4227.35)	4227.54	(4039.24)	4039.37	4173.88	4173.99	...	...
26	*4336.90*	4336.90	4137.74	4137.72	4283.21	4283.09	4085.76	4085.75	4229.37	4229.38	4033.86	4033.89	(4175.4)	4175.70	...	...
27	4338.69	4338.73	*4132.09*	4132.10	(4285.10)	4284.89	(4080.15)	4080.16	4231.11	4231.15	(4028.22)	4028.34	4177.64	4177.53	...	...
28	4340.43	4340.49	4126.34	4126.42	4286.74	4286.59	4074.43	4074.52	4232.78	4232.81	*4022.63*	4022.73	(4179.09)	4179.16	...	...
29	4342.17	4342.17	4120.75	4120.67	(4288.29)	4288.23	4068.75	4068.80	4234.32	4234.41	(4016.9)	4017.04	(4181.08)	4180.73	...	...
30	4343.76	4343.77	4114.87	4141.85	4290.00	4289.81	4062.87	4063.03	(4235.95)	4235.95	4011.14	4011.30	(4182.12)	4182.23	...	...
31	4345.28	4345.30	4109.05	4108.97	(4291.50)	4291.31	4057.00	4057.18	4237.49	4237.41	(4005.6)	4005.49	4183.82	4183.65	...	...
32	4346.69	4346.76	4102.16	4103.02	4292.91	4292.73	4051.22	4051.27	4238.85	4238.81	3999.6	3999.61	(4185.28)	4184.97	...	...
33	4348.08	4348.14	(4096.82)	4097.01	4294.23	4294.08	4045.19	4045.29	(4240.14)	4240.13	3993.8	3994.0	4186.35	4186.32	...	...
34	4349.40	4349.44	4091.06	4090.95	4295.39	4295.35	4039.24	4039.24	4241.35	4241.36	...	...	4187.49	4187.51	...	...
35	4350.67	4350.67	4084.88	4084.79	4296.56	4296.55	(4033.36)	4033.14	4242.44	4242.51	...	...	(4188.27)	4188.64	...	...
36	4351.86	4351.83	4078.53	4078.58	(4297.70)	4297.57	(4026.95)	4036.97	*4243.58*	4243.59	...	...	4189.70	4189.68	...	...
37	4352.92	4352.91	*4072.35*	4072.30	4298.72	4298.72	4020.86	4020.73	(4244.54)	4244.60	...	...	4190.71	4190.65	...	...
38	4353.93	4353.91	(4065.71)	4065.96	4299.70	4299.68	(4014.7)	4014.42	4245.61	4245.55	...	...	4191.57	4191.57	...	...
39	4354.86	4354.84	4059.56	4059.56	(4300.69)	4300.58	4008.10	4008.05	4246.38	4246.41	...	...	4192.45	4192.39	...	...
40	4355.75	4355.70	4053.11	4053.09	4301.36	4301.39	4000.41	4001.62	(4247.26)	4247.19	...	...	...	...	...	...
41	4356.54	4356.47	4046.51	4046.56	4302.14	4302.12	3994.8	3995.12	4248.00	4247.89	...	...	...	...	...	...
42	4357.28	4353.17	(4040.18)	4039.96	...	...	...	...	4248.61	4248.54	...	...	...	...	...	...
43	4357.90	4357.80	4033.30	4033.30	...	...	...	...	4249.16	4249.10	...	...	...	...	...	...
44	4358.42	4358.34	(4026.72)	4026.58	...	...	...	...	...	...	...	...	...	...	...	...
45	4358.99	4358.82	4019.72	4019.79	...	...	...	...	...	...	...	...	...	...	...	...
46		4359.21	4012.80	4012.93	...	...	...	...	...	...	...	...	...	...	...	...
50–52	4360.01	*4360.02*	...	...	4305.20	4305.39	...	...	4250.80	4250.86	...	...	4196.54	4196.49	...	...

NOTE a: Line observed (in absorption or emission). Wavelength not reported since calculated value was used to establish the wavelength scale. See text.

TABLE V. Molecular constants of CO emission-absorption bands.

Band	ν_0	$B'+B''$	$B'-B''$	$2(D'+D'')$	$D'-D''$
2−0	4260.063	3.81000	−0.035060	2.38×10^{-5}	0
3−1	4207.17	3.77495	−0.035042	2.38	0
4−2	4154.38	3.73992	−0.035024	2.38	0
5−3	4101.73	3.70491	−0.035006	2.38	0
3−0	6350.47	3.79249	−0.052576	2.38	0

$0.00061\times105=0.064$ cm^{-1}. The agreement is as close as can be expected from our semi-quantitative measurements. It should also be pointed out that the relative intensity of the isotopic absorption lines of low J and the $C^{12}O^{16}$ lines of high J are in good agreement with Penner's tables, given the natural isotopic abundance ratio 1:92. Since the spectral slit width used in measuring the 3−0 band was nearly the same as that for the 2−0 band, we may also compare the maximum absorption of the weak lines in 3−0 (about 10 percent in the R branch) with those of 2−0 to obtain a value of the relative intensities of the two bands. The result is $3-0/2-0=0.0057\pm10$ percent, which gives an integrated absorption coefficient for 3−0 of $1.64\times0.0057=(9.3\pm1)\times10^{-3}$ cm^{-2} atmos^{-1}.

The relative intensity of the emission lines may be used to test whether the various upper-state energy levels are in thermodynamic equilibrium, and to determine the "temperature" corresponding to the modulus of Boltzmann's distribution of states in various modes. For the rotational modes the transition probabilities are proportional to $(J'+J''+1)$. For the closely-spaced lines of the R branches the instrumental sensitivity and the factor ν^4 are nearly constant within each band; hence if we plot the height of each unblended line, from $J=13$ to 34, as $\ln I/(2J+1)$, *vs* the energy E' of the upper state, we should obtain straight lines of slope $1/kT$ if there is thermal equilibrium. This has been done in Fig. 7 for the spectrum of the CO−O_2 flame previously illustrated (Fig. 5). This has also been done for a number of other spectra. The accuracy of measurement, limited by flame stability, resolving power, etc., is about ±5 percent. In Fig. 7 it is seen that each of the vibrational states $v=2$, 3, and 4 are sensibly in rotational equilibrium with about the same "temperature" of 2800°K. Similar straight lines for the rotational distribution have been obtained from other flames studied, with temperatures ranging from as low as 1900°K for the outer fringes of the outer cone of CO−O_2 flames to as high as 3600°K for the inner cone of the C_2H_2−O_2 flame.

A "vibrational temperature" may also be obtained from the relative intensity of the heads or of corresponding resolved lines in the various bands. This requires a knowledge of the relative vibrational transition probabilities. These have been calculated[11–13] but with slightly discordant results, depending on the

TABLE VII. 3−0 absorption band of CO.

J''	$R(J)$ ν_{obs}	$R(J)$ ν_{calc}	$P(J)$ ν_{obs}	$P(J)$ ν_{calc}
0	...	6354.21 cm^{-1}	...	...
1	6357.84 cm^{-1}	57.85	...	6346.62 cm^{-1}
2	61.43	61.37	6342.62 cm^{-1}	42.67
3	64.80	64.80	38.64	38.62
4	68.12	68.13	34.47	34.46
5	71.41	71.32	30.23	30.20
6	74.44	74.43	25.75	25.83
7	77.44	77.43	21.26	21.35
8	80.40	80.32	16.70	16.78
9	83.10	83.11	11.98	12.10
10	85.73	85.79	07.17	07.31
11	88.31	88.37	302.37	02.42
12	90.83	90.83	297.55	97.43
13	93.20	93.19	92.44	92.34
14	95.42	95.45	87.25	87.14
15	97.51	97.59	81.92	81.83
16	399.54	99.63	...	...
17	401.39	01.56	...	...
18	403.24	03.38	...	...

TABLE VI. Isotopic lines in the 2−0 absorption band of CO.

	$C^{13}O^{16}$						$C^{12}O^{18}$					
	$R(J)$			$P(J)$			$R(J)$			$P(J)$		
J''	ν_{obs}	$\Delta\nu_{obs}$	$\Delta\nu_{calc}$	ν_{obs}	$\Delta\nu_{obs}$	$\Delta\nu_{calc}$	ν_{obs}	$\Delta\nu_{obs}$	$\Delta\nu_{calc}$	ν_{obs}	$\Delta\nu_{obs}$	$\Delta\nu_{calc}$
1	4173.93	93.61	93.56	4163.02?	93.20	93.07	...	...	...	...	...	...
2	77.38	93.80	93.71	...	...	92.89	...	...	...	...	...	...
3	...	...	93.86	*55.57*	92.75	92.72	4172.92	101.82	101.73	...	...	...
4	84.16	94.07	94.01	*51.67*	*92.59*	92.53	76.43	101.80	101.88	...	...	...
5	87.48	94.18	94.15	47.76	92.38	92.34	...	...	102.04	...	...	...
6	...	...	94.29	43.77	92.18	92.18	(82.84)	102.17	102.18	...	...	...
7	93.88	94.41	94.42	39.67	92.01	91.96	...	...	102.33	...	...	...
8	196.96	94.54	94.55	35.55	91.80	91.75	...	...	102.46	...	...	...
9	...	...	94.67	31.34	91.61	91.55	91.93	102.57	102.60	4123.77	99.18	99.21
10	202.90	94.80	94.79	27.12	91.36	91.34	...	...	102.73	19.54	98.94	98.99
11	05.70	94.99	94.90	22.82	91.12	91.12	97.87	102.82	102.85	15.19	98.75	98.76
12	(08.63)	94.99	95.01	18.44	90.89	90.91	...	...	...	10.86	98.47	98.52
13	11.31	95.16	95.11	*13.99*	90.67	90.68	...	...	...	06.37	98.29	98.28
14	...	...	95.23	*09.50*	90.42	90.46	...	...	...	...	...	...
15	16.66	95.29	95.32	(04.81)	90.29	90.22	...	...	...	...	...	...
16	...	...	95.41	4100.11	90.12	89.98	...	...	...	...	...	...
17	21.61	95.53	95.48	...	...	...	...	...	...	...	...	...

NOTE a: Line observed (in absorption or emission). Wavelength not reported since calculated value was used to establish the wavelength scale. See text.

[11] B. L. Crawford, Jr., and H. L. Dinsmore, J. Chem. Phys. **18**, 983 (1950).
[12] K. Scholz, Z. Physik **78**, 751 (1932).
[13] R. C. Herman (private communication).

TABLE VIII. Vibrational constants and levels for $C^{12}O^{16}$.

$\omega_e = 2169.81\ cm^{-1}$, $\omega_e x_e = 13.284\ cm^{-1}$, $\omega_e y_e = 0.010\ cm^{-1}$

	$G_v - G_0$ calc	$G_v - G_0$ obs		ν_0, overtone bands calc	ν_0, overtone bands obs
		2143.38[a]			
$v=1$	2143.27	2143.16[b]	3−1	4207.17	4207.17[c]
2	4260.07	4260.06[c]	4−2	4154.38	4154.38[c]
3	6350.44	6350.47[c]	5−3	4101.74	4101.73[c]
4	8414.44	8414.46[d]	...	...	...
5	10452.18	...	...	...	...

[a] Reference 3; [b] Reference 1; [c] This work; [d] Reference 2.

TABLE IX. Band heads in the CO emission spectrum.

Band	ν_{obs}, cm^{-1}	ν_{calc}, PBS	ν_{calc}, Rao
2−0	4360.01	4360.02	4359.46
3−1	4305.20	4305.29	4304.85
4−2	4250.80	4250.86	4250.09
5−3	4196.54	4196.49	4195.78

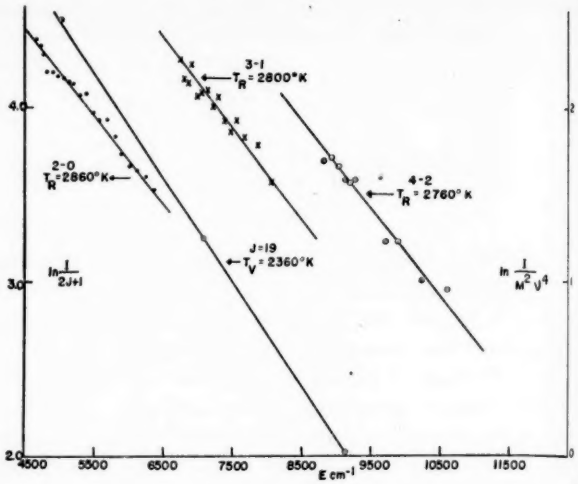

FIG. 7. Determination of "Vibrational Temperatures" T_v and "Rotational Temperatures" T_R for CO from the emission of the $CO-O_2$ flame (Fig. 5).

approximations made. In the simplest theory[11] in which both electrical and mechanical anharmonicities are introduced as perturbations on harmonic oscillator wave functions, the probability $|M|^2$ for a transition $v+n \rightarrow v$ is proportional to $(v+n)!/v!$. For the 2−0, 3−1, 4−2, and 5−3 transitions this gives intensity ratios 1:3:6:10. In the more detailed theories, using anharmonic oscillator wave functions, the probabilities deviate slightly from these integers; according to Herman,[13] the electrical anharmonicity portion is as above, whereas the mechanical-anharmonicity portion is as $1:3+28x:6+112x:10+280x$. Since for CO, $x=0.00612$, there is an uncertainty of some 10 percent in the transition probabilities. This is the same order as the experimental uncertainty in the determination of vibrational temperature, for fewer points are available to determine a slope, and the instrumental sensitivity may vary over the wider frequency range involved. In Fig. 7 we also present the results of a determination of vibrational temperature, plotting the logarithm of the intensity of the R 19 line of three bands, divided by the Herman transition probabilities $\times \nu^4$, against ϵ'. Again a fairly good straight line is obtained, but with a lower effective temperature, 2360°K, for the vibrational mode than the 2800°K that was found for rotation. This would indicate that complete thermal equilibrium has not been established. This finding is not unexpected since the observations were made in a region of the flame just above the reaction zone, where conditions definitely are not in equilibrium. In the outer cone of similar flames[5] the vibrational temperatures are nearly identical with the rotational temperatures. A more detailed discussion of the intensity distributions will be reported elsewhere.

The uncertainty in the vibrational transition probabilities does not affect the above conclusions. Somewhat better linearity of the plots was found when the x term was included, which might be taken to indicate that the mechanical anharmonicity term predominates in the expression for the first overtone intensity. It may be noted that in one of the alternative derivations of these constants,[10] the electrical anharmonicity, P_e', is nearly zero.

Since the absolute transition probabilities of the overtone bands have been determined, it is possible to calculate the expected emission intensity corresponding to thermal equilibrium at the indicated rotational or vibrational "temperatures." This leads to emissivities of the order of 0.01 for the strongest lines whereas the observed emissivity in the flames, which has not been determined quantitatively, appears to be of the same order. Further work is needed in this respect, to determine if deviations from thermal equilibrium exist between the upper and lower states involved, and if the emitted intensity may be used to determine the CO concentration and distribution in flames.

Electrical Conductivity of Silver Sulfide

MALCOLM H. HEBB
General Electric Research Laboratory, Schenectady, New York
(Received August 20, 1951)

Mixed electronic and ionic conduction in silver sulfide is examined. The importance of terminal conditions which may affect the ratio of ionic to electronic currents in experimental measurements is emphasized. In particular, either the electronic or ionic components can be completely suppressed. This is the basis of a new method of measuring the ionic and electronic conductivities independently, as functions of the chemical potential ζ of the silver component. The electronic conductivity is found to vary as $\exp B\zeta$ both above and below the transition at 177°C. However, the coefficient B changes abruptly from e/kT below the transition to $e/2kT$ above. This result can be understood theoretically in terms of the following picture: Excess silver is present mainly as dissolved atoms below the transition and as dissociated ions and electrons above. In the former case, only the electrons contribute to ζ, whereas in the latter there is a contribution both from the electrons and the ions.

INTRODUCTION

SOLID silver sulfide exhibits an electrical conductivity which is partly ionic and partly electronic. In the high temperature form (α), above 177°C, the conductivity is mainly electronic[1] and depends only slightly on temperature.[2] In the β-form below 177°C, the ionic conductivity may be a considerable fraction of the total[3] and here the conductivity varies rapidly with temperature.[4] In both forms, the conductivity is strongly dependent on composition,[2,4] being depressed by increasing sulfur content. It is the purpose of the present paper to separate the ionic and electronic conductivities and to examine particularly the dependence of the electronic conductivity on composition. The starting point for the theoretical treatment is the theory developed by Wagner[5] to account for the rate of reaction of silver and sulfur through a film or slab of solid silver sulfide.

THEORY OF MIXED CONDUCTION

We shall first give a rather simplified treatment of mixed conduction based on Wagner's theory. It is known from Hall measurements by Klaiber[6] that silver sulfide is n-type. In addition, measurements of transport numbers show that the ionic conduction is due to the motion of Ag^+ ions in both the α-phase[5] and β-phase.[3,7] The current densities due to the two carriers, electrons, and Ag^+ ions, can be written, respectively,

$$J_e = -\sigma_e \nabla\varphi$$
$$J_i = -\sigma_i \nabla(\varphi+\zeta) \qquad (1)$$

where σ_e and σ_i are the electronic and ionic conductivities. Since we wish to deal with variations in chemical composition, the electrical potential φ cannot be taken as the electrostatic potential, but is the electrochemical potential.[8] More specifically, φ is $-1/Ne$ times the partial molar free energy of electrons in the solid. Here N is Avogadro's number and e is the electronic charge. Similarly ζ is the chemical potential for neutral silver defined as $1/Ne$ times the partial free energy per gram atom for neutral silver in the solid. The sum $\varphi+\zeta$ is then the equilibrium chemical potential for silver ions.[9]

The chemical potential ζ is a function of the composition of the silver sulfide. The explicit relationship would not be easy to determine. However, the limits of ζ in the phase Ag_2S are readily established. The chemical potential ζ in the heterogeneous system, consisting of silver sulfide in equilibrium with metallic silver, will be higher by an amount $\Delta\zeta$ than it is when the silver sulfide is in equilibrium with solid or liquid sulfur. The difference $\Delta\zeta$ is $1/Ne$ times the free energy of formation per equivalent of silver sulfide from metallic silver and solid or liquid sulfur at the same temperature. In Table I are given free energies of formation[10] and calculated $\Delta\zeta$ for several temperatures.

When the composition is uniform, the chemical potential ζ in Eq. (1) is constant, and it is meaningful to speak of the total conductivity $\sigma=\sigma_e+\sigma_i$. The best

TABLE I. Isothermal free energy of formation of Ag_2S from Ag and S and corresponding difference in chemical potential for silver as function of temperature.

T	ΔF	$\Delta\zeta$
300°K	−8660 cal/mole	0.188 volt
350	−9040	0.196
400 (β)	−9420	0.204
450 (β, α)	−9680	0.210
500 (α)	−10,140	0.220
550	−10,550	0.229
600	−10,950	0.238

[1] C. Wagner, Z. physik. Chem. **B21**, 42 (1933); **B23**, 469 (1933).
[2] C. Tubandt and H. Reinhold, Z. Elektrochem. **37**, 589 (1931).
[3] C. Tubandt and H. Reinhold, Z. anorg. u. allgem. Chem. **160**, 222 (1927).
[4] H. Reinhold and H. Möhring, Z. physik. Chem. **B28**, 178 (1935).
[5] C. Wagner, Z. physik. Chem. **B21**, 25 (1933).
[6] F. Klaiber, Ann. Physik (5), **3**, 229 (1929).
[7] Tubandt, Eggert, and Schibbe, Z. anorg. u. allgem. Chem. **117**, 1 (1921); C. Tubandt, Handb. exp. Phys. XII/1 (1932).
[8] For a careful discussion of the electrochemical and electrostatic potentials for electrons in solids, see C. Herring and M. H. Nichols, Revs. Modern Phys. **21**, 185 (1949).
[9] The generalization to include a mobile anion as well as cation and to allow valence other than unity is given by Wagner. (See reference 5.)
[10] K. K. Kelley, Bureau of Mines Bulletin 406 (1937).

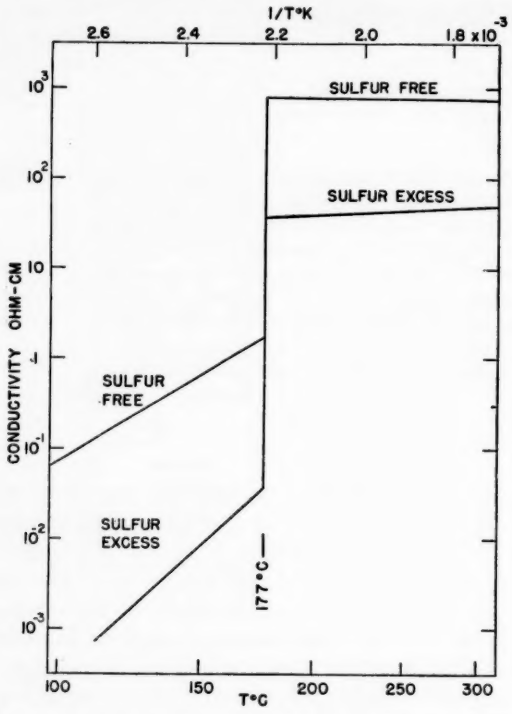

FIG. 1. Electrical conductivity of silver sulfide *versus* temperature. The upper curves marked *sulfur free* and the lower curves marked *sulfur excess* represent the upper and lower limiting conductivities corresponding to equilibrium with silver and sulfur, respectively. The temperature of 177°C represents the transition from the β-form (below) to the α-form (above).

way to avoid composition differences due to polarization is to use ac for the measurements. Published[2,4] data on conductivity of silver sulfide obtained in this way are shown in Fig. 1. In the high temperature α-form, the conductivity varies only slightly with temperature; in the low temperature β-form, the temperature variation corresponds to an apparent activation energy between 0.6 and 0.9 volt. There is a marked change in total conductivity with composition. Silver sulfide in equilibrium with silver (labeled *sulfur free*) is higher than silver sulfide in equilibrium with sulfur (labeled *sulfur excess*) by a factor between 10 and 100 in the temperature range shown.

We shall be concerned with the separation of conductivity σ into electronic and ionic parts σ_e and σ_i and of their variations with the chemical potential ζ.

IONIC CONDUCTIVITY

The ionic conductivity has not been determined nearly as accurately as the total conductivity. One method is to measure the diffusion coefficient D for the ions and to use the Einstein relation connecting D and σ_i to deduce the ionic conductivity. In this way Wagner,[11] using diffusion data from two different sources, finds 0.8 and 2.1 ohm cm for the conductivity due to the silver ions in silver sulfide at 200°C. The variation with temperature is small and corresponds to an activation energy of only 0.14 volt.[12] On the other hand, the dependence of D or σ_i on composition or on the chemical potential ζ is unknown. It is not even clear to what composition the ionic conductivities deduced by Wagner correspond. However, the structure of silver sulfide is quite open and in the α-modification particularly, there is considerable freedom in the disposition of the Ag^+ ions.[13] Consequently, it is not unreasonable to suppose that the ionic conductivity is almost independent of composition.[14] We shall outline below a method by which this dependence could be determined.

In β-silver sulfide, just below the transition temperature of 177°C, Tubandt and Reinhold,[3] using the method of transport numbers, have found that the fraction of the conductivity due to silver ions is $\nu_i=\sigma_i/\sigma=0.8$. It is known from the work of Wagner[1] that Tubandt's method of transport numbers gives erroneous results for α-silver sulfide, but it is believed that the result $\nu_i=0.8$ for the β-sulfide is reliable. It has been pointed out by Reinhold and Möhring[4] that by the nature of the experiment the result will always be the value of $\nu_i(S)$ corresponding to sulfur rich material. Assuming that the ionic component σ_i is independent of composition, we find for sulfur free material $\nu_i(\mathrm{Ag})=0.016$ since the total conductivity $\sigma(\mathrm{Ag})$ is some 50 times larger than $\sigma(S)$ at this temperature. There is some evidence[3] that ν_i is almost independent of temperature from 60°–177°C.

Since we assume σ_i independent of composition, we are attributing the rather large variation of σ with composition to the variation of σ_e alone. It will be shown below that the experimental composition dependence of σ_e deduced in this way can be explained theoretically.

TERMINAL CONDITIONS

When the terminal conditions are such that composition gradients are set up, it is not sufficient to know

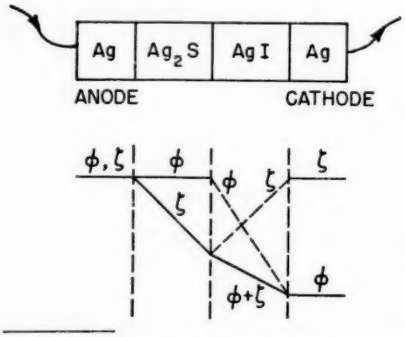

FIG. 2. Schematic arrangement for suppressing the electronic component of current in silver sulfide. The approximate distributions of electrical potential φ and chemical potential ζ are sketched below.

[11] C. Wagner, Z. physik. Chem. **B21**, 42 (1933). For experimental verification of the Einstein relation in pure ionic conductors, see W. Jost, *Diffusion und chemische Reaktion in festen Stoffen*, Steinkopff (1937); R. M. Barrer, *Diffusion in and through Solids* (Cambridge University, Press, London, 1941).

[12] C. Tubandt and H. Reinhold, Z. physik. Chem. Bodenstein Festband, 874 (1931).

[13] P. Rahlfs, Z. physik. Chem. **B31**, 157 (1935).

[14] C. Wagner, Z. physik. Chem. **B22**, 181 (1933), reaches this same conclusion for α-Ag_2S.

the total conductivity and one must use Eqs. (1) separately. Then the fractional currents carried by ions and electrons are no longer $\nu_i=\sigma_i/\sigma$ and $1-\nu_i=\sigma_e/\sigma$, and may have any value by choice of the ratio $\nabla\zeta/\nabla\varphi$ in Eqs. (1). Two special cases of interest are those for which either the electronic current J_e or the ionic current J_i is zero and the current is due entirely to the other type of carrier.

Terminal conditions which suppress the electronic component are shown schematically in Fig. 2. Tubandt used essentially this arrangement in his measurements of transport numbers, and it was the suppression of the electronic current, of which he was unaware, that led him to the erroneous conclusion that the conductivity in α-Ag_2S was mainly ionic. In Fig. 2, a slab of silver sulfide is in contact with a silver anode on one side and a slab of silver iodide backed by a silver cathode on the other. Tubandt's reason for inserting the silver iodide between silver sulfide and cathode was the experimental finding that this prevented the cathodic deposition of silver "trees" which otherwise tended to occur.*

The presence of the slab of silver iodide suppresses the electronic conductivity in the following way: The conductivity of silver iodide is ionic and caused by the motion of silver ions. Consequently, when a current is passed through the system of Fig. 2, silver ions must be withdrawn from the right side of the silver sulfide slab, leaving a deficiency of silver there. On the left side, the composition is maintained by the contact with silver. A gradient in composition or in chemical potential ζ is set up, and this causes silver ions to diffuse from the anode to the interface with the silver iodide. A steady state will be reached when the flow of silver ions by diffusion is equal to the rate at which they are withdrawn into the silver iodide. The current carried by the ions in the silver sulfide then equals the total current and the electronic current is zero. The transport of silver is in conformity with Faraday's law, as it would be for a pure ionic conductor.

Since $J_e=0$, we must take $\varphi=$ constant in Eq. (1) and

$$J=J_i=-\sigma_i\nabla\zeta,$$

where J is the total current. In the lower part of Fig. 2 are shown the distributions of φ and ζ through the two slabs. It is instructive to note that the presence of the sulfide slab causes an extra drop in φ in the iodide slab equal to the drop in ζ in the sulfide slab. This is the origin of the chemical energy which causes the current in the sulfide.

Suppose that contact is made by means of a probe at a point on the silver sulfide and its potential is measured with respect to the anode. If the probe is of platinum, it will exchange electrons, but not silver ions with the sulfide. It will then measure φ, and no potential difference with the anode will be found. Suppose, however, that the probe consists of a piece of silver iodide contacting the sulfide and backed by a piece of silver to which connection to the measuring circuit is made. It will then exchange silver ions but not electrons with the sulfide and will therefore measure $\zeta+\varphi$. Such measurements in combination with Eq. (2) would allow direct determination of σ_i as function of ζ in spite of the fact that σ_e might be several hundred times larger than σ_i. This method would be much more accurate and convenient than the measurement of the diffusion coefficient discussed above.

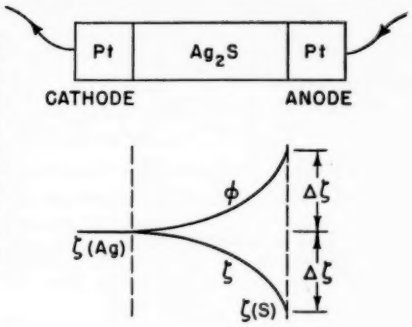

FIG. 3. Suppression of ionic current in silver sulfide. An initial transient ionic transport establishes a composition gradient through the sulfide and a layer of elemental sulfur at the anode. Potentials φ and ζ in the steady state are indicated below.

The suppression of the electronic conductivity in Fig. 2 will occur only so long as the difference in ζ across the slab of silver sulfide is less than $\Delta\zeta$ corresponding to the free energy of formation. Otherwise free sulfur can be formed at the junction between the sulfide and iodide slabs and then the electronic component need not be zero.[15]

The second terminal condition to be considered is shown in Fig. 3. In this case, the ionic component is suppressed and the current is purely electronic. A slab of silver sulfide is placed between two electrodes of inert material such as platinum or graphite. A potential applied between the two electrodes will produce a current that is partly ionic and partly electronic. As a result of the ionic fraction, the system becomes polarized. If the potential drop is small, the polarization consists of a concentration gradient through the slab. For larger potential drops, free silver and free sulfur will be formed at the cathode and anode, respectively. The polarization tends to suppress the ionic part of the current. First, the concentration gradient produces a diffusion force on the silver ions opposing the force due to the electric field. Second, the layer of sulfur deposited at the anode absorbs some of the potential drop and so reduces the drop across the slab itself. A steady state will be reached when the ionic current has been reduced to zero and the current at each point is purely electronic. If we suppose that the applied potential is greater than $\Delta\zeta$, then the potential drop through the sulfide will be $\Delta\zeta$ and the remainder will occur in the sulfur layer at the anode.

* Silver iodide is suitable for this purpose only in the α-form above 145°C. At still lower temperatures, one can use an aqueous electrolyte in a similar way. See reference 3.

[15] C. Wagner, Z. physik. Chem. **B23**, 469 (1933), discusses the breakdown of Faraday's law and gives the maximum ionic current which can be transported.

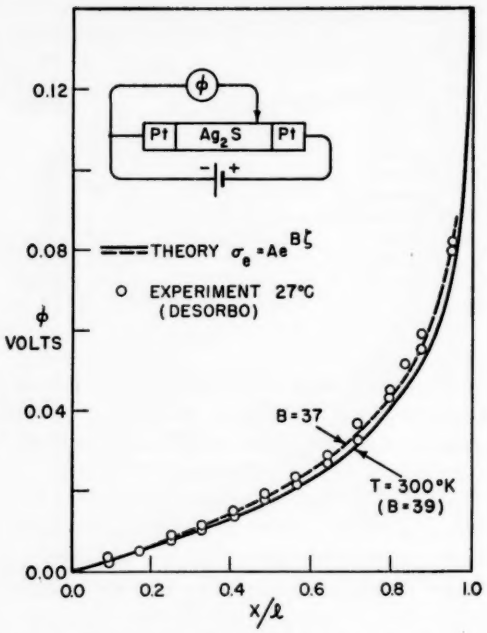

FIG. 4. Limiting potential distribution in slab of silver sulfide with suppression of ionic current. Circles are measured points. Theoretical distributions for two choices of the parameter B are given by the dashed and solid curves.

Writing the condition $J_i=0$ in Eq. (1) and integrating, we get $\zeta=-\varphi$ where the additive constant has been determined by requiring $\varphi=\zeta=0$ at the (silver) cathode. With this choice of origin, the value of ζ against the layer of sulfur at the anode is $-\Delta\zeta$ corresponding to the free energy of formation. The distributions of the electrical potential φ and the chemical potential ζ through the slab of silver sulfide are shown schematically in the lower part of Fig. 3.

Since the ionic transport has been suppressed, probe measurements of φ can now be used to find σ_e as function of $\zeta=-\varphi$. Figure 4 shows results obtained at $T=300°$K by DeSorbo[16] on a sample of β-silver sulfide 1.3 cm long with 1.5 volts applied between the electrodes. After allowing some 72 hours for a steady state to be reached, he found that the largest potential difference which could be measured between the cathode and the anode end of sulfide was only 0.1 volt. The remaining 1.4 volts drop was concentrated in a thin layer at the anode. According to our viewpoint, the actual drop in the sulfide is 0.2 volt, and the drop across the sulfur layer at the anode is the difference 1.5–0.2=1.3 volts.

Except for a constant numerical factor, the slope of the curve in Fig. 4 represents the reciprocal of electronic conductivity, $1/\sigma_e$. It is clear that σ_e decreases rapidly as $\zeta=-\varphi$ decreases from $\zeta=0$ at the silver cathode to $\zeta=-\Delta\zeta$ at the sulfur anode. We consider this dependence quantitatively in the next section.

[16] W. DeSorbo, personal communication. I am indebted to Dr. DeSorbo for permission to quote his results.

VARIATION OF CONDUCTIVITY WITH COMPOSITION

We have seen that the electronic conductivity σ_e is dependent on composition and shall now obtain a relation between σ_e and ζ for comparison with experiment. Consider an ideal stoichiometric crystal of Ag_2S containing N atoms of Ag and $N/2$ atoms of S. Let a number n_a+n of excess Ag atoms be dissolved in the crystal. We suppose that n_a of these atoms dissolve as neutral atoms and the remainder n as dissociated ions and electrons. It will be assumed that the conductivity σ_e is proportional to the number of electrons, *viz.*, n. The problem, therefore, reduces to finding the relation between the chemical potential ζ and n.

It will be convenient to use the fact that the chemical potential ζ for neutral Ag atoms is equal to the sum of the chemical potentials of the Ag^+ ions and of the electrons in the solid. The contribution to ζ by the electrons can be written[17]

$$(kT/e)\ln n+\text{terms independent of } n, \tag{2}$$

where k is Boltzmann's constant and T the Kelvin temperature. To find ζ, we must add the contribution of the n Ag^+ ions. If n is very much smaller than N, one may expect the extra ions to find places in the crystal substantially equivalent to those of the ions already there. In this case, the chemical potential of the ions will be practically independent of n and the only term dependent on n is already included in (2). Hence

$$\sigma_e\sim n\sim e^{e\zeta/kT}. \tag{3}$$

However, when n is not extremely small compared to N, the excess ions will have to occupy preferred positions.[17a] Then their contribution to ζ will also be of the form (2) and we get

$$\sigma_e\sim n\sim e^{e\zeta/2kT}. \tag{4}$$

Equations (3) and (4) are both equivalent to

$$\sigma_e=Ae^{B\zeta} \tag{5}$$

with B equal to e/kT and $e/2kT$, respectively.

TABLE II. Comparison of experimental exponent B with e/kT and $e/2kT$.

T	B	e/kT	$e/2kT$
400°K	31.7/volt	29.0/volt	···
450 (β)	25.3	25.8	···
450 (α)	14.5	···	12.9/volt
500	13.1	···	11.6
600	10.9	···	9.7

[17] See, for instance, N. F. Mott and R. W. Gurney, *Electronic Processes in Ionic Crystals* (Oxford University Press, London, 1950).

[17a] C. Wagner (private communication) has emphasized a difficulty with this argument as applied to α-Ag_2S when one attempts to sharpen it by interpreting the preferred positions as interstitial lattice sites. Then, on account of the disorder of the silver ions, the total number of interstitial ions may be appreciably greater than the number of added ions.

For comparison with the experimental results of Fig. 4, we substitute Eq. (5) into (1) and integrate, getting

$$\varphi=-(1/B)\ln[1-(x/l)(1-e^{-B\Delta\zeta})], \qquad (6)$$

where we have used the conditions:

$$J=J_e=\text{constant}$$
$$\varphi=-\zeta=0 \quad \text{at} \quad x=0$$
$$\varphi=-\zeta=+\Delta\zeta \quad \text{at} \quad x=l.$$

The broken curve in Fig. 4 is the plot of Eq. (6) for the value $B=37$/volt which gives the best fit with the experimental points. The agreement is excellent and provides good confirmation of the dependence (5). The parameter B is in satisfactory accord with the theoretical prediction of Eq. (3), *viz.*, $B=e/kT=39$/volt at $T=300°$K. The solid curve in Fig. 4 is drawn for this case.

Further information on the variation of σ_e with ζ and on the value of B is available from the conductivity data in Fig. 1. From Eq. (5) we can write

$$\sigma_e(\text{Ag})/\sigma_e(\text{S})=e^{B\Delta\zeta},$$

where $\sigma_e(\text{Ag})$, $\sigma_e(\text{S})$ are the electronic conductivities of silver sulfide in equilibrium with silver and sulfur respectively, and $\Delta\zeta$ corresponds to the free energy of formation. Knowledge of the ratio $\sigma_e(\text{Ag})/\sigma_e(\text{S})$ together with the data on $\Delta\zeta$ in Table I allows one to calculate B. The limiting conductivities shown in Fig. 1 are the total conductivities $\sigma(\text{Ag})$ and $\sigma(\text{S})$. Above the transition temperature, no appreciable error is made in identifying σ with σ_e. Below the transition, according to our earlier discussion, we can take $\sigma_e(\text{Ag})\simeq\sigma(\text{Ag})$ and $\sigma_e(\text{S})\simeq\sigma(\text{S})/5$. Table II presents values of B found in this way from data at several temperatures. For comparison with B, values of e/kT and $e/2kT$ are also tabulated. It will be seen that there is satisfactory agreement between B and e/kT for the β-silver sulfide. This is in conformity with our results at room temperature. However, at the transition temperature 177°C, there is an abrupt drop in B to about half its low temperature value and in the α-phase B is approximately $e/2kT$.

We interpret the behavior of α- and β-silver sulfide as follows: In the low temperature form (β), the dissolved silver atoms are mainly undissociated; n is small and σ conforms to Eq. (3). In the high temperature form (α), the dissolved silver atoms are dissociated into ions and electrons; n is larger and σ_e follows Eq. (4). The interpretation is supported qualitatively by the much larger conductivity in the α-form and by the different temperature dependence in the two forms.[18]

[18] H. Reinhold and K. Schmitt, Z. physik. Chem. **B44**, 75 (1939), have made careful measurements of the conductivity of α-Ag_2S as the pressure of sulfur vapor around the sample is changed. They correlate their experimental results with a theoretical dependence of the conductivity on a power of the sulfur pressure and find that the exponent is dependent on temperature. The simple power dependence breaks down when, as is the case with sulfur, the vapor consists of several molecular species. In addition, their determinations of vapor pressure are open to question, owing to pressure differences set up between sulfur reservoir and vessel containing the sample of silver sulfide. Our analysis based on use of the chemical potential is not open to these objections.

COMPOSITION OF SILVER SULFIDE

The next question to be examined is the atomic ratio of silver to sulfur in silver sulfide. Information bearing on this point is obtained from the electrical characteristics and from chemical data.

The simplest theoretical picture of semiconducting compounds requires correlation between three properties: (a) current carrier (electron, N-type or hole, P-type); (b) dependence of conductivity on pressure of electropositive or electronegative component; and (c) departure of composition from stoichiometry. The experimental agreement between (a) and (b) is good. Much less is known about (c), since departures from stoichiometry are usually too small to be determined with certainty. Silver sulfide is known by measurements of the Hall effect[6] to be N-type in both α- and β-forms. In conformity with this fact, the conductivity decreases with increasing sulfur pressure.[2,4] The best information on composition appears to be Kracek's[19] work on the phase diagram of the system silver-sulfur. He finds that the phase Ag_2S is predominantly sulfur-rich, although it may also extend to the silver-rich side at least at higher temperatures. This is in contradiction to the simple picture and results (a) and (b), which would require Ag_2S to be silver-rich throughout its range of composition.

It is possible to resolve this discrepancy by supposing that sulfur can enter the Ag_2S structure in an electrically inert form, say as dissolved sulfur molecules.[19a] The crystal is then composed of the following bodies: Ag atoms, Ag^+ ions, $S^=$ ions, S_2 molecules, e^- electrons. From the condition of electrical neutrality, the number of electrons in unit volume is

$$N(e^-)=N(\text{Ag}^+)-2N(\text{S}^=).$$

The number of potential holes which would result from converting the sulfur molecules and silver atoms to ions is

$$N(h)=4N(\text{S}_2)-N(\text{Ag}).$$

The excess of sulfur is measured by

$$X(\text{S})=N(h)-N(e^-).$$

Clearly, if $N(S_2)$ is made sufficiently large, we can have positive sulfur excess and a positive number of electrons as required by experiment.

There is no independent evidence for the existence of dissolved sulfur molecules in Ag_2S. However, it is known that excess iodine in potassium iodide occurs partly as I_2 molecules and partly as excess I^- ions. Good evidence for the I_2 molecules is obtained from

[19] F. C. Kracek, Trans. Am. Geophys. Union **27**, 374 (1946).

[19a] C. Wagner, Z. physik. Chem. **B22**, 181 (1933), has given a similar explanation.

optical absorption measurements, from the dependence of the amount of absorbed iodine on iodine pressure, and from the dependence of electrical conductivity on iodine excess.[20]

CONCLUSIONS

The thermodynamic treatment of mixed ionic and electronic conduction as given by Wagner has been considerably simplified without loss in accuracy. The important effect of terminal conditions on the ratio of ionic to electronic current has been demonstrated and used to separate the ionic and electronic conductivities. In particular, it has been emphasized that conduction in Tubandt's experiments on transport numbers in silver sulfide was the result of a gradient of chemical potential and not to an electric field. It has been concluded that the ionic conductivity in silver sulfide is not strongly dependent on composition in contrast to the electronic conductivity, which is shown to vary as $\exp B\zeta$, where ζ is the chemical potential for silver in the silver sulfide. The experimental fact that $B=e/kT$ and $B=e/2kT$ in the low and high temperature forms has been shown to be in accord theoretically with the semiconducting character of the low temperature form and the metallic nature of the high.

It is a pleasure to acknowledge indebtedness to F. E. Williams and L. Apker for discussions and suggestions on this subject.

[20] E. Mollwo, Ann. Physik (5) **29**, 394 (1937); R. W. Pohl, Proc. Phys. Soc. (London) **49**, (extra part) 3 (1937); J. H. DeBoer, *Electron Emission and Absorption Phenomena* (Cambridge University Press, London, 1935), p. 191.

THE JOURNAL OF CHEMICAL PHYSICS VOLUME 20, NUMBER 1 JANUARY, 1952

The Temperature Dependence of the Solubility of Solid Nonelectrolytes

J. H. HILDEBRAND
Department of Chemistry, University of California, Berkeley, California

(Received November 1, 1951)

The solubilities of nonelectrolytes in solutions from which chemical interactions are absent, when plotted as logarithm of mole fraction *vs* logarithm of absolute temperature, yield practically straight lines except near the melting point of the solute. This offers a superior method of smoothing out solubility data and of predicting the temperature coefficient of solubility from a single point by comparison with neighboring lines for other solvents.

An explanation is given for this behavior.

THE graphic representation of the solubility of nonelectrolytic solutions of solids by plotting the logarithm of the mole fraction of the solute, $\log x_2$, against the reciprocal of the absolute temperature has long served well[1] as a means of correlating and interpreting the experimental data. The regular family of curves obtained for the same solute in different solvents, when chemical effects are absent, was responsible for the recognition of that class of solutions known as "regular,"[2] and irregular slopes constitute evidence for the presence of a chemical, i.e., specific, intermolecular attraction. The only defect of this method of plotting is the increasing departure from linearity as solutions deviate more and more from Raoult's law. This defect can be avoided by substituting the logarithm for the reciprocal of the absolute temperature, as shown in Fig. 1[3] for violet and therefore, regular solutions of iodine. One observes that the lines for these solutions have regularly increasing slopes in going from better to poorer solvents and that they are quite straight except near the melting point in the case of solutions deviating considerably from Raoult's law. It is evident that this type of plot can serve admirably to smooth out experimental data and also to predict the temperature coefficient of solubility from a single point.

The linear relationship can be explained as follows. The top line represents the activity of solid iodine with respect to its supercooled liquid, and is therefore the solubility curve for an ideal solution of iodine, where a_2^s, the activity of solid iodine, equals its mole fraction in the saturated ideal solution, x_2^i. In what follows, the subscript 2 will be omitted, since the symbols refer solely to the solute, in this case iodine, I_2. We can express the relation between a^s and the heat of fusion, H^0-H^s, in the form $Rd\ln a^s/d\ln T=(H^0-H^s)/T$. The heat of fusion of a solid such as iodine increases as temperature increases, since the heat capacity of the liquid form is higher than that of the solid, therefore, $(H^0-H^s)/T$ changes but little with temperature. From the measurements of Frederick and Hildebrand,[4] H^0-H^s is approximately 3195 cal/mole at 25°C and 3353

[1] J. H. Hildebrand and C. A. Jenks, J. Am. Chem. Soc. **42**, 2180 (1920).

[2] J. H. Hildebrand, J. Am. Chem. Soc. **51**, 66 (1929).

[3] I first showed this type of plot on May 29, 1951, in Berlin, at the "Berliner Woche der Exakten Naturwissenschaften."

[4] K. J. Frederick and J. H. Hildebrand, J. Am. Chem. Soc. **60** 1436 (1938).

cal/mole at 50°C, but $(H^0-H^s)/T$ decreases only slightly, *viz.* 3 percent, in this interval.

Turning next to the nonideal but regular solutions, the partial molal free energy of iodine in a saturated solution, $\bar{F}$, and the molal free energy of its solid, F^s, are equal, or $\bar{F}-F^s=0$, therefore the entropy and enthalpy of solution are related by $\bar{S}-S^s=(\bar{H}-H^s)/T$. But

$$\bar{S}-S^s=-\left(\frac{\partial(\bar{F}-F^s)}{\partial T}\right)_x=\left(\frac{\partial(\bar{F}-F^s)}{\partial \ln x}\right)_T\left(\frac{\partial \ln x}{\partial T}\right)_{\bar{F}-F^s};$$

therefore,

$$\left(\frac{\partial(\bar{F}-F^s)}{\partial \ln x}\right)_T\left(\frac{\partial \ln x}{\partial T}\right)_{\bar{F}-F^s}=\frac{\bar{H}-H^s}{T}. \tag{1}$$

The free energy term, $\bar{F}-F^s$, may be split into $(\bar{F}-F^0)+(F^0-F^s)$, the sum of the free energies of fusion and dilution, whence

$$\left(\frac{\partial(\bar{F}-F^s)}{\partial \ln x}\right)_T=\left(\frac{\partial(\bar{F}-F^0)}{\partial \ln x}\right)_T,$$

but $\bar{F}-F^0=RT\ln a$, therefore,

$$\left(\frac{\partial(\bar{F}-F^0)}{\partial \ln x}\right)_T=RT\left(\frac{\partial \ln a}{\partial \ln x}\right)_T.$$

Substituting in Eq. (1), we have

$$\left(\frac{\partial \ln a}{\partial \ln x}\right)_T\left(\frac{\partial \ln x}{\partial \ln T}\right)_{\bar{F}-F^s}=\frac{\bar{H}-H^s}{RT}. \tag{2}$$

Now $(\partial \ln a/\partial \ln x)_T$ is only slightly less than 1 when x is small and Henry's law is closely approached, or even when x is larger if the solution is not far from ideal.[5] It approaches still closer to unity as temperature is increased. Finally we split the heat term for a saturated solution as we did the free energy term above and write

$$\left(\frac{\partial \ln x}{\partial \ln T}\right)_{\text{sat}}\cong\frac{\bar{H}-H^0}{RT}+\frac{H^0-H^s}{RT}. \tag{3}$$

We saw above that $(H^0-H^s)/RT$ decreases slightly in going from 25°C to 50°C. We may estimate the trend in $(\bar{H}-H^0)/T$ by aid of the equation, $\log(a/x)=(\bar{H}-H^0)/RT$ and the figures for iodine in carbon tetrachloride given by Negishi, Donally, and Hildebrand[6] which show this quotient increasing by about 7.5 percent in the same 25° temperature interval. The result is that the variations in the three terms affected by temperature are small and largely cancel so that the curves show long linear regions. This will, of course, not be the case for solutions in which chemical equilibria are present, nor will their curves have slopes fitting into the family of lines representing the physical solutions.

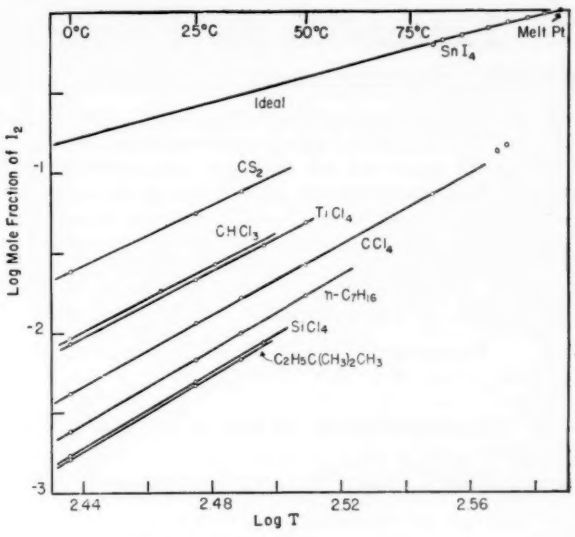

FIG. 1. The solubility of iodine.

The project of which this is a part is supported by the AEC.

[5] J. H. Hildebrand and R. L. Scott, *Solubility of Nonelectrolytes* (Reinhold Publishing Corporation, New York, 1950), Chapter III.

[6] Negishi, Donally, and Hildebrand, J. Am. Chem. Soc. **55**, 4793 (1933).

Letters to the Editor

THIS section will accept reports of new work, provided these are terse and contain few figures, and especially few half-tone cuts. The Editorial Board will not hold itself responsible for opinions expressed by the correspondents. Contributions to this section should not exceed 600 words in length and must reach the office of the Editor not later than the 15th of the second month preceding that of the issue in which the letter is to appear. No proof will be sent to the authors. A publication charge of $10.00 per Letter is made which, when honored, will entitle the Institution to 100 free reprints.

Relative Isotope Effects of C^{13} and C^{14}

WILLIAM H. STEVENS, JAMES M. PEPPER,* AND MACKENZIE LOUNSBURY
Research Chemistry Division, Atomic Energy Project, National Research Council of Canada, Chalk River, Ontario
(Received October 22, 1951)

ACCORDING to the theoretical treatment of the relative reaction velocities of isotopic molecules given by Bigeleisen,[1,2] the isotope effect resulting from substitution of C^{14} for C^{12} should be very nearly twice that resulting from substitution of C^{13} for C^{12}. The C^{14} isotope effects observed in the decarboxylation of malonic acid in two different laboratories[3,4] have been at variance, as have also been the theoretical treatments of this reaction.[5,6] Results obtained thus far in this laboratory, some of which have been published,[7–9] have indicated that the C^{14} isotope effect is larger than expected on the basis of the Bigeleisen treatment. The C^{13} effects have been studied by means of mass spectrometers where reproducibility of 0.1 percent is obtainable, whereas the C^{14} effects have been studied hitherto using counting techniques where reproducibility to 2 percent is possible only under the best of circumstances. The accuracy of the latter results is always open to some question. As yet no one has studied the C^{13} effect and the C^{14} effect in the same reaction. It seems important to make such a study. Furthermore, if sufficient C^{14} is used, both the C^{13} and C^{14} effects can be observed with a mass spectrometer, and any discrepancy caused by different analytical techniques eliminated.

Recently, Bigeleisen and Bothner-By[10] reported the C^{13} isotope effect observed in the decarboxylation of mesitoic acid in 86 percent sulfuric acid. We have prepared mesitoic acid, labelled with C^{14} in the carboxyl position to approximately 0.8 percent and have studied the isotope effects of both C^{13} and C^{14} in the decarboxylation reaction using a Nier-type 90°-deflection mass spectrometer similar to one previously described.[11] The technique used was substantially the same as that used by Bigeleisen and Bothner-By. The $C^{13}O_2/C^{12}O_2$ and $C^{14}O_2/C^{12}O_2$ ratios were measured at the same time on the same gas samples after equilibration with a water standard and were corrected for the oxygen isotopes to give the C^{13}/C^{12} and C^{14}/C^{12} ratios. The results obtained thus far are shown in Table I. The value found for the C^{13} isotope effect is very close to that obtained by Bigeleisen and Bothner-By. The C^{14} effect appears to be distinctly larger than twice the C^{13} effect. The only possible experimental error which could account for the enhanced C^{14} effect would be an impurity of mass 46 occurring in the gas obtained on complete decarboxylation and not occurring in the gas obtained from partial decarboxylation. However, scanning over a large mass range showed no peaks attributable to any impurity in the gas samples. Further experimental work on this reaction is being done. The C^{14} isotope effect will also be determined by counting techniques for comparison. A full account of this work will appear later.

TABLE I.

T°C	% Decarboxylation	C^{13}/C^{12} $\times 10^{4a}$	C^{14}/C^{12} $\times 10^{4a}$	$k12/k13^b$	$k12/k14^b$
99±0.5	>99	112.27±0.04	85.87±0.05		
99±0.5	>99	111.64±0.05	86.12±0.07		
Average		111.96	86.00		
60±0.5	13.7	108.33±0.05	78.16±0.08	1.037	1.108
60±0.5	17.5	107.97±0.06	79.23±0.07	1.039	1.094
Average				1.038±0.003	1.101±0.005
Bigeleisen and Bothner-By value				1.037±0.003	
Standard CO_2		112.54±0.04			

[a] Ratios corrected for oxygen isotopes after equilibration with standard water and relative to standard CO_2.
[b] $k12$, $k13$, and $k14$ are the reaction rate constants for the decarboxylation of the C^{12}, C^{13}, and C^{14} carboxyl mesitoic acids, respectively.

* Present address: University of Saskatchewan, Saskatoon, Saskatchewan.
[1] J. Bigeleisen, J. Chem. Phys. **17**, 675 (1949).
[2] J. Bigeleisen and T. L. Allen, J. Chem. Phys. **19**, 760 (1951).
[3] P. E. Yankwich and M. Calvin, J. Chem. Phys. **17**, 109 (1949).
[4] A. Roe and M. Hellmann, J. Chem. Phys. **19**, 660 (1951).
[5] J. Bigeleisen, J. Chem. Phys. **17**, 425 (1949).
[6] K. S. Pitzer, J. Chem. Phys. **17**, 1341 (1949).
[7] W. H. Stevens and R. W. Attree, Can. J. Research **B27**, 807 (1949).
[8] W. H. Stevens and R. W. Attree, J. Chem. Phys. **18**, 574 (1950).
[9] F. Brown and A. Holland (to be published).
[10] J. Bigeleisen and A. Bothner-By, J. Chem. Phys. **19**, 755 (1951).
[11] Graham, Harkness, and Thode, J. Sci. Instr. **25**, 119 (1947).

Microwave Spectrum and Structure of ReO^3Cl*

E. AMBLE,† S. L. MILLER, A. L. SCHAWLOW, AND C. H. TOWNES
Department of Physics, Columbia University, New York, New York
(Received October 22, 1951)

A NUMBER of microwave absorption lines caused by rhenium trioxychloride have been observed, some of which are listed in Table I. Ratios of the frequencies of these lines allow their identification as the rotational transitions $J=2\rightarrow3$, $4\rightarrow5$, $5\rightarrow6$, and $11\rightarrow12$. The nature of the spectrum shows that the molecule is a symmetric rotor.

TABLE I. Observed transitions and frequencies.

Transition	Molecule	Frequencies in mc/sec
$J=11\rightarrow12$	$Re^{187}O_3Cl^{35}$	50,246.1
	$Re^{185}O_3Cl^{35}$	50,261.4
	$Re^{187}O_3Cl^{37}$	48,584.6
	$Re^{185}O_3Cl^{37}$	48,600.5
$J=2\rightarrow3$		12,550
$J=4\rightarrow5$		20,950
$J=5\rightarrow6$	ReO_3Cl^{35}	25,120
$J=5\rightarrow6$	ReO_3Cl^{37}	24,290

Each rotational transition of ReO_3Cl is complicated by structure due to the two Re isotopes, excited vibrational states, and nuclear quadrupole effects. The presence of two Cl isotopes causes no difficulty because the separation between lines resulting from these two isotopes is large. However, since the Re atom is very near the center of mass, the isotopic shift between Re^{185} and Re^{187} is small and of the same order as the rotation-vibration splitting. Accurate measurements of the rotational constants B could most easily be obtained from the $J=11\rightarrow12$ transition because there the quadrupole hyperfine structure is relatively small and the isotopic displacement large. Doublets having the intensity ratios expected from the Re^{185}/Re^{187} isotopic abundance ratio were observed. Some other observed doublets were identified as resulting from excited vibrational effects from the dependence of their intensities on temperature.

The values of B and moments of inertia obtained from the $11\rightarrow12$ transitions are given in Table II. The molecule is a symmetric top with the axis along the Re–Cl bond, and all three structural parameters could be determined from the moments of inertia of three isotopic species. This gives 2.230±0.004A for the

TABLE II. Rotational constants B and moments of inertia for the isotopic species of ReO_3Cl.

Re	Cl	O	B in mc/sec	I in 10^{-40} g/cm^2
185	35	16	2094.23 ±0.02	241.268 ±0.002
187	35	16	2093.59 ±0.02	241.341 ±0.002
185	37	16	2025.02 ±0.02	249.514 ±0.002
187	37	16	2024.36 ±0.02	249.595 ±0.002

Re−Cl bond distance, 1.761±0.003A for the Re−O distance, and 108° 20′±1° for the Cl−Re−O angle. Errors given are thought to include both errors of measurement, and uncertainties caused by zero-point vibrations. These bond distances seem to be the first available for a rhenium compound.

In the 11→12 transition the rhenium quadrupole hyperfine structure was not resolved, but from the width of the line $|eqQ|$ was estimated as approximately 750 mc for both isotopes. From the partially resolved 4→5 and 5→6 transitions $|eqQ| \approx 800$ mc. The observed quadrupole structure is fortunately somewhat simplified for the 4→5 and 5→6 transition by the fact that the zero oxygen spin permits only states with $K=0$ and $K=3$. Of these only the $K=3$ has a large enough Stark effect to be observed with low modulation voltages. However, overlapping isotopic and excited vibrational state lines, in addition to the complication of hyperfine structure from both the Cl and Re nuclei, have so far prevented a complete solution of the hyperfine structure and a determination of the sign of the Re quadrupole coupling constant.

The bond structure of Re in this compound is probably complex, so that no unique interpretation of the observed quadrupole coupling constant can be made. However, the coupling constant caused by a valence electron can be obtained approximately from measurements on the Re atomic spectra as 3000 mc.[1] This indicates that some p character must be assigned to both the Re−Cl and Re−O bonds, since the effect of p character will then partially cancel and help reduce the quadrupole coupling constant to the observed value.

* Work supported by the AEC.
† Now of the University of Oslo.
[1] Schuler, Roig, and Korsching, Z. Physik **111**, 165 (1938).

The Electric Conductance of Liquid Iron Oxide

J. W. TOMLINSON AND H. INOUYE
Massachusetts Institute of Technology, Cambridge, Massachusetts
(Received October 18, 1951)

FISCHER and vom Ende[1] have recently published results for the electric conductance of liquid iron oxide in equilibrium with solid iron. The order of magnitude of their results is indicated by the figure 0.6 for the conductivity κ at 1390°C. Because the values of κ obtained are low in comparison with other results for iron oxides in the solid state,[2,3] and in view of the unique nature of the negative temperature coefficient of conductance, it was decided to repeat and extend these experiments.

Preliminary investigation indicated that the magnitude of the conductivity was of the order of 150 ohm^{-1} cm^{-1}. Therefore, a measuring circuit was used which was capable of measuring 10^{-3} ohm to an accuracy of 0.1 percent. The resistance was measured using the four terminal method, the current terminals being an iron rod 0.318 cm in diameter connected to the crucible and hollow central electrode 0.794 cm in diameter. Potential connections were made to the crucible edge and to the central electrode 2.5 cm above the surface of the melt by means of 0.318-cm diameter iron rods. All of the iron parts were fabricated from Armco iron. The resistance of the leads was measured by employing liquid silver as a melt, the resistance of which is of the order of 3×10^{-6} ohm[4] in the temperature range 1300–1500°C and may therefore be neglected. The cell constant was determined with tenth normal potassium chloride solution after platinum plating and platinizing the iron cell. A value of 0.128 cm^{-1} was obtained for a depth of immersion of 1 cm. This depth was used in all experiments, and the volume of the melt was kept constant at 14.9 cc. The temperature was measured by means of a calibrated platinum-platinum 10 percent rhodium alloy thermocouple located down the central electrode and protected by a porcelain sheath. Typical measured values of resistance are:

Cell containing liquid oxide	0.002047 ohm.
Cell containing liquid silver	0.001400 ohm.

Thus, the resistance resulting from the oxide is approximately one-third of the total amount measured, which is an adequately significant fraction. The justification for using a direct current method is that repeated reversal and interruption of the current did not change the resistance by a measurable amount.

The results of three independent runs on iron oxide made from C. P. iron powder and C. P. ferric oxide show a positive temperature coefficient of conductance. An average value of $\kappa=170$ ohm^{-1} cm^{-1} was obtained at 1390°C increasing to an average value of $\kappa=223$ ohm^{-1} cm^{-1} at 1490°C. It will be seen that the results of Fischer and vom Ende are in error and from a consideration of some preliminary experiments in which the current leads were included in the cell resistance, the present authors conclude that their results represent the conductance of the iron leads. A negative temperature coefficient of conductance is characteristic of solid iron in the range 200–1500°C.

The results appear to be typical of a semiconductor of the type exemplified by the solid, nonstoichiometric oxides of the transition metals.[2,5] However, further discussion will be postponed until a more detailed examination of the conduction mechanism, which is proposed, has been made. Two lines of investigation are in progress: (1) The investigation of the effect of additions of oxides of varying chemical type and valence, e.g., calcium oxide, chromium oxide, silica, etc; and (2) the investigation of the effect of changes in the oxygen to iron ratio in the melt.

[1] W. A. Fischer and H. vom Ende, Arch. Eisenhüttenw. **21**, 217 (1950).
[2] C. Wagner and E. Koch, Z. physik. Chem. **B32**, 439 (1936).
[3] E. Verwey, Nature, **144**, 327 (1939).
[4] E. F. Northrup, J. Franklin Inst. **178**, 85 (1914).
[5] N. F. Mott and R. W. Gurney, *Electronic Processes in Ionic Crystals* (Oxford University Press, London, 1948), second edition, p. 152.

Originative and Intensifier Activators in MgO Phosphors

RICHARD H. BUBE AND KENNETH F. STRIPP*
Radio Corporation of America, RCA Laboratories Division, Princeton, New Jersey
(Received October 31, 1951)

AS part of a systematic study of simple host crystal phosphor systems, magnesium oxide phosphors were prepared with each of forty-five elements (see Table I) in proportions of 0.016 and

TABLE I. Summary of impurities used.

Group I A	Li	Group VII A	Mn
Group II A	Be, Ca	Group VIII	Fe, Co, Ni, Ru, Pd, Pt
Group III A	Sc, Y, La, Ce, Pr, Nd, Sm, Eu, U	Group I B	Cu, Ag, Au
		Group II B	Zn, Cd
Group IV A	Ti, Zr	Group III B	B, Al, Ga, In, Tl
Group V A	V, Nb, Ta	Group IV B	Si, Ge, Sn, Pb
Group VI A	Cr, Mo, W	Group V B	P, As, Sb, Bi

0.60 mole percent. In most cases the impurity was introduced by slurrying finely divided $MgCO_3$ (Mallinckrodt "S.L. 5953") with a solution of the impurity (the nitrate wherever possible) and evaporating to dryness. Where this could not be done, e.g., for Si, a dry mix of $MgCO_3$ and the impurity oxide was used. Preparation heatings were carried out for 20 minutes at 1000° and 1200°C in air, and at 1000°C in hydrogen, the sample being held in a small

TABLE II. Emission colors associated with various activators in MgO.

Red	Cr, P
Orange or pink	Sm, Eu, Mn, Au
Green or blue-green	Ce, As, V
Violet	Pr, Nd
White	Y
Blue	Li, Be, Si, Sc, Ti, Zn, Ga, Ge, Zr, Nb, Ru, Ag, Cd, In, Sn, Sb, Ta, W, Tl, Pb, Bi, La

platinum boat. The samples were examined visually while excited by a spark discharge.

A faint blue luminescence emission is found for the MgO phosphor prepared without added impurity. Of the forty-five elements tested as possible activators, thirty-four give rise, under at least one of the preparation conditions, to an emission of greater intensity than that of the MgO phosphor without added impurity (see Table II); Fe, Co, Ni, and Cu act as poisons; and the remaining seven elements are ineffective as tested.

The thirty-four elements of Table II can be divided into two groups: (1) those elements giving rise to a blue luminescence emission, and (2) those elements giving rise to an emission other than blue. It is found that impurities giving rise to a blue emission are generally more efficient at the higher proportion, whereas impurities giving rise to emissions other than blue are equally or more efficient at the lower proportion.

These results may be interpreted as follows: (1) the blue emission of the MgO phosphor without added impurity is an intrinsic emission of the MgO host crystal; (2) the large number of impurities giving rise to a blue emission are intensifier activators;[1] (3) the smaller number of impurities giving rise to an emission other than blue are originative activators.[2] It is, of course, possible that some of the impurities giving rise to a blue emission may be originative activators associated with a blue emission not identical with that of the host crystal emission.

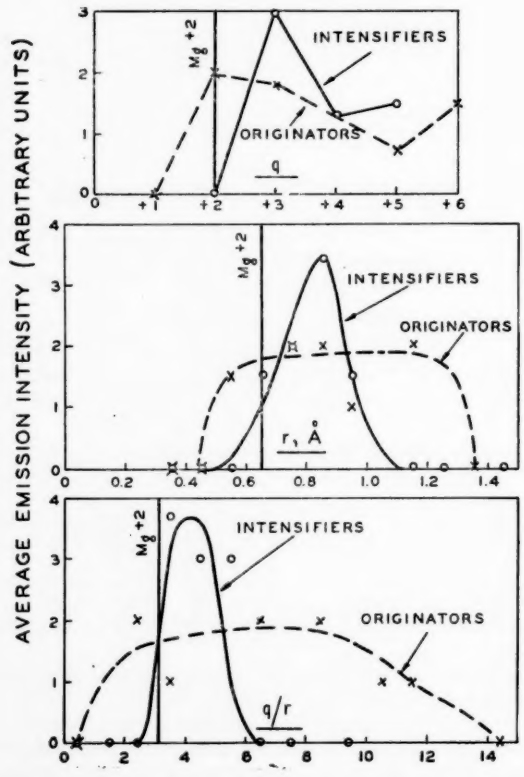

FIG. 1. The average emission intensity per impurity (visually determined in arbitrary units) as a function of the charge, q, the radius, r, and the polarizability, q/r, of the impurity.

A statistical analysis of the luminescence emission intensities associated with the incorporation of various impurities in MgO as a function of the charge, q, the ionic radius, r, and the polarizability, q/r, of the impurities,[3] shows a marked difference between those impurities classed as originative activators and those classed as intensifier activators in MgO.

It is found that impurity cations which act as efficient intensifier activators have values of r and q/r which lie within narrow limits, whereas impurity cations which act as efficient originative activators show no limitation to narrow ranges of r and q/r. A graphical presentation of the data[3] is given in Fig. 1, where the average emission intensity (visually determined in arbitrary units) per impurity is plotted as a function of the q, r, and q/r of the impurity.

These results support the concept that luminescence caused by an originative activator is associated with the activating impurity as perturbed by neighboring host crystal ions, whereas luminescence caused by an intensifier activator is associated with the host crystal ions as perturbed because of the presence of the activating impurity.

* Now at Sterling Chemical Laboratory, Yale University, New Haven, Connecticut.

[1] For definitions and other examples of intensifier and originative activators, see H. W. Leverenz, *An Introduction to Luminescence of Solids* (John Wiley and Sons, Inc., New York, 1950), pp. 239 and 240.

[2] Values of q, r, and q/r are chosen for the most probable valence state as determined by the chemistry of the impurity element.

[3] Data plotted is taken from results of preparation at 1200°C in air, for 0.60 mole percent impurity. Similar results are obtained for 0.016 mole percent impurity. Results obtained with preparation in hydrogen are not as simply analyzable, partly because of uncertainty of valence change of the impurity.

The Pyramidal B_5H_9 Structure

GEORGE H. DUFFEY
Department of Chemistry, South Dakota State College, Brookings, South Dakota
(Received October 29, 1951)

A PYRAMIDAL structure for B_5H_9 is supported by the work of Hedberg, Jones, and Schomaker[1] and Dulmage and Lipscomb.[2] The probable links in this structure are given in Fig. 1.

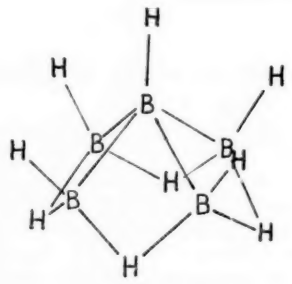

FIG. 1. Probable links in B_5H_9.

About a basal boron, orbitals having the over-all composition sp^3 and deviating somewhat from tetrahedral orbitals may be used.

About the apical boron atom, the symmetry is C_{4v}. Using the method of directed valence bonds, we may put five bond orbitals about this atom. These orbitals yield a reducible representation[3,4] which can be broken down as follows:

$$\sigma = 2A_1 + B_1 + E. \qquad (1)$$

The bond orbital used in forming the B−H bond yields the irreducible representation A_1; the other four bond orbitals yield A_1+B_1+E. The two lowest available orbitals yielding the irreducible representation A_1 are $2s$ and $2p_z$; the lowest orbital yielding the irreducible representation B_1 is $3d_{xy}$; the lowest orbitals yielding E are $2p_x$ and $2p_y$. Hence, the bond orbital directed toward the hydrogen atom may be a usual $s^n p^{1-n}$ hybrid orbital. However, an orbital directed toward a basal boron must contain $3d^4$, and the $3d$ levels lie high.

Following the molecular orbital method as used by Van Vleck,[3] we may resolve the difficulty. We fill with electron pairs only the molecular orbitals formed from $2s$, $2p_z$, $2p_x$, and $2p_y$. We might say we get effectively four bonds. One is the B—H bond. The other three bonds link the apical boron to the four basal borons.

This picture is upheld by the lack of charge on the molecule. If we assign one electron pair to each B—H bond, one electron pair to each B—H—B bond,[5] and three electron pairs to the four B—B links, we take care of all valence electrons from the five boron and nine hydrogen atoms.

[1] Hedberg, Jones, and Schomaker, J. Am. Chem. Soc. **73**, 3538 (1951).
[2] W. J. Dulmage and W. N. Lipscomb, J. Am. Chem. Soc. **73**, 3539 (1951).
[3] J. H. Van Vleck, J. Chem. Phys. **3**, 803 (1935).
[4] G. E. Kimball, J. Chem. Phys. **8**, 188 (1940).
[5] See G. H. Duffey, J. Chem. Phys. **19**, 963 (1951).

On the Scattering of H_2^+ by H_2

VERNON MYERS
The Pennsylvania State College, State College, Pennsylvania
(Received October 19, 1951)

SIMONS[1] and his students measured the scattering cross section for H_2^+ by H_2 and found it to be much larger than that expected for polarizability forces. This result does not seem to be surprising if a comparison is made with the He—He^+ interaction. There are two orbitals[2] for He—He^+, one symmetric in the nuclei and the other antisymmetric. The symmetric orbital corresponds to chemical binding. At large distances between the molecular centers, the orbitals for the H_2—H_2^+ system would be similar to those of the He—He^+ system. One might expect an appreciable attractive force at large distances for the orbital that is symmetric in the exchange of the protons from one molecule to the other. Of course, the scattering cross section is determined by an average over both orbitals, but an attractive potential for one of the orbitals could be the cause of the large scattering cross section.

[1] Simons, Fontana, Francis, and Unger, J. Chem. Phys. **11**, 312 (1943).
[2] L. Pauling, J. Chem. Phys. **1**, 56 (1933).

The Temperature Dependence of the Chlorine Quadrupole Coupling in Solid Benzene Compounds*

C. DEAN AND R. V. POUND
Harvard University, Cambridge, Massachusetts
(Received November 2, 1951)

THE resonant rf absorption resulting from transitions between levels of the nuclear electric quadrupole splitting in Cl^{35} has been investigated as a function of temperature in several solid benzene compounds. A frequency modulated superregenerative spectrometer was used, with the detected signal displayed on an oscilloscope. A persistent-screen C.R.O. tube was used as an aid to the observation of signals masked by noise. Samples were sealed in glass, inserted in the bare oscillator coil, and immersed in a bath of cooled petroleum ether, with the temperature measured by a thermocouple.

The data is presented on graphs (Fig. 1). The identification of these as Cl^{35} resonances was verified by observing the normally $5\frac{1}{2}$ times weaker Cl^{37} resonance except in the case of m-chloronitrobenzene, where the signal was apparently too weak. The observed resonance in the latter is presumed to be Cl^{35} in the absence of a companion resonance near 44.3 Mc. The ratio of the frequency of Cl^{35} to that of Cl^{37} was computed at a few points from 25° to −77°C for *p*-dichlorobenzene and for each line in the *o*-dichlorobenzene multiplets, using frequencies obtained by interpolation on large scale graphs. With chlorobenzene the melting point of the sample itself was used to provide a repeatable fixed temperature while obtaining the frequencies used in the ratio. The ratios agree within the experimental accuracy giving a value of 1.2688±0.0003,

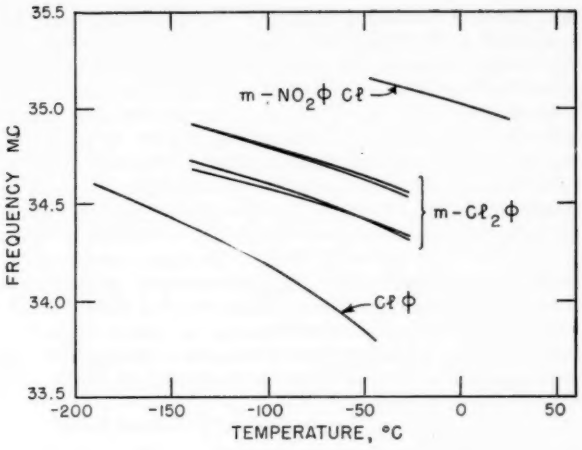

(a)

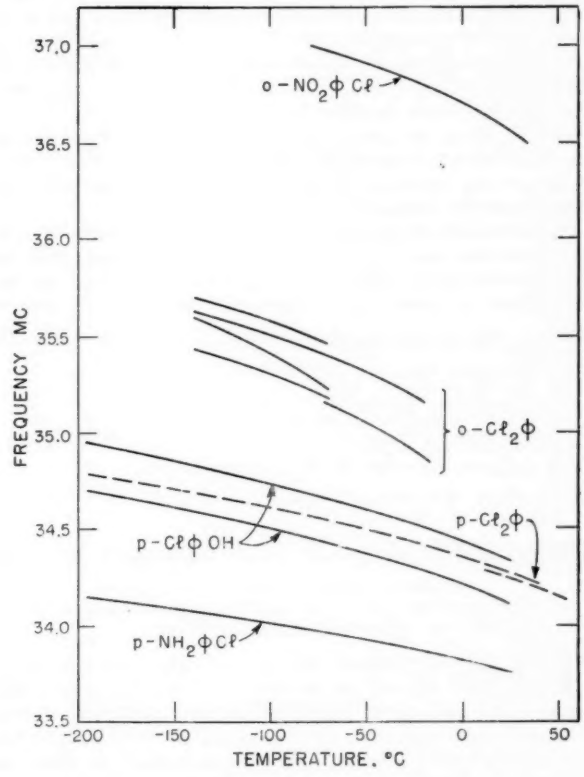

(b)

FIGS. 1(a) and 1(b). Graphs of the resonance frequency of Cl^{35} as a function of temperature in various benzene (ϕ) compounds. The experimental uncertainties of the points used for the graph were ±4 kc, and from ±1°C near room temperature to ±2°C below −100°C. In *p*-dichlorobenzene the occurrence of both phases over a range of 30°C is due to the extremely slow rate at which the transition progresses within this range, whereas the transition in o-Cl_2-ϕ takes place quickly in either direction at about −70°C.

which is to be compared with the value 1.26878±0.00015 found by Livingston[1] for several compounds at −197°C.

Since the gradient of the electric field at the Cl nucleus is predominantly caused by the Cl valence electrons, the variation of the resonance frequency among the different compounds can be interpreted in terms of a variation in the character of the Cl—C bond.[2] However, this bond character may be modified from that appropriate to the isolated molecule by the influence of intermolecular forces in the crystal,[3] and a change in crystal structure

could therefore produce a change in the bond character. The discontinuity in the *p*-dichlorobenzene curve accompanies a known phase change[4,5] and may be the result of this effect. The orientations of the Cl—C bonds in a single crystal can be determined from the Zeeman pattern of the Cl nuclear resonance, and a preliminary study with *p*-dichlorobenzene shows that the Cl—C bond directions are quite different in the two phases. A different explanation of the frequency discontinuity is that the amplitude of the thermal vibrations may be different in the two phases, which would produce a different average value of the gradient of the electric field at the nucleus in the two cases, even if the bond characters were identical. The discontinuity in *o*-dichlorobenzene probably indicates a phase change also. No reference to such a transition point has been found in the literature. Once the frequency-temperature curve is known, the sample itself is a sensitive thermometer, and this property is being used in experiments now in progress on the phase change in *p*-dichlorobenzene.

The temperature dependence of the frequencies is in qualitative agreement with the theory of Bayer,[6] in which the thermal motions of the molecules is assumed to reduce the average value of the gradient of the electric field at the nucleus. This effect makes it more difficult to evaluate fine distinctions in bond type such as are implied by the present data. It would seem that the extrapolation of each curve to absolute zero would yield a frequency truly representing the bond if this were the sole mechanism for temperature dependence. On the other hand, Townes and Dailey interpret Pound's data on the iodine resonance in I_2 as showing a gradual variation of bond character with temperature,[3,7] and such a variation may contribute to some extent to the temperature dependence of the resonance frequency in every sample.

Many thanks are due Mr. Harlan Meal of the Chemistry Department who sealed all of the samples in glass, suggested petroleum ether as a convenient nonpolar coolant, and assisted during the initial search for resonances in several of the samples.

* This work was partially supported by the joint program of the ONR and AEC.

[1] R. Livingston, Phys. Rev. **82**, 289 (1951).
[2] C. H. Townes and B. P. Dailey, J. Chem. Phys. **17**, 782 (1949).
[3] C. H. Townes and B. P. Dailey, private communication.
[4] B. D. Saksena, J. Chem. Phys. **18**, 1653 (1950).
[5] A. N. Campbell and L. A. Prodan, J. Am. Chem. Soc. **70**, 553 (1948).
[6] H. Bayer, Z. Physik **130**, 227 (1951).
[7] R. V. Pound, Phys. Rev. **82**, 343 (1951).

Dielectric Properties of Solid Hydrogen Bromide

NORMAN L. BROWN* AND ROBERT H. COLE
Metcalf Research Laboratory, Brown University, Providence, Rhode Island
(Received October 29, 1951)

THE dielectric behavior of solid hydrogen halides is of considerable interest as one aspect of the cooperative phenomena and solid phase transitions in these molecular crystals. The early work of Smyth and Hitchcock[1] on hydrogen bromide covered too narrow a range of frequencies to define the dispersion they observed below the lowest temperature phase transition at 89°K, and this prompted us to make a more extensive study over the frequency range 20 to 5×10^6 cycles/sec from 70°K to the melting point (186°K). While the work was in progress, Powles[2] reported a similar investigation. Although our results are qualitatively similar, we find significant quantitative differences.

The static dielectric constants found by us are larger than those previously reported, especially at temperatures below 100°K. The measured peak value for the transition at 89°K is about 200 and a value of 33.4 is found at 70°K, as shown in Fig. 1. In the measurements, special precautions were taken to minimize the effects of voids or cracks in the sample, as these can make the apparent values of dielectric constant much too small if the true ones are large.

As found by Powles, two dispersion regions exist at audio and radio frequencies below 89°K, both shifting rapidly with temperature. The lower frequency one is described by a circular arc locus[3] complex dielectric constant, as shown in Fig. 1 for several temperatures, and the temperature dependence of the relaxation time corresponding to the midpoint of the dispersion is expressed by a rate law with an activation energy of 2.7 kcal/mole. Although the higher frequency relaxation process is not as well defined by the data, it appears to be qualitatively similar with much smaller total dispersion.

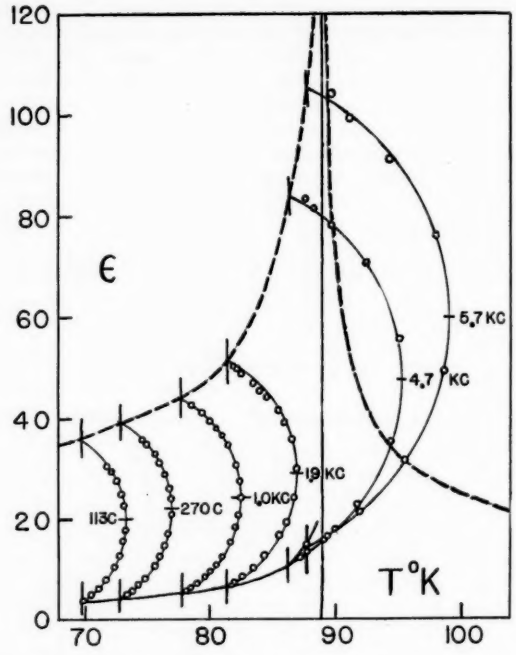

FIG. 1. Complex dielectric constant $\epsilon^*=\epsilon'-i\epsilon''$ of hydrogen bromide near the lowest temperature phase transition. The dashed line is the equilibrium dielectric constant. The complex plane loci are plotted with their real (ϵ') axes vertical at positions corresponding to the temperatures and the axes of imaginaries (ϵ'') horizontal to the same scale.

Very large dielectric constants near second-order transitions are a reasonable result of cooperative effects, as Tisza[4] has pointed out, but theories such as that of Kirkwood[5] predict much less drastic changes. In connection with this difference and with the existence of two dispersions, it seems to us important to take into account the marked anisotropy of the unit cell in the crystal lattice and of the molecular arrangement in the unit cell. In particular, the two dispersion regions are plausibly explained as arising from different principal dielectric constants parallel and normal to the *c*-axis of the nearly tetragonal structure. On the experimental side, measurements of the dispersion at temperatures below 70°K and extending to sub-audio frequencies are needed.

* Coffin Fellow, 1947–48; AEC Predoctoral Fellow, 1948–50.

[1] C. P. Smyth and C. S. Hitchcock, J. Am. Chem. Soc. **55**, 1830 (1933).
[2] J. G. Powles, Nature **165**, 686 (1950); Compt. rend. **230**, 836 (1950).
[3] K. S. Cole and R. H. Cole, J. Chem. Phys. **9**, 341 (1941).
[4] L. Tisza, Technical Report No. 127, Research Laboratory of Electronics, M. I. T. (1949).
[5] J. G. Kirkwood, J. Chem. Phys. **8**, 205 (1940).

Isotope Effect in the Cannizzaro Reaction of Carbon-14-Labeled Formaldehyde

A. M. DOWNES AND G. M. HARRIS
Tracer Elements Investigations, C.S.I.R.O., and Chemistry Department, University of Melbourne, Melbourne, Australia
(Received November 5, 1951)

ISOTOPE effect in irreversible decomposition reactions of carbon-14-labeled compounds has been detected by means of specific activity determinations of the reaction products in a number of recent investigations.[1,2] No quantitative demonstration of the effect has been reported as yet on the basis of changes in the specific activity of the residual reactant during the course of

TABLE I.

γ	S_γ/S_0	No. of samples	γ	S_γ/S_0	No. of samples	γ	S_γ/S_0	No. of samples
0.020	1.016	2	0.424	1.031	2	0.815	1.064	4
0.038	1.016	2	0.475	1.032	5	0.835	1.072	3
0.052	1.004	4	0.497	1.032	4	0.851	1.101	7
0.086	1.014	2	0.533	1.029	2	0.863	1.141	3
0.092	1.002	2	0.580	1.056	2	0.873	1.122	8
0.100	0.997	2	0.592	1.068	5	0.880	1.131	3
0.132	1.000	2	0.640	1.075	6	0.894	1.117	5
0.163	1.018	6	0.684	1.077	4	0.901	1.145	3
0.202	1.011	2	0.732	1.089	4	0.908	1.156	1
0.254	1.023	6	0.745	1.059	2	0.9180	1.145	4
0.373	1.028	8	0.791	1.052	1	0.930	1.159	8
						0.940	1.181	3

decomposition. The nature of this type of effect can be readily predicted. Let A^* and A represent labeled and unlabeled reactant compound, respectively. Suppose the reaction to be of order n with respect to this reactant, and of orders p, q, etc. with respect to any additional (unlabeled) reactants B, C, etc. If A^* is present in only trace concentration, the rate expressions for reactions involving A and A^*, respectively, will be:

$$-d[A]/dt=k[A]^n[B]^p[C]^q\cdots, \quad (1)$$

$$-d[A^*]/dt=k^*[A^*][A]^{n-1}[B]^p[C]^q\cdots. \quad (2)$$

Division of Eq. (2) by (1), and integration yields the expression:

$$S_\gamma=S_0(1-\gamma)^{\epsilon-1}. \quad (3)$$

In this, S_0 and S_γ are specific activities ($\alpha A^*/A$) of reactant initially and at fraction of total reaction γ, respectively, and $\epsilon=k^*/k$. Equation (3) is analogous to the law governing the enrichment of water in deuterium oxide during electrolysis[3] with the difference that "enrichment factor" in the present instance has a clearly defined meaning in terms of specific reaction rates.

Confirmation of the above considerations has been afforded by a radiochemical study of the Cannizzaro reaction:

$$2CH_2O+OH^-\rightarrow CH_3OH+HCO_2^-.$$

The reaction was carried out at 60.00±0.05°C, using aqueous reactant mixture initially 0.048 M in tracer-labeled formaldehyde,† and 0.520 M in sodium hydroxide. Predetermined volumes of reactant mixture, calculated to give conveniently sized samples of 2,4-dinitrophenylhydrazine or dimedone derivative of formaldehyde for radiochemical assay, were withdrawn at various stages of reaction. The progress of reaction was simultaneously followed by iodimetric titration of formaldehyde.[4] In the first type of precipitation, the reactant samples were mixed with excess hydrochloric acid, followed by addition of excess 2,4-dinitrophenylhydrazine hydrochloride reagent. The dimedone precipitations were carried out according to the procedure of Yoe and Reid.[5] The precipitates were filtered, purified by recrystallization from alcohol and washing with water, and transferred by slurry technique to standard aluminium pans for weighing and counting. Separate experiments showed that contamination of the precipitates with methyl alcohol or formate was negligible after one recrystallization and washing, and that no isotopic exchange occurred between formaldehyde and the reaction products.

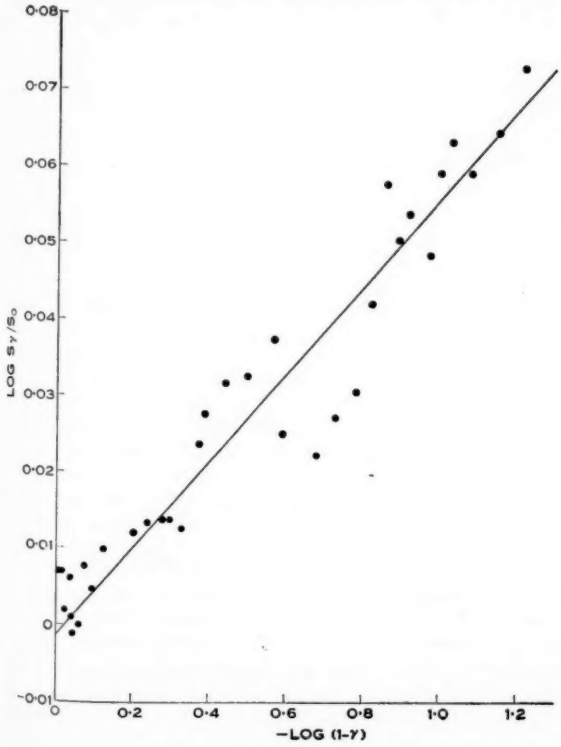

FIG. 1. Plot of $\log S_\gamma/S_0$ against $-\log(1-\gamma)$.

Counts were made using a thin mica end-window tube with constant geometry, corrections being applied for resolving time, counter sensitivity, and background. No self-absorption or back-scattering corrections were necessary, since the sample thicknesses of *ca* 1 mg/cm² varied by less than 0.2 mg/cm². It was shown that for both types of sample the errors introduced by thickness variations of this magnitude were less than 1 percent. Sufficient counts were taken to reduce the statistical probable error to less than 0.5 percent.

Several samples were prepared by each precipitation technique from the original labeled formaldehyde, reactant, and the mean specific activities of these (counts/mg/min) taken as S_0. Runs made by the two methods gave identical results within the limits of the unavoidable scatter introduced by the difficulty in obtaining reproducible sample mounting. By carrying out a good number of determinations at various values of γ, a result of reasonable statistical precision was obtainable. Table I summarizes the data, and the evaluation of ϵ is illustrated in Fig. 1. The line of best fit was determined by the method of least squares, weighting each point according to the number of samples taken at that value of γ, and it is seen to pass satisfactorily close to the origin. The slope is -0.0566, with a standard deviation of ±0.0012, whence $\epsilon=0.9434\pm0.0012$. The magnitude of this isotope effect, while smaller than that reported in some previous studies,[1] compares closely with others.[2] In any case, there is no reason to favor one value or another, since the net isotope effect in a given reaction is largely dependent on reaction mechanism, and can in fact be zero.[1,6] A full report of this work is being prepared for publication.

[1] W. H. Stevens and R. W. Attree, J. Chem. Phys. **18**, 574 (1950) and other work referred to therein.
[2] A. Roe and M. Hellmann, J. Chem. Phys. **19**, 660 (1951).
[3] A. Farkas, *Orthohydrogen, Parahydrogen and Heavy Hydrogen* (Cambridge University Press, London, 1935), p. 125.
† Formaldehyde-C¹⁴ was supplied by the A.E.C.
[4] J. F. Walker, *Formaldehyde* (Reinhold Publishing Corporation, New York, 1944), p. 259.
[5] J. H. Yoe and L. C. Reid, Ind. Eng. Chem., Anal. Ed. **13**, 238 (1941).
[6] D. R. Stranks and G. M. Harris, (to be published).

The Reaction of CH_3 and CD_3 Radicals with Hydrogen and Deuterium

T. G. MAJURY* AND E. W. R. STEACIE
Division of Chemistry, National Research Council, Ottawa, Canada
(Received October 26, 1951)

WE have investigated the reactions of light and heavy methyl radicals with hydrogen and deuterium, of the type

$$CH_3+H_2\rightarrow CH_4+H. \quad (1)$$

The photolysis of acetone (or deutero-acetone) has been used as the source of methyl radicals. By investigating the temperature coefficient of the ratio CH_4/C_2H_6[1], where ethane is formed by the reaction,

$$2CH_3\rightarrow C_2H_6, \quad (2)$$

TABLE I. Reaction of methyl radical with hydrogen isotopes.

Reaction	$P_1/P_2^{\frac{1}{2}}\times10^3$	$E_1-\frac{1}{2}E_2$ kcal
CH_3+H_2	0.7	9.2
CH_3+D_2	3.5	11.7
CD_3+H_2	2.5	10.2
CD_3+D_2	2.0	10.9

it is thus possible to arrive at the value of the activation energy difference $E_1-\frac{1}{2}E_2$. Since E_2 is almost certainly ≈0, this is equivalent to the direct evaluation of E_1. Similarly, a value is obtained for the ratio of the steric factors $P_1/P_2^{\frac{1}{2}}$, and since P_2 is now known with reasonable certainty, P_1 can be evaluated approximately. In this way the values in Table I have been obtained. The values of the activation energies in Table I are reliable to within about 0.3 to 0.4 kcal. The results indicate that the substitution of deuterium for hydrogen causes an increase in activation energy of the order of magnitude of the zero-point energy difference. The substitution of CD_3 for CH_3 makes relatively little difference.

In view of the compensating errors in E and P, somewhat more reliable conclusions regarding the isotope effect can be drawn from a consideration of velocity constant ratios, $k_1/k_2^{\frac{1}{2}}$ at a given temperature. Thus at 210°C, in the middle of the temperature range used, we have for these ratios

$$\left.\begin{aligned}\frac{CH_3+H_2}{CH_3+D_2}&=3.3\\ \frac{CD_3+H_2}{CD_3+D_2}&=3.5\end{aligned}\right\}\text{Average 3.4,}$$

$$\left.\begin{aligned}\frac{CH_3+H_2}{CD_3+H_2}&=0.71\\ \frac{CH_3+D_2}{CD_3+D_2}&=0.74\end{aligned}\right\}\text{Average 0.7.}$$

From the value of the activation energy of the reaction of CH_3 with H_2, and the bond dissociation energies $D(CH_3-H)$ and $D(H-H)$, the activation energy of the reverse reaction

$$H+CH_4\rightarrow CH_3+H_2$$

is calculated to be 7.0 ± 1.3 kcal. It seems impossible to stretch the limits of error sufficiently to reconcile this with the known slowness of the reaction of H-atoms with methane unless the steric factor for this reaction is of the order of 10^{-3} or less.

Full details, together with the results of experiments on the reaction of methyl radicals with HD will appear later.

* National Research Council Postdoctorate Fellow, 1950–51.

The Crystal Structure of Formic Acid*

F. HOLTZBERG, B. POST, AND I. FANKUCHEN
Polytechnic Institute of Brooklyn, Brooklyn 2, New York
(Received November 2, 1951)

OSCILLATION and precession diagrams of single crystals of formic acid have been obtained at −45°C using filtered Cu and Mo radiation. The low temperature x-ray camera and techniques used in investigation have been described elsewhere.[1]

The diagrams were indexed on the basis of an orthorhombic unit cell with $a_0=10.22$A, $b_0=3.62$A, and $c_0=5.34$A, all dimensions ±0.03A. The volume of the unit cell is 198A³. The assumption that there are four molecules per unit cell leads to an x-ray density of 1.54. This is in reasonable good agreement with the density computed by extrapolating from the known density of the liquid at room temperature (1.24) to that of the solid at −45°C.

Reflections of the following types were systematically absent: (*hol*) with *h* odd and (*okl*) with *k* plus *l* odd. The most probable space groups are therefore Pna and Pnam. The latter can be ruled out on steric grounds.

The arrangements of molecules in the unit cell consistent with space group Pna appear to preclude the possibility that the molecules are associated as dimers in the crystal. Preliminary calculations indicate that the molecules are arranged in the crystal in the form of infinite chains, each molecule being linked to two neighbors by hydrogen bonds. It is interesting to note that the results of a recent study of the dielectric polarization of solid formic acid have been interpreted as being incompatible with a structure having dimeric molecules as the only units.[2]

A detailed account of the complete structure determination will be published in the near future.

* This work supported by the ONR.
[1] Post, Schwartz, and Fankuchen, Rev. Sci. Instr. **22**, 218 (1951).
[2] J. F. Johnson and R. H. Cole, J. Am. Chem. Soc. **73**, 4536 (1951).

The Structure of Platinum Oxides

ERNESTO E. GALLONI AND RODOLFO H. BUSCH
Facultad de Ciencias Exactas, Físicas y Naturales, Buenos Aires, Argentina
(Received July 26, 1951)

RECENTLY, J. Waser and McClanahan[1] have given the structure of a platinum compound prepared by the method of Jörgensen.[2] They put forward the formula Pt_3O_4Na for this compound. We have studied the product obtained by Jörgensen's method since 1941, trying to check the formula Pt_3O_4 given by Galloni and Roffo[3] to an oxide found on a Pt wire. The two substances proved to be different. Our x-ray patterns of Jörgensen's oxide *are identical* with that reported by Waser and McClanahan. As a matter of fact, we have been unable to find a reasonable structure for this compound, the chemical composition of which has not been conclusively established.

In spite of the fact that the structural evidence favoring the formula Pt_3O_4Na is very satisfying, we think this formula is not possible because the compound *does not contain sodium*.

We have made a spectroscopic examination of the compound, using Hilger's spectrograph E 1, checking the spectrum obtained with that resulting from a solution containing 0.0025 mg percent sodium acetate. The persistent doublets 3302.3–3303 and 5889–5890 were selected for comparison. In the sodium acetate solution they appear very intense, but they are absent in the arc spectrum of the compound. Consequently, it is possible to state that Jörgensen's oxide does not contain appreciable amounts of sodium to fit the formula Pt_3O_4Na, which would require some 3 percent sodium.

In a footnote (p. 455), Waser and McClanahan express the opinion that the pattern reported by R. H. Busch[4] as being characteristic for PtO_2 may belong to PtO, basing their argument on a paper by Moore and Pauling.[5] They also state that the oxide studied by Galloni and Roffo[3] was not Pt_3O_4 but PtO_2. These two statements are, however, untenable, for the following reasons:

(1) *PtO_2 is a well-known substance*, extensively used in organic synthesis, easy to prepare, not very difficult to analyze, and impossible to confuse with any other oxide. The analysis of PtO_2 including determination of Pt, oxygen, and water gives results consistent with the formula PtO_2 within a few per thousands. The x-ray pattern of this substance, prepared by the method of Vorhees and Adams,[6] washing out the Pt with aqua regia and washing thoroughly with water and drying, belongs to an hexagonal structure, $c=4.19$A, $a=3.08$A, $c/a=1.36$ (Busch, Cairo, Galloni, and Raskovan).[7] We may add that this is a fact, not an opinion. The same pattern has been observed by Finch, Murison, Stuart, and Thomson[8] by means of electron diffraction. The white tetrahydrate of PtO_2, added into fused $NaNO_3$, gives the same pattern. The dioxide dihydrate obtained by anodic oxidation by Altmann and Busch,[9] heated for a long time at 350°C, gives the same pattern, as does the oxide obtained by the method of Pigeon.[10] If PtO_2 is prepared at low temperatures, it gives no pattern. The

properties and the x-ray pattern of PtO_2 are both dependent on the heat treatment.

(2) *The substance studied by Moore and Pauling[6] was probably not PtO.* They write: "PdO was prepared by the method of Shriner and Adams[11] involving fusing palladous chloride and potassium nitrate; and PtO by a similar method." . . . "The data are not sufficient to permit a rigorous structure determination to be made for PtO, but the similarity to the PdO photographs makes it highly probable that platinous oxide has the PdO structure . . . ."

The existence of PtO is questioned in Gmelin's handbook.[12] Wöhler and Frey[13] discuss the preparation of this compound and its easy oxidability. We think the method of Shriner and Adams[11] applied to H_2PtCl_4 (because $PtCl_2$ is insoluble) would give PtO_2, because of the oxidizing properties of fused KNO_3. Moore and Pauling have not analyzed the compound obtained, so it is difficult to find out what they have actually studied.

In conclusion, the structure given for PtO is not supported by sufficient experimental evidence. It is doubtful if the authors prepared PtO or not.

(3) *It is possible to prepare the hydrate of PtO by the method of Wöhler and Frey.*[13] The dehydration of this compound gives an oxide whose composition fits well the formula PtO. The x-ray pattern is platinum-like. The only difference is that the parameters of PtO are slightly enlarged with respect to Pt. Chemically, the oxide cannot be confused with platinum because it is insoluble in aqua regia, and its density is very much lower (lying between 11.5 and 14 g/cm^3). In the course of a great number of preparations of this substance, we have never found the lines reported by Moore and Pauling.

(4) *On some occasions, we have prepared the platinum oxide studied by Galloni and Roffo and have found the formula Pt_3O_4 together with the x-ray pattern reported by them.* It has been obtained by thermal decomposition of hydrated PtO_2, but it has not been possible to find a reproducible method of preparation, in spite of very numerous experiments. In two instances the right oxide has appeared, but the conditions upon which its preparation depend are not clear to us.

In conclusion, for the reasons given, we think that the compound studied by Waser and McClanahan is not Pt_3O_4Na, that the hexagonal pattern reported by Busch is caused by PtO_2, that the pattern reported by Galloni and Roffo is caused by Pt_3O_4, and finally, that the structure given to PtO by Moore and Pauling is open to discussion. Even the existence of anhydrous PtO is open to discussion.

We are indebted to Dr. J. Winkel for obtaining the spectrograms.

[1] J. Waser and E. McClanahan, J. Chem. Phys. **19**, 413 (1951).
[2] S. M. Jörgensen, J. prakt. Ch. **16**, 344 (1877).
[3] E. E. Galloni and A. E. Roffo, J. Chem. Phys. **9**, 875 (1941).
[4] R. H. Busch, Z. Naturforschung **5a**, 130 (1950).
[5] W. J. Moore and L. Pauling, J. Am. Chem. Soc. **63**, 1392 (1941).
[6] R. Vorhees and R. Adams, J. Am. Chem. Soc. **44**, 1397 (1922).
[7] Busch, Cairo, Galloni, and Raskovan, 14a. Reunión de la Asociación Física Argentina, La Plata (1949).
[8] Finch, Murison, Stuart, and Thomson, Proc. Roy. Soc. (London) **A 141**, 414 (1933).
[9] S. Altmann and R. H. Busch, Trans. Faraday Soc. **45**, 720 (1949).
[10] L. Pigeon, Ann. chim. et phys. (7), **2**, 480 (1894).
[11] Shriner and R. Adams, J. Am. Chem. Soc. **46**, 1684 (1924).
[12] Gmelin, *Handbuch der anorganischen Chemie*, eighth edition (1938), Vol. 68, part C.
[13] L. Wöhler and W. Frey, Z. Elektrochem. **15**, 133 (1909).

The Structure of $Na_xPt_3O_4$

JÜRG WASER AND EDWIN D. MCCLANAHAN, JR.
Department of Chemistry, The Rice Institute, Houston, Texas
(Received August 10, 1951)

IN the preceding note Galloni and Busch[1] report the results of a spectroscopic analysis of a platinum oxide similar to the compound recently investigated by us.[2] While their compound apparently did not contain significant amounts of sodium, we had assigned the formula $NaPt_3O_4$ to our preparation.

The presence of sodium in our compound was inferred from the following facts. An electron density projection showed the presence of a concentration of scattering matter of approximately the correct magnitude for one Na-atom per each four O-atoms. This peak could not have been caused by breaking-off errors since the Pt-contributions had been subtracted from the observed F's. Thus our projection contained neither Pt peaks nor the subsidiary features which ordinarily accompany large peaks and are caused by termination of the Fourier series. The analogous breaking-off features of the oxygen peaks are correspondingly smaller and have a negligible effect on the sodium peak. The inclusion of a scattering contribution from Na at the positions $2a$ of O_h^3 significantly improved the agreement between calculated and observed intensities. The presence of Na further explains the ionic conductivity observed by us and the sodium content Wöhler reported for his preparations.[3]

However, as indicated in our paper, the compound $NaPt_3O_4$ need not be of stoichiometric nature as far as sodium is concerned. The Na-atoms (or ions) are situated in holes formed by cubes of O-atoms, and the number of holes filled in various preparations may vary. The further possibility of filling the holes with other suitable cations exists.

Our findings may thus be reconciled with those of Galloni and Busch[1] by assuming the existence of a whole series of compounds of the formula $Na_xPt_3O_4$, $0 \leq x \leq 1$, all having the same framework of Pt and O-atoms described in our paper.[2] A more detailed investigation is, however, required to clear up completely this question of solubility of Na and possibly other cations in Pt_3O_4.

We have now had the opportunity to analyze for sodium our original very small sample of $Na_xPt_3O_4$ which had been used in the x-ray experiments. The sample was treated with strong HCl containing KI followed by boiling with aqua regia. Only a portion of the sample went into solution, the exact amount dissolved being unknown. Analysis with a Beckman flame spectrophotometer showed that the original sample contained 1.3 percent Na or more. As reported previously our preparation had been extracted several times with hot aqua regia to remove traces of Pt. The Na is therefore presumed to be part of the compound.

We wish to thank Dr. R. V. Talmage for the use of the flame spectrophotometer.

[1] E. E. Galloni and R. H. Busch, J. Chem. Phys. **19**, 198 (1951).
[2] J. Waser and E. D. McClanahan, Jr., J. Chem. Phys. **19**, 413 (1951).
[3] L. Wöhler, Z. anorg. u. allgem. Chem. **40**, 450 (1904).

Carrier-Free Radioisotopes from Cyclotron Targets. XXIV. Preparation and Isolation of $Ir^{188, 190, 192}$ from Osmium*

HERMAN R. HAYMOND, WARREN M. GARRISON, AND JOSEPH G. HAMILTON
Crocker Laboratory, Radiation Laboratory, Divisions of Medical Physics, Experimental Medicine and Radiology; University of California, Berkeley and San Francisco, California
(Received October 26, 1951)

BOMBARDMENT of osmium with 19-Mev deuterons produces, by $(d, 2n)$ and (d, n) reactions, several relatively long-lived, known, radioactive isotopes of iridium;[1,2] *viz.*, Ir^{187}, Ir^{188}, two isomers of Ir^{190}, and Ir^{192}. Radioisotopes of rhenium and osmium are also produced concurrently in relatively low yield by (n, p) and (d, p) reactions. This paper reports a method for isolation of iridium activities from irradiated osmium without the addition of stable iridium carrier.

The target was osmium metal powder (*ca.* 0.5g) in which no iridium (less than 0.01 percent) was detected by spectrographic analysis. The osmium powder was held on a grooved, water-cooled target plate by a 0.25-mil platinum foil during bombardment in the 60-inch Crocker Laboratory cyclotron.

After bombardment the osmium powder was dissolved, with heating, in a minimal amount of aqua regia. Excess nitric acid was added and the solution was heated to dryness to distill off the osmium tetraoxide. Two milliliters of nitric acid were added and

heated to dryness. Two milliliters of sulfuric acid were added and heated to fuming. Into the fuming sulfuric acid, 1 ml of HBr was added dropwise to remove radioactive rhenium. The sulfuric acid was heated to dryness. The remaining activity was taken up in 5 ml HCl and transferred to a 10-ml beaker. Twenty-five milligrams of NaCl were added and the solution was heated to dryness. The NaCl was dissolved in water to give a solution of isotonic saline suitable for biological use.

The decay periods of the isolated activity agreed with published data.[1,2] Decay half-lives of approximately 40 hours, 12.5 days, and 72 days could be resolved. No attempt was made to detect shorter periods. Identification was further verified by a chemical separation of iridium from an aliquot of the preparation using milligram amounts of rhenium, osmium, and iridium as carriers.

We wish to thank Professor G. T. Seaborg for reviewing the manuscript, Dr. T. Putnam, Mr. G. B. Rossi, and the crew of the 60-inch cyclotron for their help with the bombardments, and Miss Margaret Gee for technical assistance.

* This document is based on work performed under Contract W-7405-eng-48A for the AEC.

[1] Nuclear data, National Bureau of Standards Circular 499 (September, 1950).

[2] T. C. Chu, Phys. Rev. **79**, 582 (1950).

Erratum: Nuclear Magnetic Shielding in Fluorine and Hydrogen Compounds

[J. Chem. Phys. **19**, 1259 (1951)]

H. S. Gutowsky and C. J. Hoffman
Noyes Chemical Laboratory, University of Illinois, Urbana, Illinois

DESIGNATIONS of the F^{19} nuclear magnetic resonances in CF_3CO_2H and SF_6 are reversed in Fig. 2. Figure 2 is an oscilloscope picture of the F^{19} magnetic resonance lines in SF_6 and CF_3CO_2H, at the top and bottom, respectively, of the figure. The F^{19} resonance occurred in SF_6 at an applied field 0.81 gauss lower than in CF_3CO_2H which implies that the F^{19} nuclei are magnetically shielded 0.81 gauss more in CF_3CO_2H than in SF_6.

On the Calculation of Integral Diffusion Coefficients from Free Diffusion Experiments

Gerard Kraus
Applied Science Research Laboratory, University of Cincinnati, Cincinnati 21, Ohio

(Received October 29, 1951)

IN many instances specific diffusion rates are measured by determining concentration as a function of distance and time under conditions of free diffusion. Since the diffusion coefficient is usually a function of concentration, it is necessary to solve the equation

$$\partial C/\partial t=(\partial/\partial x)[D(\partial C/\partial x)]. \tag{1}$$

For free diffusion between two infinite volumes from an initial sharp boundary, or for the case of diffusion from a reservoir of constant concentration into a semi-infinite volume, the concentration depends only on the single variable $\xi=x/t^{\frac{1}{2}}$, and

$$D(C)=-\tfrac{1}{2}(d\xi/dC)\int_0^C \xi dC. \tag{2}$$

This equation is solved graphically,[1] with or without the use of certain mathematical devices[2] designed to improve the inherent inaccuracy of the graphical determination of the derivative $d\xi/dC$. There are instances, however, in which a single integral diffusion coefficient representing the entire diffusion process may be desired. Some workers estimate such a diffusion coefficient by the obviously incorrect procedure of evaluating D at some fixed concentration (usually half the initial concentration), using an integrated solution of Eq. (1) in which D has been treated as a constant. A correct, but laborious and somewhat inaccurate method, would be to average Eq. (2) graphically over all values of C. It is the purpose of this note to show that the desired average or integral diffusion coefficient can be evaluated directly from the data without the necessity of graphical evaluation of the derivative $d\xi/dC$.

The desired integral diffusion coefficient is

$$\bar{D}=(1/C_0)\int_0^{C_0} D(C)dC \tag{3}$$

for diffusion between concentrations $C=0$ and $C=C_0$. We now define a function $\phi(C)$ such that

$$\phi(C)-\phi(0)=\int_0^C \xi dC. \tag{4}$$

Combining (2), (3), and (4) we obtain

$$\bar{D}=-(1/2C_0)\left[\int_0^{C_0}\phi(C)(d\xi/dC)dC-\phi(0)\int_0^{C_0}(d\xi/dC)dC\right]. \tag{5}$$

Integrating the first term by parts and rearranging, we have, in view of (4),

$$\bar{D}=-(1/2C_0)\left\{\xi(C_0)\int_0^{C_0}\xi dC-\int_0^{C_0}\xi^2 dC\right\}. \tag{6}$$

If the boundary conditions are

$$C=C_0 \text{ at } x=0 \text{ for all } t$$
$$C=0 \text{ for all } x>0 \text{ at } t=0$$

then $\xi(C_0)=0$, and since $\int_0^{C_0}\xi dC$ is finite,

$$\bar{D}=(1/2C_0)\int_0^{C_0}\xi^2 dC. \tag{7}$$

If the boundary conditions are

$$C=C_0 \text{ for } x=0 \text{ to } x=-\infty \text{ at } t=0$$
$$C=0 \text{ for } x=0 \text{ to } x=+\infty \text{ at } t=0$$

conservation of mass requires that

$$\int_0^{C_0}\xi dC=0 \tag{8}$$

while $\xi(C_0)$ is infinite.[3] However by Eq. (2)

$$\xi\int_0^C \xi dC=-2D(C)\xi(dC/d\xi) \tag{9}$$

so that the first term in Eq. (6) will vanish provided that

$$\lim_{C\to C_0}(dC/d\log\xi)=0. \tag{10}$$

This condition appears to be always fulfilled in actual diffusion; hence Eq. (7) holds for either set of boundary conditions. It is readily shown that the same arguments apply if neither of the initial concentrations is zero, that is when diffusion takes place between concentrations C_1 and C_2. The result is then

$$\bar{D}=\frac{1}{2(C_2-C_1)}\int_{C_1}^{C_2}\xi^2 dC. \tag{11}$$

When differential diffusion coefficients are determined by the use of Eq. (2) the values of D at the ends of the concentration range, where $d\xi/dC$ is largest, are always uncertain; the accurate knowledge of $\bar{D}$ is then a useful aid in the estimation of these diffusion coefficients.

In view of the striking simplicity of the final result, it seems strange that the procedure described here should be unknown; however, the writer has not been able to find any reference to it in the literature.

[1] R. M. Barrer, *Diffusion in and through Solids* (Cambridge University Press, London, 1941), pp. 47–49.

[2] Eversole, Peterson, and Kindsvater, J. Phys. Chem. **45**, 1398 (1941).

[3] In some cases the original plane $x=0$ will not satisfy Eq. (8) after diffusion has taken place for some time. This difficulty is overcome by the choice of a new plane at $x'=0$ for which the above integral vanishes; see reference 1.

The Reaction of Atomic Hydrogen with Ethane

M. R. Berlie and D. J. LeRoy
Department of Chemistry, University of Toronto, Toronto, Canada

(Received October 29, 1951)

IT is generally accepted[1] that the primary reaction of atomic hydrogen with a paraffin molecule can be represented by the

elementary reaction

$$H+RH=H_2+R. \quad (1)$$

However, the determination of rate constants, steric factors, and activation energies for such reactions involves a number of difficulties which have an important bearing on the accuracy of the values obtained.

Since the rate of (1) would be given by the expression

$$\mathfrak{R}=k[H][RH], \quad (2)$$

the determination of k requires a knowledge of $\mathfrak{R}$, [H], and [RH]. Most of the published data have been obtained by the Wood-Bonhoeffer method.[1] $\mathfrak{R}$ is equated to the rate of consumption of paraffin; [H] is measured in a fixed position in the reactor and is assumed to have a constant value throughout the reaction zone; either initial or average values are used for [RH]. In a few cases average values of [H] were used,[2] based on measurements at the top and bottom of the reactor. In no case was allowance made for recombination of H-atoms.

It is clear that if a recombination reaction of the type

$$R+H(+M)=RH(+M) \quad (3)$$

occurs, the value of $\mathfrak{R}$ used will be too small. Also [H] will decrease approximately exponentially with time, and even its average value will yield a low value for k; the assumption about [RH] will have the same effect. The magnitude of the error in k arising from the above assumptions, as well as certain others which will not be discussed here, will depend on the particular paraffin and the experimental conditions used, but in general the calculated values will be low.

It might be anticipated that the error in k would have little effect on the activation energy E, calculated from the temperature coefficient through the relation

$$k=pZe^{-E/RT}. \quad (4)$$

However, only a very few studies have been made of the effect of temperature on k. The practice has been to assume that $p=0.1$ and to calculate E from data for a single temperature. This is clearly open to criticism, and in recent papers[2,3] evidence has been put forward suggesting that p might be considerably less than 0.1.

The difficulties outlined above have been largely eliminated by using the method of Dingle and LeRoy[4] for the production and detection of atomic hydrogen. Our results for ethane will be reported here in brief.

By increasing the area of the detector it was possible to remove all of the H-atoms from the stream at that point and to calculate the absolute value of [H] at any time (position in the reactor). Methane was the only product, and measurement of the amount produced up to any position of the detector permitted the calculation of $[C_2H_6]$ as a function of time. Allowance was made for the recombination of H-atoms. From the quantity of ethane and atomic hydrogen consumed it was possible to measure the extent of reaction (3) and thus to obtain the true value of $\mathfrak{R}$.

Values of k were obtained in this way for four temperatures in the range 80° to 163°C. The collision diameters were taken to be the same as those used by Trost and Steacie.[2] From the plot of $\log(k/Z)$ *vs* $1/T$ the activation energy of reaction (1) was found to be 6.2 ± 0.1 kcal per mole, the steric factor to be 3.3×10^{-3}.

For comparison, a value of k for 24°C was calculated from Eq. (4) using our values of p and E. From Table I it is seen that this is larger than the values obtained by other workers, as predicted. Full details of this work will appear in a later publication.

The authors are indebted to the Associate Committee on Scientific Research of the University of Toronto for financial assistance.

TABLE I. Comparison of rate constants for the reaction $H+C_2H_6=H_2+C_2H_5$ at room temperature.[a]

Authors	Reaction	Collision yield $\times10^8$	k cm³ molec^{-1} sec^{-1} $\times10^{17}$
Chadwell and Titani[b]	$H+C_2H_6$	1.8	1.2
Steacie[c]	$H+C_2H_6$	3.3	2.2
Trost and Steacie[d]	$H+C_2H_6$	2.0	1.3[5]
Trost and Steacie[d]	$D+C_2H_6$	3.0	2.0[2]
Taylor *et al.*[e]	$D+C_2H_6$	6.2	4.1[8]
Berlie and LeRoy	$H+C_2H_6$	9.4	6.3[9]

[a] The first five values of k were calculated from the data of Table IV, reference 2 by the relation $k=Z\times$collision yield.
[b] H. M. Chadwell and T. Titani, J. Am. Chem. Soc. **55**, 1363 (1933).
[c] E. W. R. Steacie, J. Chem. Phys. **6**, 37 (1938).
[d] See reference 2.
[e] Trenner, Morikawa, and Taylor, J. Chem. Phys. **5**, 203 (1937).

[1] E. W. R. Steacie, *Atomic and Free Radical Reactions* (Reinhold Publishing Corporation, New York, 1946).
[2] W. R. Trost and E. W. R. Steacie, J. Chem. Phys. **16**, 361 (1948).
[3] Steacie, Darwent, and Trost, Faraday Soc. Disc. **2**, 80 (1947).
[4] J. R. Dingle and D. J. LeRoy, J. Chem. Phys. **18**, 1632 (1950).

Errata: Magnetic Study of Some Organometallic Compounds of Arsenic

[J. Chem. Phys. **19**, 1051 (1951)]

MATA PRASAD AND L. N. MULAY
Chemical Laboratories, Institute of Science, Bombay, India

ON p. 1051, right-hand column, last line, "mean values" should read "mean value."

On p. 1052, left-hand column, 6th line below Table I, "characters" should read "character"; Table II,

$$[H_2N\cdot C_6H_4\cdot As{:}As\cdot C_6H_4NH_2]{:}2HCl$$

should read

$$[H_2N\cdot C_6H_4\cdot As{:}As\cdot C_6H_4\cdot NH_2]{:}2HCl;$$

and right-hand column, 1st line below Table I, for "alkyl arsines" should read "aryl arsines."

On p. 1054, caption for Figs. 1 and 2, omit the following words from the caption: "Fig. 1 (above). χ_m plotted against Z for several salts of As, Sb, and Bi" and "Fig. 2 (below) χ_m plotted against Z for the halides of As, Sb, and Bi"; right-hand column, 19th line from top, the equation should read $\chi{:}O=\chi-As{:}O(OH)_2$ $-\chi\equiv As(OH)_2$; and right-hand column, 12th line from bottom "magnitude 0.5λ" should read "magnitude -5λ."

On p. 1055, caption for Figs. 3 and 4, omit the following words from the caption: "Fig. 3 (above): χ_m plotted against Z for the oxides, sulfides, and iodides of As, Sb, and Bi." and "Fig. 4 (below): χ_m plotted against N for compounds containing the same anion."

On p. 1056, right-hand column, 22nd line from top, "χR" should read "Z_R."

Free Radical Processes in the Photolysis of Acetone

SIDNEY W. BENSON* AND CHARLES W. FALTERMAN†
Chemistry Department, University of Southern California, Los Angeles 7, California

(Received October 24, 1951)

THE mechanism for the photodecomposition of acetone in the vapor phase for the wavelength region 2000–3000A has been fairly well established,[1] but there have been differences of opinion and experimental finding concerning the region above 3000A. In particular there have been conflicting findings with regard to the nature of the primary process at the longer wavelengths. Several groups are inclined to the interpretation that the primary process above 3000A is predominantly direct dissociation into ethane and carbon monoxide.[2–4]

The nature of the primary process can be tested experimentally through a study of the photolysis of a mixture of C_2H_6CO and C_2D_6CO. A free radical mechanism should lead to 25 percent each of C_2H_6 and C_2D_6 and 50 percent $C_2H_3D_3$ in the ethane fraction.

A molecular mechanism will give none of the mixed ethane $C_2H_3D_3$. Thus from the amount of mixed ethane produced it would

be possible to calculate precisely the contribution of the two processes.

A sample of heavy acetone (>96 percent D) was prepared by successive exchanges of D_2O and light acetone. Fifty-percent mixtures of this material with C_2H_6CO were prepared in sealed quartz tubes and irradiated under the following conditions: at 2537A at 60°C and 120°C; at 3000–3400A at 35°C and 80°C.

The products after photolysis were fractionated, and the ethane samples analyzed with a mass spectrometer, using C_2H_6 and C_2D_6 samples for calibration.

It was found that the ethane distribution at all temperatures and wavelengths corresponded to within 2 percent of that predicted for a completely free radical mechanism. The conclusion is, therefore, that the primary process in the photolysis of acetone is a direct split into free radicals at all wavelengths. Further details of this work will appear in a subsequent article.

The authors wish to express their appreciation to Mr. Phillip Magee of the Chemistry Department for his aid in preparing the heavy acetone and to the Atomic Energy Commission for the sample of heavy water used. We are also indebted to Mr. Lake, Mr. Ellis, and Mr. Murrill of the Union Oil Research Group at Brea, California for conducting the mass spectrograph analysis.

* Professor of chemistry.
† Present address, Naval Ordnance Research Base, Inyokern, California.
[1] L. M. Dorfman and W. A. Noyes, Jr., J. Chem. Phys. **16**, 557 (1948); **16**, 788 (1948).
[2] R. Spence and W. Wild, J. Chem. Soc., 352 (1937).
[3] Feldman, Burton, Ricci, and Davis, J. Chem. Phys. **13**, 440 (1945).
[4] Volman, Leighton, Blacet, and Brinton, J. Chem. Phys. **18**, 203 (1950).

A Tentative Interpretation of the Magnetic Behavior of Pr_6O_{11}

KEI YOSIDA
Department of Physics, Osaka University, Osaka, Japan
(Received October 23, 1951)

SHERMAN W. RABIDEAU[1] has measured the magnetic susceptibilities of three stable oxides of praseodymium, Pr_2O_3, Pr_6O_{11}, and PrO_2 over a temperature range between 80°K and 300°K. According to his experimental results, the susceptibilities of Pr_2O_3 and PrO_2 obey the Curie-Weiss law with negative paramagnetic Curie temperatures, whereas the reciprocal susceptibility *vs* temperature plot for Pr_6O_{11} manifests a curvature, not a straight line like the other two oxides, running across the temperature axis at a positive value, though this temperature was not reached in the above experiments. The effective Bohr magneton numbers for the three oxides are all in accordance with the values expected from the Hund's or Van Vleck and Frank's theory, considering Pr_6O_{11} as a mixture of Pr^{3+} and Pr^{4+} with the ratio of 1:2.

The negative paramagnetic Curie temperatures for the sesquioxide and dioxide show these two oxides to be antiferromagnetic materials, and therefore their magnetic susceptibilities would manifest a maximum value at each antiferromagnetic Curie temperature roughly corresponding to the absolute value of the paramagnetic Curie temperature. As for the case of Pr_6O_{11}, it is considered that its magnetic behavior can be interpreted on the basis of the model proposed by the writer for the interpretation of the magnetic properties of pyrrhotite.[2] This interpretation seems to be applicable to most materials in which a weak ferromagnetism appears as their chemical compositions deviate from those of the ideal stoichiometric materials which show the antiferromagnetism, such as FeS and αFe_2O_3.[3]

The x-ray analysis of these three oxides made by J. D. McCullough[4] showed that the crystal structure of Pr_2O_3 is hexagonal and those of Pr_6O_{11} and PrO_2 are both of the cubic fluorite type, and furthermore he concluded from the observed relative intensities of the diffraction lines that Pr_6O_{11} has a structure missing one-twelfth of the oxygen ions randomly from the oxygen lattice points of an ideal structure. Therefore, in Pr_6O_{11} vacant oxygen lattice points are distributed at random. Since PrO_2, having the same crystal structure as that of Pr_6O_{11}, is an antiferromagnetic substance, it will be divided into two sublattices, each having Pr ions with + or − magnetic moment alone below its antiferromagnetic Curie temperature, also Pr_6O_{11} will be divided into two such sublattices below its antiferromagnetic Curie point. Thus if Pr^{3+} ions and Pr^{4+} ions are uniformly distributed over two magnetic sublattices in the latter substance, it will only manifest the antiferromagnetism, and its magnetic susceptibility will obey the Curie-Weiss law above the Curie point. On the other hand, in the case that Pr^{3+} ions have a tendency to occupy only one of the two magnetic sublattices below the Curie temperature, the magnetic moments on the two sublattices will not completely compensate each other on account of the different magnetic moments carried by Pr^{3+} and Pr^{4+} ions, and therefore a spontaneous magnetization equal to the difference of the magnetizations on the two sublattices will appear. L. Néel[5] called such a ferromagnetism essentially originating in the antiferromagnetism, "ferrimagnetism."

If the second situation, that Pr^{3+} ions are preferably situated on one of the two magnetic sublattices, is taking place in Pr_6O_{11}, the ferromagnetism will appear below the antiferromagnetic Curie temperature, and therefore above the Curie point. The reciprocal susceptibility will deviate from the linear Curie-Weiss law holding at the higher temperature side as the temperature is lowered, having a curvature so as to pass through zero at the antiferromagnetic Curie point, because otherwise the susceptibility at the Curie point would remain a finite value.

The experimental susceptibility of Pr_6O_{11} shows just such a ferrimagnetic feature in the temperature range between which the experiments have been made. Therefore, it is expected that this substance will become ferromagnetic below the Curie temperature which is supposed probably not to be so much lower than 80°K, while PrO_2 will become only antiferromagnetic at about this temperature. However, such an interpretation of the magnetic properties of Pr_6O_{11} mentioned above will, in future, be ascertained by the experiments in the lower temperature region.

[1] Sherman W. Rabideau, J. Chem. Phys. **19**, 874 (1951).
[2] K. Yosida, Prog. Theor. Phys. **6**, 356 (1951).
[3] K. Yosida, Physica (to be published, 1951).
[4] J. D. McCullough, J. Am. Chem. Soc. **72**, 1386 (1950).
[5] L. Néel, Ann. phys. **3**, 137 (1948).